Universidade de Aveiro Departamento de Geociências
2007

Rui Manuel do Amaral Branco de Oliveira Quartau

A plataforma submarina do Faial: Evolução morfológica e sedimentar

The insular shelf of Faial: Morphological and sedimentary evolution

Universidade de Aveiro Departamento de Geociências
2007

Rui Manuel do Amaral Branco de Oliveira Quartau

A plataforma submarina do Faial: Evolução morfológica e sedimentar

The insular shelf of Faial: Morphological and sedimentary evolution

tese apresentada à Universidade de Aveiro para cumprimento dos requisitos necessários à obtenção do grau de Doutor em Geociências, realizada sob a orientação científica do Professor Doutor Luís Menezes, Professor Associado do Departamento de Geociências da Universidade de Aveiro, com co-orientação científica do Dr. José Hipólito Monteiro, Investigador Coordenador aposentado do Instituto Nacional de Engenharia Tecnologia e Inovação, I.P.

O trabalho desenvolvido no decorrer desta tese foi suportado pelos projectos INGMAR (PLE/4/98), com financiamento da Fundação para a Ciência e Tecnologia (FCT) e pela Bolsa de Doutoramento da FCT SFRH/BD/11746/2003.

This work was supported by the INGMAR (PLE/4/98) project, financed by the Portuguese Foundation for Science and Technology (FCT) and by the FCT fellowship SFRH/BD/11746/2003.

o júri

presidente

Professora Doutora Celeste de Oliveira Alves Coelho
Professora Catedrática do Departamento de Ambiente e Ordenamento da Universidade de Aveiro

Professor Doutor Luís Filipe Fuentefria de Menezes Pinheiro
Professor Associado do Departamento de Geociências da Universidade de Aveiro

Dr. José Hipólito Monteiro
Investigador Coordenador aposentado do Instituto Nacional de Engenharia Tecnologia e Inovação

Professor Doutor Óscar Manuel Fernandes Cerveira Ferreira
Professor Associado da Faculdade de Ciências do Mar e Ambiente da Universidade do Algarve

Professor Doutor Rui Pires de Matos Taborda
Professor Auxiliar da Faculdade de Ciências da Universidade de Lisboa

Professor Doutor Fernando Joaquim Fernandes Tavares Rocha
Professor Catedrático do Departamento de Geociências da Universidade de Aveiro

Professora Doutora Cristina Maria de Almeida Bernardes
Professora Associada do Departamento de Geociências da Universidade de Aveiro

agradecimentos

Esta tese de Doutoramento não teria sido possível sem a colaboração de muitas pessoas e instituições às quais gostaria de exprimir os meus agradecimentos:

Ao Professor Luís Menezes Pinheiro por ter aceite orientar esta tese e pelo seu espírito crítico que contribuíram significativamente para a qualidade deste trabalho.

Ao Dr. Hipólito Monteiro por me ter incentivado e acreditado em mim e me ter ensinado coisas como “Difficulties are things to overcome” ou “Now, here, you see, it takes all the running you can do, to keep you in the same place. If you want to get somewhere else, you must run at least twice as fast as that!".

Ao Departamento de Geologia Marinha do Instituto Nacional de Engenharia Tecnologia e Inovação, I.P. (DGM-INETI), anterior Instituto Geológico e Mineiro onde desenvolvi a maior parte deste trabalho. Aqui cresci cientificamente e aprendi a trabalhar em equipa, mas também usufruí do excelente ambiente de companheirismo. Um grande agradecimento ao Professor Pedro Gancedo Terrinha que me trouxe para este ambiente ímpar. Ao Dr. Hipólito Monteiro, à Dra. Fátima Abrantes e ao Professor Luís Menezes Pinheiro, directores do departamento durante este período e ao seu trabalho incansável na realização do projecto INGMAR, sem o qual não teria sido possível realizar este trabalho. À Margarida Henriques por todo o apoio administrativo que me deu. Um agradecimento especial aos meus colegas do DGM-INETI: Francisco Curado Teixeira pela amizade e realização das campanhas geofísicas, Henrique Duarte e Cristina Roque pela amizade, apoio e valiosas discussões científicas, Pedro Brito, Tiago Cunha, Serguei Bouriak, Carlos Pinto, Célia Pata e Joana Gafeira, pela ajuda nos trabalhos de campo, Susana Muiños, pela ajuda nos trabalhos de laboratório.

À Secretaria Regional do Ambiente dos Açores que financiou o projecto GEMAS – Avaliação, Gestão e Monitorização de Areias Submersas do Faial, Pico e São Miguel, cujos dados permitiram a realização deste trabalho.

Um especial agradecimento ao Dr. Neil Mitchell da Universidade de Manchester pelas importantes discussões científicas que aumentaram consideravelmente a qualidade deste trabalho.

agradecimentos

Ao Departamento de Oceanografia e Pescas (DOP) da Universidade dos Açores pela amável disponibilidade com que sempre me receberam e ao seu director Dr. Ricardo Serrão Santos. Um especial agradecimento ao apoio incansável do Frederico Cardigos. Agradeço também ao Fernando Tempera que embarcou comigo nesta aventura de decifrar os mistérios da parte submarina do Faial. Agradeço também ao Dr. Igor Bashmachnikov pelas discussões sobre a Oceanografia dos Açores e ao Rogério Ferraz e Ana Meirinho pelo apoio prestado. Um agradecimento às equipas da Lancha *Águas Vivas* e Navio *Arquipélago* que tornaram sempre agradáveis e divertidas as campanhas no mar.

Agradeço também à Professora Isabel Âmbar, Professor Joaquim Henrique Dias e Professor José Teixeira da Silva do Centro de Oceanografia da Faculdade de Ciências da Universidade de Lisboa tudo aquilo que me ensinaram sobre Oceanografia. Um especial agradecimento ao Professor Joaquim Henrique Dias que teve sempre uma paciência enorme para me explicar os fundamentos matemáticos da Oceanografia.

Agradeço ao José Sampaio do Departamento de Hidrogeologia do INETI, as discussões sobre a hidrogeologia das ilhas dos Açores.

Agradeço ao Sérgio Diogo Caetano da Arena (Agência Regional da Energia da Região Autónoma dos Açores) o apoio dado na aquisição de dados e bibliografia.

Agradeço ao Dr. Sérgio Ávila do Departamento de Biologia da Universidade dos Açores as discussões sobre as variações do nível do mar.

Agradeço à Dra. Maria Emília Novo do Núcleo de Águas Subterrâneas do Departamento de Hidráulica e Ambiente do Laboratório Nacional de Engenharia Civil as discussões sobre a hidrogeologia das ilhas dos Açores e o empréstimo de bibliografia.

Agradeço à Professora Zilda França, Investigador José Manuel Rodrigues Pacheco, Professor João Carlos Nunes do Departamento de Geociências da Universidade dos Açores, pela disponibilização das suas teses de Doutoramento.

Um especial agradecimento a todos meus amigos que me apoiaram nas horas difíceis.

E por fim, mas não os menos importantes agradeço aos meus pais e à Joaninha o grande apoio que me deram.

Acknowledgements

This PhD thesis would not have been possible without the help and support of many people and institutions to whom I would like to express my gratefulness.

I am grateful to Professor Luís Menezes Pinheiro for accepting me as a PhD student and for his critical reviews that greatly improved this thesis.
I am also grateful to Dr. Hipólito Monteiro for his encouragement, personal belief and for teaching me attitudes such as “Difficulties are things to overcome” or “Now, here, you see, it takes all the running you can do, to keep you in the same place. If you want to get somewhere else, you must run at least twice as fast as that!".

I am also indebted to the Marine Geology Department of the National Institute of Engineering, Technology and Innovation, I.P. (DGM-INETI), former Geological and Mining Institute. Here, I’ve learnt how to do science and team work, but I’ve also profited from a healthy work environment. A special acknowledgment to Professor Pedro Gancedo Terrinha who introduce me to this unique environment. To Dr. Hipólito Monteiro, Dra. Fátima Abrantes and Professor Luís Menezes Pinheiro, who have been Heads of the department during this period and to their unfatigable dedication to the project INGMAR, without which it would not be possible to accomplish this work. To Margarida Henriques for the administrative support. A special acknowledgment to my DGM-INETI colleagues: Francisco Curado Teixeira for his friendship and for the technical supervision of the geophysical surveys, Henrique Duarte e Cristina Roque for their friendship, support and constructive scientific discussions, Pedro Brito, Tiago Cunha, Serguei Bouriak, Carlos Pinto, Célia Pata e Joana Gafeira, for their help in the field work, Susana Muiños, for her help in the laboratory work.

To Secretaria Regional do Ambiente who financially supported the GEMAS project – Evaluation, management and monitoring of the submarine sands of Faial, Pico and São Miguel Islands, whose data allowed the accomplishment of this work.

A special acknowledgment to Dr. Neil Mitchell of the Manchester University for the invaluable scientific discussions that greatly improved the quality of this work.

Acknowledgements

To the Department of Oceanography and Fisheries of the Azores University for its friendly welcome and to his Head, Dr. Ricardo Serrão Santos. A special acknowledgment to the unfatigable support of Frederico Cardigos. I am also thankful to Fernando Tempera who has initiated with me this adventure of finding the secrets of the depths of the Faial Island. Thanks also to Dr. Igor Bashmachnikov for the discussions over the Azores Oceanography and to Rogério Ferraz and Ana Meirinho for their support. Thanks to the crews of the R/L *Águas Vivas* and R/V *Arquipélago* who turn the sea surveys always pleasant and funny.

I am grateful to Professor Isabel Âmbar, Professor Joaquim Henrique Dias and Professor José Teixeira da Silva of the Oceanography Centre of the Science Faculty of the Lisbon University for everything that they taught me about Oceanography. A special acknowledgment to Professor Joaquim Henrique Dias that was unfatigable explaining me the mathematical fundaments of Oceanography.

I am grateful to José Sampaio from the Hydrogeology Department of INETI, for the discussions about the Azores hydrogeology.

I am grateful to Sérgio Diogo Caetano from the Arena (Regional Agency of Energy of the Azores Autonomous Region) for the support given in the acquisition of data and references.

I am grateful to Dr. Sérgio Ávila from the Biology Department of the Azores University for the discussions about sea-level oscillations.

I am grateful to Dra. Maria Emília Novo from the Groundwater Nucleus of the Hydraulic Department of the National Laboratory of Civil Engineering for the discussions about the Azores hydrogeology and for the references that she lent me.

To Professor Zilda França, Researcher José Manuel Pacheco, Professor João Carlos Nunes from the Geosciences Department of the Azores University, for making available their PhD thesis.

A special acknowledgment to all my friends that were there to support me during the difficult times.

And last but not the least to my parents and to Joaninha for all their huge support.

palavras-chave

Ilhas vulcânicas, plataforma insular do Faial, evolução da plataforma, dinâmica sedimentar actual, avaliação de inertes.

resumo

Este trabalho pretende compreender a origem e evolução das plataformas insulares de ilhas vulcânicas, particularmente a ilha do Faial, assim como a sua dinâmica sedimentar actual. Dados batimétricos e perfis sísmicos de alta resolução (*Boomer* e *Chirp*) foram usados para caracterizar geologicamente a plataforma insular do Faial. A amostragem de sedimentos na plataforma foi utilizada para descrever a distribuição granulométrica dos sedimentos e também para a criação de um modelo da sedimentação actual na plataforma insular do Faial. A caracterização geológica, assim como a variação granulométrica dos sedimentos na plataforma contribuíram para entender quais os processos responsáveis pela geomorfologia da plataforma actual. Verificou-se que a plataforma actual resulta essencialmente da interacção entre a erosão provocada pela ondulação e a progradação vulcânica da parte subaérea.

A plataforma é composta normalmente por blocos de dimensão métrica, entre a linha de costa e os 30 a 50 metros de profundidade. Estes depósitos resultam da erosão de escoadas lávicas, que nalguns casos se encontram bem preservadas, podendo ser discriminadas dos blocos através dos perfis sísmicos *Chirp*. Junto à costa estes depósitos grosseiros podem resultar também da erosão de arribas. Mais afastados da costa encontram-se os depósitos de areia e cascalho, que foram cartografados até ao bordo da plataforma.

Foi encontrada uma relação linear entre a largura da plataforma e a idade do respectivo sector subaéreo, assim como uma relação entre a eficiência erosiva da ondulação e largura da plataforma. As fontes sedimentares dos depósitos de areia e cascalho provêm essencialmente da erosão das arribas costeiras e da erosão das bacias hidrográficas. Os mecanismos de transporte e deposição na plataforma foram também âmbito de estudo e parecem estar relacionados com correntes de retorno em direcção ao largo que se formam durante as tempestades.

Formulações matemáticas simples de transporte de sedimentos foram utilizadas para definir a partir de que profundidade o transporte perpendicular à linha de costa se torna insignificante. O transporte longilitoral foi calculado para os sectores da plataforma com sedimentos finos junto à costa. Estes cálculos foram usados para definir zonas de protecção da linha de costa, de modo a impedir que a extracção de inertes nestas zonas possa pô-la em risco.

As propriedades das areias e cascalhos foram avaliadas para a sua utilização como inertes. Estes sedimentos têm uma percentagem insignificante de finos (em média menos de 1% de silte a argila). De acordo com a sua distribuição granulométrica a utilização ideal é na confecção de cimento.

keywords

Volcanic islands, Faial island shelf, shelf evolution, present-day sedimentary dynamics, aggregates evaluation.

abstract

This work focuses on the origin and development of volcanic island shelves, particularly the Faial Island shelf and also on its present day sedimentary dynamics. Bathymetric data and high-resolution seismic profiles (*Boomer* and *Chirp* data) were used to characterize the geology of the Faial Island shelf. Sediment samplings were also used to map the grain-size distribution in the shelf and contributed to develop a model of the present day shelf sedimentation. The geological characterization and the sample data were also used to infer the processes responsible for the geomorphologic variability of the shelf. It was found that the main processes molding it in the past and also in the present are wave erosion and volcanic progradation.

The shelf is normally composed by boulder deposits between the shore and 30 to 50 meters water depth. These deposits normally result form the erosion of lava flows, which in some cases are still well preserved and can be discriminated from the boulders in the *Chirp* records. Nearshore, these coarse deposits may also be the result of the erosion of cliffs. Further offshore the sandy and gravely deposits dominate and can be mapped till the shelf break. A linear relationship between the width of the shelf sectors and respective age was found as well as a relationship between wave effectiveness and shelf width for the shelf sectors of the same age. The sources of the sand and gravel deposits are discussed and appear to be mainly related to cliff erosion and erosion of the hydrographic basins. The mechanisms of transport and deposition of these sedimentary deposits are also discussed and can be assigned to downwelling returning currents that occur during storms.

Simple mathematical formulations are used to define the shelf depth at which cross-shore transport is insignificant. Longshore transport rates are also estimated for the shelf sectors were sand and gravel sediments dominate nearshore. These calculations are used to define nearshore protection buffer zones for the extraction of aggregates, which are needed for coastal protection purposes.

The sand and gravel sediment proprieties were also discussed for their use as aggregates. These sediments have a very insignificant percentage of finer material (normally less than 1% of silt and clay). Their grain-size distribution shows that they are suitable for the production of mortar.

Table of contents

List of tables

List of figures

List of symbols

a	Dimensionless coefficient in formula 58
b	Dimensionless coefficient in formula 59
$APSW$	Average present-day shelf width (*m*)
C_g	Intermediate-water group velocity (*m* s^{-1})
C_{g0}	Deep-water wave group velocity (*m* s^{-1})
C_0	Deep-water wave velocity (*m* s^{-1})
CSW	Calculated shelf width (*m*)
CER	Corrected cliff erosion rate (*mm/year*)
d_b	Breaker depth (*m*)
d_c	Closure depth of the upper shoreface for one year interval (*m*)
$d_{l,t}$	Closure depth of the upper shoreface for t years interval (*m*)
d_i	Closure depth of the lower shoreface for one year interval (*m*)
D_{50}	Median grain size of the sediment (*mm*)
D_d	Dimensionless grain diameter
ER	Erosion rate of basaltic cliffs (*mm/year*)
f	Frequency of each wave in the spectra (*Hz*)
f_i	ith Frequency of each wave in the spectra (*Hz*)
f_{ws}	Annual frequency of each wave per quadrant (%)
f_{ps}	Annual frequency of each wave period per quadrant (%)
$f(\alpha_b)$	Directionally factor
g	Acceleration due to gravity (*m* s^{-2})
h	Water depth (*m*)
h_{LS}	Closure depth of the lower shoreface for one year interval using the wave base concept (*m*)
h_{ED}	Sediment entrainment water depth (*m*)
H	Wave height (*m*)
H_s	Significant wave height (*m*)

H_{sb}	Significant wave height at the breaker line (*m*)
H_b	Root-mean-square wave height at the breaker line (*m*)
$H_s(m_0)$	Significant wave height derived from the spectral moments (*m*)
$H_s(m_0)_i$	ith Significant wave height derived from the spectral moments (*m*)
$H_s(m_0)_{av}$	Mean annual significant wave height per quadrant derived from the spectral moments (*m*)
H_{sav}	Mean annual significant wave height per quadrant (*m*)
H_{sx}	Significant wave height that is exceeded only 12 hours each year (*m*)
$H_{e,t}$	Significant wave height that is exceeded 12 hours per t years (*m*)
k	Wave number
k'	Breaker depth index
K_r	Refraction coefficient
K_s	Shoaling coefficient
L	Intermediate water wave length (*m*)
L_0	Deep-water wave length (*m*)
m_0	Variance of the sea surface elevation
M1	Mean grain size
M2	Sorting
M3	Skewness
M4	Kurtosis
PT	Percentage of time that the sea has been at a determined level (%)
Q_{LS}	Longshore sediment transport rate integrated across the surf zone (m^3 s^{-1})
Q_{LSt}	Longshore sediment transport rate integrated across the surf zone considering the annual wave frequency (Km^3 $year^{-1}$)
s	Ratio of densities of grain and water
SA	Age of the abrasional shelf (*years*)
$S(f)$	Omnidirectional wave spectrum in terms of the variance of surface elevation
$tan\beta$	Beach slope
T	Wave period (*s*)
$\overline{T}$	Mean wave period (*s*)

T_n	Scaling period for waves (*s*)
T_p	Peak spectral wave period (*s*)
T_s	Significant wave period (*s*)
T_z	Zero crossing wave period (*s*)
T_{pav}	Mean annual peak Period (*s*)
T_{pi}	ith Peak spectral wave period (*s*)
T_{sav}	Mean annual significant wave Period (*s*)
T_{sx}	Significant wave period that is exceeded only 12 hours each year (*s*)
$T_{e,t}$	Significant wave period that is exceeded 12 hours per t years (*s*)
U_{dwc}	Dimensionless critical orbital velocity
U_w	Wave orbital velocity ($cm\ s^{-1}$)
U_{wc}	Critical wave orbital velocity ($cm\ s^{-1}$)
W_{dv}	Dimensionless settling velocity
α_0	Deep-water angle between wave crests and depth contours (*degrees*)
α_b	Angle between wave crests and shoreline at breaker line (*degrees*)
ρ	Density of the water ($kg\ m^{-3}$)
ρ_s	Density of the particle ($kg\ m^{-3}$)
ρ_y	Submerged particle density ($kg\ m^{-3}$)
σH_s	standard deviation of the significant wave height
θ_{cr}	Threshold Shields parameter
$\hat{\theta}_{cr}$	Threshold factor
θ_m	Mean Shields parameter
$\theta_{\max}$	Maximum Shields parameter
θ_{wr}	Rough-flow wave Shields parameter
θ_{wsf}	Sheet-flow wave Shields parameter
μ	Dynamic viscosity of the water ($Kg\ m^{-1}\ s^{-1}$)

Chapter 1. Nature and scope of this work

1.1 Introduction

Marine aggregates extraction (sand and gravel) are becoming more and more an important mineral resource as land based resources are being depleted, polluted or subjected to more severe laws for environmental protection (International Council for the Exploration of the Sea, 2000).

In Portugal, only the shelves of the Azores and Madeira Islands are being subjected to episodic offshore exploitation where the industry has started dredging in almost all islands, without previous geological studies. For that reason, the assessment of the offshore gravel and sands deposits at Faial, Pico and S. Miguel islands has been considered a priority by the Regional Government of Azores and the GEMAS project was developed. To accomplish these objectives, a consortium was established between the Departamento de Oceanografia e Pescas (DOP) of the Azores University and the Departamento de Geologia Marinha (DGM) of the former Instituto Geológico e Mineiro, now Laboratório Nacional de Energia e Geologia, I.P. (LNEG).

The increasing demand for offshore aggregates is even more critic for the Azores Islands, since in most cases inland extractions are performed in rivers and estuaries, which are missing in these islands. Inland extractions are currently being made in piroclastic deposits, but offshore exploitation will increase in the near future as onshore quarries become depleted and laws for environment protection become more severe.

Although the initial aim of the project was restricted to the reconnaissance of the offshore aggregate resources, the data revealed remarkable geological features on the shelves of these islands and after them new questions arose. It soon became clear that a more comprehensive study had to be undertaken to understand these new scientific problems, originating this PhD project.

In order to understand the approach taken to accomplish this study, it is important to introduce first some general definitions about the processes involved in the creation, evolution and the sedimentary dynamics of continental shelves in general, and island shelves in particular.

1.2 State of the art

1.2.1 The coastal zone

The coastal zone, as defined by Inman and Brush (1973) is composed of the coastal plain, the shoreface and the continental shelf (Figure 1). The coastal plain is an area of flat, low-lying land adjacent to a seacoast and separated from the interior by a major change in topography, which is often absent in the Azorean Islands. The shoreface is the upper part of the continental shelf that is affected by contemporary wave processes and extends from the limit of wave run-up to the depth limit for wave-driven sediment transport (Cowell et al., 1999). The continental shelf is the area that extends from the toe of the shoreface to the depth at which there is a marked increase in the slope to greater depths. This zone of increasing slope is named the shelf edge or shelf break. It is a first order topographic feature because it serves as a natural boundary between two major physiographic provinces: the continental shelf and the continental slope (Southard and Stanley, 1976). These two provinces, together with the continental rise, where present, are part of the continental margin. Land areas that geologically don't belong to the continents, like oceanic islands, are often surrounded by a shallow submarine platform which, strictly speaking, is not a continental shelf and is often referred to as an insular shelf (Eisma, 1988). Depending on the island shelf morphology, the shoreface might or not be individualized from the rest of the shelf. These aspects will be discussed in more detail in the Chapter 6.

The geological framework of shelves and the origin of the shelf break have been widely discussed by Hedberg (1970), Shepard (1973), Emery (1980) and Vanney and Stanley (1983). The present day continental margins along the Atlantic and along large parts of Antarctica, Australia, India and eastern Africa

were formed after the breakup of Pangea approximately 200 Ma ago. It is generally agreed that the break bounding the shelf-slope couple is manly controlled by structural and isostatic factors resulting in downwarping, flexuring or vertical and lateral offset (Southard and Stanley, 1976).

Superimposed on this primary structural control – and thus of second order importance – is the strong imprint of Pliocene to recent geological events, which to a large degree molded the topography of the continental margins now observed. Most significant in this respect are the large-scale eustatic oscillations in sea level related to the cyclic growth and decay of ice sheets. The coastline at times of major regressions was probably located at or near the break (Southard and Stanley, 1976).

A factor of third-order importance is the effect of the present day physical shelf processes that continue to modify the superficial sedimentary cover of the shelf by eroding and transporting sediment.

The coastal zone, as it is today, is the product of the three factors exposed before, along geological times. However, some of the processes acting on the formation of a volcanic island shelf are quite different as well as it is their relative importance in the shelf evolution. These unique processes are discussed in the following section.

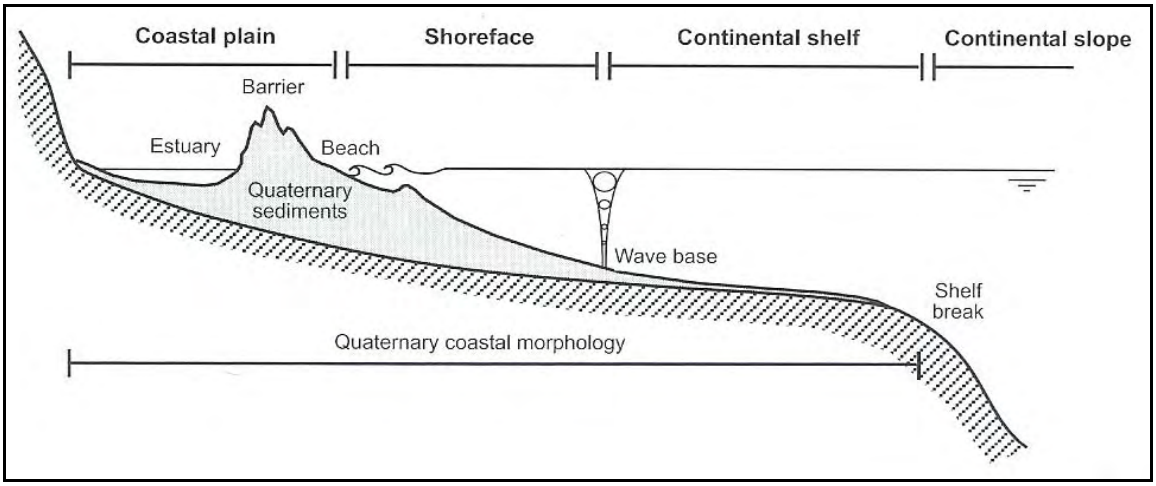

Figure 1 – Spatial boundaries of the coastal zone (Masselink and Hughes, 2003).

1.2.2 Insular shelf formation and evolution

The present–day morphology of the island shelf is the result of a continuous equilibrium between constructive and destructive processes. The constructive processes can be effusive and moderately explosive activities and also tectonic uplift movements. During the proto-insular and young insular stages, the submarine parts of volcanic islands are being constantly renewed due to the intense volcanic activity. The destructive processes may be episodic during the constructive stages, but become predominant as the island gets older. The volcanic activity becomes less frequent and the island cools and starts subsidence.

Menard (1983; 1986) suggested that the growth of a shelf reflects a long-term competition between processes infilling the shelf (e.g., progradation of lava deltas) and those enlarging it (shoreline erosion by surf, subaerial erosion of coastal cliffs and fluvial erosion on the shelf during sea-level lowstands). During early growth stages, large-scale landsliding can remove sections of the island and their associated shelves. Following the phase of active volcanism, shelves widen progressively, so that shelf widths in the Canaries and Hawaii increase in proportion to edifice age. Erosion is also faster where the swell is stronger in one direction, e.g., because of trade winds, an effect observed around Tenerife (Mitchell et al., 2003). Complicating this simple picture are the effects of sea-level variation and tectonic subsidence/uplift of the island.

The sediment stratigraphy of island shelves is even more poorly known, but various factors make shelves potentially useful natural laboratories for studying stratigraphic development. Around continental margins, stratigraphy develops from a complex interplay of tectonics, sediment supplied from the continent, transport by currents, shoreline processes and erosion during sea-level variations. The interplay between these distinct controlling factors may produce extremely different depositional architectures (Galloway and Hodbay, 1996; Johnson and Baldwin, 1986; Thorne and Swift, 1991). There are a number of reasons to expect island stratigraphy to be different and also simpler. For example, accommodation space for deposition is quite different, since the shelf is narrower and steeper than continental shelves. As the shelf is narrower, there is less attenuation of oceanic

swell from seabed friction so wave currents in shallow water are stronger. In addition, some Azorean areas have locally high rates of sediment supply from erosion of friable littoral cones. On the other hand, mainland Portugal is influenced by the Atlantic eastern boundary currents and by seasonal wind-driven upwelling and downwelling, effects that are missing or different around the Azores.

In order to understand the relative importance of the various controlling factors in the sedimentation of shelves some general processes are reviewed in detail during the following sections

1.2.3 Factors affecting the sedimentation in siliclastic shelves

Swift and Thorne (1991) proposed a general model for shelf sedimentation in which shelf facies characteristics were viewed as the result of progressive sorting operating through time as a sediment dispersal system. A dispersal system consists of three elements; sources, reservoirs and sinks connected by a transport pathway. The processes that affect the nature of the sedimentary facies on the present day siliclastic continental shelves have been discussed by Johnson and Baldwin (1986). Although the sediments in the Azores are not siliclastic in origin, the sedimentation patterns should not be very different, since there are no reefs like in the carbonate margins where these play an important role in the shelf dynamics. Furthermore, the sediments texture should be very similar to the sediments from siliclastic continental shelves and consequently the processes influencing the sedimentation on these shelves, which are reported below, should also be alike:

(1) Rate and type of sediment supply

The type and amount of sediment supplied directly from the land areas to the adjacent shelf is today largely determined by the degree to which river mouths and estuaries have readjusted to the Holocene transgression. Most present-day shelf sands were emplaced when sea-level was lower and continental, partly fluvio-deltaic deposition, prevailed over continental shelves. In the Azorean shelves the scenario might be quite different. First, there are no major rivers or

estuaries, which means that the sediment supply comes from different sources (e.g. high coastal erosion and derived from the volcanic activity) and secondly, because the accommodation space is smaller, it is not likely that large deposits have been formed before the present highstand sea-level.

(2) Physical processes

Currents and waves on the continental shelf are mainly generated by meteorological forces (winds and waves), tidal forces and other forces such as global circulation systems controlled by solar radiation. These forces generate four main types of currents: (1) oceanic circulation (semi-permanent) currents, (2) tidal currents, (3) meteorological currents, and (4) density currents (Figure 2). As already mentioned, a narrower and steeper shelf, like the one of Faial Island, may enhance some physical processes in detriment of others (e.g. swell versus tidal erosion). On the other hand, features like the Channel Faial-Pico are more easily reworked by tidal currents than by swell because of the sheltering effect of the nearby islands.

(3) Sea-level fluctuations

Sea-level fluctuations determine water-depth, which influences features such as hydraulic energy at seabed, the width of the shelf and the position of the river mouths supplying sediments. Fluctuations in the rate and extent of transgressions and regressions in the shoreline environment, which are themselves controlled by the rate of sediment supply and the rate of relative sea-level change, will significantly influence the spatial and temporal distribution of facies on the shelf (Johnson and Baldwin, 1986). During periods of lowered sea-level, coarser sediment is transported over former shelves by rivers; during periods of higher sea-level, only fine-grained sediment reaches many shelves and reworking processes predominate. Sedimentation in a volcanic island shelf during an oscillating sea-level might be different, due to the different sediment sources as well as to the distinct shelf morphology. The sea-level oscillations in volcanic islands are of remarkable importance in the way that these contribute significantly to the development of an abrasional shelf through surf erosion (Menard, 1983;

Menard, 1986) which consequently increases the accommodation space.

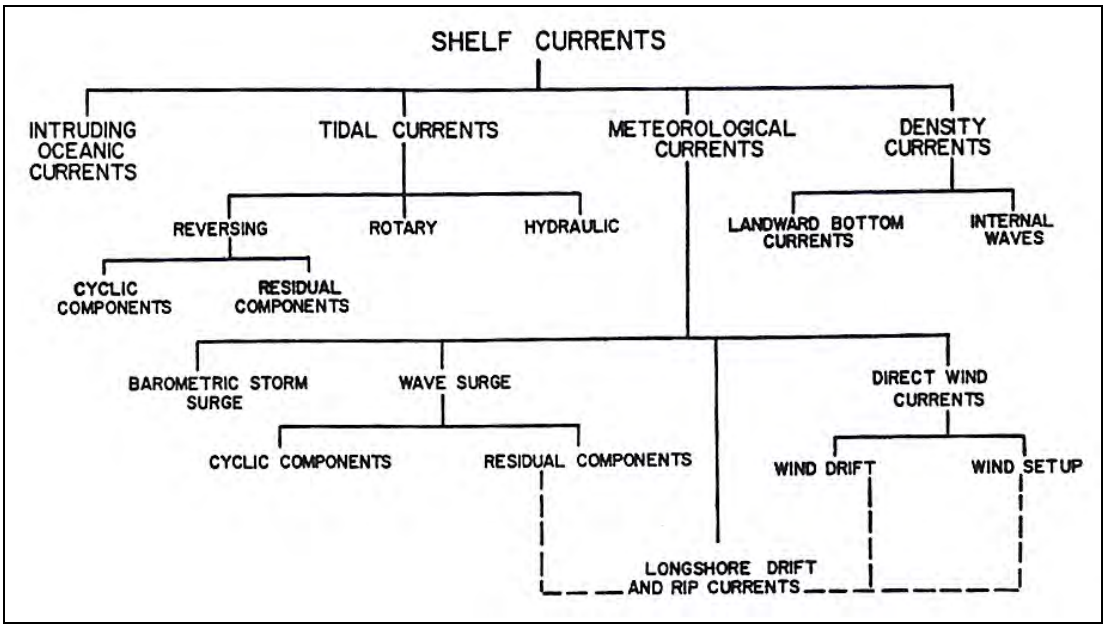

Figure 2 – Summary of the main physical processes influencing shelf hydraulic regimes (Swift et al., 1971).

(4) Climate

Climate controls shelf sediments mainly by its effects on the land areas. It determines the type and rate of weathering and erosion, thereby affecting the type of sediment available for transport. It also determines the mode of transport (water, wind or ice) which in turn affects the rate of supply of sediment to the receiving basin. Temperature and precipitation are the dominant climatic factors controlling the type of sediment on the shelf (Hayes, 1967). Marked seasonal variations also frequently control the main periods of shelf sedimentation. Menard (1983; 1986) shows some striking examples of asymmetric erosion in volcanic islands because of stronger rainfall in some parts of the coast in detriment of others. It is thus expectable to see the same effects in the Faial Island.

(5) Animal-sedimentation interactions

Shallow marine sediments are continually modified by biological and physiochemical processes, active within the biological boundary layer which extends from a few centimeters above the sediment water-interface to a few

centimeters below (Rhoads and Boyer, 1982 in Johnson and Baldwin, 1986). The boundary layer is essentially a superficial feature within which benthic activity can affect (1) the sedimentology by producing changes in grain size, sorting, fabric, water content, compaction, shear strength and bottom stability, (2) sediment transport, (3) nutrient regeneration, and (4) pollutant histories and pathways.

(6) Chemical factors

Several coastal and shelf processes have direct and indirect effects on seawater chemistry and the chemical characteristics of the shelf sediments. The major chemical components which occur in shallow marine sediments are: (1) biologically and non-biologically produced carbonates, (2) alumino-silicate minerals, (3) quartz, (4) iron and manganese hydroxide, (5) biogenic silica, and (6) biologically produced organic matter. Chemical precipitation can also cause sediment cementation and adhesion which may have an important effect on the substrate by increasing its stability and reducing its erodibility.

1.2.4 Type and intensity of the shelf hydraulic regime

From all the factors reported by Johnson and Baldwin (1986), the types of hydraulic regime are of extreme importance in controlling the sedimentation patterns. Although partly interrelated, four hydraulic regimes (Figure 3) can generally be recognized that illustrate the relative importance and interaction of both fair weather (i.e. tides, oceanic currents and waves) and storm processes:

(1) Wave-dominated shelves are controlled by seasonal fluctuations in wave and current intensity, with active sediment transport restricted to intermittent storms. Apart from those with drowned sand-rich shorelines, such as the eastern USA, fine grained sediments and small-scale bedforms predominate.

(2) Tide-dominated shelves are swept daily by powerful bottom currents enabling a wide range of bedforms to develop. In general, sand is transported more frequently and in much greater quantities than in non-tidal seas.

(3) Oceanic current-dominated shelves are characteristically narrow and more or less constantly under the influence of powerful persistent unidirectional currents which impinge on them.

(4) Storm-dominated shelves are characterized by an overprint of the other shelves regimes by storm processes, which, given a sufficiently high frequency, may produce a wholly-dominant type.

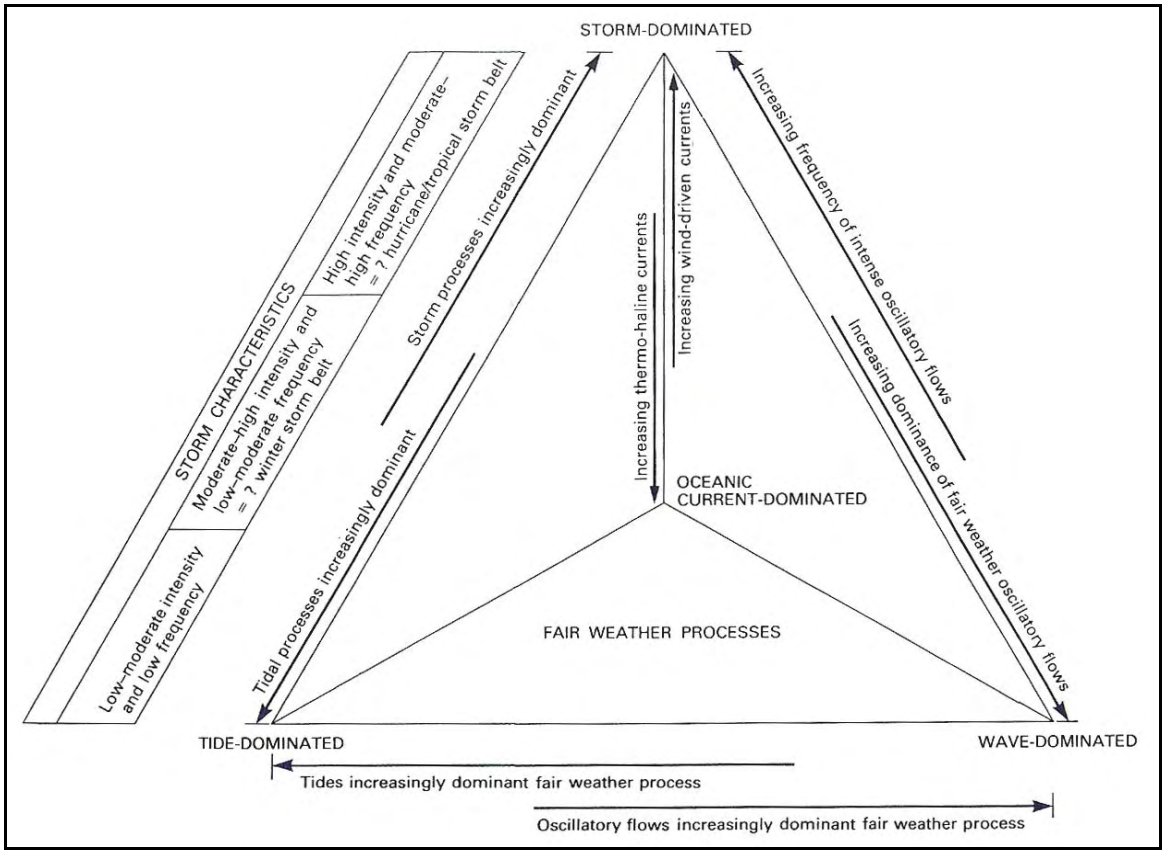

Figure 3 – Nature of the hydraulic regimes (after Johnson and Baldwin, 1986).

In the Azores the hydraulic regime is rather energetic (see Chapters 2, 4 and 6); therefore the dominant regimes expected are the wave to storm types. Nevertheless, other regimes might be present in specific areas, like in the Channel Faial-Pico where the tide-dominated regime might also be important (see Chapters 2 and 4).

1.2.5 Transport of particles across continental shelves

Depending on the shelf hydraulic regime, as well as the other controlling factors discussed before, several transport mechanisms can be present in a shelf environment. The transport of particles across continental shelves is also dependent on the shelf geometry, latitudinal constraints and the timescale of interest. For convenience, Nittrouer and Wright (1994) divided the shelf into regimes of the outer shelf, the middle shelf, the inner shelf and the surf zone (Figure 4).

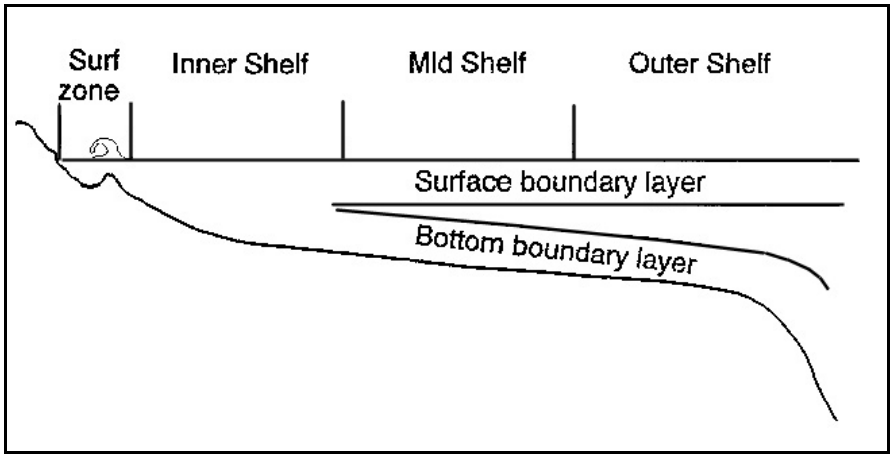

Figure 4 – Spatial relationships of the major sub regions of the continental shelf (Nittrouer and Wright, 1994).

Over the outer shelf, geostrophic flows are more important, frictional forces are small, and wave induced bottom agitation is minimal most of the time. In contrast, the inner shelf is a frictionally dominated area in which surface and bottom boundary layers overlap and may occupy the entire water column. The bottom boundary layer is the layer of the water column just above the seafloor where flows are significantly retarded by bed friction and where vertical momentum transfers are most intense whereas in the surface boundary layer, flows do not interact significantly with the sea floor. Breaking waves are the dominant source of flows within the surf zone. The mid shelf region is generally characterized by relatively steep across-shelf transitions in flow regime and by seaward decrease in the frequency and intensity of bed agitation. According to Nittrouer and Wright (1994) several physical mechanisms are responsible for the

across-shelf transport (Figure 5):

(1) Wind-driven flows

An along-shelf and southward wind with the coast to the right provokes seaward Ekman transport in the surface layer, which is accompanied by upwelling at varying depth in the northern hemisphere. With winds in the opposite direction, surface transport is landward, and seaward downwelling flows prevail at depth.

Storm winds blowing over shallow, continental shelves pile water against the coast. The result of this increase in sea level is known as storm surges. Intense wave agitation accompanies these surges, but it is the contemporaneous seaward-returning bottom current that is the significant transporting agent on the shelf. This seaward transport of nearshore sediments occurs over the inner shelf and mid shelf regions, reaching even the outer shelf during severe storms.

(2) Internal waves

Internal waves, particularly internal tides, are typically generated near the shelf break. They can have diurnal or semi-diurnal frequencies and propagate shoreward over the shelf. As they shoal over the shelf with progressively decreasing water depth, they become asymmetrical and ultimately break.

(3) Wave-orbital flows

This mechanism results from the simple back-and-forth motions from wave-induced near-bottom flows. Wave orbital asymmetries cause onshore transport inside the surf zone while outside the surf zone wave-induced transport can be in either direction.

(4) Infragravity phenomena

The dissipation of wave energy across surf zones is accompanied by the growth of energy at infragravity (0.033-0.003 Hz) frequencies. After reflection at the shoreline the released waves propagate in a seaward direction and may either escape into deep water (leaky waves) or remain refractively trapped in the shore (edge waves). Field observations in storm-driven surf zones show that suspended

sediment transport associated with infragravity motions can be 3 to 4 times larger than the associated with incident waves.

(5) Buoyant plumes

Positively and negatively buoyant plumes contribute to surface and near-bottom seaward transports of particles across shelves. The lowered relative densities of positively buoyant (hypopycnal) plumes are caused by low-salinity water outflows from rivers and estuaries. These hypopycnal surface plumes issuing from rivers and estuaries are major sources of buoyancy and sediment to the coastal ocean. Negative buoyant (hyperpycnal) plumes result from intense cooling of costal waters (e.g., by cold air outbreaks), high-salinity extrusion from freezing sea ice, and high suspended sediment concentrations (e.g., turbidity currents and related phenomena). Negative buoyancy is responsible for the highly energetic, auto suspending turbidity currents that transport large quantities of sediment to the base of the continental margin via submarine canyons. There is also evidence that negative buoyancy may contribute significantly to across-shelf sediment transport on the inner shelf during storms, when waves maintain high suspended sediment concentrations in the bottom layer of the water column. Negatively buoyant river plumes, though comparatively rare, occur off the mouths of rivers carrying unusually high suspended sediment concentrations in the bottom layer of the water column.

(6) Surf zone processes

The circulation in this zone is driven almost exclusively by forces resulting from the dissipation of breaking waves. There are three basic types of currents operating in the surf zone. Longshore currents are caused by refraction and move essentially parallel to the shore, being responsible for the greatest amount of sediment transport. Rip currents also carry a significant amount of sediment and move in generally offshore direction. Rip currents are commonly produced at the antinodes of edge waves (waves trapped in the shoreface by the topography). The third type of current is related to the type of wave activity and moves in an onshore or offshore direction depending on wave climate and location (e.g., the steeper

waves generate seaward currents and rather flat waves cause shoreward currents).

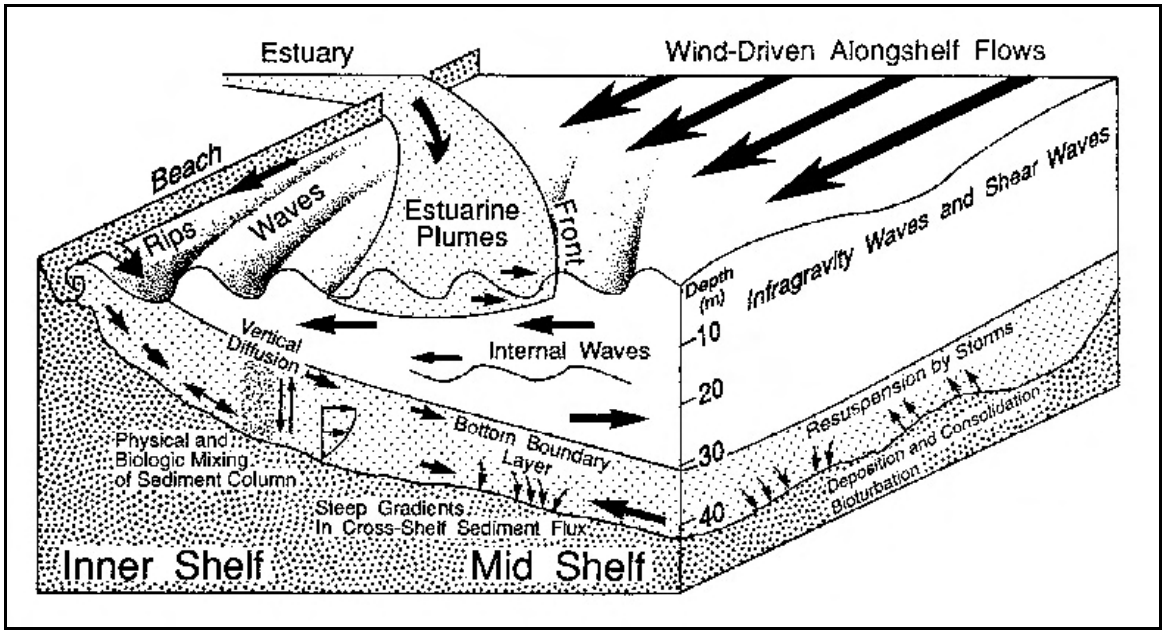

Figure 5 – Conceptual diagram illustrating the major processes responsible for across-shelf particulate transport (Nittrouer and Wright, 1994).

Seaward returning bottom currents are used in this work to explain how the sedimentary bodies found on the shelf are formed (see Chapters 4 and 6 for details). Internal waves over the shelf break are also discussed in Chapter 6 as a possible responsible for the outer shelf-coarsening pattern. The longshore transport – is used in the Chapter 6 to assess net transport directions. Although buoyant plumes are not used to explain any sedimentary pattern in the Faial shelf, negative buoyant plumes may occur when subaerial volcanic material coming from the land enter the sea (see details in section 1.2.7).

1.2.6 Nearshore sediment transport pathways

The systematic use of geomorphic and sedimentological indicators to determine the direction of long-term sediment transport along a coastline is a quick and accurate method for use in coastal management decisions, especially when no other data is available (Jacobsen and Schwartz, 1981; Taggart and Schwartz,

1988). There are various geomorphic and sedimentological indicators, although those presented here have been selected according to the relevancy of the present study.

(1) Grain size trends

There have been several approaches to model the sediment transport directions of sediments based on grain size distributions. McLaren (1981) was the first to develop a sediment transport model based on the study of combined parameters; others have followed and various modifications of the initial approach have been proposed by McLaren and Bowles (1985) Gao and Collins (1992; 1994), Le Roux (1994a; 1994b) and Poizot et al. (2006).

(2) Fetch

Fetch is the distance of open water that the wind can blow across without encountering any interfering landmass. Up to a limiting distance, the greater the fetch, the greater the wave that can be generated. Normally a good relation exists between the greatest fetch and net shore-drift direction. The sheltering effect of the islands (Léon and Soares, 2005) can be particularly important on the case of Faial Island since it is surrounded to the East and Northeast by nearby islands, respectively Pico and S. Jorge Island.

(3) Cliff morphology

Cliffs are often found along shores where wave erosion rather than deposition is the dominant coastal process. Exposed bedrock, high relief, steep slopes, and deep water are typical features of erosional shorelines, which is the case of Faial Island. Low-land areas are almost absent and the few beaches present are pocket beaches. According to Emery and Kuhn (1982) the shape of sea cliffs profiles, concavity or convexity is controlled by the relative rates of erosion by marine and subaerial processes as well as by the position of more resistant strata in the cliffs. A sharp angle at the sea-cliff base generally indicates active marine erosion, whereas a smooth curve at the base and vegetation on top of it means that subaerial erosion may dominate. These evidences are discussed

in Chapter 4 to check which of these mechanisms are dominant in the erosion of Faial coastal cliffs.

(4) Beach width and slope

Beaches tend to widen, develop one or more berms, and develop a larger backshore in their downdrift direction. The reason for this is that a long term direction of shore-drift predominates and accumulation generally prevails at the end of the drift cells while at the begging of drift sectors, erosion is usually occurring. Beach slope has a clear relation with particle size (Bascon, 1951). Beaches with finer material are less permeable to wave swash and backwash due to the smaller porosity. This decreases the amount of backwash percolation into the beach face, increasing the return surface flow volume, creating lower beach slopes due to greater sediment entrainment.

(5) Structures interrupting shore drift

Man-made or natural structures when occurring more or less perpendicular across the shoreline and large enough may impede shore drift. Sediment will accumulate on the updrift side while downdrift side will experience sediment starvation and subsequent erosion. Natural features such as lava deltas prograding in the shelf, particularly in narrow shelves like those of relatively young volcanic islands such as Faial Island, can be a common cause for sediment accumulation and erosion.

1.2.7 Submarine sedimentation in volcanic islands

Submarine sedimentation in volcanic oceanic islands such as the Azores is related to a wide spectrum of eruptive and sedimentary mechanisms. Although the sources of sediment can be easily identified - eruptive activity, coastal erosion and subaerial erosion - the mechanisms involved are quite diverse. The nomenclature used to classify these deposits is also complex and follows the terminology used by Schneider (2000):

Volcaniclastic rocks or **volcaniclastics** include all fragmental volcanic

rocks that result from any mechanism of fragmentation and are therefore defined without any genetic consideration. **Primary volcaniclastic** deposits may be defined as assemblages of fragments produced during a volcanic eruption and these can be:

(1) **Pyroclastics**, the dominant part of this group are generated by explosions at volcanic vents. Explosive activity results from the expansion of magmatic gas (magmatic eruption) or from vaporization of external water at the contact of rising magma (hydromagmatic eruption, also called phreatomagmatic eruption).

(2) **Autobreccias** are formed by frictional or extensional fragmentation of lava flows or domes during their progression. They also result from minor explosions, either magmatic or hydromagmatic during the flow of lavas.

(3) **Hyaloclastites** result from the quench shattering of lava in water, in ice or in wet sediments. Inflation and breaking into chips of pillow lavas results in the breaking through of their successive formed rims of glassy matrix that surrounds pillows and pillows fragments.

(4) **Peperites** are a kind of autobreccia generated by mixing of lava with unconsolidated wet sediment.

Autobreccias, hyaloclastites and peperitic breccias are conveniently gathered together under the term **autoclastic rocks**, as opposed to **pyroclastic rocks**. **Primary volcaniclastic** deposits being loose are easily resedimented, so pyroclastics and autoclastic when resedimented or reworked are still classified as primary volcaniclastics.

Secondary volcaniclastic or **Epivolcaniclastic rocks** are formed from fragments of volcanic origin resulting from weathering or physical erosion of coherent rocks. The main variation of this general behaviour is catastrophic flank failure during periods of activity. Such an event is the most important and rapid source of secondary volcaniclastics in the life of many volcanoes.

Volcaniclastic particles deposited in marine settings can originate both from subaerial and submarine environments. The diversity of the submarine

volcaniclastic processes is related to the succession of syn-eruptive and non-eruptive periods (Figure 6).

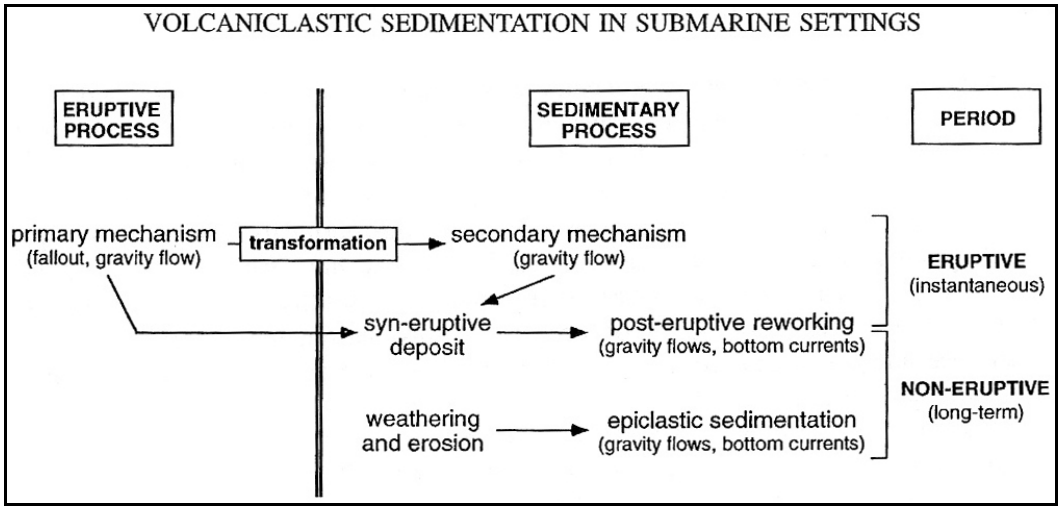

Figure 6 – Diversity and mutual genetic relationships of volcaniclastic transport mechanisms. Primary processes occur during eruptive periods. Sedimentary processes can be genetically related to transformation of primary mechanisms into gravity flows. During non-eruptive periods, primary deposits are remobilized, and older formations are eroded (Schneider, 2000).

1.2.7.1 Syn-eruptive submarine volcaniclastic sedimentation

During syn-eruptive periods, volcaniclastic material can be emplaced by primary volcanic mechanisms that can evolve into secondary but contemporaneous sedimentary processes. Rapid post-eruptive reworking of volcaniclastic deposits can occur and be genetically unrelated to an eruptive event. The processes involved in the sedimentation can be **pyroclastic falls** and **submarine pyroclastic flows** (Figure 7) and the **formation of massive hyaloclastites by lava flows** (Figure 8).

1.2.7.2 Non-eruptive submarine remobilization of the volcaniclastic material

During non-eruptive events, reworking of volcaniclastic material is also possible by mass-wasting processes (Figure 9) with subsequent alteration of pre-existing volcanic and volcaniclastic rocks.

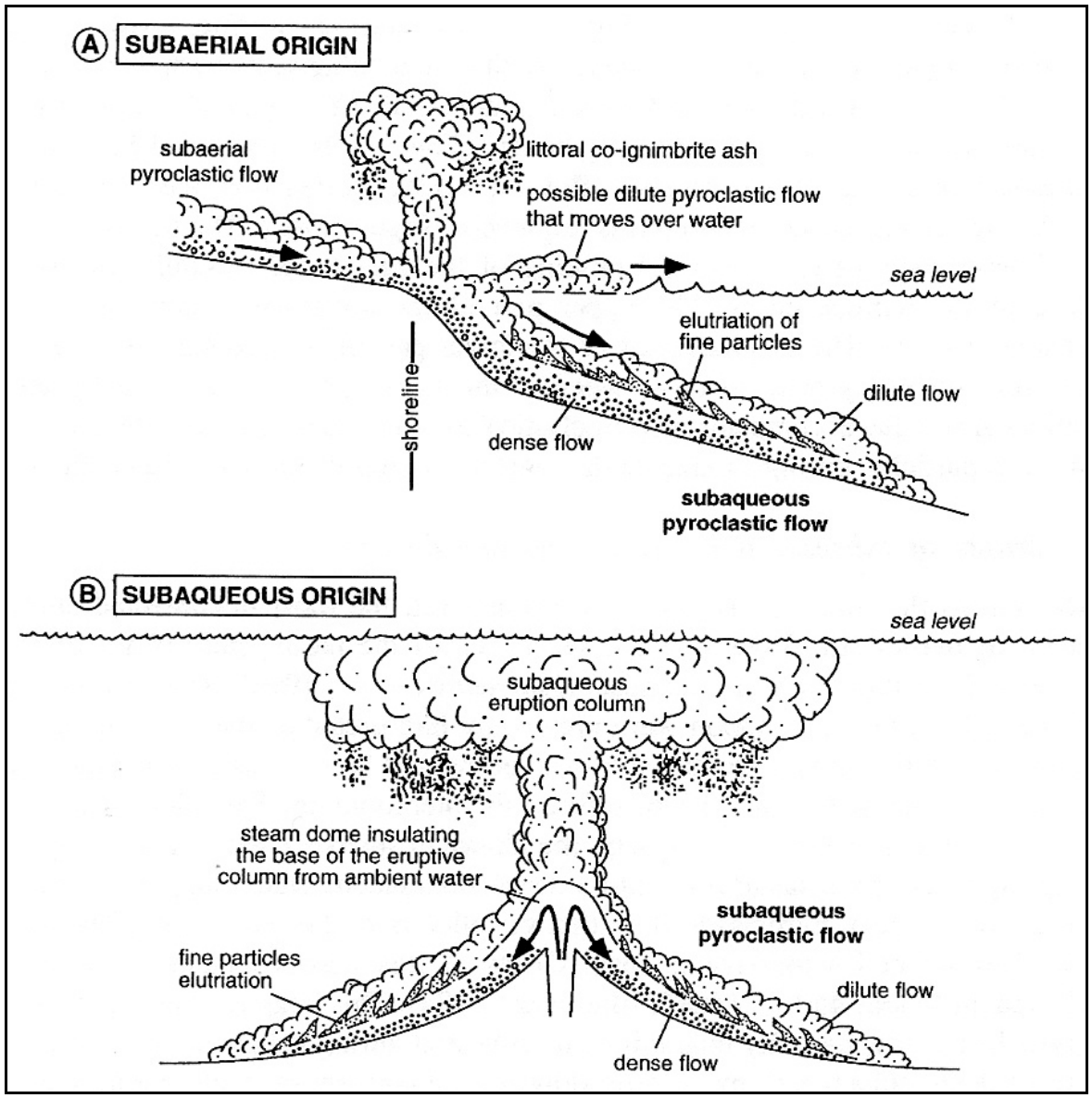

Figure 7 – Synthetic models for subaqueous pyroclastic flows. A. Pyroclastic flows of subaerial origin flow into the sea and can lead to (1) littoral explosions with formation of littoral co-ignimbrite ash, (2) a decoupling into a dense subaqueous pyroclastic flow and a dilute pyroclastic flow that moves over water, and (3) the progressive mixing of the subaqueous pyroclastic flow with water and subsequent dilution and elutriation of fine particles. B. Pyroclastic flows of subaqueous origin, which result from the collapse of the base of the submarine eruption column (Schneider, 2000)

1.2.7.3 Epiclastic sedimentation

Epiclastic material is formed by alteration and erosion of subaerial pre-existing volcanic and volcaniclastic rocks. Erosion along shorelines by wave's action is another mechanism responsible for the sedimentation of epiclastic rocks.

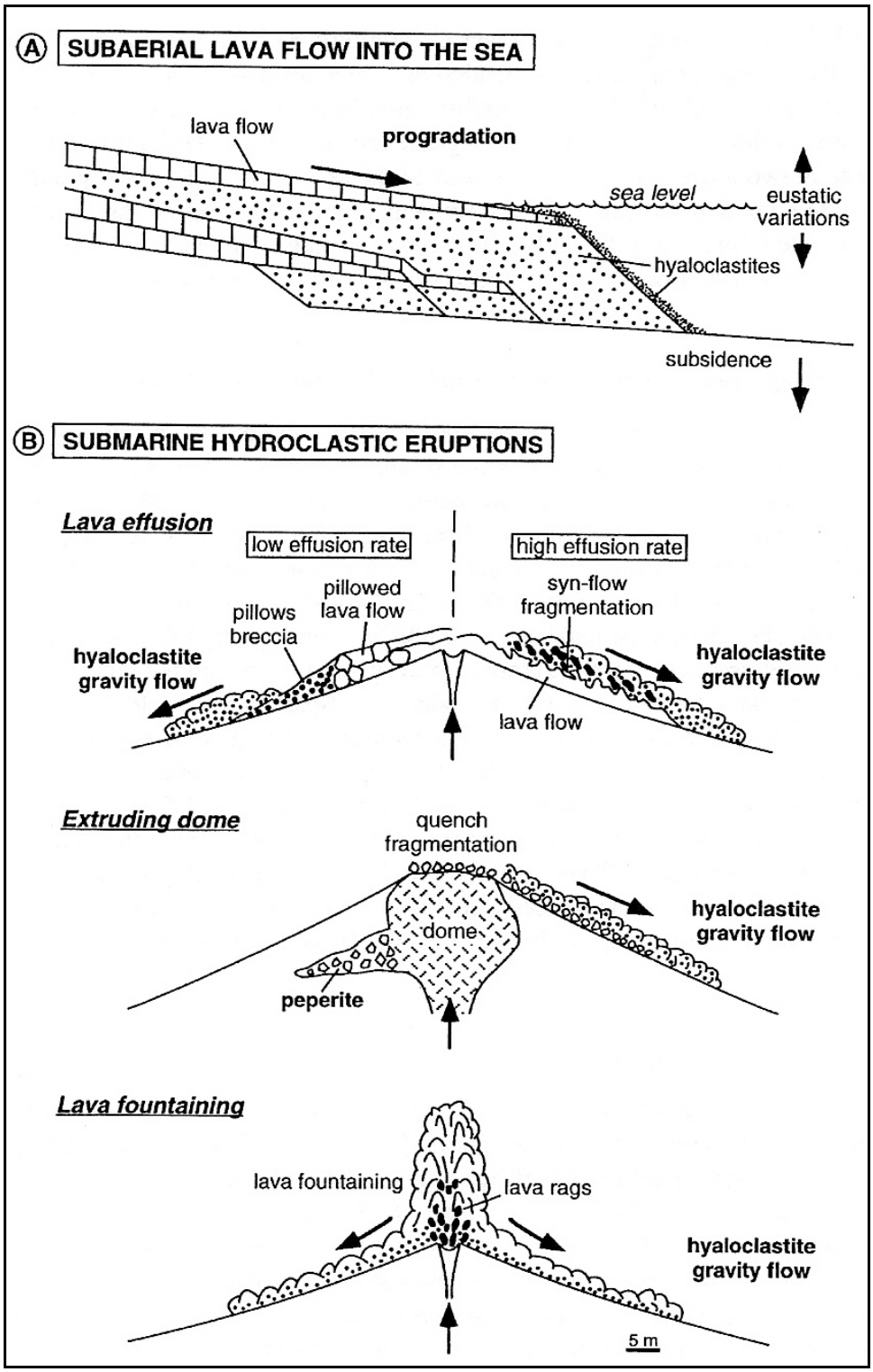

Figure 8 – Synthetic models for submarine hydroclastic volcanic activity. Hyaloclastites form by quench fragmentation when subaerial lava flows into the sea (A) and during submarine effusion of lava (B). A) Entrance of lava flows into the sea and progradation of the hyaloclastite delta. B) Submarine hydroclastic eruptions can produce hyaloclastite gravity flows by (1) brecciation of pillowed lava flows (low effusion rate), (2) in situ syn-flow fragmentation of the lava (high effusion rate), (3) quench fragmentation during subaqueous extrusion of lava domes and (4) hydroclastic fragmentation of lava rags during fountaining (Schneider, 2000).

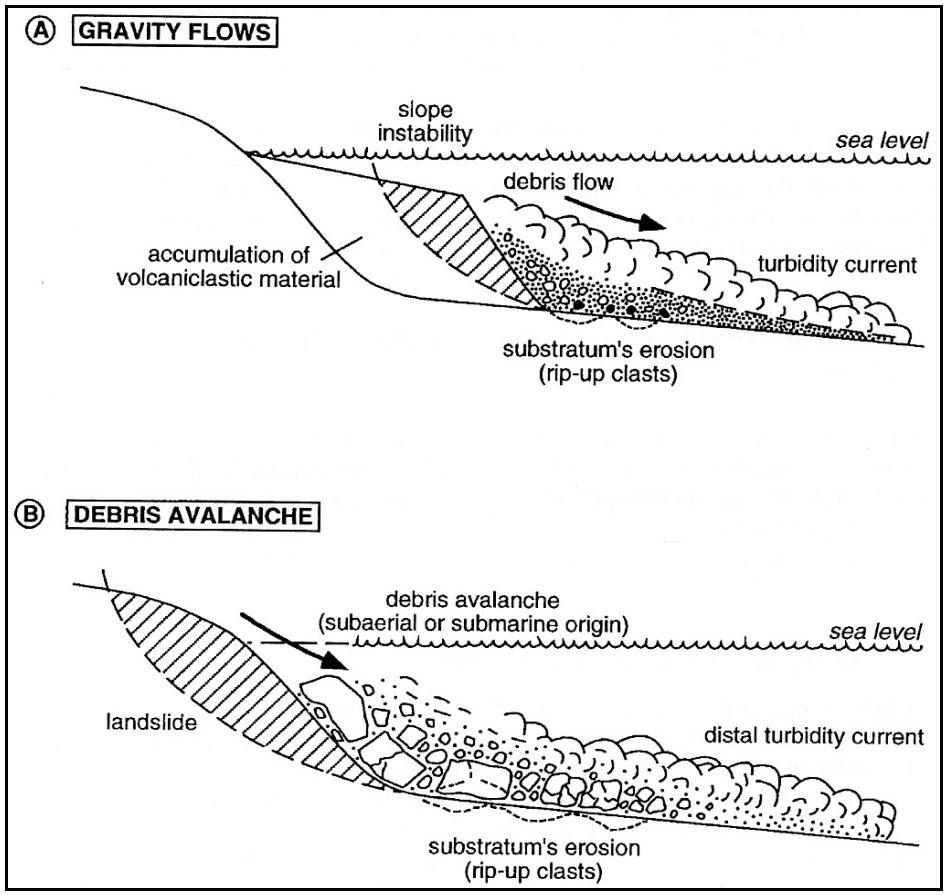

Figure 9 – Synthetic models for submarine resedimentation of volcaniclastic material during non-eruptive periods. A) Remobilization by gravity flows related to slope instability. If the volume of reworked material is important, a dense debris flow can form which can distally transform into a more dilute turbidity current. B) Remobilization by debris avalanches originated by large-scale flank collapse of a volcano in subaerial or submarine domains (Schneider, 2000).

1.2.7.3.1 Subaerial erosion

Subaerial erosion acts through the two complementary processes of chemical weathering and mechanical erosion. The yield of sediment from a drainage basin is a complex process and is related to the interaction of several variables such as the climate, tectonics, topography, lithology and land use (Louvat and Allègre, 1998).

The archipelago of the Azores has a rather smooth relief with accumulation of cratered and non-cratered cones. The few valleys are very narrow and the steeper slopes are those of the caldeiras' inner walls. The lack of wide-open valleys, meandering streams and inundation plains points to the youth of the geomorphology (Louvat and Allègre, 1998). However, some summits are very elevated and lead to steep slopes, given the small surface of the islands (e.g. the

Pico Mountain) and basaltic rocks are more easily eroded than most other crystalline silicate rocks (Dessert et al., 2003). Therefore, the places with steeper slopes and more erodible substrates are the major contributors to subaerial erosion.

1.2.7.3.2 Coastal erosion

Rocky coasts are affected by a range of processes including mechanical wave erosion, physical and chemical weathering, bio-erosion and mass movements (Trenhaile, 1987):

(1) Mechanical wave erosion is the main erosional agent in most swell and storm-wave environments, which is the case in the Azores. In addition to the removal of loose material by waves, the two principal wave effects are abrasion of rock surfaces due to the wave-induced currents and wave-generated pressure variation in the rock.

a. **Abrasion** is the scouring action of wave-induced currents and includes the sweeping, rolling, or dragging of rocks and sand across gently-sloping rock surfaces, and the throwing of coarse material against steep surfaces. The scouring effect of water is greatly enhanced if sand and/or gravel are in transport.

b. **Wave-generated pressure variation**. The impact of waves on rocks induces pressure variations that weaken the rock by causing and widening capillaries and cracks. Pieces of rock that have been dislodged due to hydraulic action can subsequently be removed from the matrix in a process know as quarrying.

The mechanical wave erosion operates most effectively at, or slightly above, the still water level. Whilst the waves, and particularly breaking or broken storm waves, perform the erosive work, tides control the water level and therefore also the level where mechanical wave erosion occurs. For greater tidal ranges the period that the tide will occupy certain level will be smaller. Therefore, the potential for mechanical wave erosion is greatest in microtidal environments (Trenhaile, 1987), which is the case of Azores (see Chapter 2).

(2) Weathering. Cliffs are subjected to alternate wetting and drying by salt spray, wave swash, tides and rain. They therefore represent suitable environments for many physical and chemical weathering processes. Chemical weathering prevails over physical weathering in hot and wet climates. The Azores climate is wet and relatively hot (see Chapter 2). In addition to this, volcanic rocks are very prone to chemical weathering.

(3) Bio-erosion is the removal of rock by organisms. This process is probably most important in tropical regions due to the enormously varied marine biota and the abundance of calcareous substrates.

(4) Mass movements. The steep slopes of rocky coasts indicate that they are unstable features prone to mass movement, such as rock falls and landslides. Rock falls are characteristic of hard rocks, especially where rocks are well-jointed and cliffs have been undercut by waves at heir base. Landslides are deep-seated failures that occur when the compressive strength of the rock is exceeded by the load on it and are often triggered by a change in moisture conditions and/or increased wave action.

According to Masselink and Hughes (2003) low cliffs erode faster than high cliffs, because less material needs to be removed to accomplish cliff recession. On the other hand higher and steeper cliffs are more prone to instability. There is also a correlation between lithology and erosion rates of cliff erosion (Sunamura, 1992), which is very clear in the coast of Capelinhos (see Chapter 2). The presence of beaches on rocky coasts acts as a buffer, causing the waves to break on the beach rather than against the cliff (Sunamura, 1976).

1.3 Objectives of this PhD thesis

This PhD project aims to understand the development of abrasion platforms in the Azores and their sediment stratigraphy, as well as to explore practical and relevant implications for the population living there, such as the offshore

aggregates evaluation and their possible exploitation impacts. Within this broad objective, the following questions represent different elements that are discussed in the chapters of this thesis:

1. In volcanically active coasts, how does the width and morphology of the shelf reflect the competition between opposing infilling and widening processes?

2. For inactive or less active coasts, does the width of the abrasion platform reflect the age of the island? Does the apparent shelf widening occur at long-term rates comparable to other volcanic islands reported by Menard (1983; 1986)? How fast are short-term rates from erosion of historical lava?

3. How does the depth of the shelf break in basement vary around the islands and does it simply reflect the depth of the sea-level during the Last Glacial Maximum or is it varied by vertical tectonic motions? Do bedrock terraces and platforms reflect earlier low- or still-stands?

4. Where do submarine landslides occur and how does their geometry and incidence reflect potential causes of slope instability or slope failure triggers, such as proximity to historical seismicity, active faults, locations of actively growing lava deltas, sources of sediment prograding, slope gradient and steepening on the uppermost slope?

5. How is sediment produced from coastal and subaerial erosion moved around shelves? Where sediment bodies are observed, how do oceanographic and sedimentary processes affect their geometry and locations? Does their spatial distribution vary because of differing wave climate or wind-driven downwelling around the coasts or because of differing sediment supply or accommodation space?

6. What is the mineralogical composition of the surface of the sedimentary bodies and how adequate are them for industrial use as aggregates?

Although during this thesis we were able to collect also data for Pico and S. Miguel Islands in the scope of the project GEMAS (Quartau and Curado, 2002; Quartau et al., 2003; Quartau et al., 2005a; Quartau et al., 2006) this PhD project concentrates on the Faial Island. Apart from the obvious lack of time to study the three islands in a single PhD thesis, Faial shows a generally remarkable difference in the age of its subaerial parts (~800 ka to recent - Madeira, 1998), which makes it ideal for testing the inferred relation proposed by Menard (1983, 1986) between the width of the abrasion platform and the age of the island.

1.4 Database and methods

This PhD project has addressed the following tasks: (1) Acquisition of geophysical and sedimentological data; (2) Data processing and interpretation; (3) Compilation of a Geographic Information System (GIS) database; (4) Geological characterization of the shelf; (5) Assessment of the importance of the several processes involved in the shelf evolution; (6) Creation of a model of the present-day sedimentary dynamics of the shelf; (7) Evaluation of the offshore aggregates potential. The several methods used in this work are briefly described in this chapter. A more detailed description can be found in the respective chapters where they were used.

1.4.1 Acquisition of geophysical and sedimentological data

1.4.1.1 Geophysical surveys

In July 2001 the DGM conducted one survey (FAPI-1), in which the author participated, to map the sediment distribution around the Faial Island (Quartau et al., 2002; Teixeira, 2001). High resolution seismic profiles were collected using a Chirp sonar system – 1.5-10 KHz, Datasonics CAP-6000W – (Figure 10) and a Boomer – EG&G 230-1 UNIBOOM – (Figure 11), onboard the R/L Águas Vivas from the DOP. A total of 500 Km of high-resolution seismic lines where acquired between 10 and 100 m water depth, being 275 km of lines from Chirp and 225 km

from Boomer (Figures 12 and 13). According to the bathymetric map available at the time of the survey (Instituto Hidrográfico, 1999) the 100 m depth contour marked the approximate break in slope of the insular shelf surrounding the island, and thus comprised a natural survey limit (Figure 40 in Chapter 2). Single beam

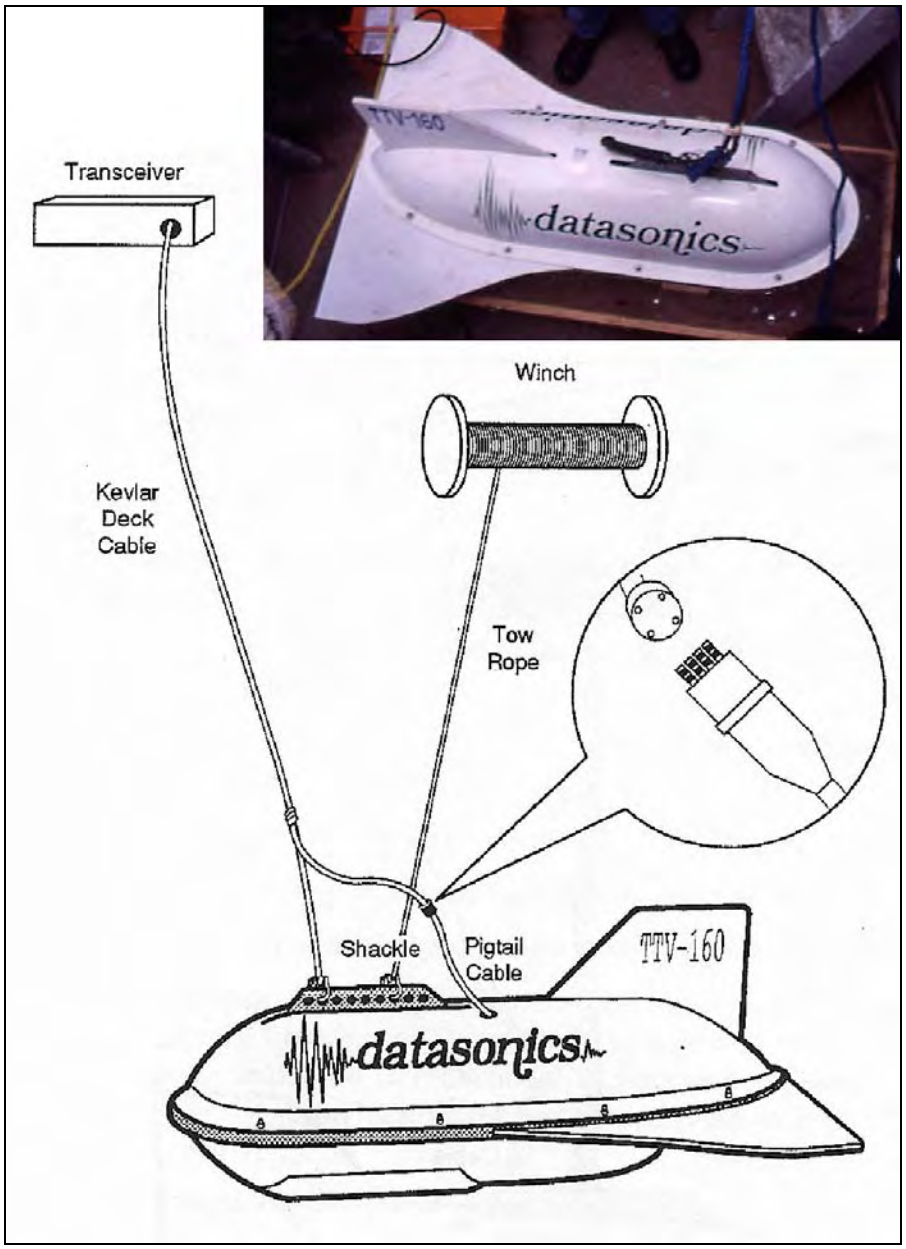

Figure 10 – Chirpsonar system used in the FAPI-1 cruise in the Faial shelf (Quartau et al., 2002; Teixeira, 2001). In the upper right side of the figure is a photo of the Chirp fish. In the lower part of the figure a scheme shows how the fish is mounted in the boat.

echo-sounder data were acquired concurrently. The survey lines were made parallel and normal to the shore. Another line was made around the island

crosscutting the previous network at approximately 40 m water depth. The area covered was about 80 km^2 and it extended from a distance of less than 0.05 km from shore to the seaward limit (~3 Km) of the study area, being the average 1.2 km wide.

During the surveys, online annotations concerning navigation, seismic acquisition and technical problems were made in the cruise log-book. Daily reports were written in the end of each survey summarizing these annotations (Quartau et al., 2002; Teixeira, 2001).

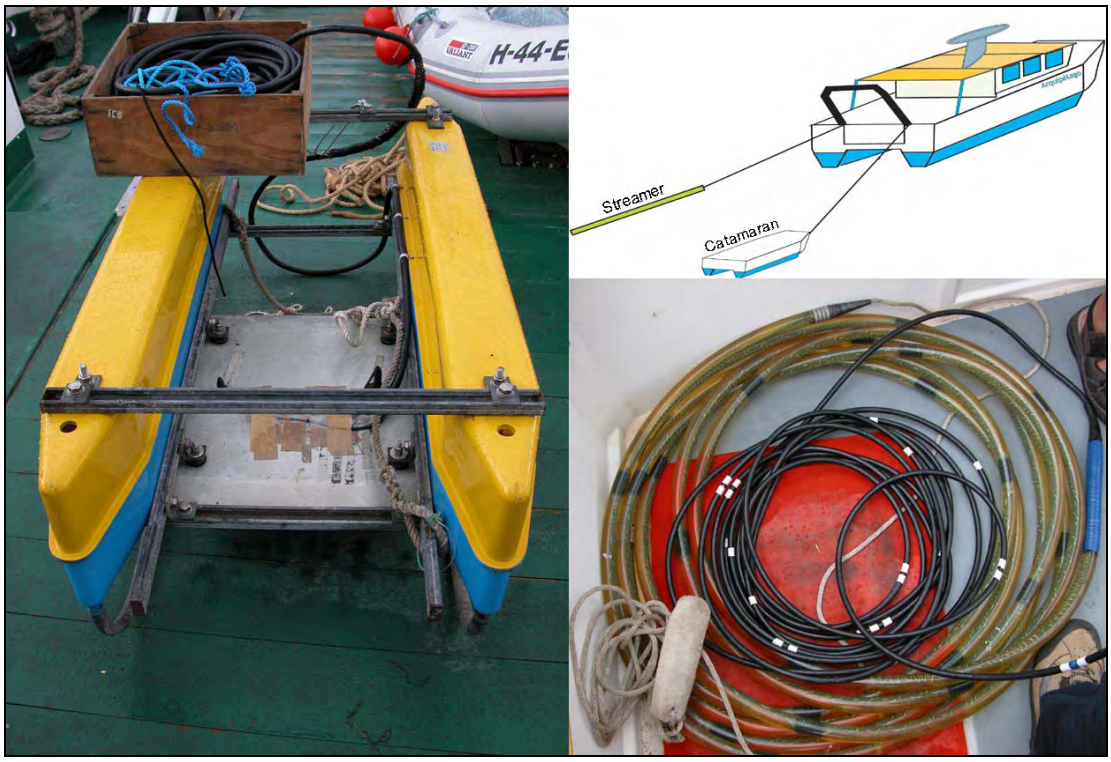

Figure 11 – Boomer system used in the FAPI-1 cruise to survey the Faial shelf (Quartau et al., 2002; Teixeira, 2001). Left photo is the catamaran where the transducer is located. Lower-right photo is the streamer, which receives the signal emitted by the transducer after reflection in sea bottom and sub-bottom layers. Upper-right picture is a scheme of how the system is mounted on a boat.

1.4.1.1.1 Navigation

Navigation was controlled using the SeaClear GPS navigation software (http://www.sping.com/seaclear/) installed on a laptop with a GPS connected through a serial cable RS-232. GPS navigation data were saved as ASCII files which included the following NMEA sentences: DBT (Depth below transducer) and

GLL (Geographic position, Latitude and Longitude). These surveys were made after the selective availability had been turned off in January 2000. Therefore positional accuracy of ± 20 m should be expected in the worst-case scenarios when using a single-frequency GPS receiver (Assistant Secretary of Defense, 2001). At the time of the survey, no procedure was made to assess the GPS errors involved. Nevertheless, during the interpretation of the data, significant errors were not found between crossing seismic lines that would suggest errors higher than ± 20 m.

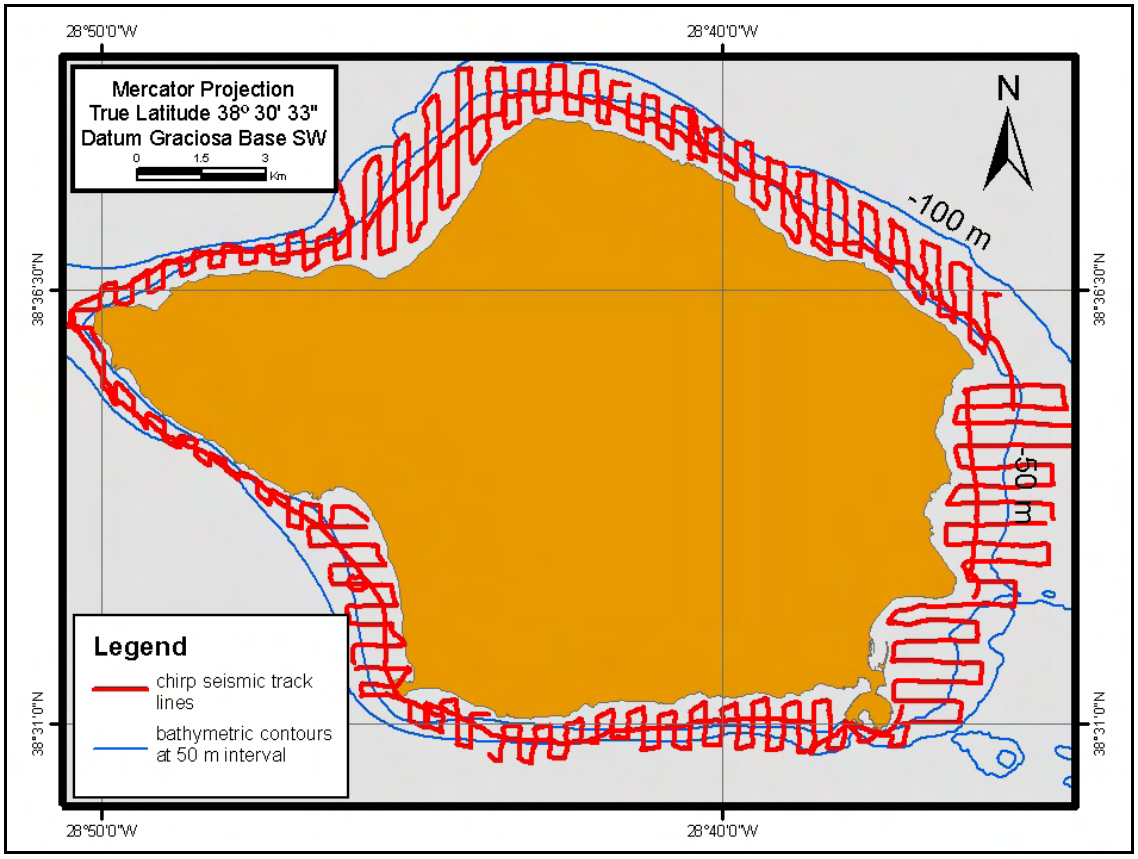

Figure 12 – Location and track lines of Chirp seismic profiles acquired during the FAPI-1 cruise in the Faial shelf (Quartau et al., 2002; Teixeira, 2001).

1.4.1.2 Sediment sampling on the shelf

Superficial sediment sampling was conducted in November 2003, aboard the R/V Arquipélago from DOP. Thirty-five stations (Figure 14) were sampled between 20 and 80 meters water depth, using a Box-corer (Figures 15 and 16) and sediment was recovered from all of them. A station form was filled for each

sampling operation, including relevant information such as GPS coordinates, operation procedure and a brief onsite description of the samples (Quartau et al., 2005b). Samples were photographed, packed inside plastic bags and weighted on the vessel. The amount of the sample recovered varied according to its grain size distribution. For samples composed mostly of sand, normally 2 to 3 kg were recovered. For coarser sediments, 3 to 10 kg were recovered, depending on its grain size distribution.

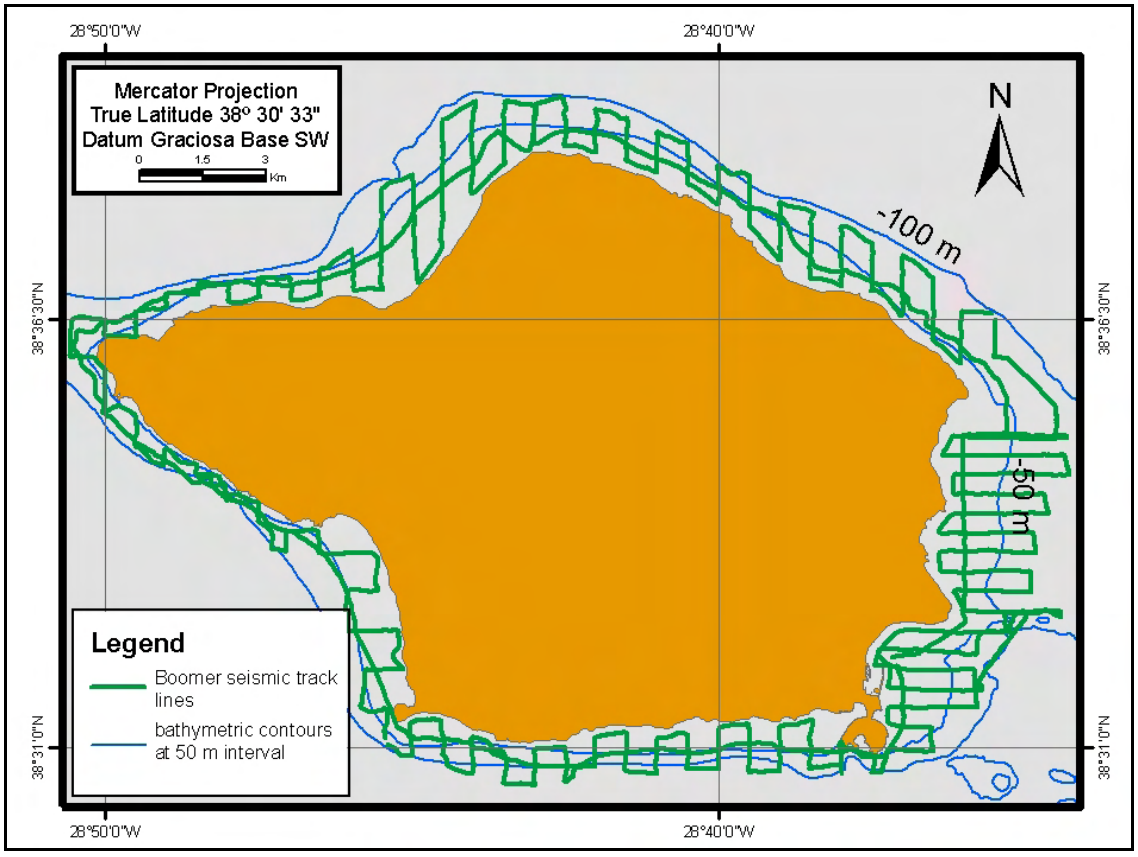

Figure 13 – Location and track lines of Boomer seismic profiles acquired during the FAPI-1 cruise in the Faial shelf (Quartau et al., 2002; Teixeira, 2001).

1.4.2 Data processing/analysis

1.4.2.1 GPS Data

GPS data positions were based on the datum WGS84 (World Geodetic System 1984). ASCII NMEA files were processed using a Visual Basic script

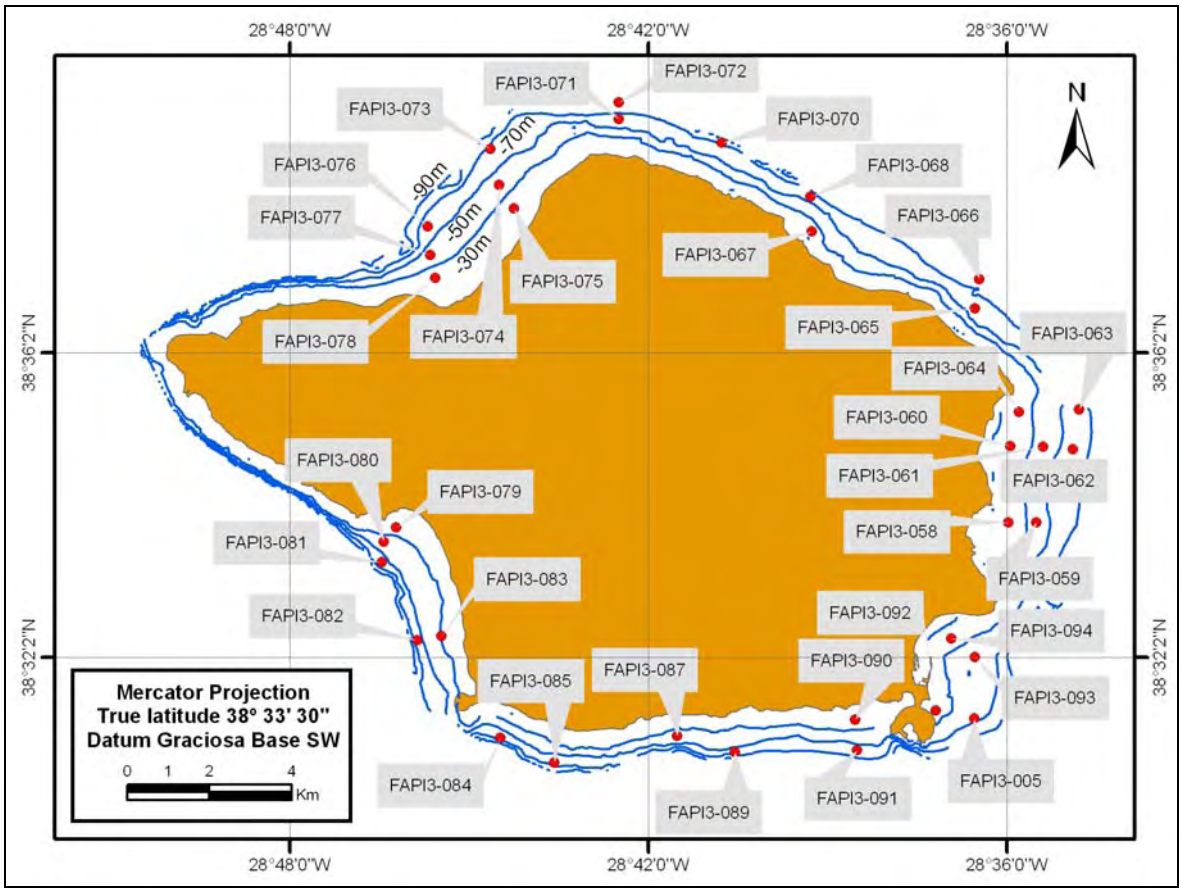

Figure 14 – Location of sediment sampling in Faial shelf realized during the FAPI-3 cruise (Quartau et al., 2005b).

Figure 15 – Example of a sample recovered during the sediment sampling of the Faial shelf realized during the FAPI-3 cruise (Quartau et al., 2005b).

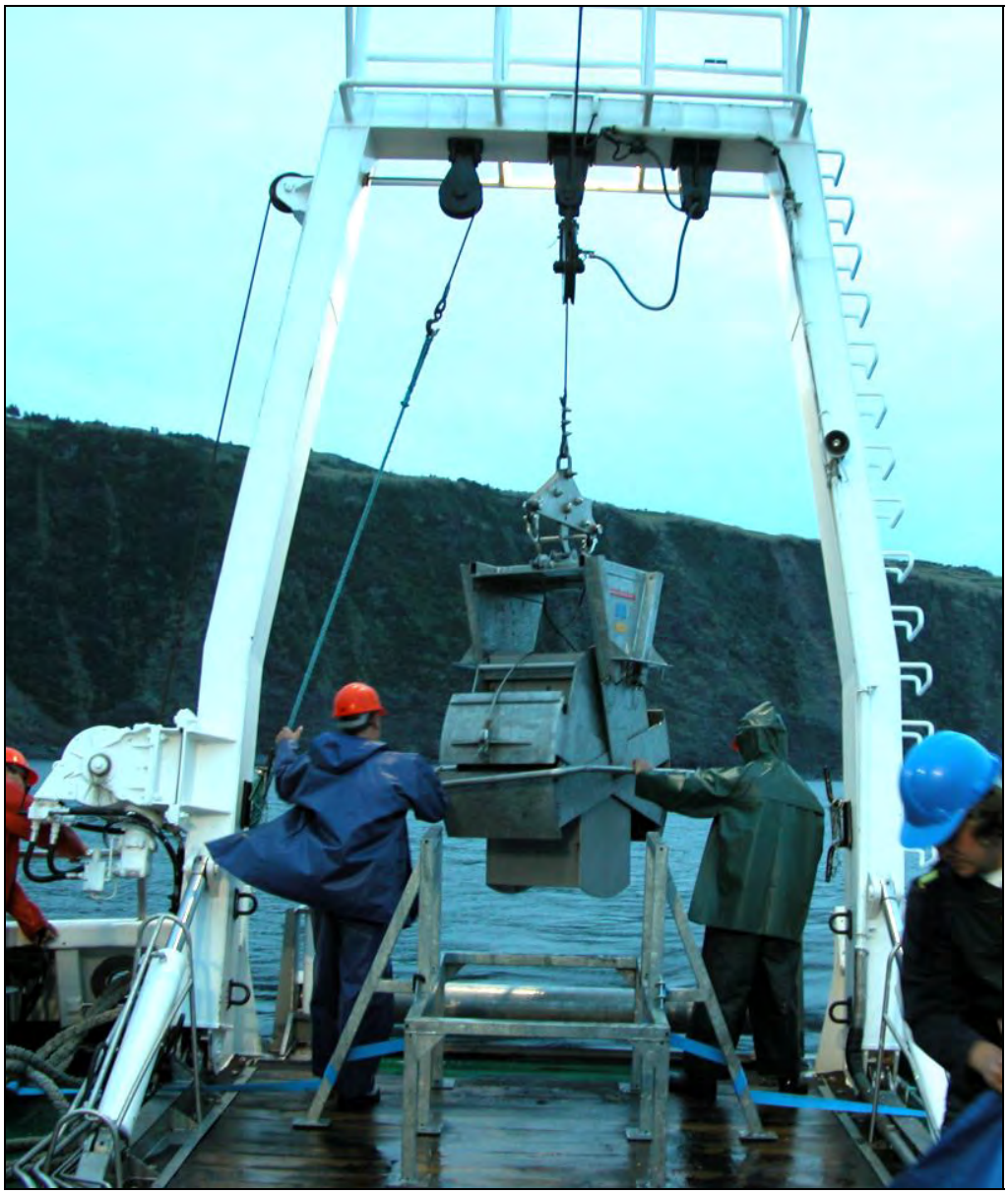

Figure 16 – Box-corer operation during sediment sampling of the Faial shelf realized during the FAPI-3 cruise (Quartau et al., 2005b).

designed to create navigation ASCII files with three columns: Timestamp (hh:mm:ss), Latitude, Longitude. GPS waypoints were plotted using ArcMap from ArcGis 9.0 GIS, to check and remove the existence of outliers.

1.4.2.2 Single beam echo-sounder

Single beam echo-sounder data was also plotted using ArcMap from ArcGis 9.0 GIS, to check the existence of outliers. When found these were deleted and no

interpolation between the data has been produced since the spatial variability of the depth can be considerable, especially in the presence of rocky bottoms.

1.4.2.3 High resolution seismic profiles

1.4.2.3.1 Chirp data

Chirp sonar data files (SEG format) were converted into standard SEG-Y format using the Chirp2SegY programme designed by Bouriak (2003).

1.4.2.3.2 Chirp seismic files positioning

Timestamp-Trace ASCII files with two columns: Shotpoint number, Timestamp (hh:mm:ss) were extracted from the SEG-Y trace headers using the Visual Basic script SEGYTable (H. Duarte, DGM).

Finally, another Visual Basic script was used to compare the timestamps of the processed navigation data and the timestamps extracted from the SEG-Y trace headers to estimate the trace positions, and to create Trace-Positioning ASCII files with three columns: Shotpoint number, Latitude, Longitude.

1.4.2.3.3 Boomer data

The seismic-reflection data was stored in 22-minutes audio cassettes using a TASCAM 234 cassette audio recorder, which saved the data into two channels: the trigger channel and the seismic data channel. The time of beginning and end of the cassettes were recorded in the log-book. The audio cassettes were digitized, using two sequential independent programmes (Bouriak, 2003). The DiGi programme, which is a strictly analogue-digital (AD) conversion that reads signal from the tapes, converts it to digital form, and stores the resulting raw sequence of digits on two files (the trigger channel and the seismic data channel). The Bmr2SegY programme, which identifies individual seismic traces within the raw digital records, converts them to a standard format and stores them as SEG-Y files.

1.4.2.3.4 Boomer seismic files positioning

The positioning of the Boomer seismic files was based on the recorded time span of the cassettes in the log-book. The beginning time of the cassette was used to distribute the traces into a Timestamp-Trace ASCII files with two columns: Shotpoint number, Timestamp (hh:mm:ss).

Subsequently, a Visual Basic script was used to compare the timestamps of the processed navigation data with the timestamps extracted from the SEG-Y trace headers to estimate the trace positions and to create Trace-Positioning ASCII files with three columns: Shotpoint number, Latitude, Longitude.

1.4.2.3.5 Boomer seismic files processing

SEG-Y seismic files have been processed using the software SPW (Parallel Geoscience Corp., version 1.8.19).

1.4.2.3.6 Landmark projects

Seismic and navigation files were prepared to match the format used by Landmark applications. An Openworks and a Seisworks project were created to import the data and make them available for interpretation.

1.4.2.4 Laboratory methods

The aim of the superficial sampling was to conduct grain size analysis, brief macroscopic description and determination of the carbonate fraction in the 35 samples collected from the Faial shelf.

All textural and compositional analyses were performed at the Marine Geology Laboratory at LNEG. The textural analysis of the superficial sediments used a dry sieving technique for material coarser than -1Φ (2 mm), whilst fine-grained material (< 2 mm) were analyzed using a Coulter Counter LS-230. Both data sets were then merged, to produce complete grain-size distributions.

The original superficial sediment samples were sub sampled (or split) to provide the sample volume required for the sieving and coulter techniques and

then were placed in a low temperature oven (40 °C to 50 °C) to dry for 24 hours. The material coarser than -1Φ were dry-sieved over intervals of 1Φ (-5 Φ, -4 Φ, -3 Φ, -2 Φ and -1 Φ sieves). This technique was chosen because samples were largely free of clay and silt and the sieving method can provide accurate results for these sediments (Folk, 1974). Calculations of the grain size statistics used the graphic method as defined by Folk and Ward (1957). In this work the term gravel is used for sediments between -1Φ and -2Φ, although according to the Udden–Wentworth sedimentary grain-size scale (Wentworth, 1922), this term is used for all the sediments coarser than -1Φ.

The calcium carbonate composition of the superficial sediments was determined by a modified method of digestion, the carbonate pump (Müller and Heidelberg, 1971 modified by L. Gaspar, DGM).

The laboratory results were used to characterize the sediments and to map their spatial distribution. This characterization provided information from their provenance and direction of transport, which are discussed in Chapter 6. In addition, it was also used to evaluate their properties as aggregates for industrial use.

1.4.3 Compilation of a Geographic Information System (GIS) database

A GIS will more readily allow measurements and spatial relations between features of different kinds of data (e.g., seismic and bathymetry) to be examined efficiently. Previous works about the Azores Islands and also data acquired during this project were compiled and put into a GIS format using for this purpose the ArcGIS 9.0 from ESRI. This includes:

1. Geological, tectonic and seismic data for the Azores archipelago.
2. Oceanographic data of the Azores. Wave and tidal data.
3. Geology and geomorphology of the subaerial Faial Island.
4. Climatological data of the Faial Island: Precipitation and wind data.
5. Geophysical and oceanographic data acquired during this PhD project.

1.4.4 Geological characterization of the island shelf

This task aimed to characterize the present day morphology of the insular shelf of Faial. The resulting maps are useful for understanding how the inter-action between the constructive and destructive processes of volcanic islands is recorded in the present day morphology, namely the shelf width and slope, as well as the spatial distribution of the rocky bottoms and sediments.

Combining different data types allows geology to be interpreted more easily. Single beam echo data, Boomer seismic files and seismic bottom echoes derived from Chirp were combined to generate basic geological maps of the island shelves.

1.4.4.1 Single beam echo data

Single beam echo data was used to produce a detailed bathymetry of the Faial shelf. This bathymetry allowed measuring the shelf width and slope of the offshore part of the island.

1.4.4.2 Boomer seismic profiles

The boomer seismic files were interpreted with the SeisWorks 2D software. The author tried to use the standard seismic and sequence stratigraphy methods (Catuneanu, 2002; Mitchum Jr. et al., 1977) to characterize the submarine deposits. The characterization of the sedimentary bodies, especially their surface morphology, geometry (shape, thickness and position in the shelf) and internal structure (seismic units and types of bounding surfaces) were pursued using these seismic interpretation techniques.

1.4.4.3 Analysis of seismic bottom echoes and interpretation

In this study the echo characters from the Chirp subbottom profiler are used to describe the submarine morphology of the shelf of Faial Island, which includes the main morphological features, the nature of the seafloor as well as its regional distribution. The different types of echoes were defined following the methodology

and classification proposed by Damuth (1980) and by Pratson and Laine (1989), including clarity and continuity of bottom echoes and seafloor morphology. An echo-character map of the region was made following three main steps. First, all available Chirp profiles from the region were examined. Portions of several boomer records were sometimes used to help clarifying doubts in the interpretation of the Chirp echoes. Secondly, a classification of the various types of bottom echoes observed was developed. Finally, the distributions of the echo types along each ship track were mapped and an echo character map was produced by connecting boundaries between various types from ship track to ship track.

1.4.4.4 Geological interpretation

The submarine geology of the shelf was used to assess the competition between constructive and destructive processes, e.g. conflict between seawards growing lava deltas and erosion by surf. The spatial distribution of the sediments and their sequence stratigraphy is also important to define the factors controlling the sediment distribution and to relate them to the Quaternary sea level fluctuations. According to Trenhaile (2001), erosional continental shelves are the product of wave erosion operating in intertidal zones that have migrated between upper, interglacial and lower glacial stage limits. It is thus expectable the formation of an abrasional shelf in the Faial Island due to the sea-level variations during the Quaternary.

In this study the shelf width was measured from the island coastline to the shelf break. Potential controls on shelf width where then studied, for example by seeing if there was a statistically significant increase in shelf width with age of the volcanic edifice. Where coastlines are of similar age, shelf width was tested for varied effects of swell. In addition, past sea-level curves were used to compare the shelf widening erosion rates of the present highstand with the longer term Quaternary erosion rates. These curves were also used to discuss the sequence stratigraphy of the sedimentary deposits that would be expectable to found on the shelf of Faial Island.

Finally, as a result of its location on an active plate boundary, the

archipelago is subject to frequent seismic activity. So, it is likely the existence of tectonic and mass-wasting morphologies. The occurrence of gullies and scarps were mapped out and tested against possible slope instability triggers, e.g., excess of load, either caused by lava flows or sediments that reach the shelf edge, active faults or density of historical seismicity.

1.4.5 Creation of a model of the present-day sedimentary dynamics of the shelf

Oceanographic conditions are of very importance for assessing the sedimentary dynamics of the shelves, especially the directions of the waves and their associated energy. Directions with higher energy waves striking the shore erode and transport sediment in that direction. The grain-size distribution of the shelf sediments is also very important when it comes to assess sediment mobility and transport directions. Simple sediment transport equations are used in this study to build a model of the sedimentary dynamics of the Faial island shelf. The model proposed combines data from the oceanographic conditions, sediment grain-size distributions and the results from the sediment transport equations.

1.4.6 Evaluation of the offshore aggregates

The assessment of the sand and gravel aggregate resources of the Azorean shelves is of very importance because these islands lack major river basins where exploitation could be made. Moreover, the increasing of environmental pressure may limit the number of exploitation sites and the volume of reserves of land-based aggregates, leaving no other option than to start dredging the submarine deposits. Therefore, the urgent need of an aggregate assessment project is obvious, namely one that will assess the amount and quality of the submarine aggregate deposits. In addition to this comes the need to study the negative impacts that the removal of sediment from the seabed can cause. It is well established in the scientific community that marine extraction can cause major changes to the natural sediment transport processes (e.g. net loss of sand, changes in wave transformation patterns may provoke coastal erosion) as well as

the destruction of benthic and fish communities.

For these reasons, the geographical distribution of the sediments was mapped and their volumes calculated. In addition, some of the sediments' physical properties were characterized to assess the range of industrial uses for these deposits. Finally, the results from the model of the sedimentary dynamics were used to define the areas where dredging can be done safely, without putting at risk the coastline.

1.5 Outline of the thesis

The organization of this thesis is based on the two main scientific problems addressed: the origin and evolution of the volcanic island shelves and the present-day sedimentation model of the Faial Island shelf. After a brief review of the more relevant issues necessary to understand the processes involved in these problems, Chapter 2 provides the geological, climatologic and oceanographic context for the analysis in the later chapters. From these, the description of the geological evolution of the emerged island is of remarkable importance since one of the objectives of this work is to investigate the relation between the present-day geology of the shelf and the emerged geomorphology.

Chapter 3 contains a geological characterization of the shelf of the Faial Island provided by the interpretation of the geophysical data. Chapter 4 summarizes the present-day processes that contributed to model the shelf, inferred by the geological features found around the submarine part of the island. Chapter 5 discusses in more detail some of the shelf features and their variability, namely the shelf width and depth of the shelf break. It also analyzes sea-level curves in order to compare short and long-term shelf widening erosion rates. In the end of the chapter, an evolutionary model of the shelf is proposed. Chapter 6 investigates the sedimentary dynamics of the shelf based on the on the grain-size distribution of the sediments and the oceanographic data. Chapter 7 discusses the potential of the sediments as aggregates, namely their quality and assesses the volumes of the offshore aggregate deposits limited by the technical and environmental restrictions. Chapter 8 discusses the implications of this study in

general terms and proposes future research directions.

Chapter 2. Geological, oceanographical and climatic setting of the study area

2.1. Geological setting of the Azores archipelago

The Azores archipelago is located in the middle of the North Atlantic Ocean between the latitudes 37º N and 40º N and the longitudes 25º W and 31º W (Figure 17). It is the result of the volcanic activity associated with the triple junction where the American, Eurasian and African litospheric plates meet. The Mid-Atlantic ridge (MAR) separates the American from the Eurasian and Africa plates. To the east of the ridge, the Azores-Gibraltar fracture zone marks the boundary between Eurasia and Africa (Krause and Watkins, 1970; Laughton and Whitmarsh, 1974).

The archipelago comprises nine islands, the Formigas islets and some submarine volcanoes. The islands emerge from the Azores volcanic plateau (Figure 18), which is a first-order morphological feature in the Atlantic basin. It has an overall triangular shape corresponding to a surface area of approximately 400 000 km^2 of elevated oceanic crust, roughly underlined by the 2000 m isobath (Lourenço et al., 1998). The plateau is mainly constructed of alkaline basalt volcanism. Geochemistry and petrology suggest a hotspot origin for this volcanism (White et al., 1976).

The plateau crosses to the west the Mid-Atlantic Ridge (MAR) and is limited to the south by the East Azores fracture Zone (EAFZ). The western group of the islands (Flores and Corvo) lie on the American plate, while the islands of the central (Terceira, Graciosa, S. Jorge, Pico and Faial) and eastern group (S. Miguel, Santa Maria and Formigas) follow a complex lineation that trends WNW–ESE from the MAR to the western limit of the Gloria Fault (Argus et al., 1989) The precise location of the western segment of the Eurasia-Africa plate boundary is still controversial. During the last three decades, several geodynamic models have

been proposed for this area relying on different approaches. Some authors have interpreted the Azores domain as a normal spreading centre (Krause and Watkins, 1970), whereas others believe it is an oblique spreading centre (McKenzie, 1972; Searle, 1980), and others support a leaky transform model (Madeira and Ribeiro, 1990).

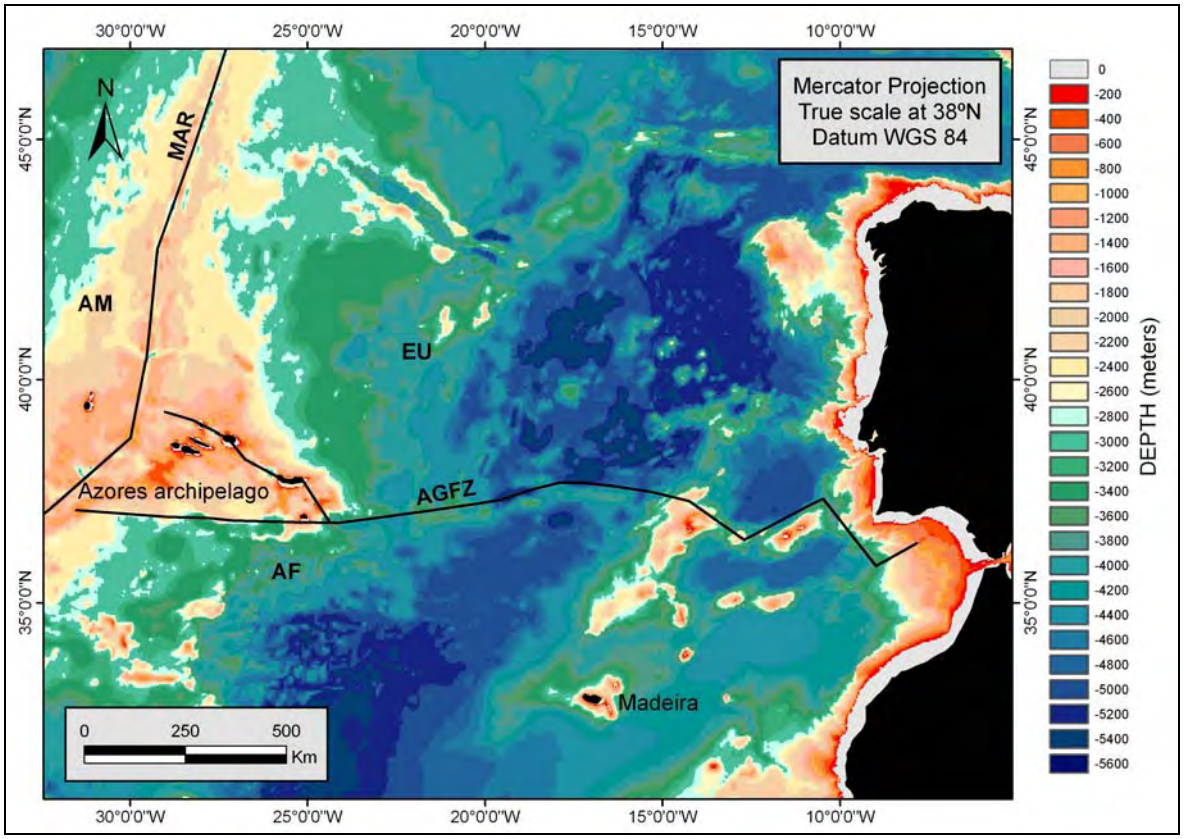

Figure 17 – Geographical and tectonic setting of the Eurasia-Africa-North America plate boundary (modified from Argus et al., 1989). AM=American plate; AF= African plate; AGFZ= Azores Gibraltar Fracture Zone; EU= Eurasian plate; MAR= Mid-Atlantic ridge. Bathymetry of the area Azores-Gibraltar from GEBCO (IOC IHO and BODC, 2003).

Recently, various works, based on bathymetric (Lourenço et al., 1998), gravity (Luis et al., 1998), and seismic (Miranda et al., 1998) data have proposed a new model for the Azores Plateau region (Figure 19). These authors state that, presently, this region is a narrow diffuse plate boundary consisting of several tectonic blocks limited by two sets of conjugated faults striking 120º and 150º. These faults established the framework for the onset of volcanism, expressing as linear volcanic ridges or as point source volcanism. This area acts simultaneously

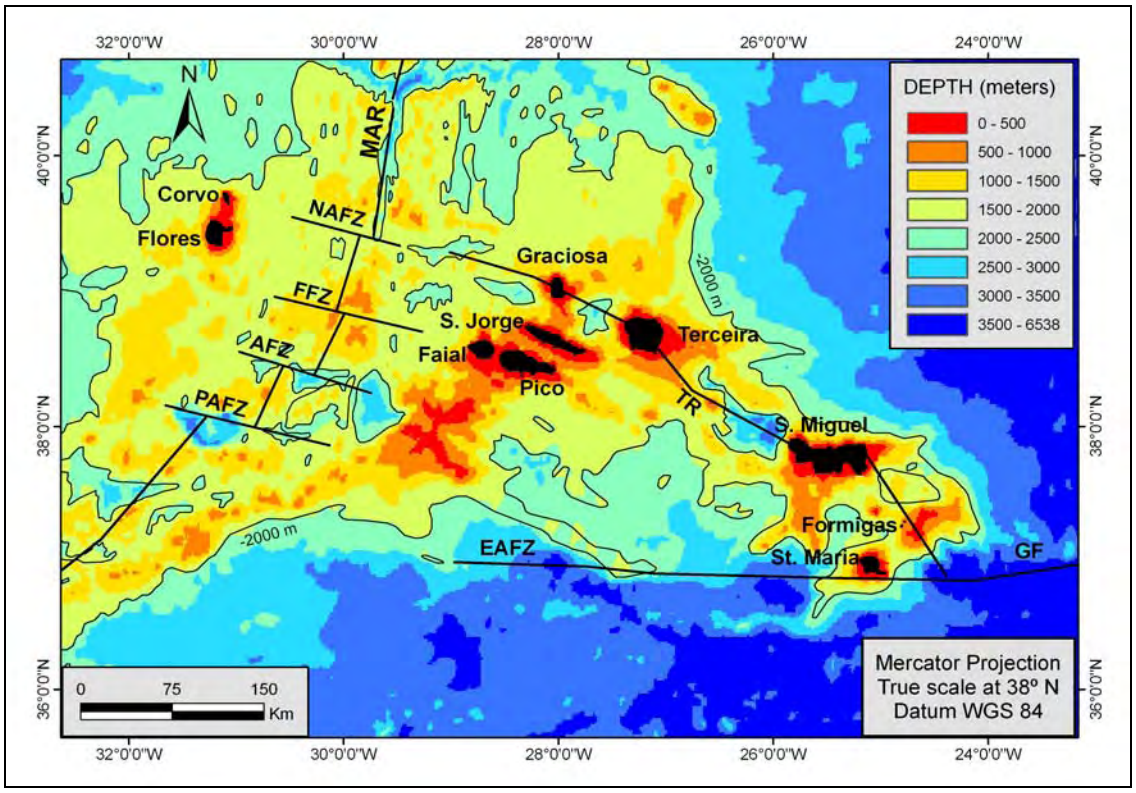

Figure 18 – Tectonic setting of the Azores archipelago (MAR modified from Luis et al., 1994; SJLT modified from Vogt and Jung, 2004). AFZ= Açor Fracture Zone; EAFZ= East Azores Fracture Zone; FFZ= Faial Fracture Zone; GF= Gloria Fault; MAR= Mid-Atlantic ridge; NAFZ= North Azores Fracture Zone; PAFZ= Princesa Alice Fracture Zone; TR= Terceira Rift. Bathymetry of the Azores archipelago from GEBCO (IOC IHO and BODC, 2003).

as an oblique ultra slow spreading center and as a transfer zone that accommodates the differential shear movement between the Eurasian and African plates from the MAR until the western tip of the Gloria fault.

Recent geodetic measurements in the central and eastern groups of the Azores Islands (Bastos et al., 1998; Pagarete et al., 1998) confirm this strain regime in the Azores triple junction. More recently, Fernandes et al. (2004; 2006) using new geodetic data revealed that Faial, Pico, S. Jorge, Terceira and S. Miguel Islands are clearly in the deformation zone whilst Graciosa Island belongs to the stable Eurasian plate and Santa Maria Island to the African plate.

2.1.1. Seismicity in the Azores area

Due to its location on an active plate boundary, the Azores archipelago is subjected to frequent seismic activity. Although most activity consists of low to

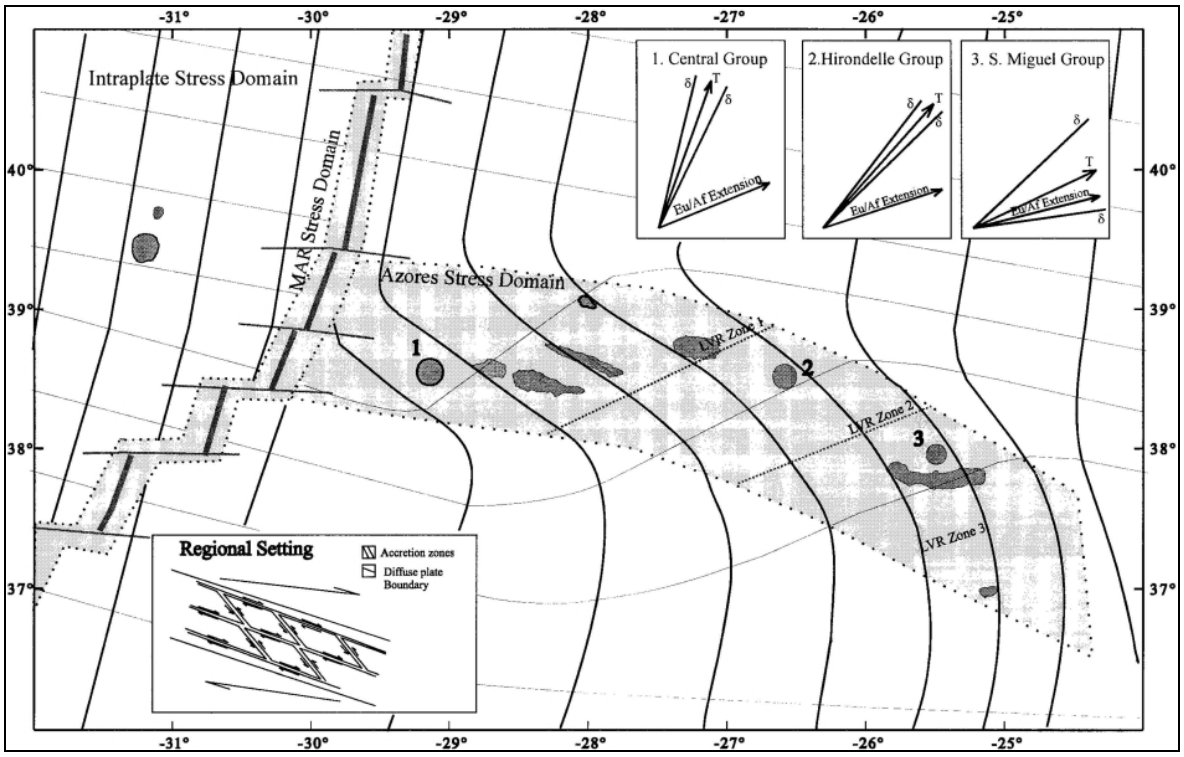

Figure 19 - Schematic stress pattern of the Azores plateau as inferred from the morphological features. Dots represent the boundaries between the different Linear Volcanic Ridge domains. Thicker lines represent maximum compressive stress orientation (σ1), thinner lines represent the minimum compressive stress orientation (σ3). The intermediate compressive stress (σ2) is vertical. Inset top are the T axis calculated from events displayed in Figure 20 in Lourenço et al. (1998) along with calculated standard deviations. The kinematic orientation of the spreading axis calculated from Nuvel-1 model (DeMets et al., 1990) in the three individualized areas is also shown for reference. Inset bottom is the schematic regional tectonic model for the Azores domain. (Lourenço et al., 1998).

moderate magnitude seismic isolated events or swarms, the islands are occasionally struck by high magnitude (M~7) earthquakes (Madeira and Brum da Silveira, 2003). The distribution of instrumental epicenters (Figure 20) shows that the present plate boundary is oriented WNW-ESE along the S. Jorge-S. Miguel alignment. Published focal mechanisms indicate: (a) dextral strike-slip with variable components of normal dip-slip in WNW-ESE oriented faults planes: (b) sinistral strike-slip with variable components of normal dip-slip in NNW-SSE oriented fault planes and (c) pure dip-slip normal events in both directions. This strain regime suggests decoupling in a transtensional regime. According to the position in time during the seismic cycle we can have pure dominant normal, dextral and sinistral strike-slip solutions on the WNW-ESE and NNW-SSE structures (Ribeiro, 2002).

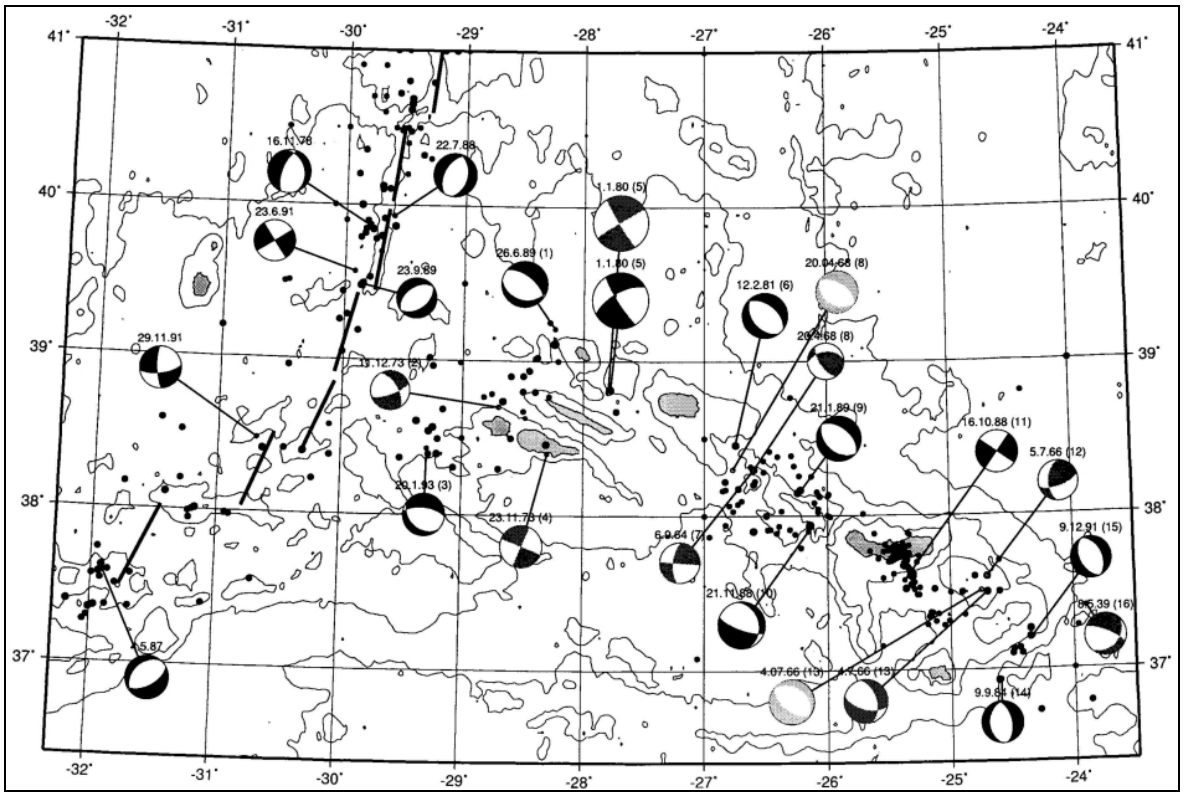

Figure 20 - Seismicity map (M>4) of the Azores plateau from 1928 until 1998, retrieved from the USGS database (Lourenço et al., 1998).

2.1.2. The origin of volcanism in the Azores archipelago

The formation of the Azores Platform may have started 36 Ma ago (Campan et al., 1993), related to the northward migration of the junction, from the latitude of the Pico Fracture Zone and East Azores Fracture Zone (see Figure 18) to its present position at the vicinity of the North Azores Fracture Zone (Luis et al., 1994). 10 Ma ago, a melting anomaly originated within the Azores hotspot provoked enhanced magmatism and played a significant role in the construction of the Azores platform (Cannat et al., 1999), consequently originating a complex spreading history (Luis et al., 1994).

The oldest isotopic ages collected in sub aerial formations for each Azorean island are given in Figure 21. The data indicate emergence of Santa Maria during the Miocene (8.12 Ma), of Formigas, S. Miguel, Terceira, Graciosa and Flores Islands in the Pliocene (respectively 4.65, 4.01, 3.52, 2.5 and 2.15 Ma) and Faial, Corvo, S. Jorge and Pico Islands in the Quaternary (respectively 0.73, 0.70, 0.55

and 0.25 Ma).

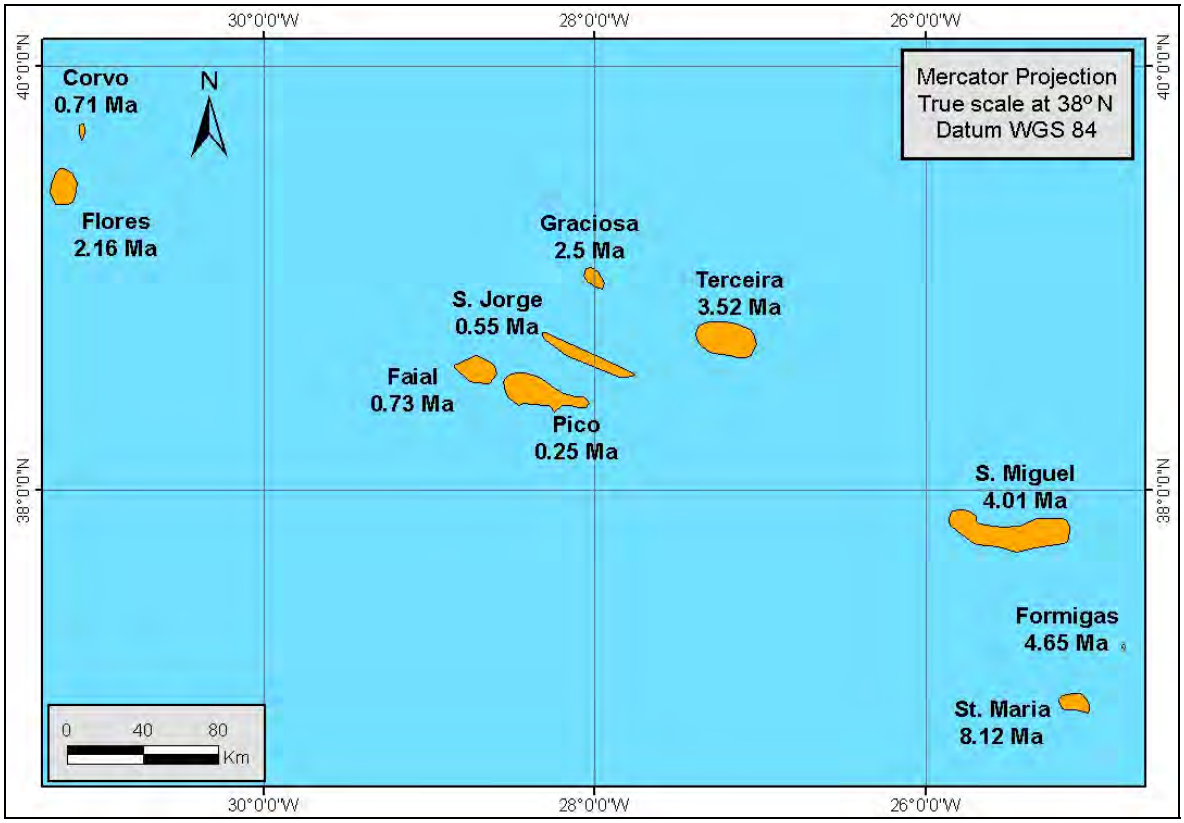

Figure 21 - Oldest radiometric ages (Ma) for each island (data collected from Abdel-Monem et al., 1968; Abdel-Monem et al., 1975; Azevedo et al., 2003; Azevedo et al., 1991; Chovelon, 1982; Feraud et al., 1980; Feraud et al., 1984; Ferreira and Martins, 1983; Forjaz, 1988; data collected from White et al., 1976).

Madeira and Ribeiro (1990) and Madeira (1998) suggest that the isotopic ages' determinations in Santa Maria may be higher than those determined by Abdel-Monem et al. (1975). Some samples may not have been collected in the oldest formations or may have been assigned to incorrect units. For the same reason, Madeira (1998) insists that in Faial, Pico and S. Jorge Islands, the isotopic ages published by Feraud et al. (1980) could be higher.

On the contrary, Johnson et al. (1998) presented new $^{40}Ar/^{39}Ar$ ages for the Nordeste complex of S. Miguel Island (between 0.78 and 0.88 Ma) which indicate a much younger volcanism than that proposed by Abdel-Monem et al. (1975) – K/Ar ages of 1 to 4 Ma. Similarly, Calvert et al. (2006) in face of new $^{40}Ar/^{39}Ar$ ages for the Cinco Picos Volcano of the Terceira Island, argues that the subaerial eruptions of this stratovolcano may have started between 0.40 and 0.50 Ma, in contrast with the age of 3.52 Ma inferred by White et al. (1976).

From what is mentioned above, it is clear that the age of the volcanism in the Azores islands is still controversial. Therefore, the assumed ages for the different volcanic regions from which the Faial Island is composed, will be used in this thesis carefully when trying to infer other geological processes (see Chapter 5).

2.1.3. Tsunami records

The Azores archipelago is highly vulnerable to tsunami hazards due to its location, active volcanism and plate-tectonics setting. First, its location on the northern mid-Atlantic makes it very vulnerable to far-sourced events namely those generated along the Iberian margin (Bryant, 2001). Furthermore, the compilations of Nunes et al. (2004) on the seismicity of the Azores show, that on average, every 70 years an earthquake with Ms exceeding 6.5 occurs. Finally, the volcanic islands are very prone to instability, with optimal conditions leading up to or contributing as potential triggers for tsunamis. De Lange et al. (2001) summarized the mechanisms associated to volcanism capable of generating large tsunamis which included the subaerial and submarine mass movements, submarine eruptions, caldera collapse, basal surges and shock waves as major sources.

Andrade et al. (2006) have built a dataset on tsunami-induced flooding of the Azores coast based on local monographs and newspapers, web citations and technical papers that cover a period from the start of the 15th century (beginning time of colonisation of the islands) till the present day. Among its major findings is the conclusion that most of the recorded tsunamis were generated by earthquakes and that the volcanic activity apparently had not generated destructive tsunamis. Since the settlement of the archipelago at least 23 tsunamis have struck the Azorean coastal zones and the highest known run-up (11–15 m) was recorded on 1 November 1755 at Terceira Island associated to the Lisbon earthquake, corresponding to an event of intensity VII–VIII (damaging–heavily damaging) on the Papadopolous–Imamura scale (Papadopoulos and Imamura, 2001). Although Andrade et al., (2006) found no evidence of volcanogenic induced tsunamis in the historical record; they agree that it would be misleading to assume that the

volcanism in the Azores had not had the power to create tsunamis. They argue

Mechanism	Source volume (km^3)	Tsunami characteristics: Wave height (m)	Period (min)	Travel distance (km)
Earthquakes	1–10	up to 17	10–40	<500
Submarine explosions	<1	1–6	1–10	<50
Pyroclastic flows (nuées ardentes)	1–100	up to 25	1–40	<250
Caldera collapse and subsidence	1–10	up to 15	short	<50
Avalanches of cold rock	<1	1–10	short	<50
Basal surges and shock waves	<1	up to 5	aperiodic	<10
Avalanches of hot rock	<1	small	short	<10
Lahars	<1	small	short	<50
Atmospheric phase coupling	?	small	15–40	>1000
Lava entering the sea	<1	very small	short	<10

Figure 22 – Mechanisms associated with volcanism capable of generating tsunami waves (De Lange et al., 2001).

Date	Source	Cause	Origin	Seismic intensity/ Magnitude	Tsunami intensity: Alexander (1993)	Tsunami intensity: Papadopoulos and Imamura (2001)	Run-up height/ tsunami height (m)	Recorded
??.07.1571	L	S		VII?	II	III–IV?	1	Smg, Ter? Gra? Sjz? Pix? Fay?
26.07.1591	L	S	37.4N/25.3W	VIII–IX	II–III	IV–V	1	Smg+other unspecified islands
24.05.1614	L	S→Ls	38.7N/27.0W	IX	III?	IV–V	**3**	Ter
21.12.1641	L	S	38.4N/28.1W		III–IV	VI–VII	**9**	Sjz
??.??.1653	L/D				III–IV?	V–VI	4	Ter
23.11.1668	L	S?	38.5N?/28.1W?		III–IV	V–VI	**7**	Sjz
??.??.1676	L	S	38.4N/27.1W		III–IV	V–VI	4	Ter
26.07.1691	L	S			II–III?	III–IV	1	Ter
01.11.1755	D	S	38.0N/10.0W	8.5–8.8	IV–V	VII–VIII	**11–15**	All islands
09.07.1757	L	S+Ls?	38.6N/28.0W	XI/7.4	II–III	IV–V	1	Ter, Gra, Fay (only)
31.03.1761	D	S	37.0N/10.0W		III	IV–V	1	Ter
??.??.1787					II?	III?	1	
23.01.1792					III–IV	V–VI	**8**	Sjz
17.02.1855	L/D				III?	V?	**5*–*10***	Ter
06.01.1856	L/D	Ss? S?			III–IV	V–VI	**10**	Sjz
03.02.1899	L/D	Ss? S?			III–IV	V–VI	**10**	Sjz
31.08.1926	L	S	38.5N/28.4W	X/5.6–5.9	I–II	II–III?	**0.5**	Fay
31.08.1931	L	S?	38.4N?/27.1W?		II–III	IV–V?	1	Fay
08.05.1939	D	S	34.3N/27.2W	VII/7.1	I	II	0.5	Ter
25.11.1941	D	S	37.5N/18.5 W	8.2	I	I–II	0.5	Ter
28.02.1969	D	S	36.0N/10.6W	7.3	II	II–III	1	Smg, Ter, Fay
26.05.1975	D	S	37.4N/17.7W	IV–V/7.9	II–III?	III–IV	1	Smg, Fay
01.01.1980	L	S	38.8N/27.8W	VIII/7.2	I	I–II	0.5	Ter

Notes: Smg — S. Miguel; Ter — Terceira; Gra — Graciosa; Sjz — S. Jorge; Pix — Pico; Fay — Faial. L — local; D — distal; S — seism; Ls — landslide; Ss — submarine slide. Tsunami run-up/height — see text for explanation.
Run-up height calculated by the authors is marked bold and *underlined*; estimates of run-up height taken from the literature or data bases and lacking confirmation by the authors are marked with an asterisk; *italics* refer to estimated or reported tsunami height; the remnant data on run-up was derived comparing the available descriptions with systems that correlate tsunami impacts on natural and human environment and structures with run-up

Figure 23 – Historical tsunami records in the Azores archipelago (Andrade et al., 2006).

that the limited instrumental and documentary data and also the small volumes released during the historical eruptions can account for that deceive. In fact, the geological record supports their assumption showing the emission of massive pyroclastic flows and caldera explosions with potential to generate high magnitude tsunamis.

2.2. Oceanographic setting of the Azores archipelago

2.2.1. Surface currents

The basic average ocean circulation pattern of the North Atlantic is an asymmetric, large scale gyre that flows to the north, on the western side, with an intense thin jet (the Gulf Stream) and to the south, on the centre/eastern side with a multibranched current system. The Gulf Stream very efficiently transports warm water of equatorial and tropical origin into the colder northern waters. The current patterns result in the high salinity, high temperature and low nutrient regime which typify the Azores. During Winter a deep mixed layer is present around 150 m and in Summer a seasonal thermocline develops around 40 to 100 m (Santos et al., 1995). The Gulf Stream is also the source of many instability processes, meanders and eddies. This picture becomes particularly complicated when this current leaves the North American coast, at about 40º to 45º N, towards the central zone of the North Atlantic where the Azores are located (Gould, 1985; Klein and Siedler, 1989).

The Gulf Stream (Figure 24) splits into two main branches at 40º N: the North Atlantic Current (NAC) and the Azores Current (AC). Each of these also divides into two further branches: NAC1 and NAC2 and AC1 and AC2 respectively. The northern part of Azores is influenced by the NAC2 and the southern one is influenced by the AC1. The general regime is from west to east (with a mean intensity of 10 cm/s at 100m water depth) but there is a clear seasonal and half seasonal oscillation of the mean direction, with periods where NAC2 dominates (current coming from northwest) and periods where AC1 is

present (current from southwest) (Alves, 1992; Santos et al., 1995).

The AC is a quasi-permanent feature throughout the year, centred between 33º and 35º N, with a variable eastward transport (Klein and Siedler, 1989). Surface mean speeds reach 30-40 cm/s decreasing to some 5 cm/s at about 700m water depth (Ollitrault, 1995). Local winds can alter significantly the AC, as well as the localization of Azores anticyclone which can have a major influence in the current direction (Instituto Hidrográfico, 2000).

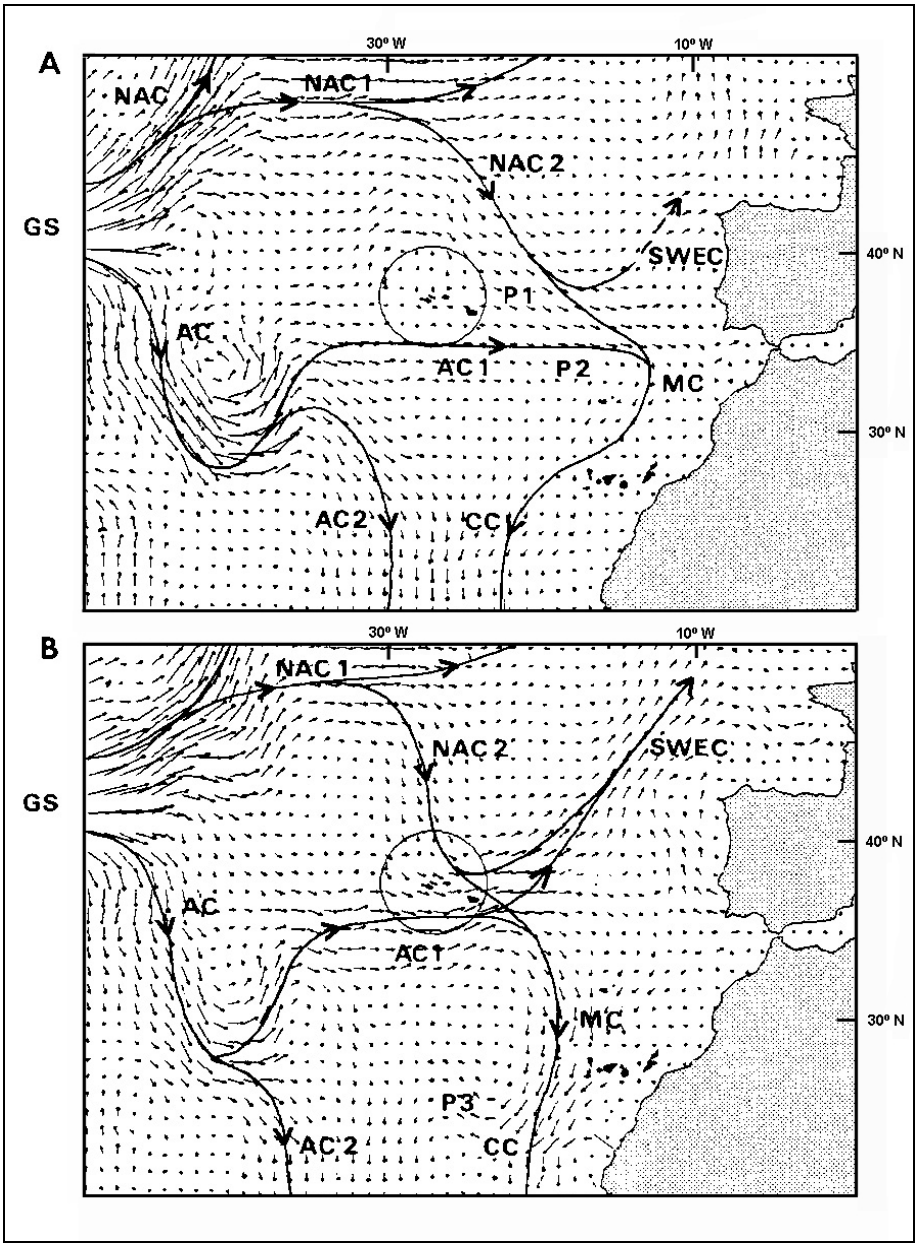

Figure 24 – Ocean currents on the area surrounding the Azores (circle locates the Azores archipelago). (A) Summer currents. (B) Winter currents. GS – Gulf Stream; NAC – North Atlantic

Current; AC – Azores Current; MC – Madeira Current; CC – Canaries Current; SWEC – Southwest European Current (after Santos et al., 1995).

2.2.2. Tides

The Azores archipelago is subjected to semidiurnal regular tides. In the Faial Island the annual mean tidal range is about 0.9 m and the annual mean tidal elevation is about 40 cm above the local mean sea level (MSL) (Instituto Hidrográfico, 2000). Consequently, this coast is subjected to a microtidal regime according to Hayes's classification (1979). In the Azores archipelago, tidal currents have not been studied yet. Nevertheless, empirical observations show that these exist, but with moderate intensity both in the flood tide and the ebb tide. In general these currents are stronger during spring tides, between the flood and ebb tides, reaching the highest velocities near the headlands of the coast. During the neap tides, the currents are weak or even do not exist (Instituto Hidrográfico, 2000).

2.2.3. Waves

Carvalho (2002; 2003) characterized the sea conditions in the Azores central archipelago during the period 1989-2002, based on the open sea-wave model (MAR3G). The model is a third generation wind-wave model that uses a square grid over a stereographic polar projection, with a node distance of 300 km at 60ºN. The grid has 20 x 22 points and for each point of the model calculates a directional spectrum of 12 directions and 13 frequencies and several wave parameters are calculated. From all the parameters supplied by Carvalho (2003) only the Significant Wave Height (H_s) and the Significant Wave Period (T_s) are required for the calculations in Chapter 6. Unfortunately, the model only provides the Significant Wave Height from spectral moments ($H_s(m_0)$) and the Peak Period (T_p) – see Tables 1 and 2. Therefore, a relationship between $H_s(m_0)$ and H_s and T_p and T_s must first be found to obtain the proper wave parameters. The significant wave height ($H_s(m_0)$) provided by Carvalho (2003) is calculated from the spectral moments (Equation 1):

$$H_s(m_0) = 4m_0^{1/2} \quad (1)$$

$$m_n = \int_0^{\infty} f^n S(f) df \quad (2)$$

Where $S(f)$ is the omnidirectional wave spectrum in terms of the variance of surface elevation and f the frequency of each wave in the spectra.

According to Tucker (1991) the use of $H_s(m_0)$ has been generally accepted since presently the majority of the records are analyzed as spectra. For a wave system whose spectrum contains only a narrow band of frequencies; $H_s = H_s(m_0)$, but for more typical sea states, 0.9 $H_s(m_0) < H_s < H_s(m_0)$. Therefore, the H_s can be substituted by the $H_s(m_0)$ in the calculations (Equation 3) without introducing significant errors.

$$H_s = H_s(m_0) \quad (3)$$

Concerning the period given from Carvalho (2003), this is the Peak period (T_p) which is the period at which the wave spectra $S(f)$ has its highest value. Fortunately, Tucker (1991) provides also the relationships for the Peak period (T_p) with the Zero crossing period (T_z) and for T_z with the Mean period ($\overline{T}$) (Equations 4 and 5). These are based on Carter's (1982) formulae derivation using the JONSWAP spectrum for the case of constant wind velocity with either limited fetch or limited duration. The equations 6 and 7 are respectively the definitions of T_z and $\overline{T}$ based on the spectral moments:

$$T_p = 1.286\ T_z \quad (4)$$

$$\overline{T} = 1.073\ T_z \quad (5)$$

$$T_z = \sqrt{\frac{m_0}{m_1}} \quad (6)$$

$$\overline{T} = \frac{m_0}{m_1} \tag{7}$$

The Significant Wave Period (T_s) is the period that corresponds to the mean wave period of one third of the highest waves in the wave spectrum. Considering the definition of the wave period parameters based on the spectra (Equations 6 and 7), T_s will lie between the values of T_p and T_z, and is most probably very similar to the value of $\overline{T}$. Therefore, the value of $\overline{T}$ will be used in Chapter 6 to substitute T_s in the calculations (Equation 8).

$$T_s = \overline{T} \tag{8}$$

Tables 1 and 2 are taken from Carvalho (2003) and represent annual averages for a period of 14 years. They are expressed into eight directional sectors (each one representing 45º) and for each sector it is represented the respective yearly percentages of the wave heights (Table 1) or periods (Table 2) (e.g. in Table 1, wave heights of 1.5 m that come from NE occur 3.71% of the year). The last two columns were calculated by the author, because their values were needed for this work. The calculations in Chapter 6 required the use of the mean annual significant wave height per quadrant (H_{sav}) and the mean annual significant period per quadrant (T_{sav}).

The H_{sav} can be determined for each quadrant in Table 1 using the following formula:

$$H_s(m_0)_{av} = \sum_{i=1}^{n} \frac{f_i \times H_s(m_0)_i}{\sum f_i} \tag{9}$$

Where $H_s(m_0)_i$ is the significant wave height and f_i its relative frequency (e.g. in Table 1, for quadrant NE, $H_s(m_0)_i$ is 0.50, 1, …..,16 m and f_i is 0.420, 2.968,….,0%). Because $H_s=H_s(m_0)$, then $H_{sav} = H_s(m_0)_{av}$.

Similarly, to calculate the mean annual peak period per quadrant (T_{pav}), the following formula was used:

$$T_{pav} = \sum_{i=1}^{n} \frac{f_i \times T_{pi}}{\sum f_i} \quad (10)$$

Where T_{pi} is the peak period and f_i its relative frequency (e.g. in Table 2, T_{pi} is 5, 6,…..,19s and f_i is 0.044, 0.685,……0%). After, Equations 4, 5 and 6 are used to determine T_{sav} after T_{pav}.

The annual wave frequency of a certain directional sector (f_{ws}) is the percentage of time in a year that waves from that sector occur and was calculated in Table 1 summing all the frequencies (f_i) of the wave heights of the respective directional sector. (e.g. in Table 1, for waves that come from NE, f_i are 0.42, 2.97,….,0.00% and the yearly frequency is 12.33%):

$$f_{ws} = \sum_{i=1}^{n} f_i \quad (11)$$

The same procedure was used to calculate in Table 2 the yearly period frequency of the directional sectors (f_{ps}).

The report of Carvalho (2002) provides also the minimum and maximum annual significant wave heights. According to the model (Figure 25), the annual prevailing wave directions come from NW and W (29% and 24% respectively). Less frequent, but also relevant are the waves from N and NE (16% and 12% respectively). The analysis of the significant wave heights along the year (Carvalho, 2002) shows a clear division of the data in four seasonal wave regimes: Autumn (September to November), Winter (December to February), Spring (March to May) and Summer (June to August). Although the waves from SW are often in fifth position in terms of decreasing frequencies, they are quite high which ranks them in the third position in terms of decreasing heights.

The Autumn (September to November) prevailing wave directions (Figure 26) comes from the NW (29%). Less frequent, but also relevant are the waves from the W, N and NE (20%, 19% and 12% respectively). During this period, the maximum significant wave heights can reach 8m, with average significant wave heights between 2 and 3 m.

Table 1 – Average annual significant wave height ($H_s(m_0)$) for the quadrant directions and respective frequencies, concerning the period 1989-2002 (Carvalho, 2003)

Significant wave Height ($H_s(m_0)$)	0.5 (m)	1 (m)	1.5 (m)	2. (m)	2.5 (m)	3 (m)	3.5 (m)	4 (m)	4.5 (m)	5 (m)	6 (m)	7 (m)	8 (m)	9 (m)	10 (m)	12 (m)	14 (m)	16 (m)	f_{ws} (%)	$H_s(m_0)_{av}$ (m)
NE	0.420	2.968	3.706	2.225	1.090	0.797	0.469	0.210	0.137	0.215	0.073	0.020	0	0	0	0	0	0	12.330	1.870
E	0.176	0.953	1.232	1.085	0.665	0.284	0.279	0.108	0.015	0.034	0.005	0	0	0	0	0	0	0	4.836	1.913
SE	0.029	0.191	0.753	0.768	0.386	0.288	0.152	0.142	0.064	0.015	0	0	0	0	0	0	0	0	2.788	2.211
S	0	0.161	0.797	0.807	0.509	0.376	0.259	0.220	0.068	0.137	0.005	0.005	0	0	0	0	0	0	3.344	2.456
SW	0.005	0.347	1.305	1.203	1.115	0.905	0.792	0.562	0.401	0.631	0.269	0.083	0.024	0.020	0.015	0.005	0	0.005	7.687	2.999
W	0.303	2.464	3.511	3.550	3.129	2.660	2.019	1.658	1.071	1.570	0.714	0.523	0.318	0.152	0.093	0.039	0.005	0	23.779	2.964
NW	0.905	5.251	5.246	4.313	3.452	2.836	2.122	1.482	0.993	1.315	0.626	0.274	0.152	0.098	0.064	0.010	0	0	29.139	2.480
N	1.002	3.545	3.496	2.851	1.858	1.217	0.777	0.460	0.328	0.342	0.132	0.073	0.020	0	0	0	0	0	16.101	2.018
Total																			100.00	

Table 2 – Average annual Peak period (T_p) for the quadrant directions and respective frequencies, concerning the period 1989-2002 (Carvalho, 2003)

Peak Period (T_p)	5 (s)	6 (s)	7 (s)	8 (s)	9 (s)	10 (s)	11 (s)	12 (s)	13 (s)	14 (s)	15 (s)	16 (s)	17 (s)	18 (s)	19 (s)	f_{ps} (%)	T_{pav} (s)
NE	0.044	0.685	2.303	3.124	2.943	1.843	0.826	0.411	0.137	0.015	0	0	0	0	0	12.331	8.626
E	0.020	0.440	1.305	1.501	1.037	0.465	0.054	0.015	0	0	0	0	0	0	0	4.837	7.988
SE	0.005	0.225	0.817	0.861	0.449	0.328	0.054	0	0	0	0	0	0	0	0	2.789	8.013
S	0.005	0.108	0.724	1.012	0.758	0.577	0.152	0.010	0	0	0	0	0	0	0	3.346	8.434
SW	0	0.166	1.169	1.359	1.545	1.584	0.993	0.543	0.225	0.078	0.015	0.005	0	0.005	0	7.687	9.321
W	0	0.484	2.132	3.208	3.833	3.574	3.418	2.826	2.039	1.081	0.689	0.318	0.132	0.044	0	23.778	10.318
NW	0.005	0.528	3.589	4.425	4.430	4.190	3.916	3.119	2.235	1.213	0.714	0.460	0.215	0.064	0.034	29.137	10.143
N	0.015	1.027	2.474	3.237	3.027	2.670	2.019	0.963	0.406	0.152	0.078	0.029	0.005	0	0	16.102	9.085
Total																100.00	

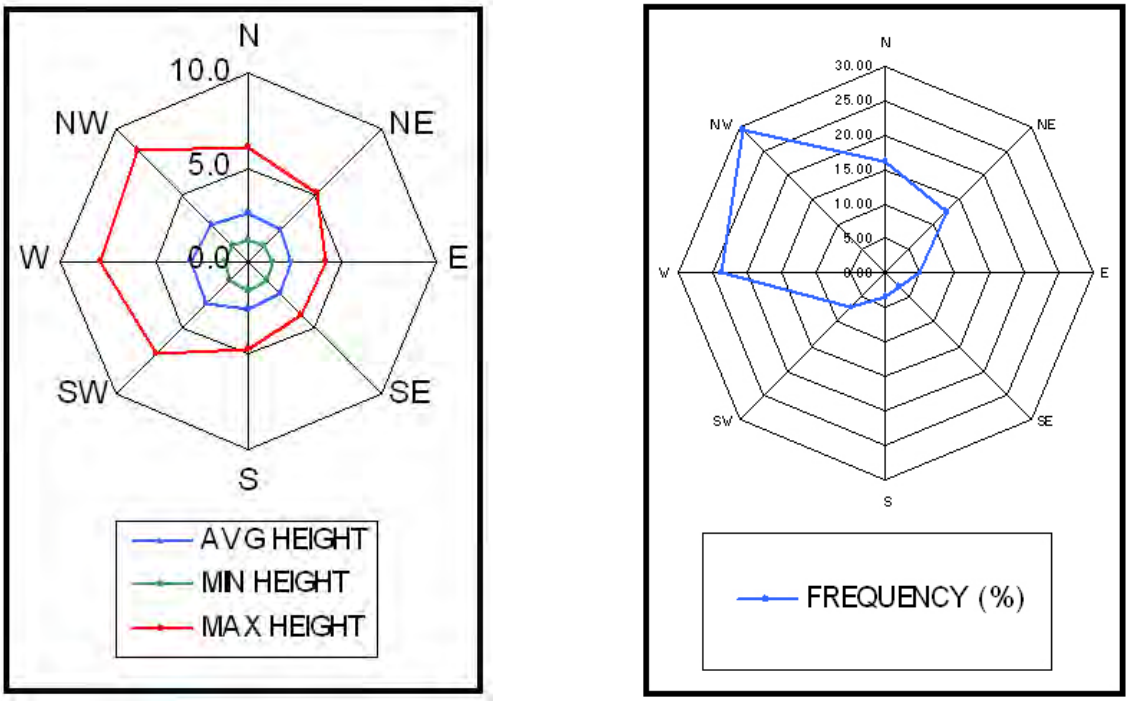

Figure 25 – Average, minimum and maximum annual significant wave heights and respective frequency (after Carvalho, 2002).

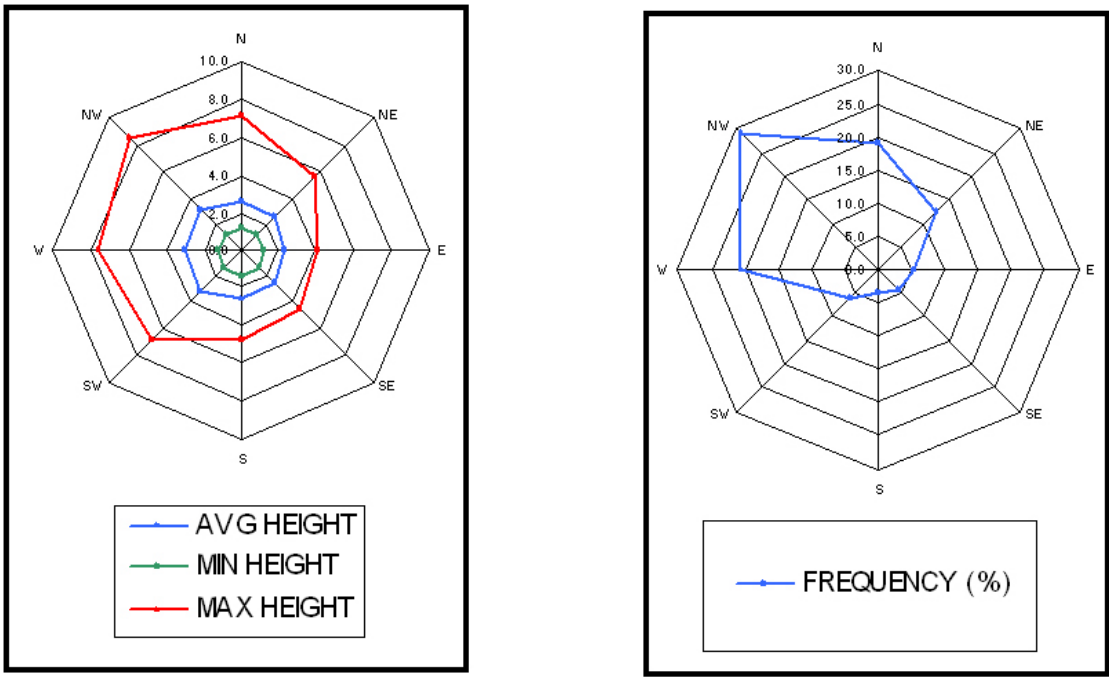

Figure 26 – Average, minimum and maximum significant wave heights and respective frequency in the Autumn (after Carvalho, 2002).

The Winter (December to February) prevailing wave directions (Figure 27) come from the W and NW (28% and 27% respectively). Less frequent, but also

relevant are the waves from the N, SW and NE (13%, 10% and 9%). During this period the maximum significant wave heights can reach 11m, with average significant wave heights between 3 and 4 m.

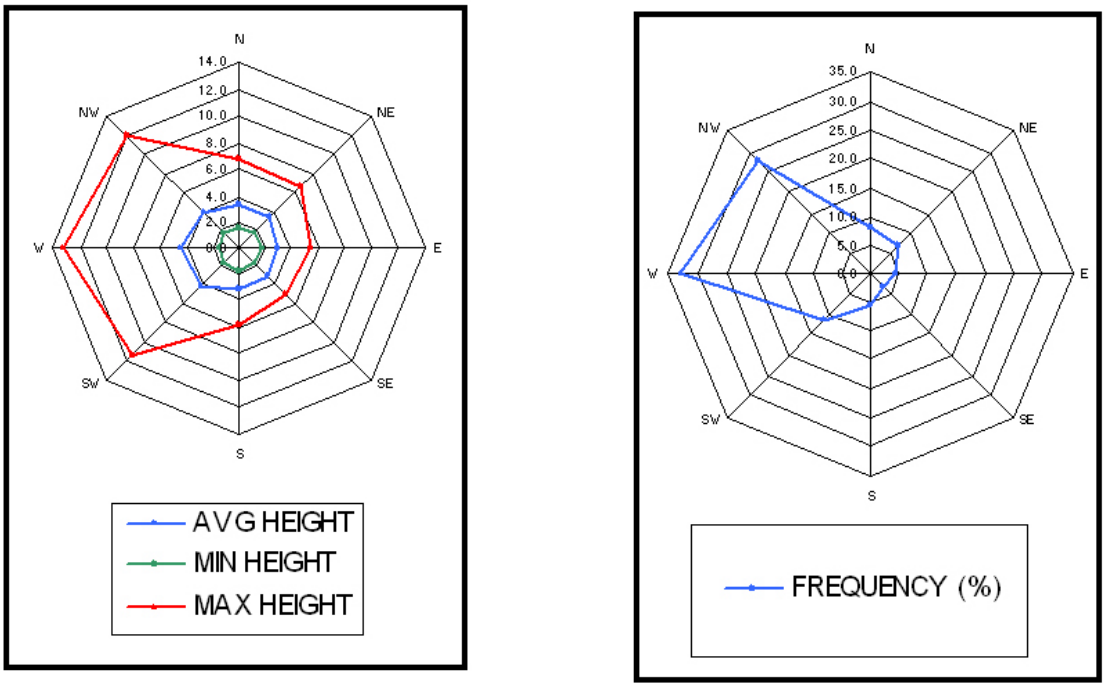

Figure 27 – Average, minimum and maximum significant wave heights and respective frequency in the Winter (after Carvalho, 2002).

The Spring (March to May) prevailing wave directions (Figure 28) come from the NW and W (26% and 23% respectively). Less frequent, but also relevant are the waves from the N and NE (18%, and 13% respectively). During this period the maximum significant wave heights don't go beyond 8m, with average significant wave heights between 2 and 3 m.

The Summer (June to August) prevailing wave directions (Figure 29) come from the NW (31%). Less frequent, but also relevant are the waves from the W, N and NE (20%, 19% and 15% respectively). During this period the maximum significant wave heights don't go beyond 5m, with average significant wave heights between 1 and 2 m.

Borges (2003) characterized the wave climate of the central group of the Azores Islands using ocean wave data available from the publication nº 700 of the U.S. Naval Oceanographic Office. He used the swell and sea observations

(Figures 30 and 31) of the mensal mean wave heights to construct the trimester graphs of the mean wave heights and frequency.

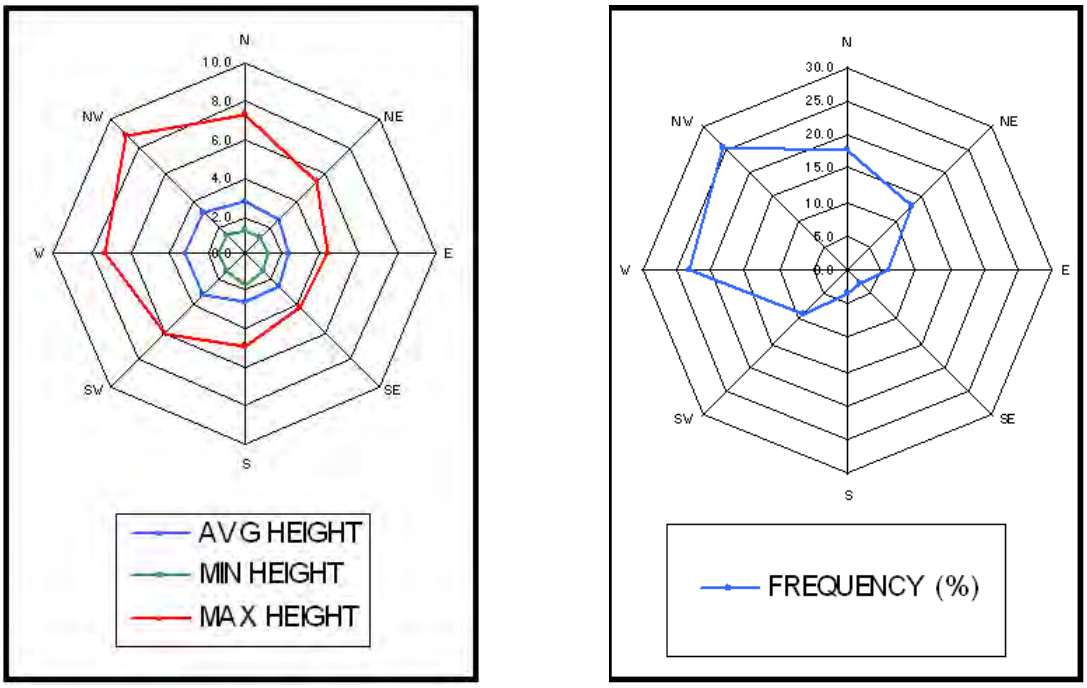

Figure 28 – Average, minimum and maximum significant wave heights and respective frequency in the Spring (after Carvalho, 2002).

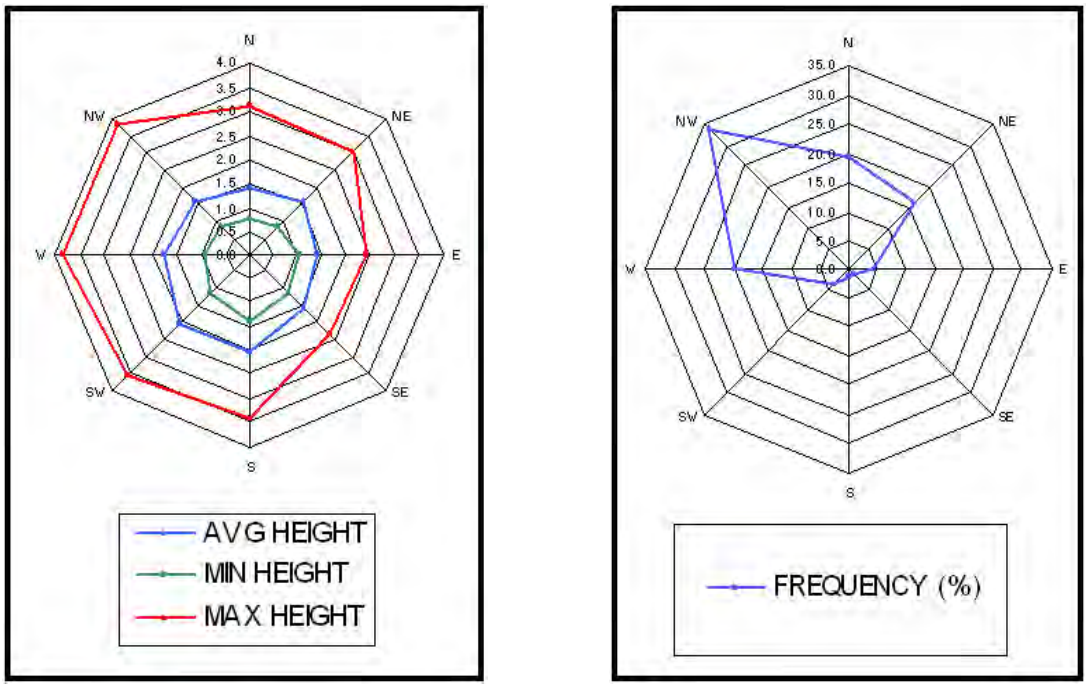

Figure 29 – Average, minimum and maximum wave heights and respective frequency in the Summer (after Carvalho, 2002).

The wave climate from Borges (2003) is presented in a different way than that produced by Carvalho (2002; 2003) making difficult the comparison between them. Nevertheless, they show almost the same results for the swell observations: the prevailing waves are those from the NW and W. The main difference is that in the MAR3G model the next prevailing waves in order of importance comes from the N whilst in the publication nº 700 they come from the SW. The sea observations are quite different, as it should be expected since these are generated by local winds. They show a predominance of the SW sector, followed by the NW, W and S in decreasing order of importance.

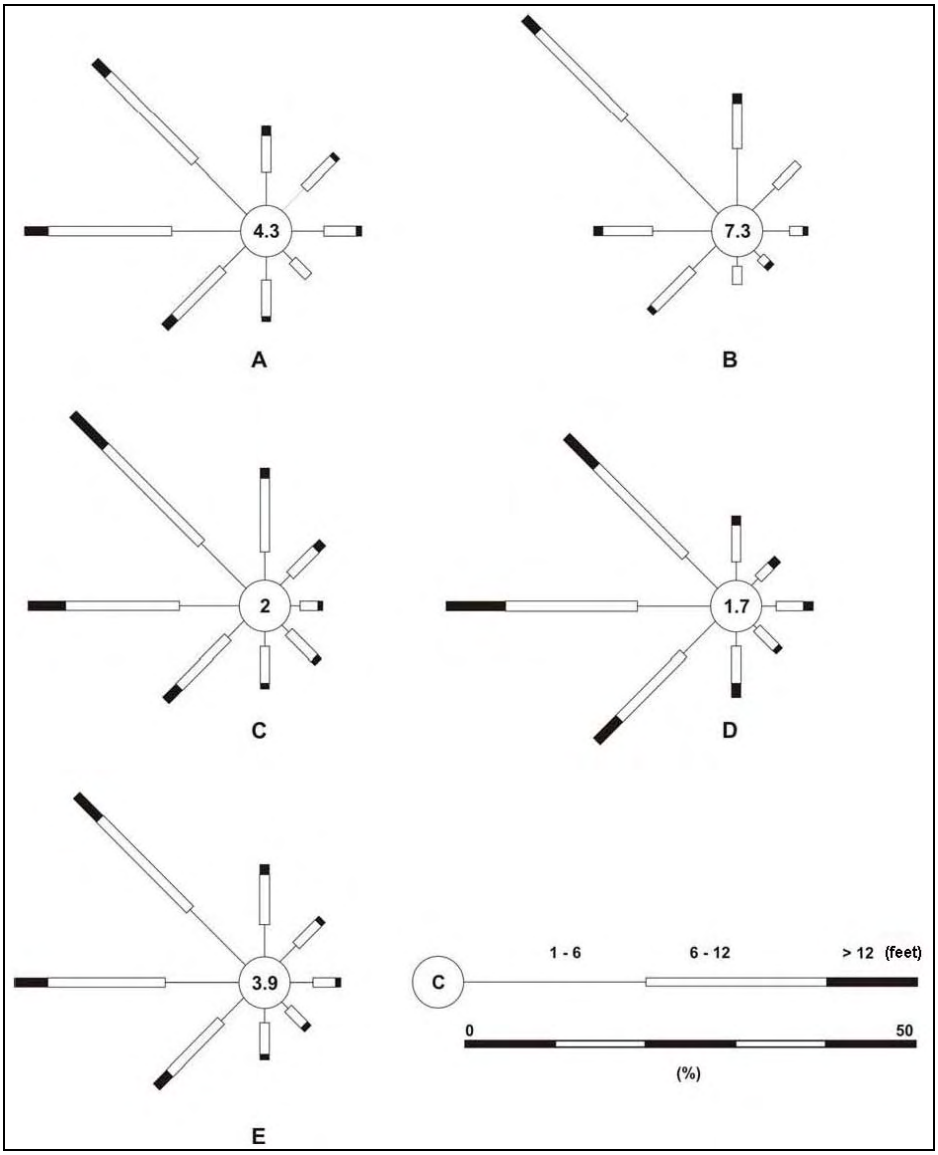

Figure 30 – Average wave heights and respective frequency for swell conditions. A – Spring; B – Summer; C – Autumn; D – Winter; E - Annual (Borges, 2003).

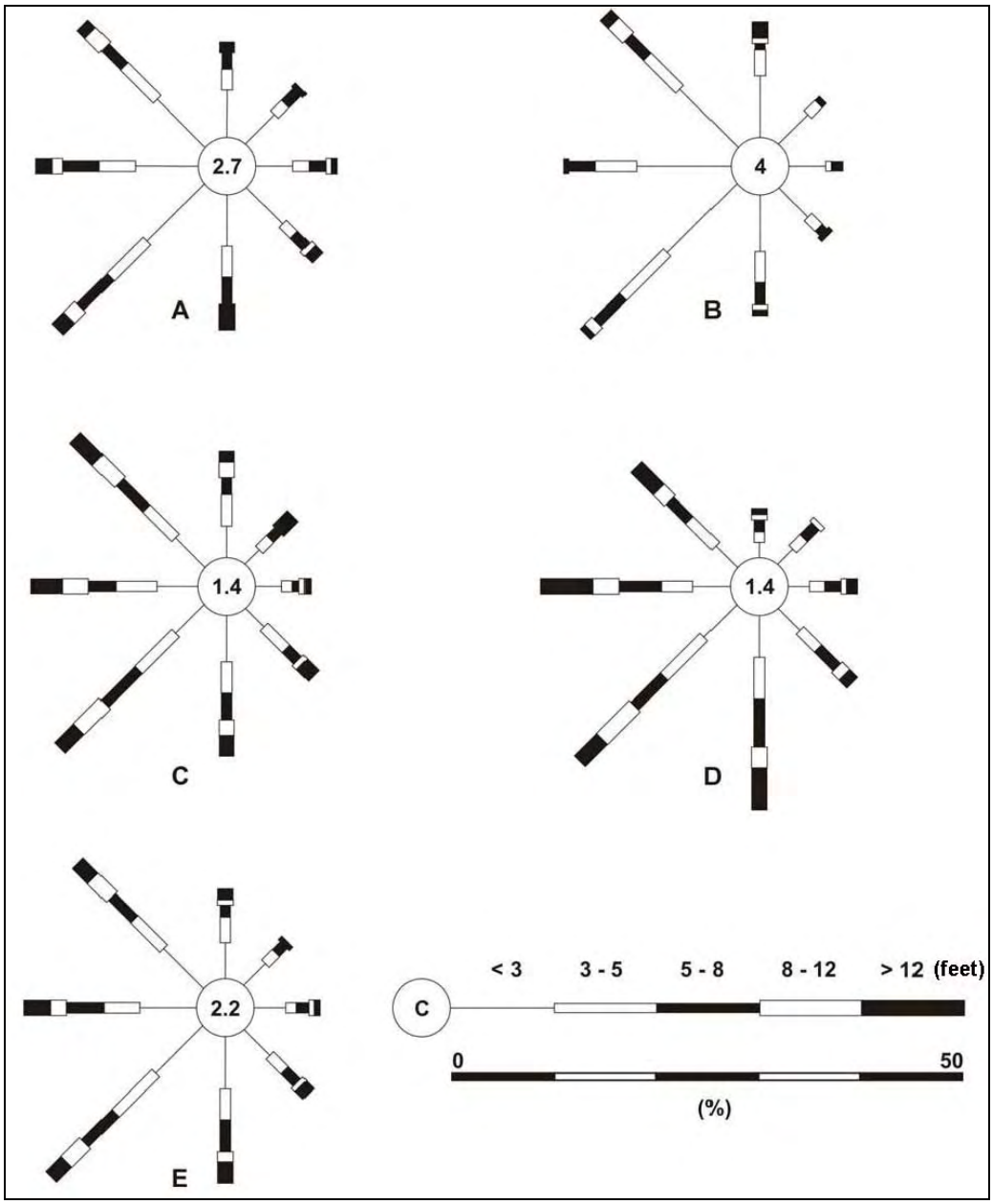

Figure 31 – Average wave heights and respective frequency for sea conditions. A – Spring; B – Summer; C – Autumn; D – Winter; E - Annual (Borges, 2003).

In spite of that, the wave data in all of them is consistent with the NW and W directions. The SW direction also appears in the three, with the frequency having more significance in publication nº 700 and the height more significance in the MAR3G model. The N and NE sector in the publication nº 700 has less importance in terms of frequency and height when compared against the MAR3G model.

Taking into account that the annual significant wave heights are in all the

quadrant directions between 1.9 and 3 m and that the mean tidal range is 0.9 m, the coast can be classified as a wave dominated coast according to the classification of Davis and Hayes (1984). Nevertheless, it is should be reminded that the tide in the channel Faial-Pico has probably a remarkable importance in the sedimentary dynamics. Although there is a lack of measurements to support this supposition, it is known that the flood currents are directed to NNE and the ebb currents to SSW, with mean velocities between 1 and 2 knots (Instituto Hidrográfico, 2000).

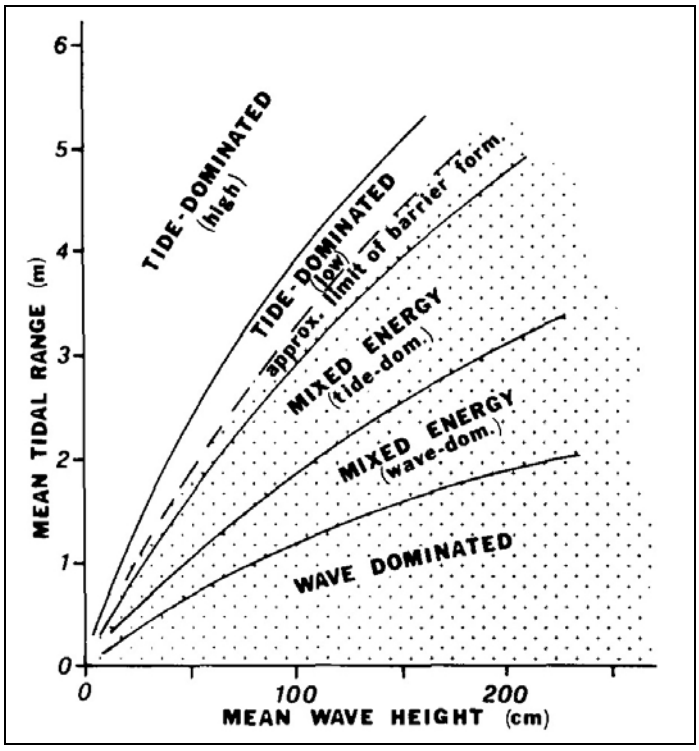

Figure 32 – General relationships between tidal range and wave height (Davis and Hayes, 1984).

2.2.4. Storminess records

Borges (2003) built a database of the historic storminess of the Azores archipelago based on the records of two Azorean newspapers. He selected the period from 1835 to 1988 and used the information from the *Açoriano Oriental* and the *Açores* newspapers. Using several statistical approaches he managed to characterize the Azores storminess for that period (Table 3) and grouped the storms into a four point intensity scale based on a classification previously made

by Andrade et al. (1996). He reached the conclusion that the low intensity storms (classes I and II) correspond respectively to 30% and 56% of the total records, whilst the more extreme events (Class IV) accounted only for 5%. Consequently a low intensity event occurs, in average, four times every five years while a violent storm occurs once every seven years. The more struck season (October to March) accounts for 76% of the entire year. During this season, December and February are the months more prone to be hit by storms (20% each), followed by November (15%), October (12%) and March (11%). The average annual frequency is 3.1 storms per year.

Table 3 - Statistical resume of the historic storminess (Borges, 2003)

Average storm duration (days)	2.3
Maximum storm duration (days)	9.0
Average frequency (Storms/year)	3.1
Extreme events frequency (Classes III and IV)	14%
Average duration of the extreme events (Class IV) [days]	1.1
Maximum duration of the extreme events (Class IV) [days]	2
Average of the extreme events (Class IV)/year	0.15
Average duration of the Class I events (days)	1.8
Average duration of the Class II events (days)	2.1
Average duration of the Class III events (days)	3.0
Number of storms	509
Number of stormy days	1166
Number of analyzed days	59536

2.2.5. Sea level variations in the Azores archipelago

In Chapter 5, a sea level oscillation curve will be used to estimate the shelf widening erosion rates. For that purpose there is the need to use a curve that covers 800 Ka, which is the oldest know subaerial age of Faial Island. There are many sea level published curves, but the problem is that many of them are based on the ratio of oxygen isotopes contained in benthic or deep sea foraminifera (Siddall, 2005). Although it is true that the ratio of $^{18}O/^{16}O$ increases in the water during glacial periods due to the incorporation of ^{16}O into the ice, there are

complications when it comes to extract the effect of ice-cycles from this ratio. The first complication is the preferential evaporation and subsequent incorporation of the lighter oxygen isotope in the ice-sheets during glacial conditions, which varies where and when the shell was formed, affecting the ocean's $^{18}O/^{16}O$ value (Bintanja et al., 2005). Secondly, differences in the isotopic ratio between water masses, coupled with changes in deep-ocean circulation, in turn affect the $\delta^{18}O$ value incorporated into the shells of benthic foraminifera (Siddall, 2005). The best option is to use sea-level curves based on fossil coral terraces, since they can provide a precise indicator of sea level when the colony lives up to the mean low sea level, as is the case of the micro-atoll formations (Chappell, 1983; Woodroffe and McLean, 1990). In other situations, the range of coral habitat may be as large as 5 to 10 m (Lighty et al., 1982; Montaggioni et al., 1997), being nevertheless more precise than using the ratio of oxygen isotopes (Chappell and Shackleton, 1986). The sea level oscillation curve from Thompson & Goldstein (2006) is the more recent and accurate curve for the last 240 Ka based on corals (Figure 33). It also uses a new approach to correct many of the problems associated with imprecise conventional U-Th ages, producing sea-level reconstructions with improved accuracy and resolution (millennium step) that confidently correlate with SPECMAP, the benchmark of $\delta^{18}O$ records (Thompson and Goldstein, 2006). This curve shows a continuous record for the first 129.3 Ka, but since there is the need to go beyond that age, another solution must be found. One hypothesis is to use another curve, for instance one based on $\delta^{18}O$ records and use a corrected proxy between concentration and sea level. The Bintanja et al. (2005) approach takes that into account, using the benthic $\delta^{18}O$ records (LR04 stack) from Lisiecki & Raymo (2005), a 5.3 Ma stack from 57 globally distributed sites and with a reliable age model calibration (Figure 34). The central assumption from Bintanja et al. (2005) is that deep ocean temperatures are related to the surface-air temperatures at high latitudes in the Northern Hemisphere by a simple, linear transformation. This enables these authors to link algorithms that describe temperatures in the deep ocean to those that calculate the ratios of oxygen isotopes in the ice sheets of the Northern Hemisphere. The authors then adjust the linked benthic and high-latitude temperatures of their coupled model iteratively, to generate the right

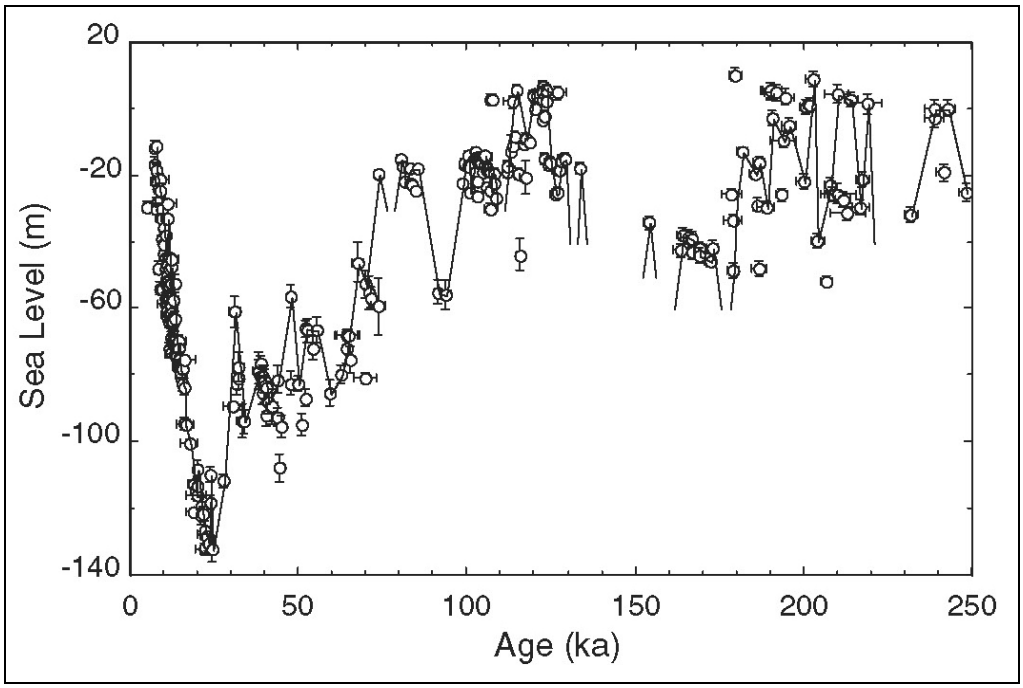

Figure 33 – Eustatic sea level curve from Thompson & Goldstein (2006). Error bars correspond to two times the standard deviation and those not visible are smaller than plotted symbols.

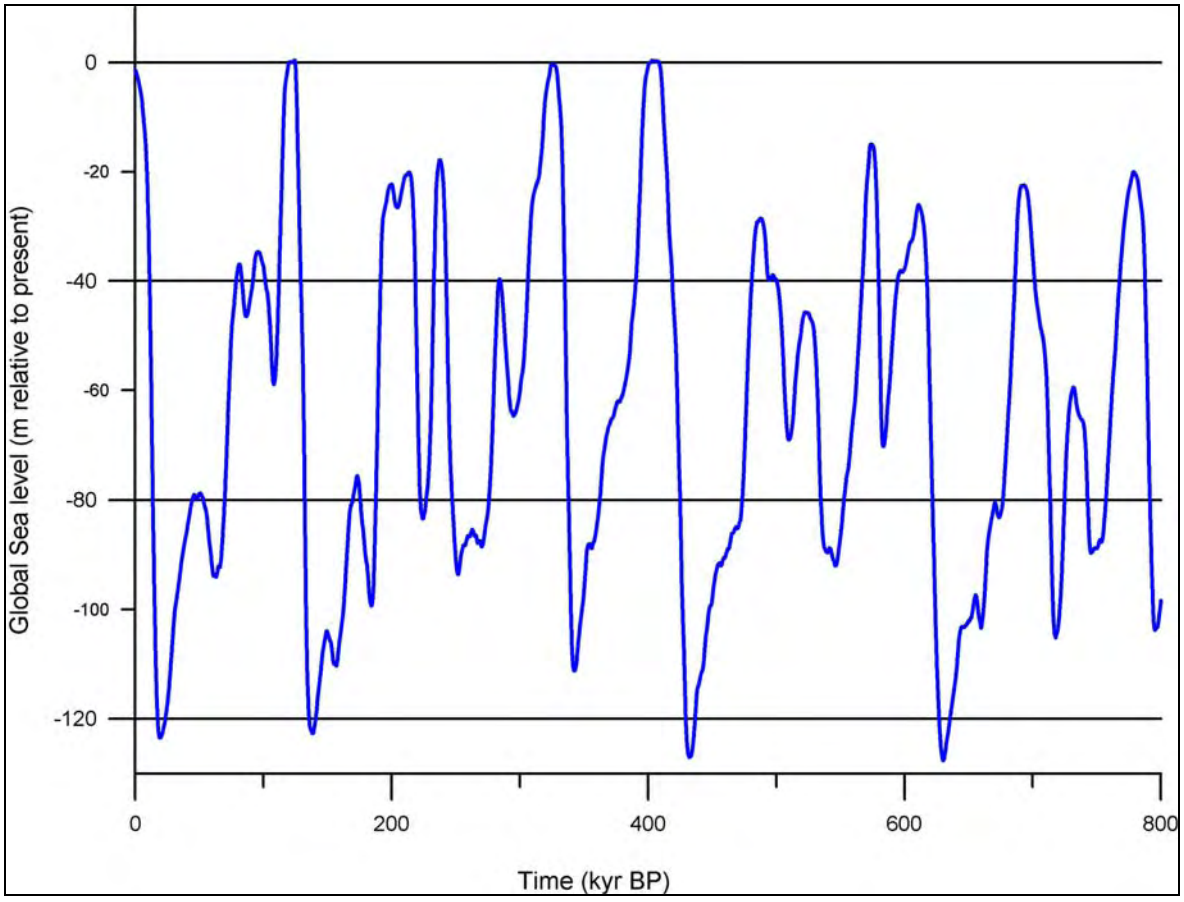

Figure 34 – Eustatic sea level curve for the last 800 Ka (after Bintanja et al., 2005).

amount of ice growth and benthic temperature to best fit the record of benthic oxygen isotope ratios, and thus arrive at mutually consistent records of temperature and ice volume at high latitudes in the Northern Hemisphere (Siddall, 2005). A similar approach had already been tried by Siddall et al (2003) in the Red Sea, reaching also good results when compared with other independent sea-level reconstructions. The Red Sea is strongly affected when lowered sea-level restricts circulation with the Indian Ocean. Therefore, Siddall et al (2003) used a conversion of a salinity record from the Red Sea, via a hydraulic model, to infer the sea-level oscillations.

The uncertainties reported so far are only a small fraction of the processes that can affect the prediction of the sea-level oscillations. There are processes mainly related with the rheological properties of the Earth that may introduce considerable variations in the sea-level depending on the geographical position of the area under study (Farrell and Clark, 1976). The magnitude and spatial extent of the ice-water mass exchange during a glacial cycle is sufficient to produce a significant deformation of the solid earth that proceeds until a state of isostatic equilibrium is reached. The surface mass flux and the associated solid earth response are commonly described by the general term Glacial Isostatic Adjustment (GIA). GIA induced sea-level changes are driven by a number of mechanisms. The ice-water mass redistribution is the most important GIA forcing. It contributes to the direct mass exchange between the ice sheets and the oceans and at the same time induces load deformations of the geoid and the solid surface. Recent improvements of the traditional sea-level theory of Farrell & Clark (1976) have had an impact on the predictions of sea-level changes. These include the change in the Earth's rotation vector which acts to deform the geoid and the solid surface (Milne and Mitrovica, 1998b), the water influx into regions vacated by a retreating marine-based ice margin (Milne et al., 1999) and the impact of a time-varying shoreline, which depends on the detailed ocean-continent geometry and bathymetry (Milne and Mitrovica, 1998a). In the near-field regions, the uplift of the solid surface during and following ice load removal is the dominant process resulting in a sea level fall of up to hundreds to several hundreds of meters (Lambeck and Chappell, 2001; Milne et al., 2002). In contrast, the addition of

glacial meltwater to the global oceans, either by isostatic effect of water loading or simple water excess, is the dominant contribution to the observed sea-level rise in far-field regions (Lambeck and Chappell, 2001; Milne et al., 2002). These examples are, of course, a simplified view of the end-members of the global sea level response. It is likely to expect that at mid-latitude places like the Azores, these two components of the GIA sea-level contribute with different magnitudes creating a more complex signal. It would be difficult to make previsions for mid-latitude places since operational models for glacial rebound with lateral variation do not yet exist and different parameters may need to be used according to the representative mantle conditions (Lambeck and Chappell, 2001). Furthermore, significant and systematic discrepancies between previous predictions of sea-level change subsequent to the last glacial maximum and observations are recorded even in far-field regions (up to 14 m), suggesting that also here the several components that control the sea-level play a significant role (Bassett et al., 2005; Milne et al., 2002). In conclusion, the relative sea level change therefore exhibits complex spatial patterns, even when the localities lie relatively near to each other (Lambeck and Chappell, 2001). Pflaumann et al. (2003) present a comprehensive new Sea Surface Temperature reconstruction of the Atlantic for the last glacial period. It shows that sea ice was restricted to the north western margin of the Nordic seas during glacial northern summer, while the central and eastern parts were ice-free. During northern glacial winter, sea ice advanced to the south of Iceland and Faeroes (between 50º and 60º N). This does not mean that this had to be the case during more extreme glacial cycles like MIS 12 (474–427 Ka). However, it is pretty likely that during most of the glacial times the polar front did not reach the Azores islands. According to Dennielou et al. (1999) the Azores Plateau was located south of the maximum extension of the polar front which was at 42ºN.

Presently, there are also other processes that affect the sea level surface and although they are now constant, they may have varied in the past. The marine geoid is the sea undulating surface related to the gravity field that reflects differences below the surface of the Earth (e.g., density). This surface (Figure 35) can account for sea level variations of almost 200 meters between two ocean

regions thousands of kilometers apart (Cullen and Moore, 2001). Superimposed over this surface is the sea surface height, also called the dynamic topography. It is defined as the height of the sea surface relative to the geoid and is directly caused by ocean currents (Figure 36). Differences of one meter are recorded around the North Atlantic due to wind and buoyancy (heat and freshwater) forcing, resulting in a nonzero dynamic topography and a corresponding circulation of the ocean (Bingham and Haines, 2006).

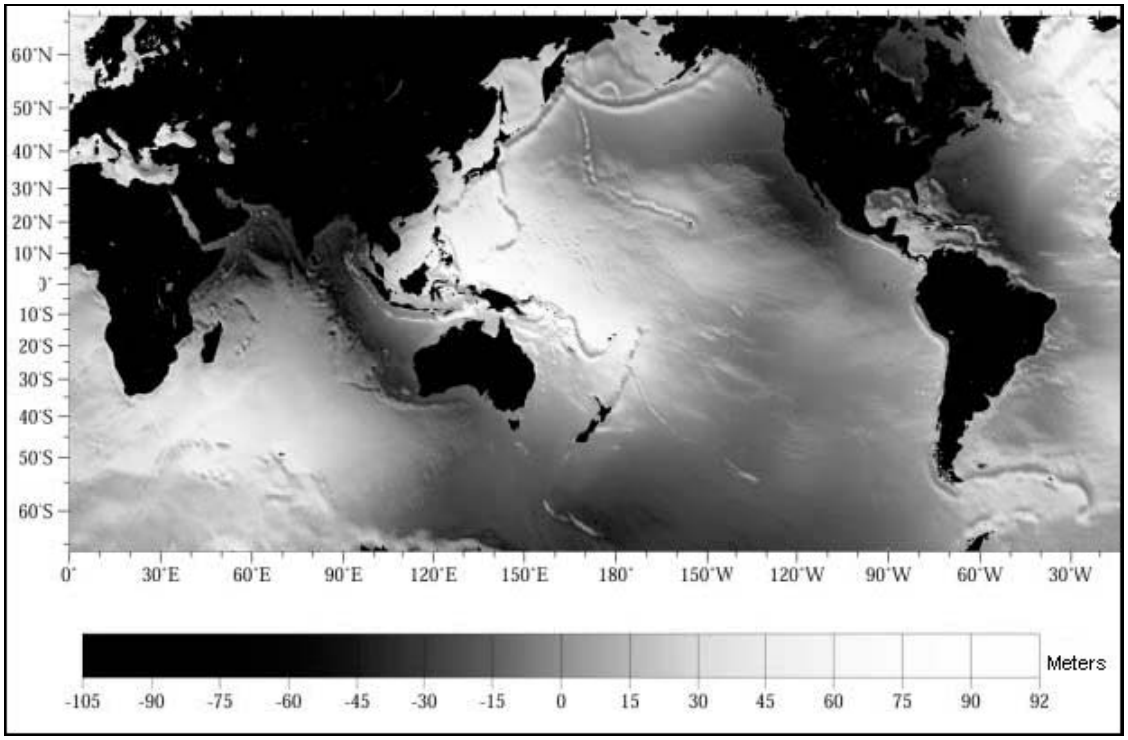

Figure 35 – Global mean sea surface from ERS-1 geodetic phase data (Cullen & Moore, 2001).

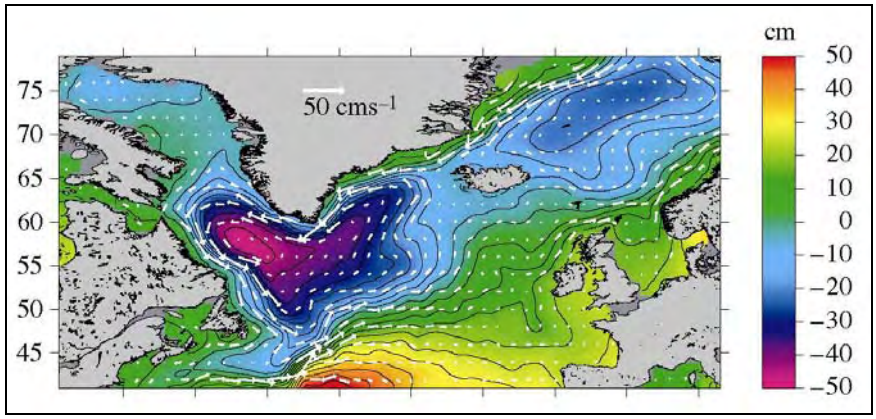

Figure 36 – Composite MDT (mean dynamic topography) for the period 1993-2001 over the North Atlantic (Bingham & Haines, 2006).

In the Azores region a high resolution mean sea surface, named AZOMSS99, has been derived using altimeter data from ERS-1 and ERS-2 35-day cycles, spanning a period of about four years, and also data from an ERS-1 geodetic mission (Fernandes et al., 2000). It shows that the mean sea surface near Faial Island is 58 meters above the zero reference level of the Earth's ellipsoid (Figure 37). This data also shows that the mean sea surface in the Azores may vary by 10m (see Figure 37) and that using sea-level variations extracted from cores in this area may introduce this amount of error and we are only considering the error transmitted by the mean sea surface variation. The sum of all the errors (if possible) resulting from using local cores in the Azores would be considerable. Therefore, it is preferable to use a compilation of results from different ocean basins and latitudes that would average out local effects. Taking this into account, the sea-level curves from Thompson and Goldstein (2006) and from Bintanja et al. (2005) were chosen as the ones that would introduce fewer errors in the modeling. The resulting sea-level curve is a compilation which includes the first 129.3 Ka of the curve of Thompson and Goldstein (2006) and from 129.3 Ka to 800 Ka the curve of Bintanja et al. (2005).

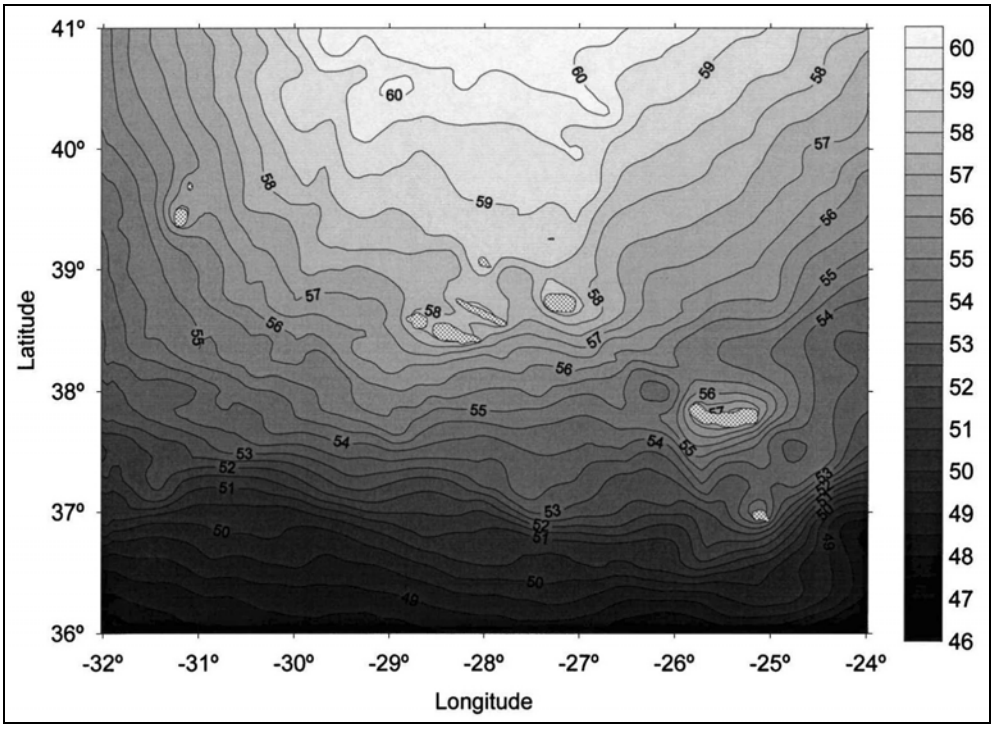

Figure 37 - Regional geoid of the Azores archipelago (Fernandes et al., 2000).

However, the author is aware that these sea-level curves do not include most of the corrections for the uncertainties discussed above. Nevertheless, the emphasis in Chapter 5 is not to reproduce the details of an Azorean sea-level curve, but to have a rough estimation of the amount of time that sea has been at the different levels (with 10 m interval).

2.3. Climatic Setting of the Azores archipelago

The Azores archipelago is located in the Northern Hemisphere subtropical anticyclones zone, under the direct influence of the Azores anticyclone. During most of the year (September to March), the polar-front jet often migrates to south and the Azores region is affected by low-pressure systems causing stormy weather and intermittent periods of high winds. It is during this season that three quarters of the total annual precipitation occurs. During late Spring and Summer, the Azores climate is influenced by the Azores anticyclone and there is less rain (Ferreira, 1981; Santos et al., 2004).

The islands are characterized by an oceanic temperate climate, with mild temperatures all year round, at low altitudes, and a rather wet climate. The distribution of rain is highly controlled by topography (the precipitation is 20 to 25% higher in the northern slopes than the southern), rainy at high altitudes and drier in coastal areas. In fact, one of the main processes responsible for the production of precipitation in these islands is the ascent of moist air over the islands terrain. The climate can be considered as oceanic cold in the higher areas where precipitation is higher and temperature decreases, with temperature decreasing 0.6 ºC and the precipitation increasing 250 mm every 100 m. The annual precipitation ranges between 800 mm and 2200 mm (Bettencourt, 1979).

2.3.1. Wind

The highest wind velocities occur from January to March and are related with the bigger horizontal gradient of the atmospheric pressure in the North Atlantic during this period.

In Horta Observatory (Figure 38A) the highest frequency is from SW (21.9%) being the highest velocities from the SW and S, with annual mean values of about 30 km/h. The annual mean days with velocities equal or above 36 km/h (force 5 in the Beaufort's scale) and equal or above 55 km/h (force 7 in the Beaufort's scale) are respectively 119 and 28 (Instituto Hidrográfico, 2000). In Madalena Observatory (Figure 38B) the highest frequency is from SW (24.3%) being the highest velocities from SW, with annual mean value of about 24 km/h.

The SW and S prevailing winds are consistent with the generation of local sea waves coming from the SW and S (see Figure 31 to compare) shown in Borges (2003). However, the other prevailing directions of local sea waves shown in Figure 31 are not consistent with those of Horta and Madalena observatories, which may indicate that the data presented by Borges (2003) may not apply for all the islands of the central archipelago.

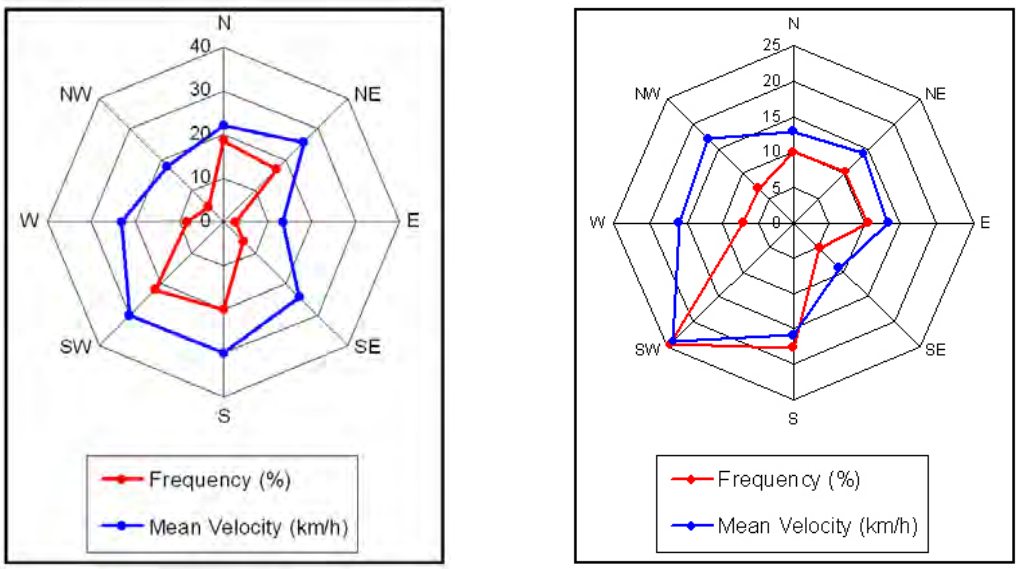

A B

Figure 38 - Average annual wind speeds and respective frequency. A) Horta Observatory (Faial Island). B) Madalena Observatory (Pico Island). Data provided from the Horta and Madalena observatories of the Instituto de Meteorologia.

2.3.2. Soil erosion rates in the Azores archipelago

The Azorean soils are mainly Andisols, i.e. soils that have formed in volcanic ash or other volcanic ejecta (Madruga et al., 2001).

Fontes et al. (2004) used modelling and direct measurement to obtain

values of runoff and erosion on pasture lands, the predominant cover of the Azorean cultivated soils. Results show that under pasture, runoff is < 1% of total rainfall but increases sharply to near 20% of the rainfall when the soil is tilled and not protected by vegetation. The sediment produced by erosion corresponded to less than 50 kg/km^2/year under pasture cover, but increased to almost 150 ton/ km^2 during the period of 8 months when the soil was disturbed by tillage and less protected by vegetation.

Louvat & Allègre (1998) estimated erosion rates for three drainage basins in S. Miguel Island. They used the chemical composition of the river waters sampled to infer chemical denudation rates of 26-50 ton/km^2/year. Using a steady-state model of erosion that assumes a relationship between chemical and mechanical erosion rates, they reached a rate of mechanical erosion of 70-500 ton/km^2/year.

2.4. The Faial Island

The Faial and Pico Islands define the subaerial section of a major WNW-ESE topographic lineament that extends over 100 km, from 10 km west of Capelinhos in Faial Island to 10 km east of Ponta da ilha in Pico Island (Figure 39). To the east, this lineament changes direction to NW-SE as the Pico submarine volcanic ridge, with approximately 83 km long and 9.6 km wide (Stretch et al., 2006). This ridge seems to be predominantly formed from fissure eruptions along the ridge axis, with lava flowing down its flanks (Stretch et al., 2006).

Both islands rise from a depth of 1200-1600 m and extend over an area of about 2000 km^2, whereas the subaerial parts are a mere 660 km^2.(Pico's surface is about 480 km^2 and Faial's is 180 km^2).

In contrast to the fairly well known geological evolution of the subaerial part of the island, the submarine portion has remained almost unknown till the present time. The only data source available to understand its submarine development was the hydrographic map of the Faial Island (Instituto Hidrográfico, 1999). The approximate shelf extent of the island is shown by the 100 m contour (Figure 40), where an obvious increase in slope (higher than five degrees), reflects the shelf edge. One exception is the northeast part of the shelf where the shelf limit

changes abruptly from the 100 m to the 200 m contour. Another exception is the southern part of Faial where the E-W shelf edge occurs at the 50 m contour. The third exception is the eastern part of the Faial Island where the shelf extends beneath the channel Faial-Pico and merges with the western shelf of the neighboring Pico Island.

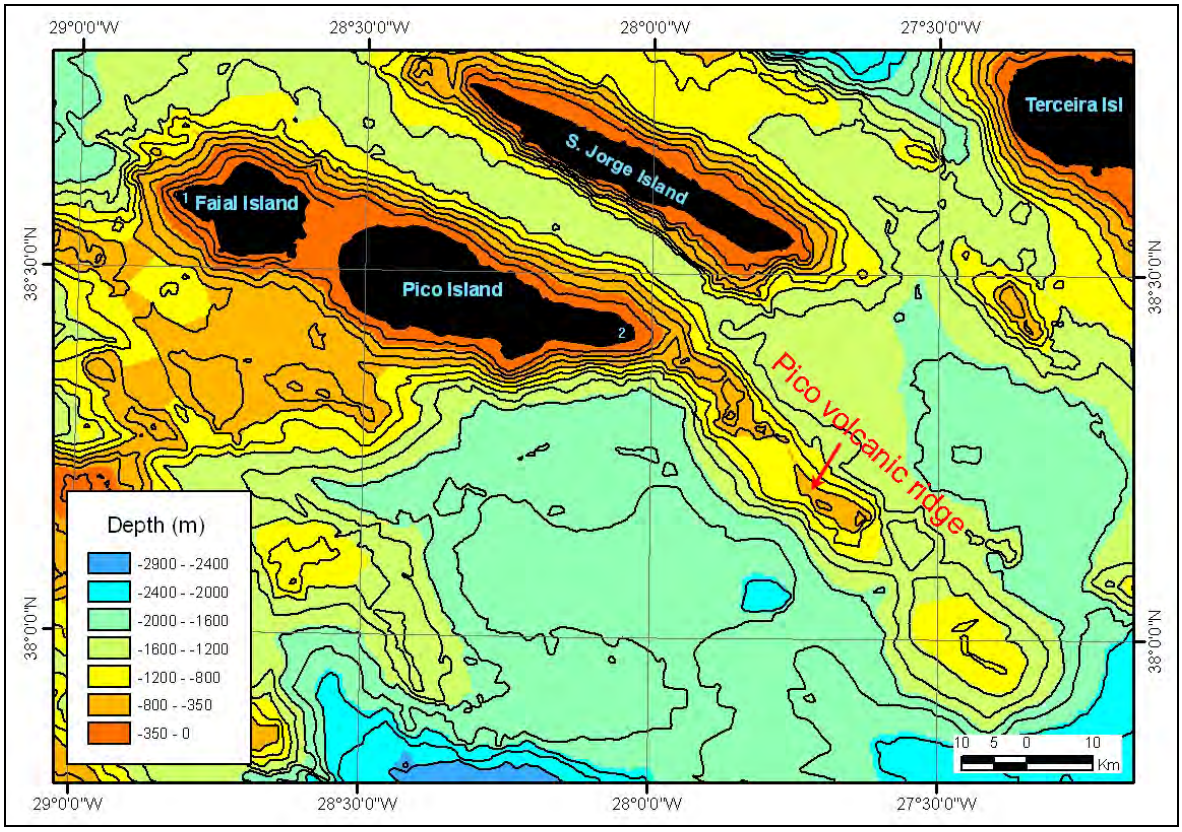

Figure 39 – Faial-Pico topographic lineament and Pico submarine volcanic ridge. 1. Capelinhos; 2. Ponta da Ilha. Bathymetric curves are spaced 200 m. Bathymetry of the Azores archipelago from GEBCO (IOC IHO and BODC, 2003).

The channel Faial-Pico (Figure 41) is the submarine extension of the two islands. It constitutes an 8 km-wide shelf between the islands and the adjacent coasts whose depths vary from 200 meters at both entrances to an average of 80 meters in the middle. There is a clear bathymetric separation into two sectors by a WNW-ESE lineament between the Ponta da Espalamaca and the Madalena village. The northern sector has an average depth of 80 meters in its axis, whilst the southern is deeper, falling immediately to 130 m south of the lineament. Apparently this lineament is composed of submarine cones of the surtseyan type

(Nunes, 1999). The more prominent cone is the Baixa do Norte with 50 m height and its peak only 16.2 m below sea level. Westerly of Baixa do Norte there are also other prominent features in the same alignment with peaks just 41 and 46 m below sea level. Easterly of Baixa do Norte are the subaerial features of the WNW-ESE lineament, the Ilhéus da Madalena which are also surtseyan cones. In the southern sector there is a remarkable bathymetric feature which also corresponds to a submarine cone (Nunes, 1999), the Baixa do Sul, with 90 m height and its peak only 7.1 m below sea level.

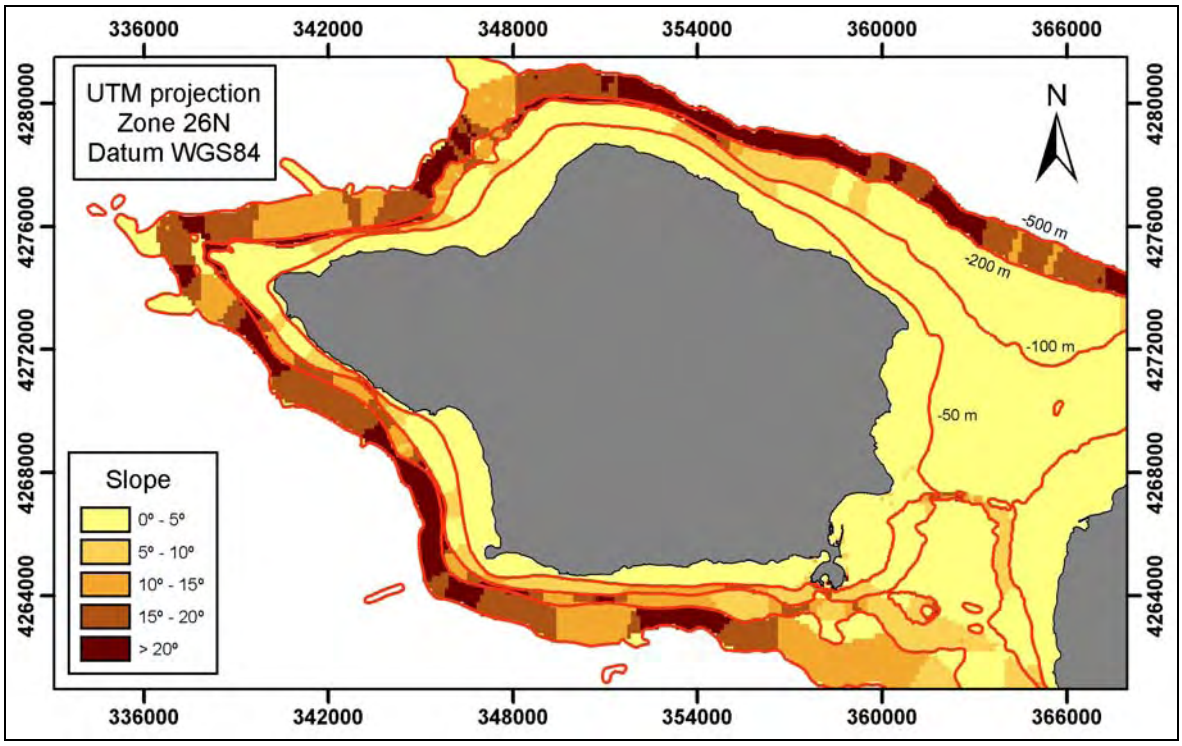

Figure 40 – Slope of the submarine area of Faial Island obtained from the hydrographic map of Instituto Hidrográfico (1999), using ArcGis 9.0 GIS running the 3D Analyst extension. In red are the bathymetric curves.

2.4.1. Geomorphology of the Faial Island

The island of Faial has approximately a pentagonal shape, elongated along the WNW-ESE direction with a maximum length of 21 Km and width of 14 km. The sub-aerial part of the island can be divided into four different physiographic regions (Figure 42): **Caldeira Volcano, Pedro Miguel Graben, Horta-Flamengos-Feteira Region and Capelo Peninsula** (Madeira, 1998). Although Madeira (1998) has

only divided the island into four regions, the author decided to differentiate the coastline into eight different sectors plus a subdivision of one of them. This division is based on the geological mapping of the shelf (see Figure 57 in Chapter 3) and it is the reason why there is a detailed description in this Chapter of the defined coastal sectors that composed the island. The subaerial description of these sectors will be useful to understand some of the differences found on the shelf, because there is, as it will be discussed in Chapters 3, 4 and 5, a high degree of correspondence between the shelf geology and the emerged geomorphology.

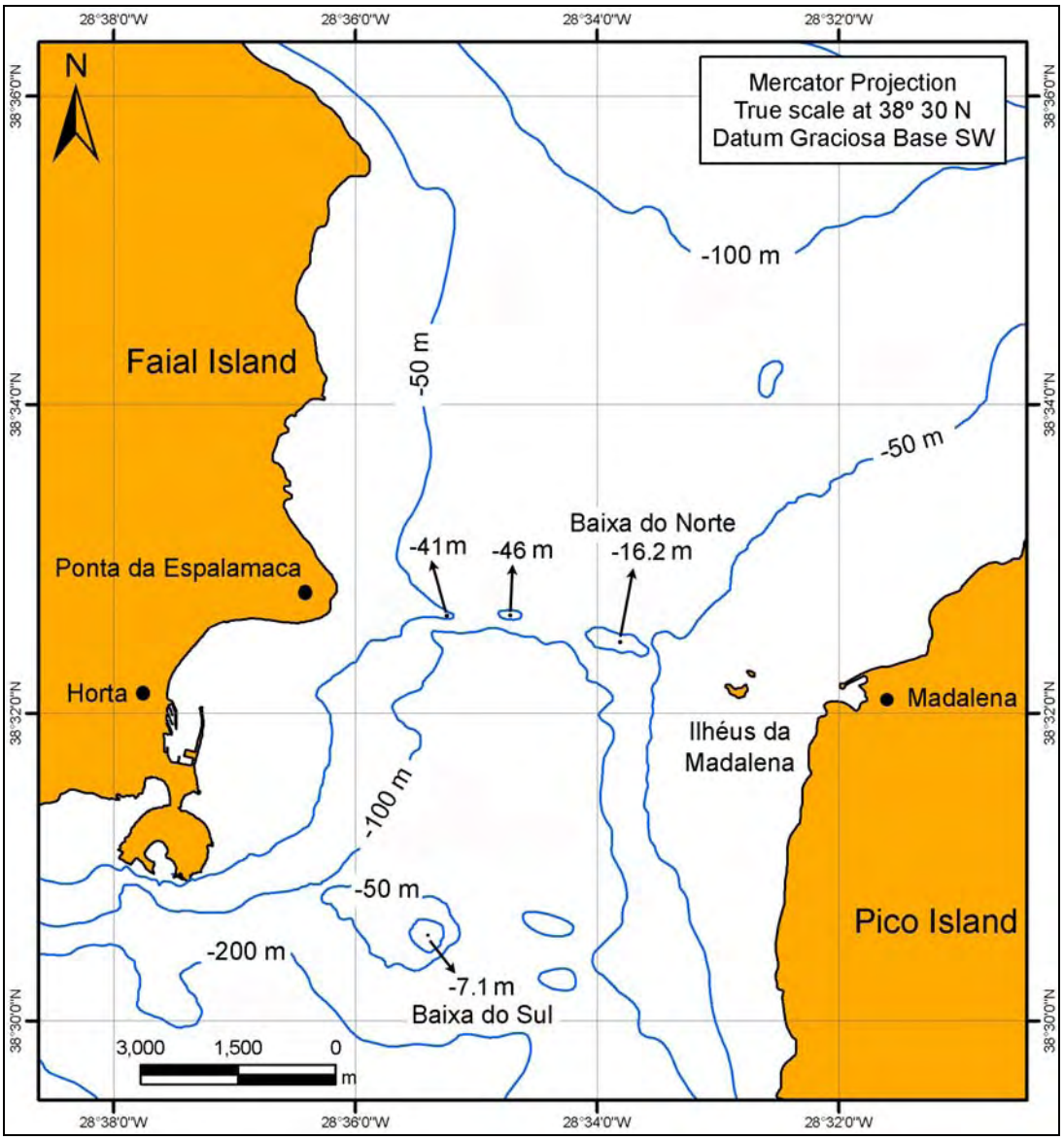

Figure 41 – Channel Faial-Pico (after Instituto Hidrográfico, 1999), showing the WNW-ESE lineament composed of submarine elevated features which are thought to be surtseyan cones.

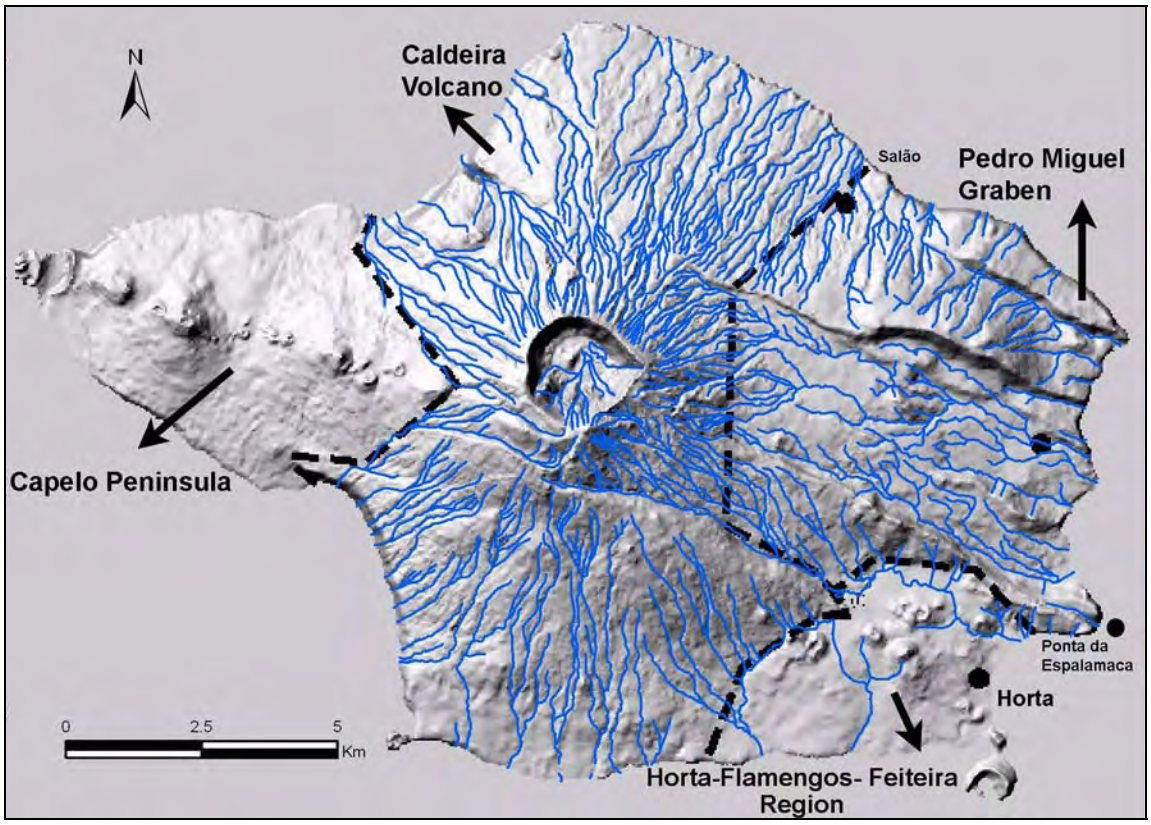

Figure 42 – Physiographic regions of the Faial Island shown on a DTM map of island (after Pacheco, 2001). The hydrographic network is taken from the topographic maps of the Instituto Geográfico do Exército (2001a; 2001b; 2001c; 2001d).

The **Caldeira Volcano** is a stratovolcano which dominates the central part of the island and constitutes the main relief, reaching 1043 m at Cabeço Gordo. It has 15 Km in diameter at sea level and the summit is truncated by a 2 km wide caldera. It is composed by a range of volcanic rocks that includes basalts to trachytes and can be divided into two volcanostatrigraphic units (Madeira, 1998). The lower unit, the Cedros Volcanic Complex (Cd in Figure 43), is mainly composed of sub aerial basalt to benmoreite lava flows and some scoria cones and trachytic domes. According to Féraud et al. (1980) and Chovelon (1982) this unit ranges from 470 Ka to 11 Ka. The upper unit, the Caldeira Formation (p and i in Figure 43), corresponds to a Holocene sequence of trachyte pumice fall deposits, phreatic and phreatomagmatic breccias, surges, ignimbrites and lahars, emplaced by explosive eruptions (sub-plinian style from the formation of the summit caldera). The radiocarbon dating made by Madeira et al. (1995) revealed ages that range from 10 to 1 Ka. Pacheco (2001) presents a finer stratigraphy of

the Caldeira Formation, dating it from 16 Ka to the present and assigning it to the Grupo Superior do Complexo Vulcânico dos Cedros (Figure 44) and also assigning the Cedros Volcanic Complex to Grupo Inferior do Complexo Vulcânico dos Cedros.

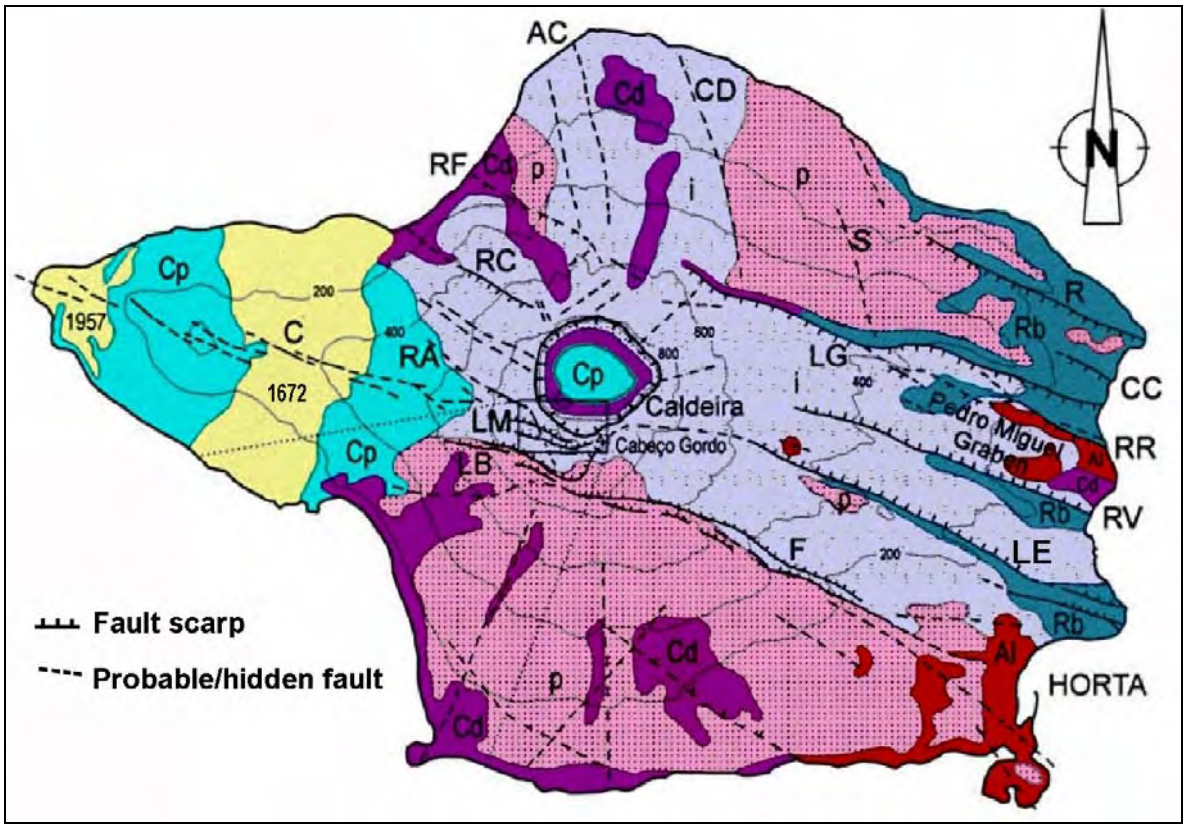

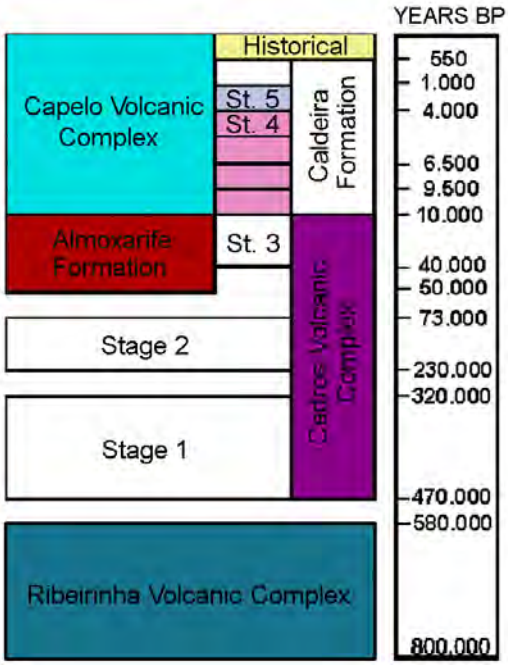

Figure 43 – Simplified geology of Faial Island (after Madeira, 1998; after Madeira and Brum da Silveira, 2003). Volcano stratigraphic units: Rb - Ribeirinha Volcanic Complex; Cd - Cedros Volcanic Complex; Al - Almoxarife Formation; p - pumice fall, phreatic, phreatomagmatic, breccia and surge deposits from Caldeira Formation; i - 1200 years BP pumice fall, ignimbrite and associated lahars from Caldeira Formation; Cp – Capelo Volcanic Complex, including 1672 and 1957 historic eruptions. Identification of faults: R - Ribeirinha; CC - Chã da Cruz; LG - Lomba Grande; RR - Ribeira do Rato; RV - Rocha Vermelha; E - Espalamaca; F - Flamengos; LB - Lomba de Baixo; LM - Lomba do Meio; RA - Ribeira do Adão;C - Capelo; RC - Ribeira das Cabras; RF - Ribeira Funda; AC - Água-Cutelo; CD - Cedros; S - Salão.

Although, Pacheco's (2001) thesis has a more up to date stratigraphy and

nomenclature for the recent products of the Caldeira Volcano, the adopted stratigraphy in this work is from Madeira (1998). The reason is because in Madeira and Brum da Silveira (2003) mapping (p and i in Figure 43), the recent products of the Caldeira Volcano show a geographical distribution that is useful to understand their influence on the shelf sedimentation (see Chapter 4).

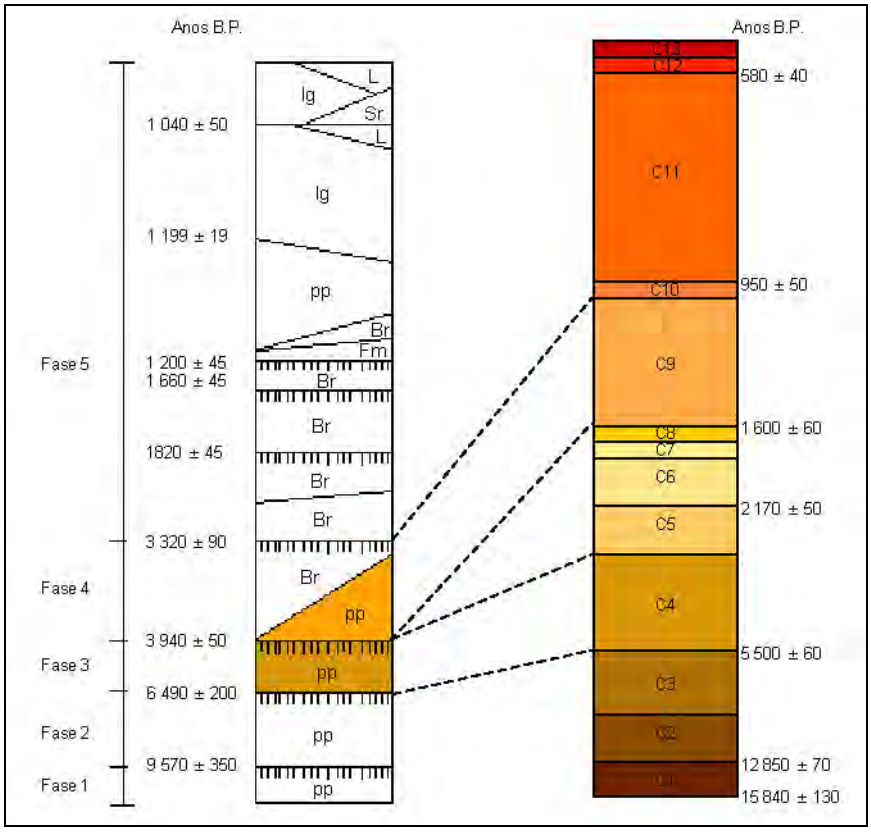

Figure 44 – Stratigraphic correlation between the Caldeira Formation (Madeira, 1998) and the finer stratigraphy of the Grupo superior do Complexo Vulcânico dos Cedros of Pacheco (2001). PP-Pumice fall deposit; Br – Explosion breccia; Ig – ignimbrite; Sr – Surge deposit; L – Lahars deposit; Fm – Freatomagmatic deposit (Pacheco, 2001).

At its surface, the **Caldeira Volcano** is almost completely covered by the Caldeira Formation (Figure 43) whose thickness can reach 100 m in the northern part of the caldera, diminishing towards the littoral zone. On the top of this Formation, stream drainage has developed eroding the superficial pyroclast deposits and reaching the lava flows of Cedros Volcanic Complex beneath. The drainage has a radial pattern (Figure 42), although in some places the tectonic control reveals its influence, with drainage showing considerable angles to the steepest slopes. These streams are ephemeral over much of the year and end

over suspended valleys on the littoral cliffs. The littoral zone is manly constituted by rocky cliffs and often shows accumulation of rock debris at the base of the cliffs and can be divided into four coastal segments.

The segment between Baía da Ribeira das Cabras and Ponta dos Cedros has a NE-SW direction and is slightly concave (Figure 45). The cliffs are developed in the lava flows of Cedros Volcanic Complex and can reach 60 m at Ponta dos Cedros, increasing to Baía da Ribeira das Cabras where they can reach 300 m. There is a remarkable incision (gullying) of Ribeira Funda and also Ribeira das Cabras on the cliff. Lava flows from a recent unit (the Capelo Volcanic Complex) have prograded into the sea (where is now the Fajã village) and acted as a buffer zone to marine erosion (Figures 43 and 45), protecting the old cliff of Baía da Ribeira das Cabras. This protection against marine erosion was enough to build a small beach in front of Ribeira das Cabras, composed of sand near the Fajã village and boulders towards its northeastern sector.

The segment between Ponta dos Cedros and Salão fishing Port has a WNW-ESE direction and is slightly convex (Figure 46). The cliffs are also developed in the lava flows of Cedros Volcanic Complex and can reach 30 m at Salão Port, increasing to Ponta dos Cedros where they can reach 60 m.

The segment between Varadouro and Morro do Castelo Branco has a NNW-SSE direction and is slightly concave (Figure 47). The cliffs are also developed in the lava flows of Cedros Volcanic Complex and can reach 230 m at the northern sector, decreasing to Morro do Castelo where they can reach 60 m.

The streams make small incisions (gulling) on the cliffs. Similarly to Baía da Ribeira das Cabras (Figure 45), the old cliffs of Varadouro are protected by the progradation into the sea of lava flows (represented in the Figure 47 by the low-lying and irregular coast just next to Varadouro) of the Capelo Volcanic Complex. This allowed also the building of a small beach (dot in the Figure 47) in front of the Varadouro thermal Spa, composed of sand in its western tip and pebbles towards its eastern tip. The Morro do Castelo Branco is a small peninsula linked to the land by a narrow isthmus. It is an erosion relief more resistant to wave attack due to its nature – a trachytic dome.

The segment between Morro do Castelo Branco and the geodetic pillar of

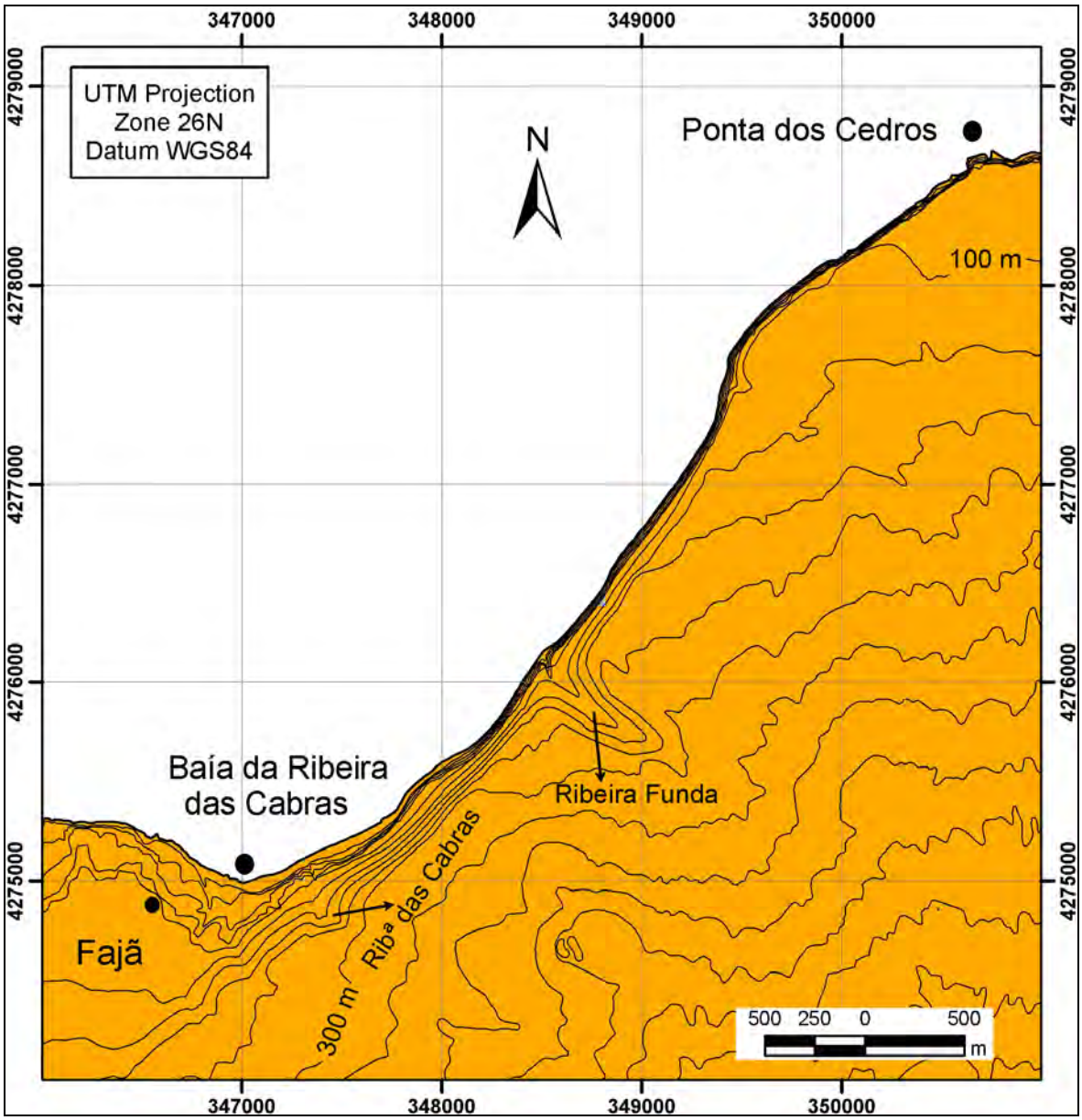

Figure 45 – Coastal segment between Baía da Ribeira das Cabras and Ponta dos Cedros (after Instituto Geográfico do Exército, 2001d). Black lines represent contours spaced every 10 m below 50 m height and spaced 50 m above 50 m height.

Rocha Alta has a W-E direction and is slightly convex (Figure 48). The cliffs in this segment are less developed, with heights from 10 to 50 m, sculpted in the lava flows of the Cedros Volcanic Complex. One coastal segment, south of the Horta airport has no cliffs, suggesting that also here there was recent progradation of the volcanism into the sea (see Chapters 4 and 5).

The old cliffs from the Caldeira Volcano used to extend from the Fajã village (Figures 43 and 45) to the eastern part of Cabeço do Capelo (black square in

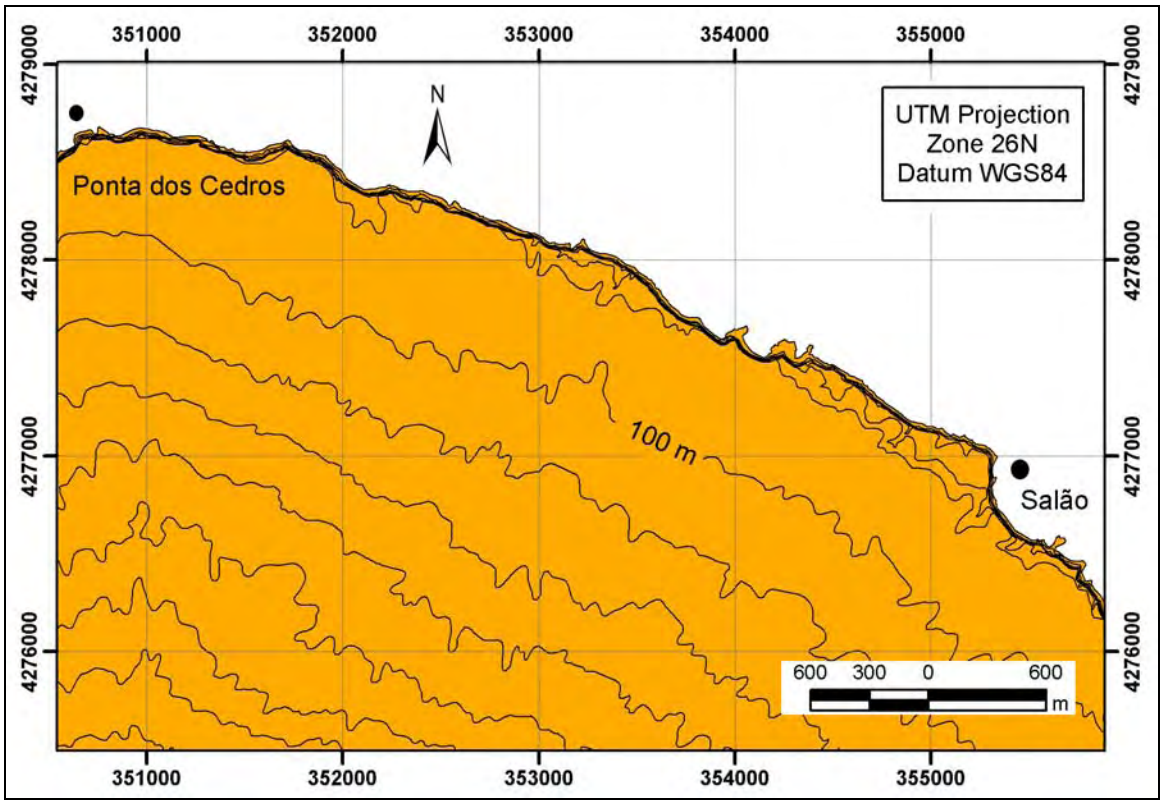

Figure 46 – Coastal segment between Ponta dos Cedros and Salão fishing Port (after Instituto Geográfico do Exército, 2001d). Black lines represent contours spaced every 10 m below 50 m height and spaced 50 m above 50 m height.

in Figure 52) and from this place to Varadouro (Figures 43 and 52), before being covered by the more recent flows of the Capelo Volcanic Complex.

Although in Figure 43 the Caldeira Formation covers almost the Cedros Volcanic Complex, near the cliffs of the Caldeira Volcano region the thickness of the cover has almost no expression.

The **Pedro Miguel Graben** region comprises the eastern area of Faial, from the Salão village to Ponta da Espalamaca (Figure 42). It is a rather complex region since the explosive and effusive materials from the Caldeira Volcano lay on top of the lava flows of the oldest volcanic structure of the island, the Ribeirinha shield volcano (800-580 Ka old; Féraud et al., 1980). It is predominantly composed of sub aerial hawaiitic lava flows mapped under the designation of Ribeirinha Volcanic Complex (Rb in Figure 43). This region is characterized by a WNW-ESE trending graben structure composed of seven normal dextral faults. The graben is partially fossilized by Holocene pyroclastic fall and flow deposits from the Caldeira Formation in the central area of the island.

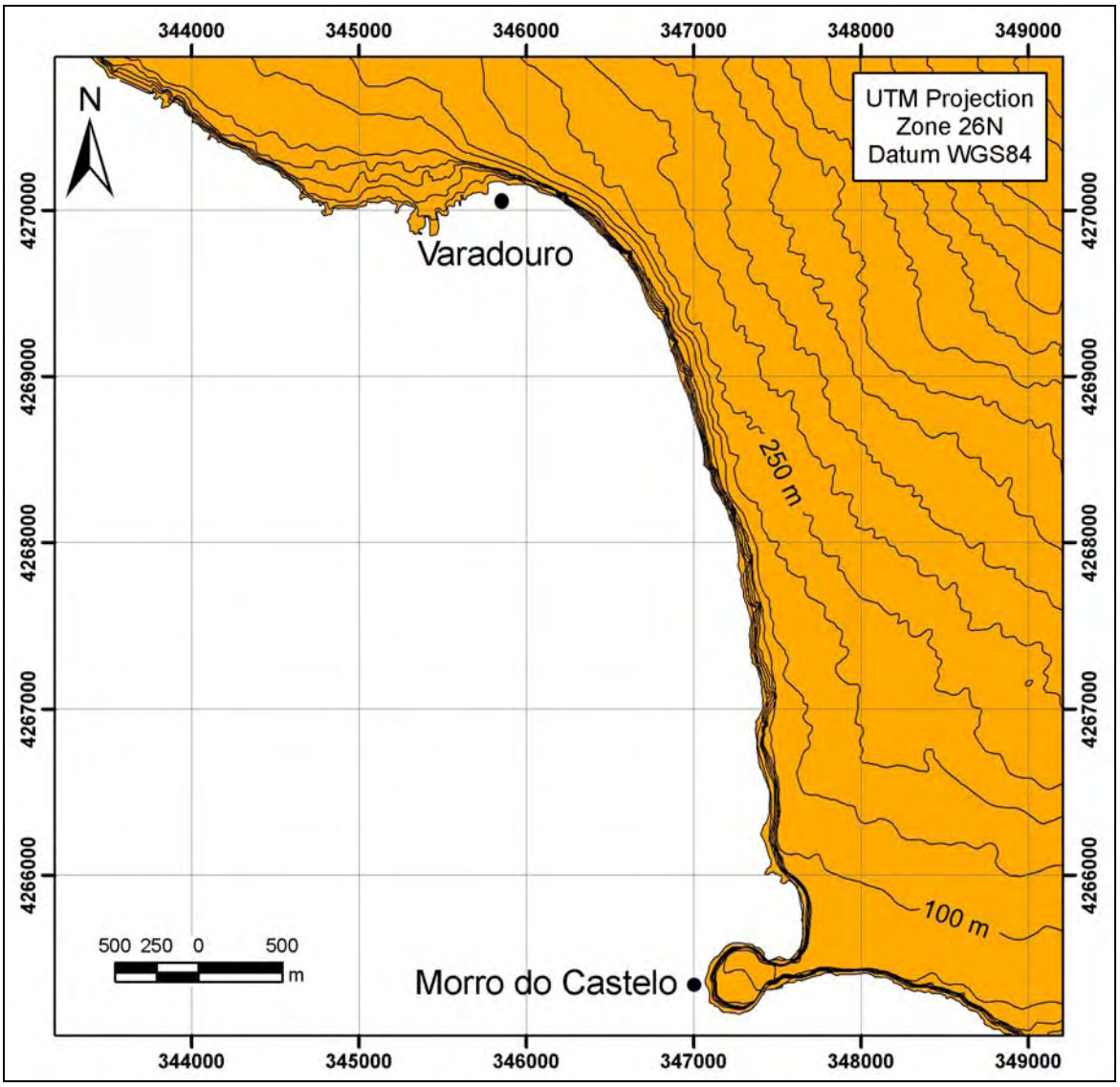

Figure 47 – Coastal segment between Varadouro and Morro do Castelo Branco (after Instituto Geográfico do Exército, 2001a; Instituto Geográfico do Exército, 2001d). Black lines represent contours spaced every 10 m below 50 m height and spaced 50 m above 50 m height.

The drainage pattern is controlled by the normal faults that constitute the graben, following the base of the fault scarps (Figure 42). The stream drainage north of Lomba Grande is well developed (Figures 42 and 43), eroding the superficial pyroclast deposits and reaching the lava flows beneath (Madeira, 1998). It is less developed between the Lomba Grande and Lomba da Espalamaca (Figures 42 and 43) because it cuts very recent materials from the Caldeira with 1200 years (Madeira, 1998).

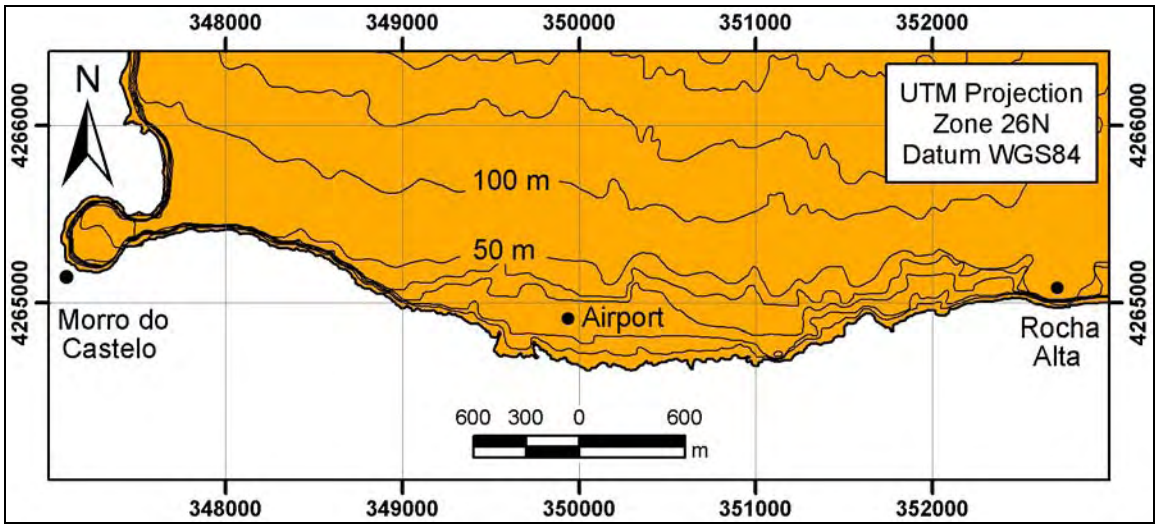

Figure 48 – Coastal segment between Morro do Castelo Branco and the geodetic pillar of Rocha Alta (after Instituto Geográfico do Exército, 2001a). Black lines represent contours spaced every 10 m below 50 m height and spaced 50 m above 50 m height.

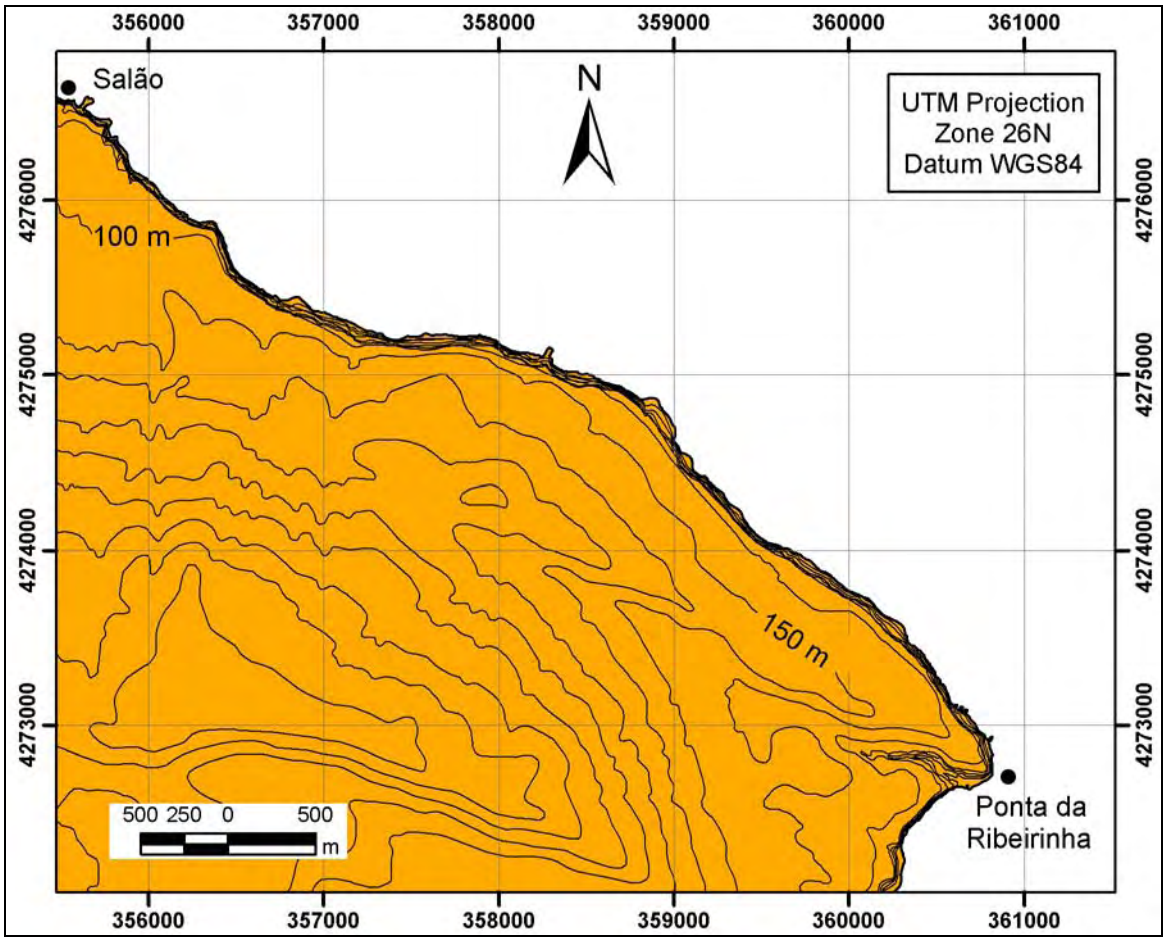

Figure 49 – Coastal segment between Salão fishing port and Ponta da Ribeirinha (after Instituto Geográfico do Exército, 2001c). Black lines represent contours spaced every 10 m below 50 m height and spaced 50 m above 50 m height.

The littoral zone is manly constituted by rocky cliffs and often shows accumulation of rock debris at the base of the cliffs. The littoral can be divided into two coastal segments.

The segment between Salão fishing port and Ponta da Ribeirinha is more irregular than the previous ones, nevertheless revealing a NNW-SSE trend (Figure 49). The height of the cliffs is quite variable, ranging from 30 m at the Porto do Salão to 120 m in Ponta da Riberirinha. The more concave segment can reach up to 150 m.

The segment between Ponta da Ribeirinha and Ponta da Espalamaca is very irregular with heights ranging from 0 to 120 m (Figure 50). The cliffs normally have accumulation of rock debris at the cliff toe and in some areas several pocket beaches have developed. There are, from north to south, two boulder beaches, the Porto da Boca da Ribeira and the Praia da Rocha Vermelha and four sandy beaches, Porto Pedro Miguel, Foz da Grota da Relvinha, Praia dos Inglesinhos and Praia do Almoxarife. The Praia do Almoxarife is fed by the Ribeira da Praia which has a well developed alluvial plain that extends 500 m landward. The southern tip of Almoxarife beach is composed of boulders that result from the erosion of Ponta da Espalamaca headland.

The **Horta-Flamengos-Feteira** region (Figure 42) is characterized by a set of scoria cones surrounded by low slope areas formed by the accumulation of pyroclasts deposits and lava flows from a basaltic fissural unit, the Almoxarife Formation (Al, in Figure 43). This Formation comprises Hawaiian/Strombolian volcanism that overlies the southeastern slope of the Caldeira volcano and the southertn part of Ribeirinha Volcano. This region is covered in the western part by a thin blanket of pyroclasts from the Caldeira Formation (Figure 43). The only available age for this formation is a low quality K/Ar date of 30 ±20 Ka (Feraud et al., 1980). The Almoxarife Formation also appears (Figure 43) in the tectonic block of Praia de Almoxarife (between Espalamaca fault and Rocha Vermelha fault which is not seen at the scale of the map of Figure 43) and in the central part of the Pedro Miguel Graben (Madeira, 1998).

The Horta Bay (Figure 51) is protected at the northern part by Ponta da Espalamaca headland and at the southern by Monte da Guia. This entire bay used

to have a sandy beach before the urbanization of this area (Madeira, 1998). Now, the only remaining of this beach is the sandy beach of Conceição fed by the Ribeira dos Flamengos in the northern part of bay.

The Monte da Guia is a small peninsula (a surtseyan cone) linked to the land by a narrow isthmus. This isthmus is composed of sand in its western part where it forms a bay and the famous sandy beach of Porto Pim. The eastern part of the isthmus has also a small unnamed pocket beach composed of pebbles.

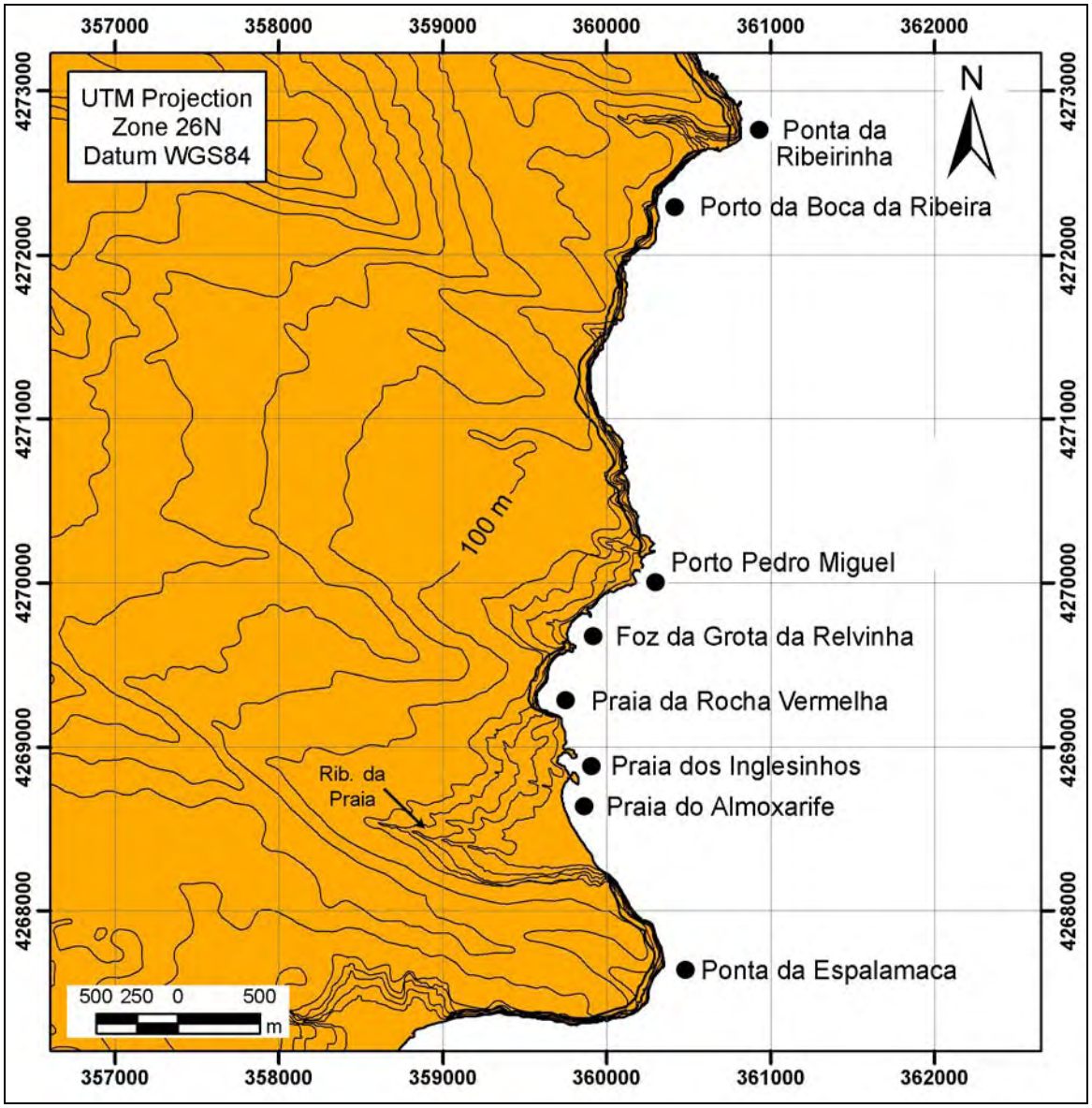

Figure 50 – Coastal segment between Ponta da Ribeirinha and Ponta da Espalamaca (after Instituto Geográfico do Exército, 2001b; after Instituto Geográfico do Exército, 2001c). Black dots represent beach locations. Black lines represent contours spaced every 10 m below 50 m height and spaced 50 m above 50 m height.

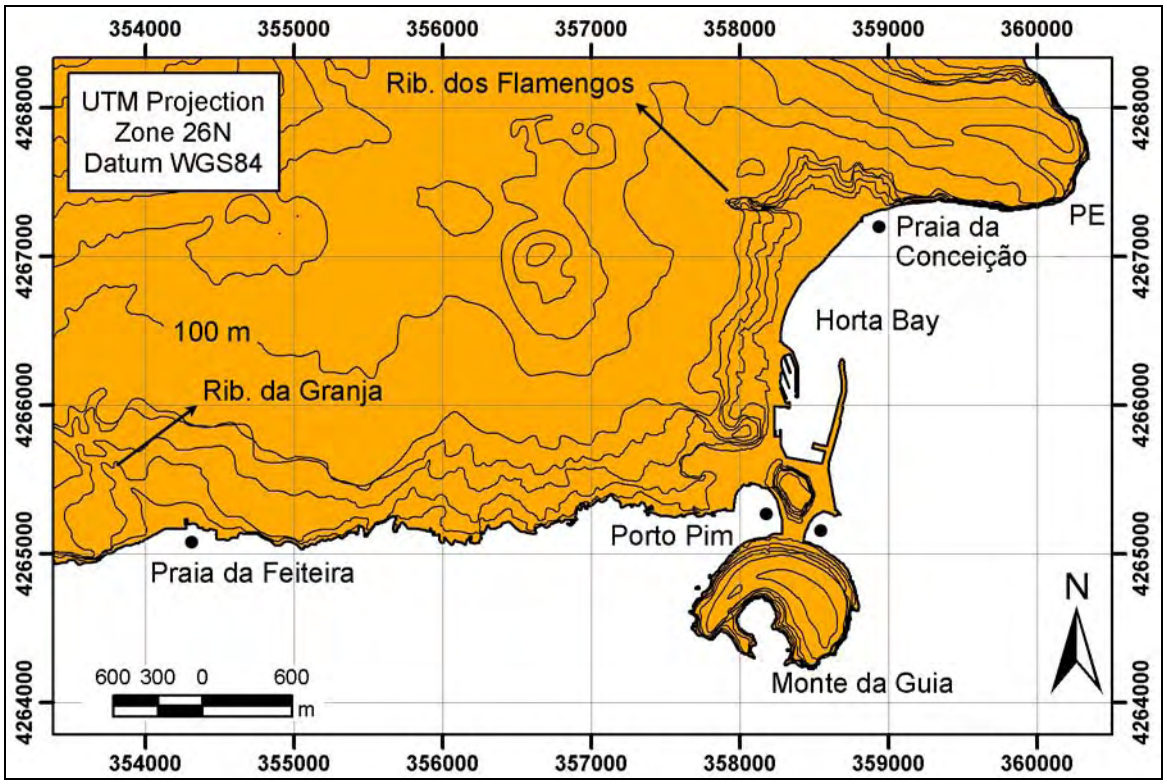

Figure 51 – Coastal segment of the Horta-Flamengos-Feteira region between Ponta da Espalamaca (PE in the map) and 1 km west of Praia da Feteira (after Instituto Geográfico do Exército, 2001a; Instituto Geográfico do Exército, 2001b). Black dots represent beach locations. Black lines represent contours spaced every 10 m below 50 m height and spaced 50 m above 50 m height.

The segment between Monte da Guia and Feiteira (Figure 51) has very low cliffs less than 30 m) cut into the lava flows of the Almoxarife Formation. These are plunging cliffs punctuated with several small pocket beaches on this coastal segment. The biggest and the only sandy beach is the Feiteira, whose sediments are fed by the Ribeira da Granja.

The hydrographic network in this region is almost absent; the few exceptions are the Ribeira dos Flamengos and the Ribeira da Granja.

The **Capelo Peninsula** is located on the western region of Faial and is formed by a dextral en échelon alignment (WNW-ESE direction) of basaltic Hawaiian/Strombolian and surtseyan cones that form the central spine of this peninsula (Figures 42, 43 and 52). The activity from these cones spread lava flows both to the north and south, enlarging the area of the primitive island (which before 10 ka only reached the black dot in Figure 52). The eastern half of the peninsula is built on the west slope of the Caldeira volcano, which means that the other

western half has started as submarine eruptions. These materials belong to the Capelo Volcanic Complex (Cp in Figure 43), whose age is less than 10000 years (as it overlies the oldest pyroclasts of Caldeira Formation), and includes two historical eruptions (1672 and 1957 in Figure 43). There is alternation between the later deposits of the Caldeira Formation and these from the Capelo Volcanic Complex in the eastern sector of the Capelo Peninsula. Capelinhos lies on the most westerly tip of the island and started as a classic surtseyan event in which rising basaltic magma came into contact with sea water to produce violent eruptions of ash, lapilli and steam (Cole et al., 1996; Cole et al., 2001). The Surtseyan activity changed to magmatic Strombolian activity when seawater was prevented from accessing the vent, by the piling of the submarine pyroclastic deposits. At least three tuff cones were formed, with each new cone being built to the east of the previous one. The first two cones were destroyed by collapse events and the third tuff cone still remains today.

This area, due to its youth and the resistance of the geology (mainly basaltic flows), does not have a well-developed hydrographic network. Therefore, the drainage occurs along the morphology structures of the flows or can be criptorreic through subterranean lava tubes (Madeira, 1998). The littoral zone is manly constituted by rocky cliffs and often shows accumulation of rock debris at the base of the cliffs. The littoral can be divided into two coastal segments.

The segment between Baía da Ribeira das Cabras and Capelinhos has a WSW-NNE direction and has two sandy beaches, one in the northern part of the Capelinhos volcano and the other just east of the old cliff before the Capelinhos eruption (Figure 52). In the older sector of the Capelo Volcanic Complex the cliffs range from 30 to 120 m whilst in the littoral covered by the lava flows of 1672, the sea has already cut cliffs that reach 5 to 50 m height (Madeira, 1998).

The segment between Capelinhos and Varadouro has a WNW-SSE direction and one sandy beach in the southern part of the Capelinhos volcano (Figure 52). To the SSE there are two beaches, manly composed of pebbles and is also very frequent the accumulation of rock debris at the cliff toes. The littoral covered by the lava flows of 1672 has cliffs of 20 to 45 m height and the older sector of Capelo Volcanic Complex has cliffs from 5 to 90 m height.

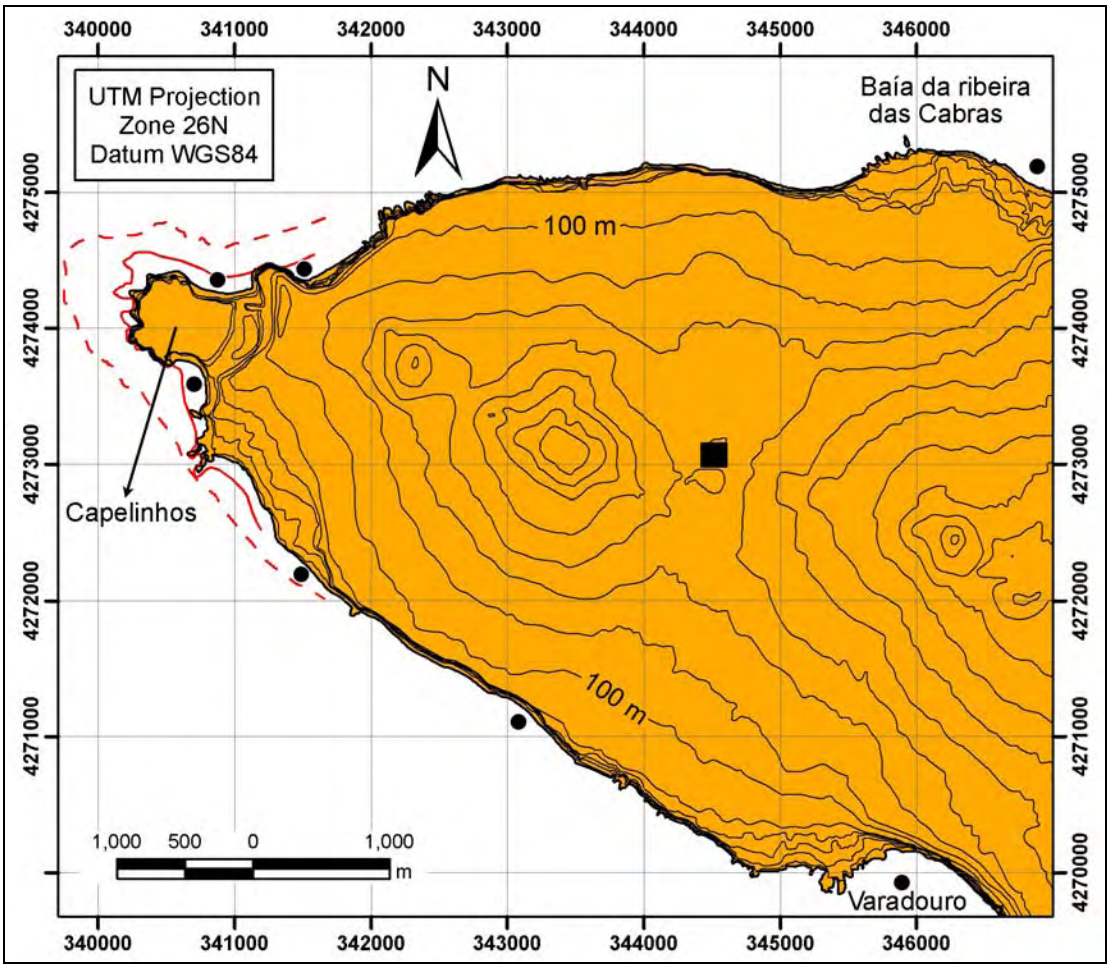

Figure 52 – Coastal segment of the Capelo Peninsula between Varadouro and Baía da Ribeira das Cabras (from Instituto Geográfico do Exército, 2001d). The hatched red line corresponds to the coastline of November 1958 limit and the solid red line the coastline of 1981 (from Machado and Freire, 1985). Black dots represent beach locations. Black lines represent contours spaced every 10 m below 50 m height and spaced 50 m above 50 m height.

According to Machado e Freire (1985) the littoral zone of the Capelinhos volcano has been eroding with a rate of 20 m/year. These rates were derived from five topographical surveys during 1958 and 1981 (see 1958 and 1981 coastline in Figure 52). Using the 2001 coastline from the map of Instituto Geográfico do Exército (2001d) it is possible to estimate a rate of 10m/year for the last 20 years when comparing against the 1981 coastline.

2.4.2. Tectonic setting of the Faial Island

The eastern part of Faial Island is characterized by a WNW-ESE trending graben structure (Pedro Miguel Graben) composed of seven normal dextral faults

(Figure 43). Other WNW-ESE important faults are located south of the caldera and in the western part of the island. There is also a less important, secondary conjugate fault system, trending NNW-SSE to NW-SE, composed of normal left lateral faults. Their geomorphic expression is less developed and the fault lengths are smaller.

2.4.3. Climatic setting of the Faial Island

According to Coutinho (2000) the density of the observation stations is not adequate to the dimension of the island. There are only two meteorological stations, six udometric stations and two climatologic stations to characterize the Faial climate. Nevertheless, Coutinho (2000) has calculated the water balance based on real data and using several statistical approaches to interpolate the missing data. He estimated values for the precipitation, actual evapotranspiration and the surplus water that will generate runoff on these 10 stations. Annual precipitation ranges from 980 to 1031 mm/year in the coastal area and 2860 mm at 700 m above sea level. The precipitation recorded from September to March represents 70 to 75% of the total precipitation. The mean annual temperature is 17.5 ºC and the temperature decrease is 0.6 ºC every 100 m of altitude. Mean annual actual evapotranspiration and surplus estimated by the methods of Thornthwaite (1948), Turc (1955), and Coutagne (1954), is respectively 736 and 244 mm/year at 60 m above sea level, reaching 711 and 2049 mm/year at 700 m.

2.4.4. Oceanographic setting of the Faial Island

In section 2.2.3, the review of the wave climate has shown the direction and height of the predominant waves for the Azores central archipelago. However, the different coastal sectors of the island are subjected to more than one wave directional component and therefore to compare its vulnerability to erosion, two parameters must first be calculated, the Directional annual wave frequency (DAWF) and the Directional annual maximum wave height (DAMWH). The coastal sectors presented in Figure 53 are defined in the following Chapter (see Figure 57 and text for explanation in Chapter 3) where a letter for reference has been

assigned to each one. DAWF and DAMWH (Table 5) were calculated for all these sectors using the respective wave directional components that each sector is exposed, which can be three to four depending on the sector orientation (Figure 53). For sector E these two parameters were not calculated because this sector suffers from the sheltering effect of the nearby Pico and S. Jorge Islands.

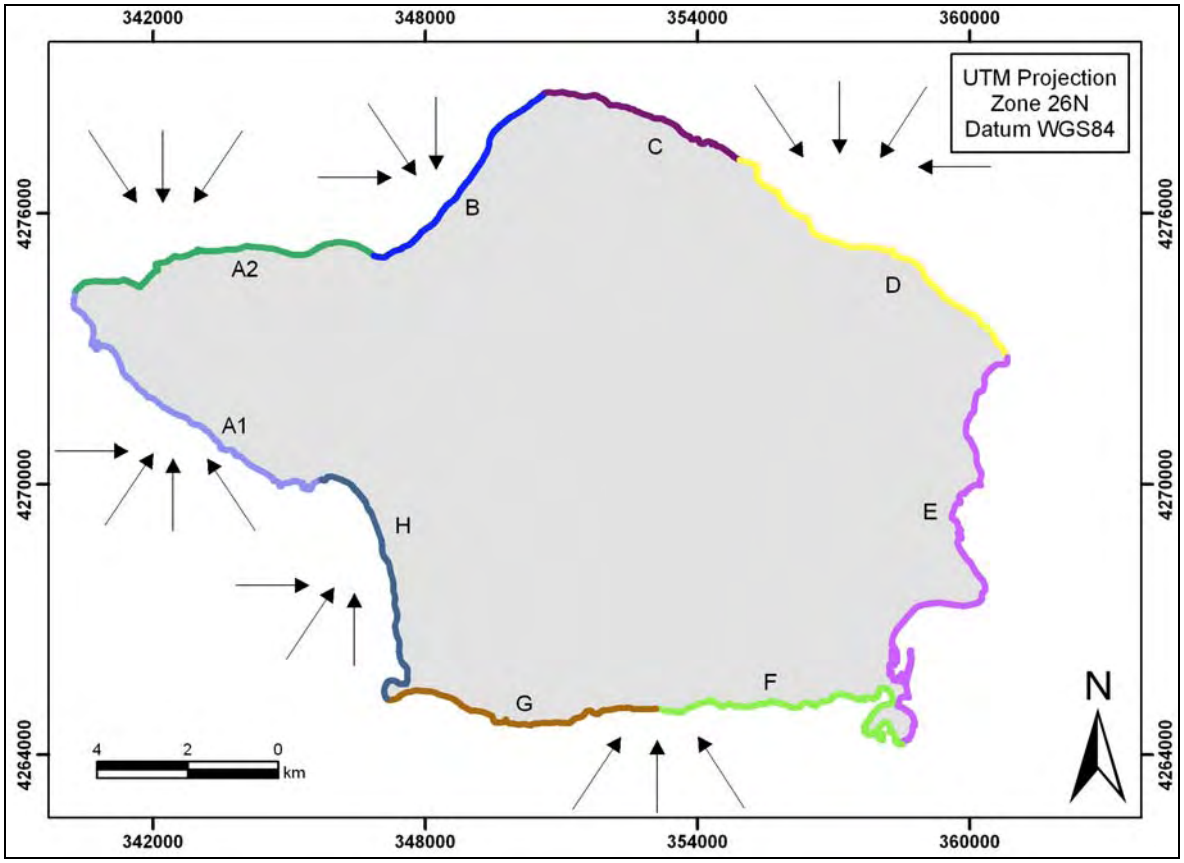

Figure 53 – Coastal segments defined in Chapter 3 and the wave directions used to calculate the Directional annual wave frequency (DAWF) and the Directional annual maximum wave height (DAMWH).

The DAWF is calculated using Table 1 simply by summing the annual wave frequency (f_{ws}) of each of the directional components that affect the respective coastal segments (e.g., in Table1 for coastal sector B, the f_{ws} of the W, NW and N are summed which gives 69.2%). Table 4 is from Carvalho (2002) and represent the annual averages of the Maximum Wave height regarding a period of 14 years and is used to calculate the DAMWH. The calculation is simply a weighted mean of the Annual Maximum Wave height of each coastal sector (e.g., in Table 4 for coastal sector B, the frequencies of the W, NW and N are multiplied by the

respective wave height and the result divided by the sum of the frequencies of the quadrants involved).

Table 4 – Annual maximum significant wave height and respective frequency (Carvalho, 2002)

	Maximum significant wave height	Frequency (%)
N	6.06	16.03
NE	5.14	12.19
E	4.05	5.00
SE	3.92	2.79
S	4.65	3.35
SW	6.89	7.49
W	7.95	24.02
NW	8.24	29.13

Table 5 - Directional annual wave frequency (DAWF) and the Directional annual maximum wave height (DAMWH) calculated for the different coastal sectors

Sectors	DAWF (%)	DAMWH (m)
A1	37.60	7.26
A2	81.35	7.15
B	69.02	7.63
C	62.41	6.74
D	62.41	6.74
F	13.82	5.73
G	13.82	5.73
H	34.81	7.41

One of the mechanisms described in Chapter 1 for the cross-shelf transport of sediments was the downwelling offshore currents provoked by the piling of water against the coast during storm surges where intense wave agitation affects the coastline. Youssef (2005) studied the physical environment of two sites on the southern coast of Faial. He used current meters deployed at 19 and 23 meters depth to characterize the bottom currents at these depths. During 10 months (from August to June) these sensors measured the bottom current at these two sites and found several extreme bottom current events, the majority of them (80%) related with the increase of the significant wave heights and directed offshore (Figure 54). The highest bottom velocity (200 m/s) was recorded during 24th March, during a

period in which the significant wave height reached 5.12 m. It is likely to expect even higher bottom velocities since according to Carvalho (2002) the annual maximum significant wave heights can reach up to 8 m.

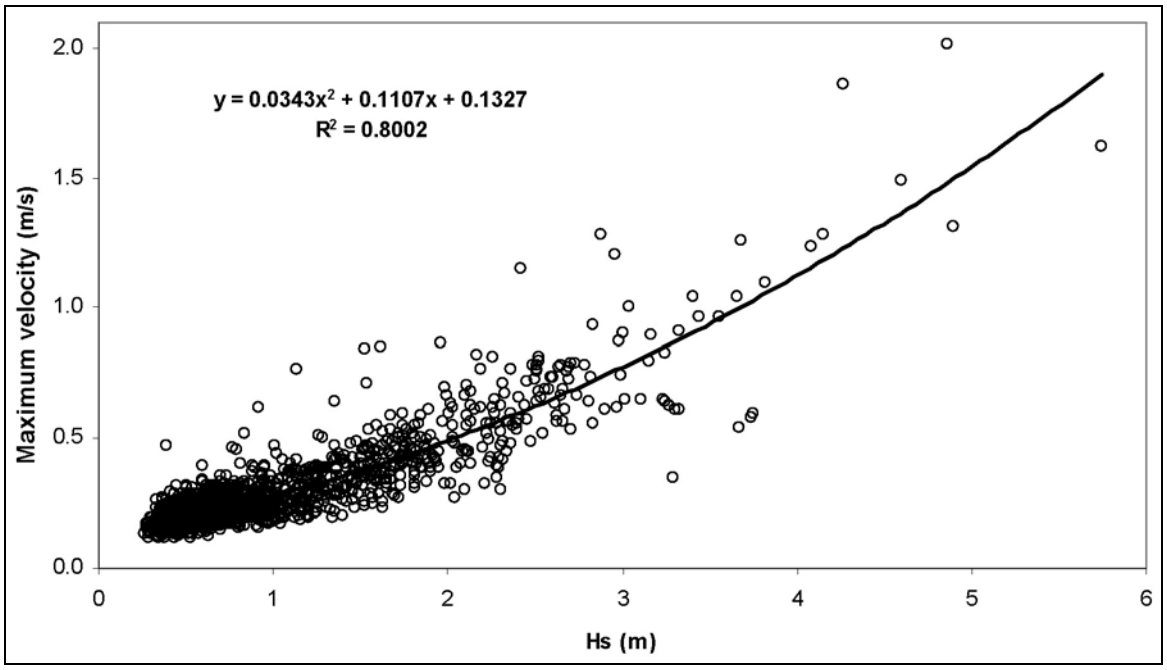

Figure 54 – Relationship between the measured maximum bottom current velocity and the significant wave height (Youssef, 2005).

2.5. Summary

The aim of this chapter was to introduce the state of the art of the scientific knowledge of the Faial Island and the surrounding physical environment. The amount of information exposed was selected concerning its relevance for the scientific problems under study.

First, the tectonic and volcanic setting of the Azores archipelago is outlined to understand the geological origin of the Faial Island. Within this general view, the historical records of earthquakes and tsunamis were mentioned because of their relevance for the evolution of the subaerial as well as the submarine part of the island.

Secondly, the Azores oceanographic environment is also described in detail. The importance of the waves, tides and surface currents in the modeling of

the coastline and the shelf environment is taken into account when facing differences in the coastline of the same volcanic terrains.

Thirdly, the climatic setting of the Azores is also addressed in this chapter because the type of weathering is directly related with the climate. The subaerial erosion rates are needed to fully understand its role in the contribution of sediments to the shelf deposits. The sea-level variations are of extremely importance because it is the oscillating level of the sea through wave erosion that is responsible for the development of an abrasional shelf. The lowest sea levels control the depth of the shelf break, while intermediate stillstands are responsible for the presence or absence of erosional terraces and the longer periods of highstand favor the widening of the shelf.

Finally, the geomorphology of the emerged part of the Faial Island as well as the age of the different volcanic regions is delineated. The subaerial geomorphology is the result of the subaerial processes that have impinged on it. In addition, the age of the terrains normally shows a linear relationship between their age and the degree of evolution of the shelf sectors. Both are good indicators of the expected shelf development because it is often found a high degree of geological correspondence between the subaerial and the submarine part of the island.

Chapter 3. Bathymetric and high-resolution seismic characterization of the Faial shelf

3.1. Introduction

The bathymetric and high-resolution seismic profiles acquired on the scope of the project GEMAS were used to produce a basic geological characterization of the Faial shelf. The chirp and Boomer interpretation of the bottom echoes permitted not only to define the geological composition of the shelf but also to infer some of the processes responsible for the present-day morphology of the shelf, which is discussed in the foregoing chapter. The interpretation of the Bommer seismic profiles also allowed the mapping of the thickness of the sand and gravel deposits. The integration of the different data sets permitted to define eight distinct shelf sectors based on the shelf width and slope and also on the geological composition of each sector. It was also found a geological correspondence between the defined shelf sectors and the subaerial geomorphology which is discussed in the Chapters 4 and 5.

3.2. Limitations of the geophysical data

The data used in this chapter to describe the submarine geology of the Faial Island includes single beam echo-sounder data and also Chirp and Boomer high-resolution seismic profiles.

The bathymetric data obtained in this work covers almost all of the submarine area of the Faial Island between the coastline and the 100 m contour. In some areas the data does not reach the 100 m water depth whilst in others it goes beyond that depth, which means that the shelf has not been fully covered. For that reason, it is not possible to make a complete bathymetric analysis of the shelf on the areas where the shelf break has not been mapped. According to

Teixeira (2001), during the acquisition of the Chirp seismic profiles in the FAPI-1 cruise some operational parameters such as the Bottom Hardness Reference, the Hardware Power Gain and the Chirp Length were systematically changed. That variation may have produced different values for the Reflectivity and Bottom loss parameters registered by the Chirp as well as differences in the acoustic clarity of the echo characters for the exactly same seafloor areas scanned. This has caused difficulties in the interpretation of the echo characters. Consequently, these drawbacks were taken into account, especially when trying to deduce different types of grain size for the sedimentary floors based on the acoustic clarity of the echo characters. Furthermore, the records of the Chirp profiles rarely show the existence of subbottom reflectors, which are due to the fact that Chirpsonars have difficulty in penetrating coarse-grained sediments. This is confirmed by Damuth and Hayes (1977), that mention sands or gravels as very good reflectors of sound energy and consequently little or no sound penetrates to buried sediment interfaces when using high-frequency depth systems (3.5-12 kHz).

Another drawback was the electrical noise introduced by the power generators during the acquisition of the Boomer seismic profiles. The consequence was a low signal-to-noise ratio for some of the data, which resulted in poor images of the Boomer seismic profiles in some areas of the shelf, also difficulting the interpretation (e.g. Figure 74 and other examples in section 3.3.4). Further details on the acquisition and processing of the data can be consulted in Chapter 1 and also in Teixeira (2001) and Quartau et al. (2002).

3.3. Geophysical mapping

3.3.1. Bathymetry

Single beam echo-sounder data was used to produce a detailed bathymetry of the Faial shelf using an ArcGis 9.0 GIS running the 3D Analyst extension. Initially, a Triangular Irregular Network (TIN) was obtained, using as TIN vertices the depth points recorded along each ship's track. The digital elevation model (DEM) of the shelf was gridded converting the TIN to a raster with the cell grid

output size to 100 m. In order to measure accurately the position and depth of the shelf break in a consistent manner, the definition of Wear et al. (1974) was adopted (figure 1.C in Southard and Stanley, 1976). In this definition the shelf break is defined as the point of the first major change in gradient at the outermost edge of the shelf (Figure 55). In the case of the Faial Island, the shelf slope in the various sectors is variable (Figure 57) which means that the point of the first major change in gradient at the outermost edge of the shelf corresponds to distinct values in slope for the different sectors. Since in the sectors that have the highest shelf slopes, this point correspond to the shelf areas that exceed 5º in slope, this value was adopted as defining the shelf break of the submarine bathymetry of the Faial Island.

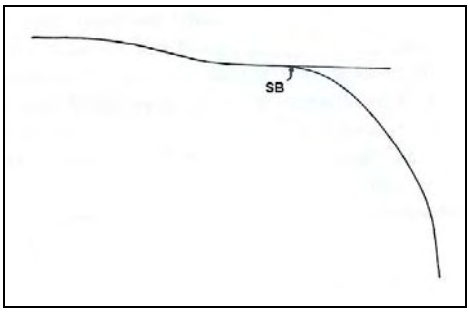

Figure 55 – Method adopted to define the shelf break (SB), (after Southard and Stanley, 1976).

The data reveals a bathymetry (Figure 56) which is roughly similar to the one produced by the hydrographic map (Instituto Hidrográfico, 1999) of the Faial Island. It disagrees, however, with what was suggested by the slope map based on the lower resolution bathymetry of the Instituto Hidrográfico (see Figure 40 in Chapter 2). The shelf edge is not always at uniform depths (-100 m) around the island, although it is normally marked by gradients exceeding 5 degrees (Figure 56 and 57). In some of the areas of the Faial shelf with data gaps (Figure 57), the shelf edge was inferred using the slopes derived from the Instituto Hidrográfico map (Figure 40).

The higher resolution bathymetry and the slope derived from it show distinct shelf features making it possible to distinguish different shelf sectors (Figure 57), based on the shelf width and slope, which are described in more detail in section

3.3.4. This sector division shows also a high degree of correspondence with the different features found by the interpretation of the echo character (Figure 72), the sedimentary thickness map (Figure 76) and the emerged geomorphology supporting this shelf division (see Chapter 2, description in section 3.3.4 and Chapter 4).

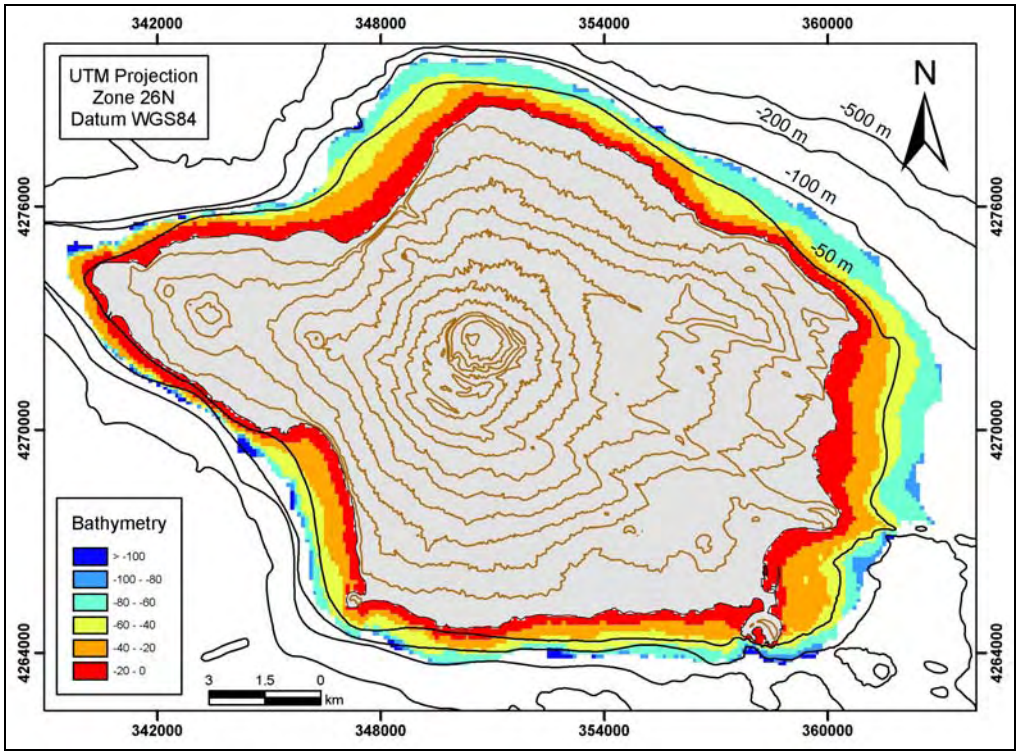

Figure 56 – High-resolution bathymetry of the Faial Island (pixel size 100 m) created with the data acquired in the FAPI-1 cruise, using the ArcGis 9.0 GIS running the 3D Analyst extension. The black lines are bathymetric curves taken from the Instituto Hidrográfico map (1999). The brown lines are hypsometric curves spaced 100 m, taken from the maps of Instituto Geográfico do Exército (2001a; 2001b; 2001c; 2001d).

3.3.2. Classification and mapping of echo types

3.3.2.1. Chirp records

A total of 10 different echoes have been identified on the basis of seafloor topography, surface bedforms and acoustic character of the seafloor. They have been grouped into four major classes, depending on their acoustic response. This classification followed the methodology proposed by Damuth (1980) and by Pratson and Laine (1989).

3.3.2.1.1. Type I – Distinct bottom echoes

Type I-A: Distinct, continuous, sharp bottom echo with no or few diffuse sub-bottom reflectors (Figure 58). This type of echo is generally located between 30-50 m water depth and the shelf break and is commonly bounded upslope by echo type III-A (Figures 61, 62 and 72). The surface echo shows nearly flat or gently sloping topography near the echo III-A, passing seaward to a convex downward break in slope to the shelf edge, which in some cases can reach 10º in slope (Figures 104, 109 and 112). More rarely, this echo type may appear nearshore and when this happens, it normally covers the entire shelf (Figure 72). Very often,

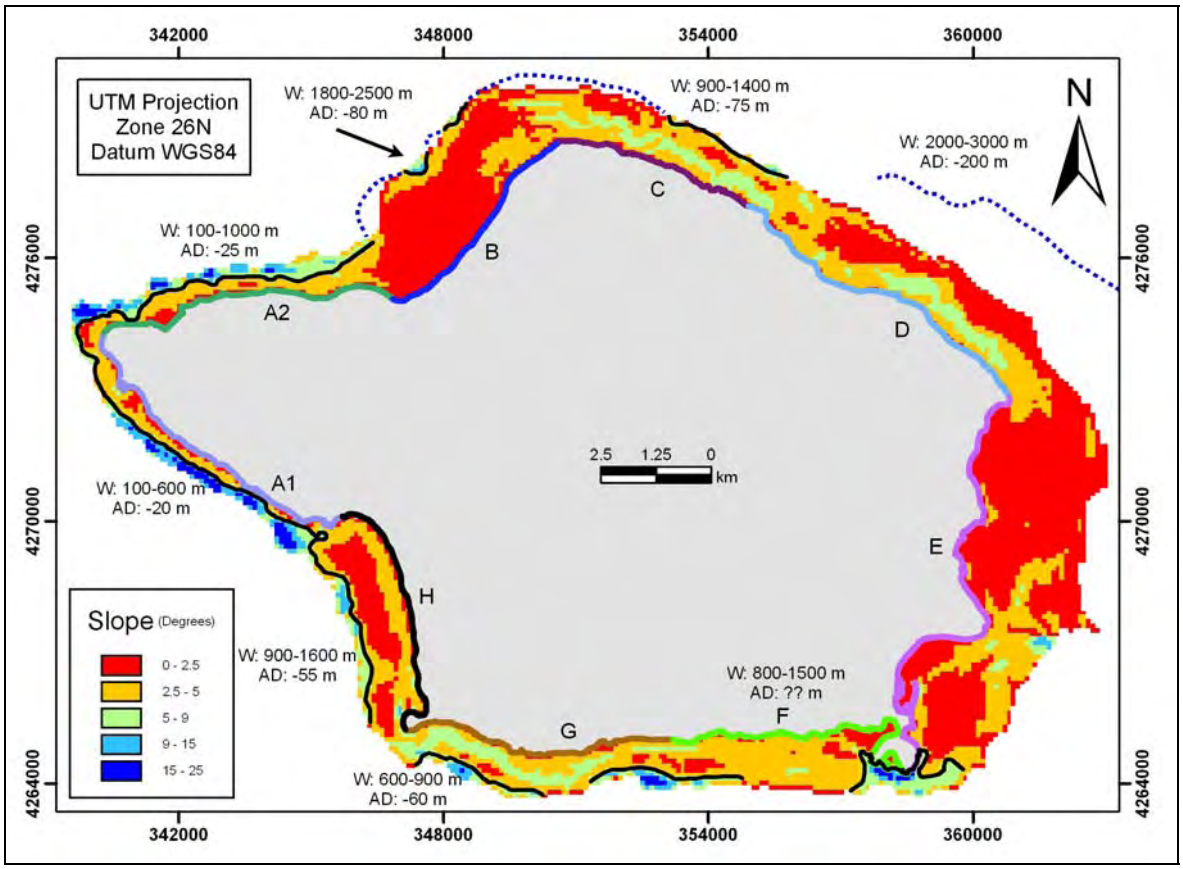

Figure 57 – Slope of the Faial shelf based on the bathymetric data of Figure 56, using the ArcGis 9.0 GIS running the 3D Analyst extension. The bold black line marks the shelf edge mapped where the slope is higher than 5º. The bold blue dotted line marks the inferred shelf edge based on the Instituto Hidrográfico map (1999). The different bold colored lines bordering the Faial coastline and the respective letters are the different shelf sectors defined. W means shelf width and AD average depth of the shelf break.

the surface echo shows irregularities that appear to be wavy bedforms (Figure 58). However, these irregularities can also be due to heave artifact. In fact, annotations

of swell occurring in some of the days have been recorded in the log-book of the FAPI-1 cruise and the dimensions of these bedforms are compatible with swell waves (2 m height and 30 m wavelength on average). Unfortunately, these annotations were not made systematically which makes it difficult to assess if these are in fact bedforms or just heave artefacts. There is also a change in the clarity of the echo at the shotpoint 9850 which may be related to a change in the sediment characteristics'. This seaward change coincides with a subbotom reflector that intersects the sea-bottom at the same point. This subbotom reflector probably corresponds to a coarser sediment than the one above it which explains the more prolonged echo seaward of the intersection.

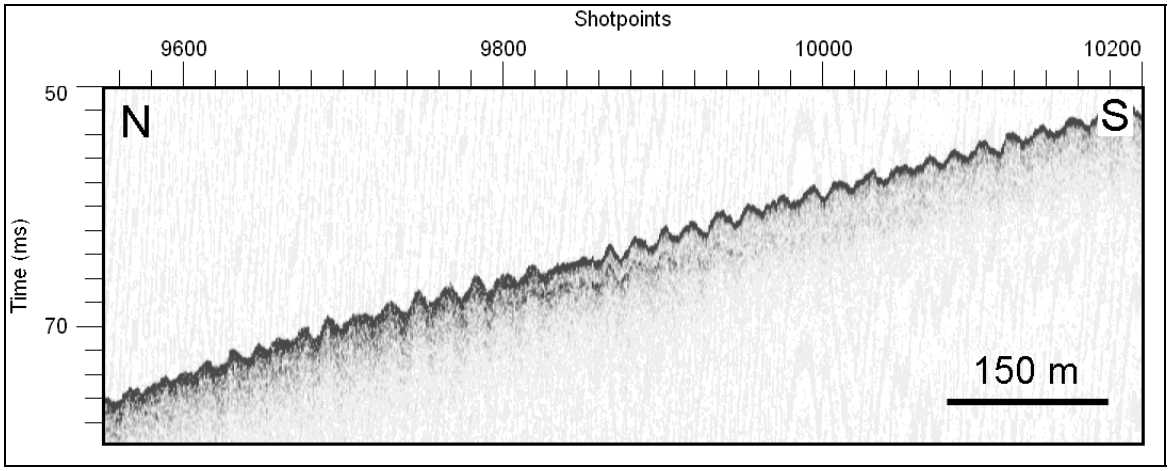

Figure 58 – Chirp seismic profile showing echo type I-A. These echoes are interpreted as sands and gravels (see location of the profile in Figure 72 and text for explanation).

Type I-B: This type of echo (Figure 59) is very similar to echo type I-A (Figure 58), but with a different geometry. It shows a slight elevation of no more than 3m from the surrounding seafloor (the echo type I-A), but with a sharper and less prolonged echo. The surface echo also shows more prominent wavy bedforms than those of the surrounding echo type I-A. It occurs in the areas where the echo type I-A dominates and immediately donwslope of the echo type III-A (Figure 72).

3.3.2.1.2. Type II – Indistinct bottom echoes

Type II-A: Indistinct, continuous, prolonged echo with no apparent sub-bottom reflectors (Figure 60). This type of echo appears in a restricted area of the island

shelf, offshore the Capelo Peninsula (see Figure 42 in Chapter 2 for location) and always associated with the echo types III-A and III-B. Because the geographical variability of this three echoes offshore the Capelo Peninsula is very high, the author did not discriminate these echoes and assigned them to a composite echo (see echo type IV-A in section 3.3.2.1.4).

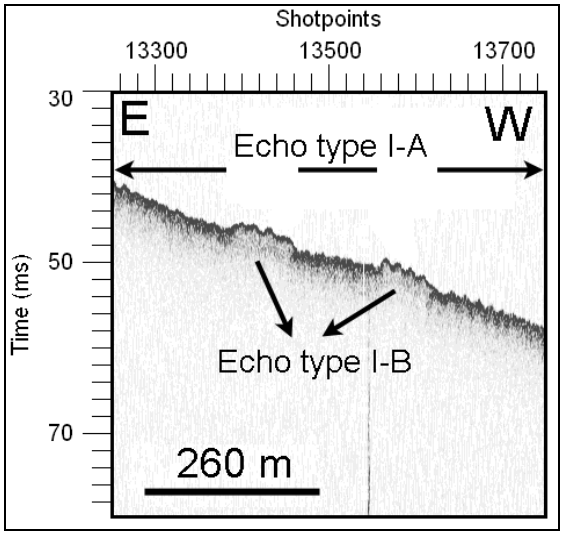

Figure 59 – Chirp seismic profile showing echo type I-B. These echoes are interpreted as sands (see location of the profile in Figure 72 and text for explanation).

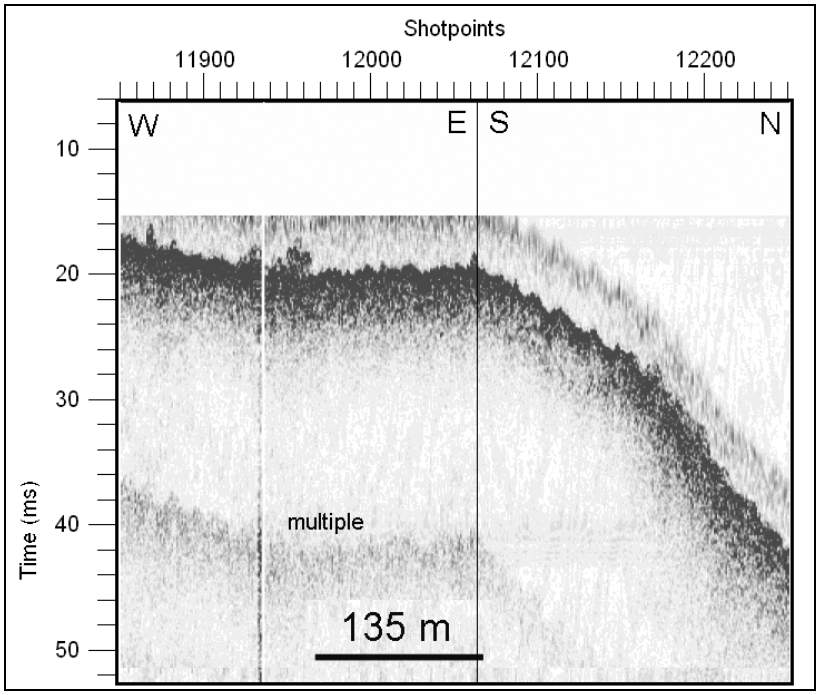

Figure 60 - Chirp seismic profile showing echo type II-A. These echoes are interpreted as pebbles and cobbles (see location of the profile in Figure 72 and text for explanation).

According to Damuth and Hayes (1977), when the shelf is dominated by coarse-grained sediments such as sands or gravels, no sub-bottom reflectors appear in the echograms (which is the case for most of the echo types I-A and I-B). The reason is because these sediments are very good reflectors of sound energy and consequently little or no sound penetrates to buried sediment interfaces. Damuth (1975) has showed that regions characterized by more prolonged echoes and no sub-bottom reflectors (type II-A) are covered by even coarser sediments. It is thus expectable to find associated to echo type I-A and I-B sand and gravels, whilst to echo type II-A pebbles and cobbles (Table 6). Echo type I-B which has a sharper and less prolonged echo, is most likely the result of the sea-bottom reflection of finer sands than the one produced by the echo type I-A (Table 6). Results of sediment sampling (see Chapter 6) confirmed that echo types I-A are in fact areas where sand and gravels dominate. Areas where echo type II-A was present were not sampled to prevent damaging the box-corer which is not suitable for sampling sediments coarser than gravels. The areas where echo type-B is found were also not sampled.

3.3.2.1.3. Type III – Hyperbolic bottom echoes

Type III-A: This type of echo shows regular, very intense overlapping hyperbolae with little varying vertex elevations and very prolonged echo without sub-bottom reflectors. Each hyperbola is generally less than 3 m in relief and 1-2 m in wavelength (Figures 61 and 62). This type of echo generally appears nearshore, extending offshore to depths at around 30-50 m (Figure 72). In the offshore direction these echoes show steeper slopes, with size, spacing and elevation of the hyperbola gradually decreasing downslope. Sometimes these slopes may present a step-like geometry (Figure 62).

Type III-B: This type of echo shows more irregular hyperbolae and with more greatly varying vertex elevations than echo type III-A. Each hyperbola is generally less than 10 m in relief and 50 m in wavelength (Figure 63). It also shows a very prolonged echo without sub-bottom reflectors. This type of echo generally appears nearshore, associated with echo type III-A, although in some cases can be located

more seaward, on the transition from echo type III-A to echo type I-A (Figure 72).

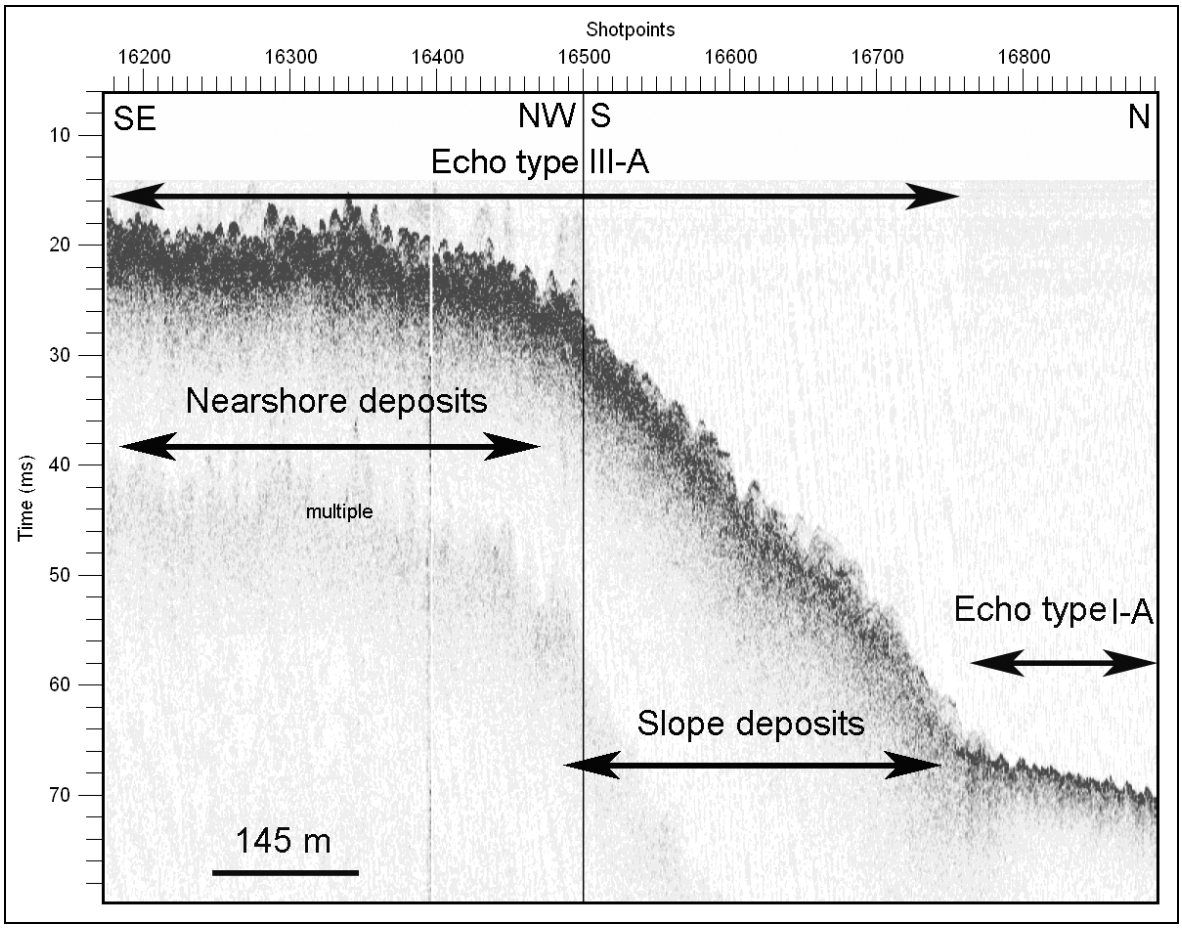

Figure 61 – Chirp seismic profile showing echo type III-A and echo type I-A. Echo types III-A are interpreted as coarse clastic deposits (see location of the profile in Figure 72 and text for explanation).

Type III-C: This type of echo shows irregular single hyperbolae with widely varying size and spacing above the seafloor (Figure 64). Each hyperbola generally shows very strong surface, prolonged echo with no apparent sub-bottom reflectors. Some of the echo types III-C may be covered by sediments and in that case show a distinct, continuous, sharp bottom echo. This type of echo appears in a restricted area of the island shelf, near the surtseyan cone of Monte da Guia (MG in Figure 72).

Type III-D: This type of echo shows irregular, intense overlapping hyperbolae with varying vertex elevations and a very prolonged echo with no apparent sub-bottom

reflectors. Each hyperbola generally exhibits a rounded top surface with a bubble-like geometry (Figure 65). The individual hyperbola is normally less than 10 m in relief and 20 m in wavelength. This type of echo appears in a restricted area of the island shelf, next to the trachytic dome of Morro do Castelo (MC in Figure 72).

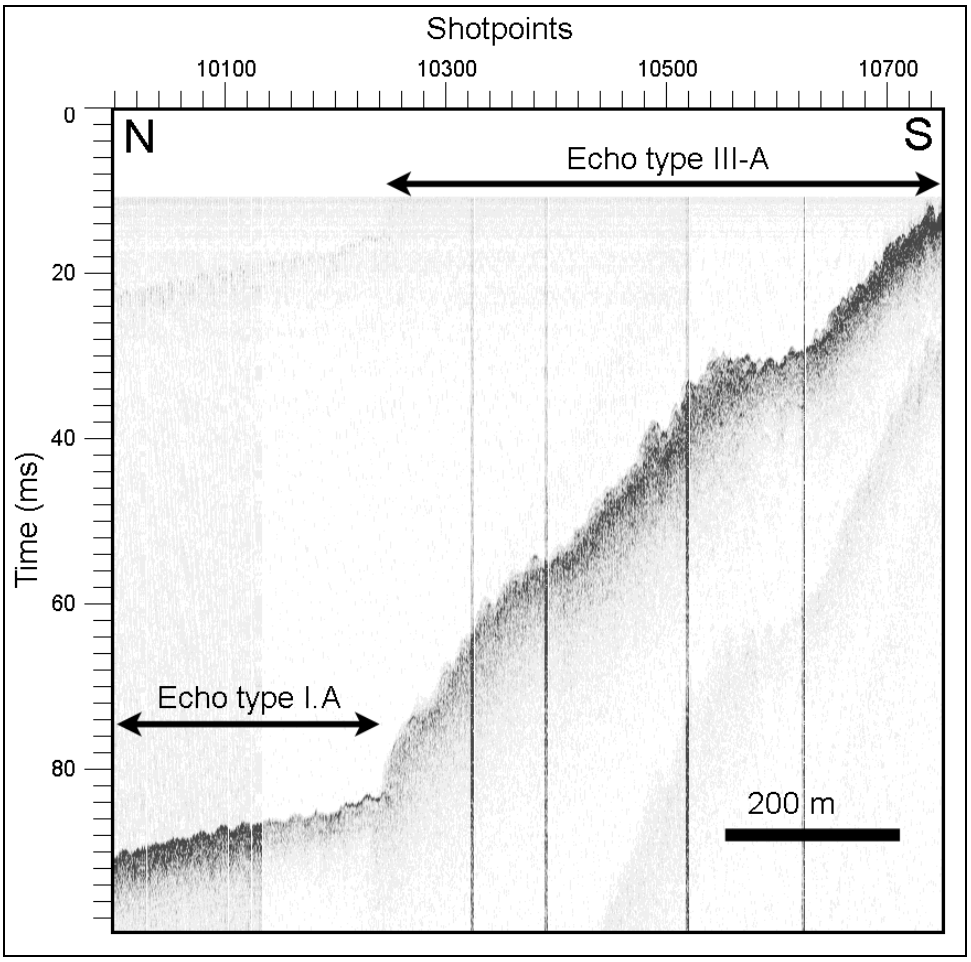

Figure 62 - Chirp seismic profile showing echo type III-A with step-like geometry and echo type I-A. Echo types III-A are interpreted as coarse clastic deposits (see location of the profile in Figure 72 and text for explanation).

Hyperbolic echoes are either caused by rugged sea-floor topography or by undulating sea-floor surfaces (Damuth, 1980). The strongly reflective single or irregular overlapping hyperbolae with widely varying vertex elevations above the seafloor are suggestive of basement highs or outcrops and have no relationship to near-bottom sedimentation processes (Damuth, 1975; Damuth, 1980).

The small size and very intense overlapping hyperbolae from echo type III-A may be returned by the presence of coarse clastic deposits on the sea-floor,

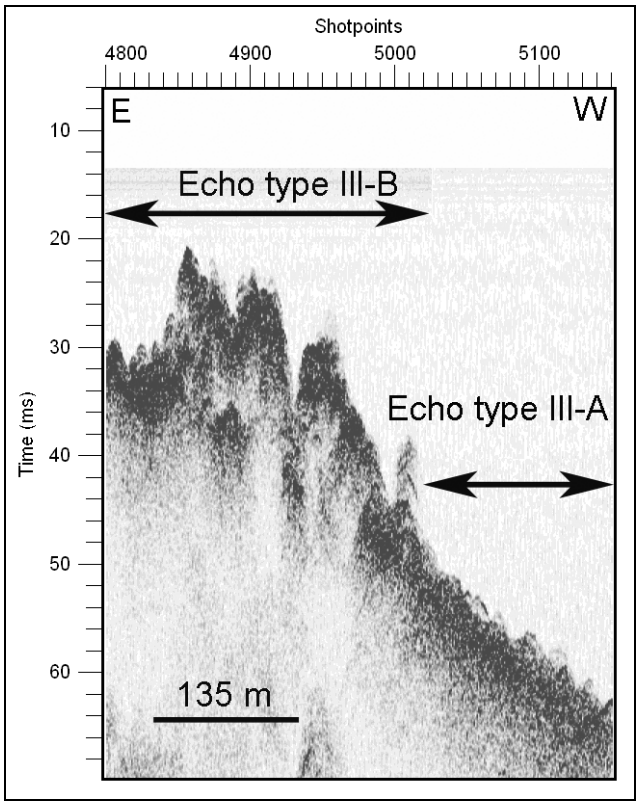

Figure 63 - Chirp seismic profile showing echo type III-A and echo type III-B. Echo types III-B are interpreted as lava flows (see location of the profile in Figure 72 and text for explanation).

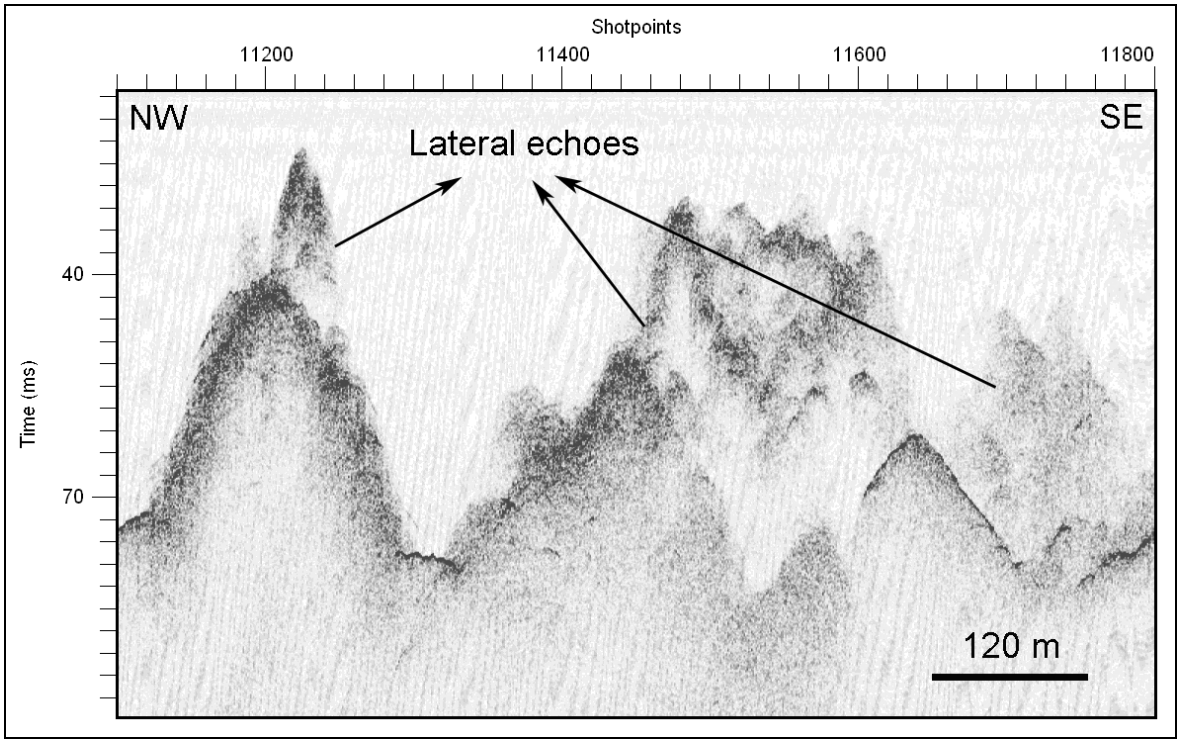

Figure 64 - Chirp seismic profile showing echo type III-C. Echo types III-C are interpreted as submarine cones (see location of the profile in Figure 72 and text for explanation).

with blocks of boulder-size. Damuth (1980), Pratson and Laine (1989), Chough et al. (1997), Lee et al. (2002) have all associated this type of echo to mass-movement deposits, namely debris flows. The nearshore deposits are probably rock debris that result from the retreat of the cliffs. Further offshore these echoes may represent lava flows that have been hardly eroded and the returning echo may either be the result of the smoothing of the lava surface irregularities or the presence of block debris due to the dismantlement of the lava flows. It is probable that in the higher slope areas these rock debris turn downslope into mass-flow deposits (Figure 61). Sometimes the echo type III-A presents a step-like geometry (Figure 62) suggesting that these deposits may have been formed due to the piling of several lava flows, which are now smoothed or covered by rock debris. The author believes that it is possible to find nearshore deposits that either result from the cliff retreat or the dismantlement of lava flows. It is however impossible to distinguish between these two processes, because the echo signal will be the same for the coarse clastic deposits (boulder size) that result from both mechanisms.

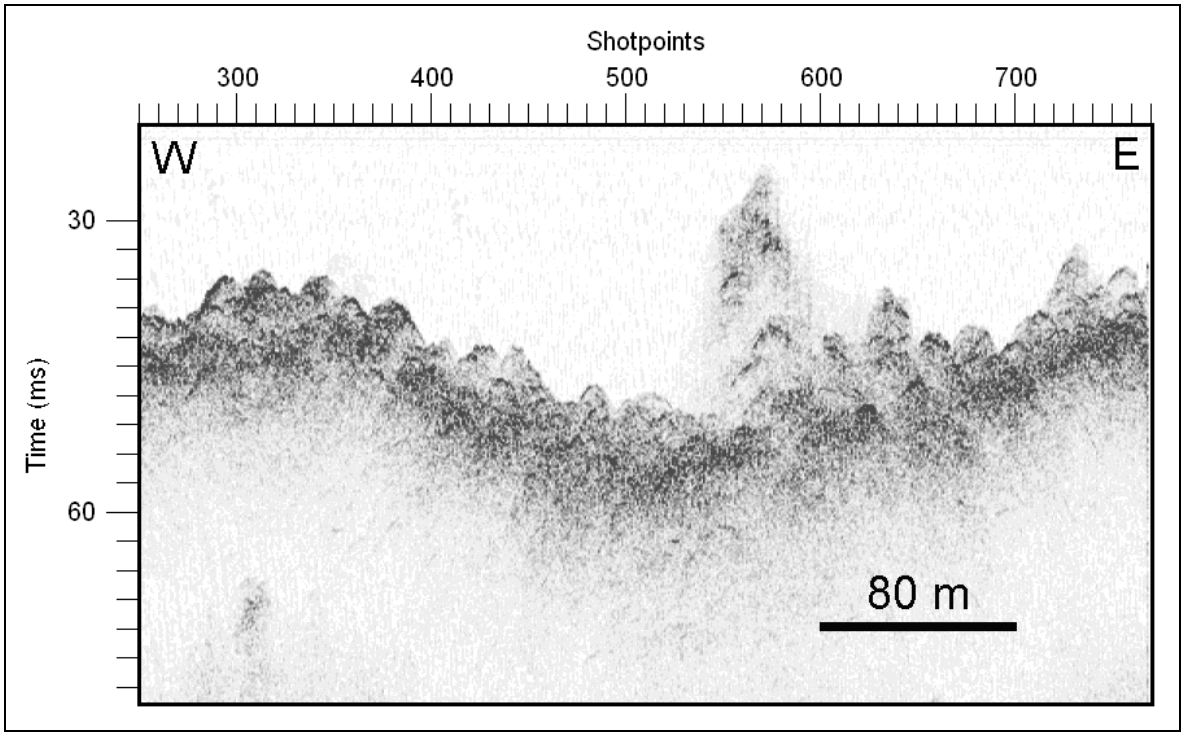

Figure 65 - Chirp seismic profile showing echo type III-D. Echo types III-C are interpreted as lava domes (see location of the profile in Figure 72 and text for explanation).

Mitchell et al. (2007) have shown a remarkable variety of submarine lava flows in the Pico island's shelf with data collected from a multibeam sonar (Figure 66). Chirp seismic profiles collected during FAPI-2 cruise (Quartau et al., 2003), also in the scope of the GEMAS project, cross the multibeam bathymetry which makes possible the comparison between the two types of geophysical data. The FAPI-2 chirp seismic profiles show less defined echoes as the ones from FAPI-1 cruise because some operational parameters were maintained constant and with low values. Nevertheless, it is possible to compare the echoes from both surveys. Chirp seismic profiles (Figure 67) crossing these lava flows in Pico's shelf revealed similar features to echo types I-A and II-A (Figure 58 and 60) III-A, (Figures 61 and 62) and III-B (Figure 63).

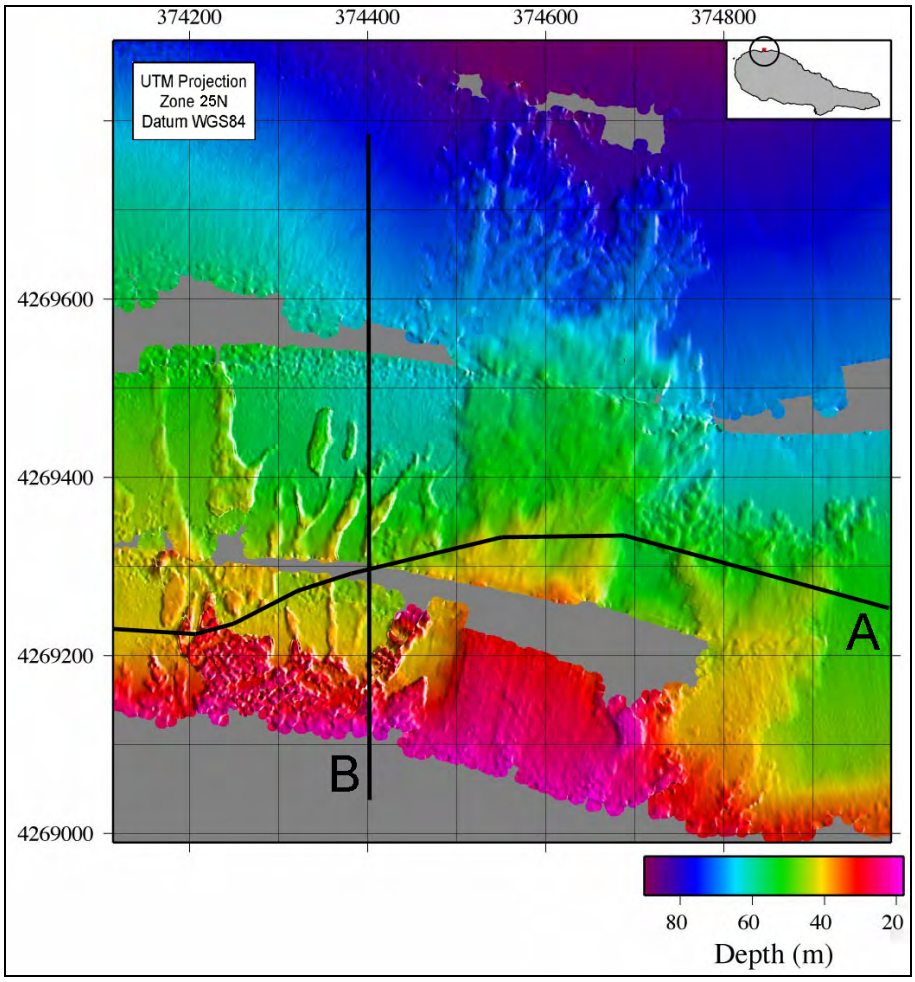

Figure 66 – Lava flows on the offshore NW sector of Pico Island. These show a relief when compared with the surrounding sedimentary area (location on the top-right inset of the figure). Bold black lines (A and B) represent the tracks of the chirp seismic profiles from Figure 67(after Mitchell et al., 2007).

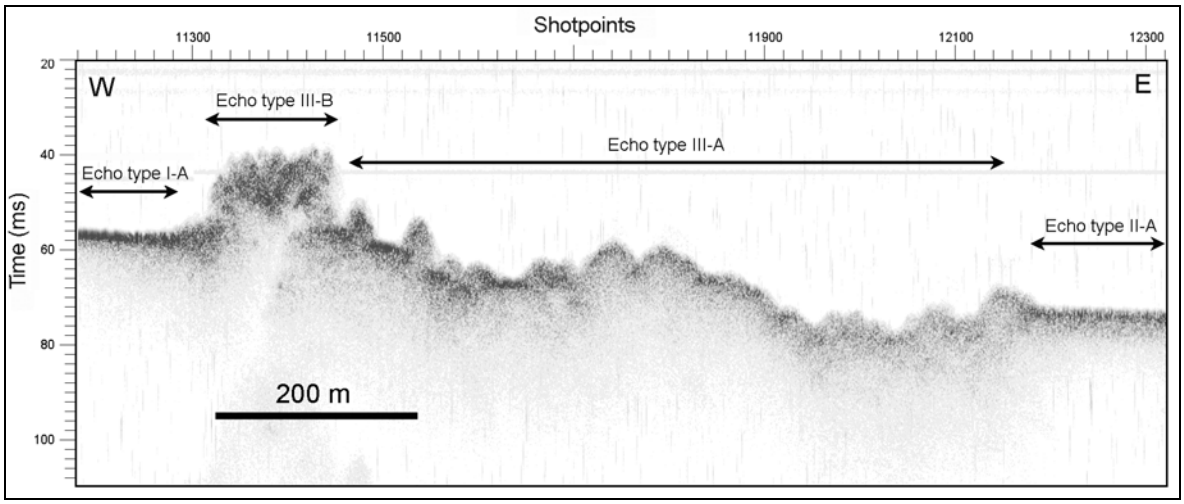

A

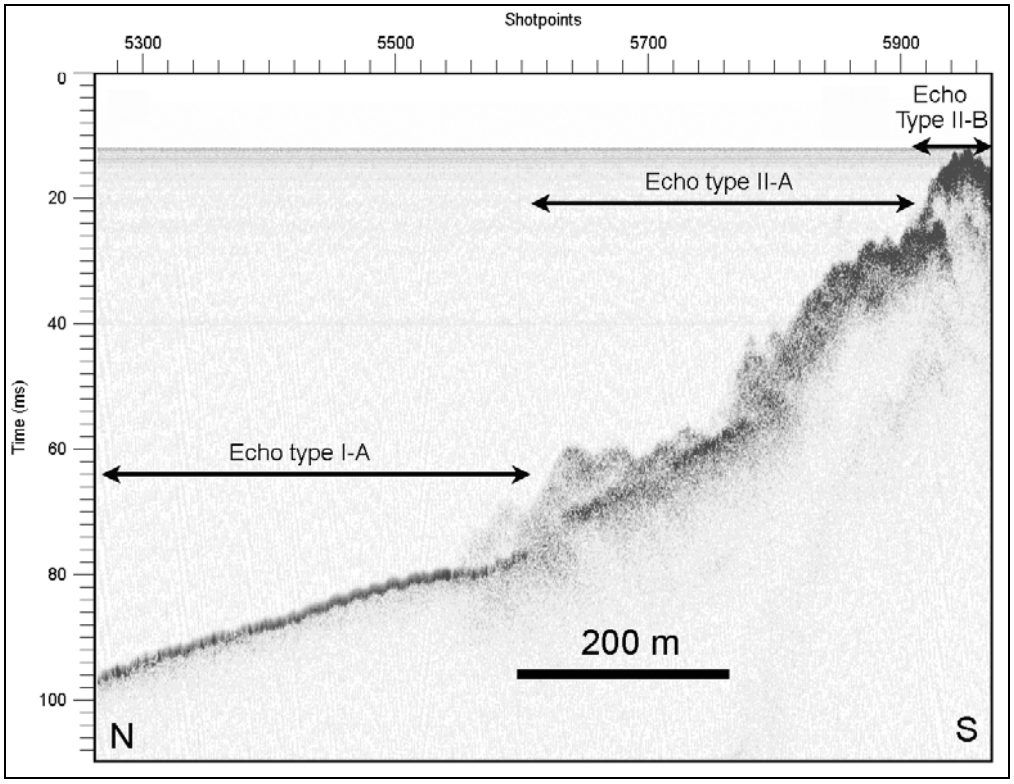

B

Figure 67 – Chirp seismic profiles A and B (see location on Figure 66). The echo types III-A and III-B correspond in the multibeam bathymetry to higher relief areas interpreted by Mitchell et al. (2007) as lava flows. The low-relief areas are interpreted by Mitchell et al. (2007) as sediments and correspond in the chirp profiles to echo types I-A and II-A.

Therefore, the type, size and return of the hyperbolic returns of echo type III-B suggest that it may be caused by the irregularities on the surface of lava flows (Table 6). In this case the hyperbolae are higher, wider and more spaced than the ones from echo type III-A. The echo type III-A appears also in areas where

Mitchell et al. (2007) interpret as lava flows (Figures 66 and 67). However, this echo shows smaller and less spaced hyperbolas than echo type III-B and the author believes that it might represent lava flows with smoother surfaces probably because they have been hardly eroded. Echo type III-A might also represent the presence of block debris due to the dismantlement of the lava flows (Table 6). In the presence of echo type III-A, it is impossible to say which of the two interpretations are right. Nevertheless, both interpretations suggest erosive processes and echo type III-A will be associated to them (see Table 6 and Figure 77).

The bigger height and width of the hyperbolae from echo type III-C (Figure 64) may indicate the existence of submarine cones (Table 6), resultant from the activity of the near surtseyan cone of Monte da Guia (MG in Figure 72 and see section 2.4.1 in Chapter 2).

The bubble-like geometry of the hyperbolae from echo type III-D (Figure 65) is in concordance with the geometry found in lava domes (Table 6). According to Tilling (1985) volcanic or lava domes are formed by relatively small, bulbous masses of lava too viscous to flow any great distance; consequently, on extrusion, the lava piles over and around its vent. To support even more this supposition is the possible near source: the trachytic dome of Morro do Castelo (MC in Figure 72 and see section 2.4.1 in Chapter 2).

The type III echoes, as already mentioned, are normally located in the more nearshore areas. These echoes are quite visible in the slope map of Faial shelf (Figure 57) because they roughly correspond to the nearshore areas with slopes between 2.5 and 9º (compare slope map of Figure 57 with echo map of Figure 72).

3.3.2.1.4. Type IV - Composite bottom echoes

These types of echoes are distinctively morphological, and do not fall in any of the general categories described above, being often a combination of more than one single type of echo.

Type IV-A: Echo type IV-A (Figure 68) is located in the offshore area of Capelo Peninsula (see section 2.4.1 in Chapter 2 and Figure 72), a very recent zone with

no more than 10 Ka. This type of echo is in some areas similar to echo type III-A and III-B (Figures 61, 62 and 63), with irregular hyperbolae generally less than 10 m in relief and 50 m in wavelength. It shows alternation between these hyperbolae and echo type I-A and II-A (Figures 58 and 60). Since in the offshore area of Capelo Peninsula, there is a frequent alternation between echo types I-A, II-A, III-A and III-B (Figure 68), it was impossible to map all these changes at the scale used in this work. Consequently, the author decided to create another class of echo, the type IV-A which combined all these echoes. In the offshore direction the echoes show very steep slopes and turn to regular and very intense overlapping hyperbolic, becoming also very indistinct and prolonged. Similarly to echo type III-B, the hyperbolae appear to be associated to the irregularities of lava flows (Table 6). The areas where echo type II-A is present may be covered by deposits of pebbles and cobbles or even boulders in the case of echo type III-A that probably result from the dismantlement of the lava flows (Table 6). The areas covered by the echo type I-A are probably covered by sand and gravels (Table 6). The echoes presented in the slope areas may be once again the result of mass-flow deposits.

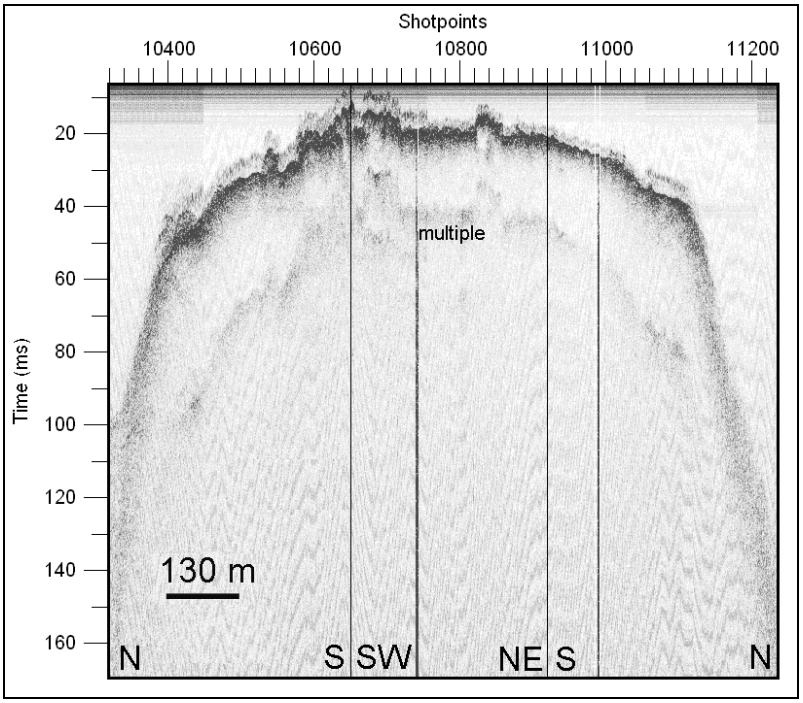

Figure 68 - Chirp seismic profile showing echo type IV-A. Echo types IV-A are interpreted as alternation between, lava flows, coarse clastic deposits that result from the dismantle of the lava flows and sands and gravels (see location of the profile in Figure 72 and text for explanation).

Type IV-B: This type of echo consists in sharp, continuous steeply dipping echo which may correspond to scars and scarps bounded downslope by irregular blocky or hyperbolic masses (Figure 69). These scarps with displaced masses generally exhibit step-like geometry. According to Mulder and Cochonat (1996), the scars and scarps, the blocky or hyperbolic morphology of the displaced masses with deformed or transparent internal reflectors are typically characteristic of slides and slumps (Table 6).

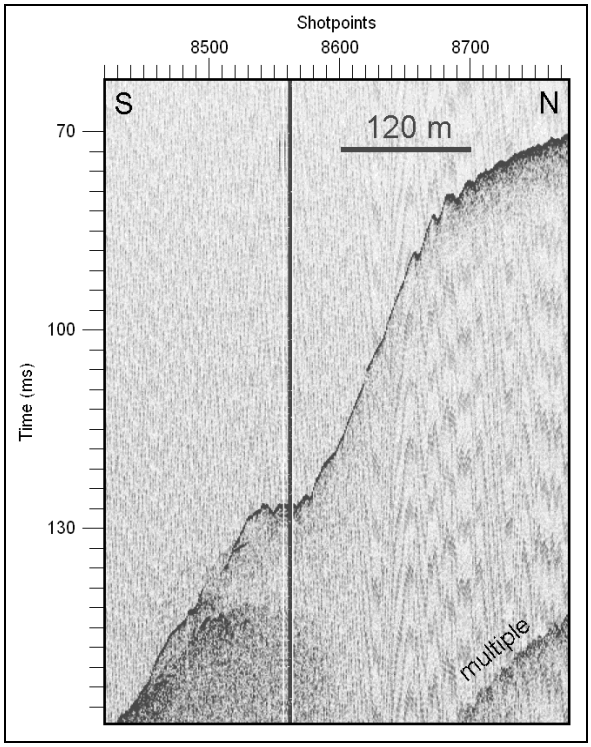

Figure 69 - Chirp seismic profile showing echo type IV-B. Echo types IV-B are interpreted as the result of slides or slumps (see location of the profile in Figure 72 and text for explanation).

Type IV-C: This echo type comprises irregular, blocky, lumpy or hyperbolic masses, laterally wedged, that are often acoustically transparent. Below the sea surface these masses exhibit a varied degree of deformation, with disrupted internal reflections. The deformed or transparent sub-bottom echoes of the displaced masses are characteristic of slide/slump deposits (Mulder and Cochonat, 1996). However, according to Fernando Tempera of DOP (personal communication) the data collected from multibeam sonar (Mitchell et al., 2003) showed here large sand-waves with WNW-ESE direction. Since the chirp track-

lines have W-E and N-S directions in this area (see Figures 12 and 72), it is likely to expect the hyperbolic echoes with sub-bottom reflectors because the data was acquired obliquely to these bedforms. What remains difficult to explain is the sub-bottom deformation of these masses with the disrupted internal reflections. Apparently these bedforms are parallel to the main graben structures that are found on the Pedro-Miguel Graben region (see Figures 42 and 43), which has been proved as seismically active (Madeira and Brum da Silveira, 2003). It is very likely that these faults extend offshore and their movement has caused irregularities on the sea-floor, conditioning the emplacement of these bedforms. Whenever these faults move, they may disturb the deposits above producing the chaotic masses seen on the echo type IV-C (Table 6).

3.3.2.2. Boomer records

A similar bottom echo technique, as the one used for the chirp data, was implemented to distinguish sea-floor bottoms. Although the Boomer seismic profiles, due to their lower resolution, are not adequate enough to distinguish many types of sea-floor bottoms, they were used whenever there were doubts in the chirp interpretation or in areas where the chirp seismic profiles were missing. Two main echoes were identified (Figure 71):

Type B-1: Distinct, continuous, sharp bottom echo with frequent sub-bottom reflectors

Type B-2: This type of echo shows regular, very intense overlapping hyperbolae with little varying vertex elevations and very prolonged echo without sub-bottom reflectors.

Echo type B-1 has been interpreted as resulting from reflection on sedimentary bottoms (sand and gravel) and can be assigned to echo types I-A, I-B and II-A from the echo chirp interpretation. **Echo type B-2** is interpreted as resulting from reflection of lava flows/coarse clastic bottoms and can be assigned to echo types III-A, III-B, III-C, III-D and IV-A from the echo chirp interpretation.

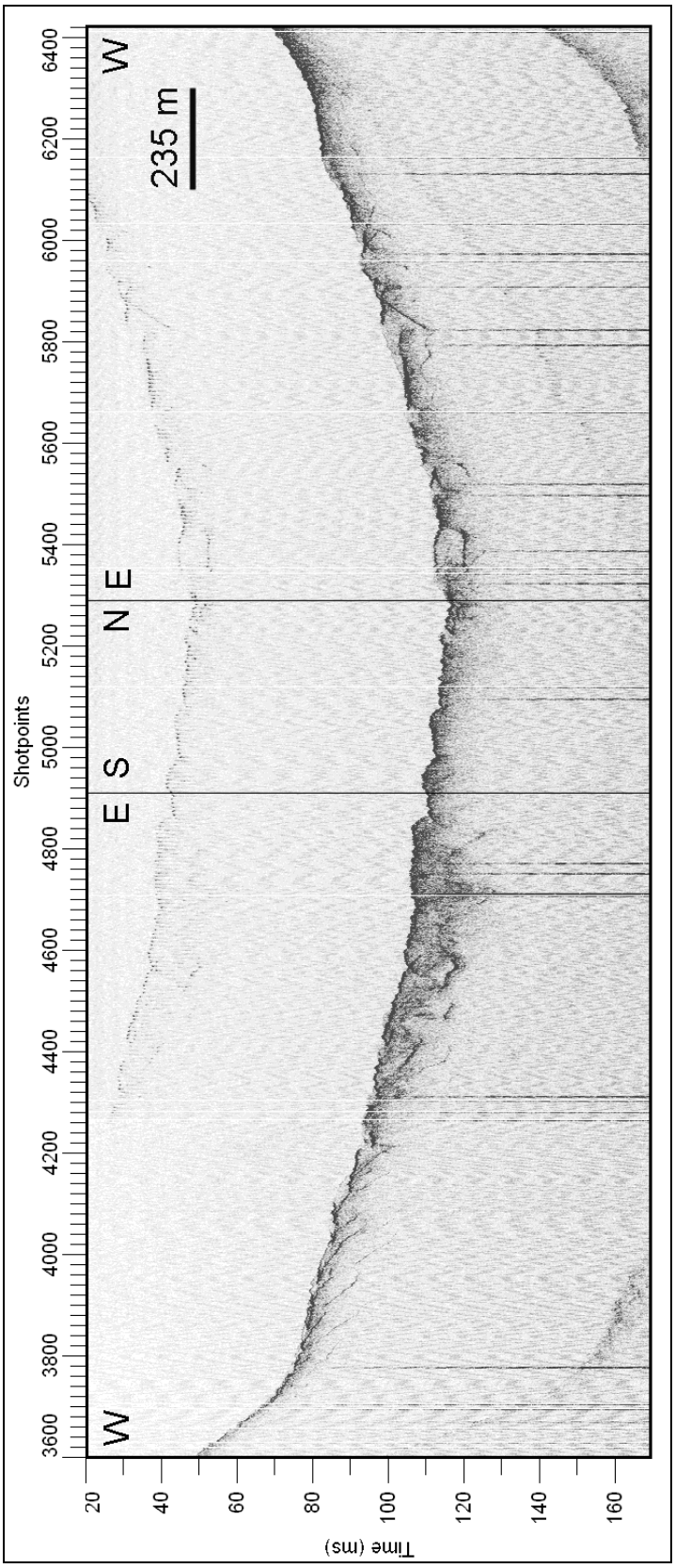

Figure 70 - Chirp seismic profile showing echo type IV-C. Echo types IV-C are interpreted as a sand-wave field emplaced over irregularities of the sea-floor of tectonic origin (see location of the profile in Figure 72 and text for explanation).

Table 6 – Classification, description, general physiographic distribution and interpretation of the geological processes of each chirp echo type.

ECHO CLASS & TYPE	GENERAL DISTRIBUTION	INTERPRETATION	PROCESSES
I. DISTINCT			
I-A: Sharp continuous single echo	Middle to outer shelf; more rarely nearshore	Sand and gravels	Depositional
I-B: Very sharp and continuous single echo	Middle shelf; just offshore echo type III-A	Sands	Depositional
II. INDISTINCT			
II-A: Prolonged and continuous echo	Entire shelf sector A	Pebbles and cobbles	Depositional
III. HYPERBOLIC			
III-A: Small and regular overlapping hyperbola	Nearshore to middle shelf	Boulders	Erosive; Mass-wasting
III-B: Medium irregular single hyperbola	Nearshore to middle shelf	Lava flows	Volcanic progradation
III-C: Large irregular single hyperbola	Next to Monte da Guia and offshore Ponta da Espalamaca	Surtseyan cones	Volcanic cones
III-D: Small and irregular overlapping hyperbola	Nearshore to middle shelf; next to Morro do Castelo	Lava domes	Volcanic progradation
IV. COMPOSITE			
IV-A: Intercalation of distinct, indistinct and hyperbolic echoes	Entire shelf sector A	Lava flows and pebbles, cobbles and boulders surrounding them	Volcanic progradation; Erosive
IV-B: sharp, continuous steeply dipping echo bounded downslope by irregular blocky or hyperbolic masses	Outer shelf to slope	Sediment slide/ debris flow deposits	Mass-wasting
IV-C: Irregular, blocky, lumpy or hyperbolic masses, laterally wedged.	Middle to outer shelf; in the channel Faial-Pico	Sand waves and debris flows	Depositional; Mass-wasting

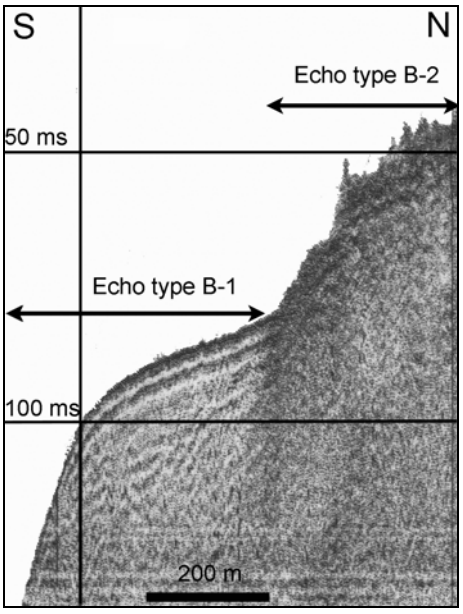

Figure 71 – Echo types defined in a Boomer seismic profile. Echo type B-1 has been interpreted as resulting from reflection of sand and gravel deposits and Echo type B-2 is interpreted as resulting from reflection of lava flows/coarse clastic bottoms. See location on Figure 76.

Based on the echo classification scheme (Table 6), all the chirp and Boomer profiles were interpreted and the resulting map produced (Figure 72). Several examples of the chirp profiles are shown in section 3.3.4 to support the geological interpretation and the description of the defined shelf areas.

3.3.3. Shelf sedimentary deposits

The author tried to apply the classic seismic stratigraphy techniques (Mitchum Jr. et al., 1977a; Mitchum Jr. et al., 1977b) and also the more recent seismic sequence stratigraphy models (Catuneanu, 2002) for the interpretation of the Bommer seismic profiles.

In the sedimentary areas, the seismic profiles were interpreted and one seismic unit has been defined. Figure 73 shows one example representative of the mapped deposits in the shelf. It is a surface deposit lying above a well defined, continuous and high amplitude reflector. This unit has a sigmoidal shape perpendicular to the shore and trends parallel to the shore. It is thicker at intermediate depths (between 40 and 60 m water depth), thinning nearshore as well as offshore. Nearshore, the unit terminates against the rocky outcrops through

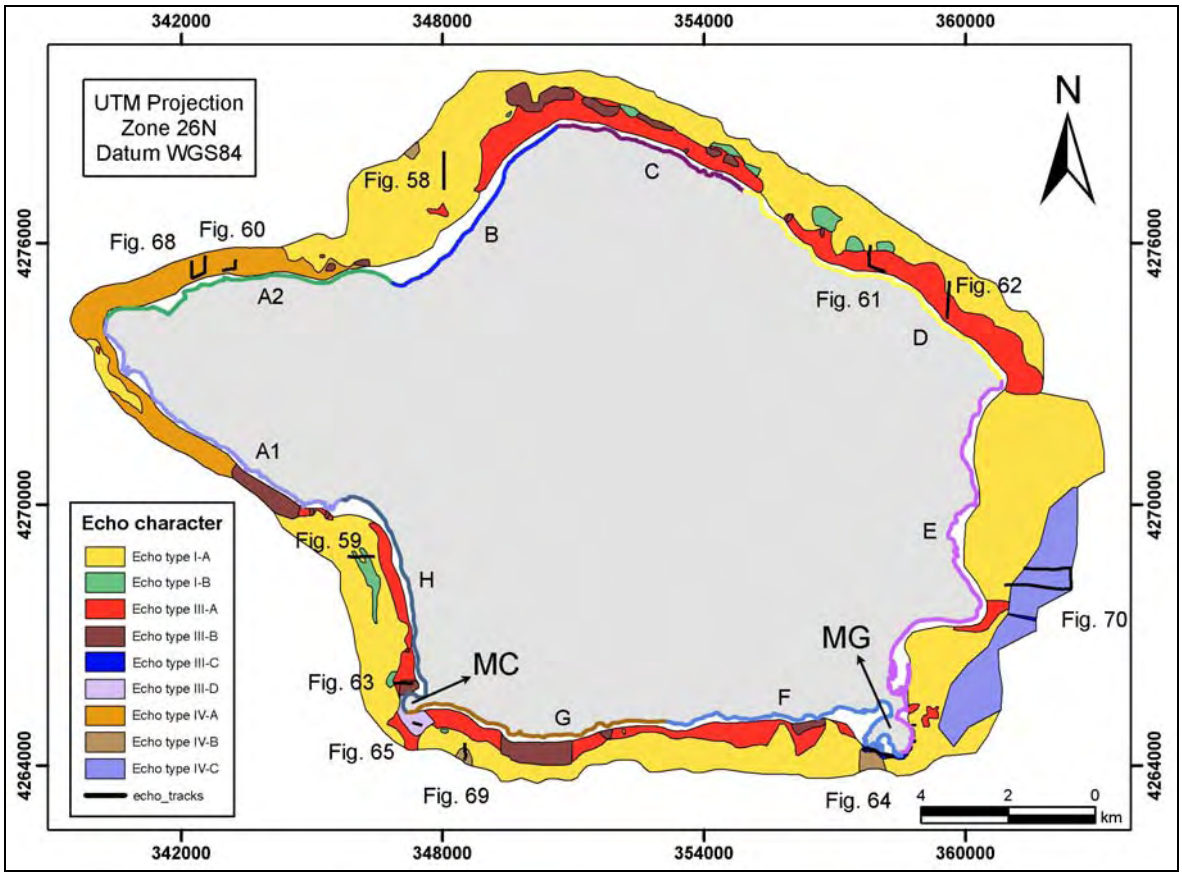

Figure 72 – Echo character map of the Faial shelf. Black lines correspond to chirp seismic navigation of the echo figures. MC – Morro do Castelo. MG – Monte da Guia. The different bold colored lines bordering the Faial coastline and the respective letters are the different shelf sectors defined.

coastal onlap. In the offshore direction, the unit almost disappears on the shelfedge with what appear to be downlap terminations. The downlap terminations are not well imaged in the seismic profiles; they are mainly inferred by the thinning of the unit offshore. The seismic unit shows internal reflectors with low amplitude and poor lateral continuity. Although, in some profiles it is possible to distinguish some reflections that are discordant with the internal reflectors of the seismic unit defined (Figures 86, 106, 115 and 116), these reflections do not have lateral continuity and no other seismic unit was defined. The lack of lateral continuity of these reflections may be attributed to the poor resolution of the seismic data. Alternatively, these reflections might just be a local change in the sedimentary pattern and do not correspond to other unit. Therefore, the application of the traditional seismic and sequence stratigraphy techniques is very limited and only one seismic unit was mapped to obtain the sedimentary deposits thickness.

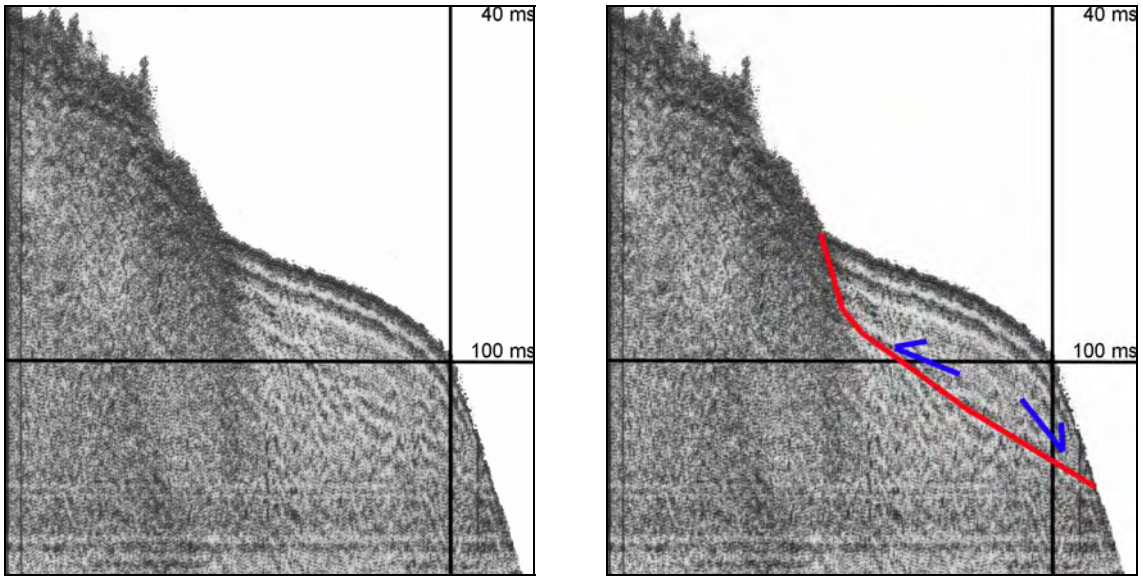

Figure 73 – Geometry of the seismic unit. A: Non-interpreted Boomer seismic profile. B: Interpreted Boomer seismic profile. The red line represents the basement of the seismic unit and the blue arrows seismic reflections terminating against the basement (the left arrow shows coastal onlaps and the right arrow the inferred downlap terminations). See location on Figure 76.

As already mentioned in section 3.2, in some areas the poor quality of the Boomer seismic profiles (e.g. Figure 74) did not permit the fully mapping of the shelf, leaving some interpretation gaps. Although the sea bottom was covered by sediments, confirmed by the echo interpretation of chirp and Boomer seismic profiles (see Figure 58 for chirp echo interpretation and Figure 74 for Boomer seismic interpretation) it was often impossible to follow a basement reflector and the corresponding areas were filled with the light green color in the Figure 76.

In other areas, the medium quality of the Boomer seismic profiles permitted the mapping of the sedimentary deposits, but with some uncertainty because the basement reflector is not always well defined (red hatched line in Figure 75). These areas with a certain degree of uncertainty correspond to all the mapped deposits in the shelf sectors B, C, D and E (Figure 76). In the shelf sectors F, G and H the seismic profiles have good quality and the sedimentary deposits were interpreted relatively easily (see example in Figure 73 from sector G and location on Figure 76). The use of the software tools of the SeisWorks 2D from the Landmark workstation permitted to refine and detect errors from the previous interpretation from Quartau et al. (2002). The past interpretation has been made

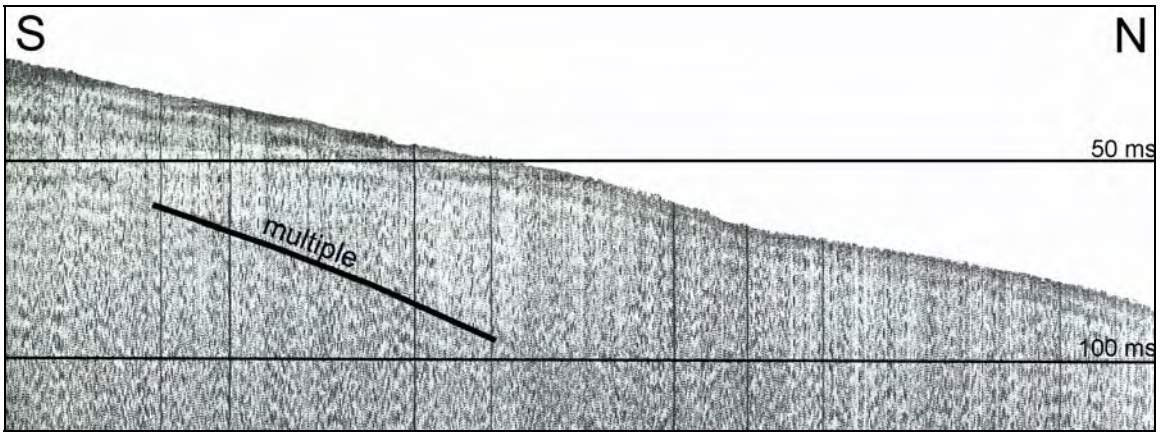

Figure 74 – Low-quality Boomer seismic profile where it is not possible to define the basement reflector of the seismic unit. See location on Figure 76.

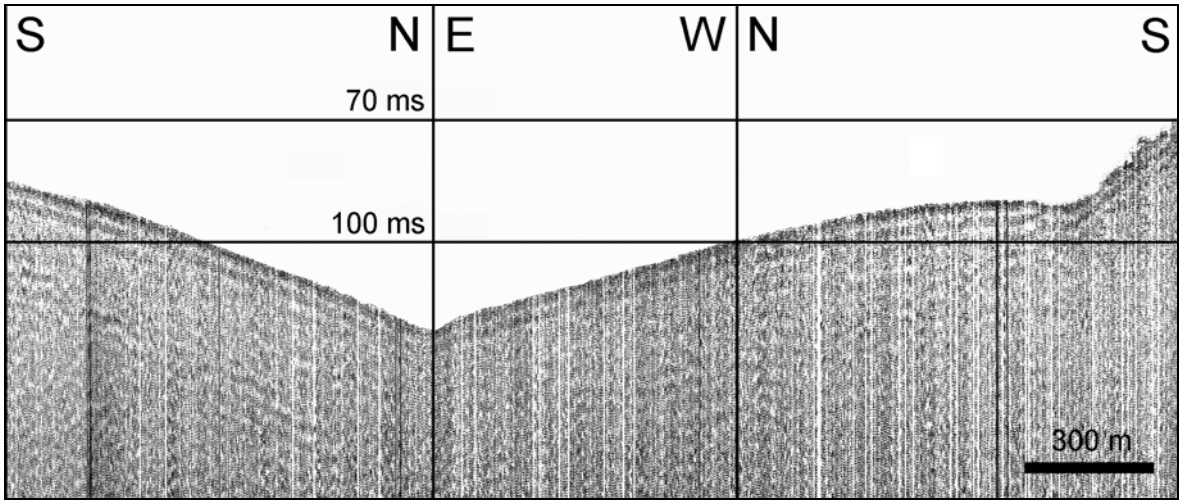

A

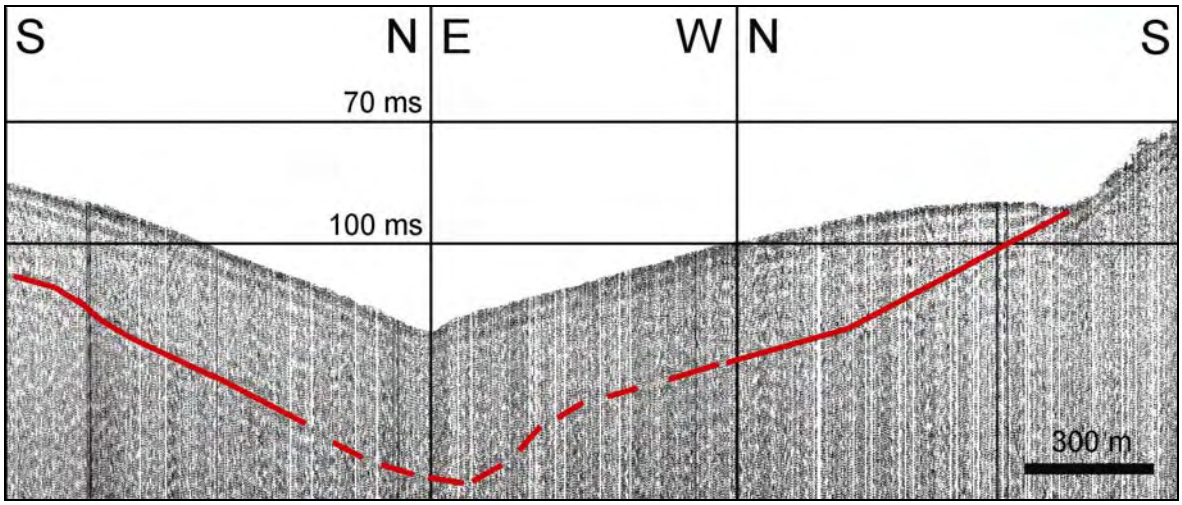

B

Figure 75 - A: Non-interpreted Boomer seismic profile. B: Interpreted Boomer seismic profile. The red line represents the basement of the seismic unit. See location on Figure 76.

using only analogue data that resulted from the EPC printer. The poor quality analogue data was more susceptible to errors in the interpretation since it had very deep reflectors that revealed, in the light of the new digital data, to be artifacts. Consequently, an erroneous basement reflector has been followed in some areas, increasing wrongly the sediment thickness.

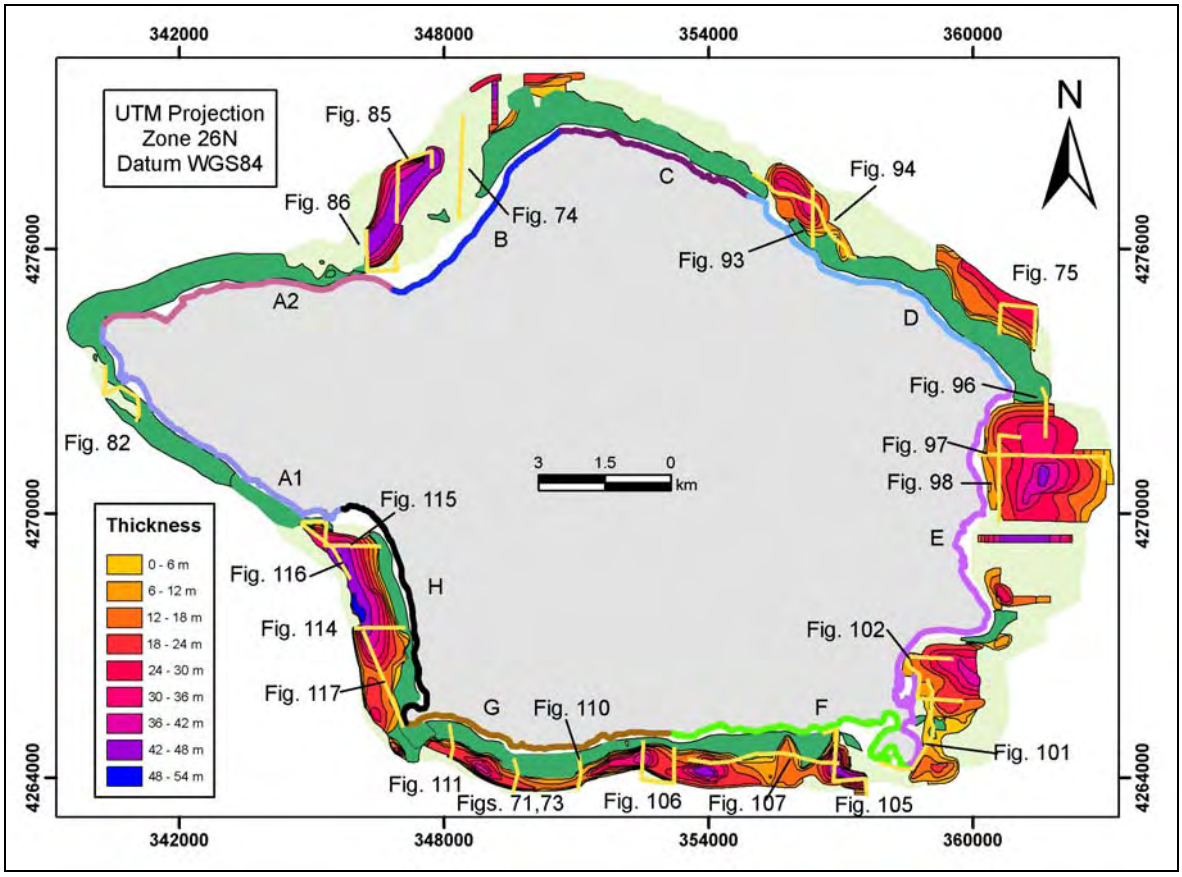

Figure 76 – Sedimentary thickness map produced in ArcGis based on the interpretation of the Boomer seismic profiles. Green areas correspond to lava flows/coarse clastic deposits interpreted with the chirp and Boomer seismic profiles. Light green areas correspond to sedimentary areas interpreted with the chirp and Boomer seismic profiles where no information exists about thickness of the deposits due to the poor quality of Boomer seismic profiles. Yellow lines are the track lines of some examples of the Boomer seismic profiles shown in the text. The different bold colored lines bordering the Faial coastline and the respective letters are the different shelf sectors defined.

Hamilton and Bachman (1982) found sound velocities from 1700 m/s for very fine sands and 1800 m/s for coarse sands from the shelf and slope of the main ocean basins. Since the sediment samples from the Faial shelf did not reveal sediments finer than sands (see Chapter 6), an average sound velocity of 1800 m/s must be a more realistic value. Nevertheless, it should be emphasized that

that some of these buried deposits may already be consolidated and could have a higher value. Therefore, the sound velocity value used for the estimation of the sedimentary thickness was 1800 m/s, resulting in a map that shows the thickness and the geographical distribution of the sediments (Figure 76).

All the medium and good quality Boomer seismic profiles were interpreted and the resulting thickness map produced (Figure 76). Several examples of the Boomer seismic profiles are presented in section 3.3.4 to support the interpretation and the description of the shelf areas.

3.3.4. Geological description of the Faial shelf

A geological map of the shelf of Faial Island (Figure 77) has been produced on the basis of the new bathymetric data acquired, the sea-floor features shown by the echoes and the distribution of the sedimentary deposits. Using an integrated and systematic approach that uses the information resulting from both the geological submarine mapping and the emerged area, the shelf was separated into sectors that have distinct submarine features, which commonly show a correspondence with the emerged geology. Each sector has been attributed a letter for reference (Figures 57, 72, 76 and 77), which will be used in the text to facilitate the future descriptions of these areas. The information represented in the map of Figure 77 not only shows the basic geological constitution of the shelf but tries also to extrapolate the physical processes responsible for the present-day morphology of the shelf.

Sector A is the shelf area that corresponds onshore to the Capelo Peninsula, between the Ponta do Varadouro and Fajã Village (see Figure 52 in Chapter 2 and Figure 77). The shelf has a 3 to 5 degree slope and the shelf edge is marked by an increase in the slope that can reach more than 15 degrees (Figure 57). The water depth at the shelf break ranges from 20 to 45 m on the northern sector and 10 to 35 m on the southern sector (Figure 56). It was subdivided into two sub-sectors (A1 and A2) based on the shelf width and also on the processes that molded the shelf that appear to be a little different in each case (see Figure 56 for bathymetry, Figure 57 for slope and Figure 77 for geological interpretation).

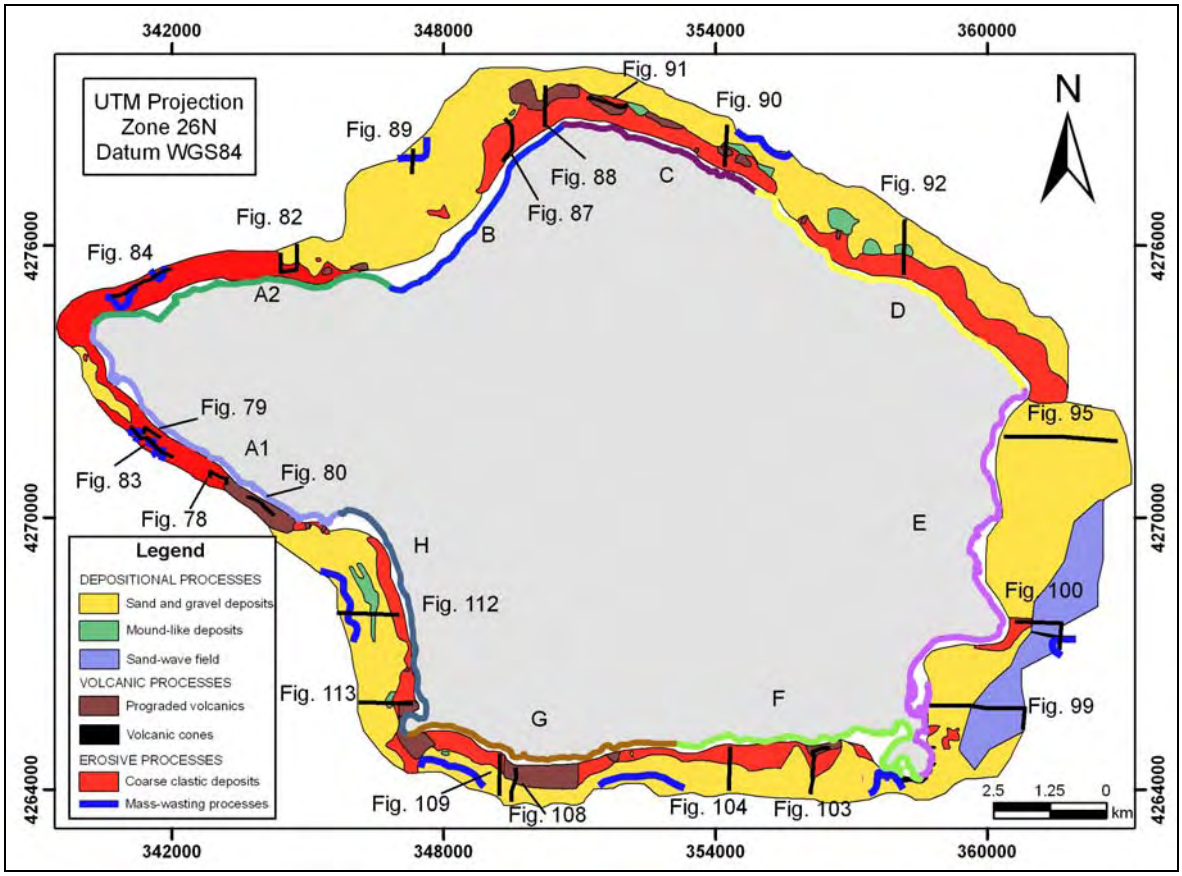

Figure 77 – Geological map of the Faial shelf, produced in ArcGis, based on the interpretation of the new bathymetric data and the chirp and Boomer seismic profiles. Black lines are the track lines of some examples of chirp seismic profiles. The different bold colored lines bordering the Faial coastline and the respective letters are the different shelf sectors defined.

The southern sub-sector (A1) is narrower, 300 m wide on average, ranging from 100 to 600 m (Figure 57). The echo interpretation (Figures 72, 78 and 79) revealed that this sector is covered by preserved lava flows mixed with coarse clastic sediments (boulders) and finer sediments (sand to cobbles) that probably resulted from the erosion of the lava flows. The eastern part of sector A1 appears to be completely covered by very well preserved lava flows (Figures 72 and 80). This hypothesis is based on the presence of the echo type III-B all over this area and also a narrower shelf when compared with the other areas of the A1 sector. The narrower shelf is probably the result of the progradation of the lava flow of 1672 AC (see Figure 43 in Chapter 2) into the sea. The western part of sector A1 has a wide area, below 20 m water depth that is covered with fine sediments (echo type A-1 in Figure 72). The Boomer echo interpretation (Figure 81) revealed the

presence of sands and gravels. Unfortunately, the data is of poor quality, giving no information about the thickness of the deposits in the area.

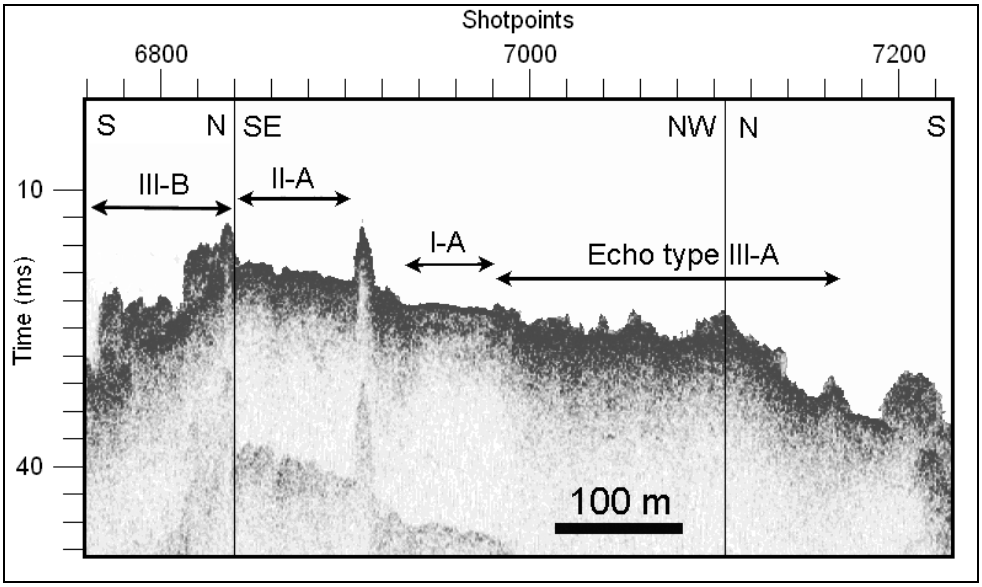

Figure 78 – Chirp seismic profile from sector A1 showing that this sector is composed by the combination of several echo types which were classified together as Echo type IV-A. Echo type IV-A is interpreted to result from the presence of lava flows mixed with the products of their erosion. See location in Figure 77.

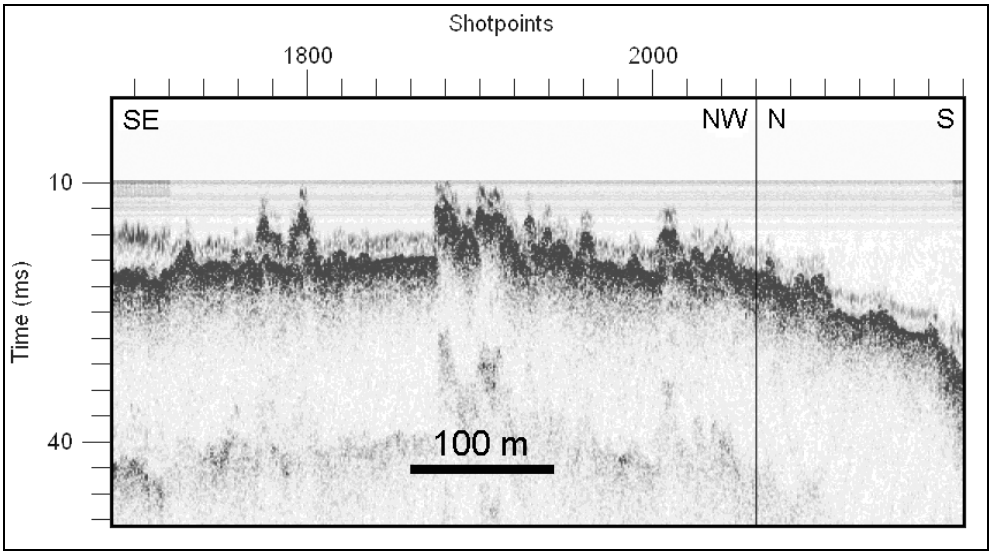

Figure 79 - Chirp seismic profile from sector A1 showing that this sector is composed by the combination of several echo types which were classified together as Echo type IV-A. Echo type IV-A is interpreted to result from the presence of lava flows mixed with the products of their erosion. See location in Figure 77.

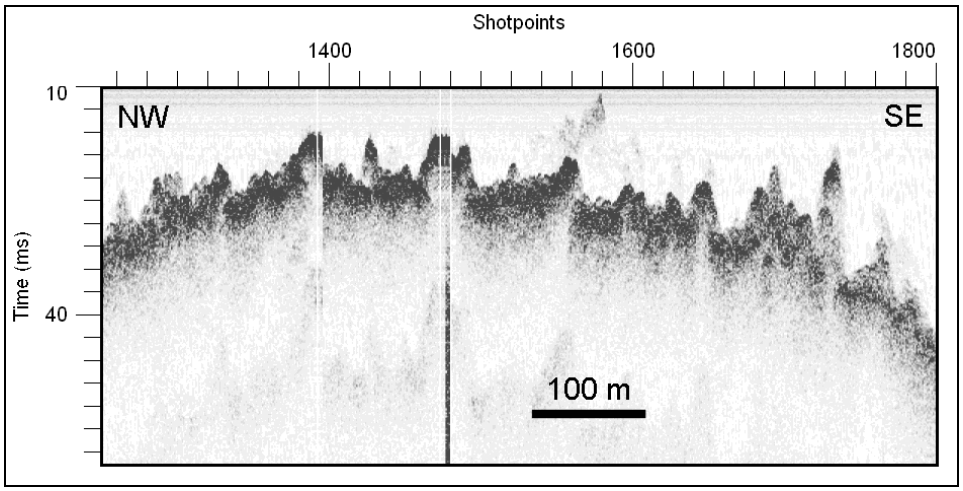

Figure 80 - Chirp seismic profile from sector A1 showing that this sector is exclusively composed by the echo type III-B. Echo type III-B is interpreted to result from the presence of well preserved lava flows. See location in Figure 77.

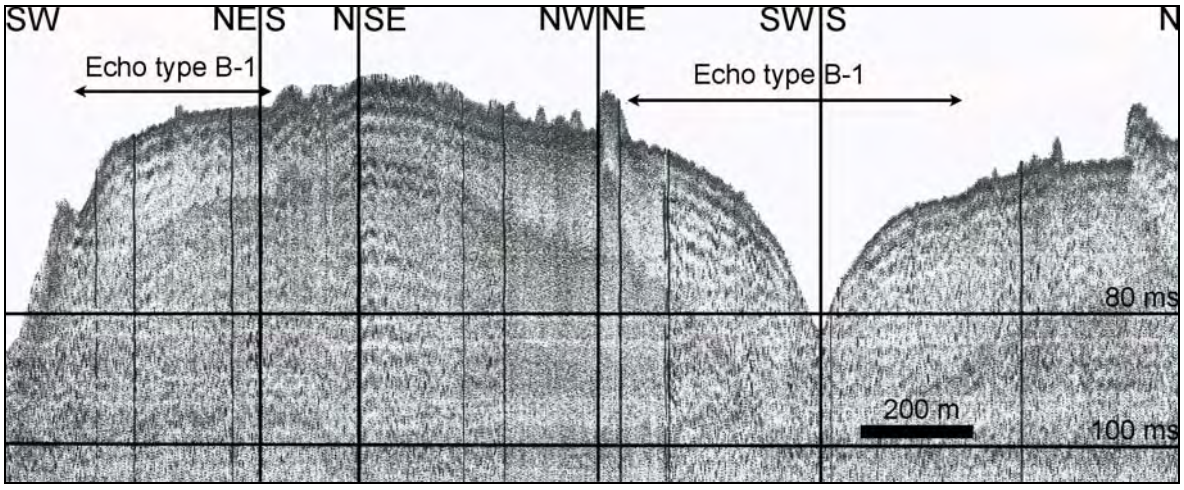

Figure 81 – Boomer seismic profile showing the sedimentary area in the sector A1 (echo type B-1). See location on Figure 76.

The northern sub-sector (A2) has a wider shelf, 450 m wide on average, ranging from 100 to 1000 m (Figure 57). The echo interpretation (Figures 81 and 84) revealed that this sector is almost covered by preserved lava flows mixed with coarse clastic sediments (boulders) and finer sediments (sand to cobbles) that probably resulted from the erosion of the lava flows. The eastern area of the A2 sub-sector is quite different. Nearshore, the shelf has the same characteristics (Figure 82), but below the 20 meters water depth, the shelf is filled with finer sediments (sand and gravels). The shelf edge in both sub-sectors is extensively incised by gullies (Figures 83 and 84).

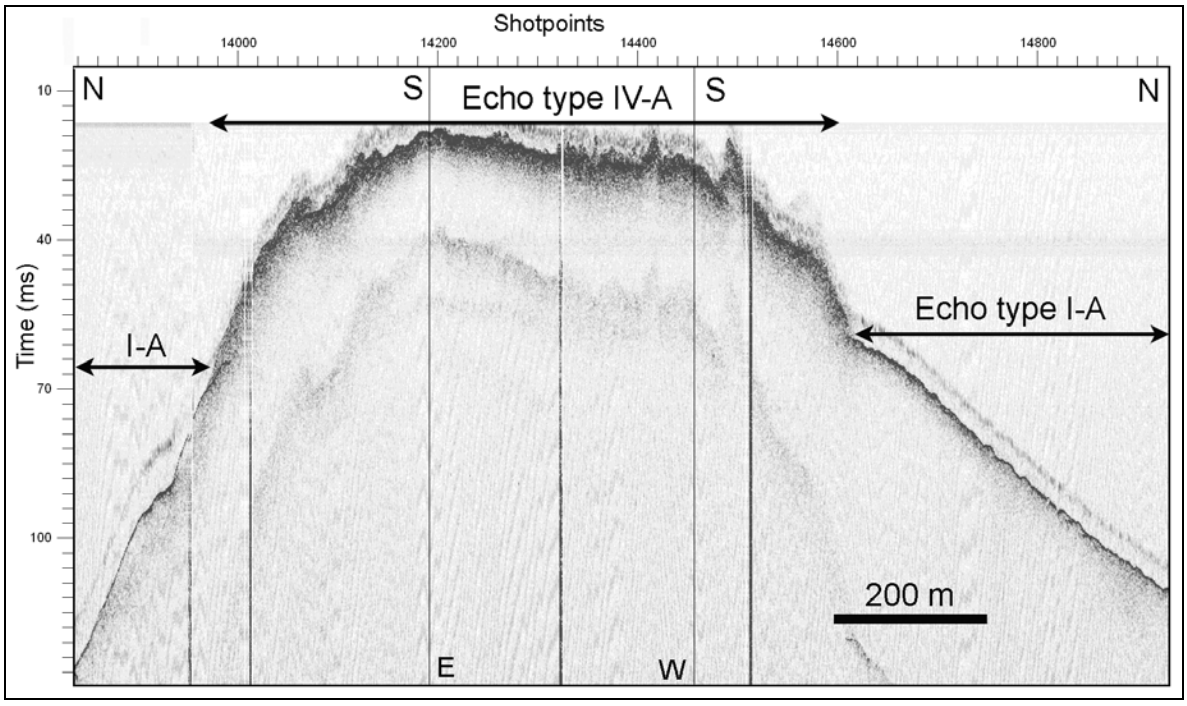

Figure 82 - Chirp seismic profile from the eastern part of sector A2 showing that this sector is composed by the echo type IV-A and I-A. Echo type IV-A is interpreted to result from the presence of lava flows mixed with the products of their erosion and echo type I-A from the presence of finer sediments (sand and gravels). See location in Figure 77.

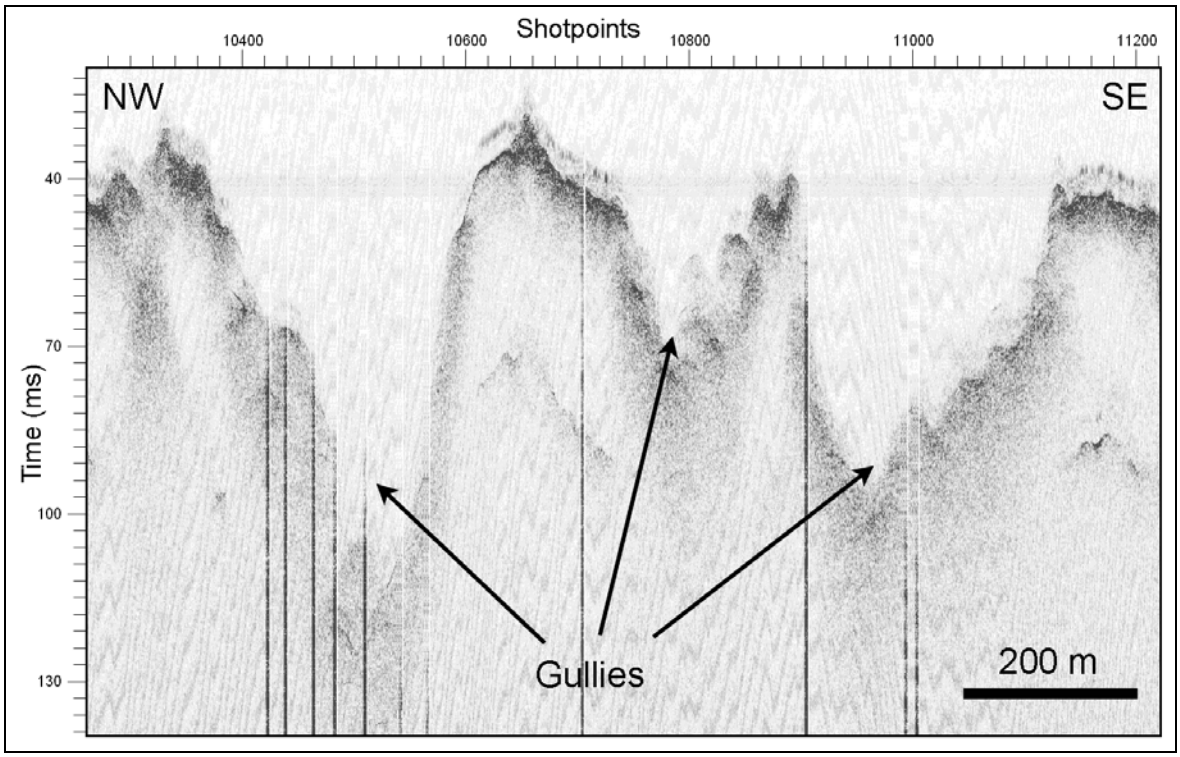

Figure 83 - Chirp seismic profile from sector A1 showing that this sector is extremely incised by gullies. See location in Figure 77.

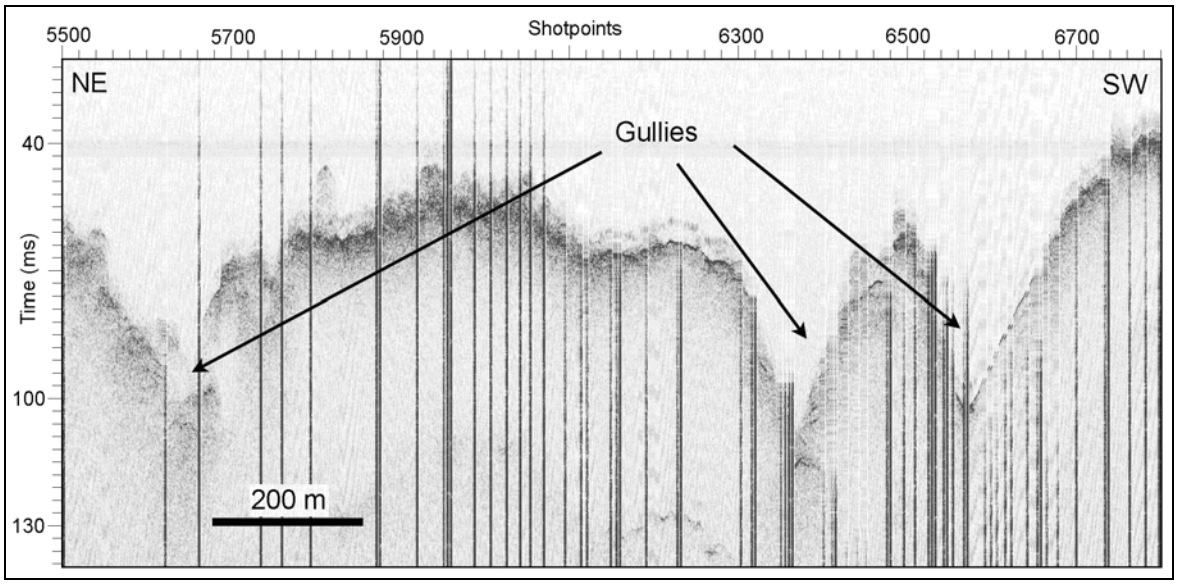

Figure 84 - Chirp seismic profile from sector A2 showing that this sector is extremely incised by gullies. See location in Figure 77.

Sector B is the shelf area that corresponds onshore to the area between Fajã village and Ponta dos Cedros (see Figure 45 in Chapter 2 and Figure 77). The southwestern part is a rather uniform area, with slopes normally below 3 degrees (Figure 57) and covered by sand and gravels (Figures 58 and 72). These sedimentary deposits show a NE-SW trend (Figures 76, 85 and 86), parallel to the shoreline, reaching 45 meters thick at 60 meters water depth. Further offshore as well as onshore the bodies seem to loose their expression in thickness, although the thicknesses have not been entirely mapped, due to poor quality of the data (Figure 74). In the northeast segment, close to Ponta dos Cedros, the slope ranges from 3 to 5 degrees (Figure 57) due to the nearshore presence of coarse clastic deposits (boulder-size) that extend beyond the 50 meters water depth (Figures 77 and 87). Further offshore, other sedimentary bodies appear, but were not well mapped. Between the coarse clastic deposits and the sedimentary bodies, there is an area of well preserved lava flows (Figures 77 and 88). On the entire sector B, the shelf edge can only be mapped in two small segments (Figure 57). One of them resembles a head scar of a landslide (arrow in Figure 57), also shown by the hydrographic map (see Figure 40 in Chapter 2) and in a Chirp seismic profile as echo type IV-B (Figure 89). The shelf width is at least 2000 m in this sector and the shelf break appears at 80 meters water depth (red line Figure

57). The slopes derived from the hydrographic map of the Instituto Hidrográfico (Figure 40 in Chapter 2) suggest that the shelf width can reach 2500 m and the shelf break can also be deeper (green line on Figure 57).

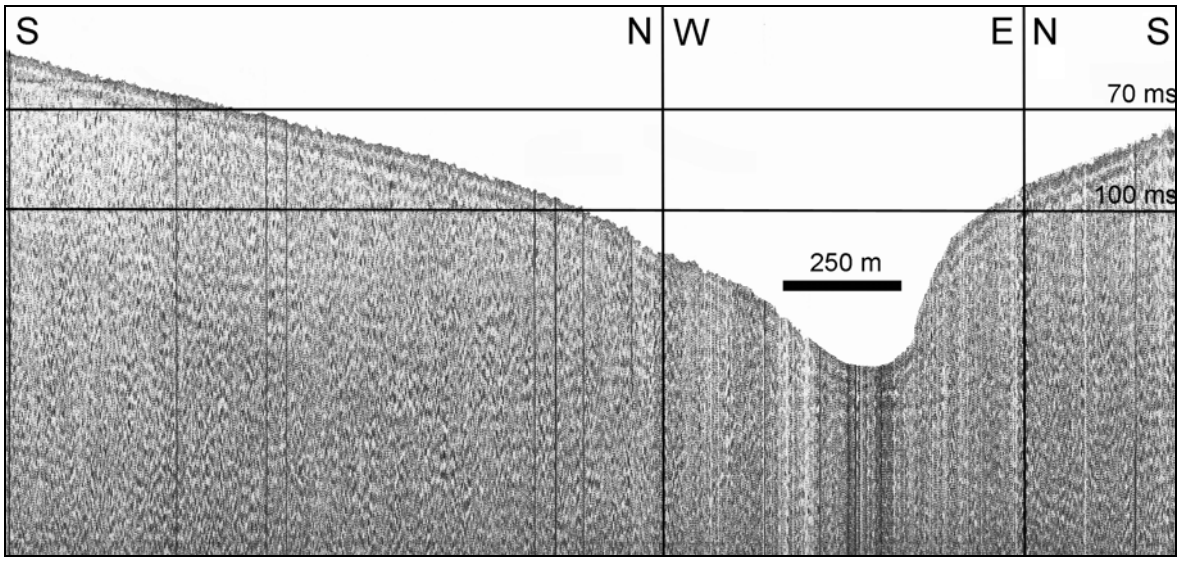

A

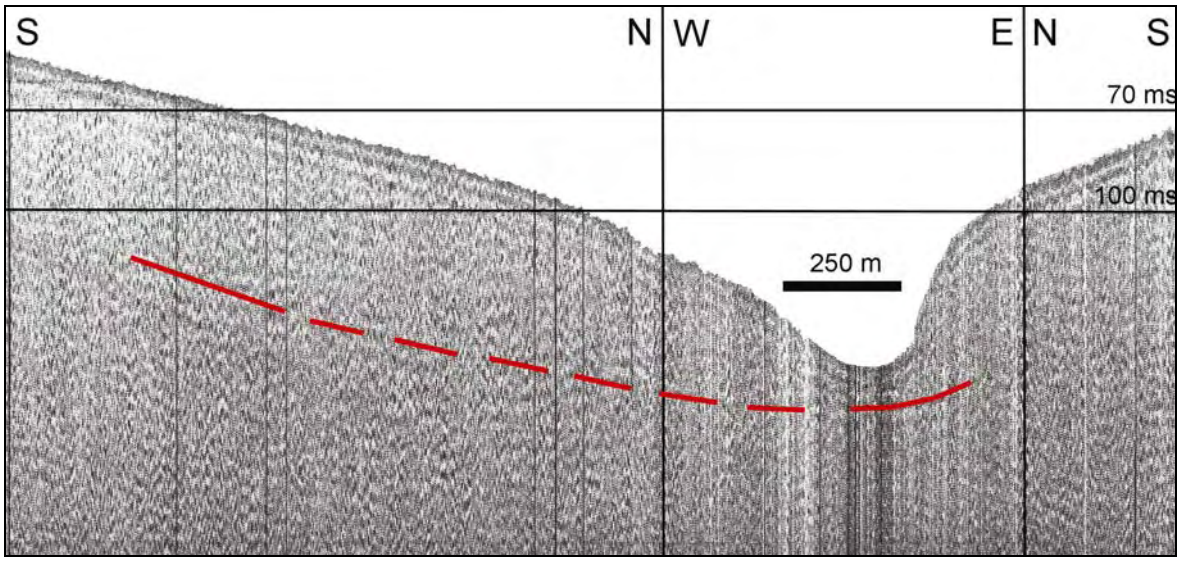

B

Figure 85 – Boomer seismic profile on sector B, showing the mapped sedimentary unit that thins offshore. A: Non-interpreted seismic profile. B: Interpreted seismic profile. The red line represents the basement of the sedimentary unit. See location on Figure 76.

Sector C is the shelf area that corresponds onshore to the area between Ponta dos Cedros and the headland located 750 m northeast of the geodetic pillar Vigia (see Figure 46 in Chapter 2 and Figure 77). Steeper submarine slopes ranging from 3 to 6 degrees flank the island nearshore to a depth of about 50

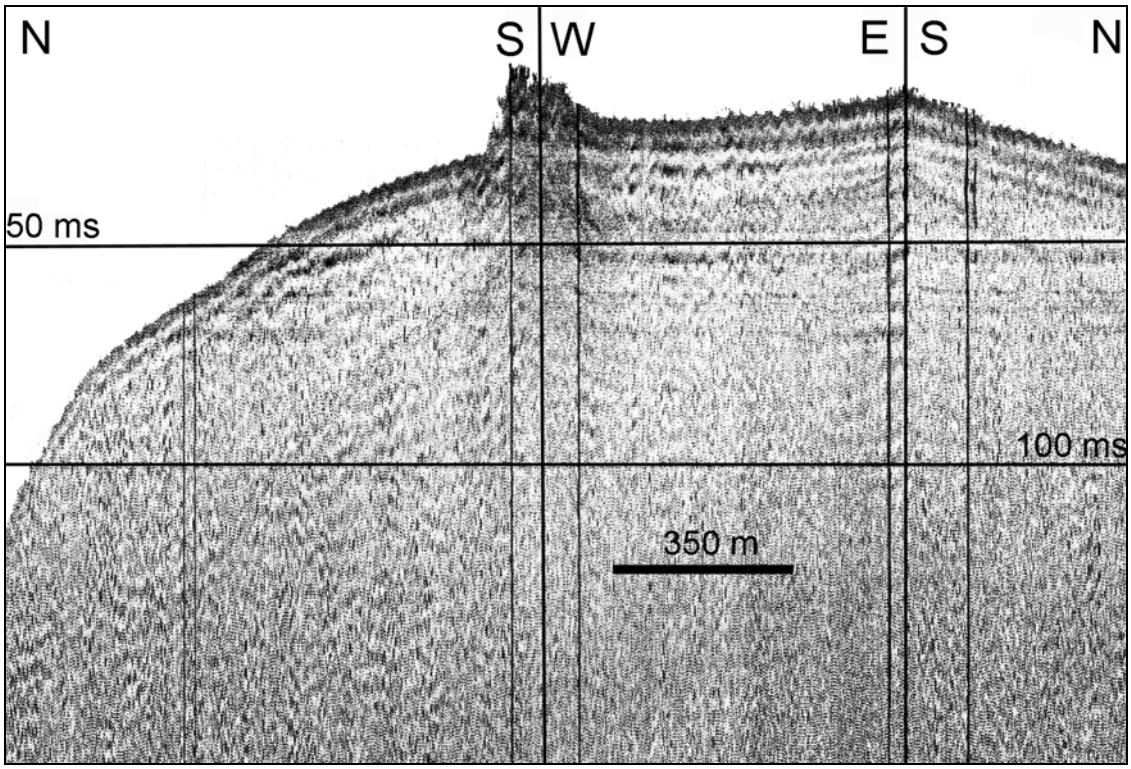

A

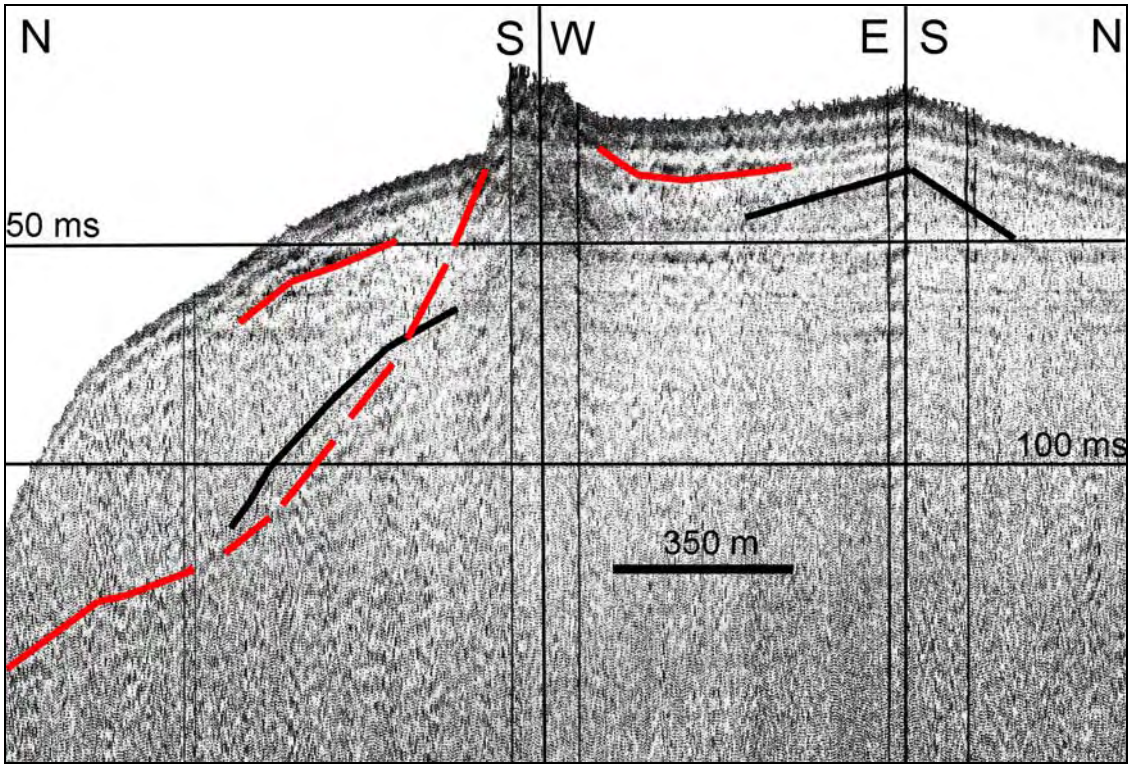

B

Figure 86 - Boomer seismic profile on sector B, showing the mapped sedimentary unit that thins both onshore and offshore. Inside the major unit it is possible to see one shallower reflection, probably other sedimentary unit. A: Non-interpreted seismic profile. B: Interpreted seismic profile. The red line represents the basement of the seismic unit. The black line represents the multiple of the sea-floor reflection. See location on Figure 76.

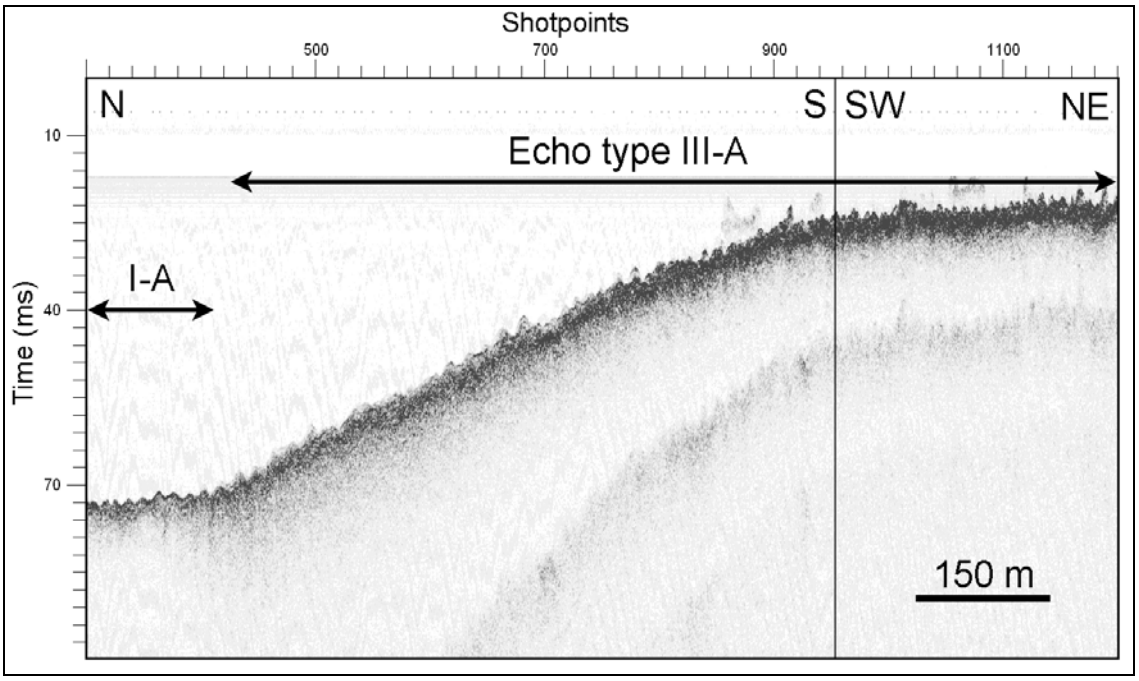

Figure 87 - Chirp seismic profile from the northeastern part of sector B showing that this area is composed nearshore by the echo type III-A and further offshore by the echo type I-A. Echo type III-A is interpreted to result from the presence of coarse clastic deposits (boulder-size) and echo type I-A from the presence of finer sediments (sand and gravels). See location in Figure 77.

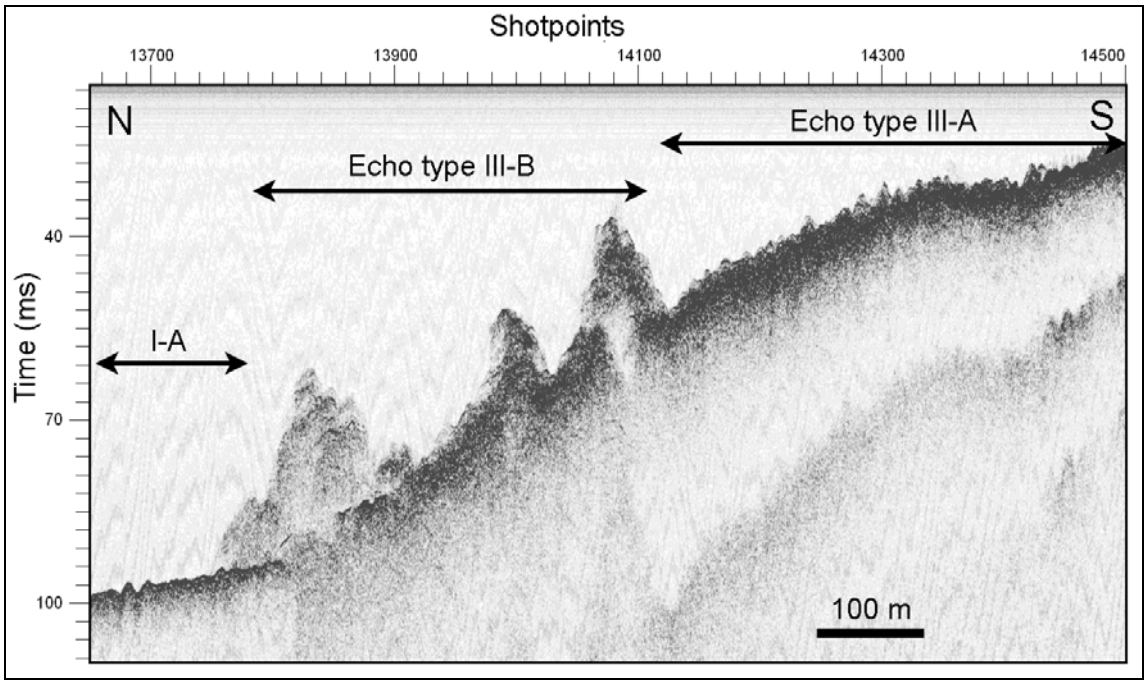

Figure 88 - Chirp seismic profile from the more eastern part of sector B showing that this area is composed nearshore by the echo type III-A, further offshore by the echo type III-B that passes in the deeper areas to echo type I-A. Echo type III-A is interpreted to result from the presence of coarse clastic deposits (boulder-size), echo type III-B from the presence of well preserved lava flows and echo type I-A from the presence of finer sediments (sand and gravels). See location in Figure 77.

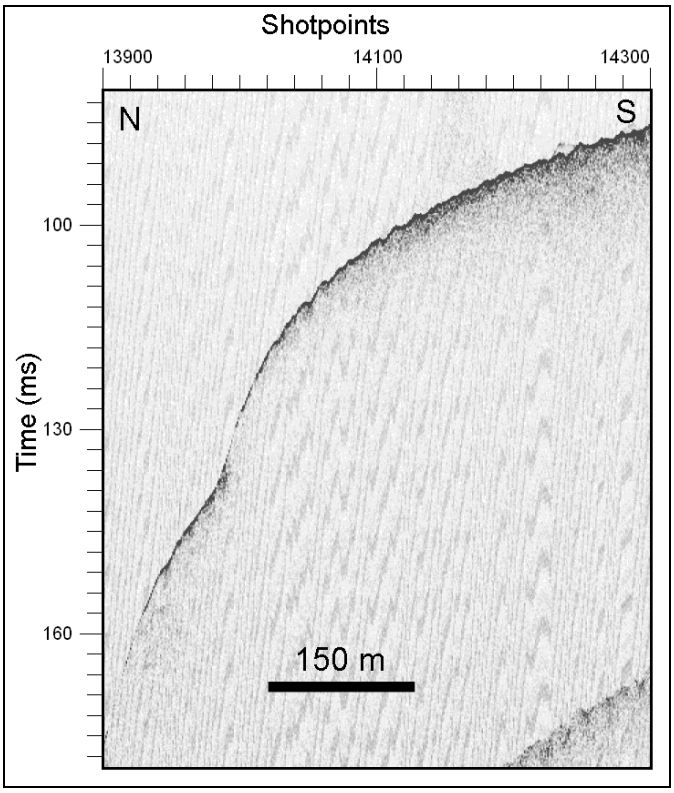

Figure 89 - Chirp seismic profile from the outer shelf of sector B showing that this area is composed by the echo type I-A. Echo type I-A is interpreted to result from the presence of finer sediments (sand and gravels). Approximately at shot 13990 the sea-floor shows a change in slope which suggests the presence of a scarp upslope like the one defined in the echo type IV-B. See location in Figure 77.

meters (Figures 56 and 57). Beyond this depth a smoother surface with an over-all gradient below 4º extends offshore. The nearshore steeper slopes correspond mainly to coarse clastic deposits and the adjacent offshore smoother slopes to sand and gravel deposits (Figures 57, 77 and 90). Between the coarse clastic deposits and the sedimentary bodies, there areas of well preserved lava flows (Figures 77 and 91). It also appears in this sector, between the coarse clastic deposits/lava flows and the sand and gravels from echo type I-A, the mound-like and frequently elongated sedimentary deposits of the echo type I-B (Figure 90). In this sector the sedimentary bodies were almost not mapped due to poor quality data (Figure 76). Similar to the previous sector, the shelf edge can only be mapped in some parts of the shelf (red line in Figure 57). In these areas, the shelf edge lies at 75 m water depth and 900 m from the coastline (Figures 56 and 57). In the western part of the area, the shelf break is inferred by the slopes derived from the hydrographic map of the Instituto Hidrográfico (Figure 40 in Chapter 2).

Here, the shelf width can reach 1400 m and the shelf break can also be deeper (green line on Figure 57).

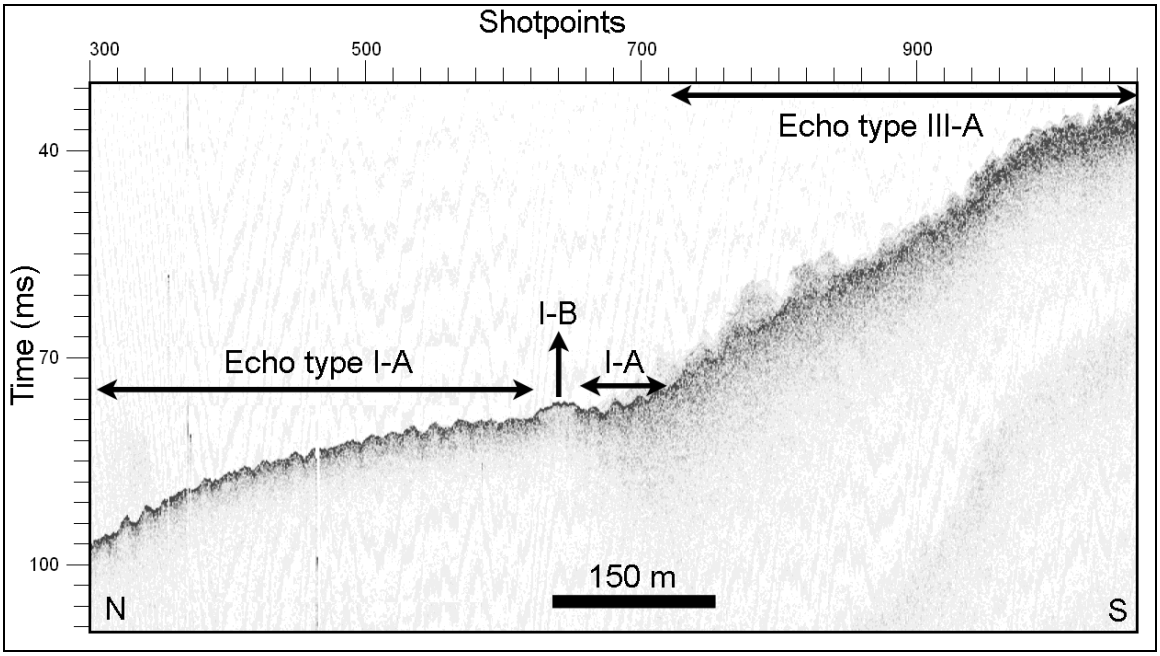

Figure 90 - Chirp seismic profile crossing the entire sector C showing that this area is composed nearshore by the echo type III-A, passing offshore to echo type I-A. Echo type I-B appears in some areas between the echo types III-A and I-A. Echo type III-A is interpreted to result from coarse clastic deposits (boulder-size), echo type I-A from sand and gravels and echo type I-B from sands. See location in Figure 77.

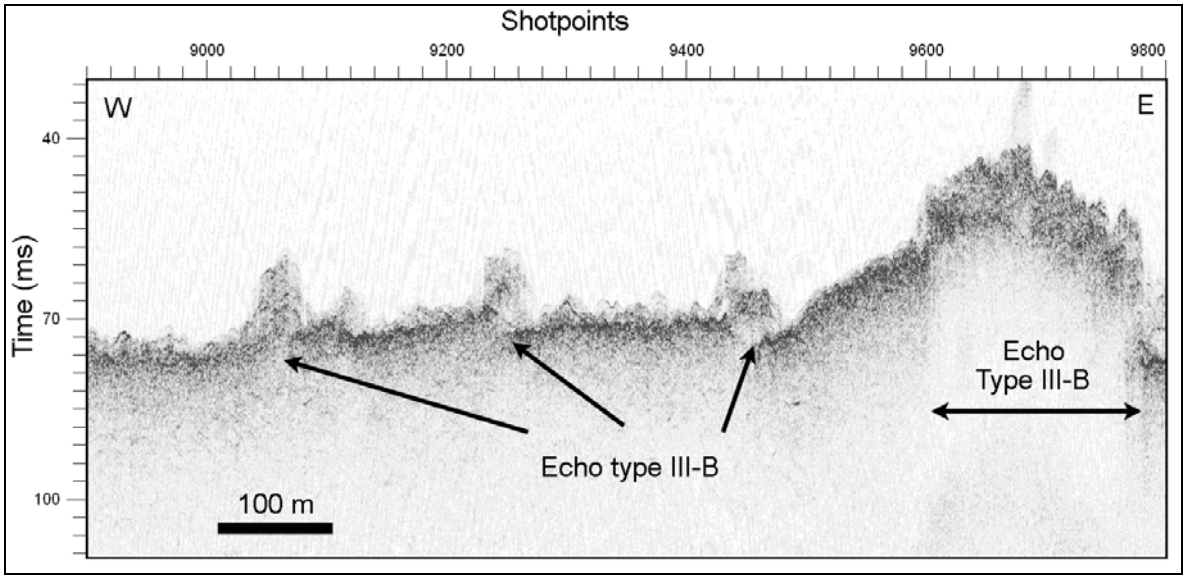

Figure 91 - Chirp seismic profile showing that there are well preserved lava flows (echo type III-B). The other echoes in the profile correspond to the type III-A which are interpreted as coarse clastic deposits (boulder-size) that result from the erosion of the lava flows. See location in Figure 77.

Sector D is the shelf area that corresponds onshore to the area between the headland located 750 m northeast of the geodetic pillar Vigia and Ponta da Ribeirinha (see Figure 49 in Chapter 2 and Figure 77). Steeper submarine slopes, ranging from 3 to 7 degrees, flank the island nearshore to a depth of 35 to 65 meters (Figures 56 and 57). These correspond to a variable 0.50 km-wide belt of coarse clastic deposits (Figures 77 and 92). Beyond these depths a smoother gradient below 2º (Figure 57), extends offshore, revealing the presence of sand and gravels (Figures 72 and 92).

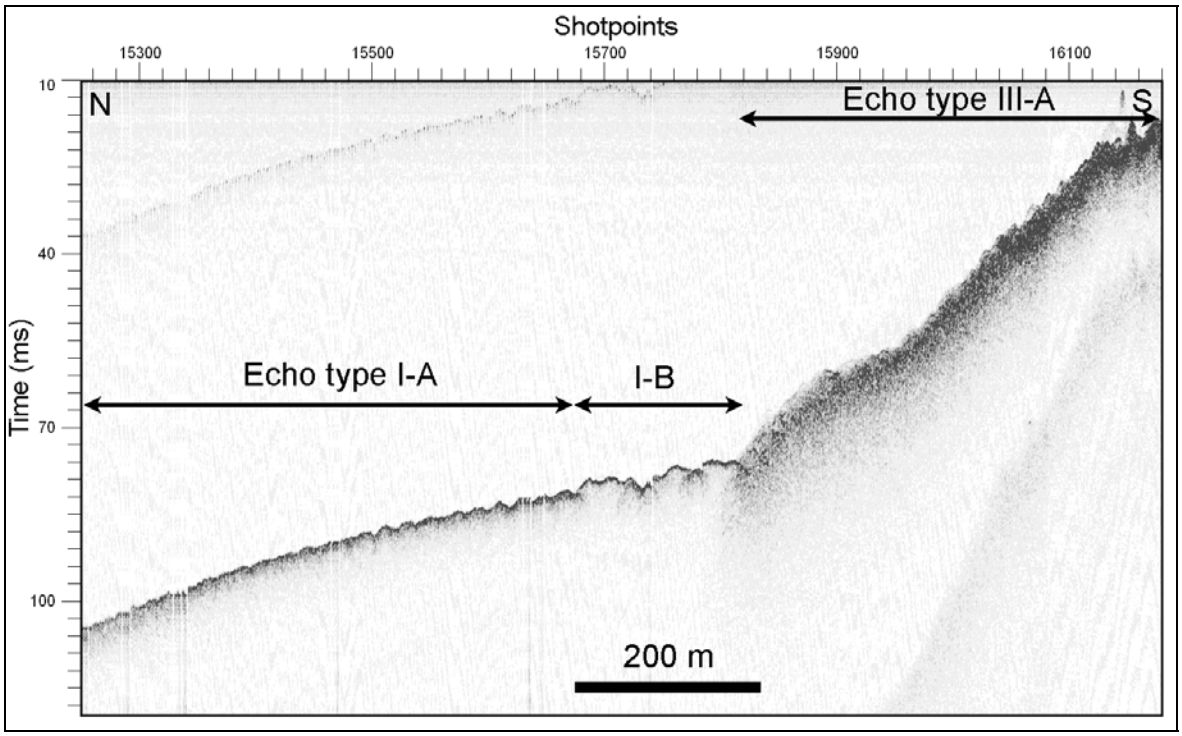

Figure 92 - Chirp seismic profile crossing the entire sector D showing that this area is composed nearshore by the echo type III-A, passing offshore to echo type I-A. Echo type I-B appears in some areas between the echo types III-A and I-A. Echo type III-A is interpreted to result from coarse clastic deposits (boulder-size), echo type I-A from sand and gravels and echo type I-B from sands. See location in Figure 77.

Similar to the previous sector, only small sedimentary bodies have been mapped; one in the western area (Figures 76, 93 and 94) and other in the eastern area of sector D (Figures 76 and 75). The western body has a NNW-SSE trend, parallel to the shoreline, reaching 35 meters thick at 40 meters water depth. The eastern also trends NNW-SSE, parallel to the shoreline, reaching 25 meters thick at 80 meters water depth. Both bodies seem to decrease in thickness further

onshore and offshore, although the latter is not fully mapped seaward. Between the sand and gravels and the coarse clastic deposits are small patches of the mound-like deposits revealed by the echo type I-B (Figures 77 and 92). Contrary to the previous sectors, the shelf edge was not reached in this area. So, one can

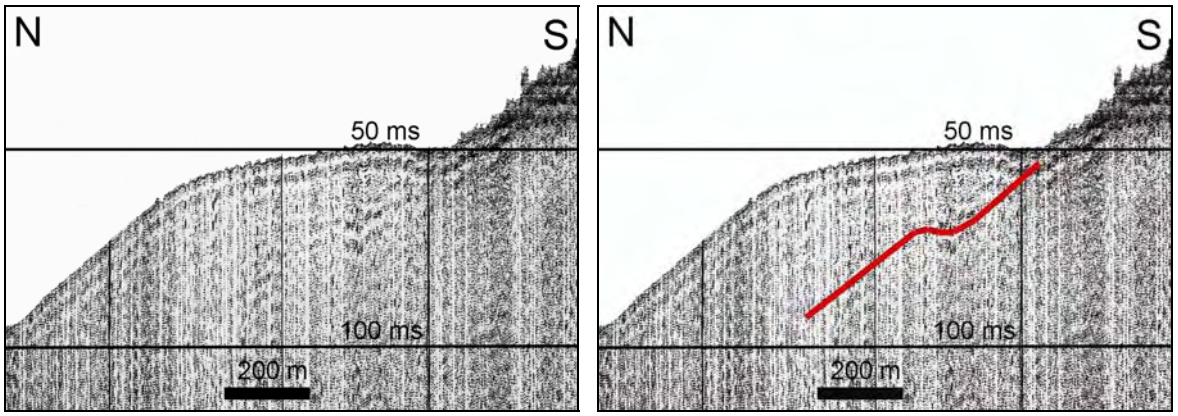

Figure 93 – Cross-shore Boomer seismic profile on sector D, showing the sedimentary unit thinning nearshore. A: Non-interpreted seismic profile. B: Interpreted seismic profile. The red line represents the basement of the seismic unit. See location on Figure 76.

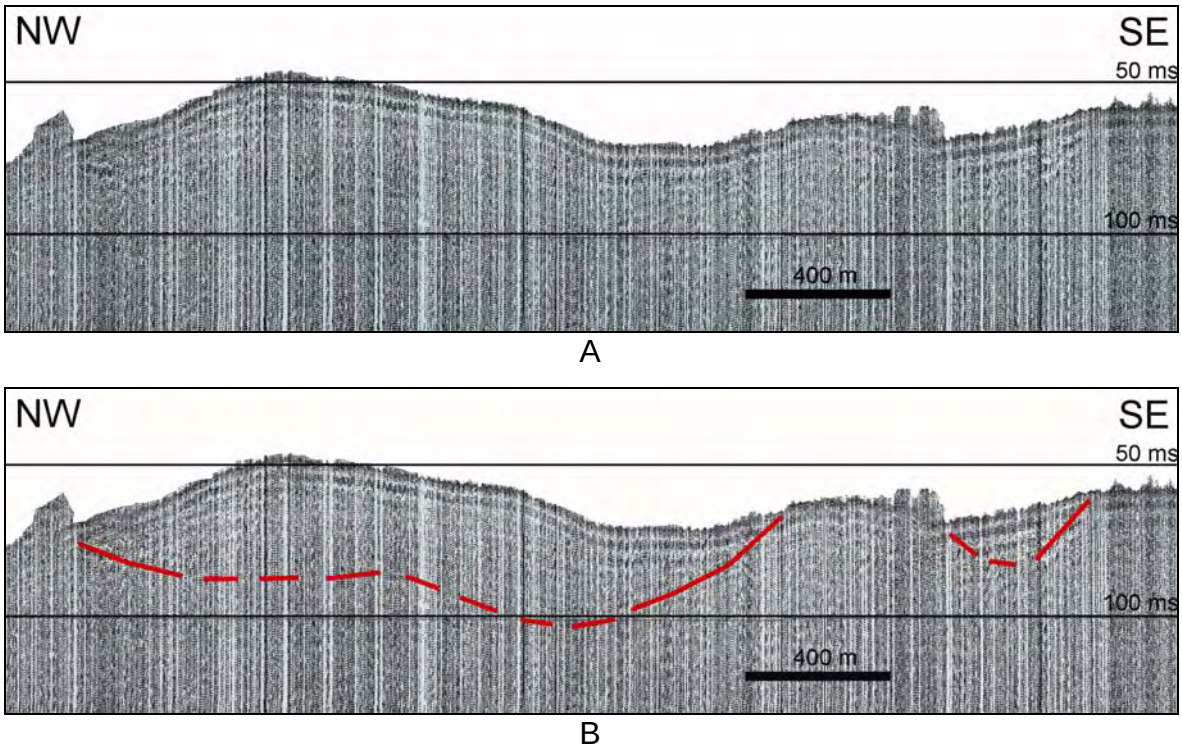

Figure 94 - Longshore Boomer seismic profile on sector D showing the lateral variation of the sedimentary unit. A: Non-interpreted seismic profile. B: Interpreted seismic profile. The red line represents the basement of the seismic unit. See location on Figure 76.

expect at least, a shelf width of 1800 m in the more extended areas, where 85 m water depth has been probed (Figures 56 and 57). The shelf edge may be inferred from the Instituto Hidrográfico map (see Figure 40 in Chapter 2 and green line Figure 57), lying at 200 m water depth and within 2 to 3 km of the coastline.

Sector E is the shelf area that corresponds onshore to the area between Ponta da Ribeirinha and Monte da Guia (see Figures 50 and 51 in Chapter 2 and Figure 77). This sector corresponds to the eastern part of the channel Faial-Pico. It was not fully surveyed and corresponds to less than one fourth of the total area of the channel. The area surveyed can be divided in two sub-sectors; a northern one, between Ponta da Ribeirinha and Ponta da Espalamaca (Figure 50 in Chapter 2) and a southern one, between Ponta da Espalamaca and Monte da Guia (see Figure 51 in Chapter 2). The northern sub-sector is a smooth area (Figures 56 and 57), sloping below 2º, except the area northeast of Ponta da Espalamaca where slopes from 3º to 5º can be found between 30 to 50 m water depths. This sub-sector is almost entirely covered by sand and gravels (Figures 72 and 95) and a sedimentary body has been mapped (Figures 76, 96, 97 and 98) in its northern part. It is roughly parallel to the shoreline and reaches 45 meters thick at 50 meters water depth, decreasing in thickness both landward and seaward.

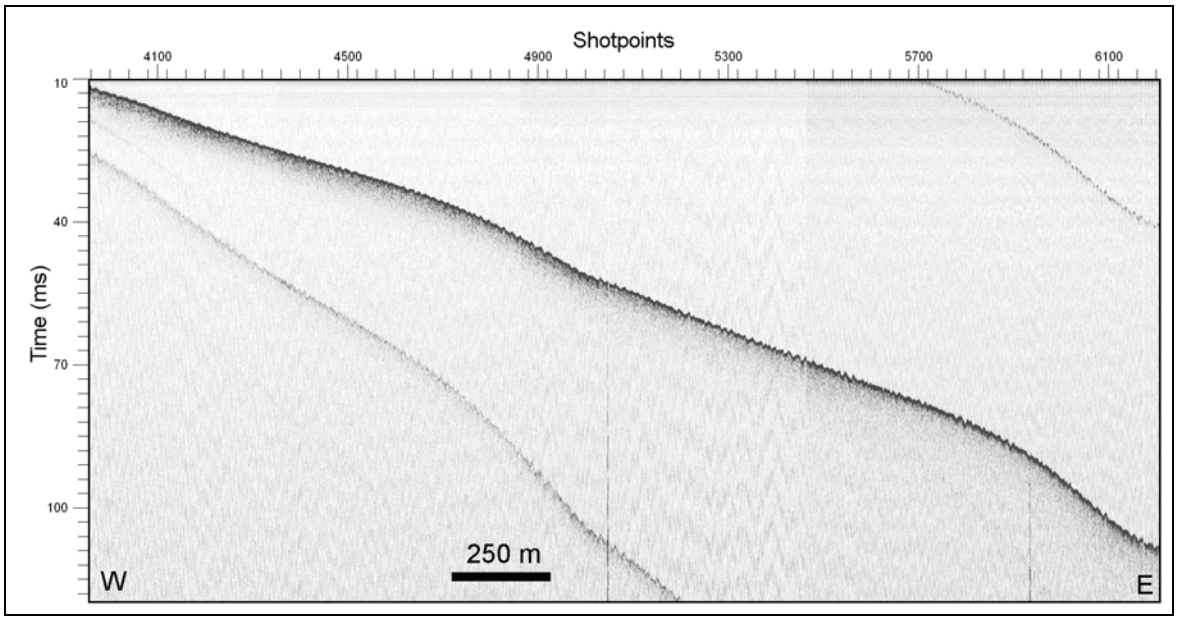

Figure 95 - Chirp seismic profile from the northern area of sector E showing that this area is composed by the echo type I-A. Echo type I-A is interpreted to result from the presence of sand and gravels. See location in Figure 77.

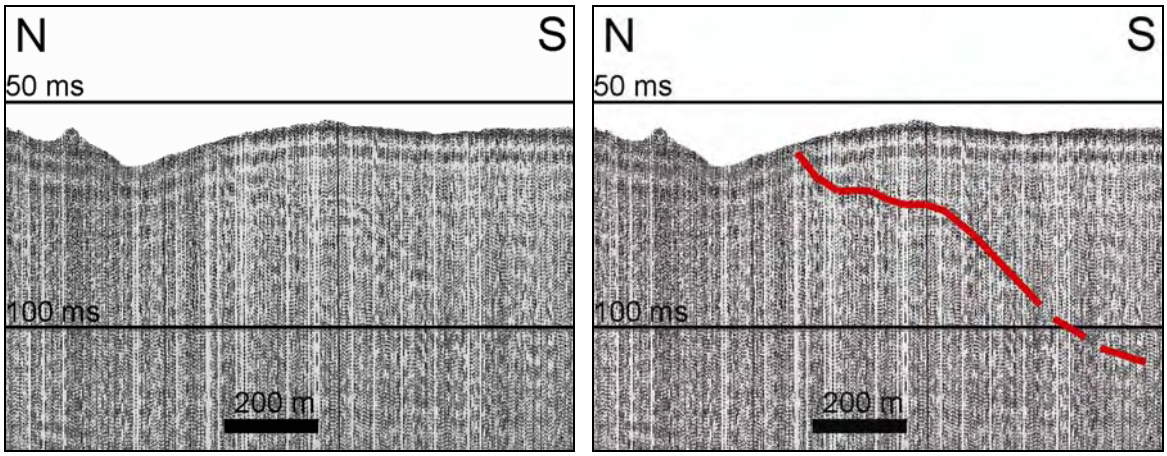

A B

Figure 96 – Boomer seismic profile on sector E showing the sedimentary unit thinning towards coarse clastic deposits. A: Non-interpreted seismic profile. B: Interpreted seismic profile. The red line represents the basement of the seismic unit. See location on Figure 76.

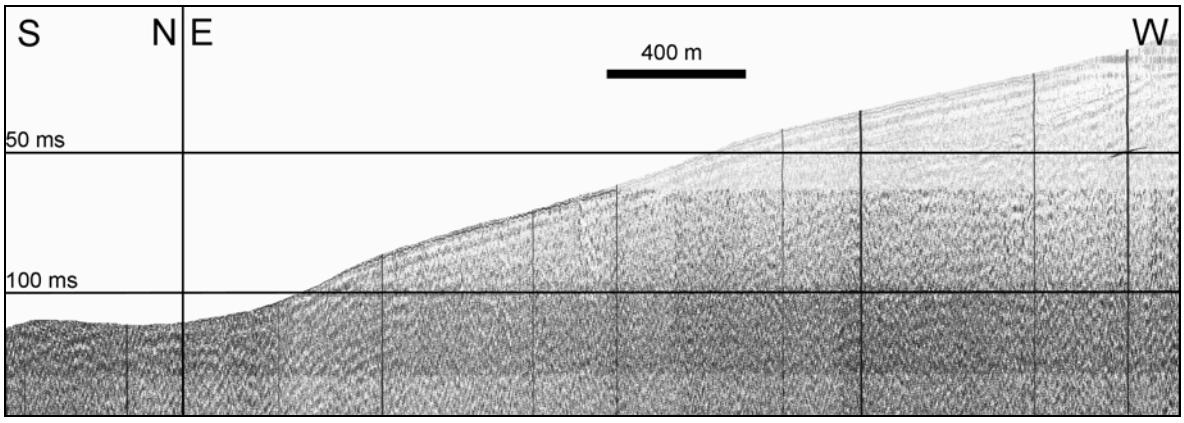

A

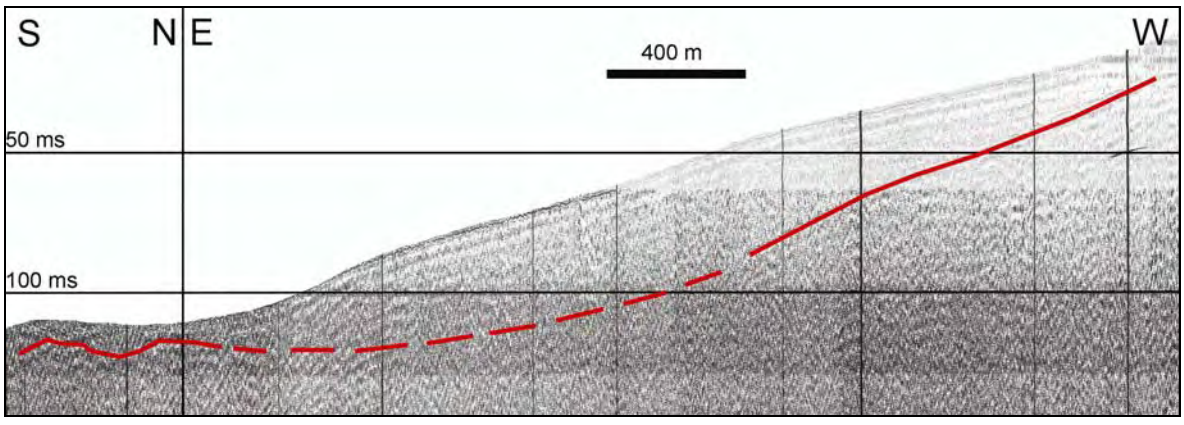

B

Figure 97 – Cross-shore Boomer seismic profile on sector E showing the sedimentary unit thinning both onshore and offshore. A: Non-interpreted seismic profile. B: Interpreted seismic profile. The red line represents the basement of the seismic unit. See location on Figure 76.

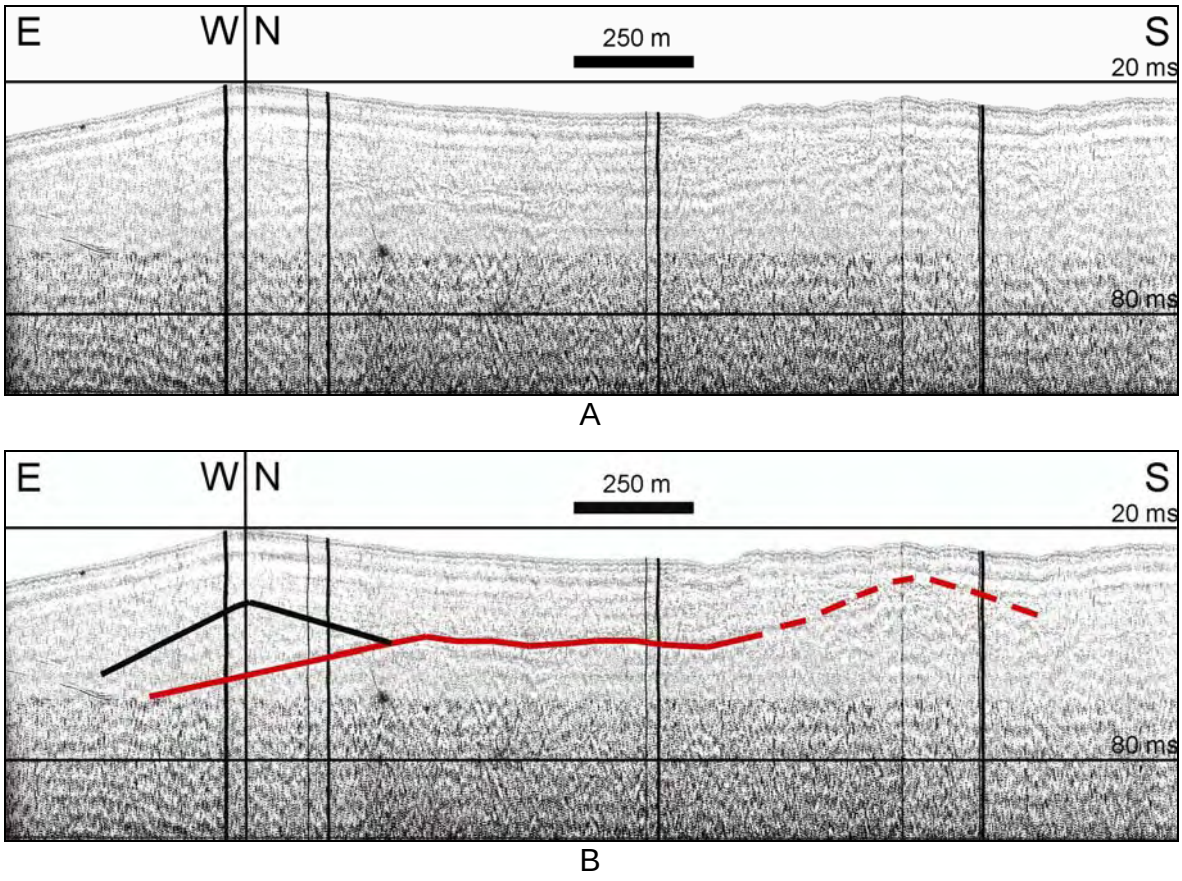

Figure 98 - Boomer seismic profile on sector E showing the lateral variation of the sedimentary unit nearshore. A: Non-interpreted seismic profile. B: Interpreted seismic profile. The red line represents the basement of the seismic unit. The black line represents the multiple of the sea-floor reflection. See location on Figure 76.

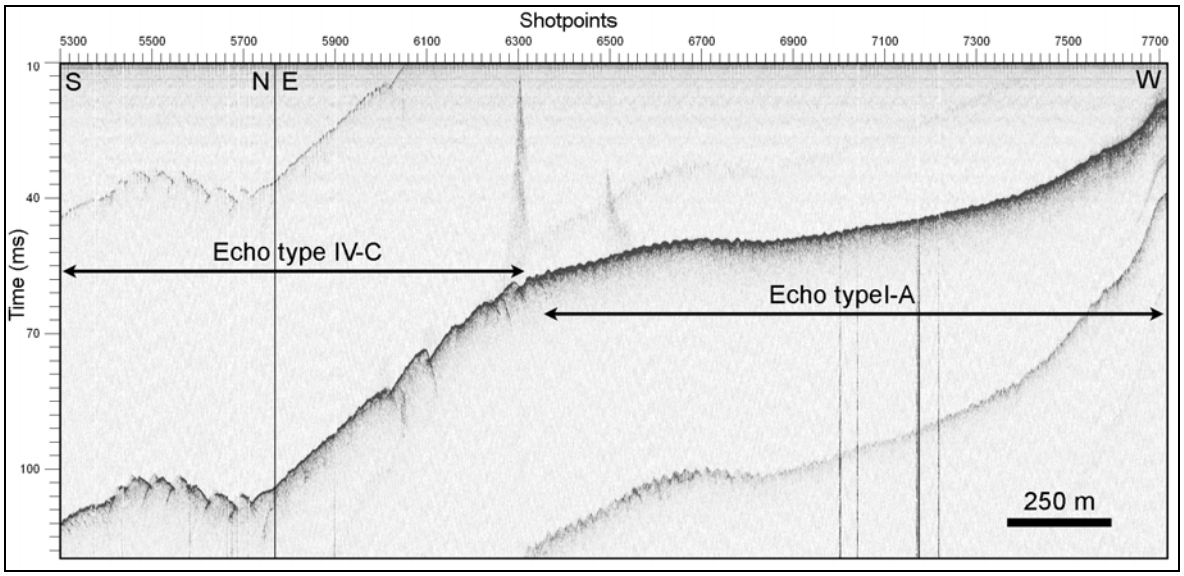

Figure 99 - Chirp seismic profile of the southern area of sector E showing that nearshore this area is composed by the echo type I-A and further offshore by the echo type IV-C. Echo type I-A is interpreted to result from the presence of sand and gravels and echo type IV-C from a sand-wave field. See location in Figure 77.

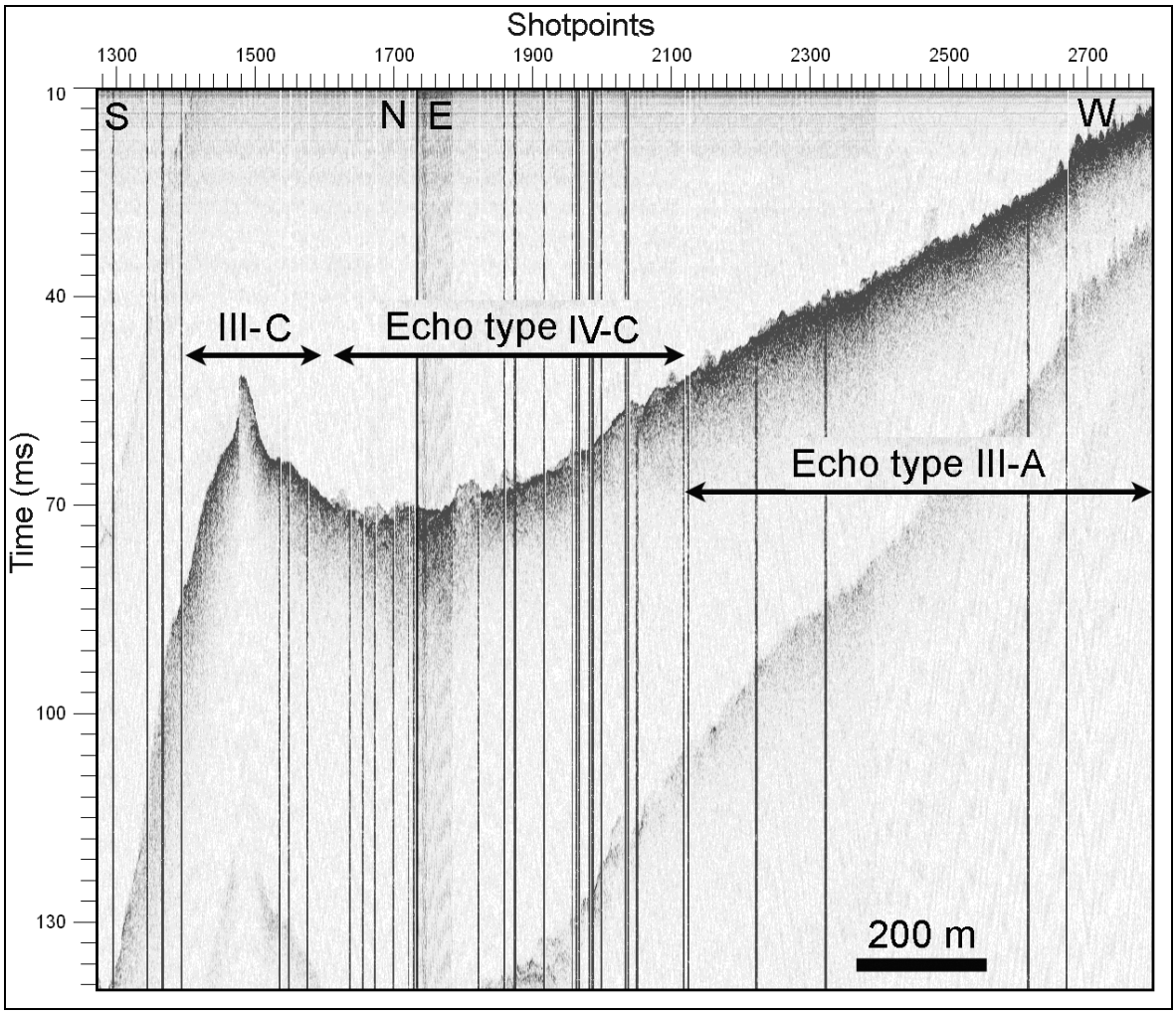

Figure 100 - Chirp seismic profile offshore of Ponta da Espalamaca showing that nearshore this area is composed by the echo type III-A, further offshore by the echo type IV-C and the echo type III-C. Echo type III-A is interpreted to result from coarse clastic deposits (boulder-size), echo type IV-C from sand-waves and the echo type III-C from a submarine cone. See location in Figure 77.

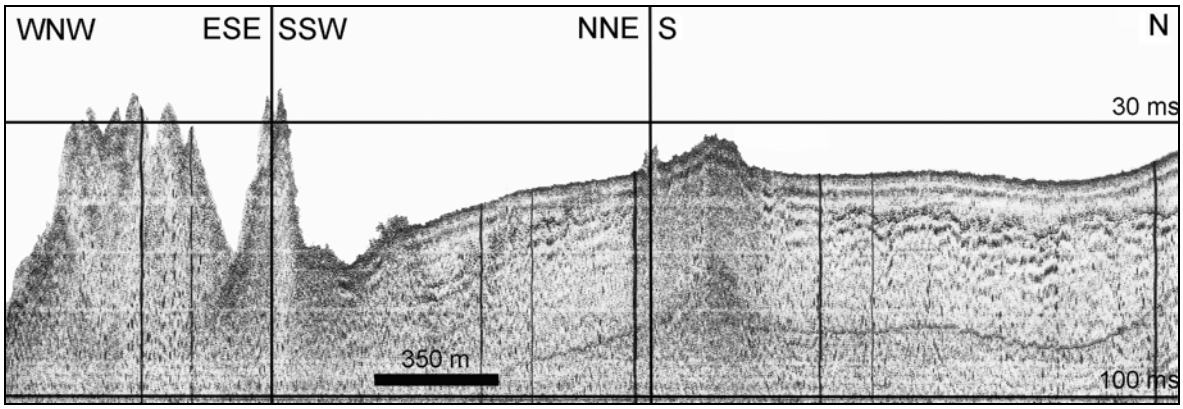

A

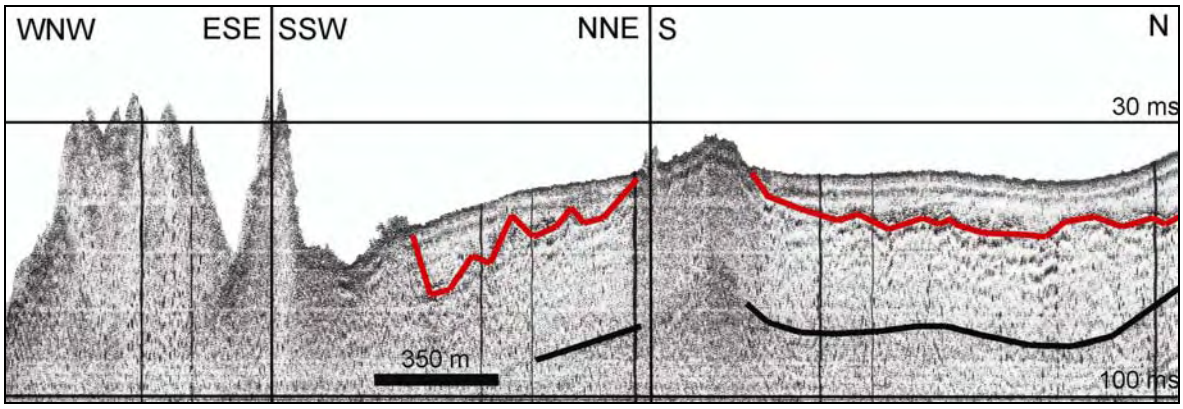

B

Figure 101 - Boomer seismic profile on sector E showing the lateral variation of the sedimentary unit nearshore. A: Non-interpreted seismic profile. B: Interpreted seismic profile. The red line represents the basement of the seismic unit. The black line represents the multiple of the sea-floor reflection. The rocky outcrops mentioned in the text are those in the N-S section of the profile. The volcanic cones from section WNW-ESE are the submarine part of Monte da Guia and belong to sector F. See location on Figure 76.

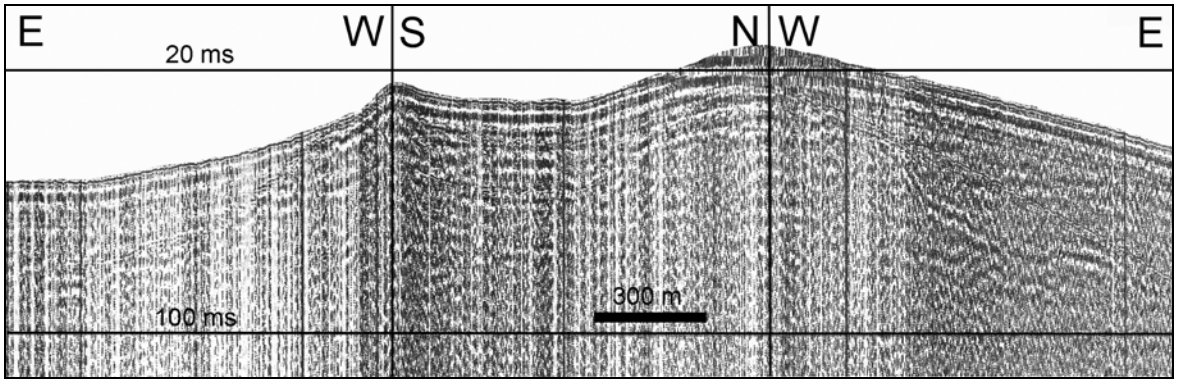

A

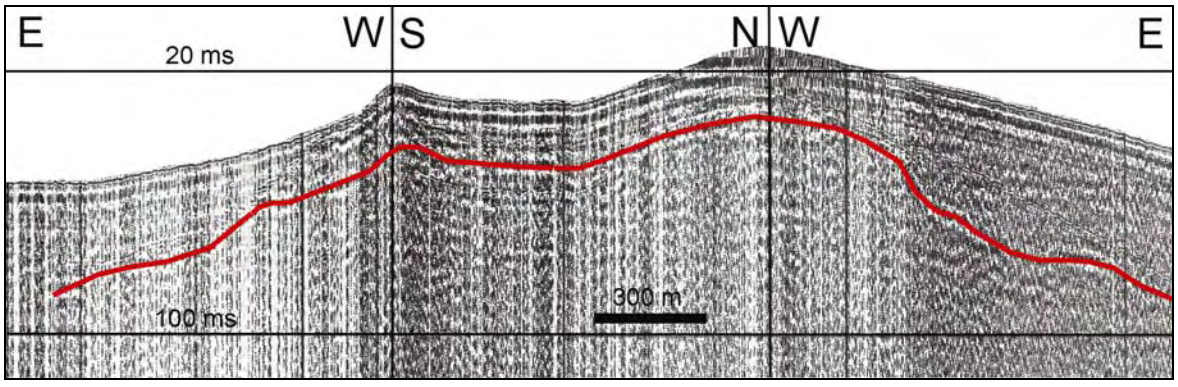

B

Figure 102 – Boomer seismic profile on sector E showing the lateral variation of the sedimentary unit thinning nearshore. A: Non-interpreted seismic profile. B: Interpreted seismic profile. The red line represents the basement of the seismic unit. See location on Figure 76.

Splitting the northern from the southern sub-sectors is the submarine rocky

development of Ponta da Espalamaca (Figures 56, 57, 77 and 100), with high slope gradients that can reach values higher than 10º between 50 and 100 m water depths. As already mentioned in section 2.4 of Chapter 2, these high slope gradients correspond to a bathymetric separation of the sub-sectors made by a lineament of submarine cones which is visible in Figure 100 as the echo type III-C. The southern sub-sector shows a rather smoother area, sloping below 2º in front of the city of Horta, reaching even less than 1º between 30 and 40 m water depths (Figures 56 and 57). This area is almost entirely covered by sand and gravels (Figure 77), speckled by some rock outcrops (Figures 76 and 101). It is within these depths that a sedimentary body has been mapped reaching a thickness of 40 meters (Figures 76, 101 and 102). Beyond these depths the slope increases offshore reaching almost 6º offshore Monte da Guia. In almost the entire sector the offshore sedimentary cover has large wavy bedforms that trend WNW-ESE that are apparently conditioned by the main graben structures that are found on the Pedro-Miguel Graben region (Figures 70, 77 and 99).

Sector F is the shelf area that corresponds onshore to the area between Monte da Guia and the coastline 1 km west of Porto da Feiteira (see Figure 51 in Chapter 2 and Figure 77). This sector shows a rather uniform area with slopes ranging between 2 to 4º (Figure 57). It is normally composed nearshore by a 300 to 700 m wide-belt of coarse clastic deposits (Figures 77 and 104), being the exception a nearshore well preserved lava flow in the eastern part of sector F (Figures 77 and Figure 103). Further offshore the sand and gravels dominate (Figures 77, 103 and 104). The western sedimentary body trends W-E and reaches 45 meters thick at 60 meters water depth, decreasing its thickness both landward and seaward (Figures 76, 106 and 107). The eastern body has a more complicated geometry, trending roughly NW-SE, where it reaches 45 meters thick between 30 and 70 meters water depth, decreasing its thickness, both landward and seaward (Figures 76, 105 and 107). Between these two larger bodies, lies an area of relatively thin sedimentary cover, no more than 15 meters thick. The shelf edge has been mapped near Monte da Guia and in the western sub-sector. Just south of Monte da Guia, a very steep area can be found nearshore, higher than 12º in slope (Figures 56 and 57), that corresponds to the southern limit of the

submarine extension of Monte da Guia (Figures 57, 77 and 101). Further offshore, on the western part of Monte da Guia, the slope decreases to 8º and an embayment can be seen (Figures 56, 57 and 77). This embayment is carved on an area composed by sand and gravels and its shape suggests the presence of mass-wasting processes. Once again, this feature is also detectable on the hydrographic map (see Figure 40 in Chapter 2). The shelf edge in sector F has not been mapped in all its extension. The areas where it has been done, it was found a shelf width of 1500 m in the more extended areas with the shelf break at 70 m water depth.

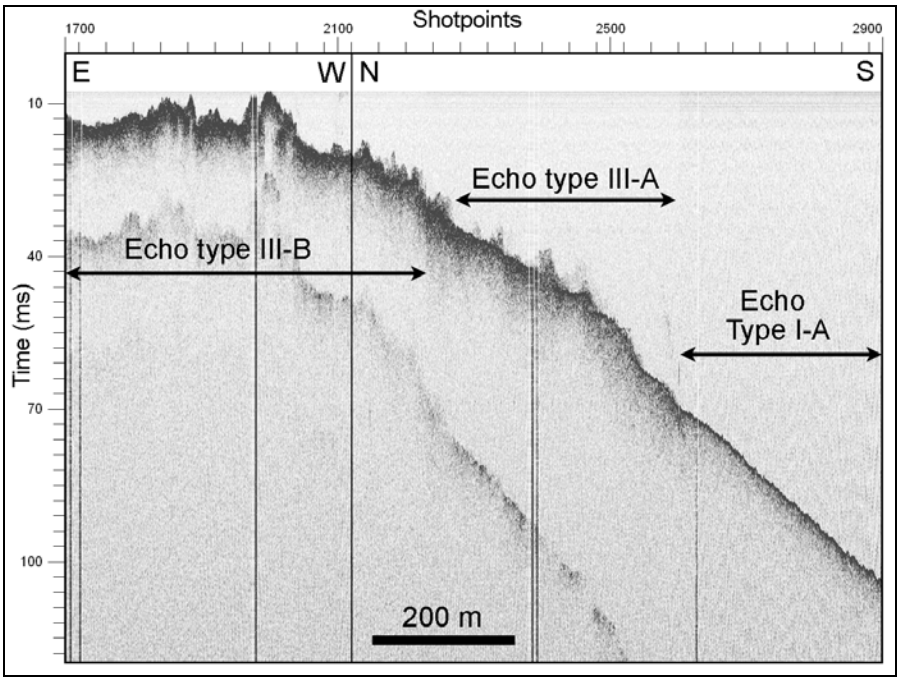

Figure 103 - Chirp seismic profile crossing the sector F showing that this area is composed nearshore by the echo type III-B, further offshore by the echo type III-A that gives place in the deeper areas to echo type I-A. Echo type III-B is interpreted to result from the presence of well preserved lava flows, echo type III-A from coarse clastic deposits (boulder-size) and echo type I-A from the presence of sand and gravels. See location in Figure 77.

Sector G is the shelf area that corresponds onshore to the coastline 1 km west of Porto da Feiteira and Morro do Castelo (see Figure 48 in Chapter 2 and Figure 77). The western sub-sector shows steep submarine slopes ranging from 4 to 6 degrees that flank the island nearshore to a depth that ranges from 30 to 60 meters (Figures 56 and 57). These steeper slopes correspond to lava flows (Figures 77 and 108) and to coarse clastic deposits (Figures 77 and Figure 109)

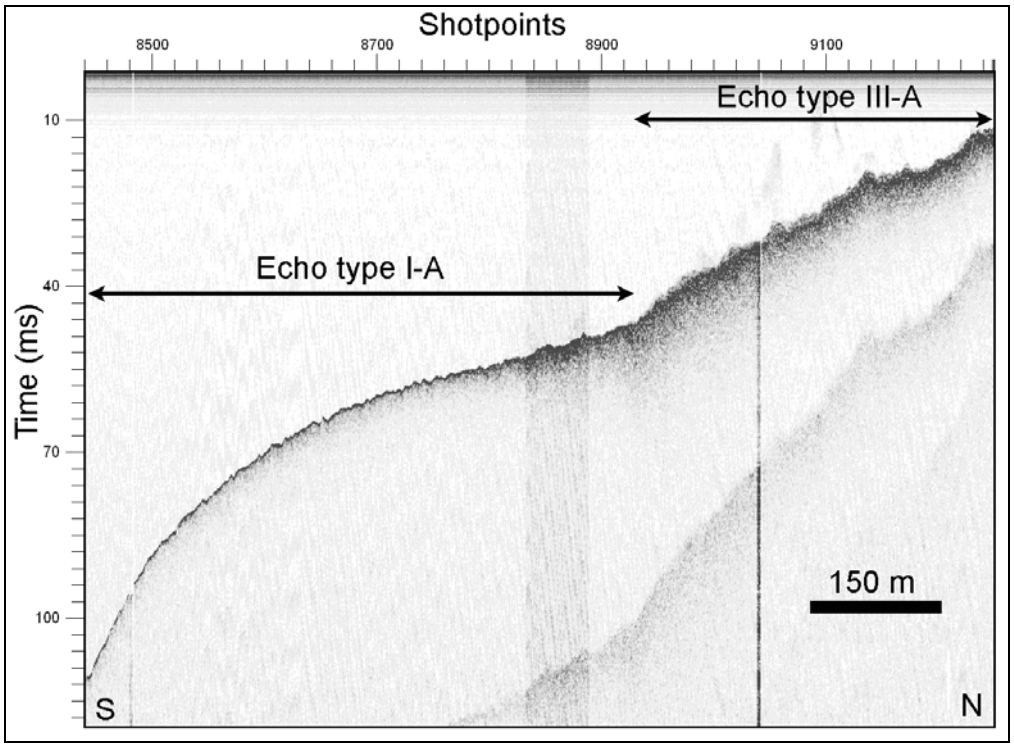

Figure 104 - Chirp seismic profile crossing the sector F showing that this area is composed nearshore by the echo type III-A and further offshore by the echo type I-A. Echo type III-A is interpreted to result from the presence of coarse clastic deposits (boulder-size) and echo type I-A from the presence of sand gravels. See location in Figure 77.

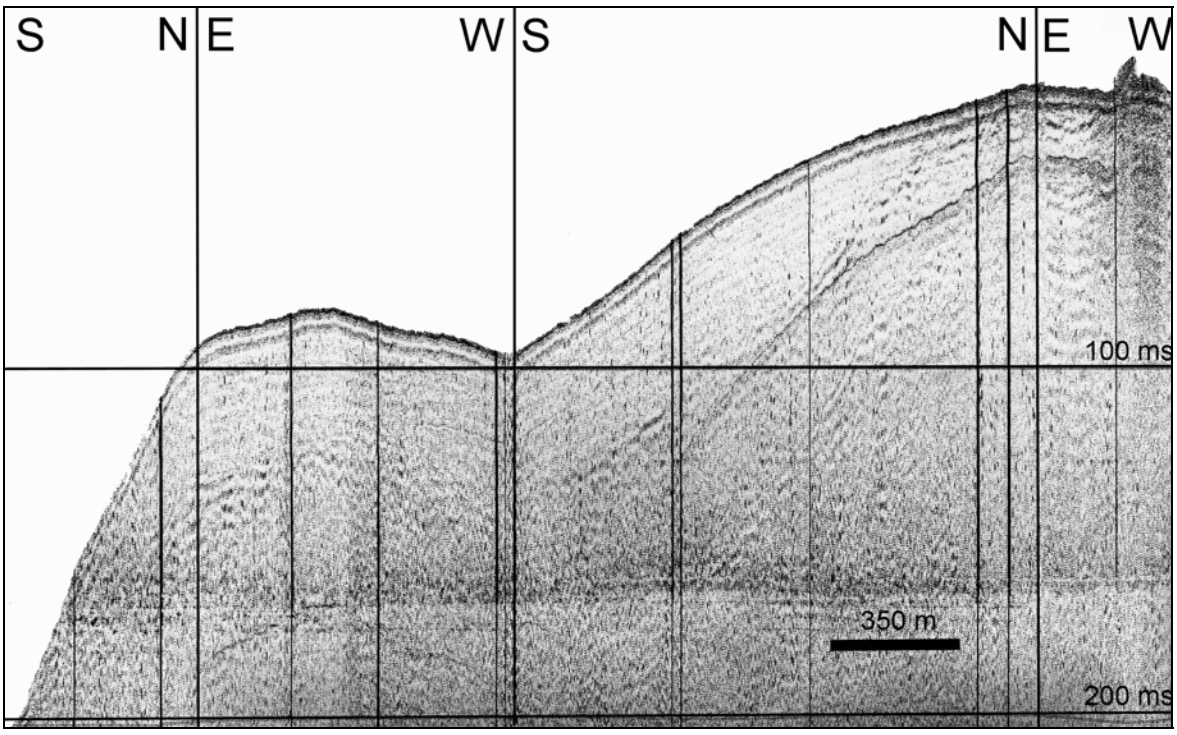

A

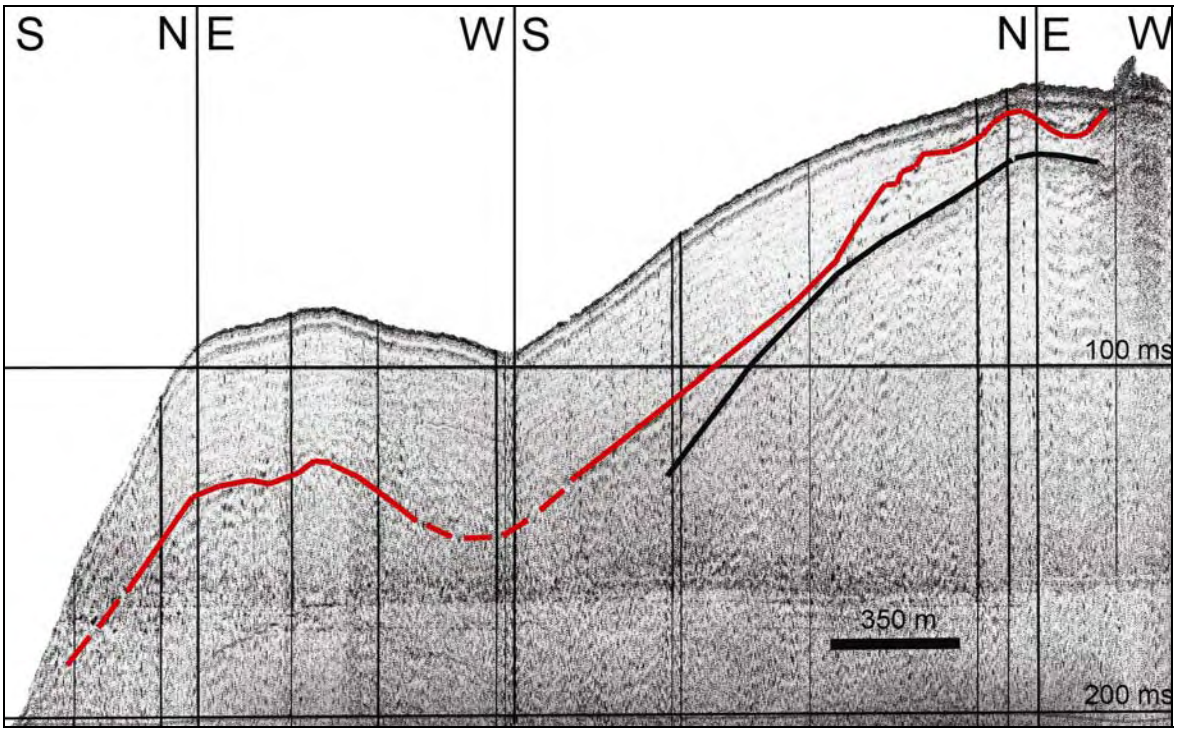

B

Figure 105 - Boomer seismic profile on sector F showing the sedimentary unit thinning both nearshore and offshore. A: Non-interpreted seismic profile. B: Interpreted seismic profile. The red line represents the basement of the seismic unit. The black line represents the multiple of the sea-floor reflection. See location on Figure 76.

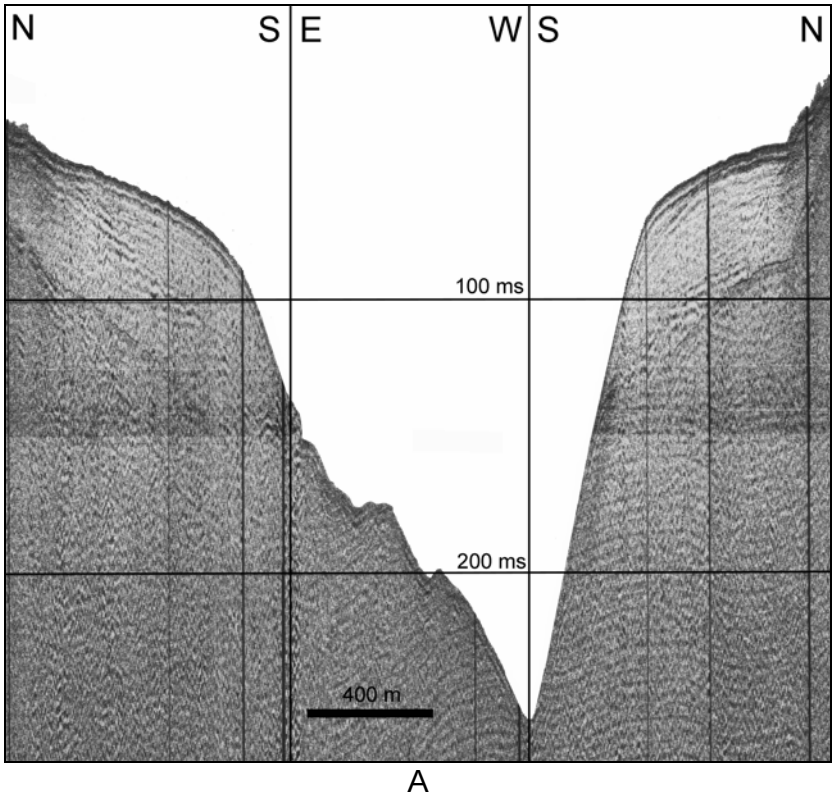

A

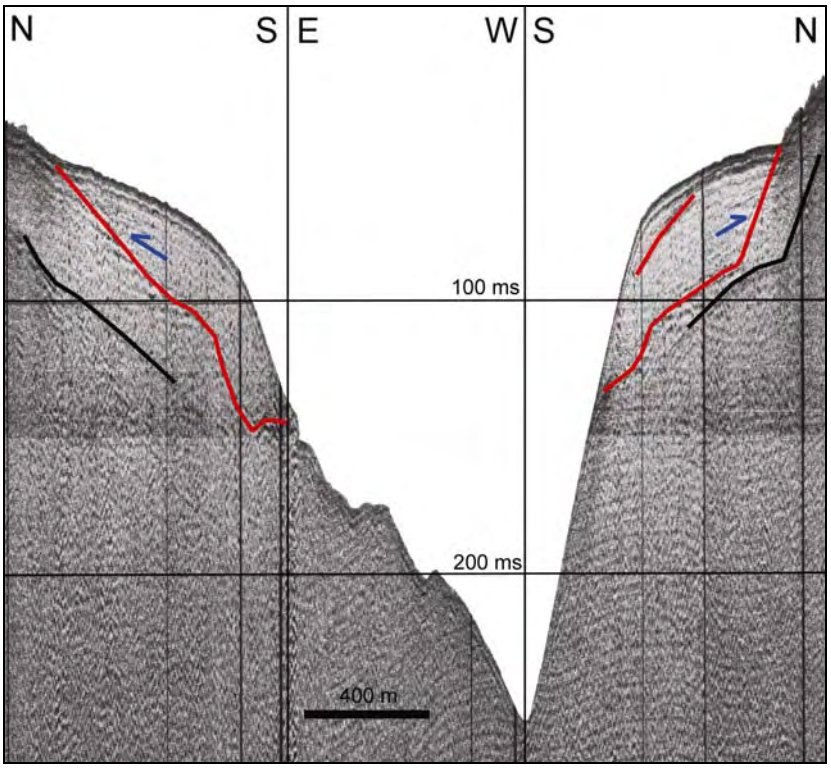

B

Figure 106 - Boomer seismic profile between sectors F and G showing the sedimentary unit thinning both nearshore and offshore. In the S-N section of the profile it is possible to see a a shallower reflection that might be attributed to another sedimentary unit A: Non-interpreted seismic profile. B: Interpreted seismic profile. The red line represents the basement of the seismic unit. The black line represents the multiple of the sea-floor reflection. The right sedimentary body belongs to sector F while the left one is already on the sector G. See location on Figure 76.

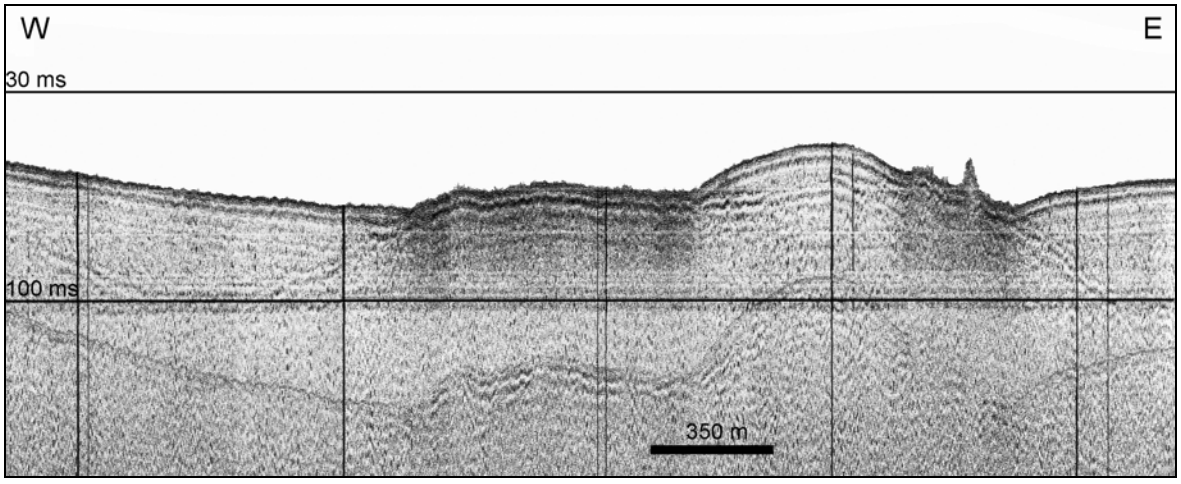

A

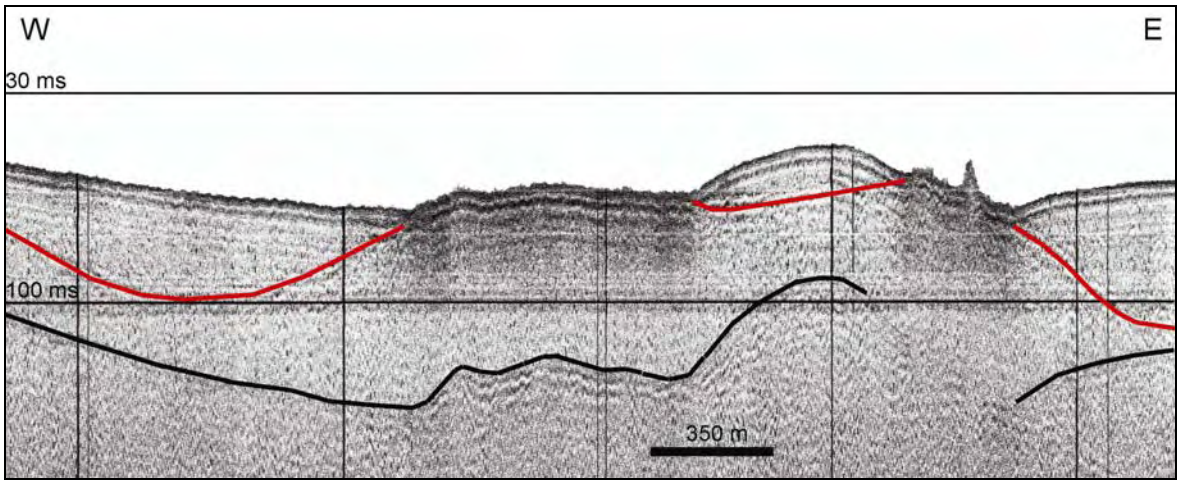

Figure 107 - Boomer seismic profile on sector F showing the longshore variation of sedimentary unit. A: Non-interpreted seismic profile. B: Interpreted seismic profile. The red line represents the basement of the seismic unit. The black line represents the multiple of the sea-floor reflection. See location on Figure 76.

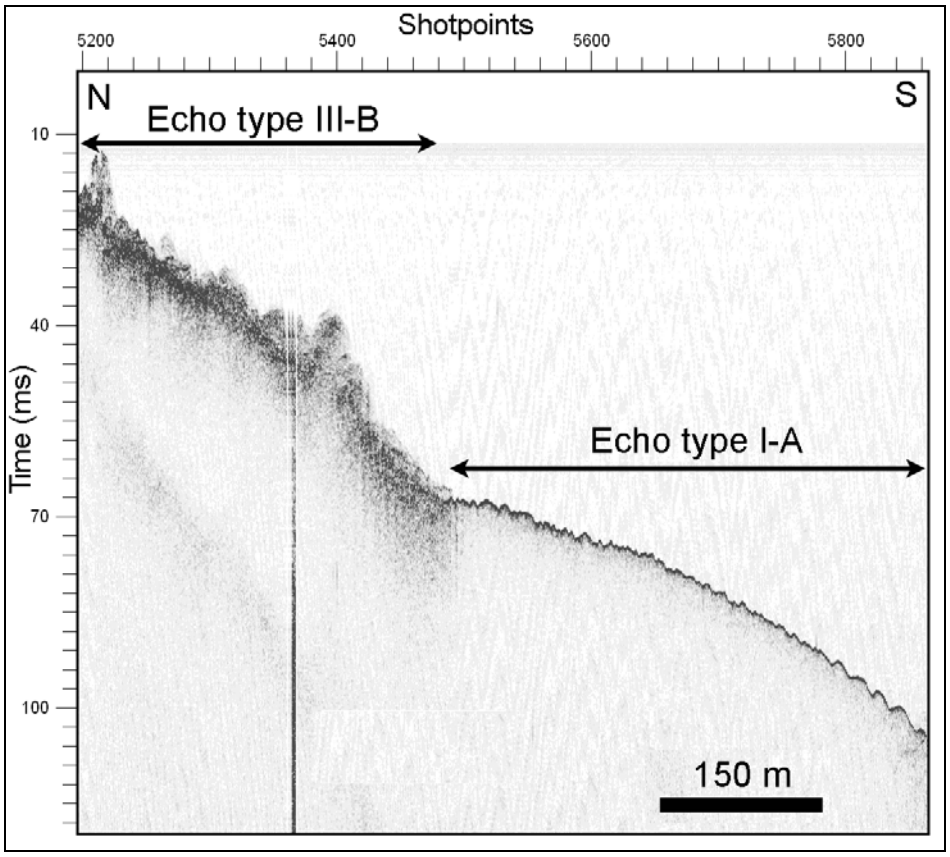

Figure 108 - Chirp seismic profile crossing the sector G showing that this area is composed nearshore by the echo type III-B and further offshore by the echo type I-A. Echo type III-B is interpreted to result from the presence of well preserved lava flows and echo type I-A from the presence of sand and gravels). See location in Figure 77.

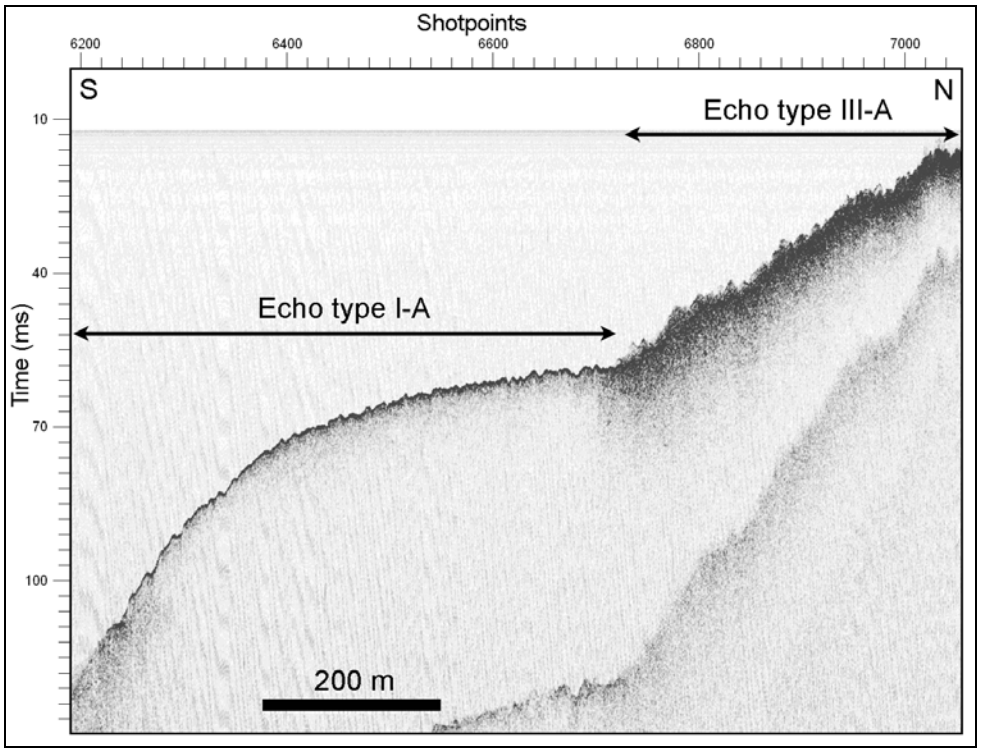

Figure 109 - Chirp seismic profile crossing the sector G showing that this area is composed nearshore by the echo type III-A and further offshore by the echo type I-A. Echo type III-A is interpreted to result from the presence of coarse clastic deposits (boulder-size) and echo type I-A from the presence sand and gravels). See location in Figure 77.

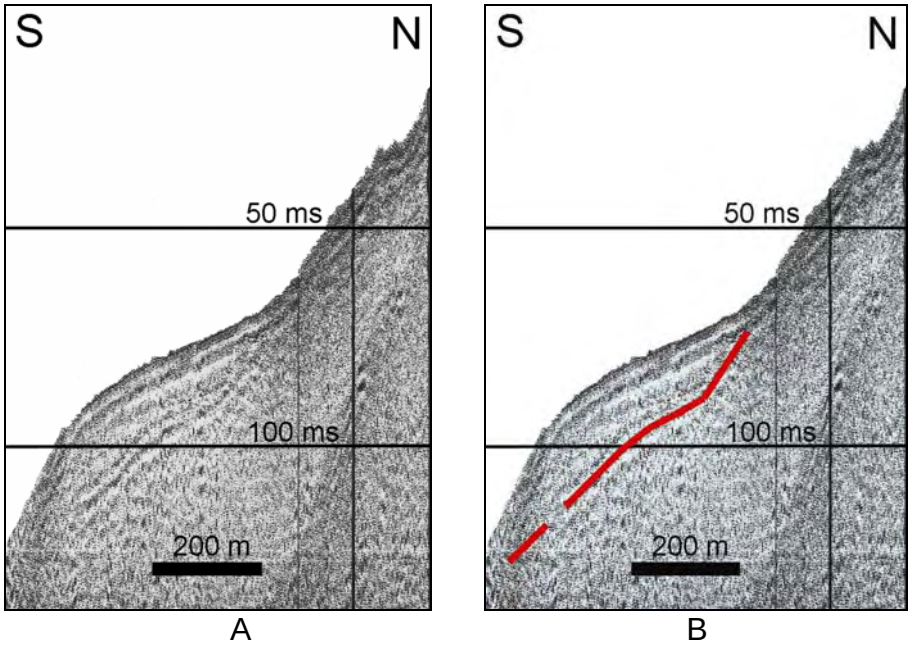

Figure 110 – Cross-shore Boomer seismic profile on sector G showing the sedimentary unit thinning both nearshore and offshore. A: Non-interpreted seismic profile. B: Interpreted seismic profile. The red line represents the basement of the seismic unit. See location on Figure 76.

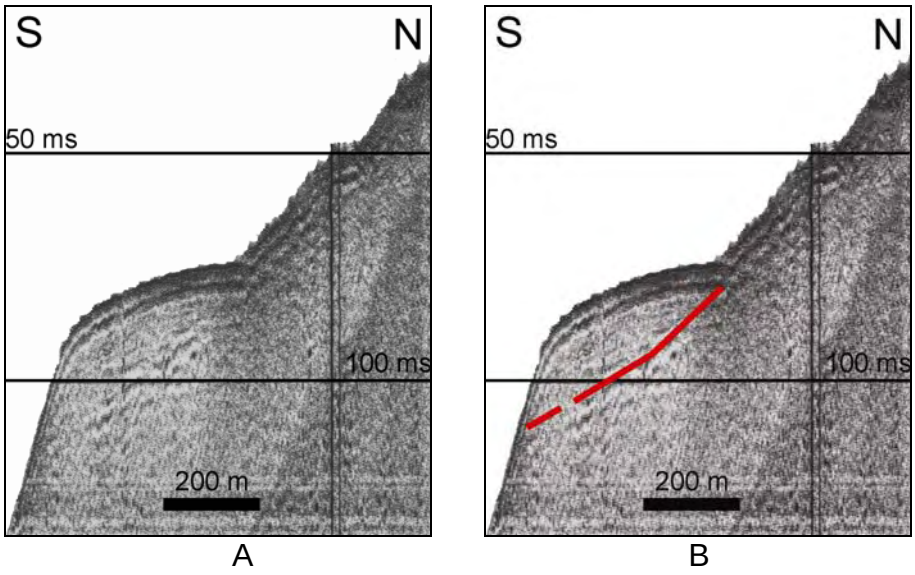

Figure 111 - Cross-shore Boomer seismic profile on sector G showing the sedimentary unit thinning both nearshore and offshore. A: Non-interpreted Boomer seismic profile. B: Interpreted Boomer seismic profile. The red line represents the basement of the seismic unit. See location on Figure 76.

that are replaced offshore by a sedimentary bottom through a change in slope. Beyond these depths a smoother gradient between 2 to 4º covered by sand and gravels (Figures 77, 108 and 109), extends offshore till the shelf edge, where it increases to slopes higher than 5º (Figures 56 and 57). The sedimentary basins trend parallel to the shore with two main bodies (Figures 76, 110 and 111), one in the western part that reaches 40 meters thick at 70 meters water depth, and another in the eastern part that reaches 40 meters thick at 40 meters water depth. Between these two bodies, a thin deposit of sediment occurs, only 15 meters thick. In this sector the shelf edge has been almost fully covered, appearing on average at 60 m water depth. Here, the shelf width varies between 600 and 900 meters (Figures 56 and 57).

Sector H is the shelf area that corresponds onshore to the area between Morro do Castelo Branco and Ponta do Varadouro (see Figure 47 in Chapter 2 and Figure 77). Nearshore, the submarine slopes range from 3 to 4 degrees usually within 30 water depth m (Figures 56 and 57) and correspond to coarse clastic deposits (Figures 77 and 112). Nearshore, westward of the Morro do Castelo Branco are well preserved lava flows (Figures 77 and 113). Further away from the coastline, between 30 and 50 m water depth, the slope decreases to

values below 2º, where sand and gravels dominate (Figures 77, 112 and 113). At depths higher than 50 m the slope increases again, reaching the shelf edge at 60 m water depth. Seaward of the coarse clastic deposits, at water depths below 30 m, a sedimentary body develops with NNW-SSE direction, reaching 50 meters thick at 60 meters water depth (Figures 76, 114, 115, 116 and 117). Its thickness decreases both landward and seaward. Near the coarse clastic deposits (echo type III-A in Figures 72, 112 and 113), within the sedimentary bottom revealed by the presence of the echo type I-A are elongated mound-like deposits parallel to the shoreline, revealed by the presence of the echo type I-B (Figures 72, 112 and 113). The shelf width in the areas where the shelf edge has been mapped is between 900 and 1600 meters. The shelf break appears on average at 55 meters water depth.

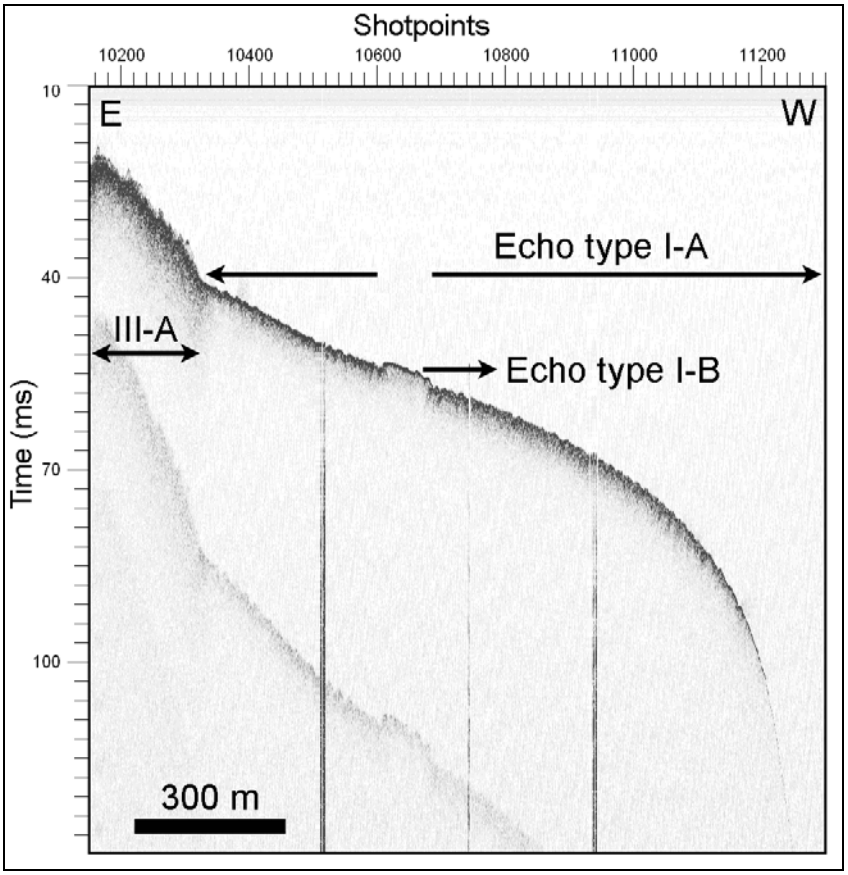

Figure 112 - Chirp seismic profile crossing the entire sector H showing that this area is composed nearshore by the echo type III-A, passing offshore to echo type I-A. Echo type I-B appears in some areas, between the echo types III-A and I-A. Echo type III-A is interpreted to result from coarse clastic deposits (boulder-size), echo type I-A from sand and gravels and echo type I-B from sands. See location in Figure 77.

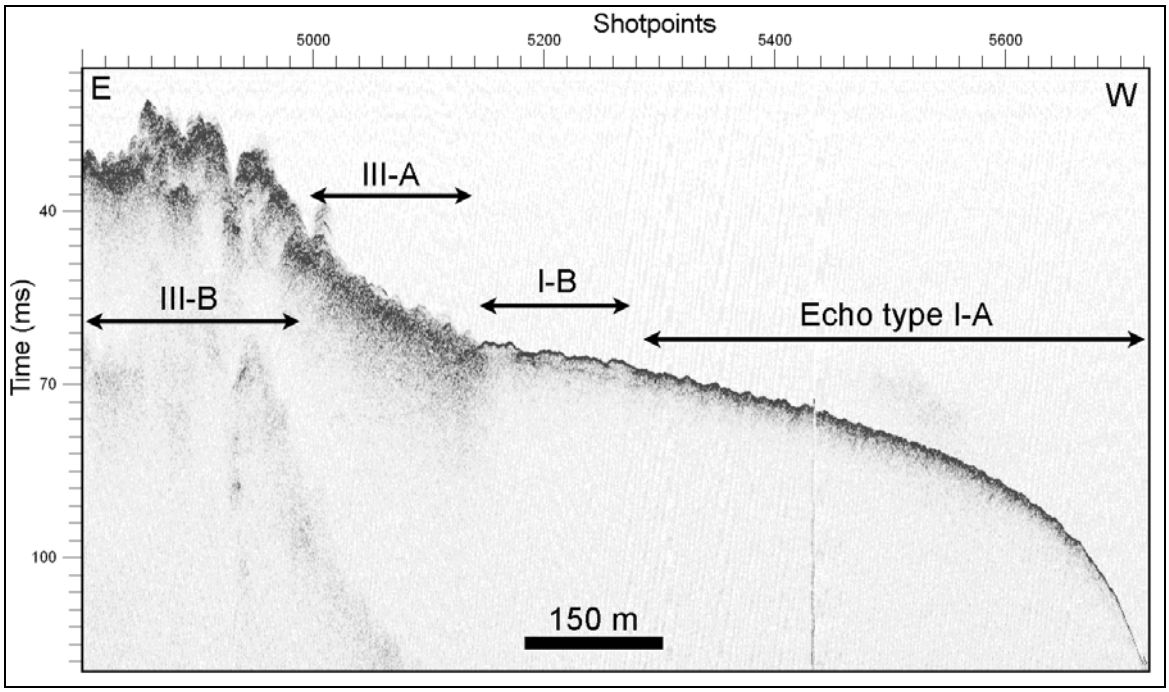

Figure 113 - Chirp seismic profile crossing the sector H showing that this area is composed nearshore by the echo type III-A and further offshore by the echo type I-A. Echo type I-B appears in some areas, between the echo types III-A and I-A. Echo type III-A is interpreted to result from coarse clastic deposits (boulder-size), echo type I-A from sand and gravels and echo type I-B from sands. See location in Figure 77.

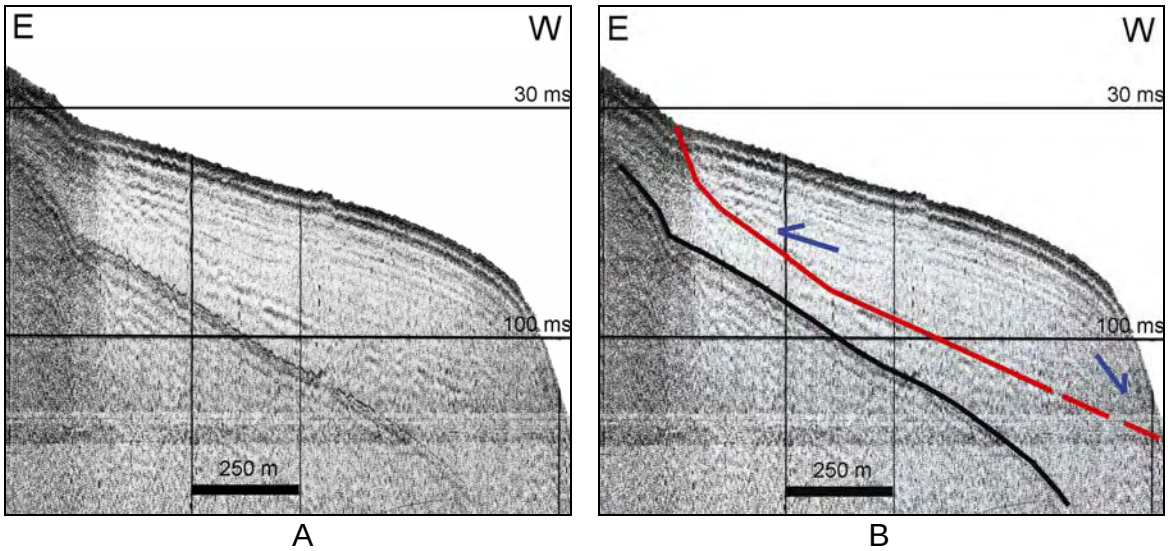

Figure 114 - Cross-shore Boomer seismic profile on sector H showing the sedimentary unit thinning both nearshore and offshore. A: Non-interpreted seismic profile. B: Interpreted seismic profile. Red line represents the basement of the seismic unit. The black line represents the multiple of the sea-floor reflection. See location on Figure 76.

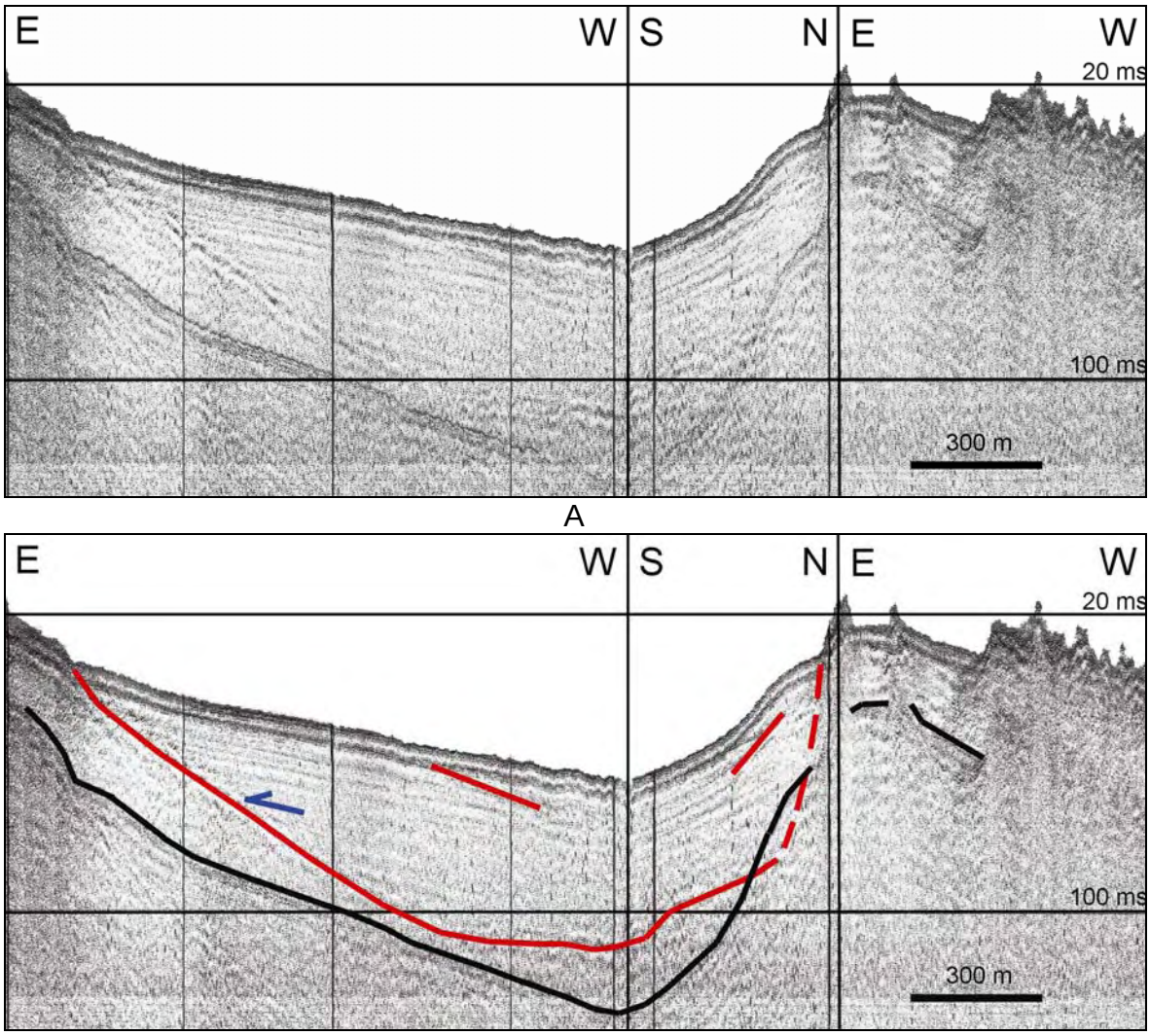

Figure 115 - Boomer seismic profile on sector H showing the sedimentary unit thinning both nearshore and offshore. It is possible to see other shallower reflections that might represent other sedimentary unit. A: Non-interpreted Boomer seismic profile. B: Interpreted Boomer seismic profile. Red line represents the basement of the seismic unit. The black line represents the multiple of the sea-floor reflection. See location on Figure 76.

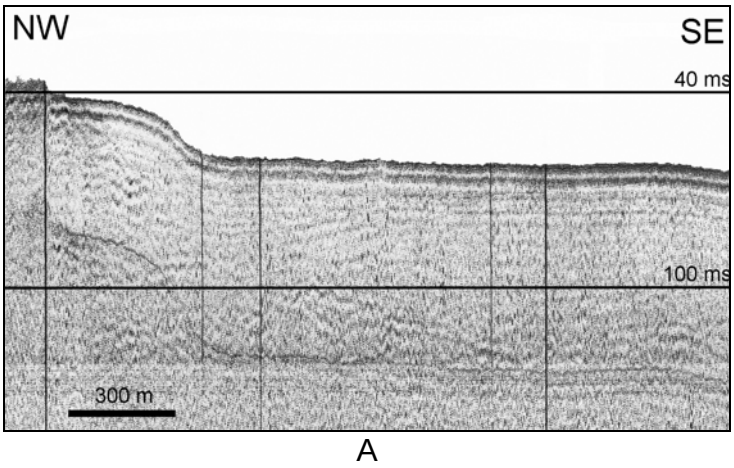

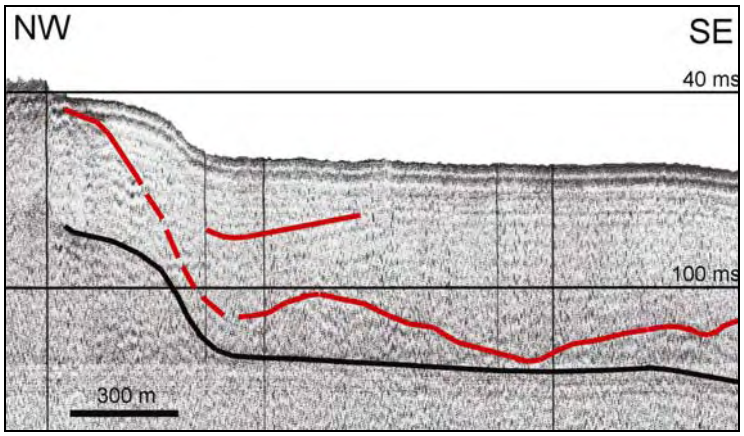

B

Figure 116 – Longhsore Boomer seismic profile on sector G showing the sedimentary unit thinning nearshore. It is possible to see other shallower reflection that might represent other sedimentary unit. A: Non-interpreted seismic profile. B: Interpreted seismic profile. Red line represents the basement of the seismic unit. The black line represents the multiple of the sea-floor reflection. See location on Figure 76.

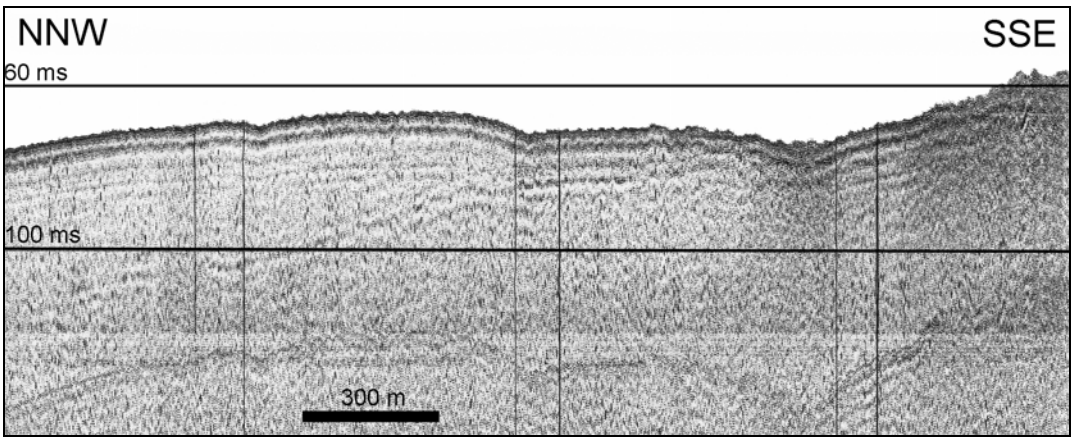

A

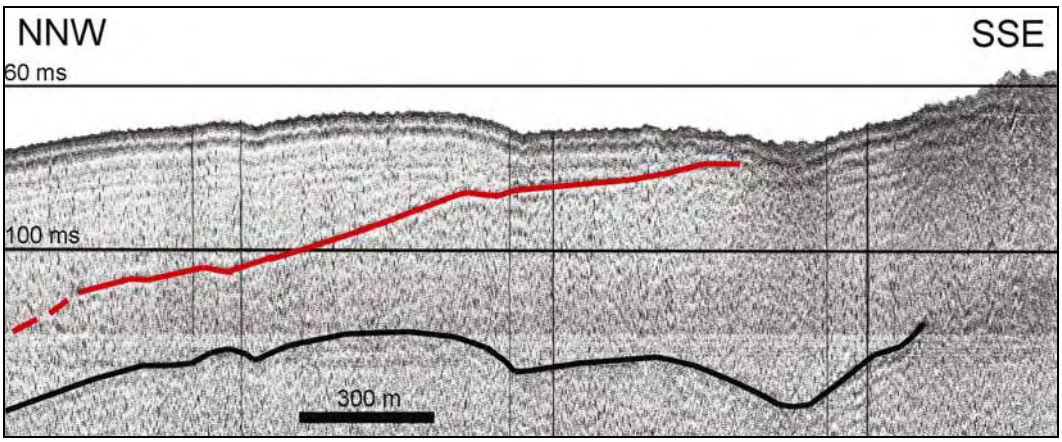

B

Figure 117 - Longhsore Boomer seismic profile on sector G showing the sedimentary unit thinning towards coarse clastic deposits. A: Non-interpreted seismic profile. B: Interpreted seismic profile. Red line represents the basement of the seismic unit. The black line represents the multiple of the sea-floor reflection. See location on Figure 76.

Chapter 4. Present-day processes controlling the shelf morphology

4.1. Introduction

There have been yet very few worldwide geological studies of the shelves of volcanic islands. The investigation of the shelf around the Faial Island offers a unique opportunity to discuss and compare the roles of widely varying parameters such as volcanism, earthquakes, waves, climate, types and amount of sediment and inherited topography in the evolution of the shelf. The combined mapping of the bathymetry, the bottom echo character and the geographical distribution of the sedimentary bodies have provided an important contribution for the discussion that follows about the role of the physical parameters that control the geological differences found on the shelf.

4.2. Coastal erosional processes

The coastline of the Faial Island is mostly rocky and shows signs of coastal retreat. The most obvious evidence of retreating, comes from the topographical surveys of Machado and Freire (1985) in the littoral zone of the Capelinhos volcano that found erosion rates of 20 m/year during the period of 1958 to 1981 (see Figure 52 from Chapter 2). All the other costal sectors (Figures 118, 119, 120, 122 and 123) show frequent accumulation of a small subaerial belt of rock debris at the base of the cliffs, even in places where the shelf is exclusively covered by sediments. They also show a sharp angle at their base that result from mass-wasting activities. The presence of all these rock debris at the cliff bases suggests that these are eroding essentially through mass-wasting processes that generate large blocks instead of fine sediments. Possible causes can be related to high rates of **marine erosion** (cliff undermining), **earthquakes** triggered by

volcanism or local tectonics and **cliff weathering**.

Marine erosion is a constant destabilizing agent, since erosion at the sea-cliff base erodes the bedrock, removes debris, steepens the coastal slope and produces instability that results in persistent recession (Bray and Hooke, 1997). The presence of very coarse sediments at the base of the Faial cliffs enhances the scouring effect at their base, promoting the instability. On the other hand, low cohesive strength deposits such as hyaloclastites, pyroclastic layers, and littoral cones (e.g. Capelinhos, Monte da Guia) are highly susceptible to subaerial erosion (Keating and McGuire, 2000). Even more resistant cliffs are prone to erosion if they have steeper slopes. Higher cliffs retreat more rapidly (though still slower than soft cliffs) because they generate higher shear stresses and are affected by larger landslides (Richards and Lorriman, 1987 in Keating and McGuire, 2000). Dramatic slope failures occur most often where the slope angle exceeds twenty degrees (Keating and McGuire, 2000). Not surprisingly, 85% of the cliffs of Faial have slopes higher than 20 degrees which make them good candidates for frequent landsliding (Figures 118 to 124). These causes explain why some coastal zones of the Azorean Islands have high erosion rates with several examples reported. In S. Miguel Island, the average rate of retreat is 0.21 m/year, but can reach, in some cases, rates as high as 1.01 m/year (Borges, 2003). According to Malheiro (2006) the south coast of Faial is mainly formed by compound pahoehoe lava flows, made up of thin units, with interbedded lenses of clinkers and fragmented lava, which are easily eroded by wave action and winds. Consequently, various littoral caves are formed (Figure 121), some of large size (at least 10-m long), extending under the road that connects the town of Horta to the airport. The other sectors of the Faial coast are also prone to cliff erosion and consequently, 76.2% of these, were classified by Borges (2003) as secondary coasts, molded by marine erosional processes, using the modified coastal classification of Shepard's (1973),

Earthquakes are the most obvious triggers for the generation of onshore landslides (Malamud et al., 2004). Historical compilations of seismicity in the Azores show that, on average, every 70 years an earthquake with Ms exceeding 6.5 occurs (Nunes et al., 2004). The historical records from Faial show intensities

Figure 118 - Coastal cliffs from sector B. The cliffs are composed of alternation of lava flows and more friable materials. The cliffs are very steep and their bases show a vertical angle caused by mass-wasting processes with accumulation of rock debris (Fernando Tempera © *ImagDOP*).

Figure 119 - Coastal cliffs from sector D. The cliffs are composed of alternation of lava flows and friable materials. The cliffs are very steep and it is possible to see at their bases a vertical angle caused by mass-wasting processes with accumulation of rock debris (Fernando Tempera © *ImagDOP*).

Figure 120 - Coastal cliffs from sector E. The cliffs are very steep and show at their toes a belt of pebbles (Fernando Tempera © *ImagDOP*).

Figure 121 - Coastal cliffs from sector F. The cliffs show various littoral caves that form because of erodible material that composes them (Fernando Tempera © *ImagDOP*).

Figure 122 – Very steep coastal cliffs of sector G. It is possible to see a more friable material sandwiched between two lava flows. The cliff show at their toes, accumulation of rock debris due to mass-wasting processes (Fernando Tempera © *ImagDOP*).

Figure 123 – Coastal cliffs from sector H. The cliffs are very steep and their bases show often a sharp angle and accumulation of rock debris due to mass-wasting processes (Fernando Tempera © *ImagDOP*).

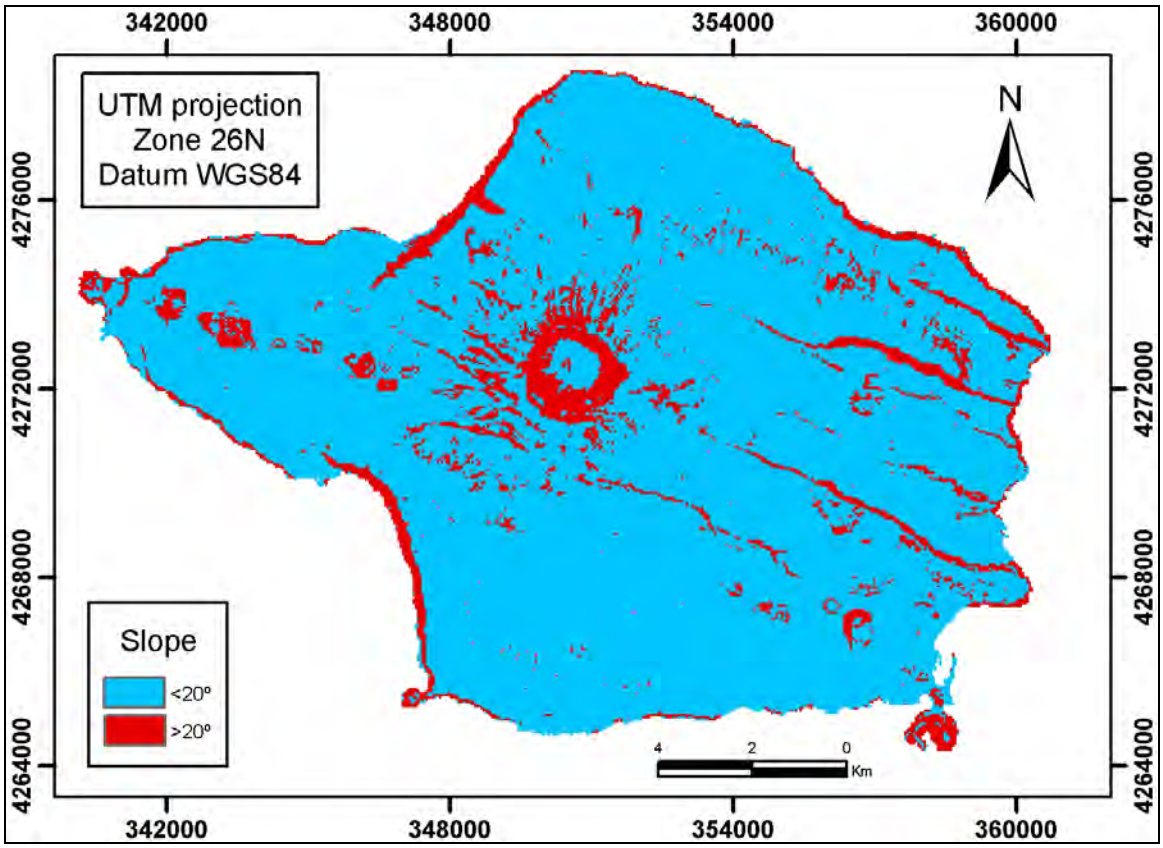

Figure 124 – Faial Island subaerial slope map based on the altimetry of the Instituto Geográfico do Exército map (2001a; 2001b; 2001c; 2001d), using the ArcGis 9.0 GIS running 3D Analyst extension. This figure shows that most of the cliffs in Faial have slopes higher than 20º.

of, X (1926), VII (1945), VIII/IX (1958), VIII/IX (1998) of the Modified Mercalli Scale

and magnitude 5.8 on the Richter scale for the 1998 earthquake. As a cliff is steadily undermined at its base, it will progressively become more unstable until a relatively small trigger is enough to make it collapse. Because the Azores are a moderate to high seismicity region, even when the cliffs are not very unstable the rate of cliff landsliding might be considerable. According to Malheiro (2006), some of the major landsliding events in the Azores are typically triggered by earthquake-induced ground shaking. Valadão et al. (2002) produced a landslide density map of S. Miguel Island based on historical documents, aerial photographs and field observations. A significant portion of them are localized in the sea cliffs (Figure 125) and appear to be triggered by earthquakes whether or not associated to volcanic eruptions. Some of the earthquake-triggered landslides in 1998 Faial event were located along the steep coastlines of Faial and S. Jorge Islands (Malheiro, 2006). According to Coutinho (2000) the 1998 earthquake has provoked retreats of 10 meters in the cliffs close to the offshore epicenter (coastal sector D), showing that seismicity plays a significant role in cliff landsliding on the Azorean islands. Malamud et al. (2004) suggests that bedrock landslides and massive rock falls are the dominant contributors to the long-term erosion in seismically active tectonic zones. They estimate erosion rates of 0.01–0.7 mm/year related to onshore landslides adjacent to plate boundary strike-slip fault zones and according to Borges et al. (2007), the Faial Island falls within a zone (30°W to 27°W) where earthquakes show a predominant strike–slip motion with extension in the direction NE-SW. Although Malamud et al. (2004) work does not directly apply to coastal cliff landslides it is obvious from the works of Coutinho (2000) and Malheiro (2006) that earthquakes contribute to coastal retreat in the Faial Island. The majority of the landslides provoked by the 1998 earthquake referred by these two authors are located in the coastal sector D which means that probably coastal sectors with orientation NNW-SSE (such as C and D) are more prone to earthquake induced landslides. The reason for this might be the predominant strike–slip motion with extension in the direction NE-SW that earthquakes provoke in the Faial zone (Borges et al., 2007), which is perpendicular to the direction of the coastal C and D sectors (see Figure 77 for sectors definition). This NNW-SSE direction is also expressed as fault scarps in other areas of the island (see other NNW-SSE

alignments with slopes higher than 20º in Figure 124 and compare them with the mapped faults in Figure 43 in Chapter 2).

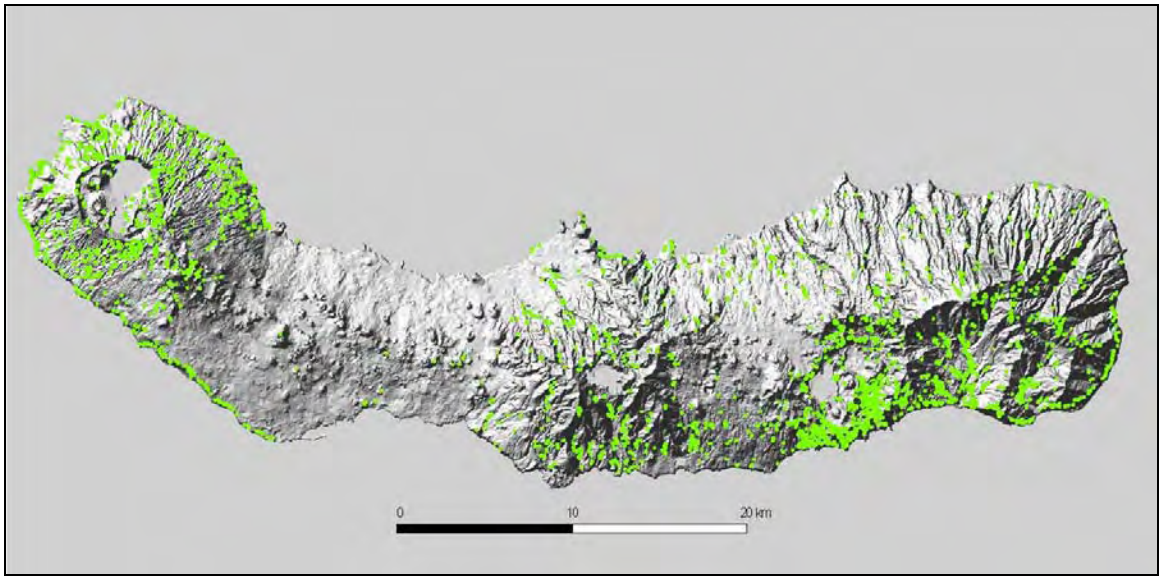

Figure 125 - Landslide Density Map for S. Miguel Island. Each green dot represents one landslide. A total of 2818 events are shown (Valadão et al., 2002).

Precipitation is also an important environmental factor in weathering and ultimately cliff failure. Increased precipitation will increase the alteration of rock to clays and increase pore pressure in the rocks (Keating and McGuire, 2000). Indeed, Valadão et al. (2002) and Malheiro (2006) report that the intense and long-duration precipitation is another reason for the triggering of major landslides in Azores. In addition to the high annual precipitation rates in Faial (980 to 1031 mm/year in the coastal area and 2860 mm at 700 m above sea level), the high mean annual high temperatures (17.5 ºC) and high mean annual relative humidity (≈80%) contributes significantly to weathering and consequently to landsliding.

In conclusion, the Faial Island is very prone to cliff erosion through mass-wasting processes due to its geologic and climatic setting. It remains however to assess which of the three processes mentioned (marine erosion, earthquakes induced landslides and precipitation) are predominant in the cliff retreat. According to Emery and Kuhn (1982) a sharp angle at the sea-cliff base generally indicates active marine erosion, whereas a smooth curve at the base and vegetation on top of it means that subaerial erosion may dominate. Furthermore, steep cliffs tend to

form where marine processes are important, whereas convex profiles develop if subaerial processes are most important (Emery and Kuhn, 1982). The coastline of Faial is dominated by steep coastal cliffs (with angles normally higher than 20º - see Figure 124) and with a sharp angle at the base, which means that the dominant process responsible for coastal retreat is marine erosion. Furthermore, in microtidal regimes the waves are more effective at eroding the cliffs, because the period that the tide will occupy certain level is bigger (Trenhaile, 1987), which is the case for the Faial Island (see section 2.2.2 in Chapter 2). It is also possible that earthquakes have a major role in the cliff retreat. This supposition is highly supported by the evidences mentioned by Malheiro (2006) and by Coutinho (2000), especially the coastal sectors with NNW-SSE direction. In addition, the compilation of Andrade et al. (2006) showed that most of the recorded tsunamis were generated by earthquakes, which reveals the importance of the earthquakes in the modelling of the coastline. Although the volcanic rocks are very prone to chemical weathering and the Azores climate is wet and relatively hot, it appears that the subaerial erosion is less predominant and this fact is supported by the cliff morphology.

4.3. Shelf processes

4.3.1. Shelf sedimentary model

As mentioned in Chapter 1, the island shelf origin is normally linked to a decrease of the island volcanism. The erosive processes (surf erosion linked to the sea level oscillations) increase in proportion to the volcanic processes, initiating an incipient shelf by cutting the island subaerial slopes. Since the volcanic phases that originated most of the subaerial part of the island are considerably old (800 Ka for the Pedro Miguel Graben region and 470 Ka for the Caldeira Volcano – see Figure 43 in Chapter 2) the respective adjacent shelf sectors have probably also began their formation long ago. Consequently, the morphology and geological composition of these shelf sectors must reflect their considerable age.

It is today well known, the concept of stratigraphic cyclicity where the work of Mitchum Jr. et al. (1977) have shown that most continental margins present several depositional sequences whose formation is in great part related to eustasy. Sequence stratigraphy provides a tool to classify the architecture of these sedimentary successions. This new methodology has shown that depositional sequences, bounded by unconformities and correlative conformities, can be subdivided into systems tracts (Van Wagoner et al., 1988), which origin is also strongly related to eustasy. During this period the Azores has suffered several sea-level oscillations (see Figure 34 in Chapter 2). Therefore it ought to be expectable to find on the shelf several depositional sequences, which could have expression in the Boomer seismic records as more than one sedimentary unit. There are presently five sequence stratigraphic models (Catuneanu, 2002) that are currently in use (Figure 126). Their main differences remain in the style of conceptual stacking of strata into sequences (Figure 127). The diversity of the sequence models may in part be attributed to the fact that their proponents draw their own research experience from different types of basins (Catuneanu, 2002). It is not the purpose of this work to discuss the merits and limitations of these models, but to use them to classify the sedimentary unit defined in the Faial shelf. Therefore, for simplicity of the classification, the model of Posamentier and Vail (1988) was chosen for the discussion that will follow. This model seems more suitable for the Faial shelf because it is based on the architectures of divergent continental margins as opposed to the models of foreland (Plint and Nummedal, 2000; Van Wagoner et al., 1988) and rift basins (Embry, 1995). According to the model of Posamentier and Vail (1988) during an entire sea-level cycle three main systems tracts should be recorded on the shelf: the Lowstand System Tract (LST), the Transgressive System Tract (TST) and the Highstand System Tract (HST). Knowing that the lack of preservation of System Tracts is a common problem of the stratigraphic record (Catuneanu, 2002), the more recent system tracts are more likely to stay intact. Since today we are facing highstand conditions, the system tracts more likely to be preserved in order of priority, are the HST, TST and finally the LST. Therefore, the only sedimentary unit defined by the interpretation of the Boomer seismic records is more likely to belong to a HST. This system tract

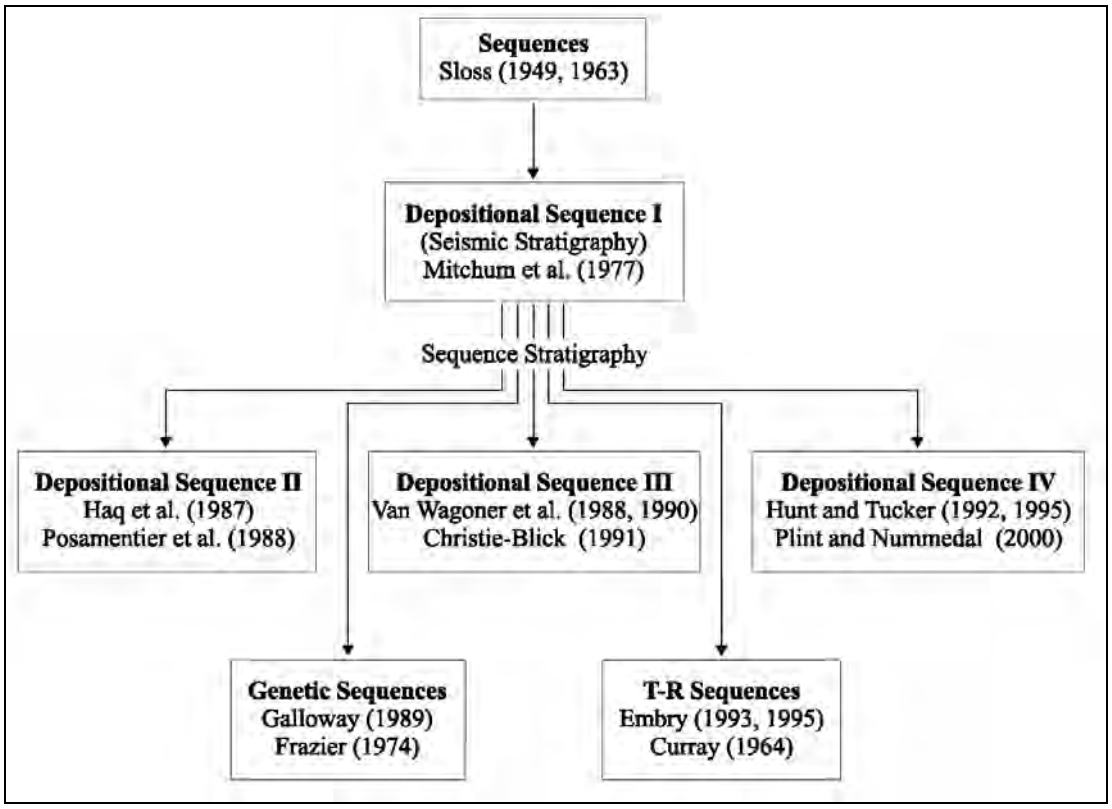

Figure 126 – Family tree of the various sequence stratigraphic models (Catuneanu, 2002).

Events \ Sequence model	Depositional Sequence II	Depositional Sequence III	Depositional Sequence IV	Genetic Sequence	T-R Sequence
	HST	early HST	HST	HST	RST
end of transgression	TST	TST	TST	TST	TST
end of regression	late LST (wedge)	LST	LST	late LST (wedge)	RST
end of base level fall	early LST (fan)	late HST (fan)	FSST	early LST (fan)	
onset of base level fall	HST	early HST (wedge)	HST	HST	

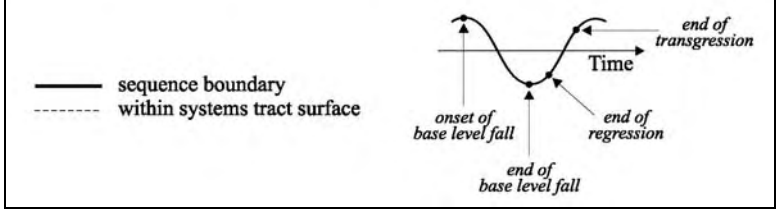

Figure 127 - Position of sequence boundaries, as well as the subdivision into systems tracts, for the sequence models currently in use (Catuneanu, 2002).

was probably formed during the last 7.5 Ka, which, according to the curve of Thompson and Goldstein (2006), is the moment when the present stillstand began. Although from 7.5 Ka to the present, the sea-level rose 11m, it is nevertheless a stillstand, when compared with the rapid rise that started at 23.1 Ka (Figure 128).

After a rapid rise of sea level, a surface of non-deposition may be developed before the progradational deposits of the stillstand are laid down. This surface is then covered by the progradational deposits and recognized by the downlap of these overlying deposits due to their seaward advance (Figure 130A). A relative stillstand of sea level is an apparently constant position of sea level with respect to the underlying initial surface of deposition and is indicated by costal toplaps (Figure 130A). If a relative stillstand occurs after a rise that is more rapid than the rate of deposition, the result is onlap instead of toplap (Vail et al., 1977). Therefore, the geometry of the sedimentary unit defined (coastal onlaps in Figures 129 and 130B) is in aggreement with a rapid rise of sea-level and a low or even absent rate of deposition (from 23.1 Ka to 7.5 Ka, see Figure 128).

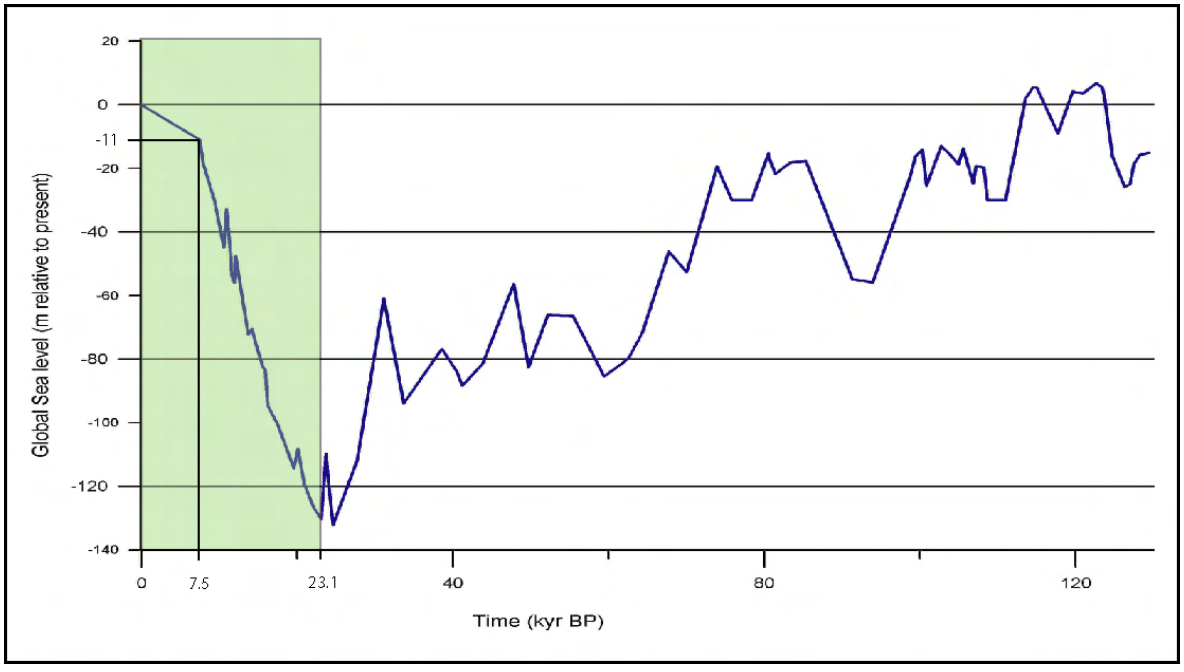

Figure 128 – Curve from Thompson and Goldstein (2006) that shows the last complete sea-level cycle. Colored rectangle represents the last sea-level rise that started at 23.1 Ka.

The regional positions of proximal onlap (onlap in the direction of the source of the sediment supply) and distal downlap (downlap in a direction away from source of sediment supply) commonly mark the lateral beginning and the lateral ending of deposition of a given stratum or unit (Mitchum Jr. et al., 1977b). This geometry is the same as the present in the sedimentary unit defined (Figures 129 and 130B) and reveal what seems to be a progradational geometry towards offshore. The sedimentary bodies have a sigmoidal shape in cross-shore profile, with the highest thickness normally near the shelf break and what seem to be downlap reflectors in the offshore part (Figure 129). Hernández-Molina et al. (2000) have described prograding bodies in the Spanish coast, but with a slightly different geometry. The Spanish bodies' are characterized by seaward dipping progradational clinoforms while the Faial bodies show a aggradational pattern in the inner and middle shelf and only in the outer shelf they seem to show a progradational geometry with downlaps towards the base of the sedimentary unit (Figure 130B). The aggradational pattern of Faial sedimentary bodies is explained by the absence of deposition (see section 4.3.2) during the rapid rise of sea level (from 23.1 Ka to 7.5 Ka), which left enough accommodation space for the sedimentation start aggrading instead of prograding.

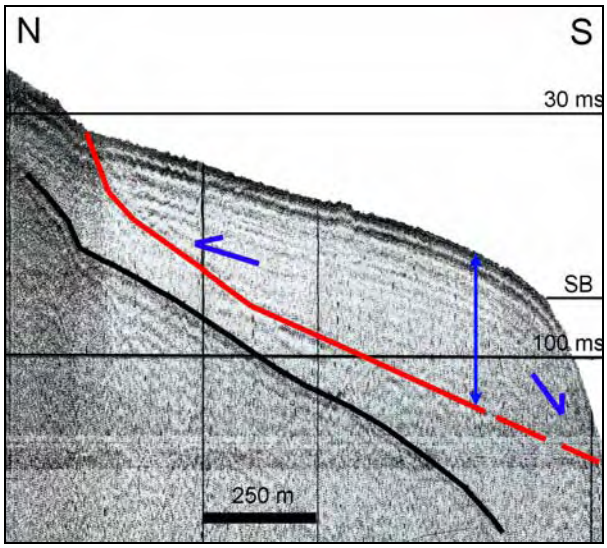

Figure 129 - Interpreted Boomer seismic profile showing the geometry of the sedimentary unit defined (see the non-interpreted seismic profile in Figure 114). The red line represents the basement of the sedimentary unit. The left blue arrow represents the onlap of reflectors against the basement and the right arrow the downlap. The vertical blue bar represents the section of the profile where the sedimentary body is thickest. SB means shelf break. See location on Figure 76.

Hernández-Molina et al. (2000) named their sedimentary bodies as the infralittoral prograding wedges (IPW), because they lie in the infralittoral zone, between the shoreface and the inner continental shelf. In terms of sea-floor morphology the IPW forms a low-angle slope which represents the infralittoral prograding environment, extending to a strong break in slope at water depths of 20-25 m in the Mediterranean areas and 30-35m in the Atlantic areas. The IPW bodies are considered to have originated in storm-generated currents (downwelling currents), which produce a seaward sediment transport.

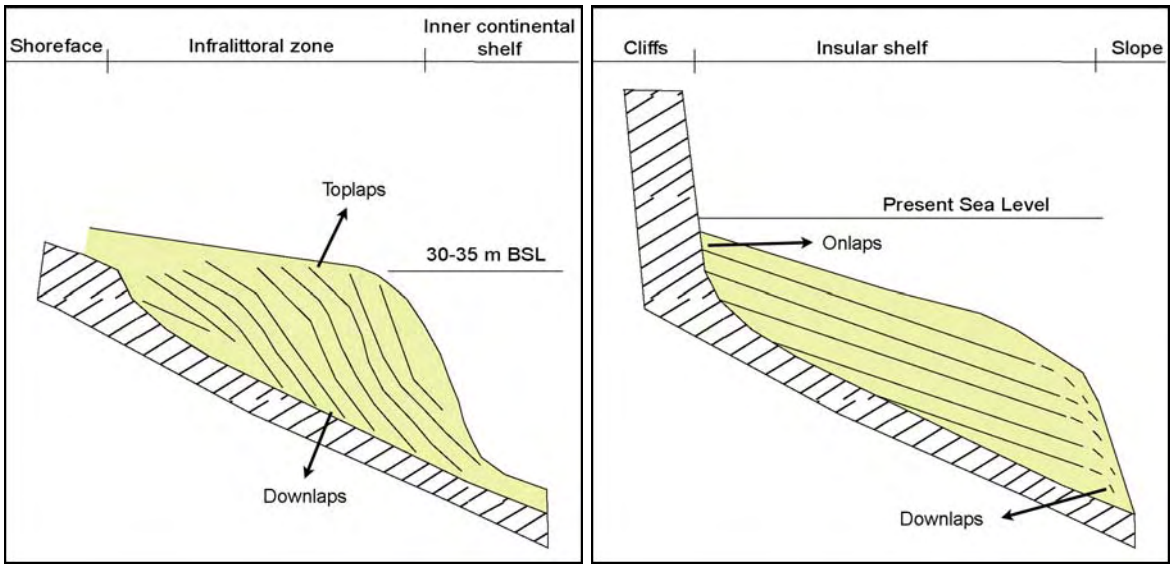

Figure 130 – A) Example of the Spanish sedimentary bodies showing a seaward dipping progradational clinoform geometry (adapted from Hernández-Molina et al., 2000). BSL means below sea level. B) Example of the Faial shelf sedimentary bodies showing aggradational geometry in the inner and middle shelf and progradational geometry in the outer shelf.

These authors have shown that storm-generated currents can produce prograding sedimentary bodies. The author believes that the same mechanism was responsible for the formation of the Faial sedimentary bodies. The Faial shelf is narrower and consequently with less accommodation space, which may explain why these bodies have prograded further offshore (the depositional shelf break is normally found between 65 to 80 meters water depth – see Figure 57 in Chapter 3 and discussion in Chapter 5). In addition, the higher energetic environment of the shelf produces stronger storm-generated currents (see section 2.4.4 in Chapter 2)

supporting even more this mechanism as the main responsible for the generation of these sedimentary bodies.

4.3.2. Preservation potential of the previous depositional sequences

The previous discussion showed that the geometry of the sand bodies mapped on the shelf sectors F, G and H (which are the best characterized sectors by the interpretation of the Boomer seismic profiles) is typical of highstand deposits. Although the sedimentary bodies of the other sectors have not been fully characterized, the same geometry in the Boomer seismic profiles, points out to a similar origin. What is difficult to explain, is why the previous depositional sequences are not recorded in the shelf, since during the last 800 Ka the shelf has suffered several well defined sea-level cycles (see Figure 34 in Chapter 2).

In high-frequency eustatic cycles, sea level fluctuations occur faster than the earth can respond to them, altering the resulting stratigraphic successions. Numerical investigations indicate that several factors can significantly affect the architecture of sequences, their thicknesses and the relative importance of transgressive and regressive deposits (Carey et al., 1999; Steckler, 1999). These factors include tectonics, sea level changes, constant sediment supply, isostasy, compaction and the effects of erosion and deposition. In the case of volcanic islands like Faial, sediment supply appears to be mostly from marine and subaerial erosion (see also section 4.3.4) during the sea-level highstands. The reason is that when the sea level drops sediment supply becomes sparse due to low erosion of the paleo-marine cliffs left behind and lack of major river systems to transport these few sediments to the shelf. Moreover, the reduced precipitation during glacial periods starves even more the shelf deposits. At the same time, the low rate of subsidence in almost all of the shelf sectors (see section 5.5) and a narrow shelf creates little space for accommodation of sediments. Consequently, during sea level falls, the lack of sediment supply prevents the formation of large LST. On the other hand, when the base level falls below the shelf break (which has always been the case, see Figure 34 in Chapter 2) the preservation potential of the falling stage strata that accumulates on the shelf is very small, making the LST very

reduced or inexistent (Catuneanu, 2002). Furthermore, the presence of a narrow insular shelf and highly energetic like the one of Faial enables faster transport of sediment offshore, with regressive ravinements sweeping away the highstand sediments from the shelf. Therefore, during sea level drops, not only LST deposits are formed, but the highstand deposits may be lost to the slope by downweling currents during storms.

During sea-level rises, the erosion faces a starved rocky area, which makes difficult the generation of sediments. Accordign to Zecchin (2007), shelf settings characterized by low sediment supply and/or intensive wave reworking have normally thin transgressive deposits. The importance of the sediment supply is well expressed by the scheme of Cattaneo and Steel (2003) which shows how the ratio between accommodation and sediment supply controls the thickness of the transgressive deposits (Figure 131). Therefore, during transgressions, the resultant deposits of the Faial shelf are thin and scattered, possibly below the resolution of the Boomer records. Not surprisingly, the simulation of slow coastal erosion is characterized by transgressive deposits poorly preserved and the coincidence of the transgressive ravinement with the regressive ravinement (Carey et al., 1999).

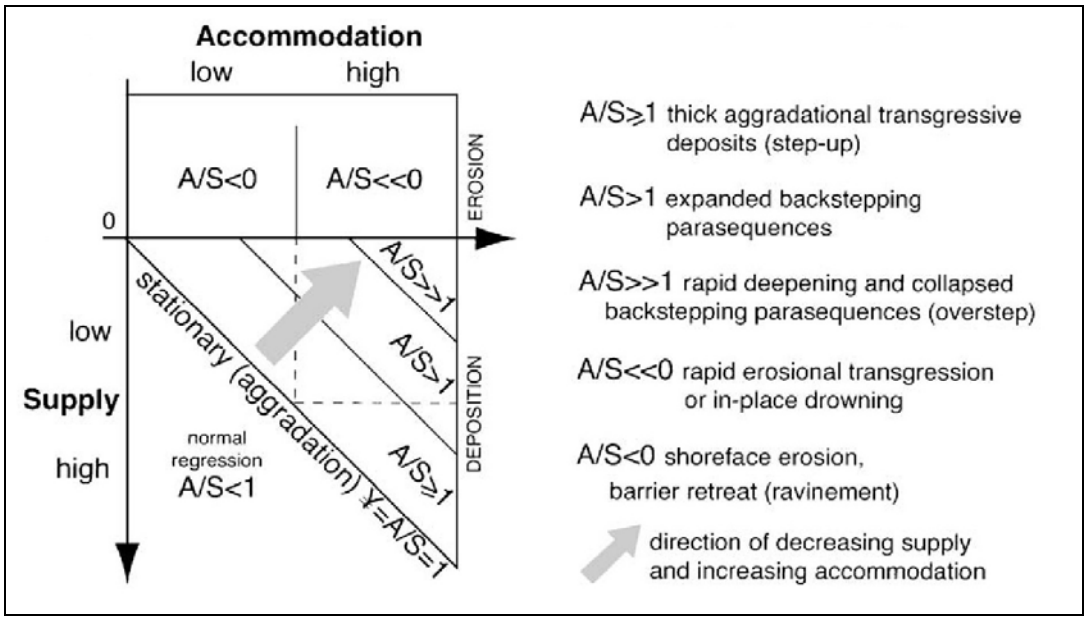

Figure 131 – Theoretical cases of transgression (after Cattaneo and Steel, 2003). Depositional regime is expressed as the Accommodation-Supply ratio (A/S). In this case, the transgression can lie within or above the line of erosion (A/S >>1, A/S<0 or A/S<<0).

In conclusion, the reason for the lack of preservation of System Tracts in the Faial Island shelf can be accounted for by small accommodation space, high wave energy and low sediment supply during sea levels below the present highstand.

4.3.2.1. The sand-wave field in the channel Faial-Pico

The sedimentary deposits that lay on the shelf sector E (Figure 77 in Chapter 3) are believed to have formed through the same mechanism as the one described in section 4.3.1. Nevertheless, they show distinct features from the other sectors, such as a sand-wave field with bedforms trending WNW-ESE. The direction of these bedforms is compatible with the direction of the flood (NNE) and the ebb (SSW) tide currents. However, the echo interpretation of the chirp seismic profiles revealed below the sea surface, masses that exhibited a varied degree of deformation, with disrupted internal reflections (see Figures 70 and 77 in Chapter 3). This deformation may be associated to the movement of the graben faults from the Pedro Miguel Region that probably extend offshore. The subaerial reactivation of the graben faults is tectonically active and well described by Madeira and Brum da Silveira (2003). A remarkable evidence of the offshore extension of the graben faults is the WNW-ESE lineament offshore Ponta da Espalamaca (see section 2.4 and Figure 41 in Chapter 2) that extends to the Madalena village, which according to Nunes (1999) is formed by submarine cones of the surtseyan type. Furthermore, the echo interpretation revealed the presence of submarine cones (see Figures 77 and 100 in Chapter 3) in this lineament. In this particular case the fault planes appear to have facilitated the emplacement of these surtseyan cones. According to Pacheco (2001) there is still ongoing submarine gas emanation east of Espalamaca headland which means that this volcanic lineament is still active. These references are a further evidence of the offshore activity of the WNW-ESE faults. The movement of these faults could have created a stepping sea-floor that may have conditioned the emplacement of these bedforms during the movement of sediments by the tidal currents.

4.3.2.2. The mound-like deposits

These sediment bodies are distinctly mounded and elongated in shape (Figures 59 and 72). They are normally located at the base of the coarse clastic deposits (Figures 77, 90, 92 and 113), although some are located further offshore (Figures 77 and 112). They are present in the sectors C, D and H, within the sedimentary deposits of sand and gravel, between 30 to 50 meters water depth. These deposits were not sampled during the FAPI-3 survey. Nevertheless, their echo character (I-B) suggests that they are composed of finer sediments than those from the surrounding sea floor, probably fine sands. Unfortunately, the Boomer seismic profiles, due to their poor resolution, do not show their internal geometry, which makes it difficult to assess their origin. The landward steep slope of the coarse clastic deposits is manly composed by rock debris, so it is expectable that the sediments in the base of the slope will be very poorly sorted since they probably result from mass-wasting processes along the slope. The origin of these deposits could be accounted for by the seaward bottom currents. These currents can periodically exceed the threshold velocities needed to erode the finer sediments at the base of the coarse clastic deposits and transport them offshore. There are evidences in other places of the world of sand ridges formed by other processes than nearshore ones. Sand ridges on the middle continental self of the Middle Atlantic Bight have been reported to form by sedimentary processes that occur at these depths (Rine et al., 1991).

4.3.3. The interplay between the erosive and the constructional processes

According to Menard (1983) the shelves of volcanic islands evolve by competition between erosive and constructional processes. The erosive processes contribute to the formation and enlargement of the shelves (Figure 132). At any time of the enlargement of the shelf, constructional processes, mainly volcanic progradation (Figure 133) and sedimentation (Figure 134), may fill partial or all the space left by the erosive processes, reducing the shelf width.

In the Faial Island there are parts of the shelf that are purely abrasional and

others where the competition between these two processes is balanced and ongoing. The southwestern part of sector B is an area of the shelf that was probably cut by these erosive processes and shows no signs of volcanic progradation. It has very high and steep cliffs (100 to 300 meters – see Figure 45 in Chapter 2), which are the result of the abrasional processes mentioned before and shows no presence of lava flows or the products of their erosion in the shelf. It

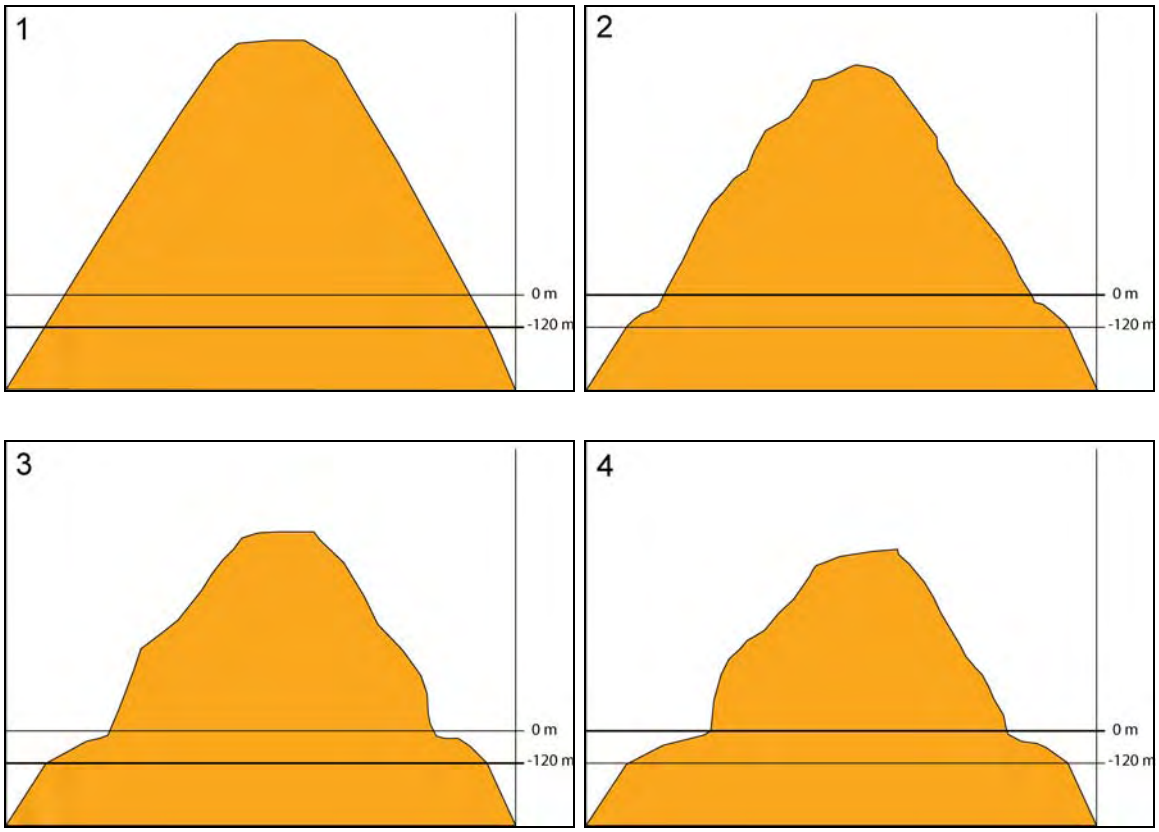

Figure 132 – Schematic cross-section of an island showing the formation of an abrasional shelf through surf erosion during the sea-level oscillations. (1) Formation of the subaerial island – sea level is at -120 m. (2) Beginning of the shelf incision during the sea level rise from -120 m to 0 m. (3) Enlargement of the shelf during the sea level drop from 0 m to -120 m. (4) New enlargement during the sea level rise from -120 m to 0 m. Between 1 and 4 the onshore part of the island is also reworked by the subaerial erosion.

is covered by a blanket of sediments (similar to Figure 134), only uncovered by a very small speckle of rock outcrops (Figure 77). Similarly, sector E seems to be absent of volcanic progradation (Figure 77). On the other hand, sectors A1, A2, C, D, F, G, H and the northeastern part of sector B show examples of recent volcanic progradation (Figure 77). These areas have lava flows (echo type III-B) covering small parts of the shelf at varied depths (Figure 77). According to Mitchell et al.

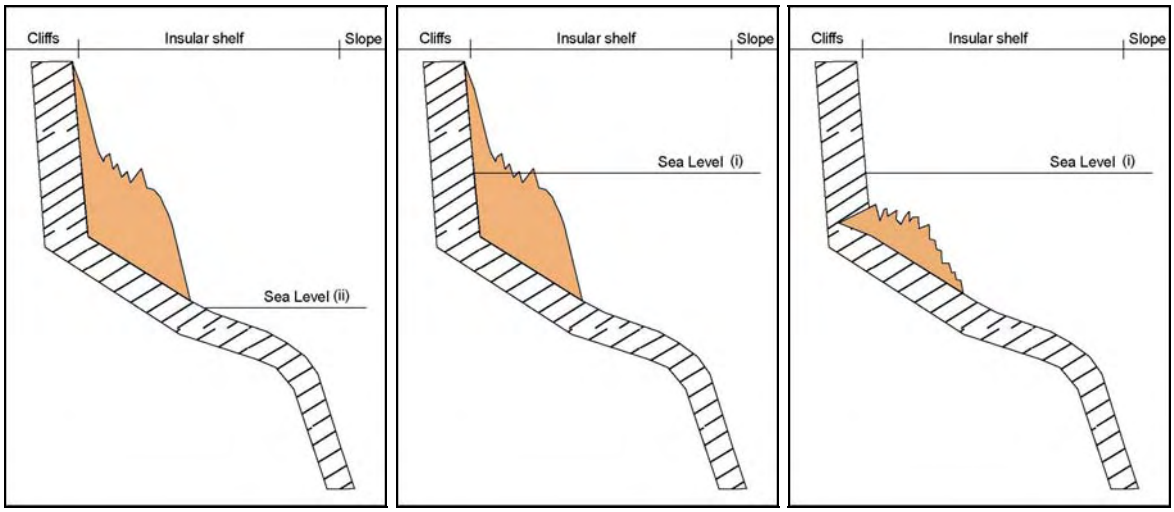

Figure 133 – Three possible options for the emplacement of lava flows in the shelf. A) Emplacement of subaerial flows on the shelf with a sea-level lower than today. B) Subaerial flows penetrating the sea and moving offshore along the shelf. The sea level is above the emplaced lavas. C) Submarine flows originated from near-shore tube openings or vents.

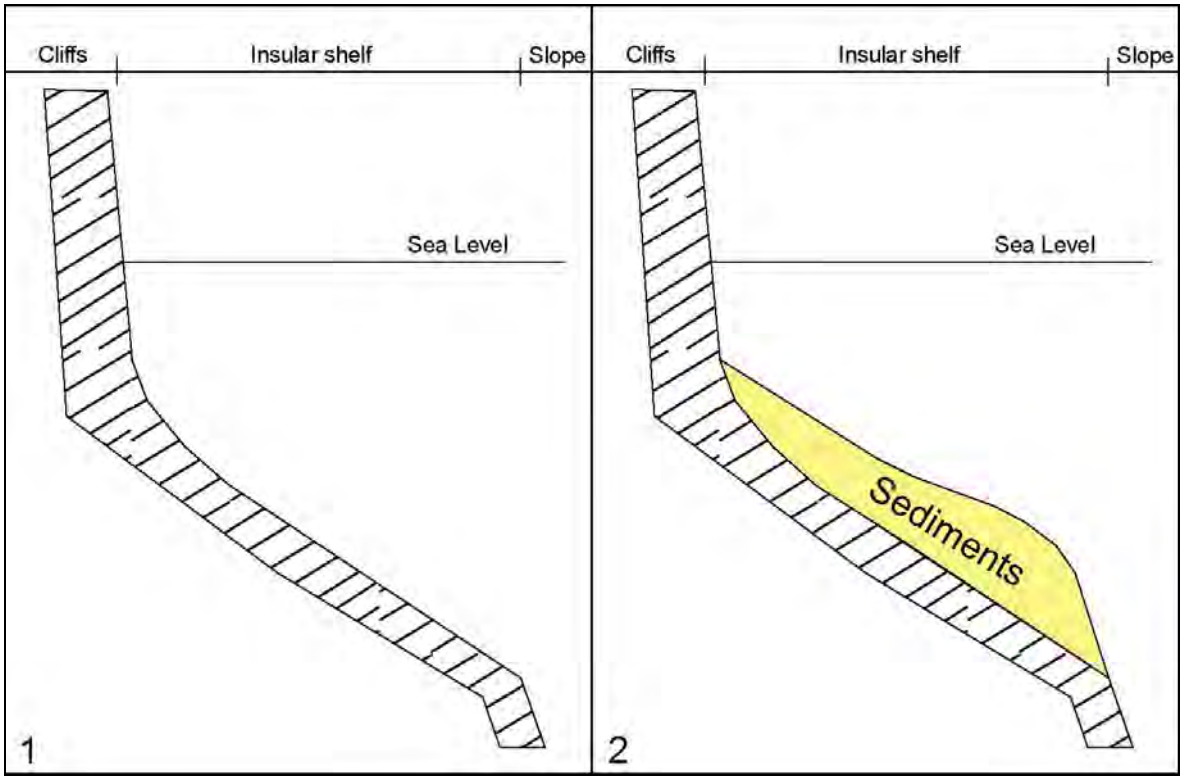

Figure 134 –In a shelf already formed, sediments may accumulate from subaerial origin or from erosion of submarine lava flows like those in Figure 133.

(in press) the observed strong surf erosion of historical flows around the world suggests that these submarine lava flows are not pre-Holocene subaerial flows

because they could not have survived the sea level changes that took place since the formation of these shelf sectors (see section 4.2 in Chapter 4 for the discussion about the age of the sectors). These authors think the submarine lava flows were probably formed in the Holocene, when the sea-level was similar to today, from subaerial flows penetrating the sea (Figure 133B) or from near-shore tube openings or vents as submarine flows (Figure 133C). However, in the case of the Faial Island such flows appear to be strongly dismantled since they are much dispersed and it is not possible to follow an entirely preserved flow from the coastline to the middle or outer shelf (except in sectors A1 and G – see Figure 77). They could either be isolated flows or belong to bigger flows that were partially remobilized by surf, forming abundant clastic deposits around them (echo type III-A, see Figures 72 and 77) during times of varying sea level (similar to example 3 in Figure 135).

In conclusion, since most of the Faial shelf is covered by coarse clastic deposits (Figure 77), the author believes that these result from the erosion of lava flows. These flows might have emplaced subaerially when the sea-level was lower than today (Figure 133A) or from subaerial flows penetrating the sea (Figure 133B) or even submarine flows that came from near-shore tube openings or vents (Figure 133C), when the sea-level was above their emplacement depth. Later, they were eroded by surf erosion as the sea-level varied across them. The more nearshore deposits might also result from landslide flows of the coastal cliffs. The small and isolated lava flows that are still preserved might have resisted to the passage of a varying sea-level or were emplaced by submarine eruptions. Well preserved lava flows that cover almost the entire shelf (like those of sector A1 and G) are more likely to have formed after the sea-level reached the present level, which allowed them to stay intact.

The time and mechanism of emplacement of the lava flows will generate different types and geometric relations of the geological composition of the shelf:

1. Nearshore predominance of coarse clastic deposits up to 30-50 meters water depth and below these depths predominance of sand and gravel deposits. In this case, over a clean abrasional shelf (example 1 in Figure 135), there is volcanic

progradation from subaerial source that penetrates the sea and reduces the shelf width (example 2 in Figure 135). Then, as the sea level oscillates, there is erosion of the shelf and consequently the lavas are dismantled, giving origin to coarse clastic deposits (example 3 in Figure 135). Finally, the sea-level reaches its present level and a sedimentary body deposits (example 4 in Figure 135).

2. Nearshore predominance of lava flows up to 30-50 meters water depth and below these depths predominance of sand and gravel deposits. In this case, over a clean abrasional shelf (example 1 in Figure 136), a sedimentary body deposits during the present sea-level (example 2 in Figure 136). Then, over the sedimentary deposit there is volcanic progradation from subaerial source that penetrates the sea and reduces the shelf (example 3 in Figure 136). Finally, surf erosion removes the subaerial part of the lava flows (example 4 in Figure 136). The result seen in a Boomer seismic profile is the same as the example 4 of Figure 135, because the seismic signal does not penetrate rocky bottoms and only the part S_2 of the sedimentary body will be seen in the seismic profile. This is probably the case for the area in sector G that has a big lava flow that reaches the middle shelf (Figure 77).

3. The shelf is dominated by lavas intercalated with coarse clastic deposits, which is the case for sectors A1 and A2. Because the subaerial part of the island is very recent (10 Ka to the present) the shelf is still poorly developed, comparable to the example 2 of Figure 132 (with the difference in this case that the sea level was at 40 meters water depth when the shelf started its formation – see discussion of this implication in Chapter 4). As the sea level rose an incipient shelf was formed and probably at the same time lava flows were prograding over the shelf. The lava flows that are now in these shelves might have resisted to the passage of the varying sea-level or were emplaced with a sea-level higher than its present emplacement depths (as the example B in Figure 133). The coarse clastic deposits around the preserved lava flows result from their erosion during the sea-level rise.

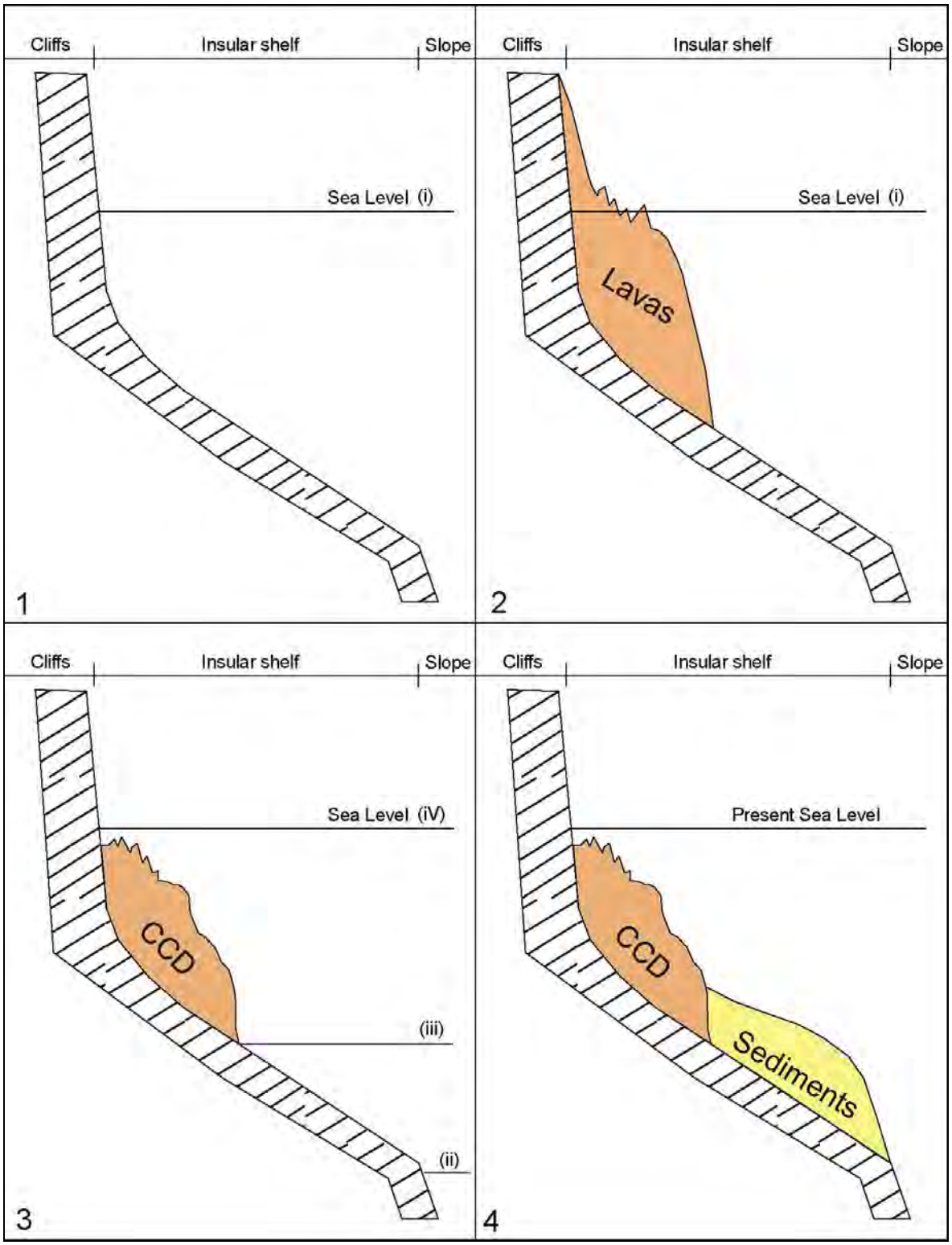

Figure 135 – Abrasional shelf with nearshore coarse clastic deposits and offshore blanket of sediments. In this model the lavas flow (brown area) into the shelf from subaerial origin (2); the sea level oscillates (i, ii, iii and iv) eroding all the shelf, including the lavas that give origin to coarse clastic deposits (CCD) (3); and during the present sea-level the sedimentary bodies (yellow area) deposit (4).

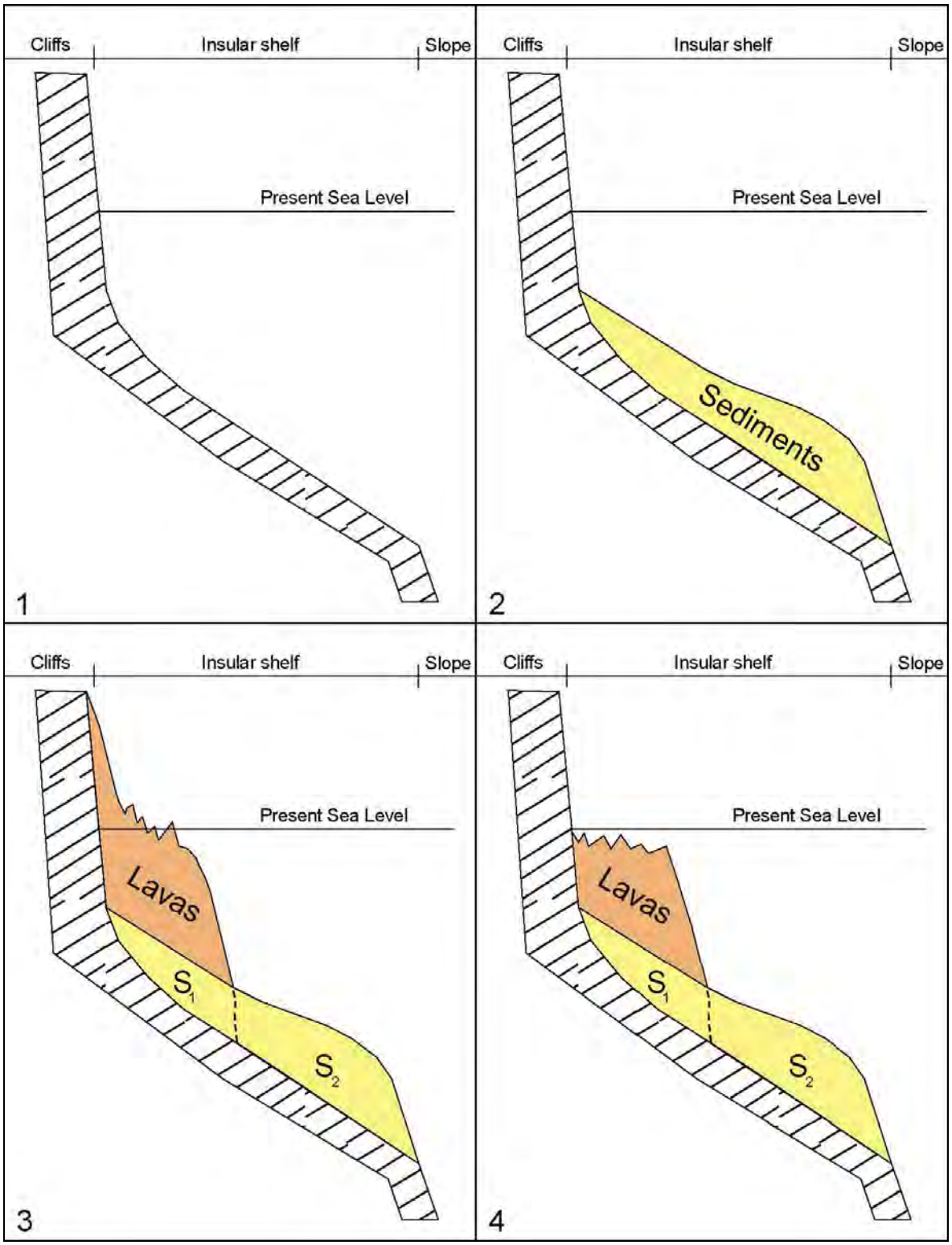

Figure 136 – Abrasional shelf with nearshore volcanic progradation and offshore blanket of sediments. In this model the sedimentary bodies (yellow area) deposit during the present sea-level (2); lavas flow (brown area) into the shelf from subaerial origin and cover the S1 part of the sedimentary deposit, leaving the S2 part uncovered (3); Surf erosion removes the subaerial part of the lava flows (4).

4.3.4. The sedimentary sources of the sand and gravel deposits in the shelf

The presence or absence of sand and gravel deposits in the shelf is mainly related to three processes: subaerial erosion of the hydrographic basins, erosion of the shelf prograded volcanics and landslide flows from coastal cliff failure. The subaerial erosion of the hydrographic basins is normally a source of finer sediments (sands and gravels). The erosion of the shelf prograded volcanics may or not be a source of fine sediments. According to Moore et al. (1973), interaction of lava with surf generates a lot of sand directly by quenching of lava. The lava is often very friable because of abundant fractures so, it easily erodes out. However, if there is a lot of massive lava without a high density of fractures, it may be more resistant and the surf erosion generates coarser deposits and consequently it will take longer time for erosion to transform these coarser deposits into finer sediments. The nearshore coarser deposits may also result from landslides of coastal cliffs, although the granulometry of the deposits greatly depends on the cliff composition. The Faial cliffs are normally composed by intercalation of basaltic lava flows with pyroclastic deposits (Figures 118 to 123). Nevertheless, there is not quantitative information about the percentage of the different types of deposits that compose the cliffs. Nor about the type of lava flows that have prograded onto the shelf. There are still other mechanisms that might explain the presence of sand and gravel deposits in the shelf. These mechanisms have been reviewed in the section 1.2.7 of Chapter 1 and are related to the syn-eruptive sedimentation or non-eruptive remobilization of volcaniclastic material from subaerial origin. The relative importance of all these mechanisms is very difficult to assess due to lack of detailed knowledge about the subaerial and submarine geological evolution. Due to the scarcity of the information, the author will only try to relate the precipitation data with the presence of sand and gravels nearshore, because this is the only reliable and quantitative information available at this stage. In addition, the high runoff values (see section 2.4.3 of Chapter 2) estimated by Coutinho (2000) and the highly erodible superficial deposits that cover most of the subaerial part of island (i and p in Figure 43) suggest that subaerial erosion might be important.

The residence time of the sand and gravels near the coastline is probably low due to the seaward returning currents that occur during storms, already discussed in the section 4.3.1. The evidence for that low residence time is the absence of submarine sediments smaller than cobbles or pebbles in the majority of the nearshore areas (Figures 77 and 137). However, the absence of submarine fine sediments may also be related with an abnormal rate of recent volcanic progradation. In these areas, the inner shelf is covered by lava flows and by the products of their erosion, most often coarse clastic deposits. A good example is the sector A, which abrasional shelf is very incipient because erosion has not had enough time to transform the coarse clastic deposits and the lava flows (Figure 77) that compose the shelf into finer sediments.

Only the sectors B, D, E, F and H have sandy and gravely sediments covering the sea floor near the coastline (Figure 137), which indicates that, in these sectors the subaerial contribution of sediments may be higher and/or there has not been much volcanic progradation. Sector B has no coarse clastic deposits in their southwestern and central part, but as we move eastwards the contribution of these deposits increases. Looking at the annual precipitation map (Figure 137) of the Faial Island it is clear that the submarine areas from sector B that have adjacent inshore yearly precipitation values higher than 1200 mm are covered with finer sediments. The same happens for the submarine areas covered by sediments in the sectors D and H (Figure 137).

Surprisingly, all the submarine area of sector E is covered by sediments but the adjacent inshore areas have lower precipitation values. However, if we look to a 3D view of the eastern sector of Faial (Figure 138), the drainage pattern is controlled by the normal faults that constitute the graben structures (compare with Figure 42 in Chapter 2). The stream drainage is well developed and follows the base of the fault scarps. These watercourses are supplied by erosion of the superficial pyroclast deposits of Cedros Volcanic Complex (see Figures 42 and 43 in section 2.4.1 of Chapter 2) that occur upstream (Figure 138) due to the high precipitation values near the caldera. In addition, sector E is also less exposed to surf due to the sheltering effect of Pico and S. Jorge Islands; therefore sediments might not be transported offshore so rapidly. It is also the oldest subaerial area of

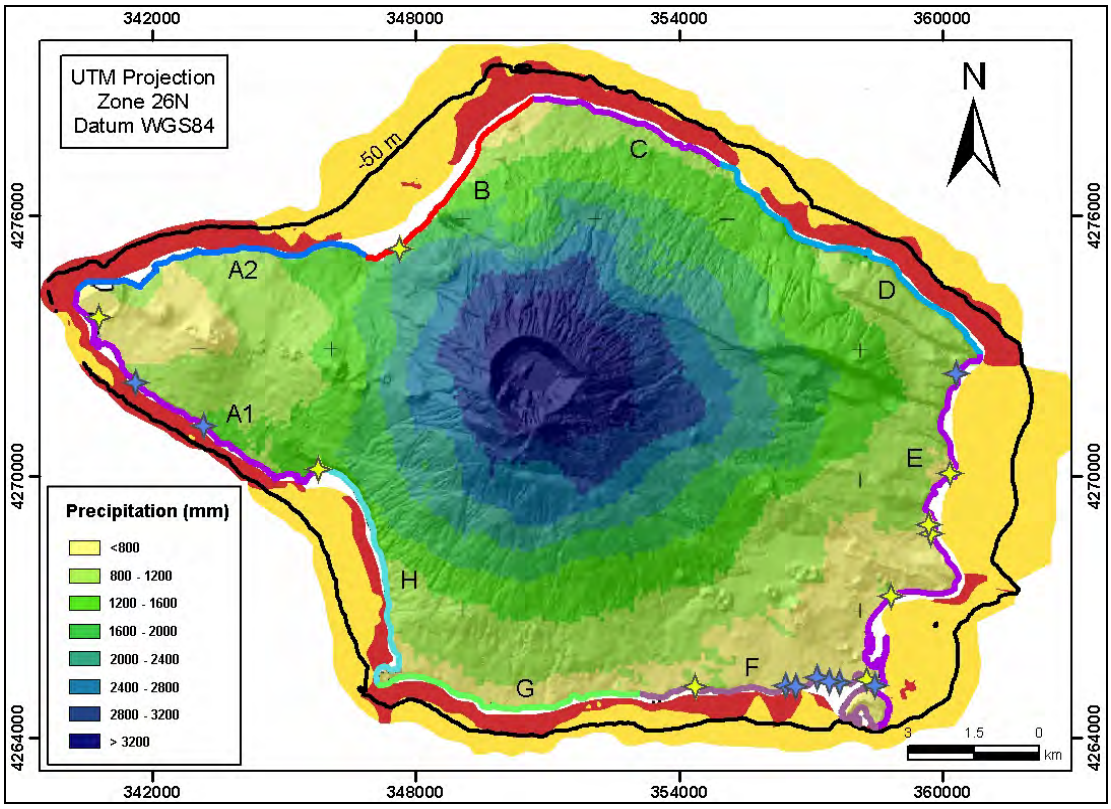

Figure 137 – Annual average precipitation map of the Faial Island and relation with the submarine sedimentary cover. Areas in yellow on the shelf are covered by sands and gravels. Areas in reddish brown are covered by lava flows and coarse clastic deposits. The yellow stars represent sandy beaches and the blue stars pebble and cobble beaches. The bold coastal lines and the respective letters represent the different coastal segments. (Precipitation map taken from http://www.climaat.angra.uac.pt/).

the Faial Island which means that probably it has not had recent volcanic progradation into the shelf.

The onshore part of sector A, due to its youth (not more than 10 Ka) and the resistance of the fresh basaltic flows, does not have a well-developed hydrographic network (see section 2.4.1 in Chapter 2). In fact, although it has precipitation values higher than 1200 mm in the eastern inshore areas, the sea bottom has very few sand and gravels. The onshore eastern part of sector F and southern part of sector E are also very youth (the Horta-Flamengos-Feteira Region is not older than 30 Ka) and without a well-developed hydrographic network (see section 2.4.1 in Chapter 2). Nevertheless, they have a sedimentary cover of sands and gravels, probably due to the constitution of their subaerial parts, more prone to erosion. Their subaerial parts are characterized by a set of scoria cones surrounded by low slope areas formed by the accumulation of pyroclasts deposits

and lava flows.

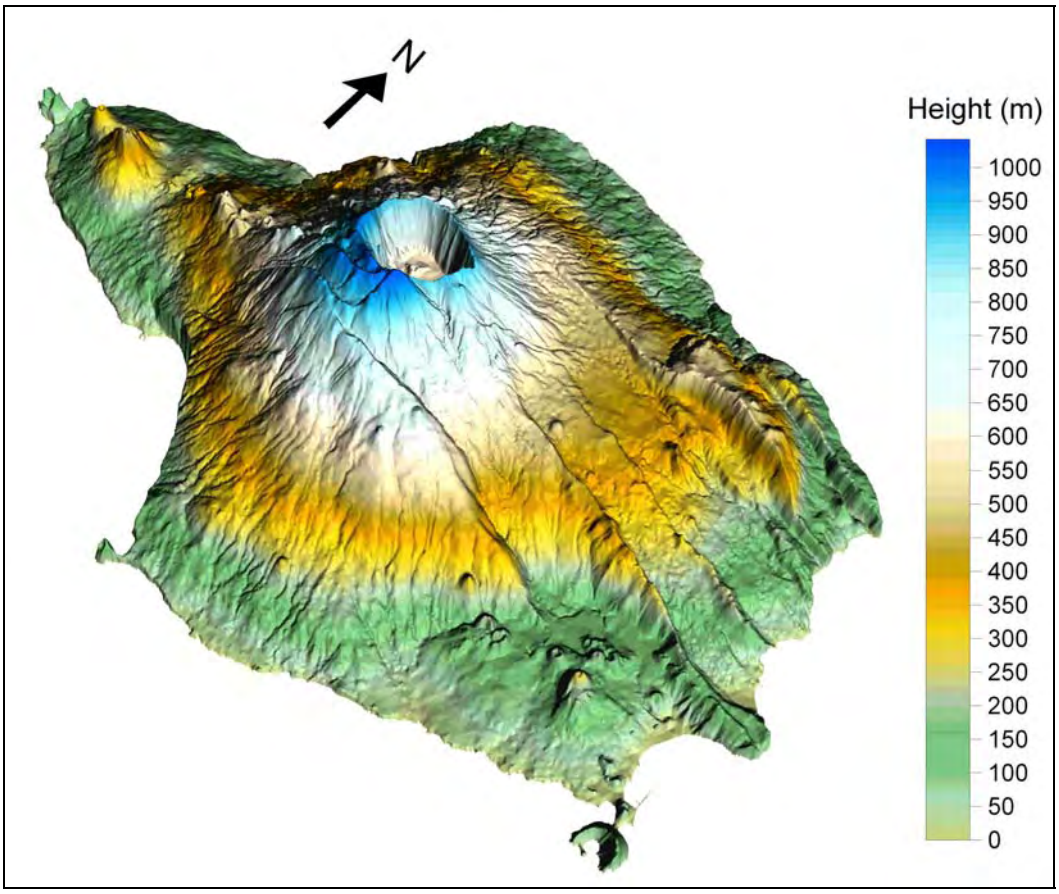

Figure 138 – DTM of the subaerial part of the Faial Island showing that the drainage pattern on sector E (see Figure 137 for location) is controlled by the graben faults (data from Instituto Geográfico do Exército, 2001a; 2001b; 2001c; 2001d).

It is clear that the subaerial input of sediments may have played an important role in the supply of finer sediments to some areas of the shelf sectors B, western D, E and northwestern H, because there is a obvious relation between higher precipitation rates and sands and gravel nearshore. These inshore areas also show the steeper slopes (except on sector D, see Figure 139) and erodible substrates (cover of friable material from the Caldeira Formation – see section 2.4.1 from Chapter 2) making them good sources of sedimentary output for the shelf. It is also evident that the sector E has a higher input of fine sediments than sectors B, western D and western H due to the better developed hydrographic network of the Pedro Miguel Graben Region that discharges over the northern part of sector E. The sector E is also a good example of asymmetric erosion in the

Faial Island. However, contrary to what is suggested by Menard (1983) that it results from stronger rainfall in some parts of the coast in detriment of others, in this case the tectonics and the age of the area play a more important role. The areas of the inshore sectors B, D and H have higher precipitation rates, but because they are more recent (superficial deposits have 10 Ka as opposed to 800 Ka of sector E – see section 2.4.1 from Chapter 2) and less affected by tectonics, they are more preserved. Not surprisingly, the few scattered pocket beaches (Figure 139) that exist in the Faial Island are mostly located in the embayed areas that have inshore high precipitation rates. It is also in these places that the sandy beaches occur, although almost all of them turn to pebble and cobble beaches during the winter.

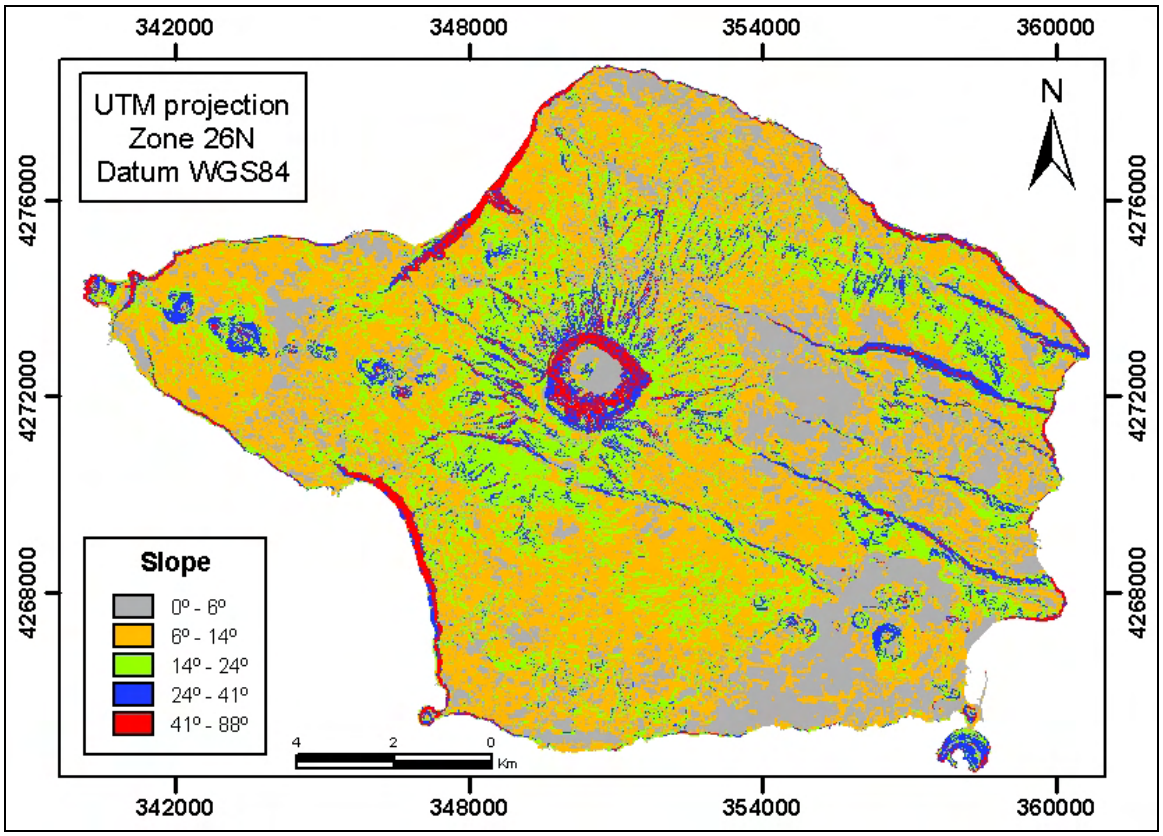

Figure 139 – Faial Island subaerial slope based on the altimetry of the Instituto Geográfico do Exército maps (2001a; 2001b; 2001c; 2001d), using the ArcGis 9.0 GIS running the 3D Analyst extension. This figure shows that the higher subaerial slopes are those related with riverine erosion directed to the shelf sectors B, E and H (see Figure 137 for shelf sectors legend).

Marine erosion is also probably important in the contribution of sand and gravels to the shelf. It appears to be the main process acting on cliff retreat

(section 4.2) and the sectors B and northwestern H show very high cliffs (see Figures 45 and 47 in Chapter 2) in areas where sand and gravels dominate nearshore. The source of these nearshore deposits can be afforded to erosion of these cliffs which seem to have retreated more than other sectors that have lower cliffs. In the section 5.6 of Chapter 5 the sources of sands and gravels are discussed again using subaerial and cliff erosion rates to assess the contribution of these two mechanisms to the shelf. The transport of sediments can also explain the presence or absence of these deposits in some areas of the shelf and these implications are discussed in the Chapter 6.

4.3.5. Cross-shelf sedimentary patterns

The concept of wave-graded continental margins, with the seafloor sediment coarsening from offshore mud to shoreface sand is well know since the nineteenth century (Stanley et al., 1983). According to these authors, the mudline position is the depth on the outer continental margin where proportions of clayey silt, silty clay and clay no longer increase significantly with depth. This position shows a high variability and is dependent on three most consistently important factors: shelf width, sediment supply (reworked coastal and shelf derived as well as fluvial) and magnitude of fluid energy on the shelf, shelfbreak and upper slope. High-energy conditions prevent deposition of mud and erode and winnow it from the shelf. Moreover, in a narrow shelf the offshore spillover will puts the mudline even further than on a wide shelf. In addition, if the river sediment supply is low, there will also be a lack of fine-grained sediment deposition on the shelf.

The frequent recovery of coarse sands and gravel from samples of the outer shelf of Faial (see Chapter 6) shows that the concept of Stanley et al. (1983) of wave graded shelves does not apply to the shelf of Faial. In fact, the presence of coarse sands and gravel in the outer shelf is an evidence of continuous reworking along the shelf and possible shelf spillover. The high energetic conditions described on Chapter 2, a narrow shelf (less accommodation space) and the lack of developed river systems are the great responsibles for the absence of fine sediments on the shelf. In addition, the volcanic activity (both subaerial and

submarine), may have also contributed to the increase of coarser sediments.

The cross-shore spatial variability of the sediments in Faial is discussed in more detail in Chapter 6.

4.3.6. Shelf break retreat

There is also evidence of mass-wasting processes and gullying at or near the shelf break of the Faial Island. Evidences include headwall embayments (Figure 140) at the shelfbreak with slopes within the embayment generally steeper than those from the adjacent areas and some chirp seismic profiles (Figures 84 and 89) crossing these embayments. Figure 84 shows a long-shore chirp profile revealing the presence of several gullies and Figure 89 is a cross-shelf profile that shows a change in slope at 140 ms, suggesting the presence of a scarp upslope. Figure 83 is also a long-shore chirp profile (see Figure 77 for location) that reveals the presence of several gullies on sector A1. The A1 and A2 sectors due to very high slopes and unstable material (mostly eroded lava flows) are very prone to the generation of mass-wasting processes.

Possible causes for the generation of these submarine landslides include seismicity and sedimentary loading that can cause oversteepening and instability near the shelfbreak. It is well know that storm surges move the material offshore loading the submarine slopes. According to Damuth and Embley (1981) the rapid overbank deposition of fine sediments leads to oversteepening and triggers mass-movement deposits. Vanney and Stanley (1983) related the erosion at the shelfbreak with the spill-over of material seawards across it. They suggest that the spill-over triggers sediment failure and, in turn, a landward retreat of the shelf break and the formation of gullies on the uppermost slope. Pratson et al. (1994) and Pratson and Coakley (1996) proposed that canyon initiation began with depositional oversteepening and localized failure of the upper continental slope. It is known that high sedimentation rates produces a buildup of excess pore water pressure making very easy the deposits to failure (Laberg and Vorren, 1993). Well-developed canyons on the western flank of Monserrat Island are related by Le Friant et al. (2004) to have formed by the collapse of shelf sediments in

response to sediment loading. On the other hand Einsele (1990) found that many fine-grained, but low-cohesion, slope sediments have a high liquefaction potential, and dynamic loading caused by earthquakes may lead to gravity flows.

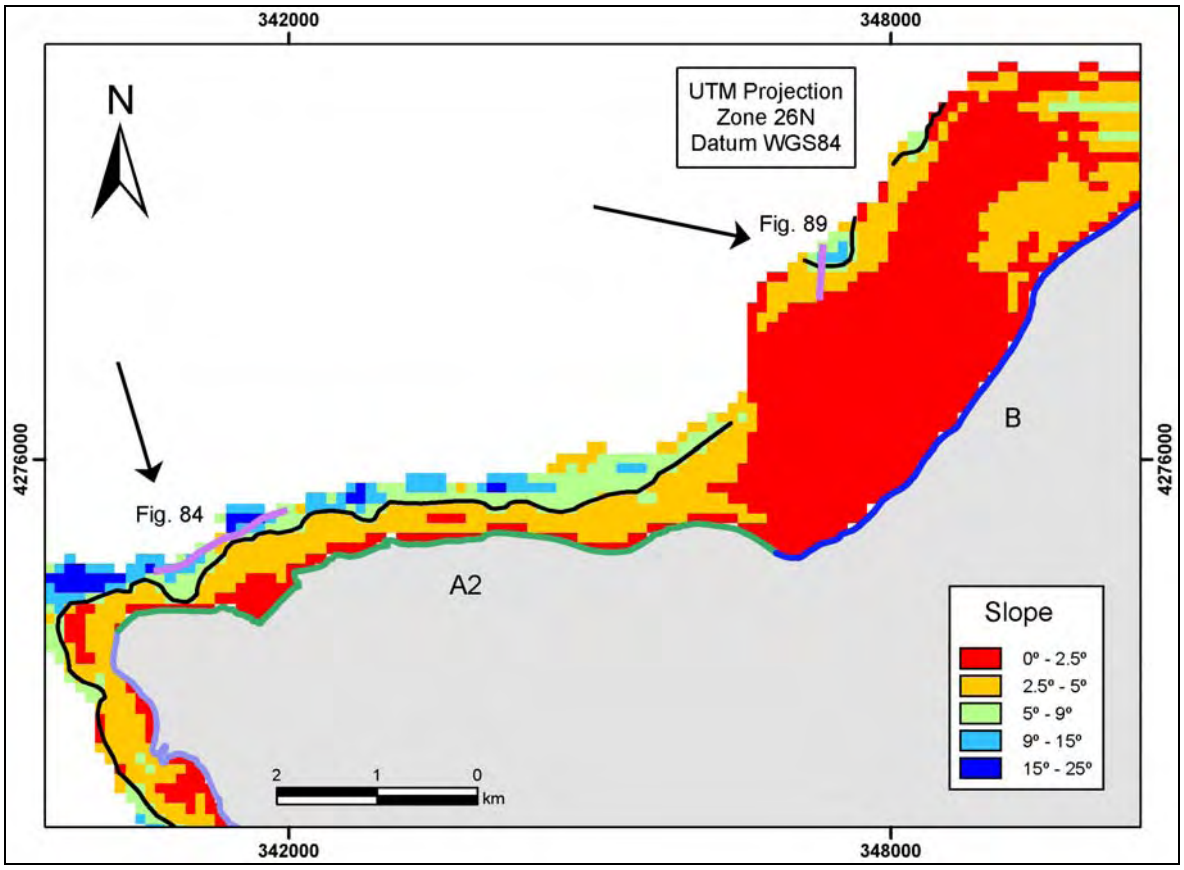

Figure 140 – Detail of the slope map of Figure 56, showing headwall embayments suggestive of landslides. The bold black line marks the shelf edge, the arrows identify the embayements and the purple lines are the tracks lines of the chirp seismic profiles.

As already mentioned in section 4.3.5 the shelf of the Faial Island has the ideal physical conditions (high energy and narrow shelf) for the accumulation of material at the shelf break and shows evidences of sediment moving offshore (coarse sands and gravel at the outer shelf of Faial) and possible spillover. It appears that the combination of abundant earthquakes (as described in Chapter 2) and a high sedimentation rate are the most likely explanation for the sediment instability in the outer shelf.

4.3.7. Shelf hydraulic regime

According to Johnson and Baldwin (1986) wave-dominated shelves are those controlled by seasonal fluctuations in wave and current intensity, with active sediment transport restricted to intermittent storms, where fine grained sediments and small scale bedforms predominate. Storm-dominated shelves are struck by high intensity and moderate/high frequency hurricane and tropical storms, where bigger bedforms and coarse grained sediments dominate. The shelf of Faial may be classified as wave-dominated shelf although it presents some features of a storm-dominated shelf. There are not big bedforms in the shelf, except for the Channel Faial-Pico where these may be related to the strong tidal currents. However, this does not mean that the storms do not have an important role in the shelf dynamics. The width of the sedimentary cover in the shelf is very small, with average widths less than 1 km, which makes it less suitable to the generation of large scale bedforms. There are however megaripples (according to Reineck and Singh's classification, 1975) with lengths up to 30 m (Figure 58) in the shelf and the sedimentary cover is normally coarse-grained (see details in Chapter 5), although the lack of fine-grained sediments is a consequence of the limited fluvial sources. Still, the most supporting evidences for the storm influences in the shelf dynamics are the historical records and model forecasts. According to Borges (2003) classes 1 and 2 storms occur 4 times each five years and classes 3 and 4 once every 7 years. Classes 1 and 2 correspond to storms characterized by significant wave heights ranging from 4 to 7 m and classes 3 correspond to storms characterized by significant wave heights equal or exceeding 10 m. The MAR3G model (Carvalho, 2003), predicted 15 days of significant wave heights equal to 5 m every year and every 2 years 1 day of significant wave heights equal to 10 m. The instrumentally recorded storm of 26/27 February 2005 (Instituto Hidrográfico, 2005) showed continuous significant wave heights higher than 5 m during 19 hours, with the maximum significant wave height and maximum wave height registered, respectively 7.66 and 15.09 m.

In conclusion, the evidences described above permit to classify the shelf of Faial as a wave to storm dominated regime. The implications of this were also discussed in this chapter: coastal retreat associated to wave erosion,

sedimentation associated to seaward bottom currents that occur during storms, predominance of coarse grained sediments all over the shelf, sediment accumulation over the shelf break that generates instability and possible spillover.

Chapter 5. Origin and evolution of the insular shelf of Faial

5.1. Introduction

Although the modern continental margin is a product of many millions of years of sediment deposition and erosion and over this time the environments have changed dramatically, many present margin shapes seem to reflect recent and ongoing geological processes. Furthermore, seismic patterns for most margins show that changes to the overall shape of a margin through time tend to be incremental, cumulative, and slow. Therefore, unless the rates of deposition or erosion on the continental slope are extremely high, some portion of the modern morphology must be inherited from the previous underlying form (O'Grady et al., 2000). Consequently, it is expected that the abrasional processes responsible for the development of the insular shelf of Faial have left an imprint on the present-day morphology. That imprint is probably well preserved on the more remarkable morphological features of the shelf, namely the shelf width and the shelf break.

The aim of this chapter is to discuss these features and to assess which were the processes that have conditioned the final morphology of the shelf. One of the processes addressed is the shelf widening rates and for that reason the sources of sand and gravel are once again discussed based on the new rates presented. Finally, an evolutionary model of the shelf is proposed with basis on the previous discussions.

5.2. Shelf width

As already stated in Chapters 1 and 4, Menard (1983) put forward the idea that the shelves of volcanic islands evolved by competition between constructional and erosional processes. The effects of sea-level variation, tectonic subsidence

or uplift and isostasy of the island will of course complicate the simplicity of this model. When the volcanic activity becomes less frequent, the island cools and subsides. Meanwhile, erosion starts and subsidence can be opposed by isostatitc compensation due to unloading of the eroded material. On the other hand, renewed volcanism can promote subsidence due to increase of crustal loading. At the same time, eustatic changes in sea level can cause relative emergence or submergence in a range of few hundred meters.

Despite the complexity of the subject, Menard (1983) compiled data from several volcanic islands and compared the age of the coastal sectors against the respective shelf width. Taking into account the numerous uncertainties that this type of analysis may be affected by, he found a linear erosion rate of 0.6 mm/year for the Canary Islands, 1.1 mm/year for the reefless Hawaiian Islands and 1.7 mm/year for Marquesas Islands. More recently, Dickson (2004) studying the development of talus slopes around the Lord Howe Island referred to a 10 km wide platform which has been volcanically inactive for the last 6 Ma. Applying Menard's simple calculations (1983), Lord Howe Island shelf has been eroding with a rate of 1.7 mm/year.

These figures suggest that many island shelves around the globe have erosion rates between 0.6 and 1.7 mm/year, simply by comparing their shelf width against the age of the adjacent coastal terrains. This is assuming that the present-day shelf break is somehow inherited from the previous underlying form, created after the main volcanic activity has stopped, thus giving rise to the initial development of an erosional shelf. The existence of this concordant coastal retreat rates for oceanic islands so diverse, poses the following question: Should one expect similar values for the Azorean Islands? Or the similarity between these figures is just a mere coincidence?

There is however some difficulty in developing an accurate uncertainty analysis for the calculation of the erosion rates. The difficulty remains in knowing the precise time that the erosional shelves have begun to develop. To overcome this difficulty four main assumptions have been taken into account:

1. The older ages of the diverse coastal sectors referred in the bibliography

correspond to the time when the main volcanism has ceased and the shelves have begun to form.

2. The K-Ar datings are accurate enough to make this analysis. That might not be true as discussed in the section of Chapter 2.1.2.
3. The present-day shelf break is inherited from the previous underlying form created in the initial development of the erosional shelf (i.e. no major modification has occurred).
4. There has not been any volcanic episode strong enough to reset the abrasion platforms after their creation.

5.2.1. Relationship between shelf width and shelf age

In chapter 2, a review of the emerged geology of the Faial Island showed that the present day island is composed by four different geomorphological regions that correspond to different stages of volcanism. Following Menard's view (1983) that older islands would have wider shelves, the width of the shelf was measured and compared with the age of the adjacent coastline in the four geomorphological regions. It is assumed that a shelf sector that is adjacent to a determined geomorphological region has the same age of the oldest rock dating found in the region. The shelf edge mapping was presented in Chapter 3 (see red line in Figure 141) and the values presented in Figure 141 and Table 7 are the minimum and maximum distances of the shelf edge to the coastline for each sector. As already mentioned in Chapter 3 the shelf edge was not entirely mapped in some sectors, therefore for these unmapped sectors the shelf width might even be higher. In some of the unmapped areas of the shelf, the shelf edge was well represented by the slope changes in the slope map derived from the hydrographic chart of the Instituto Hidrográfico (see Figure 40 in Chapter 2 and green line in Figure 141) and those shelf widths were also taken into account in Table 7.

The older emerged terrain is the **Pedro Miguel Graben region** which has on its base the remnants of the older Ribeirinha shield volcano which begun its subaerial formation around 800 Ka (Madeira and Brum da Silveira, 2003). Assuming an age of 800 Ka and a width between 2000 to 3000 m for the abrasion platform, an erosion rate of 2.5 to 3.8 mm/year is obtained. The sector E lies on

the Channel Faial-Pico and for that reason this kind of analysis cannot be made since there is no shelf break of erosional origin in the Channel.

Table 7 – Minimum and maximum erosion rates based on the shelf age and respective shelf width of the different shelf sectors

Sectors	Shelf Age (Ka)	Minimum shelf width (m)	Minimum erosion rate (mm/year)	Maximum shelf width (m)	Maximum erosion rate (mm/year)
A1	10000	100	10.0	600	60.0
A2	10000	100	10.0	1000	100.0
B	470000	1800	3.8	2500	5.3
C	470000	900	1.9	1400	3.0
D	800000	2000	2.5	3000	3.8
F	30000	800	26.7	1500	50.0
G	470000	600	1.3	900	1.9
H	470000	900	2.5	1600	3.4

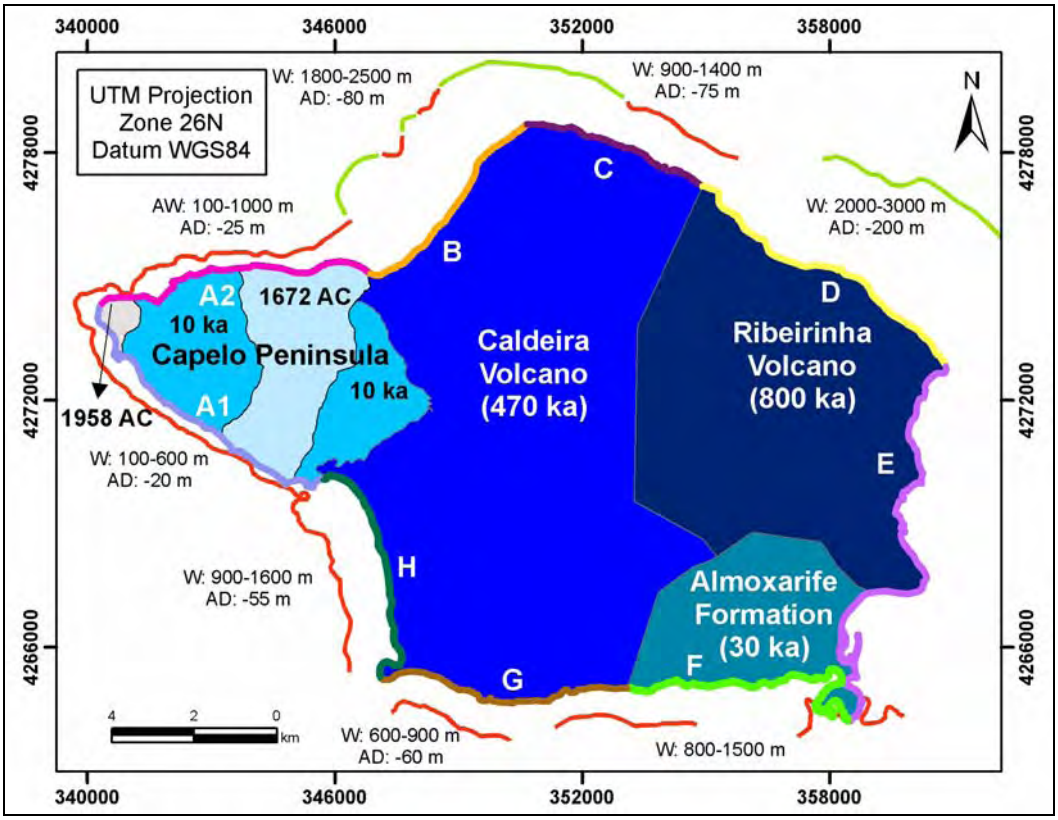

Figure 141 – The shelf edge variability of the Faial shelf and its relation with the subaerial geology. The red line represents the shelf edge mapped in this work. The green line represents the inferred shelf edge based on the Instituto Hidrográfico map (1999). The bold colored lines around the coast of Faial and the white capital letters represent the different shelf sectors. The different blue areas inside the island represent the four geomorphological regions that compose its subaerial part. W means shelf width and AD average depth of the shelf break.

The second older emerged terrain, the **Caldeira Volcano** is at least 470 Ka and has a shelf width of 1800 to 2500 m at the sector B, a shelf width of 900 to 1400 m at the sector C, a shelf width of 600 to 900 m in the sector G and a shelf width of 1200 to 1600 m at sector H. Assuming an age of 470 Ka and the shelf widths of the abrasion platforms for the respective sectors, an erosion rate of 3.8 to 5.3 mm/year is found for sector B, 1.9 to 3.0 mm/year for sector C, 1.3 to 1.9 mm/year for sector G and 2.5 to 3.4 mm/year for sector H.

The third older emerged terrain is the **Horta-Flamengos-Feteira** region with an age of 30±20 Ka. Assuming an age of 30 Ka and a width of the abrasion platform between 800 to 1500 m, an erosion rate of 26.7 to 50 mm/year can be found.

The younger emerged terrain is the **Capelo Peninsula** whose age is less than 10 Ka and has several historic eruptions. The shelf width ranges from 100 to 600 m for sector A1 and from 100 to 1000 m for sector A2. Assuming an age of 10 Ka and the shelf widths of the abrasion platform for the respective sectors, an erosion rate of 10 to 60 mm/year is obtained for sector A1 and 10 to 100 mm/year for sector A2.

Although Menard's observations that older volcanic terrains tend to have wider shelves is generally confirmed for the Faial shelf (Figure 142), all the shelf sectors show exceptions to this rule. For example, **Horta-Flamengos-Feteira** region has a wider shelf than the shelf sector G, although it is younger. The same happens for almost all the shelf sectors, there are shelf sectors whose maximum width is bigger than the minimum width of older sectors (see Table 7). There also some shelf sectors that show erosion rates much higher (10 to 100 mm/year for the shelf sectors A1 and A2 and 26.7 to 50 mm/year for the shelf sector F) than those calculated from Menard (1983). Another singularity that was found was the remarkable difference in the shelf widths for sectors of the same age (e.g. the differences found between sectors B, C, G and H - see Table 7). If one considers that the sectors that share the same age have had synchronous volcanism, the differences found on the shelf width have to be explained by other processes that have played a more significant role on the widening of these platforms. Finally, the average rate of shelf widening of the volcanic islands (0.6 - 1.7 mm/year) compiled

by Menard (1983) is smaller than the one measured in the older shelf sectors (B, C, D, G and H) of the Faial Island (1.9 - 5.3 mm/year). The reasons for these differences may be explained by the youth of the Faial Island (just 800 Ka old) when compared with the islands that Menard used in his study (most had more than 1 Ma, up to 16 Ma). According to Menard (1986), as the shelf increases in age (and consequently in width), the rate of the shelf widening decreases with time because the wave attenuation is higher and consequently less energy reaches the coastline.

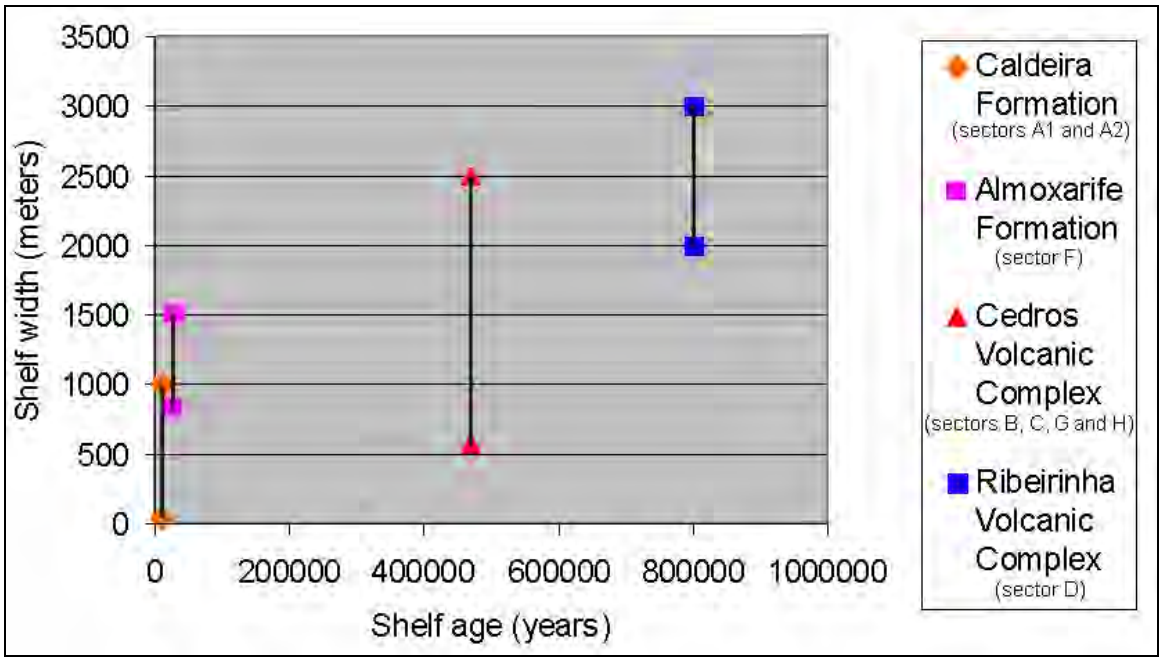

Figure 142 – Relation between shelf width and age of the shelf sectors in the Faial Island. Each different symbol represents the minimum and maximum width of the shelf sectors that share the same age.

The shelf widening erosion rates are the result of three distinct processes acting on the coastal cliffs: they include marine erosion, cliff sub-aerial erosion and river erosion, which may of course have varied for the different sectors. There are however two important factors that Menard (1983) showed to account for considerable differences in the shelf width. The windward sides of the islands normally show higher erosion rates, due to increased surf and subaerial erosion. The windward side is also more prone to rainfall, and hence increasing river erosion. The higher intensity of subaerial erosion produces deeper valleys on the

windward side and waves can erode headlands between valleys to cut a broad shelf much faster than they would in the continuous high cliffs of the lee side (Menard, 1983). Sunamura (1977) has also shown a positive relationship between wave-induced cliff erosion and the erosive force of the waves.

5.2.2. Relationship between shelf width and shelf energy

In chapter 2, a review of the wave conditions in the Azores central archipelago has shown the direction and height of the predominant waves and the Directional Annual Wave Frequency (DAWF) and the Directional Annual Maximum Wave Height (DAMWH) were calculated (see Figure 53 and Tables 4 and 5 in section 2.4.4 of Chapter 2). From the analysis of the Figure 143, a somewhat linear relationship between the shelf width and the DAWF may be found, explaining the variability of the shelf width. In order to have a better relationship, the shelf of sector C should be wider than sector H, which is not the case (see dashed line in Figure 144). The relationship between the shelf width and the DAMWH shows a better linear relationship (Figure 144) for the sectors C, G and H because there is a swap between sectors C and H. However, the sector B falls out of the relationship (see dashed line in Figure 144). The coastal areas of the sectors B and H are submitted to higher precipitation rates (see Figure 137 in Chapter 4), which mean that part of the shelf widening may be accounted to cliff subaerial erosion in these sectors. Therefore if the component of the cliff subarerial erosion in the Figure 143 could be weighted and removed, the graph would show a better relationship (Figure 145). This probably means that wave frequency plays a bigger role than wave height in coastal retreat.

Submitting sectors A1 and A2 to the same analysis, we found again a linear relationship between shelf width and wave predominance. Sector A2 is submitted to higher wave frequency and wave heights (see Table 4 and Table 5 in section 2.4.4 of Chapter 2) and consequently on average has a wider shelf (see Table 7).

In conclusion, there appears to be a linear relationship between shelf width and wave energy for the shelf sectors of the same age, in which the wider shelf sectors are the ones submitted to higher wave energy. It also appears to exist a linear relation between shelf width and age of the shelf sectors, with older sectors

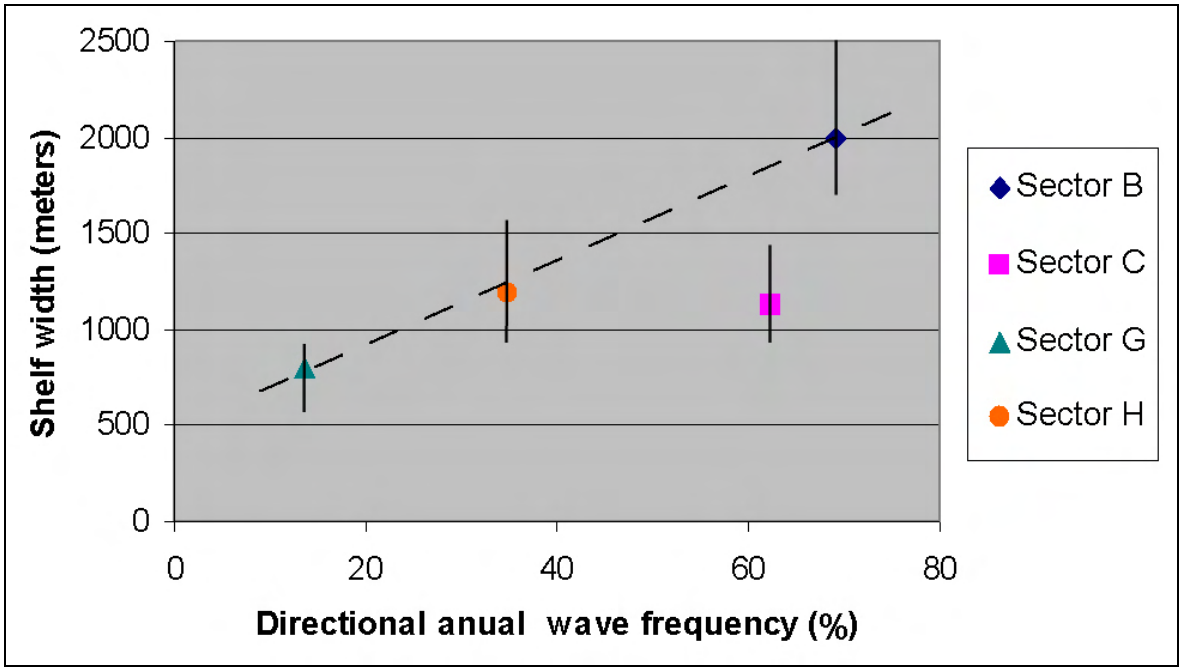

Figure 143 – Relationship between the shelf width and the directional annual wave frequency (DAWF). The position of the symbols represents the average width and the vertical lines that cross them the variability of the shelf width. The hatched line represents the best-fit of the linear relationship.

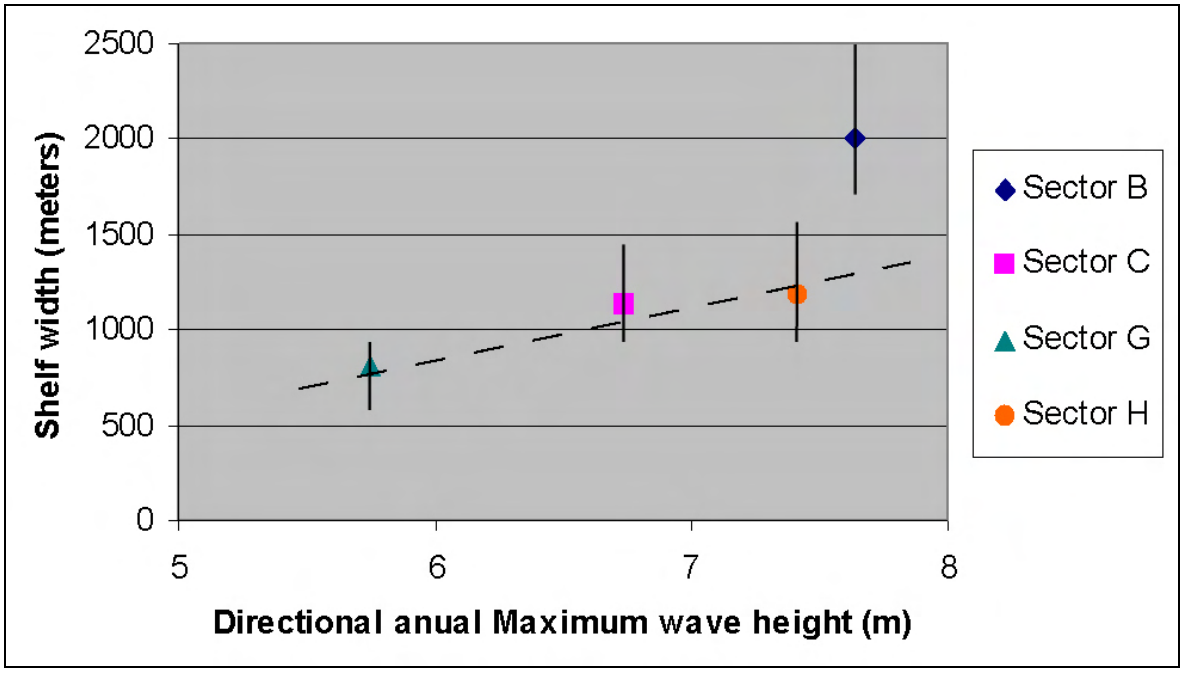

Figure 144 - Relationship between the shelf width and the Directional annual maximum wave height (DAMWH). The position of the symbols represents the average width and the vertical lines that cross them the variability of the shelf width. The hatched line represents the best-fit of the linear relationship.

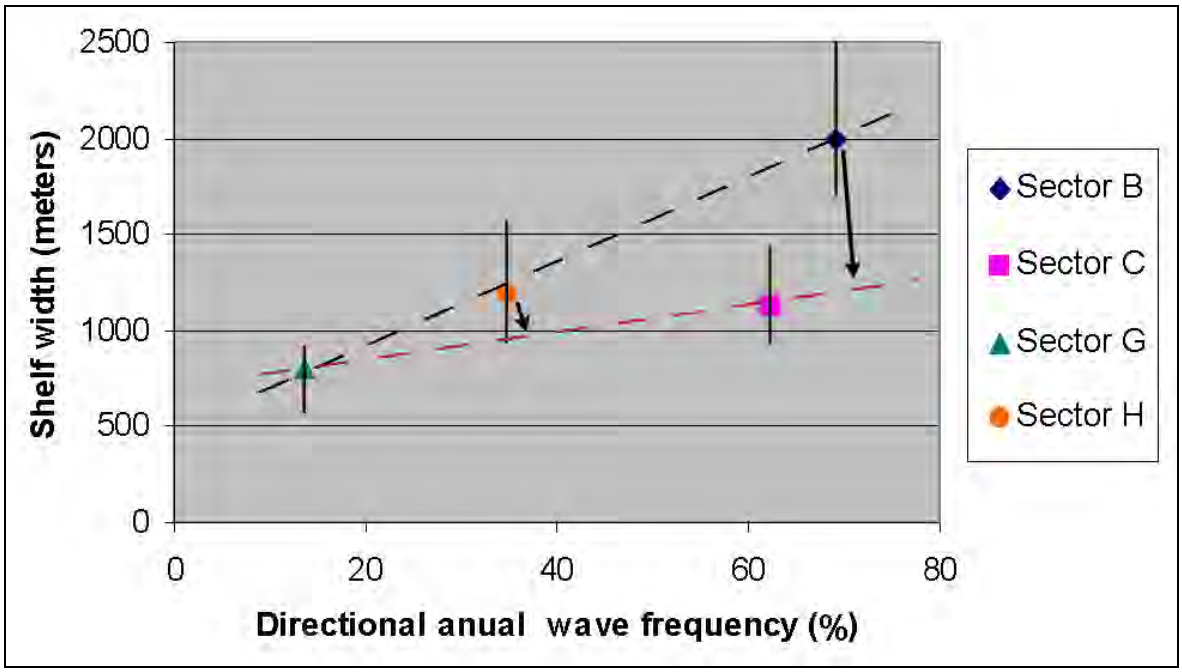

Figure 145 - Relationship between the shelf width and the directional annual wave frequency (DAWF). The position of the symbols represents the average width and the vertical lines that cross them the variability of the shelf width. The black-hatched line represents the best-fit of the linear relationship. The red-hatched line represents the best-fit of the linear relationship if the contribution of the subaerial cliff erosion to the shelf width was removed.

having wider shelves (Figure 142). The imperfections in the linearity of these relationships (shelf width-shelf age and shelf width-shelf energy) would have probably been caused by original distinct slopes and volcanic compositions. If the flanks of the volcano have low gradients, there is less material for coastal erosion to remove, hence potentially faster coastal retreat rates. The variable resistance of the substrate to erosion would also have produced different coastal erosion rates (Sunamura, 1992). Furthermore, other factors may account for disturbing the calculations which are uncertainty in subsidence rate, possibility of some lava flows having covered the shelf and resetting the geomorphology, pyroclastic materials on the shelf, etc.

It is also possible that climate variability has changed the wave energy around the island which complicates the present relationship between shelf width and shelf energy. Dennielou et al. (1999) showed that in the last three glacial periods, the Gulf Stream carried fine particles at depths shallower than 1500 m, south of the modern Gulf Stream. Similarly, Schiebel et al. (2002) showed that planktic foraminifers from multi-cores over the last 290 Ka indicate a southward

shift of the Azores Front during glacial times, the presence of transitional water masses south of the Azores islands and a southward shift and a weakening of the Azores Current. According to Crowley (1981), the variations in the ocean circulation around the Azores during the seven glacial advances of the last 150,000 years can be explained in terms of increased Gulf Stream/North Atlantic Current velocities advecting warmer waters into the study area. The increased velocities may have been due to a combination of increased wind stress, increased baroclinicity of surface waters, and steepening of the thermocline due to increased cooling of water (18°C) south of the Gulf Stream. All these authors report changes of the ocean circulation in the Azores related to the glacial events. It is possible that the variations in the wind pattern may have changed the resulting wave energy that reaches the coastline and are therefore also responsible for the less good linear relationship between the shelf width and shelf energy.

5.2.3. Extreme shelf widening erosion rates

As mentioned before, there are three sectors (sectors A1, A2 and F) that have very high shelf widening erosion rates (10 to 100 mm/year) when compared with those estimated (0.6 and 1.7 mm/year) by Menard (1983).

The shelf sector F (Figure 141) is wider than some of the older sectors of the shelf (shelf sectors C and G) and shows higher erosion rates (Table 7). The Almoxarife Formation (see Figure 43 and text in Chapter 2) comprises Hawaiian/ Strombolian volcanism and most of it appears in the Horta-Flamengos-Feteira region (Figure 141), probably covering part of the southeastern slope of Caldeira volcano (470 Ka old) and the southern remainings of Ribeirinha volcano (800 Ka old). Therefore, it is possible that when this volcanism has started 30 Ka ago, a considerable abrasion platform was already cut on the volcanic buildings of Caldeira and Riberinha Volcano with the coastline of that time landwards of the present-day one. This volcanism could have started on land, on top of one or both the older volcanic buildings and prograded seaward building what is now the Horta-Flamengos-Feteira region, resetting part of the older abrasion shelves of Caldeira and Ribeirinha volcano (see Figures 164 and 165).

The offshore part of Capelo Peninsula (sectors A1 and A2) shows a great

variability in the shelf width ranging, from 100 to 1000 m (Figure 141 and Table 7). This fact may be explained because this peninsula has been formed by the accumulation of several lava flows over the last 10 Ka and their diachronic pattern may account for the variability in the shelf width. One good example is the southeastern end of the sector A1 where the narrowest values of the shelf can be found (Figure 141). This area has onshore a recent volcanic lava flow (1672 AC) which has probably caused volcanic progradation over the shelf (arrow in Figure 146). On the northern side, where the flow reaches the coast, the adjacent shelf is considerably wider probably because the progradation did not occur so extensively. These facts are confirmed by the echo analysis in chapter 3 (see Figures 77, 80 and 82 in Chapter 3) that showed that the southeastern part of the A1 sector has well preserved lava flows and opposite of it, in the sector A2, the lavas did not advanced much further offshore.

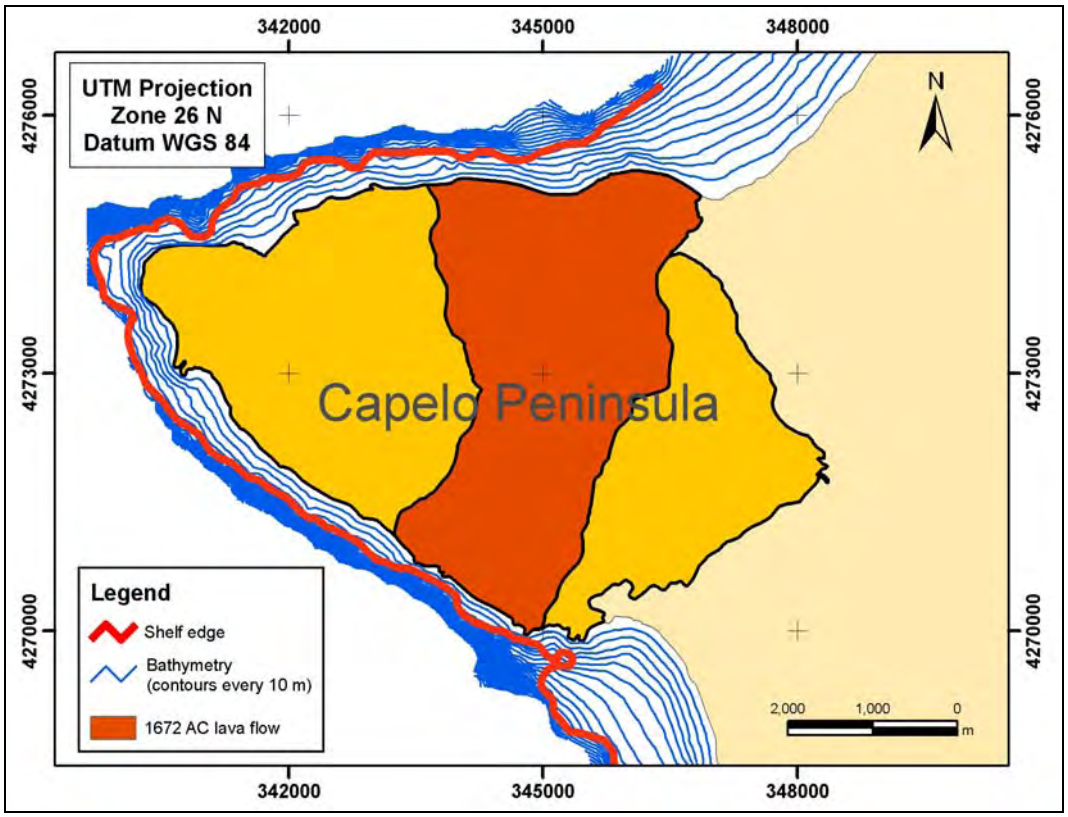

Figure 146 – An example of how the shelf width variability of the Capelo Peninsula is related with the diachronism of the volcanism. The 1672 AC lava flow has prograded south into a previous cut shelf, decreasing the shelf width in this area (marked by the arrow). In the northern part it has not prograded further offshore and therefore did not decrease much the width of the previous shelf.

Despite the fact that the shelf growth offshore the Capelo Peninsula (sectors A1 and A2) has been diachronic, it nevertheless shows very high erosion rates (10 to 100 mm/year) and there is not a simple explanation like the one found for the sector F. The other older sectors show erosion rates much smaller (between 1.3 and 5.3 mm/year, see Figure 141 and Table 7). There should be an explanation for the discrepancies in the erosion rates of the sectors A1 and A2 relative to the other older sectors (B, C, D, G and H). The easiest explanation is to assume that the volcanic complexes in the sectors B, C, D, G and H did not form in a single event (geologically speaking) and repeated volcanism has reset for several times the abrasion platforms. Another explanation is to assume that the abrasional shelves formed in the sectors B, C, D, G and H are not the result of the cumulative erosion during the entire sea-level cycle, but that erosion only occurs during highstand conditions. Therefore the high erosion rates of the sectors A1 and A2 represent highstand conditions because when the shelf started to form 10 Ka ago the sea-level was rising and at 7.5 Ka ago it was already at 10 m below the present sea-level. It is possible to presume that after a first complete cycle of sea-level oscillation (drop and rise) the shelf widening rates of the sectors A1 and A2 would become progressively smaller, because during most of the time of the cycle, the erosion promoted by the sea does not reach the present cliffs. The first hypothesis is impossible to assess because there is not detailed geological knowledge of the subaerial evolution of the Faial Island. The second hypothesis is easier to check and one way to untangle this is to compare these high erosion rates with the ones found presently at the sea cliffs.

To test the second hypothesis one must turn to Borges work (1997, 2003). He used aerial photographs to calculate erosion rates over a time period of 44 years for several coastal segments in S. Miguel Island (Azores). There, he found a great variety of figures, with average erosion rates of 0.21 m/year and realized that the differences found had to do with the natural variability of the cliffs studied and in some cases with the wave climate. Another conclusion from Borges's work (1997, 2003) was that when analyzing different time spans he would get different erosion rates. The S. Miguel erosion rates are in fact very high, but are difficult to relate to the erosion rates of the sectors A1 and A2 because there is not a detailed

description of the areas under study. Luckily, Borges (2003) describes in detail two cases, the cliff of Rocha Quebrada and the cliff of Rocha dos Campos. These descriptions are useful to compare with Faial's coastal sectors, since they are two end-members representative of volcanic cliffs. The cliff of Rocha Quebrada is 20 m height and represents a cliff less prone to erosion since it is constituted manly by basaltic lava flows and has an average erosion rate of 60 mm/year. On the other extreme is the cliff of Rocha dos Campos, which is 50 to 70 m height, more prone to erosion once it is manly constituted by pumice pyroclasts and has an average erosion rate of 140 mm/year. These figures are more similar with those measured in the sectors A1 and A2, especially the ones from Rocha Quebrada, which cliff composition does not differ much from the Capelo cliffs. The heights of Capelo cliffs are however extremely variable, between 10 and 120 m. Although the differences in the shelf width of the Capelo Peninsula can be attributed to the diachronic volcanism, some of the variability in the erosion rates may also be explained by the cliff heights, with the higher cliffs being less prone to erosion.

In order to test this second hypothesis the composite sea-level curve described in the section of 2.2.5 of Chapter 2 is used to recalculate the erosion rates for all the sectors, assuming that the widening of the shelf is only occurring when the sea-level is around the present level. Figures 147 and 148 try to explain in a schematic way, why most of the widening of the shelf occurs during highstand conditions (sea level around the present level). First, let us consider a stepping sea-level curve like the one of Figure 147, with sea-level starting at -140 m and an initial slope profile of the island (Figure 148). As the sea-level rises (orange part of the curve in Figure 147) it starts eroding areas of the initial profile (orange triangles in Figure 148). When it reaches the 10 m, it starts a descending cycle (blue part of the curve in Figure 147) and continues eroding (blue areas in Figure 148) the previous shelf formed during the sea level rise. From the Figure 148, it is obvious that after one rise and drop of sea-level, the erosion at the present sea-level (0 m) is three times bigger than the erosion made at shallower depths and for that contributes the three stillstands at the present-level (0 m when it rises, at 10 m and again at 0 m when it drops) compared with only one at each shallower depth. The implication of this phenomenon is that after several cycles of sea-level oscillations

what it really counts for the widening of the shelf are the highstand conditions (Figure 148). In this work, it will be considered highstand conditions when the sea-level is between -10 and 10 m relative to the present sea-level.

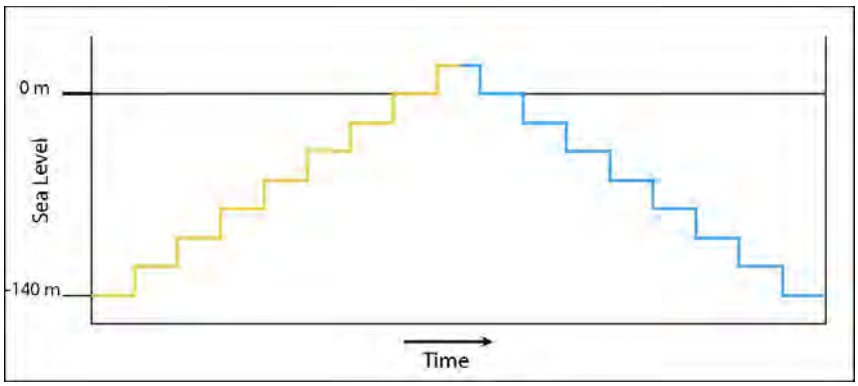

Figure 147 – Hypothetic sea-level rise and drop with vertical steps of 20 meters. The orange part of the curve corresponds to a sea-level rise and the blue part to a sea-level drop.

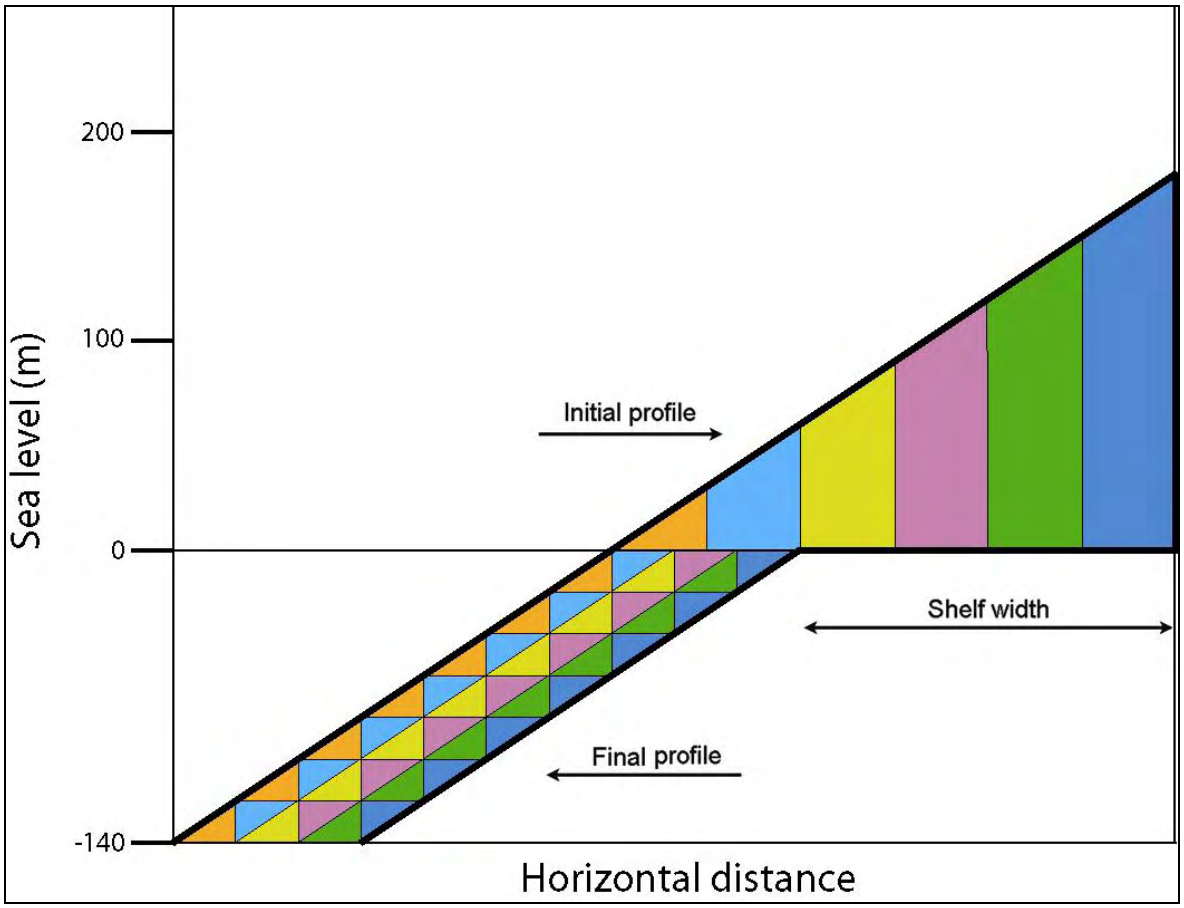

Figure 148 – Schematic model of the development of an abrasional shelf, using the curve of Figure 147. Each color corresponds to a cycle of sea-level rise or sea level drop (e.g the orange color represents the erosion made by a sea level rise from -140 to 10 m and the light blue the erosion made by a sea level drop from 10 to -140m and so on).

5.3. Sea-level curves and estimation of net erosion rates

Menard (1983) was not the first to propose that some continental shelves were wave-cut features. Before him, Shepard (1973) had already made that suggestion and following this assumption others authors (Sunamura, 1978; Trenhaile, 2001) have modeled the formation of erosional continental shelves by mechanical wave erosion during the sea-level glacially induced fluctuations. Storms et al., (2002) have showed the importance of substrate slope in coastal evolution through sea-level oscillations. According to these authors, barrier coasts develop only on gentle slopes, whereas steeper slopes give rise to a closed coastline or even cliff formation. Numerical modeling by Trenhaile (2001) suggested that shelves cut into rock should be significantly narrower and more steeply sloping than depositional shelves, which is also the case of Faial Island when compared with the continental margins (O'Grady et al., 2000).

Trenhaile's modelling (2001) assumed that the enlargement of the abrasional shelf was continuous during an oscillating sea-level. However, as has been discussed in section 5.2.3, there are evidences that probably the enlargement of the shelf is only occurring when the sea is at the present high level (± 10m). Therefore, the main question is: Is it or not plausible that over the 470 Ka of the Caldeira Volcano and the 800 Ka of the Ribeirinha Volcano the coastline has only been retreating during highstand conditions? Table 8 shows the amount of time that the sea has been at different depths from the present to 470 Ka. These calculations result from using the generalized sea-level curve for the last 130 Ka based on a U/Th coral datings (Thompson and Goldstein, 2006) and the curve from Bintanja et al (2005), from 130 Ka to 470 Ka. The same procedure (the curve of Bintanja et al., 2005) was used to generate Table 9 to calculate the amount of time that sea level has been at different depths from 470 to 800 Ka.

The estimation of the percentage of time that the sea-level has been at different levels makes possible the calculation of the net cliff erosions integrated over the time. This calculation will be done for the different coastal sectors of the Faial Island and the selected depths (10 to -10 meters) were chosen assuming that when the sea level is below these depths no erosion is occurring on the

Table 8 – Percentage of time that sea has been at different levels (10 m interval) for the period of 470 Ka (based on Thompson and Goldstein, 2006, for the last 130 Ka and Bintanja et al., 2005, from 130 Ka to 470 Ka).

Sea-level variations from 0 to 470 Ka			
Depth 1	Depth 2	Nº of Ka years	% of time
10	0	20.94	4.46
0	-10	19.17	4.09
-10	-20	29.34	6.26
-20	-30	41.84	8.92
-30	-40	26.31	5.60
-40	-50	33.18	7.06
-50	-60	28.35	6.03
-60	-70	34.48	7.34
-70	-80	40.54	8.63
-80	-90	65.40	13.91
-90	-100	51.50	10.94
-100	-110	30.18	6.41
-110	-120	30.02	6.38
-120	-130	12.44	2.65
-130	-140	6.31	1.34
Total		470.00	100.00

Table 9 – Percentage of time that sea has been at different levels (10 m interval) for the period of 470 to 800 Ka (based on Bintanja et al., 2005).

Sea-level variations from 470 to 800 Ka			
Depth 1	Depth 2	Nº of years	% of time
10	0	0.00	0.00
0	-10	0.00	0.00
-10	-20	6.84	2.07
-20	-30	25.30	7.67
-30	-40	26.32	7.98
-40	-50	34.69	10.51
-50	-60	42.87	12.99
-60	-70	49.34	14.95
-70	-80	32.26	9.78
-80	-90	22.01	6.67
-90	-100	37.11	11.25
-100	-110	29.68	8.99
-110	-120	9.93	3.01
-120	-130	9.24	2.80
-130	-140	4.40	1.33
Total		330	100

coastline because the waves cannot reach the cliffs. From Figure 34, the sea level has remained between -15 m and -28 m water depth from 470 to 800 Ka. Consequently, it will be considered highstand conditions for the retreat of the paleo-coastline of the Ribeirinha Volcano when the sea-level was between -10 and -30 m relative to the present sea-level.

Table 10 shows the estimation of the width of the abrasion platform for the different coastal segments of the Faial Island. The calculus of the shelf width (*CSW* - Equation 12) was made assuming an erosion rate of 60 mm/year, using the percentage of time that the sea-level remained at a certain level (between 10 and -10 m water depth for the Caldeira and Ribeirinha Volcano during the last 470 Ka, and between -10 and -30 m water depth for the Ribeirinha Volcano for the period

Table 10 – Calculated Shelf Width (*CSW*) using the erosion rate from Borges (1997, 2003) and the Corrected Erosion Rate (*CER*) based on the *CSW* (see text for details)

Coastal Sectors	*SA* (years)	*APSW* (m)	*PT* between 10 and -10m	*PT* between -10 and -30m	*ER* (mm/ year)	*CSW* (m)	Difference between *CSW* and *APSW*	*CER* (mm/y ear)
A1	10000	400	100		60	600	100	40
A2	10000	500	100		60	600	100	50
B	470000	2100	8.55		60	2411	311	52
C	470000	1100	8.55		60	2411	1311	27
D	800000	2500	8.55	9.74	60	4340	1840	35
F	30000	1100	100		60	1800	700	37
G	470000	800	8.55		60	2411	1611	20
H	470000	1300	8.55		60	2411	1111	32

$$CSW\left(\text{Calculated shelf width}\right) = \frac{ER}{1000} \times \frac{SA \times PT}{100} \qquad (12)$$

ER - Erosion rate of basaltic lava flow cliffs (60 mm/year) from Borges (1997, 2003).

SA – Age of the abrasional shelf (years).

PT – Percentage of time that sea-level has been at -10 to +10 m (0-470 Ka), -30 to -10 m (470-800 Ka) or 100% (30 Ka to recent).

$$CER\left(\text{Corrected erosion rate}\right) = \frac{APSW \times ER}{CSW} \quad (13)$$

$APSW$ – Average present-day shelf width (m).

470-800 Ka). For the sectors A1, A2 and F, which are very recent (see age in Table 10), the sea-level is always rising and during all that time since their formation the surf erosion is widening their incipient shelves and for that reason the percentage of time used is 100%.

The CSW (Equation 12) using the erosion rate (60 mm/year) taken from Borges (1997, 2003) shows that using this value over the period of time that corresponds to a certain sea-level where the retreat of the coastline is occurring (-10 to 10 m for the period 0 to 470 Ka, -10 to -30 m for 470 to 800 Ka and 100% for 30 Ka to recent), gives an approximate value of the present-day shelf width. It proves to be a good estimation for the sectors A1, A2 and B, but not so good for the other sectors. The differences found may be explained by diverse erosion rates caused by the distinct factors mentioned before, which may include different original slopes and different composition of the volcanic buildings, different wave energy attack and different height of the cliffs being retreated. In fact, if we calculate the Corrected Erosion Rate (CER - Equation 13), values between 20 and 52 mm/year may be found, which are very similar to those reported by Borges (1997, 2003). The Equation 12 for sector F gives 1800 m and this value might be compatible with the present shelf width, considering a lower erosion rate (37 mm/year). However, in the section 4.2.3 it was considered the hypothesis that a considerable abrasion platform was already cut on the volcanic buildings of Caldeira and Riberinha Volcano (Figure 163) when the Almoxarife Formation prograded into the sea. Considering the higher maturity of the shelf in sector F (few well preserved lava flows, a large area with coarse clastic deposits and a high thickness of sediments – see Figures 76 and 77 in Chapter 3) when compared with sectors A1 and A2, this hypothesis remains valid.

Therefore, this type analysis appears to suggest that the erosion rates measured by Borges (1997, 2003) are compatible with the long-term erosion rates found by Menard (1983) and also with those measured in the older sectors of the

Faial Island, i.e. assuming that the shelf enlargement is only occurring when the sea is near its present high level. In addition, if high erosion rates as those suggested by Borges (1997, 2003), for instance 60 mm/year, were eroding the shelf during the entire cycle of sea-level oscillation, the Faial Island (14 to 21 km wide) would have been completely wiped out within 200 to 300 Ka. Only a very high effusion rate could explain the permanence of the Faial Island above sea-level.

Nevertheless, it is important to be cautious when analyzing these results. Several processes that contribute to cliff erosion were not included in the simulation and their effects cannot be evaluated. These include isostatic compensations, initial topography and composition of the volcanic buildings, accumulation and movement of loose sediments on the shelf and shelf break retreat. All these simplifications aim to reduce the complexity of the model and facilitate the analysis of the basic processes in the simulation. The author realizes the considerable uncertainty of this estimation, but thinks that is nonetheless better than having no estimate at all.

5.4. Depth of the shelf break

Dietz and Menard (1951) discussed the existence of the shelf break and proposed an abrasional origin due to surf erosion, formed during lowstands when the sea-level was 10 m or less above the break. According to them, this depth is related not to the wave-base limit but to the vigorous abrasion reflected by wave-breaking, which, in the most extreme cases, can break at these water depths.

Pickrill (1983) analyzed the morphology of several nearshore profiles from lakes and semi-enclosed bodies of water. His aim was to draw similarities between the small-scale terraces found in almost all profiles and the continental shelf. He found in almost all profiles a shallow nearshore platform whose depth increased slowly seaward, marked at the outer edge by a change to a steep gradient on the offshore slope. He also showed that the width of the shelf increases logarithmically with effective fetch. This study supports the evidences discussed in section 5.2.2 concerning the relationship between shelf width and wave effectiveness (whether

it is related to wave frequency or wave height).

Pickrill's terrace model represents the morphology produced during just one period of relative stable sea level, whilst the topography of the insular shelf has evolved in response to processes operating over thousands of years, including several transgressions and regressions. Assuming that the island shelf is a wave-cut platform, the depth of the shelf break is a result of isostasy as well as the combined effect of erosion (and deposition) over the period of all the sea level changes since the main volcanic activity has stopped. Moreover, the shelf break is considered as the seaward limit of continental or insular margins where subaerial processes (waves, wind, rivers, ice) have left a considerable imprint at low sea-level stands along with marine depositional events and mass-wasting processes during high sea-level stands (Southard and Stanley, 1976; Vanney and Stanley, 1983).

Trenhaile (2001) used a mathematical model to investigate the effect of glacially induced fluctuations in sea level on the evolution of wave-cut shore platforms and erosional continental shelves during the Quaternary. He showed that the breaks in slope are produced by the accumulated action of waves over many similar glacial stages and have a high preservation potential. Therefore, the shelf edge is considerable old and is not the product of a single low sea level in the late Quaternary, which means that probably the position of the present-day shelf edge of the Faial Island has not changed much since the shelf begun to form.

The shelf break has been mapped in the sectors A, B, C, D, F, G and H (Figure 141) and it is often a sedimentary feature (Figure 77 in Chapter 3). When the shelf break is a sedimentary feature it is normally called the depositional shelf break (Steckler et al., 1993) or offlap break (Vail et al., 1991). This feature is not dependent from sea level change but from sediment supply. Taking that into account, the Boomer seismic profiles that reached the shelf break have been analyzed in order to check if the shelfbreak is a depositional or an erosional feature (Figures 149, 150, 151, 152, 153 and 154). The position of the depositional shelf break represented in the Figures 149 to 154 is merely indicative since its mapping was based on the shelf bathymetry where the slopes exceeded 5º. Only the sectors G and H have Boomer seismic profiles crossing the shelf break and for

that reason the discussion that will follow is concentrated on these shelf sectors.

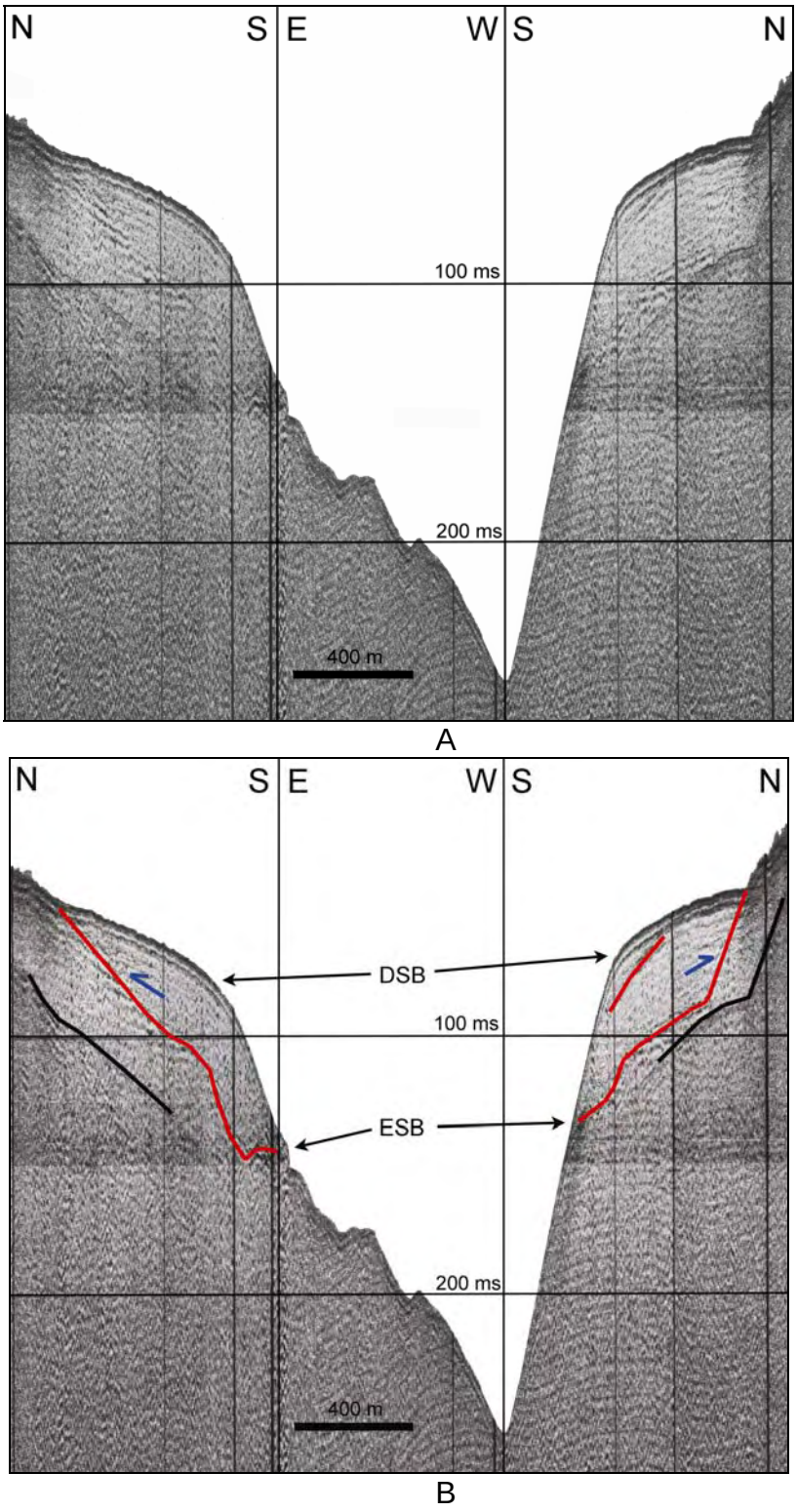

Figure 149 –Boomer seismic profile (A – non-interpreted, B – interpreted) showing the Depositional shelf break (DSB) and the Erosional shelf break (ESB). The red line represents the base of the seismic unit defined. See location on Figure 157.

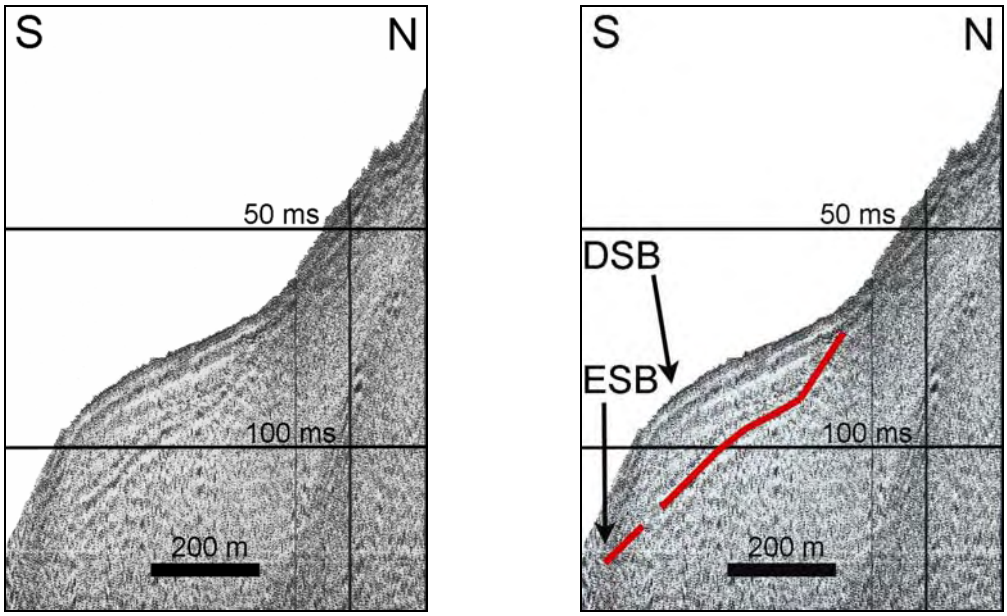

Figure 150 – Boomer seismic profile (A – non-interpreted, B – interpreted) showing the Depositional shelf break (DSB) and the Erosional shelf break (ESB). The red line represents the base of the seismic unit defined. See location on Figure 157.

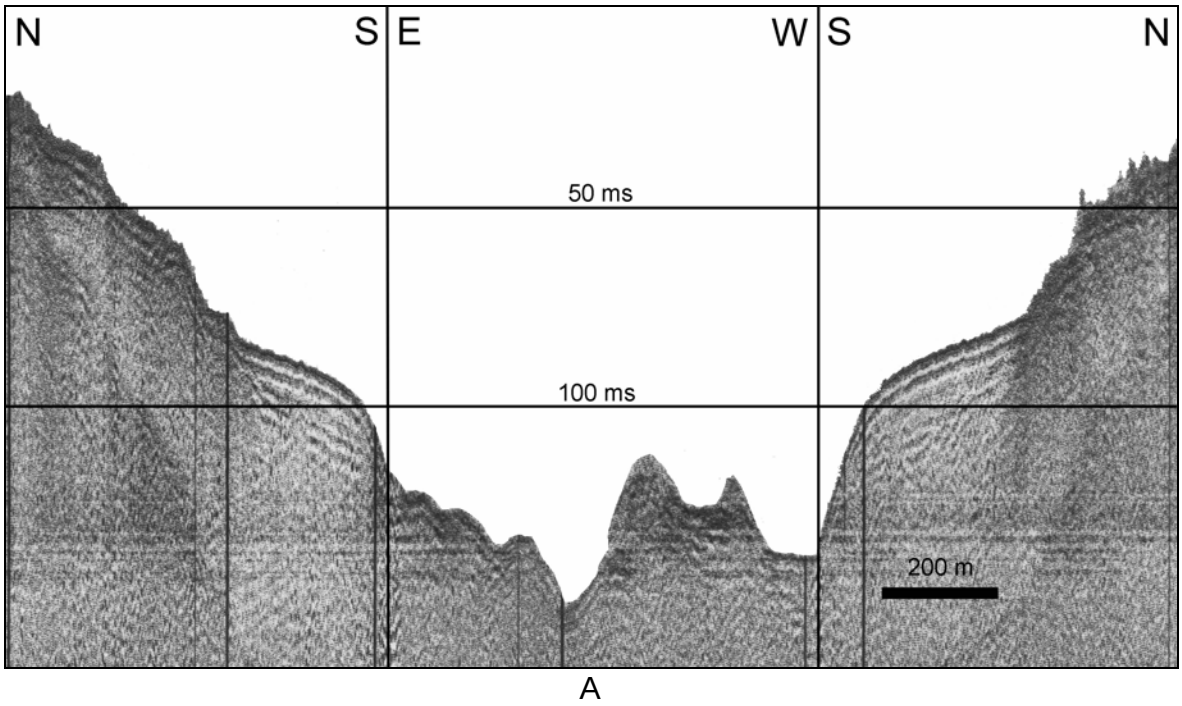

Figure 155 shows the percentage of time that the sea level has been at different levels during the last 470 Ka, based on Table 8. A brief analysis of this figure shows that the sea has been a significant amount of time (16%) between the -80 and -90m water depth, when compared against the other depths.

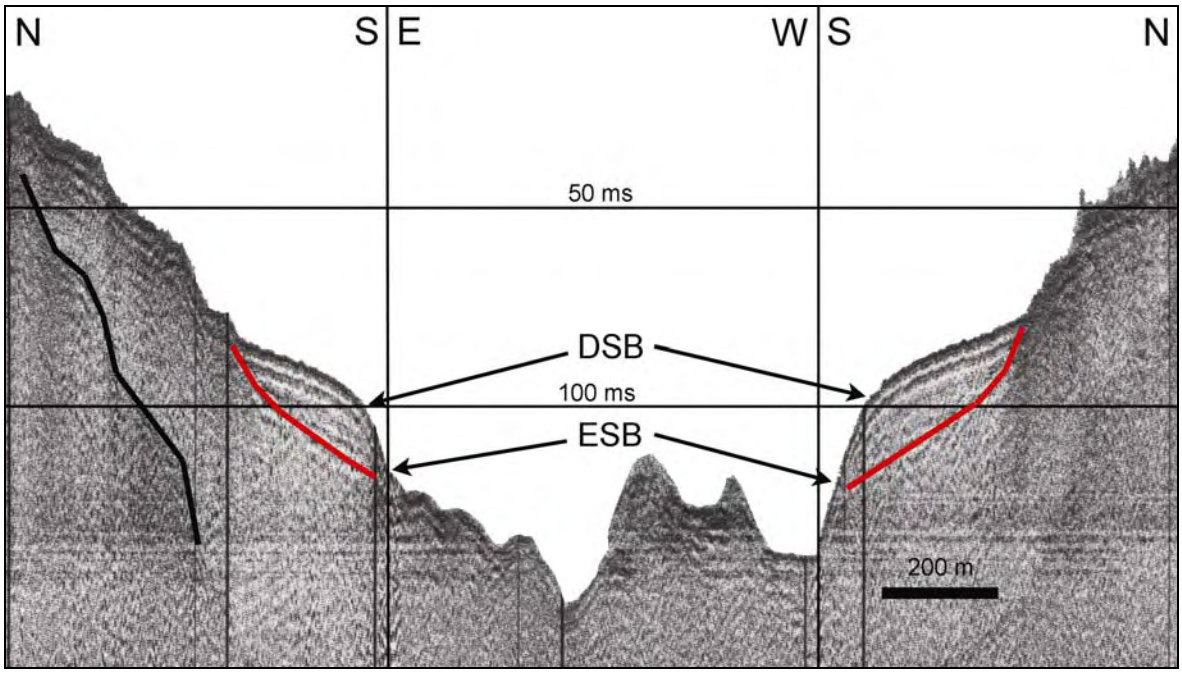

B

Figure 151 – Boomer seismic profile (A – non-interpreted, B – interpreted) showing the Depositional shelf break (DSB) and the Erosional shelf break (ESB). The red line represents the base of the seismic unit defined. See location on Figure 157.

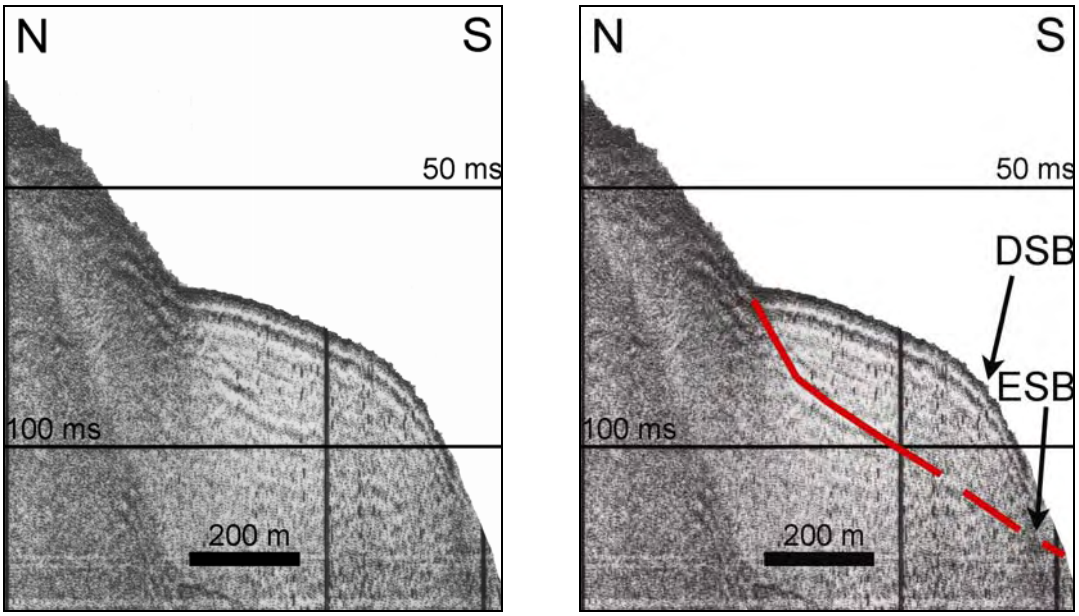

A B

Figure 152 – Boomer seismic profile (A – non-interpreted, B – interpreted) showing the Depositional shelf break (DSB) and the Erosional shelf break (ESB). The red line represents the base of the seismic unit defined. See location on Figure 157.

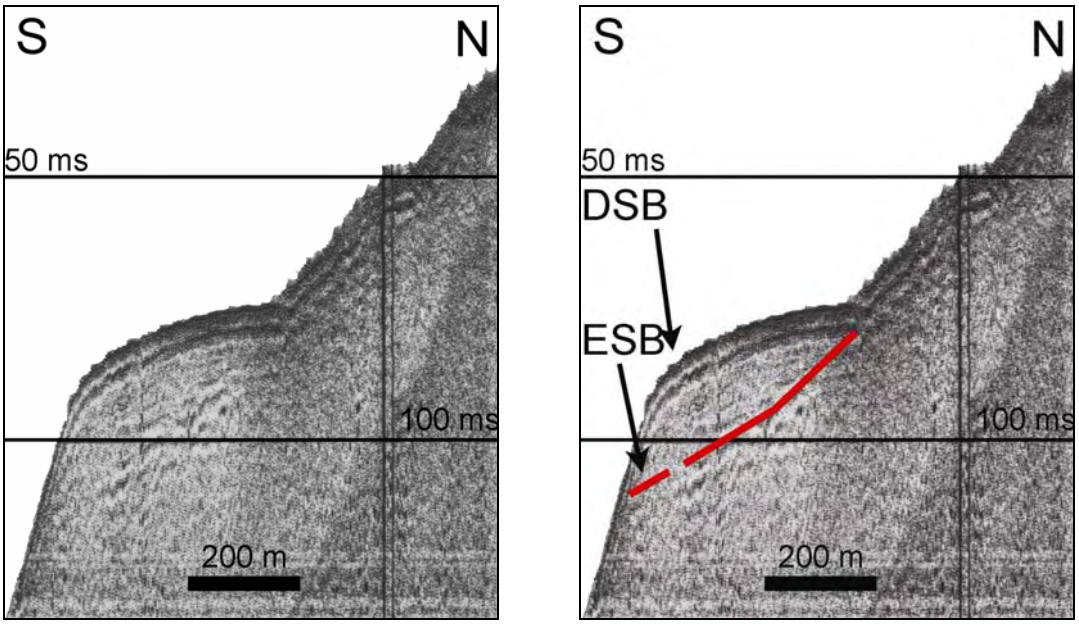

Figure 153 – Boomer seismic profile (A – non-interpreted, B – interpreted) showing the Depositional shelf break (DSB) and the Erosional shelf break (ESB). The red line represents the base of the seismic unit defined. See location on Figure 157.

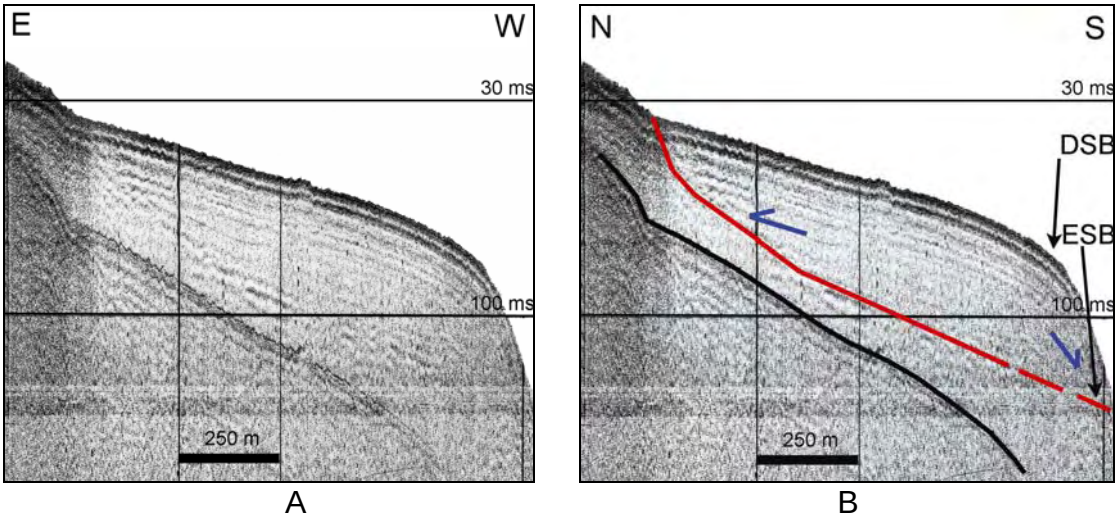

Figure 154 – Boomer seismic profile showing (A – non-interpreted, B – interpreted) the Depositional shelf break (DSB) and the Erosional shelf break (ESB). The red line represents the base of the seismic unit defined. See location on Figure 157.

Therefore, it would be expectable to have the erosional shelf break between these depths. However, the contemporary processes can change in a minor degree the position and shape of the shelf break, whether by progradation due to high sedimentation rates, whether by retrogradation due to mass-wasting failures.

In the border between the sector F and G, the depth of the erosional shelf break below the sedimentary wedge is at 115 and 100 meters water depth

(Figures 149 and 157). On sector G the depth of the erosional shelf break is between 90 and 95 meters water depth (Figures 150, 151, 152, 153 and 157) and on sector H is at 96 meters water depth (Figures 156 and 157). The erosional shelfbreak is found at distances from the depositional break that vary from 115 to 260 meters. As expected from the analysis of the sea-level variations in sectors G and H the depth of the relict shelf break falls roughly near the range forecasted (80-90 meters water depth).

The erosional shelf break at 100 and 115 m is somewhat deeper and is located in the transition between the sectors F and G. However, as it has been already discussed in section 5.2.3, the shelf in sector G is probably younger (470 Ka) than the one from the sector F (800 Ka), which means that the latter could have suffered subsidence. Therefore, the transition zone between one shelf sector that has suffered subsidence (G) and other that has not (F) is probably smoothed by erosion and for that reason it shows a slow deepening towards the east.

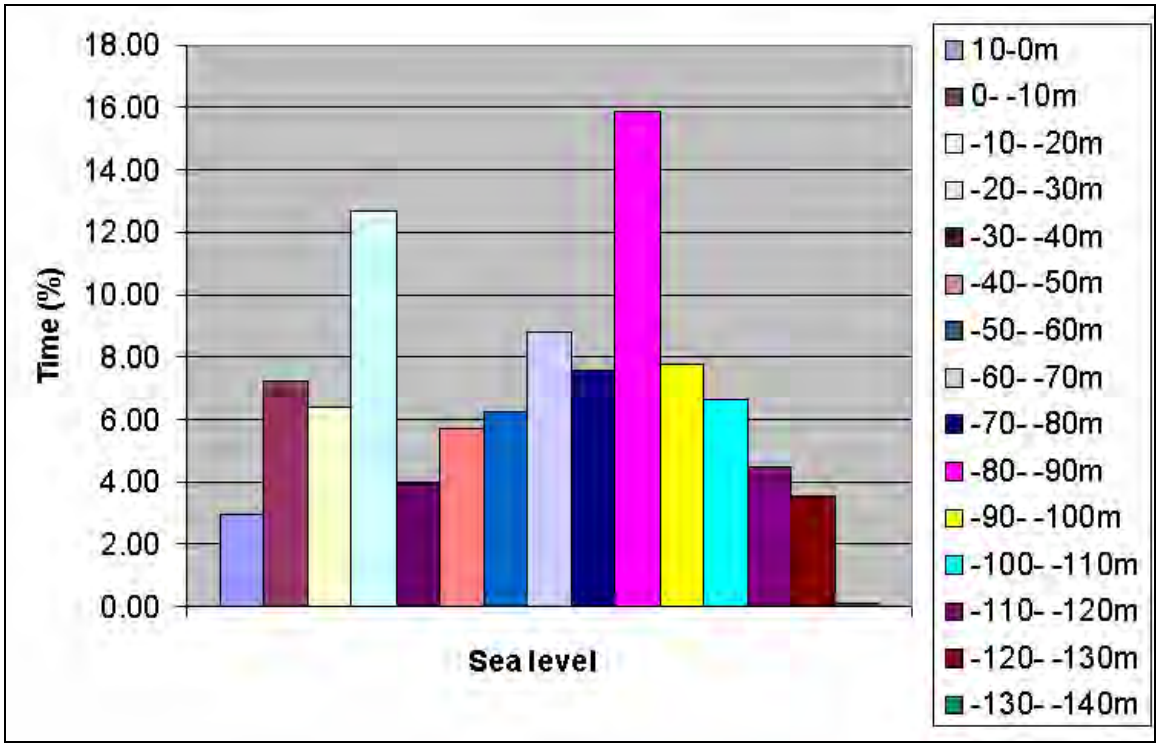

Figure 155 – Percentage of time during the last 400 Ka that the eustatic sea level has been at different depths (data from Table 8).

Figure 156 shows the percentage of time that the sea level has been at

different levels during the last 800 Ka. Assuming that the sea level has also been a considerable amount of time (16%) between the 80 and 100 m water depth (Figure 156), when compared against the other depths, the shelf break at sector D should also be found between these depths. On the contrary, it is found at 200 m water depth (Figure 141), which may be explained by subsidence. Given the assumed older age of the shelf in sector D (800 Ka), it is expected, as Menard (1983) suggested, that as the volcanism decreases, the island cools and initiates subsidence. Furthermore, the weight of the volcanic material that formed the Cedros Volcanic Complex, which occupies more than 50% of the island, would also have contributed to that subsidence. Assuming that the shelf break has subsided 100 m during a time period of 330 Ka, the subsidence rate of 0.3 mm/year can be obtained. The reason to use the 330 Ka period is because the shelf breaks of B, C, G and H which have formed around 470 Ka do not appear to have suffered much subsidence since their formation.

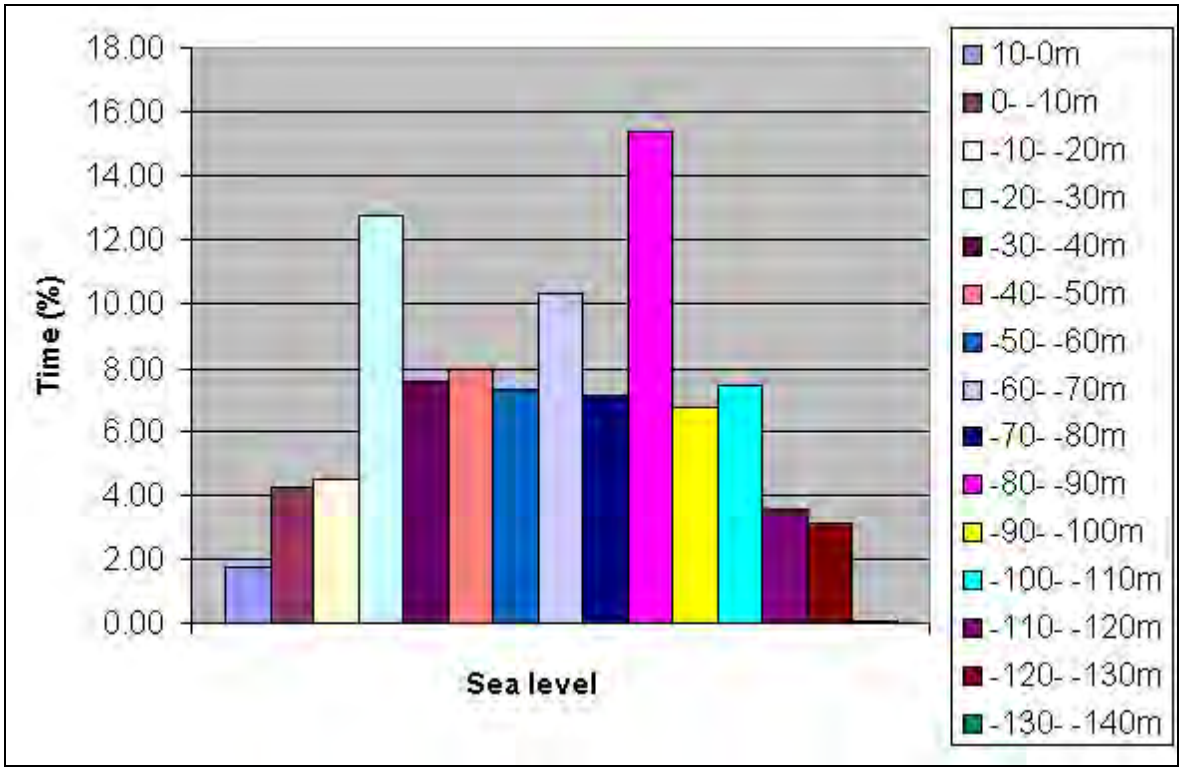

Figure 156 - Percentage of time during the last 800 Ka that the sea level has been at different depths (data from Table 9).

Although only small segments of the shelf break have been mapped in

sector B and sector C (red line in Figure 141), it appears that in these sectors the shelf break might be found, if mapped, at higher depths than those found in the sectors G and H. That is confirmed by the shelf break mapping (green line in Figure 141) based on the Instituto Hidrográfico map (1999), although this map due to the poor resolution does not allow obtaining its depths. In the sectors G and H, the depositional shelf break is found at 65-70 m, whilst the unmapped area of the sectors B and C were mapped until the 85 m water depth and no break feature (depositional or erosional) has been found. Once again, it appears that subsidence is the most plausible mechanism, to explain this discrepancy. The problem is that these four sectors have the same age and a mechanism must be found to generate subsidence on the north of the island but not on the south. This will be discussed in more detail in the following section.

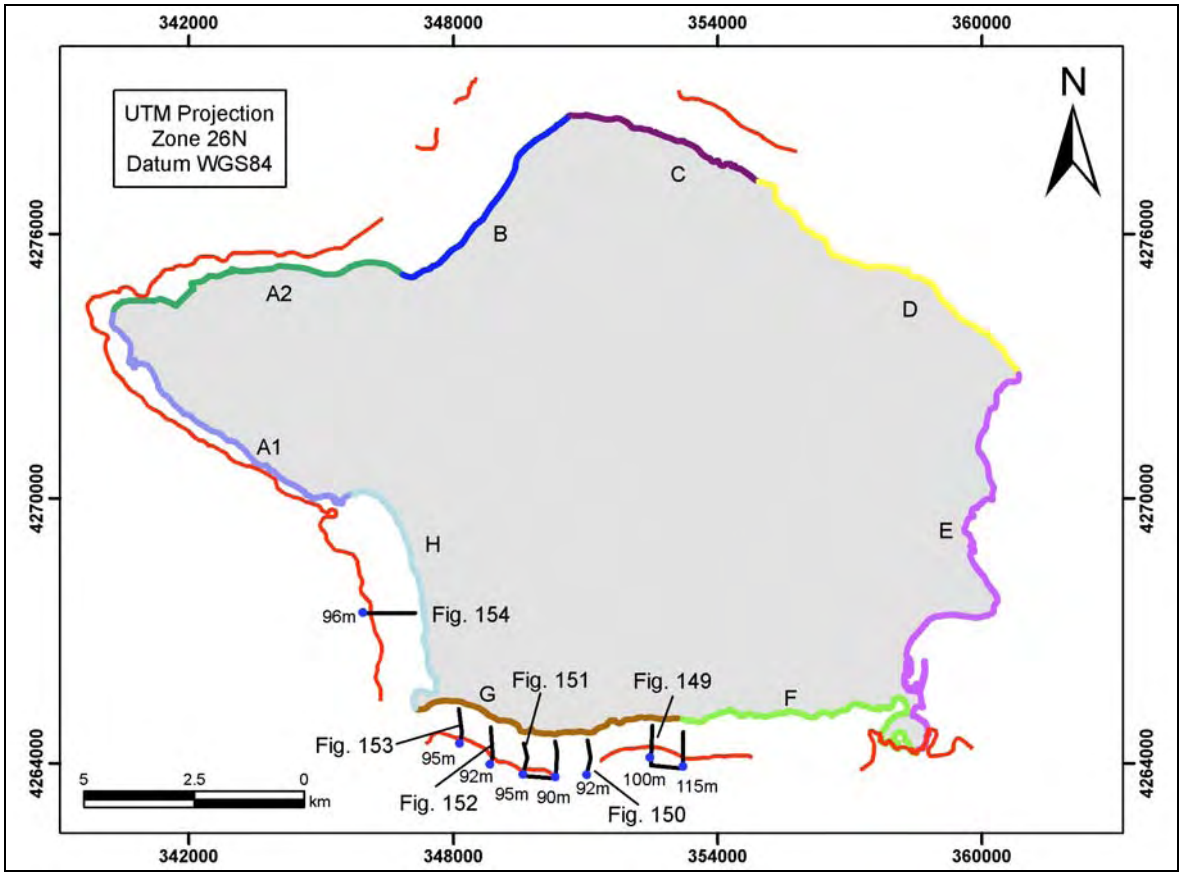

Figure 157 – The blue dots represent the places where the erosional shelfbreak has been mapped from the Boomer seismic profiles (next to them are the depths of the erosional shelf break). The red line represents the bathymetric shelfbreak mapped on this work. The corresponding figures of the seismic profiles are also shown on this map.

The shelf break of the sectors A1 and A2 is on average at 20 and 25 meters water depth respectively. Looking at the sea-level curve from Thompson & Goldstein (2006), it is easy to see that the sea was at 38 meters water depth at 10 Ka (Figure 128 in Chapter 4). This discrepancy can only be explained by the fact that the volcanism in this area has not been synchronous. Both shelves might have had lavas prograding offshore until the sea-level was at the respective present-day shelf break depths which made the start of the abrasion platform later.

5.5. Subsidence rates

The subsidence rate calculated for sector D, assuming that the shelf break should be presently at 80-90 meters water depth, is 0.3 mm/year, which is a considerably high value according to Pauly and McEdward (1990). These authors compiled data of subsidence from oceanic volcanic islands and have shown that older islands are almost stable with subsidence rates of 0.005 mm/year. In contrast, younger islands can reach values as high as 0.2 mm/year whilst average subsidence rates are 0.05 mm/year. Menard (1983) has also calculated average rates of subsidence for a variety of Pacific plate islands based on estimates of reef thickness made from bathymetric profiles and obtained subsidence rates of 0.04 to 0.23 mm/year. The subsidence rate of an island is directly connected with its activity. An island that is volcanically active has subsidence rates up to two orders of magnitude greater due to isostatic adjustment to the load added by the growing island. A good example is the active volcano of Hawaii that subsides at a rate of 1.2-4.1 mm/year (Moore and Fornari, 1984).

Deep drilling in S. Miguel Island (Azores) showed subsidence rates of 1 mm/year, when transition from subaerial to submarine lavas was found at 786 m below present sea-level. Once again, this high value reveals that subsidence arises primarily from crustal loading due to addition of volcanic material (Muecke et al., 1974). Moreover, São Miguel's closest neighbor, Santa Maria, which is currently inactive, shows uplift due to isostatic rebounding, as volcanic islands do when they become extinct (Muecke et al., 1974). Nevertheless, this explanation may not be that simple since S. Miguel overlies on what some authors believe to

be the Terceira Rift (TR, see Figure 18 in Chapter 2), formed either by pure extensional regime (Buforn et al., 1988; Krause and Watkins, 1970; Udías, 1980; Udías et al., 1986) or by transtensional regime (Argus et al., 1989; Laughton and Whitmarsh, 1974; McKenzie, 1972; Searle, 1980). More recently Vogt & Jung (2004) suggested that the TR is a hyper-slow (4 mm/yr) hotspot-dominated oblique spreading axis. According to Vogt & Jung (2004) the TR is a 550 km long, generally WNW trending line of alternating volcanic massifs (of which Graciosa, Terceira and São Miguel islands are the highest) and basins. These deep basins (Fig. 1 from Vogt & Jung, 2004 and Fig. 4 from Lourenço et al., 1998) that separate the islands and seamounts along the TR may well simply be the holes left vacant by volcanoes during volcano growth around them by sagging and extension (Vogt and Jung, 2004).

Luís et al. (1994) work revealed several northward migrations of the Eurasia–Africa–North America triple point, from a past location near 37°N up to its present location in the Faial Fracture Zone (FFZ, see Figure 18 in Chapter 2). According to these authors, the Faial and Pico are very young islands located along the projected trace of the FFZ and probably built in a transtensional mode, recorded geologically in the Faial graben structures (Luis et al., 1994). Recently, new GPS data (Fernandes et al., 2006) seem to support the Pico–Faial alignment of the triple point deduced from the magnetic modeling of Luís et al. (1994), which may account for the high subsidence value recorded on the sector D.

It is also reasonable to assume that the fissural volcanism in the Capelo Peninsula would also have contributed to the subsidence of the northwest sector of the island through loading since its main body is not in the center of the island but displaced to the northwest part (see Figure 168). This explanation could account for the differences of the depth of the shelf break between the northern and southern sectors of the Caldeira volcano region, discussed in the previous section.

An alternative explanation to the shelf break variability can be due to the selective preservation of former sea levels. Wave and rock strength function as filters that determine the amount of time that the sea must be at a particular elevation to produce significant erosional forms (Trenhaile, 1987). Therefore,

depending on local wave conditions, geology and submarine morphology, waves may be effective erosional agents during a low sea level stand in some areas along a coast, but not in others (Trenhaile, 2001). These mechanisms could explain the differences between the sectors A1 and A2 from the Capelo Peninsula and between the sectors B, C and F, G from the Caldeira Volcano. The sectors with higher wave frequency (see Figure 143 and Table 4 in Chapter 2) show higher shelf break depths (A1, B and C) when compared with others of the same age that have lower wave frequency (A2, F and G). However, it can not explain the shelf break from sector D at 200 meters water depth, which can only be explained by differential subsidence, either by crustal loading due to addition of the volcanic material from Capelo Volcano, or by the transtensional regime, as suggested by Luis et al. (1994).

5.6. Relation between the sand and gravel volumes on the shelf and the estimated cliff and subaerial erosion rates

In Chapter 3 the sources of the sands and gravels in the shelf have been discussed. At that time, the cliff erosion rates were not yet estimated and the possible sources were mainly related to the onshore precipitation. Also in Chapter 3, the mechanism of deposition and age of the sedimentary bodies was discussed and attributed to seaward downwelling currents that acted during the last 7450 years. During this period the island has been releasing sediments to the shelf either by coastline erosion, land subaerial erosion or associated to volcanic processes. In order to confirm the availability of sediments during this short period of time, the volume of material eroded from the cliffs and from the subaerial erosion of the hydrographic basins adjacent to the cliffs is calculated. The figures obtained, are compared to the volume of the sand bodies found on the adjacent shelf.

The submarine deposits from sectors F+G and H were almost completely mapped (Figure 76 in Chapter 3) and for that reason their volume can be estimated and compared with the volume of material resultant from the erosional

processes. The volume of the sediments was calculated using the ArcGis 9.0 GIS running the 3D Analyst extension which gave 106×10^6 m^3 of sediments for sectors F+G of and 101 $\times10^6$ m^3 for sector H.

5.6.1. Cliff erosion

The cliff erosion was calculated using the Corrected Erosion Rates estimated on section 5.3. These erosion rates are the sum of several processes acting on the coastline, namely wave erosion, cliff weathering and earthquake induced landslides. On sector H the cliff heights vary from 230 m on the NNW extreme till 60 m on the SSE extreme. Three topographic profiles (H1, H2 and H3 in Figure 158) were used and the area of the respective parallelograms was calculated. Using these three areas as unitary volumes (corresponding to 1 m of coastline) and the H1 and H3 as end-member and H2 as a middle member, the in-between values were calculated using a linear interpolation technique for each meter of coastline from a total of 5400 meters of coast. The value for the annual cliff retreat (32 mm) was the same for entire coastline, since the shelf width is relatively constant in this sector, suggesting that the entire cliff is retreating at the same rate.

The calculated volume of eroded material from the cliffs on sector H during the last 7450 years was 218×10^6 m^3 (Table 11).

The sectors F and G have cliff heights more or less constant, with an average of 30 meters. It might be expected that both sectors show similar erosion rates using the shelf width as proxy. This is not the case as discussed in section 5.2, due to the uncertainty in estimating an erosion rate for the sector F. Nevertheless, to simplify the calculations necessary to estimate the erosional contribution of these sectors to the volume of the sand bodies found on the shelf, it was assumed that sector F has the same erosional rate as sector G. Using for both sectors the Corrected Erosion Rate of 20 mm/year during 7450 years, over a cliff extension of 11500 meters, a volume of eroded material of 51.5×10^6 m^3 was obtained.

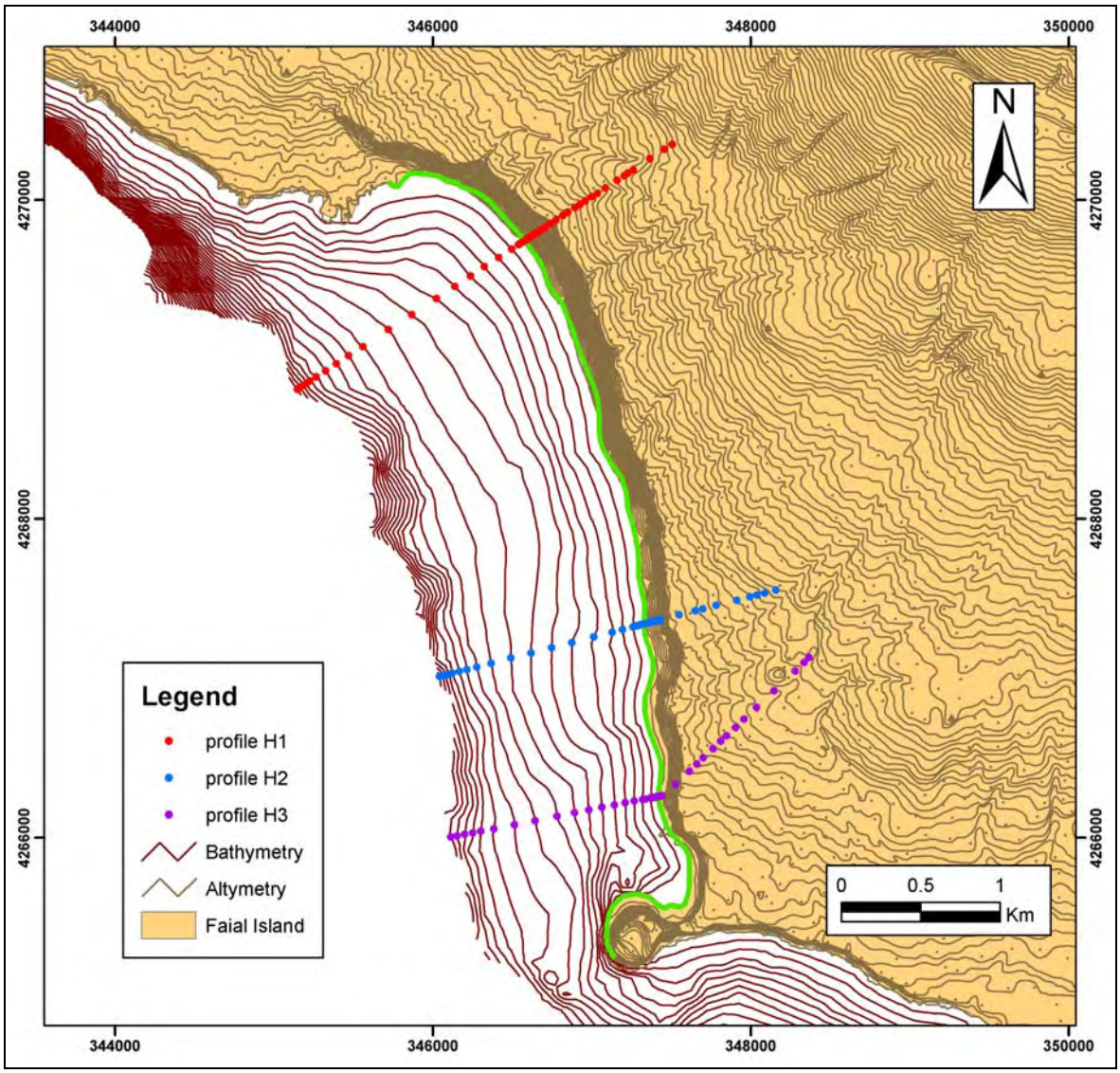

Figure 158 – Topographic profiles used for the calculations of the cliff area eroded. Green line is the delineation of the sector H.

As discussed in the section 4.3.4 of Chapter 3, the Faial cliffs are composed by intercalation of basaltic lava flows with pyroclastic deposits. Since, there is no quantitative information about the percentages of each type of these volcanic deposits, it is assumed in this study for the simplicity of the calculations that 50% of the cliffs are composed by pyroclasts. Therefore, the erosion of the cliffs of sector H would contribute 109×10^6 m^3 for the submarine sand and gravel deposits and the erosion of the cliffs of sector F+G would contribute with 25.7×10^6 m^3.

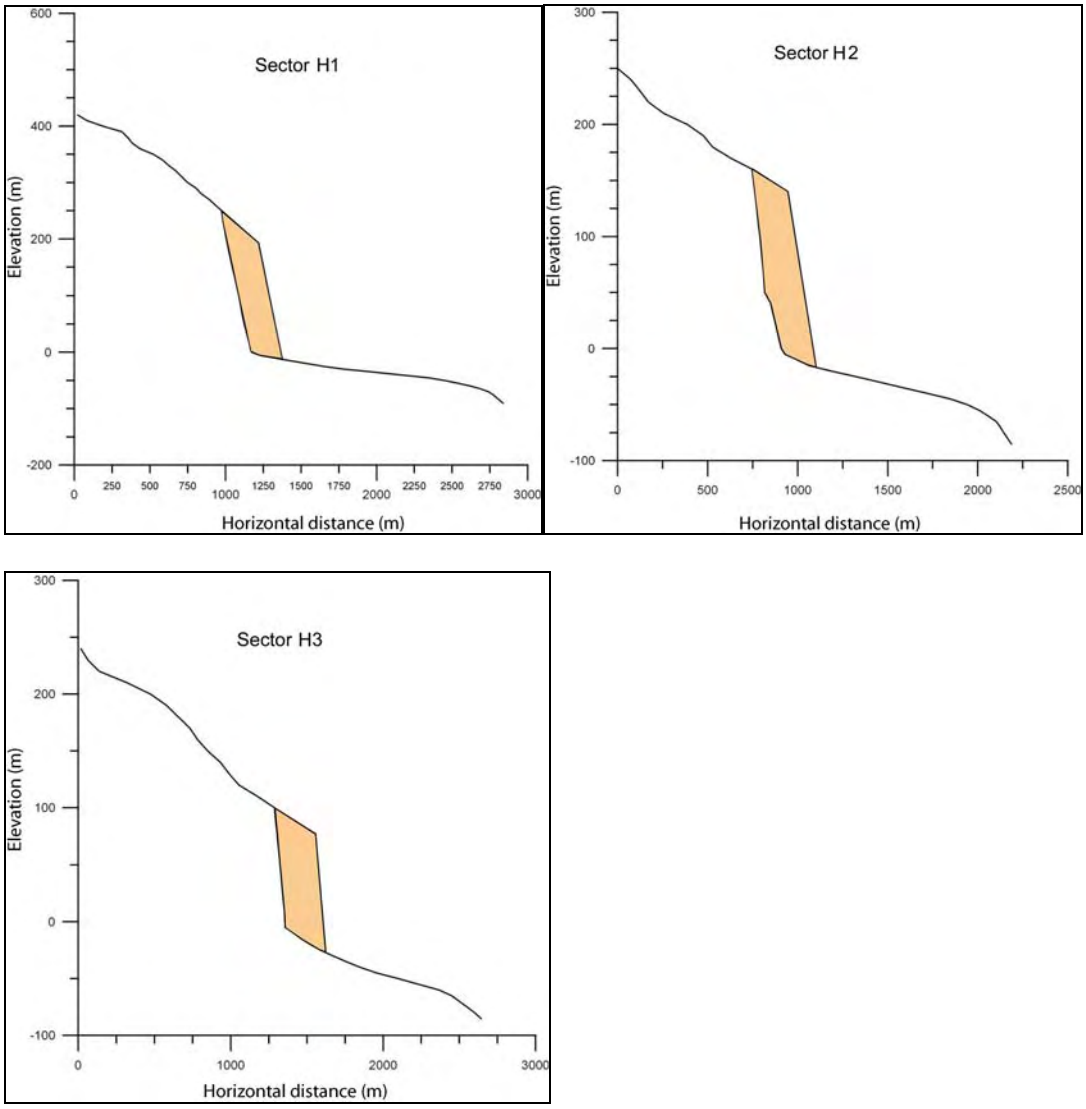

Figure 159 – Cliff areas (brown polygons) of the sectors H1, H2 and H3 eroded during the last 7450 years.

Table 11 – Summary of the cliff erosion occurring at sectors F+G and H

Sectors	Corrected erosion rate mm/year	Nº of years	Cliff retreat (m)	Average Cliff height	Cliff area eroded (m^2)
Profile H1	30	7450	223	230	51290
Profile H2	30	7450	223	175	39025
Profile H3	30	7450	223	100	22300
Total H					218×10^6 m^3
F+G	20	7450	149	30	51.4×10^6 m^3

5.6.1.1. Contribution from cliff weathering

Douglas et al. (1991) investigated the specific mechanism by which subaerial processes erode precipitous basaltic sea cliffs. According to these authors, first, microfractures develop and are eroded by processes such as swelling, oxidation of iron, hydration, and freeze-thaw. Gradual enlargement of the microfractures then leads to instability, and rock falls occur through gravity. Subaerial erosion can be inferred from published erosion rates of basalt scarps that are subject only to subaerial erosion processes. In southeast Australia, scarps have generally retreated at rates of 12–28 m/million years (Young, 1983; Young and McDougall, 1985), although Nott et al. (1996) noted considerably slower erosion rates at the Shoalhaven Gorge (0.3 m/million years). Basalt scarps in central Queensland, Australia, have retreated at rates of up to 130 m/million years (Young and Wray, 2000), and rates of 50–95 m/million years have been recorded at Drakensberg, South Africa (Fleming et al., 1999). Assuming these values as reference and using the highest value found by these authors (95m/million years), the subaerial erosion during the last 7450 years, would account only for 0.7 m of cliff retreat and a volume of eroded material of 684.000 m^3 for sector H. This value represents only 0.31% of the 218×10^6 m^3 estimated (Table 12). For the sectors F and G the volume of eroded material would be 242.000 m^3, which represents only 0.47% of the 51.5×10^6 m^3 estimated (Table 12).

5.6.1.2. Contribution from earthquakes

The cliff erosion also includes material resulting from landslides induced from earthquakes. It is nevertheless impossible to estimate this contribution. However, the report made by Coutinho (2000) of a 10 meters retreat in a sea cliff after the 1998 seismic event and the work of Malheiro (2006), suggests that seismicity is of considerable importance in the process of cliff retreat.

5.6.2. Subaerial erosion

There are no records of the subaerial erosion in the hydrographic basins of the Faial Island. Nevertheless, as it was discussed in section 4.3.4 of Chapter 3,

this process appears to be responsible for the presence of sand and gravel deposits nearshore the shelf sectors B, D, E and H. To estimate their contribution to the submarine deposits, the areas of the two hydrographic basins have been determined to use in the calculation of the subaerial erosion (Figure 160).

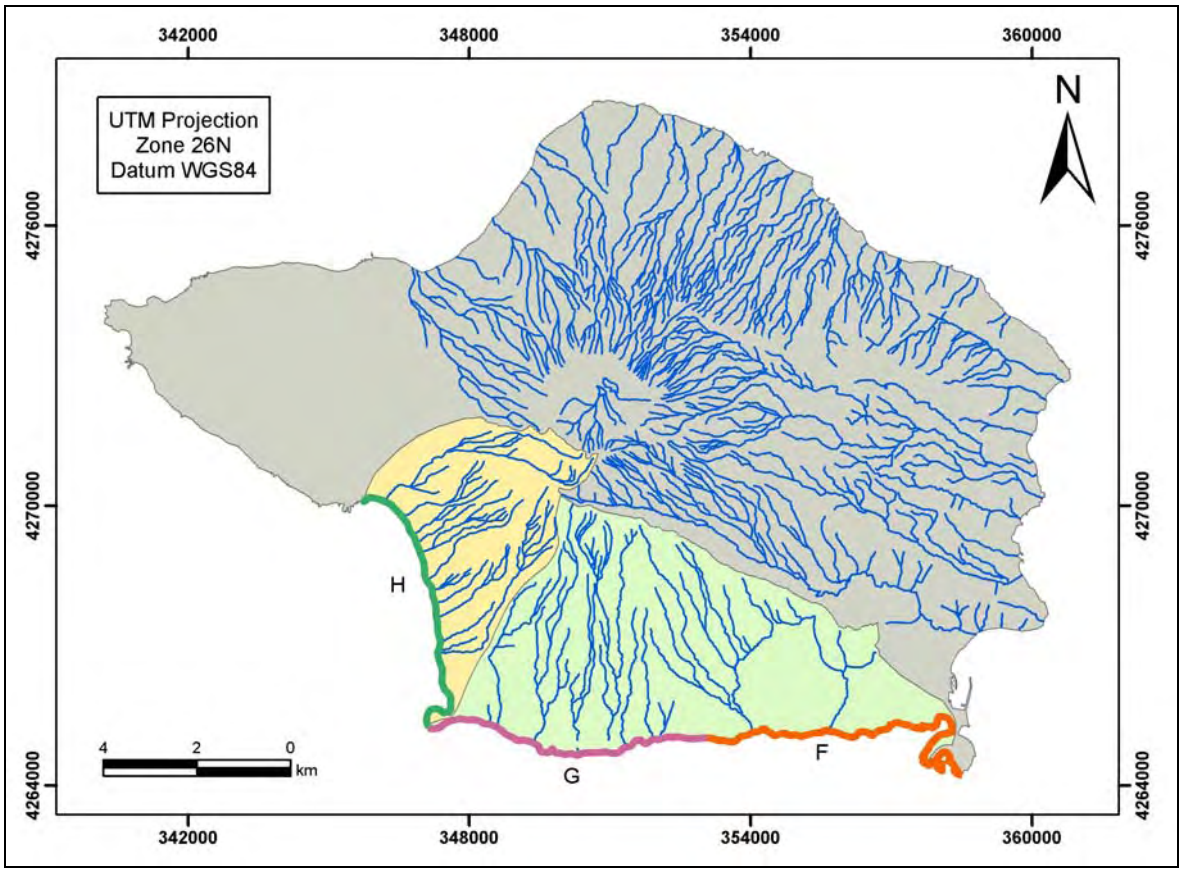

Figure 160 – Hydrographic basins responsible for the delivery of sediments to coastal sectors F+G and H.

It is possible to infer the subaerial erosion in these basins using some published values of subaerial erosion in S. Miguel (Louvat and Allègre, 1998) and Terceira Islands (Fontes et al., 2004). Their methods are described in detail in the section 2.3.2 of Chapter 2. Louvat & Allègre (1998) estimated erosion rates of riverine mechanical erosion of 70-500 ton/ km^2/year. Fontes et al. (2004) estimated erosion rates of less than 50 kg/ km^2/year under pasture cover, but increased to almost 150 ton/km^2/year when the soil was disturbed by tillage and less protected by vegetation. Both authors obtained values with similar magnitudes for unprotected soils, 70-500 ton/ km^2/year for Louvat & Allègre (1998)

and 150 ton/ km^2/year for Fontes et al. (2004). However, one should consider that the soil in these hydrographic basins was once covered with evergreen forests (Haggar, 1988) and only since the settlement in the 15th century were these replaced by pastures. Therefore, the value of 50 kg/km^2/year would probably be a good estimate for the erosion on these basins. It would be anyway an overestimation since the ancient land cover would retain more water than the pastures. The calculated volume of material eroded from the hydrographic basins F+G and H, based respectively on a surface area of 33.1 km^2 and 15.2 km^2 is respectively 287.000 m^3 and 138.000 m^3 (Table 12).

Table 12 represents a summary of the volume of sediments in the shelf sectors F+G and H and an estimate of their possible sources. The first and most obvious impression when analyzing these values is that sectors F+G have on the shelf four times the volume of sediments than the prediction made from the erosional sources and that Sector H has on the shelf more or less the same volume than its prediction from cliff erosion. The other obvious remark is that the contribution of the subaerial erosion of the hydrographic basins to the submarine deposits is insignificant (less than 1% of volume of the shelf deposits).

Table 12 - Volume of submarine deposits and estimation of the possible sources.

	Submarine deposits	Hydrographic basin erosion	Erosional cliff components							
			Wave attack		cliff weathering		Landslides induced earthquakes		Total Cliff erosion	
	Vol.*	Vol.*.	Vol.*.	%	Vol.*.	%	Vol.*.	%	Vol.*.	
Sector F+G	**105.9**	**0.1**	?	?	0.2	0.5	?	?	**25.7**	100
Sector H	**101.6**	**0.3**	?	?	0.7	0.3	?	?	**109**	100

* Vol. represents volume of sediments in millions of m3

The discrepancies for the sectors F+G can be explained whether by using a Corrected Erosion Rate higher than 20 mm/year or by finding other source for the

sediments than those presented on Table 12. The section 2.4.1 of Chapter 2 showed that adjacent to the shelf sectors F+G lye two volcanostatrigraphic units, the Caldeira Formation and the Almoxarife Formation, composed of very friable material. So, apparently both units could have contributed with volcaniclastic sedimentation processes, either by syn-eruptive submarine volcaniclastic sedimentation or non-eruptive submarine remobilization of the volcaniclastic materials, supplying the necessary sediments to reach the shelf volume of 105.9×10^6 of m^3.

The contribution of the cliff eroded material in Sector H is similar to the volume of sediments found on the shelf and like the sectors F+G, the volcaniclastic sedimentation processes from the Cedros Volcanic Complex have not be taken into account. There is also evidence that hydrographic basin erosion plays an important role in the contribution of sand and gravel deposits to the shelf (see discussion in section 4.3.4 in Chapter 3). Therefore, it means that probably the Corrected Erosion Rate should be lower if considering the contribution of the volcaniclastic sedimentation processes and the erosion of the hydrographic basins.

In section 5.6.2 it was used a low value for the erosion of the hydrographic basins (50 kg/ km^2/year) assuming that the soils were protected by vegetation. However, like it was discussed in the last two paragraphs, the hydrographic basins are covered by the highly erodible deposits of either the Caldeira Formation or Almoxarife Formation that have been emplaced by explosive eruptions during the last 10 Ka. Therefore, the erosion value of Fontes et al. (2004) for unprotected soils (150 ton/km^2/year) is probably not that unlikely as it sounded in the first place. The calculated volume of material eroded from the hydrographic basins F+G and H, using this value is respectively 92×10^6 m^3 and 42×10^6 m^3, which is more than enough to obtain the volume of the submarine deposits, if considering the cliff erosion rates of Table 11.

In conclusion, the cliff erosion rates for the sectors F+G are probably higher than 20 mm/year and also the hydrographic basin erosion rates (in the order of some ton/km^2/year) to obtain the volume of the submarine deposits. The cliff erosion rates of the sector H is probably lower than 30 mm/year if one accounts

also the contribution of the hydrographic basin erosion, in the order of some ton/km^2/year. It remains, however, impossible to evaluate the respective contribution of each process due to lack of data. It is also possible that some of the volcanism in the last 10 Ka have provided sediments directly to the shelf either by syn-eruptive submarine submarine volcaniclastic sedimentation or by non-eruptive submarine remobilization of the volcaniclastic material emplaced on the shelf (see section 1.2.7 in Chapter 1). The role of the landslide induced earthquakes and the wave attack on the overall value of cliff retreat is not easily perceived. It is likely that wave attack is the major contributor for cliff retreat; what is not clear is how lower would be the erosion rates without earthquakes. Very obvious is the insignificance of the subaerial weathering of the cliffs (0.3-0.4×10^6 m^3) to the total value of the submarine deposits. The probability that some percentage of the sediments that reach the shelf may be lost to the slope is also high. That possibility was already discussed in section 4.3.6 of Chapter 4 due to the evidence of mass-wasting processes and gullying on the shelf break.

5.7. Evolutionary model of the Faial insular shelf

The analysis of the shelf geology in the Chapter 4 and especially the discussion concerning the shelf width versus shelf age in the present chapter permitted the development and proposal of an evolutionary model for the shelf of Faial Island. This evolutionarily model is based on the assumption that the shelf is abrasional in origin and results from the balance between erosive processes and volcanic progradation. There are seven time windows presented in this model and each one corresponds to the oldest age of the different subaerial volcanic stages described in Chapter 2. The last time window is the present-day situation. The distances of the coastline to the shelf break on most of the time windows are merely schematic and do not correspond to real measurements.

At 800 Ka ago the Ribeirinha shield volcano reached its maximum horizontal subaerial expression marked by the mapped shelf breaks in sector D and F in Figure 161. From 800 Ka to 470 Ka wave erosion associated to sea-level changes formed an abrasion platform around the slopes of Ribeirinha volcano

(Figure 162). At 470 Ka ago the Caldeira Volcano (composed of the Cedros Volcanic Complex) reached its maximum horizontal subaerial expression, covering a significant part of the Riberinha shield volcano. The limits of its horizontal subaerial expression are marked by the shelf breaks at sectors B, C, G and H (Figure 162). From 470 Ka to 30 Ka an abrasion platform has formed around the slopes of Caldeira Volcano (Figure 163). At the same time, the platform around the Ribeirinha volcano also increased (Figure 163). At 30 Ka, fissural volcanism emplaced the Almoxarife Formation on the top of the southeastern slope of the Caldeira Volcano and the southern slope of the Ribeirinha volcano (Figure 164). A significant part of the volcanism of the Almoxarife Formation has probably prograded offshore covering the platforms cut on the slopes of Ribeirinha and Caldeira volcanoes (Figure 164). From 30 Ka to 10 Ka all the platforms slightly enlarged (although at the scale of Figure 168 it is not possible to see) around the subaerial part of the island. At 10 Ka the Capelo Volcanic Complex started to form, covering the western part of the Caldeira volcano and resetting some parts of the platforms cut on the slopes of the Caldeira volcano (Figure 166). The limits of its horizontal subaerial expression are marked by the shelf breaks at sectors A1 and A2 (Figure 165). From 10 Ka to the present, the sea-level rose from - 38 m to the present sea-level, forming an incipient platform on the offshore part of Capelo Peninsula. In 1672 AC, a lava flow that has started on the central part of the Capelo Peninsula, prograded, both north and south, into the sea (Figure 167). The southern progradation was more extensive, resetting almost the southeastern incipient platform. In 1958 AC, a surtseyan eruption (the Capelinhos volcano) increased the western part of the Capelo Peninsula. Even the Capelinhos volcano, a recent offshore advance of the island, has already been eroded, forming also here an abrasion platform (Figure 168).

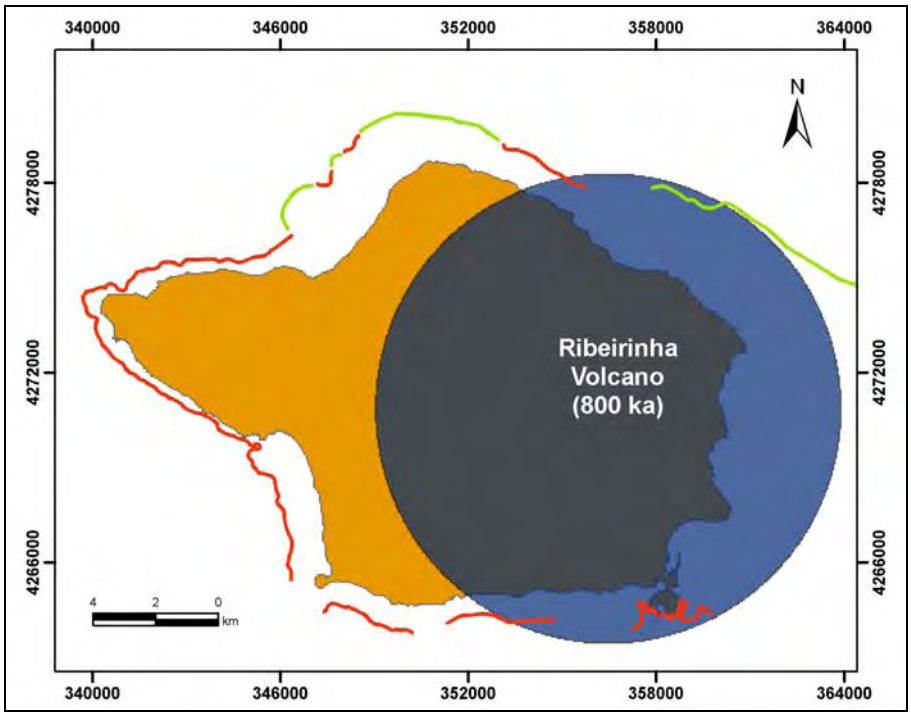

Figure 161 – Time slice at 800 ka. Dark blue circle represents the maximum development of the subaerial Ribeirinha Shield Volcano. The red line is the measured depositional shelf-break and the green line is the inferred shelf-break based on the Instituto Hidrográfico map (1999). The light brown area is the present-day subaerial part of the Faial Island.

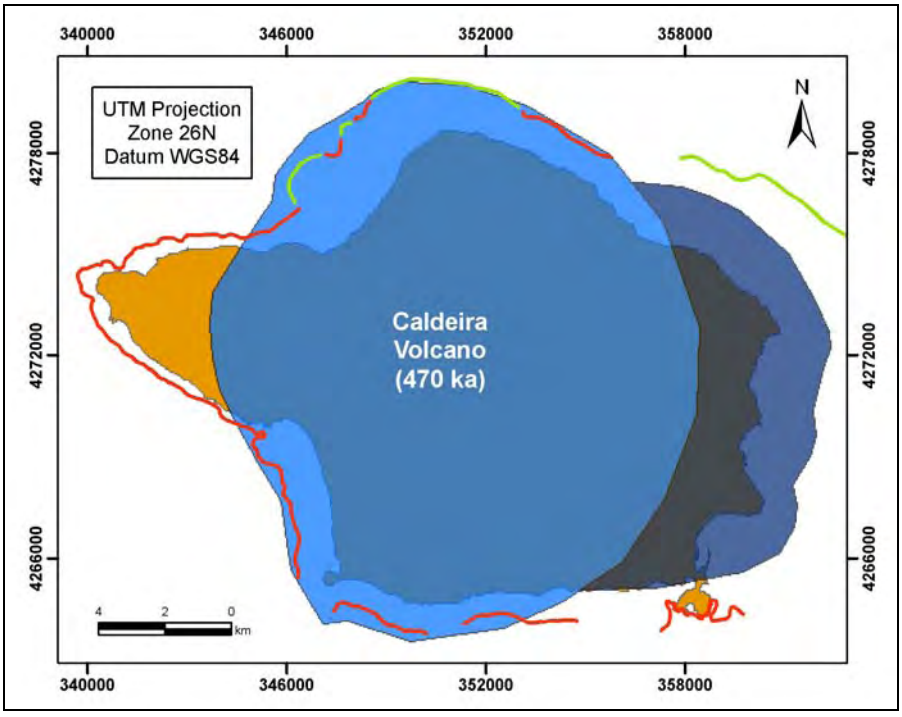

Figure 162 – Time slice at 470 ka. Lighter blue polygon represents the maximum development of the subaerial Caldeira volcano. Dark blue polygon represents the Ribeirinha Shield Volcano partly eroded by an abrasional shelf formed from 800 Ka to 470 Ka. The red line is the measured depositional shelf-break and the green line is the inferred shelf-break based on the Instituto Hidrográfico map (1999). The light brown area is the present-day subaerial part of the Faial Island.

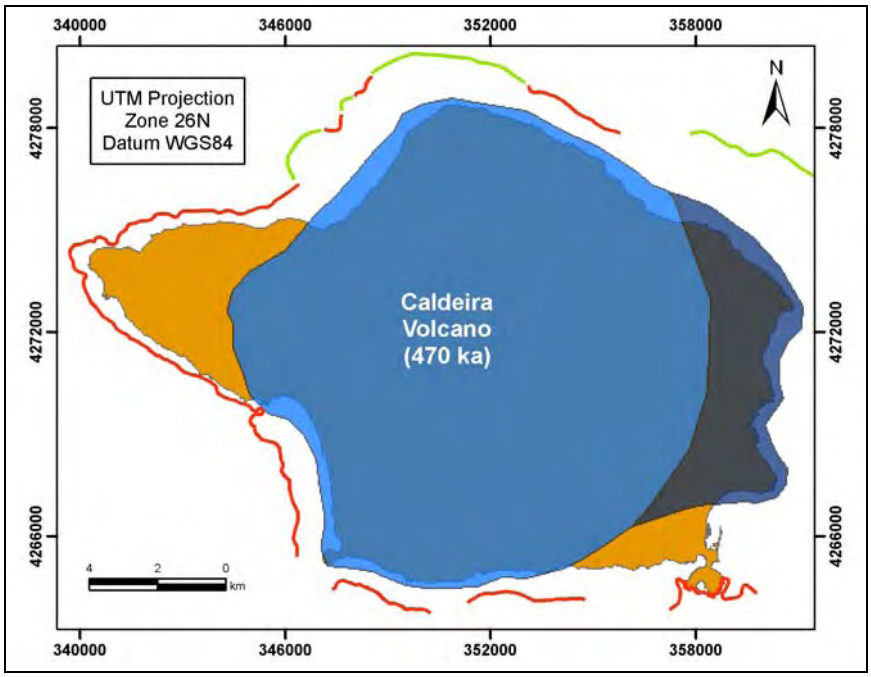

Figure 163 – Time slice at 30 ka. Lighter blue polygon represents the Caldeira volcano partly eroded by an abrasional shelf from 470 Ka to 30 Ka. Dark blue polygon represents the Ribeirinha Shield Volcano that continued to be eroded from 470 Ka to 30 Ka by an abrasional shelf. The red line is the measured depositional shelf-break and the green line is the inferred shelf-break based on the Instituto Hidrográfico map (1999). The light brown area is the present-day subaerial part of the Faial Island.

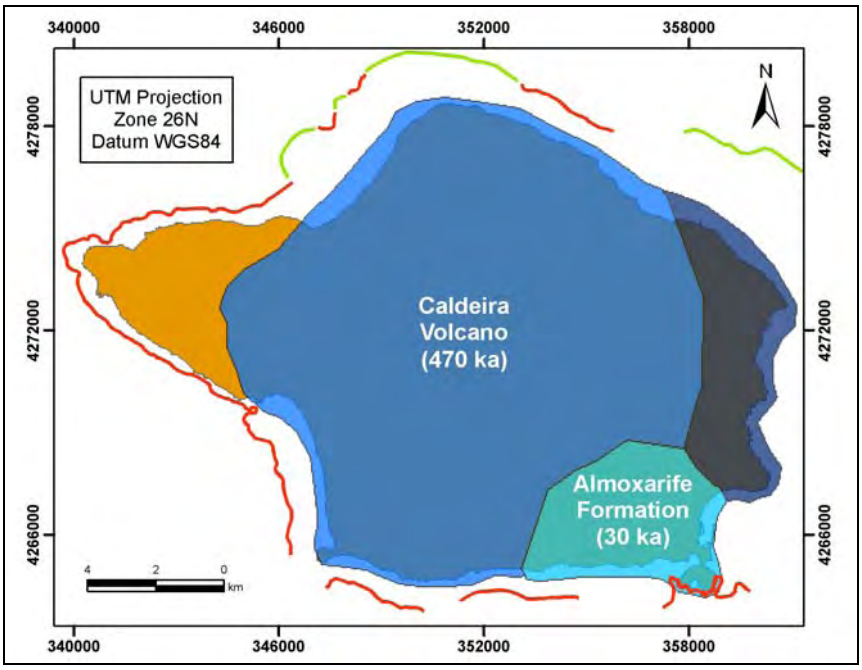

Figure 164 - Time slice at 30 ka. Maximum development of the subaerial volcanism of Almoxarife Formation with progradation onto the abrasion platforms of Caldeira and Ribeirinha volcanoes. Continuation of the development of the abrasional platforms surrounding the Ribeirinha and Caldeira Volcano. The red line is the measured depositional shelf-break and the green line is the inferred shelf-break based on the Instituto Hidrográfico map (1999). The light brown area is the present-day subaerial part of the Faial Island.

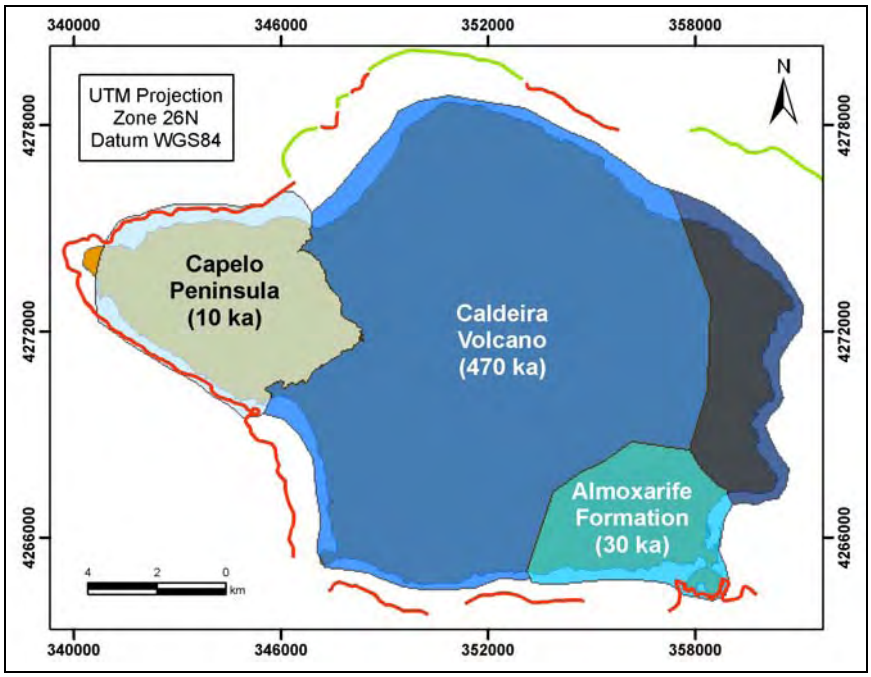

Figure 165 - Time slice at 10 ka. Maximum development of the subaerial Capelo Volcanic Complex Continuation of the development of the abrasional shelf surrounding the Ribeirinha Shield Volcano, the Caldeira Stratovolcano and the Almoxarife Formation. The red line is the measured depositional shelf-break and the green line is the inferred shelf-break based on the Instituto Hidrográfico map (1999). The light brown area is the present-day subaerial part of the Faial Island.

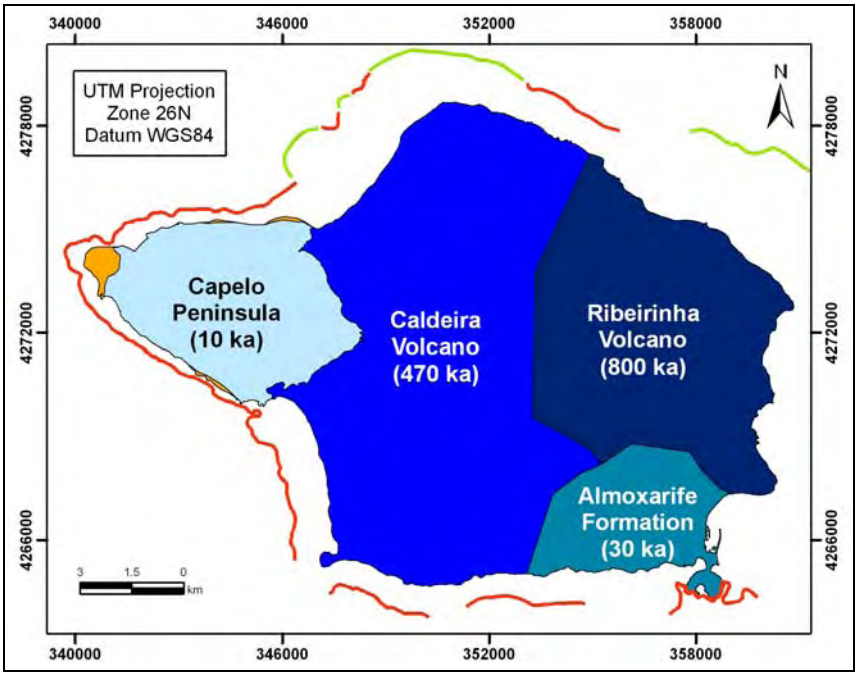

Figure 166 - Time slice at 1672 AC. Development of the abrasional shelf surrounding the Ribeirinha Shield Volcano, the Caldeira Stratovolcano, the Almoxarife Formation and the Capelo Volcanic Complex. The red line is the measured depositional shelf-break and the green line is the inferred shelf-break based on the Instituto Hidrográfico map (1999). The light brown area is the present-day subaerial part of the Faial Island.

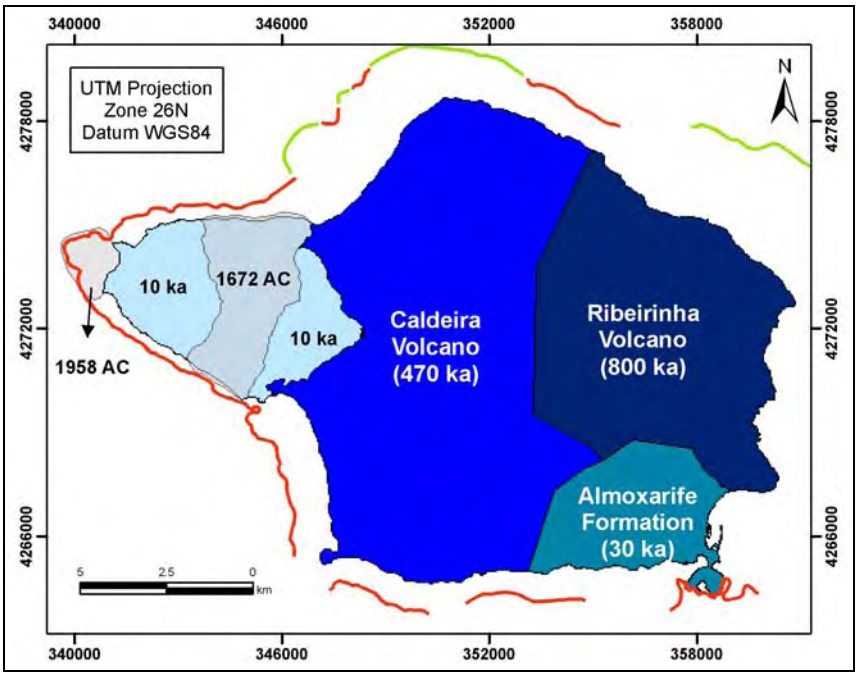

Figure 167 - Time slice at 1672 AC and 1958 AC. Historical lava flow of 1672 AC and Capelinhos eruption at 1958 AC. Development of the abrasional shelf surrounding the Ribeirinha Shield Volcano, the Caldeira Stratovolcano, the Almoxarife Formation and the Capelo Volcanic Complex. The red line is the measured depositional shelf-break and the green line is the inferred shelf-break based on the Instituto Hidrográfico map (1999).

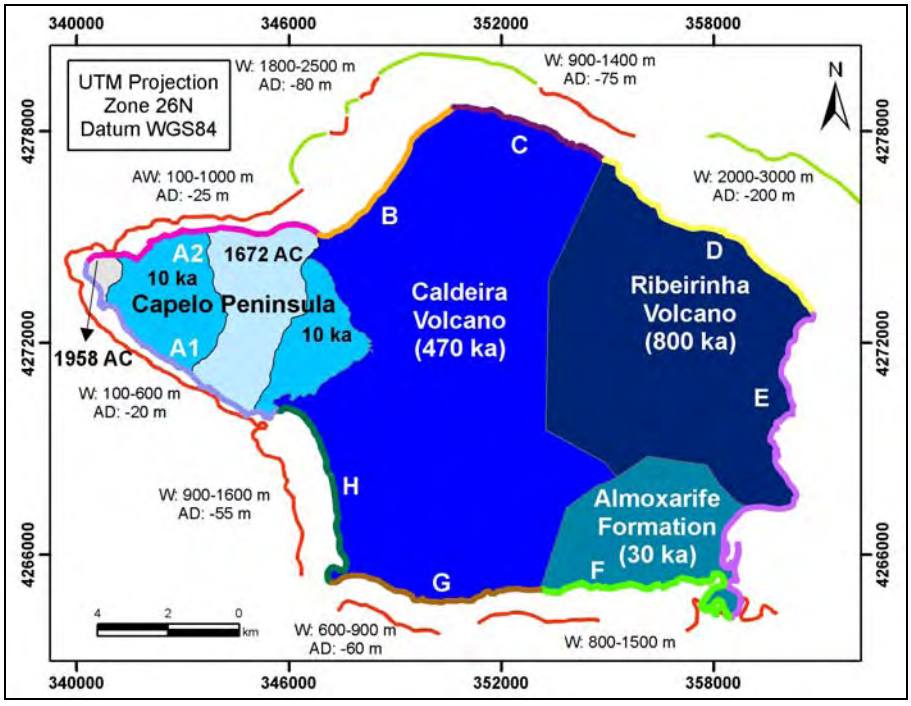

Figure 168 – Present-day situation of the shelf. The red line is the measured depositional shelf-break and the green line is the inferred shelf-break based on the Instituto Hidrográfico map (1999). W – Width of the shelf; AD – Average Depth of the shelf break. The different blue polygons represent the different subaerial stages of volcanism in the Faial Island. The bold color lines bordering the coastline of Faial Island represent the landward limits of the shelf sectors defined in Chapter 3.

Chapter 6. Shelf sedimentary dynamics

6.1. Introduction

The superficial sedimentary cover of the Faial shelf is described in this chapter and the reasons for its peculiar sedimentary pattern are discussed. The seaward limits of the cross-shore transport of sediments are estimated and a relation is proposed between these limits and the cross-shore sedimentary variation. The longshore transport of sediments is calculated for the sectors with nearshore sediments and simple bathymetry. All these characterizations aim to understand the present-day shelf dynamics and to help in the evaluation of these sediments as aggregates and limit their potential dredging areas in Chapter 7.

6.2. Characterization of the shelf sedimentary environments

One of the main purposes of this investigation was to study the part of the insular shelf of Faial that is composed of sand and gravel. For that purpose Box-Core samples were collected between 20 and 80 meters water depth (see Figure 14 in Chapter 1) in order to study the distribution patterns of sediment texture and composition. The samples were taken along cross-shore transects spaced between 300 and 1000 m, up to 80 m offshore and along-shore transects spaced between 1000 and 4000m. The grid sampling was chosen to be irregular because it was adjusted according to the specific characteristics of each shelf sector, based on the interpretation of the seismic and bathymetric data. For each of the samples several statistical parameters were calculated. The mean, sorting, skewness and kurtosis were calculated using the moment measures on the whole sediment distribution using the Folk and Ward method (1957). For that purpose the Visual Basic program GSSTAT (Poppe et al., 2004), available from the International Association for Mathematical Geology web-site was used to calculate these

moment statistics. The Visual Basic program SEDCLASS (Poppe et al., 2003), also available from the International Association for Mathematical Geology web-site was used to generate automatically the Folk's classification system of sediments (1954) based on gravel-sand-silt-clay ratios.

6.2.1. The shelf grain-size distribution

Table 13 presents the percentages of each size fraction in the samples using the phi scale defined by Krumbein (1938) and the Folk's classification system (1954) based on gravel-sand-silt-clay ratios, while Table 14 presents the corresponding moment statistics (mean, sorting, skewness and kurtosis, respectively M1, M2, M3 and M4), the description of the samples based on the moment statistics classification of Folk (1974) and the carbonate calcium percentage of each sample.

A brief analysis of the results shows that there are no samples finer than medium sands (Table 14 and Figure 169). In fact, 54% of the samples collected revealed sediments that are medium sands, 17% that are coarse sands, 26% that are very coarse sands and 3% that are granules according to the Udden-Wentworth scale (1922). Moreover, when using the Folk's classification ternary diagram (1954), 54% of the samples fall into the category of slightly gravely sand, 34% fall into gravely sand and 12% into sandy gravel (Table 13 and Figure 170). Apparently, the presence of coarse sediments in the Faial shelf points out to a rather energetic depositional environment as already discussed in section 2.4.4 of Chapter 2 and section 4.3.7 of Chapter 4.

When analyzing the grain-size distribution as a function of water depth, it is clear that the samples are coarser at greater water depths. In fact, 77% of the samples coarser than medium sands (smaller than 1Φ) are located between the water depths of 50 and 80 meters (Figure 171). Even when analyzing each shelf sector separately, the samples tend to be coarser offshore in almost all sectors, sector B being the only exception the (Figures 172, 173, 174, 175 and Figure 176). There is a clear increase of the mean grain-size after the 50 meters water depth. The Standard Deviation also shows a raise with increasing water depth, although it

is not so clear in some shelf sectors. The Skewness is fairly constant around the 0 value, which means that the sediment distribution is nearly symmetrical in all the cases, resembling a normal Gaussian curve. The Kurtosis value is less constant

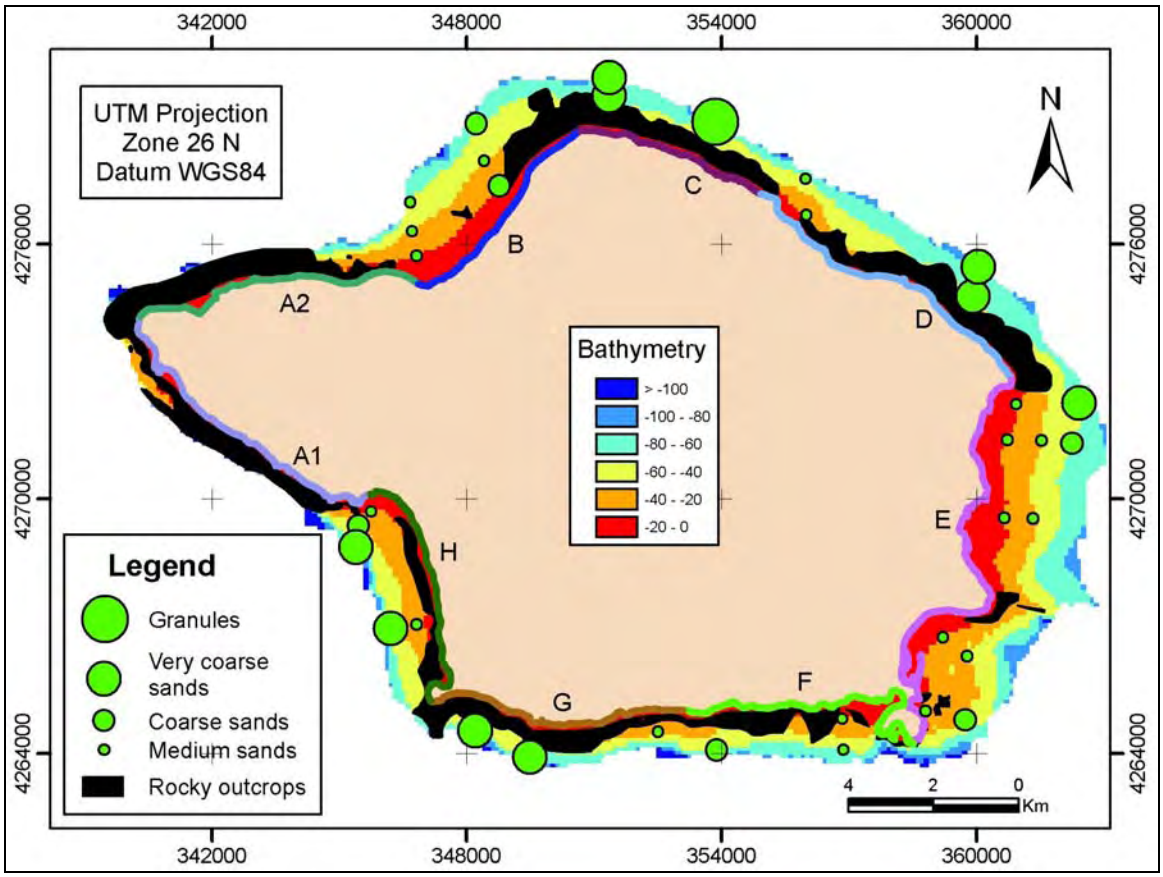

Figure 169 – Mean grain size (M1) distribution of the samples in the shelf. The rocky outcrops correspond to the lava flows and coarse clastic deposits interpreted in Chapter 3.

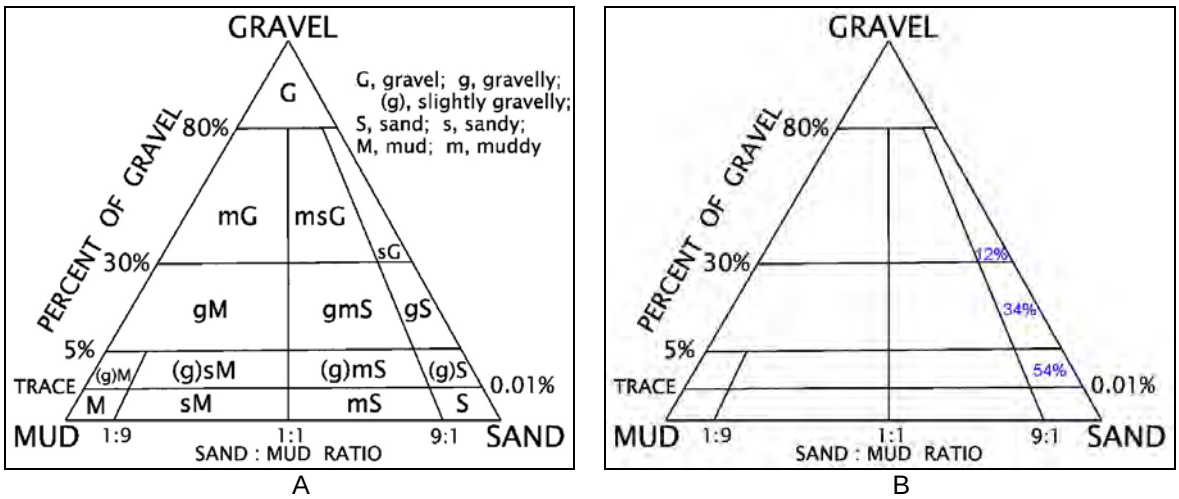

A B

Figure 170 – A: Folk's (1954) classification ternary diagram. B: Folk's (1954) classification of the Faial shelf samples showing that these have a significant percentage of gravels.

Table 13 - Percentages of each size Φ fraction and the Folk's classification system (1954).

SAMPLEID	5Φ	4Φ	3Φ	2Φ	1Φ	0Φ	-1Φ	-2Φ	-3Φ	-4Φ	-5Φ	Gravel (%)	Sand (%)	Silt (%)	Folk's Classification
FAPI3_005	1.78	1.32	18.49	43.24	10.55	9.97	5.41	4.18	1.74	2.03	1.27	14.63	83.57	1.78	Gravelly sand
FAPI3_058	0.6	1.39	35.94	56.51	5.52	0.02	0.03	0	0	0	0	0.03	99.38	0.6	slightly gravelly sand
FAPI3_059	0.48	1.1	18.72	46.33	22.59	10.57	0.22	0	0	0	0	0.22	99.31	0.48	slightly gravelly sand
FAPI3_060	1.16	8.14	47.06	27.85	10.02	5.63	0.11	0.04	0	0	0	0.15	98.7	1.16	slightly gravelly sand
FAPI3_061	0.56	1.7	40.58	36.7	8.27	11.81	0.38	0	0	0	0	0.38	99.06	0.56	slightly gravelly sand
FAPI3_062	0.37	0.25	2.78	39.48	42.62	13.88	0.58	0.04	0	0	0	0.62	99.01	0.37	slightly gravelly sand
FAPI3_063	0.17	0.11	0.89	17.15	44.75	18.74	2.03	0.46	1.02	6.32	8.34	18.17	81.64	0.17	Gravelly sand
FAPI3_064	1.47	10.36	36.12	31.44	14.54	5.81	0.21	0.04	0	0	0	0.25	98.27	1.47	slightly gravelly sand
FAPI3_065	0.14	0.15	0.38	1.11	23.79	57.14	15.45	1.61	0.24	0	0	17.3	82.57	0.14	Gravelly sand
FAPI3_066	0.25	0.57	1.4	1.26	17.24	66.3	11.8	1.1	0.07	0	0	12.97	86.77	0.25	Gravelly sand
FAPI3_067	0.75	1.91	23.86	52.13	18.24	3.01	0.09	0.01	0	0	0	0.1	99.15	0.75	slightly gravelly sand
FAPI3_068	0.5	1.51	21.04	52.61	20.29	3.96	0.06	0.03	0	0	0	0.09	99.41	0.5	slightly gravelly sand
FAPI3_070	0	0.24	1.64	5.88	13.01	24.39	19.91	21	9.19	3.36	1.39	54.85	45.16	0	Sandy gravel
FAPI3_071	0.05	0.17	1.8	6.25	14.08	41.51	23.44	10.34	2.2	0.15	0	36.13	63.81	0.05	Sandy gravel
FAPI3_072	0	0.1	0.84	4.25	15.16	42.3	24.04	9.86	2.93	0.5	0	37.33	62.65	0	Sandy gravel
FAPI3_073	0.12	0.15	1.37	17.34	40.9	20.49	9.37	6.11	2.87	1.29	0	19.64	80.25	0.12	Gravelly sand
FAPI3_074	0.25	0.51	8.81	49.19	37.35	3.83	0.06	0	0	0	0	0.06	99.69	0.25	slightly gravelly sand
FAPI3_075	0.24	0.34	4.81	40.05	47.22	7.12	0.17	0.06	0	0	0	0.23	99.54	0.24	slightly gravelly sand
FAPI3_076	0.78	3.35	36.12	49.49	9.3	0.94	0.02	0	0	0	0	0.02	99.2	0.78	slightly gravelly sand
FAPI3_077	0.35	1.5	18.97	57.82	19.53	1.8	0.03	0	0	0	0	0.03	99.62	0.35	slightly gravelly sand
FAPI3_078	0.33	1.19	12.74	44.07	35.38	6.19	0.1	0	0	0	0	0.1	99.57	0.33	slightly gravelly sand
FAPI3_079	0.41	1.31	14.04	49.52	29.72	4.83	0.12	0.06	0	0	0	0.18	99.42	0.41	slightly gravelly sand
FAPI3_080	0.29	0.76	5.39	20.41	38.26	28.1	4.29	1.96	0.55	0	0	6.8	92.92	0.29	Gravelly sand
FAPI3_081	0	0.29	1.94	9.78	35.09	37.38	9.96	4.56	1.01	0	0	15.53	84.48	0	Gravelly sand
FAPI3_082	0.09	0.09	0.46	5.57	30.15	42.25	14.18	5.68	1.52	0	0	21.38	78.52	0.09	Gravelly sand
FAPI3_083	0.22	0.74	11.12	49.45	32.67	5.53	0.22	0.04	0	0	0	0.26	99.51	0.22	slightly gravelly sand
FAPI3_084	0.17	0.61	4.41	9.23	17.23	25.8	24.16	15.52	2.64	0.23	0	42.55	57.28	0.17	Sandy gravel
FAPI3_085	0.37	0.29	4.13	18.71	24.58	26.24	7.83	3.35	14.49	0	0	25.67	73.95	0.37	Gravelly sand
FAPI3_087	0.69	3.65	36.14	32.21	10.05	11.33	2.92	1.64	1.38	0	0	5.94	93.38	0.69	Gravelly sand
FAPI3_089	0.59	0.87	9.82	27.44	23.78	21.95	7.59	6.57	1.29	0.1	0	15.55	83.86	0.59	Gravelly sand
FAPI3_090	0.53	2.53	36.13	43.38	12.64	4.42	0.24	0.09	0.04	0	0	0.37	99.1	0.53	slightly gravelly sand
FAPI3_091	0.42	1.88	26.11	46.63	15.02	8.97	0.89	0.08	0	0	0	0.97	98.61	0.42	slightly gravelly sand
FAPI3_092	1.24	2.94	38.96	40.42	8.83	7.38	0.18	0.03	0	0	0	0.21	98.53	1.24	slightly gravelly sand
FAPI3_093	1.31	6.15	35.9	29.14	11.85	9.72	3.96	1.7	0.26	0	0	5.92	92.76	1.31	Gravelly sand
FAPI3_094	0.59	3.24	43.54	42.28	5.91	4.29	0.17	0	0	0	0	0.17	99.26	0.59	slightly gravelly sand

Table 14 - Moment statistics of Folk (1974) (M1, M2, M3 and M4), description of the samples based on the Udden-Wentworth grain-size classification (1922) and the carbonate calcium percentage.

SAMPLEID	M1	M2	M3	M4	Description	Carbonate (%)
FAPI3_005	0.92	1.64	-0.5	1.29	Coarse sand; Poorly sorted; Strongly coarse skewed; Leptokurtic	29.00
FAPI3_058	1.84	0.58	0.14	0.96	Medium sand; Moderately well sorted; Fine skewed; Mesokurtic	5.10
FAPI3_059	1.27	0.93	-0.16	1.09	Medium sand; Moderately sorted; Coarse skewed; Mesokurtic	22.45
FAPI3_060	1.98	0.97	-0.29	1.21	Medium sand; Moderately sorted; Coarse skewed; Leptokurtic	10.20
FAPI3_061	1.62	1.02	-0.34	1.19	Medium sand; Poorly sorted; Strongly coarse skewed; Leptokurtic	12.24
FAPI3_062	0.81	0.74	-0.08	0.97	Coarse Sand; Moderately sorted; Near symmetrical; Mesokurtic	10.20
FAPI3_063	-0.28	1.77	-0.56	1.97	Very coarse sand; Poorly sorted; Strongly coarse skewed; Very leptokurtic	3.06
FAPI3_064	1.85	1.06	-0.13	1.07	Medium sand; Poorly sorted; Coarse skewed; Mesokurtic	8.16
FAPI3_065	-0.4	0.69	0.01	1.21	Very coarse sand; Moderately well sorted; Near symmetrical; Leptokurtic	5.10
FAPI3_066	-0.41	0.62	0.1	1.47	Very coarse sand; Moderately well sorted; Fine skewed; Leptokurtic	10.20
FAPI3_067	1.56	0.77	-0.02	1.16	Medium sand; Moderately sorted; Near symmetrical; Leptokurtic	5.10
FAPI3_068	1.47	0.78	-0.05	1.18	Medium sand; Moderately sorted; Near symmetrical; Leptokurtic	5.10
FAPI3_070	-1.27	1.59	-0.03	0.98	Granule; Poorly sorted; Near symmetrical; Mesokurtic	7.14
FAPI3_071	-0.71	1.15	-0.02	1.27	Very coarse sand; Poorly sorted; Near symmetrical; Leptokurtic	6.12
FAPI3_072	-0.78	1.08	-0.12	1.22	Very coarse sand; Poorly sorted; Coarse skewed; Leptokurtic	6.12
FAPI3_073	0.02	1.29	-0.34	1.25	Coarse sand; Poorly sorted; Strongly coarse skewed; Leptokurtic	3.06
FAPI3_074	1.14	0.68	-0.03	1.01	Medium sand; Moderately well sorted; Near symmetrical; Mesokurtic	3.06
FAPI3_075	0.93	0.67	0.05	0.96	Coarse sand; Moderately well sorted; Near symmetrical; Mesokurtic	0.00
FAPI3_076	1.84	0.69	0.03	1.03	Medium sand; Moderately well sorted; Near symmetrical; Mesokurtic	3.06
FAPI3_077	1.49	0.7	0	1.24	Medium sand; Moderately well sorted; Near symmetrical; Leptokurtic	3.06
FAPI3_078	1.17	0.79	0.01	1.03	Medium sand; Moderately sorted; Near symmetrical; Mesokurtic	0.00
FAPI3_079	1.27	0.77	-0.04	1.09	Medium sand; Moderately sorted; Near symmetrical; Mesokurtic	0.00
FAPI3_080	0.42	1.01	0.04	1.05	Coarse sand; Poorly sorted; Near symmetrical; Mesokurtic	0.00
FAPI3_081	-0.07	1.01	-0.04	1.24	Very coarse sand; Poorly sorted; Near symmetrical; Leptokurtic	4.08
FAPI3_082	-0.34	0.97	-0.1	1.18	Very coarse sand; Moderately sorted; Coarse skewed; Leptokurtic	4.08
FAPI3_083	1.18	0.74	-0.07	1.06	Medium sand; Moderately sorted; Near symmetrical; Mesokurtic	3.06
FAPI3_084	-0.65	1.48	0.1	0.98	Very coarse sand; Poorly sorted; Fine skewed; Mesokurtic	10.20
FAPI3_085	-0.45	1.85	-0.29	1.19	Very coarse sand; Poorly sorted; Coarse skewed; Leptokurtic	12.24
FAPI3_087	1.4	1.3	-0.4	1.13	Medium sand; Poorly sorted; Strongly coarse skewed; Leptokurtic	12.24
FAPI3_089	0.45	1.42	-0.15	1.02	Coarse sand; Poorly sorted; Coarse skewed; Mesokurtic	22.45
FAPI3_090	1.74	0.83	-0.13	1.11	Medium sand; Moderately sorted; Coarse skewed; Leptokurtic	8.16
FAPI3_091	1.46	0.95	-0.19	1.22	Medium sand; Moderately sorted; Coarse skewed; Leptokurtic	16.33
FAPI3_092	1.8	0.89	-0.2	1.24	Medium sand; Moderately sorted; Coarse skewed; Leptokurtic	10.20
FAPI3_093	1.5	1.32	-0.35	1.14	Medium sand; Poorly sorted; Strongly coarse skewed; Leptokurtic	22.45
FAPI3_094	1.92	0.78	-0.17	1.23	Medium sand; Moderately sorted; Coarse skewed; Leptokurtic	4.08

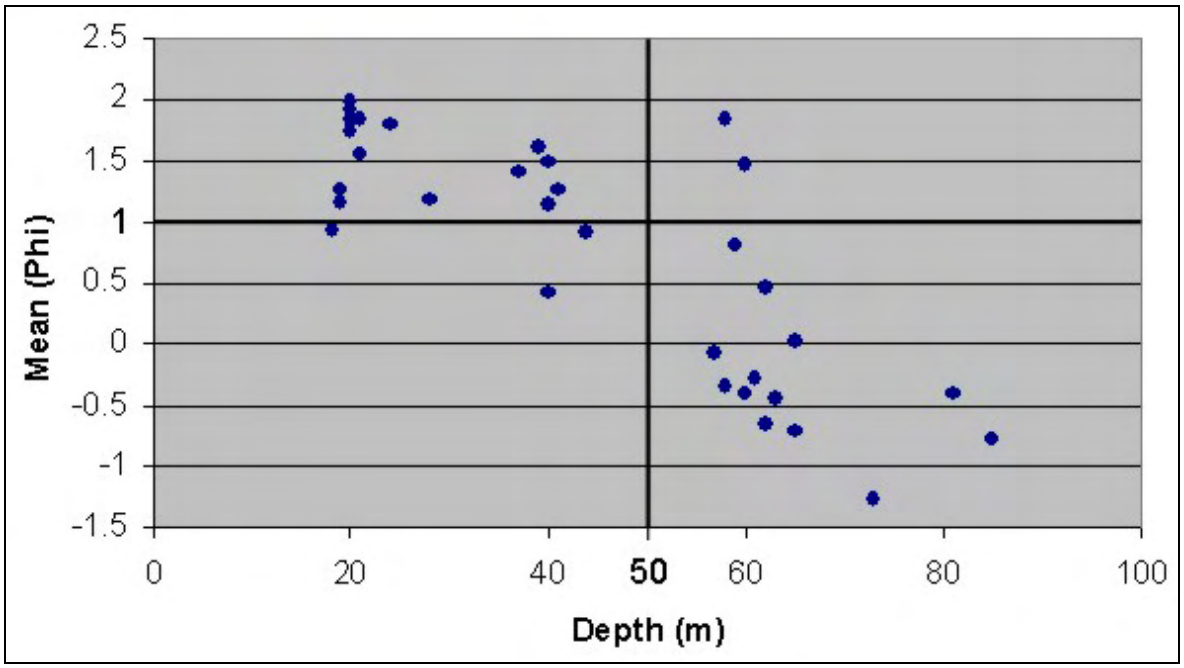

Figure 171 – Mean size (M1) plotted against water depth of the Faial shelf samples. The bolder black lines show that the majority of the samples coarser than medium sands (1Φ) are located below 50 meters water depth.

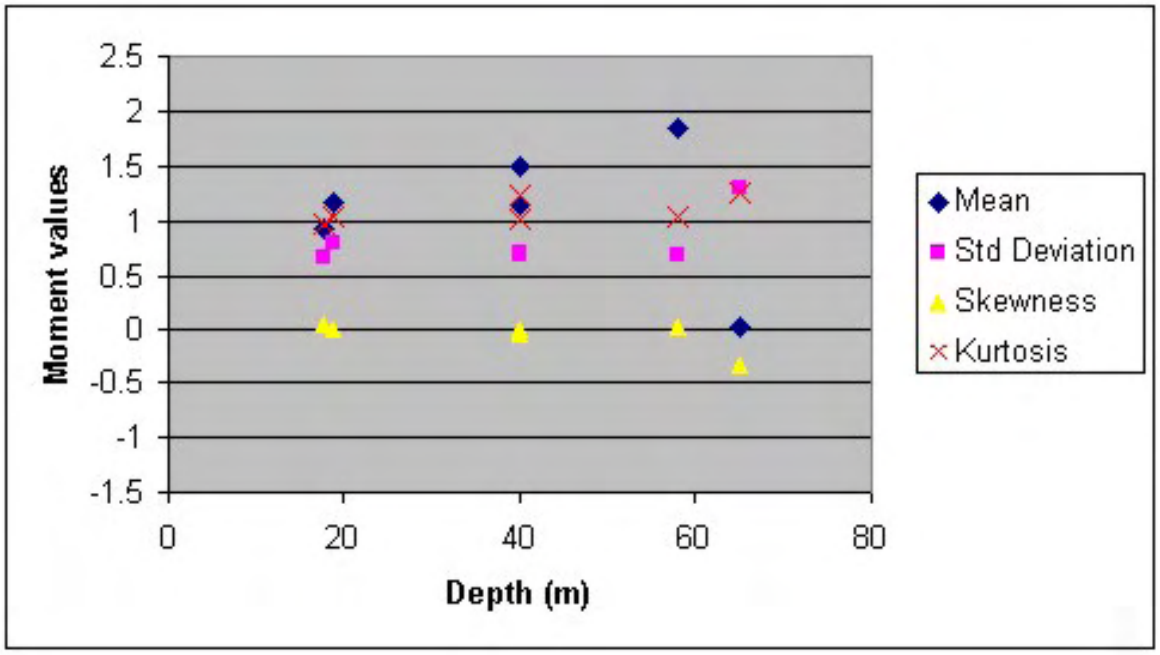

Figure 172 - Mean size (M1), Standard Deviation (M2), Skewness (M3) and Kurtosis (M4) plotted against water depth for the shelf sector B.

but is around 1 and 1.5, which means that the distributions are slightly leptokurtic.

Figure 177 shows the percentage of carbonate calcium of the samples in

the shelf, which is due to the presence of carbonate skeletal particles. It is however difficult to explain why there is such variability along the shelf due to the absence of habitat mapping in the Faial shelf.

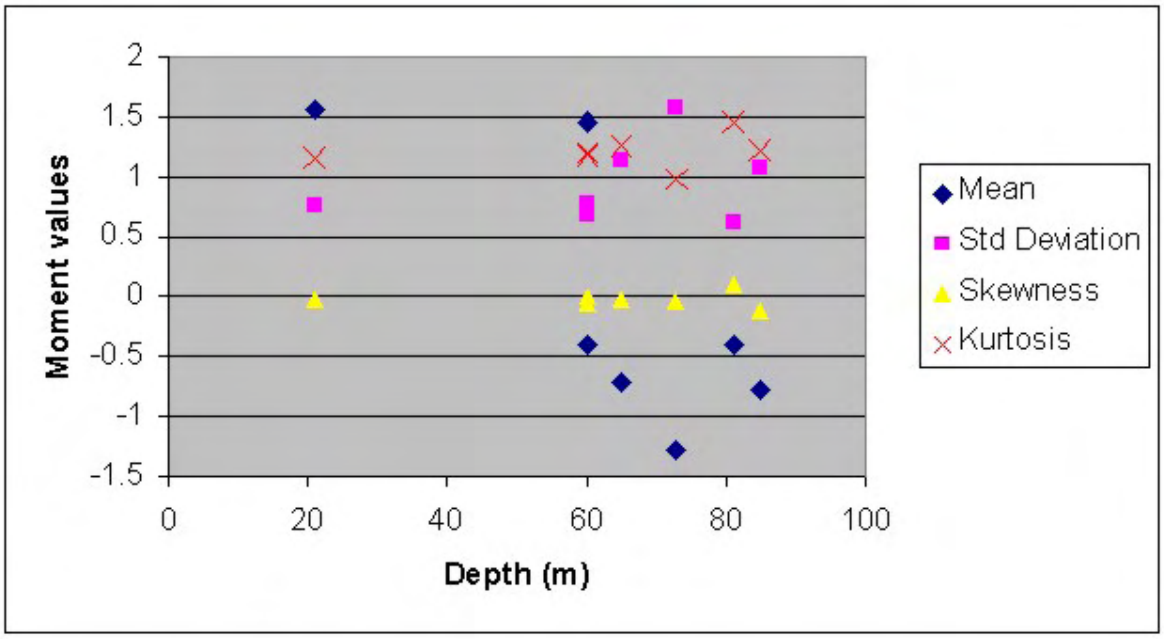

Figure 173 - Mean size (M1), Standard Deviation (M2), Skewness (M3) and Kurtosis (M4) plotted against water depth for the shelf sectors C and D.

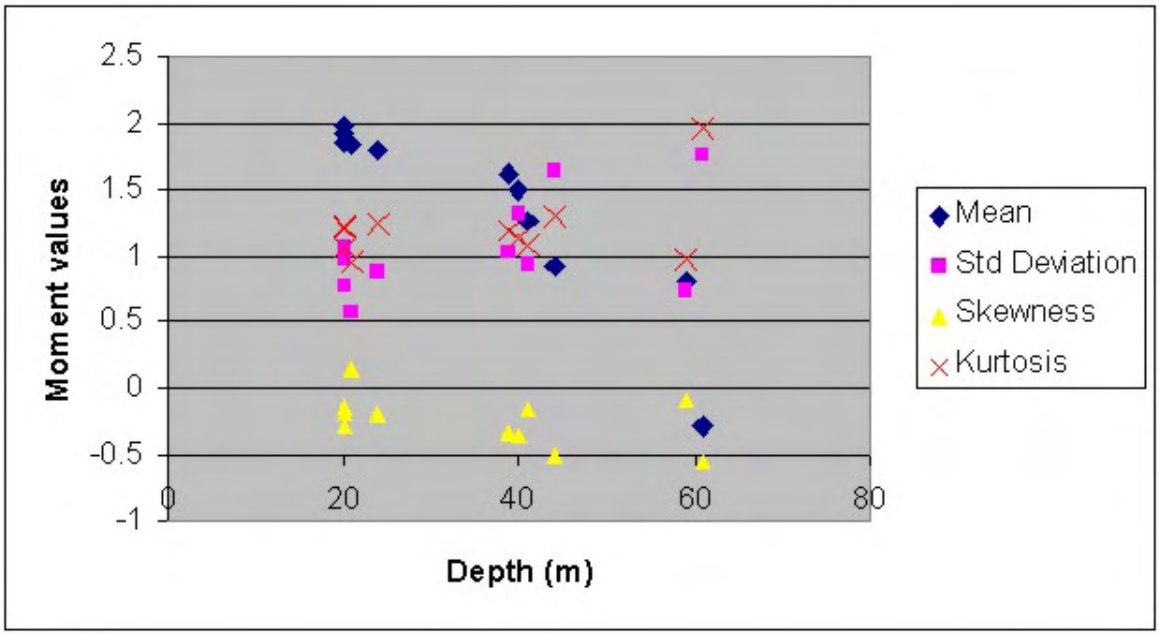

Figure 174 - Mean size (M1), Standard Deviation (M2), Skewness (M3) and Kurtosis (M4) plotted against water depth for the shelf sector E.

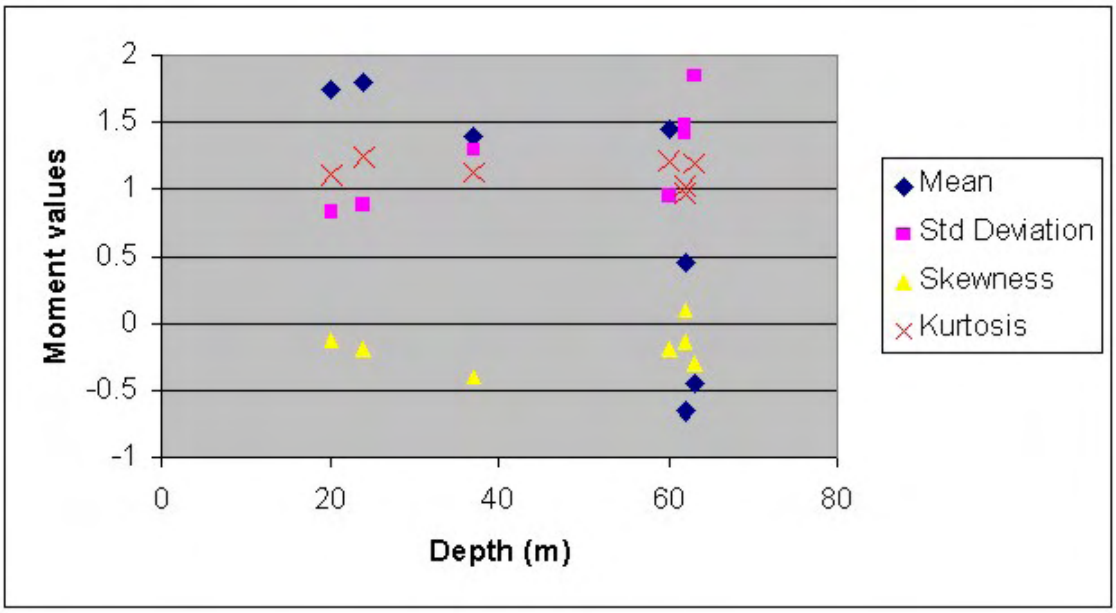

Figure 175 - Mean size (M1), Standard Deviation (M2), Skewness (M3) and Kurtosis (M4) plotted against water depth for the shelf sectors F and G.

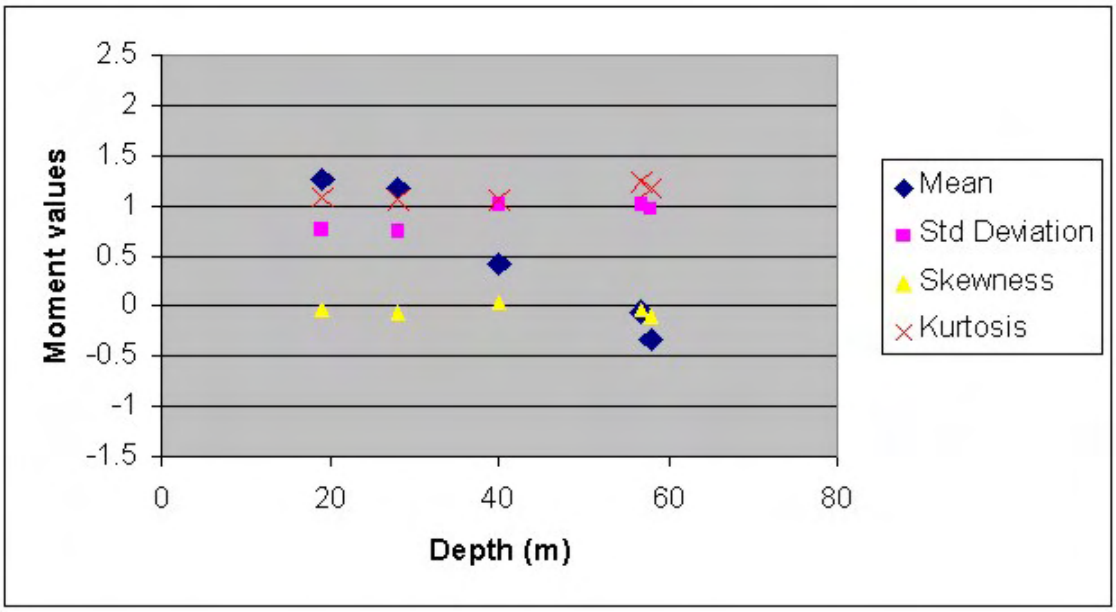

Figure 176 - Mean size, Standard Deviation, Skewness and Kurtosis plotted against depth for shelf sector H.

6.2.2. Processes responsible for the cross-shelf sedimentary pattern

According to Leeder (1999), weather-dominated shelves tend to show a general offshore decrease in grain size. Although much of the present continental

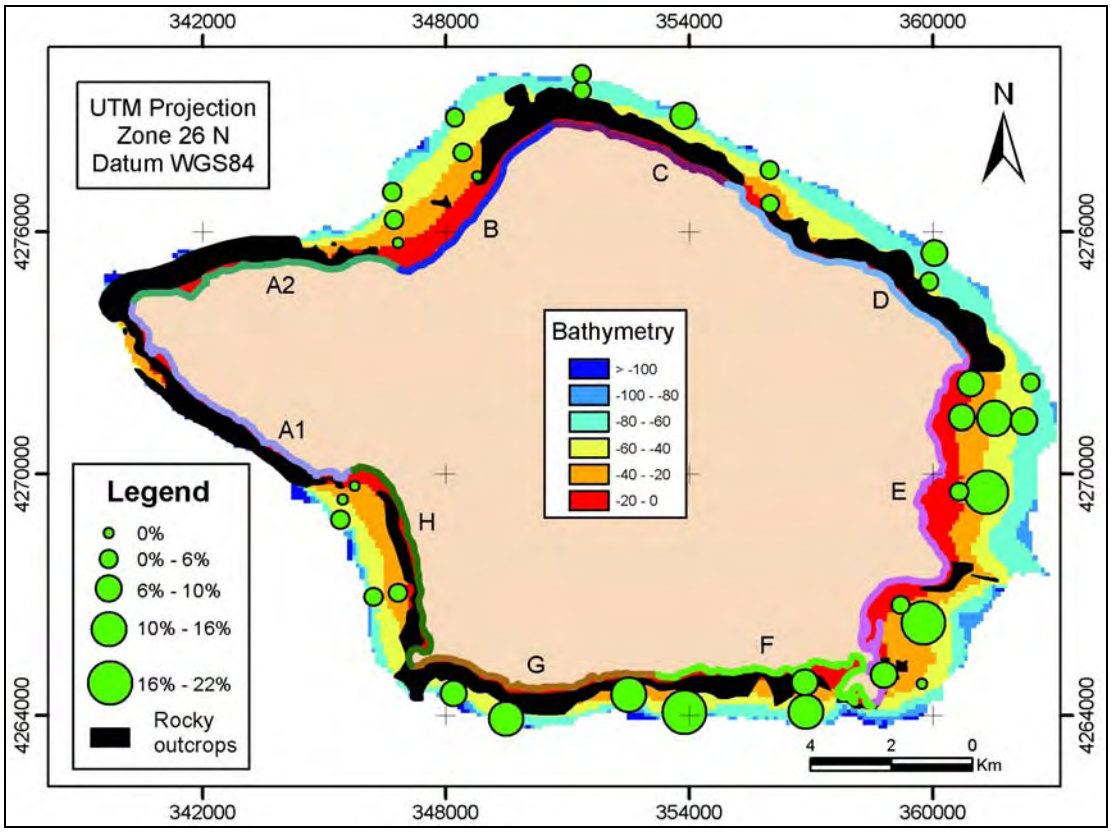

Figure 177 – Carbonate percentages from the Faial shelf samples. The rocky outcrops correspond to the lava flows and coarse clastic deposits interpreted in Chapter 3.

shelf contains relict or palimpsest sediments (Emery, 1968; Swift et al., 1971), those parts of the inner-shelf where sediment is accumulating today should show such a seaward-fining profile (Figure 178), reflecting the balance between grain size, water depth and wave energy (Dunbar and Barrett, 2005).

Surprisingly, being the Faial shelf a wave to storm-dominated system, the sampling has shown the absence of this offshore-fining profile. On the contrary, the data shows an offshore-coarsening profile, especially below 50 meters water depth. The simplest explanation is to assume that at higher depths the presence of relict or palimpsest sediments dominates. Relict sediments are sediments that were deposited long time ago in equilibrium with their environments, most likely when the sea level was lower than today. As the sea-level rose, the sedimentary environments changed and the sediments are no longer in equilibrium (Emery, 1968). Therefore, the coarse sediments that are presently at greater depths could have been formed in a shoreface environment that with the rise of sea-level has changed to an outer shelf environment.

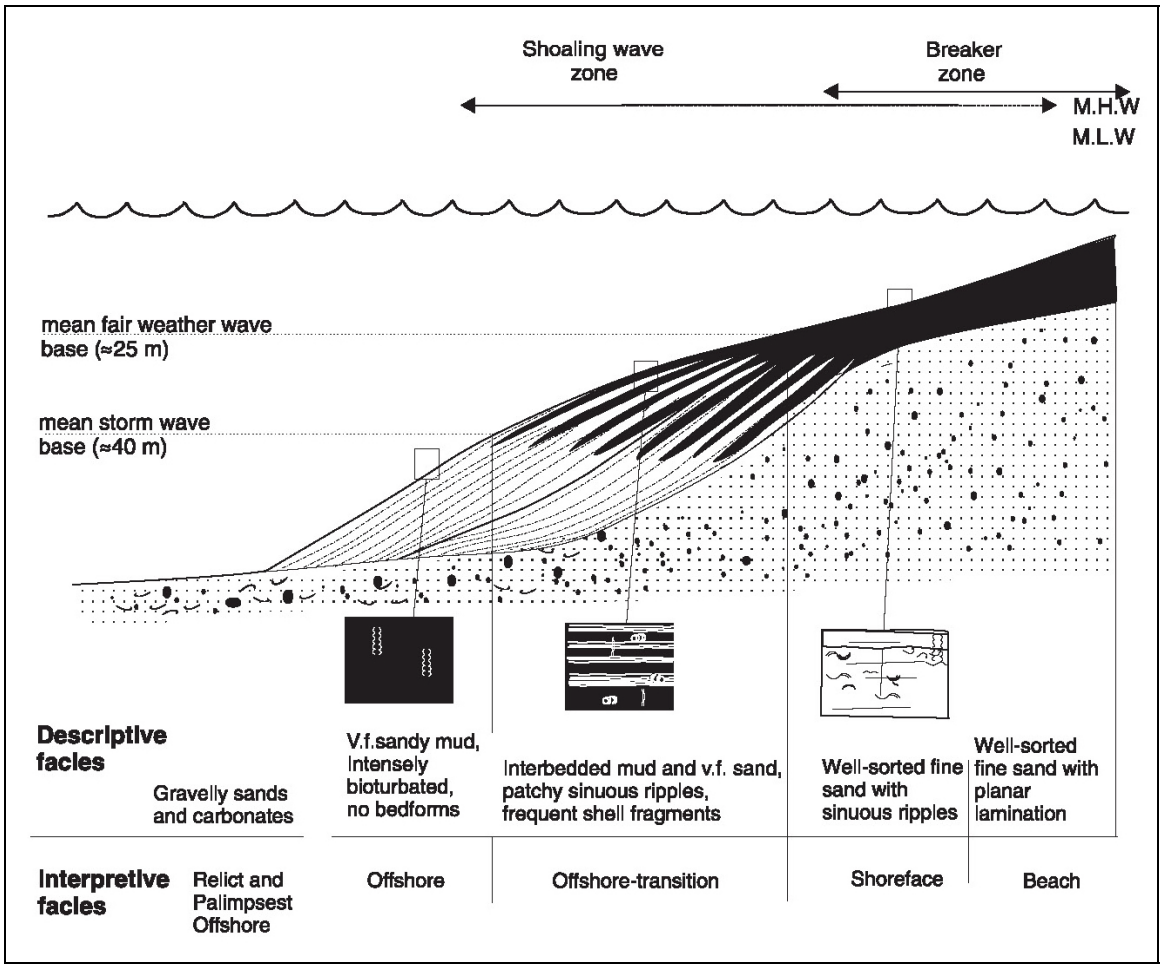

Figure 178 – Schematic diagram of the development of a wave-graded shelf and the normal textural pattern of the sea-floor sediment (Dunbar and Barrett, 2005).

A relict origin is normally attested by coarse well-sorted sands lying seaward and deeper than finer and less well-sorted sands (Emery, 1968). In fact, the sediments from the Faial shelf are coarser offshore but they are also more poorly sorted (Figures 172, 173, 174, and 176). Moreover, they do not show staining of grains by iron oxide and pitting by solution (see section 7.3 of Chapter 7), which, according to Emery (1968), are good indicators of a relict origin. Nor, as it is referred by Swift et al. (1971), the shells compounding the sediments show any signs of abrasion, corrosion and encrustation by bryozoan and polychaete tubes. Consequently, the relict origin does not seem a good explanation for the presence of coarser sediments offshore and another mechanism must be found to explain this trend.

The study of continental shelves has shown that their sedimentary

sequences basically consist of beds displaying storm-induced depositional structures intercalated with mud and shale layers. At short time scales, sediment redistribution across the shelf is controlled by hydrodynamic processes, i.e. waves, tides, geostrophic currents during storm events, whilst at longer time scales and 1-100 m sequence scale the controlling factors are the accommodation space and availability of sediments (Quiquerez et al., 2004). Several studies demonstrated that winter storms are the agent causing much of the sediment dispersal on coastal shelves. The effects of these storms are observable from shoreface to water depths greater than 200m, at several tens of kilometres (Nittrouer and Wright, 1994). Side-scan surveys after an intense winter storm at the Scotian shelf showed the presence of hummocky megaripples in a region previously mapped as featureless (Amos et al., 1996). These megaripples were linked to the storm, which produced 7 m high significant waves. Box cores through the megaripples revealed a well-defined tempestite bed 0.3 m thick overlying a lag layer of 4-cm diameter pebbles (Amos et al., 1996). However, Lee et al. (1998) have shown that these highly energetic events responsible for redistributing sediments to the shelf have a very low recurrence. Conversely, fair-weather period is rather constant all over the year and bioturbation and swell waves contribute significantly to the smoothing of depositional profiles by favouring resuspension of the sediments (Amos et al., 1996; Gagan et al., 1988). Lee et al. (1998) have also shown that it is the interplay between the low recurrence groups of storm events and the steady onshore feed of sediments from the shoreface during fair-weather conditions that appear to play an important role on medium- and long-term profile evolution at Duck beach, California. Furthermore, the onshore feeding of sediments in Duck beach was not significantly affected by individual storms during the fair-weather conditions, which lasted up to 4 years. On the contrary, the responsible for the significant changes were the high energetic storm group events.

The mechanisms of which sediments are redistributed across the modern shelves during the passage of storms are well established (Cookman and Flemings, 2001). A range of wind stress orientations are present during the passage of the storm and it can produce upwelling or downwelling (Figure 179B) at different locations and at different times during a storm’s history. In the example

of Figure 179A, shore-parallel wind stress drives a current at the sea surface which is acted upon by the Coriolis force, causing the current to veer to the right. This rotating flow adjacent to the water surface is called the surface Ekman layer (Figure 179A) and the onshore component of the flow causes pilling of water on the coast (coastal set-up). The resulting water surface gradient drives an offshore current which extends throughout the entire water column and veers to the right, producing a geostrophic flow oriented parallel to the shore. Below one Ekman depth (D) is the geostrophic core where the interlayer shear stress goes to zero. Near the sea floor, frictional forces retard the geostrophic flow, and the Coriolis force causes the current to veer to the left. In this bottom Ekman layer, flow is oriented obliquely offshore (Figure 179A).

It is clear that the Faial shelf is subjected to a very high energetic regime; big storms struck the Azores (see section 2.2.4 of Chapter 2) and downwelling currents were recorded associated to them (see section 2.4.4 of Chapter 2). Therefore, four mechanisms often associated to storms could explain the coarsening-offshore trend in the Faial shelf:

1. It is possible to assume that a very energetic event or group of events may have swept off the shelf of Faial dispersing coarse sediments all over it. Strong storm winds push surface waters landward and coastal setup results. The resulting water surface gradient drives a downwelling offshore current which transports sediments seaward. These extreme energetic events that affect the entire shelf have probably a low frequency, much less than 1 per year. Only a big storm could provoke downwelling currents strong enough to transport such coarse sediments (coarse sands to granules) across the entire shelf. In fact, as already discussed in section 2.2.4 of Chapter 2, violent storms occur once every seven years. Nevertheless, it does not explain the transition between the dominance of medium sands above 50 meters water depth to coarser sediments below this depth (Figure 171).

2. Although most of the storm-bed models describe deposits which thin and become more finely grained with increasing water depth and distance from

shore due to offshore directed storm-surge ebb-flow, Gagan et al. (1990; 1988) have shown that other patterns are also possible. They showed that theWinifred storm-layer in the central Great Barrier Reef, Australia, becomes thicker and more coarsely grained offshore. According to these authors, the cross-shelf changes in thickness, texture and composition of the Winifred storm bed were controlled by the changing response of a variable shelf substrate rather than by shore-normal changes in the current velocity. Furthermore,

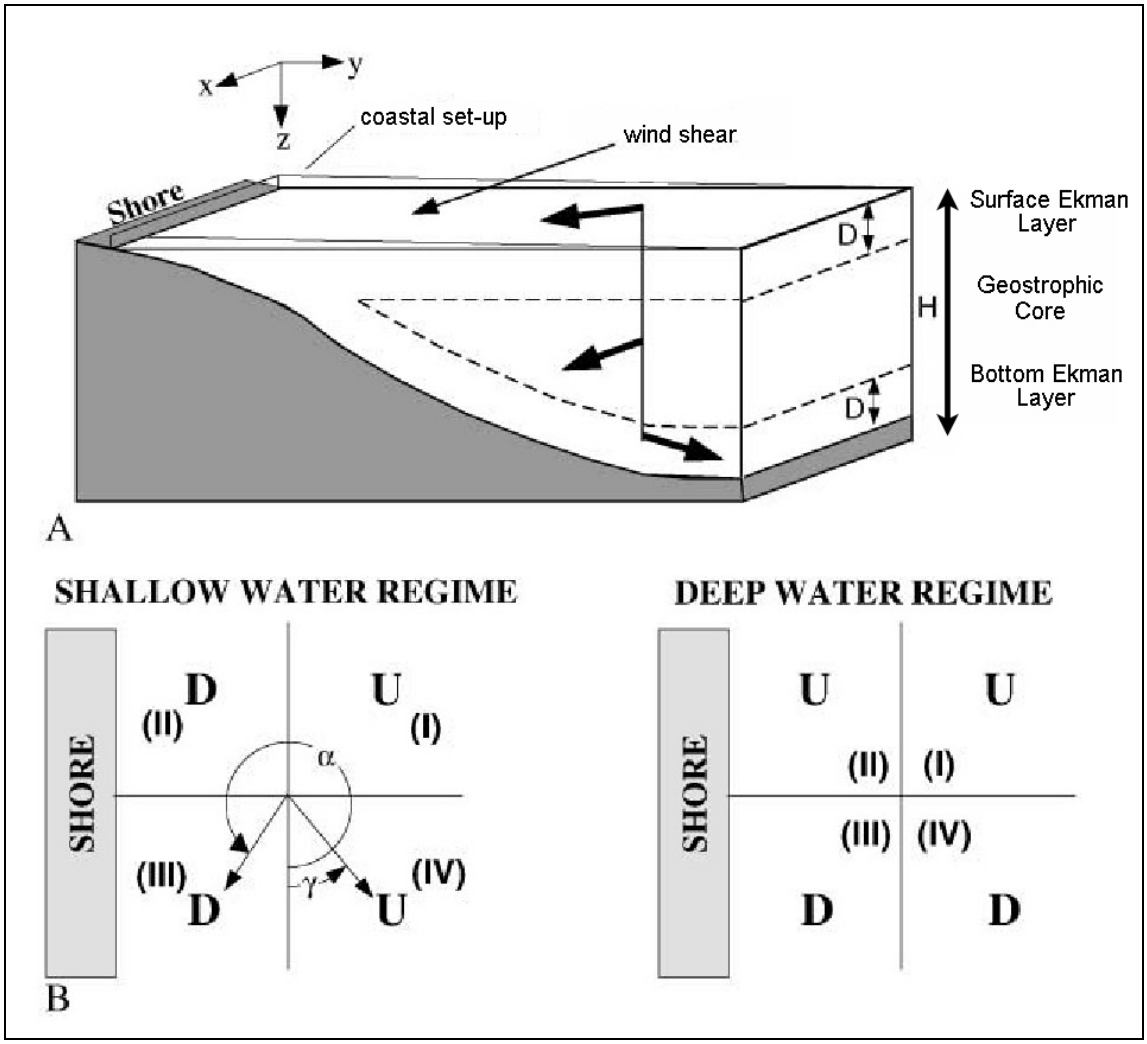

Figure 179 – A - In the northern hemisphere, downwelling (thick arrows show flow direction) results from steady wind oriented to right as observer faces seaward. Ekman layers develop at water surface and sea bed in response to boundary shear stresses. Geostrophic core has a constant shore-parallel velocity. B - Downwelling (D) occurs in deep and shallow regime if the wind is oriented (a) in quadrant III. Upwelling (U) occurs in deep and shallow regime if the wind is in quadrant I. If wind orientation is in quadrant II or IV, upwelling can occur in shallow zone and downwelling in deep zone (or vice versa) (Cookman and Flemings, 2001).

resampling one year after showed preservation of the Winifred storm layer nearshore and rapid reworking offshore below fair-weather wave-base. This work shows that different shelf substrates may respond differently to storm currents, resulting in storms beds that have significantly lateral variations in thickness, texture and composition. However, the surface of the sand and gravel deposits of the Faial shelf, except for the coarsening offshore pattern and the varying calcium carbonate percentage, show a rather cross-shelf uniform composition. The sediments are basically medium to coarse sands composed of dark volcanic minerals and a variable percentage of skeletal carbonate particles. The seismic interpretation also showed homogenous sedimentary deposits. Although they present varied thickness, their geometry and internal structure (see section 4.3.1 in Chapter 4) is the same all over the shelf. Therefore, it would not be very convincing to explain the present-day sedimentary pattern of the Faial shelf by the existence of a previous variable shelf substrate.

3. As mentioned before, the downwelling currents directed offshore during storms are known to be the major responsibles for the sediment redistribution in the continental shelves. There might be however transport of sediments in any direction, depending on the intensity, orientation (relative to the shoreline) and duration of the storm winds. Probably unlikely, but possible, is to assume the presence of strong winds blowing in the offshore direction resulting in the predominance of upwelling currents that would transport finer sediments onshore leaving the coarser offshore. In fact, the predominant wind directions (higher frequencies and velocities) in the Faial Island (see section 2.3.1 in Chapter 2) are those orientated towards S to SW and N to NE. The Coriolis effect would cause net transport of surface and bottom waters approximately directed W-E, which would only explain the fining landward trend in the shelf sectors E and H (see Figure 169 for coastal orientation), leaving the sedimentary pattern in the remaining sectors unexplained. Moreover, most of the onshore transport of sand is attributed to wave asymmetry, whilst upwelling currents are considered to be a process of secondary importance (Niedoroda

et al., 1985).

4. Another possible explanation is to consider that the shelf break in Faial Island is a zone of active sedimentation. The majority of the detailed surveys on the outer margins have provided evidence of recent sediment displacement at and near the shelf break (Southard and Stanley, 1976). Furthermore, there is also a wide variety of data showing that relict sediment has been reworked since the rise in sea level and continues to be modified at present resulting in palimpsest sediment (Swift et al., 1971). Southard and Stanley (1976) reviewed the physical processes at the shelf break capable of sediment entrainment and transport at the shelf break. Several kinds of water movements seem to be distinctive here. These distinctive processes when superimposed on bottom currents caused by tides, waves and winds that are known to be typical of the outer shelf environment, act to increase bottom sediment movements that seem to be characteristic of the shelf edge. Tidal currents, especially on low-latitude, gently sloping shelves, tend to be stronger on the outer shelf than nearshore. Bottom currents produced by migration of the atmospheric pressure-induced wave that migrates beneath a major storm moving in the offshore direction can result in a current on the order of 10 cm/s concentrated on the shelf break. Both theory and experiment suggest that internal waves of tidal or shorter period propagating shoreward in thermoclines produce intensified near-bottom velocities near the shelf edge as they steepen and break. Large eddies generated at shear zones between major currents on the shelf and in adjacent open-ocean should locally increase bottom velocities in the shelf break region (Southard and Stanley, 1976). In conclusion, there seem to be several processes that may be responsible for the winnowing of fine sediments near the shelf break leaving behind the coarser fractions. Furthermore, the shelf break in Faial Island occurs on average at depths that vary between 55 and 80 meters (see Figure 57 in Chapter 3) which correspond precisely to the range of depths where the coarser sediments dominate.

From what has been discussed above, it appears that the most likely explanation of the offshore coarsening trend is the conjugation of two of the four

mechanisms described. First, the existence of low recurrence and very energetic events transport coarse sediments across the entire shelf of Faial through downwelling currents. Then, transport of sediments at the shelf break (which was mapped between 55 m and 80 m water depth – see Chapters 3 and 5) to the slope provokes the winnowing of fine sediments between the 50 and 80 meters water depth, causing the coarsening pattern found at these depths. Since the very energetic events do not occur often (much less than one per year), the areas below 50 meters water depth have not yet received sediments from the downwelling currents. This would allow the outer shelf to be covered by sediments with grain-size distribution similar to ones that are above 50 meters water depth, homogenizing the entire sedimentary cover of the shelf.

6.3. Cross-shore sediment transport in the Faial Island shelf

The seaward limit to significant sediment transport in sandy coastal regions is of fundamental importance to understanding long and cross-shore sediment budgets and modeling coastal evolution. The significance of the shoreface lies in the role it plays in the exchange of sand with the continental shelf and whether the offshore zone is a net source or a sink for beach sands (Cowell et al., 1999). The shoreface (Figure 180) can be defined as the upper part of the continental shelf that is affected by contemporary wave processes and extends from the limit of wave run-up to the depth limit for wave-driven sediment transport (Cowell et al., 1999).

The shoreface can be subdivided into an upper and lower section. The upper shoreface, referred to as the littoral zone by Hallermeier (1981), is defined as the region in which erosion and accretion result in significant (i.e. measurable) changes in the beach profile during a typical year. The lower shoreface, referred to as the shoal zone by Hallermeier (1981), experiences little sediment transport processes under typical wave conditions, but significant morphological changes can occur during extreme storm events.

The boundary between the upper and lower shoreface is referred to as the

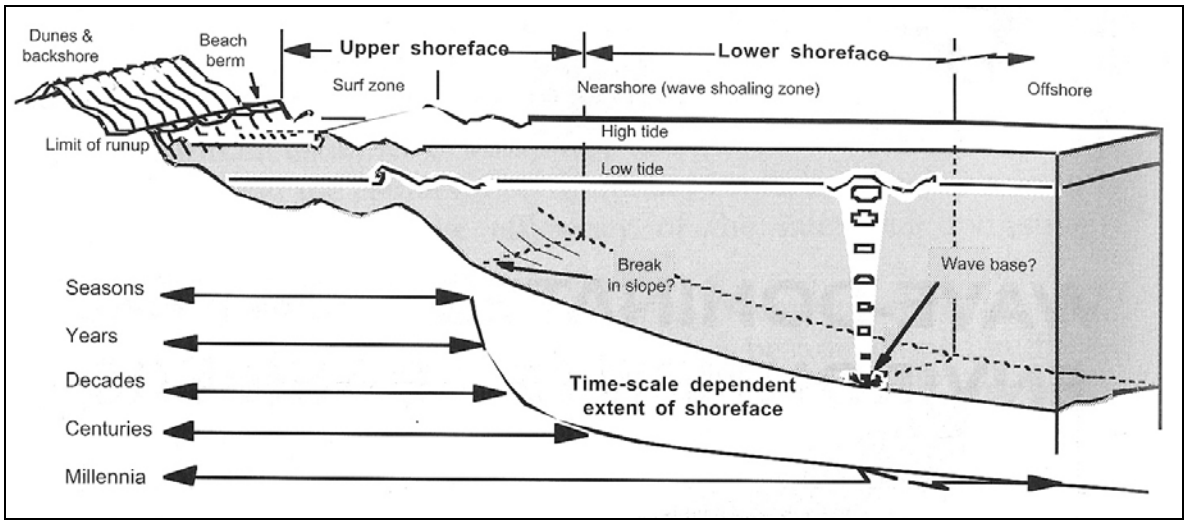

Figure 180 – Definition of the upper and lower shoreface profiles and the time scale of interest in the positioning of their limits (after Cowell et al., 1999).

depth of closure (or closure depth) and can be used to infer a seaward limit to significant cross-shore sediment transport (Nicholls et al., 1998). According to Hallermeier (1981), at the closure depth one should not expect vertical variations higher than 0.3 m during a typical year. In the absence of repetitive submarine beach profiles to determine the depth at which morphological change is insignificant (less than 0.3 m), Hallermeier (1981) proposed that the depth of closure d_c could be predicted using the annual wave climate according to Equation 14:

$$d_c = 2.28H_{sx} - 68.5\frac{H_{sx}^2}{gT_{sx}^2} \quad (14)$$

Where H_{sx} is the nearshore significant wave height that is exceeded only 12 hours each year (e.g. one should look in the data for the highest waves of the record that occur with this frequency: 12h/(365days×24h)×100%=0.137%), T_{sx} is the associated wave period and g the acceleration due to gravity. Equation 14 was generalized to a time-dependent form by Stive et al. (Equation 15, 1992):

$$d_{l,t} = 2.28H_{e,t} - 68.5\frac{H_{e,t}^2}{gT_{e,t}^2} \quad (15)$$

Where: $d_{l,t}$ is the d_c over t years; $H_{e,t}$ is the significant non-breaking wave height that is exceeded 12 hours per t years, (0.137/t)% of the time; $T_{e,t}$ is the associated wave period and g the acceleration due to gravity.

It has been shown in several studies that the predictive equations for the d_c (Equations 14 Equation 15) provide good estimations although they use simple wave parameters (Hallermeier, 1981; Nicholls et al., 1998). However, these studies have also revealed uncertainties in this estimation, which allows for the following considerations (Capobianco et al., 2002; Cowell et al., 1999):

- The depth of closure is time and space-scale dependent and generally the lateral (shore-normal) migration of the theoretical closure depth increases with time-scale (Figure 181a). The stretching of the theoretical closure depth also involves seaward shift of this limit during storms (Figure 181b) and landward shift during fair-weather conditions.

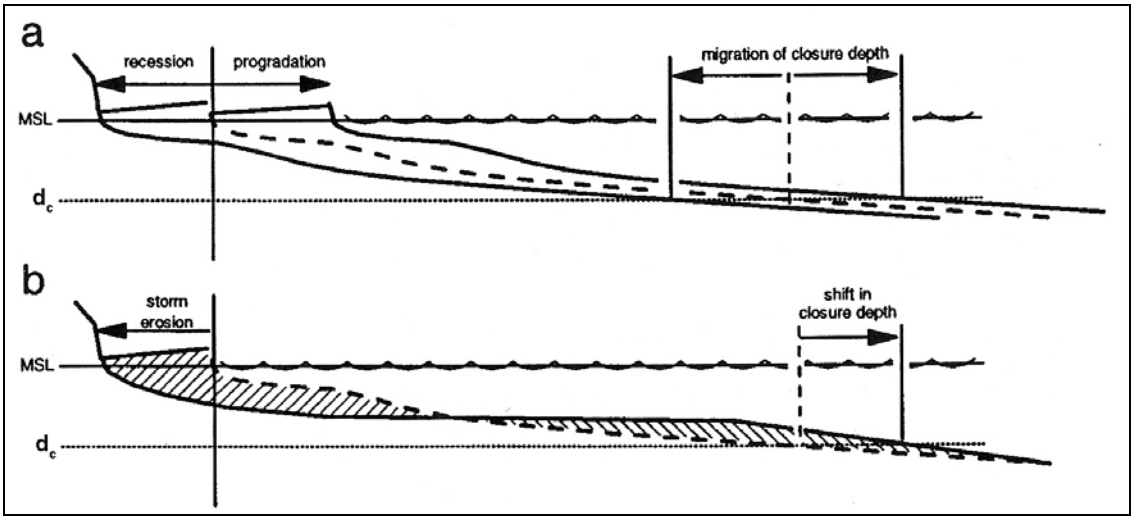

Figure 181 – Movements in the seaward boundary of the closure depth: (a) at intervals significantly longer than the annual time scale; (b) seaward displacement of the closure depth due to a severe storm with a return interval greater than 1 year. (Cowell et al., 1999).

- The depth of closure is a morphodynamic boundary, not a sediment transport boundary. Sediment transport occurs seaward of the closure depth, especially during storms. However, the closure depth is a good empirical indicator of an increasing capacity for shoreward sediment transport at any point within the limits of closure.

- At small scales, the depth of closure is usually the product of bar migration due to surf zone processes (Nicholls et al., 1998). As the scale increases, so does beach-nearshore profile translation and ultimately shoreface processes come to control the location of closure.
- In two-dimensional situations, the analytical formulation for d_c (Hallermeier, 1981) provides robust estimates of the limit of closure for individual erosional events up to the annual time-scale (Nicholls et al., 1998). Between annual and decadal scales, it continues to act as a limit, but with an increasing tendency for overprediction. The d_c only considers cross-shore redistribution of sediment and is invalid in areas which are accreting rapidly due to longshore supply of sand.

6.3.1. Estimation of the seaward limit of the upper shoreface

The wave-climate data (Carvalho, 2003) used to estimate the seaward limit of the upper shoreface (closure depth - d_c) includes the annual average hindcast of $H_s(m_0)$ and the T_p for the period of 1989-2002 (Tables 1 and 2 in Chapter 2). As already discussed in the section 2.2.3 of Chapter 2, there is the need to use in the calculations the H_s and T_s; therefore, the Equations 3, 4, 5 and 8 (see Chapter 2) are used to convert $H_s(m_0)$ into H_s and T_p into T_s. Since the hindcast data provides a period bigger than one year, it is possible to use the Equation 15 from Stive et al. (1992) to estimate the d_c for a 14 year period. Including an enlarged period is important, because it will take into account more energetic events although there is the risk of overestimation for the d_c. Nevertheless, overestimation can be a safer approach when it comes to decide at which depth aggregates can be explored without putting at risk the coastline (see Chapter 7). Therefore, the d_c is calculated for each coastal sector, using the values of H_s and T_s that are exceeded only 12 hours during the 14 years period (which are referred respectively as $H_{e,t}$ and $T_{e,t}$ in the Equation 15). For instance, to calculate the NE H_s that is exceeded only 12 hours during the 14 years period – (0.137/14)% of the time - one should look for the highest waves in the record that have a frequency of 0.00978% (e.g. in Table 1

the NE $H_s(m_0)$ must result from a linear interpolation between 7 m (0.020%) and 8 m (0%), which gives 7.51 m and since H_s = $H_s(m_0)$, the value is the same – see Table 15). To calculate the NE T_s that is exceeded only 12 hours during the 14 years period – (0.137/14)% of the time - one should look for the highest periods in the record that have a frequency of 0.00978% (e.g. in Table 2 the NE T_p must result from a linear interpolation between 14 s (0.015%) and 15 s (0%), which gives 14.51 s and using Equations 4, 5, and 8 the value 11.97s is found – see Table 15).

The closure depth estimated with Equation 15 (Table 15) gives values between 10 m (coastal sector perpendicular to the SE direction) to 26 m (coastal sector perpendicular to the W direction). In reality, this kind of analysis only makes sense for coastal sectors that have nearshore sands and these are only present in the coastal sectors B, E and H (see sectors orientation in Figure 169). Therefore, in a typical year, sectors B, E and H should not have vertical variations higher than 0.3 m below the respective water depths of 24 m, 11 m and 20 m.

Table 15 - Estimation of closure depth based on Equation 15. The represented quadrants are relative to wave ray directions.

	$H_{e,t}$ (m)	$T_{e,t}^*$ (s)	$d_{l,t}^*$ (m)
NE	7.510	11.973	14.373
E	5.840	10.304	11.070
SE	5.350	9.862	10.141
S	5.960	10.029	11.120
SW	11.040	12.808	19.978
W	13.720	15.669	25.923
NW	12.040	16.445	23.705
N	8.510	13.901	16.783

The transition from the upper to the lower shoreface is generally not characterized by a change in morphology. However, the theoretical closure depth may correspond to a distinct break in sediment characteristics (Niedoroda et al., 1985). Upper shoreface sands are usually well-sorted and similar to beach

sediments, and tend to display a seaward-fining trend. In many places, the seaward fining of sediments occurs down to an abrupt transition at a depth similar to d_c, seaward of which coarser, poorly sorted sand may be found. In this work, a detailed sampling is not available (samples were always taken below 20 m water depth) to check if the transition from the upper to the lower shoreface shows such a change in the sediment characteristics.

6.3.2. Estimation of the seaward limit of the lower shoreface

As mentioned before, the lower shoreface does not suffer significant vertical changes (less than 0.3 m) in a typical year. Furthermore, its seaward limit represents the depth of sediment immobility during a normal year. Only during extreme storm events, significant changes can occur in the lower shoreface and sediments can be transported beyond the seaward limit of it. Because the seaward limit of the lower shoreface depends greatly on the time scale of interest (Figure 180), it is less straightforward to define. However, in the absence of other clear-cut definitions, it is useful to turn to another of Hallermeier's (1981) criteria for estimating this limit (Cowell et al., 1999). Based on a synthesis of theoretical and field studies, Hallermeier (1981) estimated that the limiting depth for the on-offshore transport of sand by waves throughout a typical year is given by:

$$d_i = (H_s - 0.3\sigma H_s)T_s(g / 5000D_{50})^{1/2} \quad (16)$$

Where H_s is the nearshore annual average significant wave height; σH_s is the standard deviation of H_s, T_s is the associated wave period, g the acceleration due to gravity and D_{50} is the size of the median sediment (in meters) determined from a sand sample taken in a water depth (h) of $h=1.5\ d_c$. The H_s for each quadrant (corresponds to H_{sav} in Chapter 2) is calculated from Table 1 in Chapter 2 using Equation 9. To calculate the standard deviation of the H_s per quadrant (σH_s), first one must calculate each monthly average significant wave height per quadrant, using also Equation 9. This is possible because Carvalho (2003)

provides tables similar to Table 1 but with monthly average significant wave heights (these are averages from January to December for the 14 year period - 1989-2002). Then, the values of each monthly average significant wave height per quadrant are used to calculate the annual standard deviation of H_s. The median size used in the calculations was derived from the nearest sample of the required water depth h, since very often there were no samples at this water depth. The T_s for each quadrant (corresponds to T_{pav} in Chapter 2) is calculated from Table 2 in Chapter 2 using the Equation 10 and then Equations 4, 5 and 8.

Table 16 shows the estimations for the seaward limit of the lower shoreface where these vary between 29 and 49 meters water depth. In this case, the differences are primary related with the annual variation of the value of H_s for the distinct directional sectors.

Table 16 - Estimation of the offshore limit of the lower shoreface based on the Equation 16. The represented quadrants are relative to wave ray directions.

	H_s (m)	T_s(m)	σ Hs	D_{50} (m)	h=1.5 d_c (m)	d_i (m)
NE	1.870	7.197	0.678	0.000342	20.930	28.730
E	1.913	6.665	0.599	0.000242	16.090	32.850
SE	2.211	6.685	0.598	0.000261	14.740	37.238
S	2.456	7.037	0.576	0.000295	16.120	41.403
SW	2.999	7.777	0.893	0.000403	28.780	46.817
W	2.964	8.609	1.034	0.000426	37.660	48.984
NW	2.480	8.463	0.944	0.000438	34.700	39.316
N	2.018	7.580	0.779	0.000342	24.570	32.407

However, one question remains. How representative was the grain diameter used for the calculations, considering the variable nature of the sediment distribution on the lower shoreface? A simple alternative approach to defining the seaward limit of the lower shoreface is through the application of the wave base concept, where wave base is defined as water depth beyond which wave actions ceases to stir the sediments bed (Cowell et al., 1999). Conventionally, this limit is taken to be where the water depth (h_{LS}) is half the deep-water wave length (L_0) - Equation 17 - which corresponds to the deep-water transition to intermediate-

water waves.

$$h_{LS}=L_0/2 \quad (17)$$

The general expression for wave length according to linear Airy wave theory is (Dean and Dalrymple, 1991):

$$L = \frac{gT^2}{2\pi}\tanh\left(\frac{2\pi}{L}\right) \quad (18)$$

And for the special case of deep-water waves, $\tanh(2\pi / \mathrm{L}) \to 1$, so that wave length simply becomes:

$$L_0 = gT^2/2\pi \quad (19)$$

Where L_0 is the deep-water wave-length, T the period and g the acceleration due to gravity (9.81 m/s^2). For this case it will also be used the T_{pav} of Chapter 2 and then use the Equations 4, 5 and 8.

The seaward limit of the lower shoreface (Table 17) calculated with this method is very similar for some sectors, whilst for others it shows some significant differences (e.g. 16.6 m difference for waves coming from NW). Nevertheless, both methods put more or less this limit between 30 and 50 m, depending essentially on the values of the wave height and period for Equation 16 and period for Equation 17.

Figure 182 shows theoretical curves based on the Equation 16 for all wave directions and grain size distributions. The curves were drawn with the values of H_s and T_s for each quadrant (Table 16) and using increasing theoretical values of D_{50}. If one looks to the curve generated by the southwestern waves (sector H), the area above the dark red curve represents all the sediments that at the respective depths and grain size do not suffer transport in a typical year; they are only

Table 17 - Estimation of the offshore limit of the lower shoreface based on of the wave base concept using Equation 17. The represented quadrants are relative to wave rays directions.

	L_0 (m)	T (s)	h_{LS} (m)
NE	80.797	7.197	40.399
E	69.292	6.665	34.646
SE	69.712	6.685	34.856
S	77.243	7.037	38.621
SW	94.329	7.777	47.165
W	115.597	8.609	57.798
NW	111.721	8.463	55.861
N	89.619	7.580	44.809

transported during extreme storms events. The area below the curve represents all the sediments that the respective depths and grain size, suffer transport, although by definition the transport in the lower shoreface is not very significant in terms of quantity. If one looks to the graphic of the Figure 171, it is obvious that the sediments are coarser below 50 meters water depth. And if one plots those sediments in a graph (Figure 183) like the one of the Figure 182 it is also obvious that the shelf sediments below 30 m water depth do not suffer transport for the lower energy wave quadrant (sector E) and even for the second higher energy wave quadrant (sector H), all the samples below 50 m water depth are immobile. Therefore, in a typical year, depending on the shelf sectors, below 30 meters water depth (e.g. sector E) or 50 meters water depth (e.g. sector H), the respective sector shelf sediments are immobile. One tends immediately to find a parallelism between the offshore limit of the lower shoreface in the more energetic sectors and the distinct change in the characteristics of sediments below 50 meters water (Figure 171 and Figure 183). It appears that the offshore limit of the lower shoreface for the second higher energetic shelf sector (sector H, d_i = -46.8 m) roughly coincides with the coarsening trend below 50 meters water depth. This evidence supports the hypothesis discussed in the section 6.2.2, that only during extreme storm events the shelf below 50 meters water depth is affected by the

transport of sediments. Otherwise, the sedimentary cover would be homogenized every year and the grain-size distribution would also be the same all over the shelf.

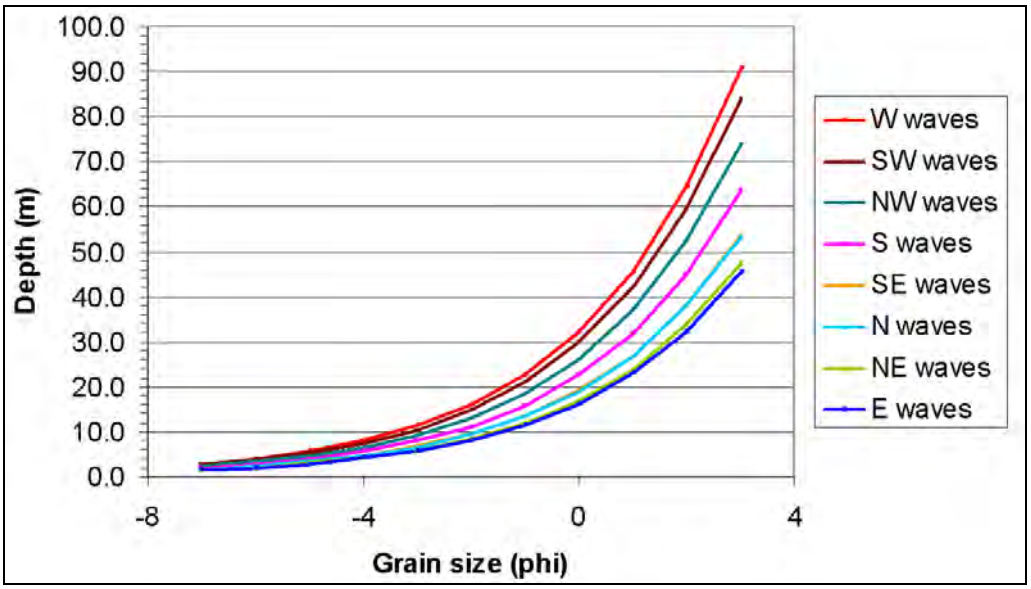

Figure 182 – Theoretical curves for all wave quadrants based on Equation 16 using the values of H_s and T_s for each quadrant expressed in Table 16 and increasing values of D_{50}.

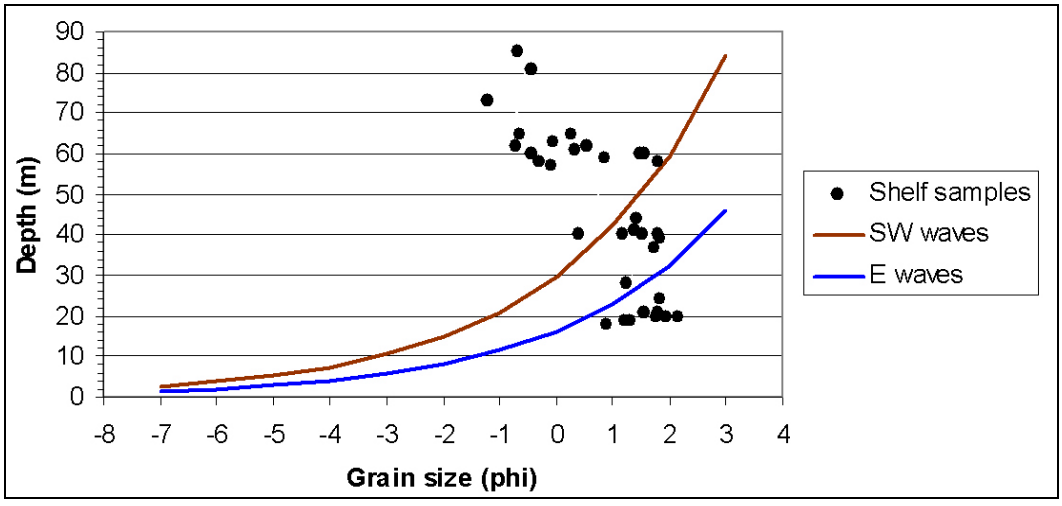

Figure 183 - Theoretical curves for the second higher and the lower energy wave quadrants (respectively SW and E) based on Equation 16 and the Faial shelf samples plotted.

From what as been discussed above, it seems that the shoreface in the Faial Island extends down to 50 meters water depth, which is, in some shelf sectors, almost the entire shelf area. Therefore, it does not make sense to individualize the shoreface from the rest of the shelf like it is shown in Figure 180.

6.3.3. Estimation of sediment entrainment depth during storm events

The offshore limit of the lower shoreface is not a guarantee of sediment immobility, since during extreme storms, sediment transport can occur well beyond this limit. It would be interesting to have a notion of how deep can storms (for instance the storm which wave height is exceeded only 12 hours in 14 years) affect sediment mobility. This wave height was chosen because the aim is to calculate the entrainment depth for low occurrence and high energetic storms. In order to get an accurate value for it, it was decided to use the approach of the grain settling velocity to predict the entrainment threshold of sediments on a plane bed by oscillatory waves. For that purpose it is necessary to calculate the critical wave orbital velocity (U_{wc}). The U_{wc} can be determined from the equations of Le Roux (Le Roux, 2001; Le Roux, 2005):

$$D_d = D_{50}\left(\rho g \rho_y / \mu^2\right)^{1/3} \tag{20}$$

$$W_{dv} = \left(0.0236 D_d - 0.37\right) \qquad \text{for } 2.9074 < D_d < 22.9866 \tag{21}$$

$$W_{dv} = \left(0.08255 D_d - 5.4\right)^{2/3} \qquad \text{for } 22.9866 < D_d < 134.9215 \tag{22}$$

$$U_{dwc} = 0.0246 W_{dv}^{-0.55} \tag{23}$$

$$U_{wc} = -0.01\left[\left(U_{dwc} g D_{50} \rho_y\right)^2 / \left(\rho\mu / T\right)\right] + 1.3416\left[\left(U_{dwc} g D_{50} \rho_y\right) / \left(\rho\mu / T\right)^{0.5}\right] - 0.6485$$

for U_{wc} < 50 cm/s (24)

$$U_{dwc} = 0.027 W_{dv}^{-0.6757} \qquad \text{for } U_{wc} \text{ up to 150 cm/s} \tag{25}$$

$$U_{wc} = -0.002\left[U_{dwc}^{2} g^{2} D_{50}{}^{2} \rho_y^2 T / \rho\mu\right] + 1.0702\left[U_{dwc} g D_{50} \rho_y \left(T / \rho\mu\right)^{0.5}\right] \quad (26)$$

Where ρ is the density of water (1.026 kg/m^3 is the value for 15 ºC and 35 ppt of salinity that will be used in the calculations); ρ_y is the submerged particle density, i.e. ρ_s-ρ, with ρ the water density and ρ_s as the particle density (3.2 is the density value for the mineral pyroxene, one of the major constituents of basaltic sands); μ is the fluid dynamic viscosity of the water (μ= $\rho\nu$, and ν is the kinematics' water viscosity with the value of 1.2 m^2/s × 10^{-6} for 15 ºC and 35 ppt of salinity, which will be used in the calculations); D_{50} is the median grain diameter in cm; T is the period in seconds and the value used in this calculation is taken from Table 15 (because it is in this table that are calculated the periods that are only exceeded 12 hours in 14 years).

When the critical wave orbital velocity (U_{wc}) is equal to the amplitude of the wave orbital velocity (U_w) just above the bed, then the particle is entrained and is able to suffer transport. According to the Linear Wave Theory the equation for the wave orbital velocity (U_w) of a monochromatic wave is:

$$U_w = \frac{\pi H}{T \sinh\left(k h_{ED}\right)} \quad (27)$$

Where H is the wave height, *sinh* is the hyperbolic sine, $k = 2\pi/L$ is the wave number, T is the wave period, L is the wavelength and h_{ED} the water entrainment depth. The H and T used in the calculations are the ones derived from Table 15.

Since it not easy to calculate k, Soulsby (1997) suggests an abacus (Figure 184) from which U_w can be calculated directly from the input parameters H, T, h_{ED} and g for a monochromatic sea (that will be used in this work) and the JONSWAP spectrum. After calculating U_{wc}, the procedure is the following; since h_{ED} is not known, first, T_n/T is calculated, giving increasing arbitrary values to h_{ED} in Equation 28:

$$T_n = \sqrt{\frac{h_{ED}}{g}} \quad (28)$$

Then, using the graph of the Figure 184, the value of $U_w \times T_n/2H$ (y-axis) for a monochromatic sea is taken after the value of T_n/T (x-axis); next assuming for instance that $U_w \times T_n/2H = 0.2$, U_w can be calculated with the following formulae:

$$U_w = 0.2 \times 2H/T_n \quad (29)$$

Or, generalizing:

$$U_w = Y \times 2H/T_n \quad (30)$$

This procedure is repeated giving increasing values to h_{ED} in Equation 28 until U_{wc} is found to be equal to U_w (Equation 30) and the final value of h_{ED} is found.

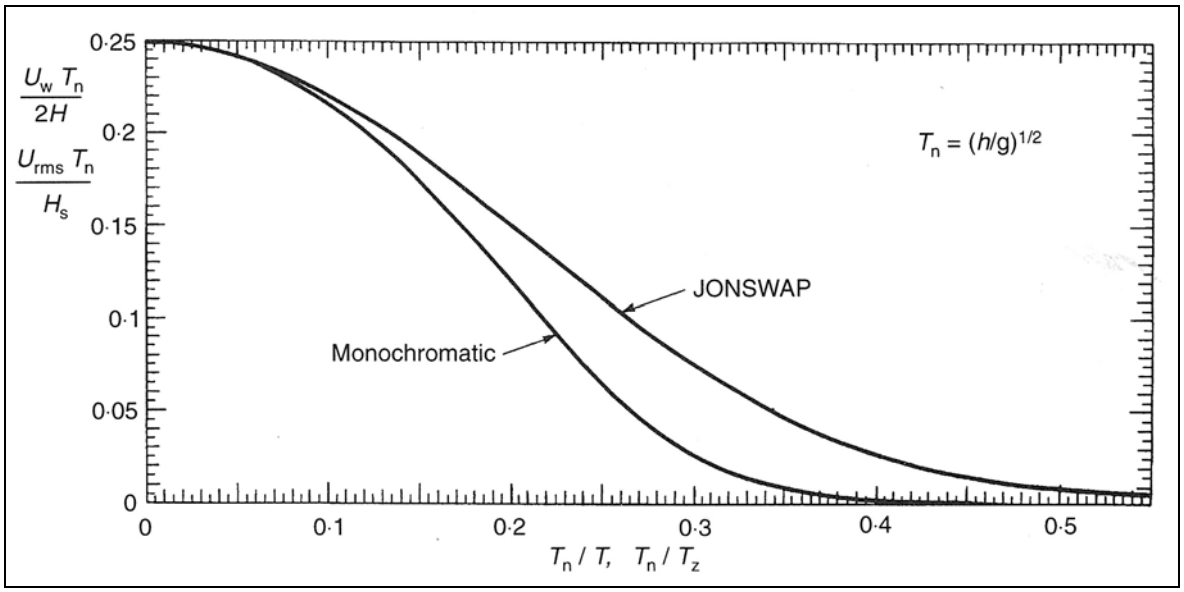

Figure 184 – Abacus for determining U_w for monochromatic waves (this case) using the input parameters $U_w T_n/2H$ and T_n/T (from Soulsby, 1997). U_w is determined with the following relationship $U_w = 2H/T_n \times Y$ with Y as the value taken from the curve in the vertical axis.

The grain-size of the sediments chosen, were derived from the natural variability found on the shelf. It was chosen the median diameter (D_{50}) of the finer, middle and coarser sediment to cover the complete size distribution of the set of samples.

The results from Table 18 show that the storms (coming from NW) which H_s

and T_s are only exceeded 12 hours every 14 years are able to entrain sediment between 84 to 164 meters water depth depending on the grain size. The D_{50} values used in the calculations of Table 18 correspond more or less to 2Φ to -1Φ, which are the grain-size distribution of the Faial shelf (see Figure 171 and Figure 183).

It would also be interesting to have a notion of how deep can yearly storms (for instance the storm which wave height is exceeded only 12 hours each year) affect sediment mobility. This would tell if normal storms are able to entrain sediments below 50 meters water depth or not. Therefore, the same calculation was made for storms which H_s and T_s are only exceeded 12 hours each year (Table 19 for storms coming from NW and Table 20 for storms coming from NE) and the results show that these are able to entrain sediment between 54 to 118 meters water depth for storms coming from NW and 65 to 32 meters water depth for storms coming from NE. These directions were chosen because they represent the higher (NW storms) and the lower (SE storms) energetic shelf sectors of the Faial Island. Table 20 shows that more than half of the Faial shelf samples below 50 meters water depth are not entrained. Being more precise, according to Table 20 the samples coarser than 1 mm (0 Φ) are only entrained above 57 meters water depth (see in Figure 171 that eight samples that are below 50 meters meet these criteria – coarser than 1 mm and below 57 meters). For yearly storms coming from NW, there are more shelf samples entrained below 50 meters water depth (Table 19), although not all of them are entrained (samples coarser than 2.34 mm are not entrained below 54 meters water depth). In conclusion, the Tables 19 and 20 show that there are shelf sediments that are entrained below 50 meters water depth and others that are not. However, that does not mean that the yearly stormy waves are able to generate currents strong enough to transport them at these depths. To test if these wave-induced currents would transport sediments below 50 meters water depth a more complex hydrodynamic model would be needed and that is out of the aims of this work. The author's suspicion is that yearly storms are not able to transport sediments below 50 meters water depth and the confirmation would give a broader support to what was discussed in the section 6.2.2 and 6.3.2, that only during extreme and low occurrence storm

events (in this case that occur only 12 hours every 14 years) all the sediments of the Faial shelf are entrained and transported all over the shelf.

Table 18 – Entrainment depth (h_{ED}) for NW storms occurring 12 hours every 14 years, for the selected grain sizes using the critical wave orbital velocity U_{wc} from Le Roux (2001; 2005) and the abacus of Soulsby (1997)

D_{50} (mm)	D_d	W_{dv}	U_{dwc}	T (s)	Hs (m)	U_{wc} (m/s)	T_n/T	$U_w T_n/2H$	h_{ED} (m)
0.25	5.98	1.21	0.02	17.50	12.04	0.38	0.25	0.066	164
1.00	23.94	5.91	0.01	17.50	12.04	0.44	0.24	0.074	154
2.34	56.01	11.86	0.01	17.50	12.04	1.20	0.18	0.145	84

Table 19 – Entrainment depth (h_{ED}) for NW storms occurring 12 hours every year, for the selected grain sizes using the critical wave orbital velocity U_{wc} from Le Roux (2001; 2005) and the abacus of Soulsby (1997).

D_{50} (mm)	D_d	W_{dv}	U_{dwc}	T (s)	Hs (m)	U_{wc} (m/s)	T_n/T	$U_w T_n/2H$	h_{ED} (m)
0.25	5.98	1.21	0.02	14.60	8.26	0.37	0.24	0.080	118
1.00	23.94	5.91	0.01	14.60	8.26	0.44	0.23	0.086	110
2.34	56.01	11.86	0.01	14.60	8.26	1.13	0.16	0.163	54

Table 20 – Entrainment depth (h_{ED}) for NE storms occurring 12 hours every year, for the selected grain sizes using the critical wave orbital velocity U_{wc} from Le Roux (2001; 2005) and the abacus of Soulsby (1997).

D_{50} (mm)	D_d	W_{dv}	U_{dwc}	T (s)	Hs (m)	U_{wc} (m/s)	T_n/T	$U_w T_n/2H$	h_{ED} (m)
0.25	5.98	1.21	0.02	10.90	5.55	0.36	0.24	0.079	65
1.00	23.94	5.91	0.01	10.90	5.55	0.43	0.22	0.096	57
2.34	56.01	11.86	0.01	10.90	5.55	0.98	0.17	0.156	32

6.4. Longshore sediment transport

When waves break in the surf zone they release momentum giving rise to a *radiation stress*. For waves incident obliquely on the shoreline there is a longshore component of the *radiation stress*, whose gradient produces a longshore current

within (and just outside) the surf zone which is balanced by friction within the bed (Soulsby, 1997). This in turn drives sediment along-shore as a littoral drift. The longshore sediment transport rate (Q_{LS}) measures the littoral drift across an area normal to the shoreline. Variations in Q_{LS} along the shoreline cause recession or advance of the shoreline in question. The CERC formula (Coastal Engineering Research Centre, 1984) is the most widely used method to calculate the total sediment transport Q_{LS} integrated across the width of the surf zone. However, it does not include dependencies on grain size, beach slope and wave period and, although it proves valuable for the transport of sediments by suspension, for grain sizes bigger than 0.5 mm it has a tendency for overestimation (Soulsby, 1997). Damgaard and Soulsby (1997) proposed a formula for bedload longshore sediment transport which has probably a better applicability for Faial shorefaces. The reason is that most of the samples taken on the shelf revealed sediments coarser than 0.5 mm, which means that the transport mechanism will be manly beadload instead of suspension. The resulting formula is:

Q_{LS} = maximum of Q_{LS1}, Q_{LS2a} and Q_{LS2b} (31)

$$Q_{LS1} = \frac{0.19\left(g \tan\beta\right)^{1/2}\left(\sin 2\alpha_b\right)^{3/2} H_b^{5/2}\left(1-\hat{\theta}_{cr}\right)}{12\left(s-1\right)} \quad \text{for } \hat{\theta}_{cr} < 1 \quad (32)$$

$$Q_{LS1} = 0 \quad \text{for } \hat{\theta}_{cr} \geq 1 \quad (33)$$

$$Q_{LS2a} = \frac{0.24\, f(\alpha_b) g^{3/8} D_{50}^{1/4} H_b^{19/8}}{12\left(s-1\right) T^{1/4}} \quad \text{for } \theta_{wr} \geq \theta_{wsf} \quad (34)$$

$$Q_{LS2b} = \frac{0.046\, f(\alpha_b) g^{2/5} H_b^{13/5}}{12\left(s-1\right)^{6/5} (\pi T)^{1/5}} \quad \text{for } \theta_{wr} < \theta_{wsf} \quad (35)$$

$$Q_{LS2} = 0 \quad \text{for } \theta_{\max} < \theta_{cr} \quad (36)$$

Where:

$$\hat{\theta}_{cr} = \frac{16.7\theta_{cr}\left(s-1\right)D_{50}}{H_b(\sin 2\alpha_b)(\tan\beta)} \quad (37)$$

$$f(\alpha_b) = (0.95 - 0.19\cos 2\alpha_b)(\sin 2\alpha_b) \quad (38)$$

$$\theta_{wr} = \frac{0.15H_b^{3/4}}{\left(s-1\right)g^{1/4}(TD_{50})^{1/2}} \quad (39)$$

$$\theta_{wsf} = \frac{0.004H_b^{6/5}}{\left(s-1\right)^{7/5}\, g^{1/5}T^{2/5}D_{50}} \quad (40)$$

θ_w = maximum of θ_{wr} and θ_{wsf} (41)

$$\theta_m = \frac{0.1H_b(\sin\alpha_b)(\tan\beta)}{\left(s-1\right)D_{50}} \quad (42)$$

$$\theta_{\max} = \left[\left(\theta_m + \theta_w \sin\alpha_b\right)^2 + \left(\theta_w \cos\alpha_b\right)^2\right]^{1/2} \quad (43)$$

$$\theta_{cr} = \frac{0.3}{1+1.2D_d} + 0.055\left[1-\exp(-0.02D_d)\right] \quad (44)$$

$$H_b = H_{sb}/\sqrt{2} \quad (45)$$

Where $tan\beta$ is the beach slope, α_b is the angle between wave crests and shoreline at breaker line, H_{sb} is the significant wave height at the breaker line, s is the ratio of densities of grain and water (1.026 kg/m^3 is the density value for water at 15 ºC and 35 ppt of salinity and 3.2 kg/m^3 is the density value for the mineral pyroxene), D_{50} is the median grain diameter (the value used is from the nearest sample of the upper shoreface), T is the average annual peak period (T_{pav}) which can be calculated by Equation 10 (see Chapter 2). From all the variables required for Equation 30 to Equation 45, the only unknowns until now are the $tan\beta$, α_b and

H_b.

The beach slope ($tan\beta$) was calculated using the definition of closure depth. The slope was calculated for the upper shoreface using as the inshore limit the coastline and the offshore limit the closure depth estimated in Table 15. Therefore, upper shoreface profiles were made for each shelf sector using the bathymetric data of Figure 56 in Chapter 3 to calculate the distance between the coastline and the closure depth. More complex to calculate are the values of α_b and H_b. For that purpose, the methodology suggested in the exercise II-1-1 from the U.S. Army Corp of Engineers (2003b) and exercise II-3-1 from the U.S. Army Corp of Engineers (2003a) was used. First, the deep-water wavelength (L_0) was calculated using Equation 19:

Then, the intermediate water wavelength (L) was calculated:

$$L = \frac{gT^2}{2\pi}\tanh\left(\frac{2\pi d_b}{L}\right) \tag{46}$$

With d_b being the water depth at breaker line. Since d_b is not yet known, the value of 2m will be used in the beginning of the calculations. The use of Equation 46, involves however some difficulty since the unknown L appears on both sides of the equation. Since d_b/L_0 is known, the following relationship (Equation 47) is used to estimate d_b/L by trial and error (for instance if d/L_0 = 0.5, random values of L will be given until the right hand-side of Equation 47 reach 0.5 or the nearest value with an approximation of 5 decimals and finally L is found).

$$\frac{d_b}{L_0} = \frac{d_b}{L}\tanh\left(\frac{2\pi d_b}{L}\right) \tag{47}$$

Once L and L_0 are calculated it is possible determine the shoaling coefficient K_s:

$$K_s = \left(\frac{C_{g0}}{C_g}\right)^{1/2} \tag{48}$$

$$C_{g0} = \frac{1}{2} C_0 \tag{49}$$

$$C_0 = 1.56T \tag{50}$$

$$C_g = \frac{1}{2}\left(1 + \frac{4\pi d_b / L}{\sinh(4\pi d_b / L)}\right)\frac{gT}{2\pi}\tanh\left(\frac{2\pi d_b}{L}\right) \tag{51}$$

Where C_{g0} is the deep-water wave group velocity, C_0 is the deep-water wave speed and C_g is the intermediate-water group velocity. Then the angle α_b can be determined by the following relationship (Equation 52):

$$\frac{\sin\alpha_b}{C} = \frac{\sin\alpha_0}{C_0} \tag{52}$$

$$C = \frac{L}{T} \tag{53}$$

Where C is the shallow-water wave speed and α_0 is the deep-water angle between wave crests and depth contours. Once sin α_b is known it is possible to calculate the refraction coefficient (K_r):

$$K_r = \left(\frac{1-\sin^2\alpha_0}{1-\sin^2\alpha_b}\right)^{\frac{1}{4}} \tag{54}$$

Finally, the significant wave breaker height (H_{sb}) can be determined with the following equation:

$$H_{Sb} = HK_sK_r \tag{55}$$

Where H is the mean annual significant deep-water wave height and was

estimated using Equation 9 from Chapter 2. Now, it is possible to estimate the breaker depth (d_b) with the Equation 56 taken from Dean and Dalrymple (1991) after Weggel (1972):

$$H_{Sb} = k' d_b \tag{56}$$

$$k' = b - a\frac{H_b}{gT^2} \tag{57}$$

$$a = 43.8 \times \left(1 - e^{-19\tan\beta}\right) \tag{58}$$

$$b = 1.56 \times \left(1 - e^{19.5\tan\beta}\right)^{-1} \tag{59}$$

The value of the breaker depth (d_b) calculated using Equation 56 is checked against the value initially estimated to be used in Equation 47 (2m). If different, the value just determined is substituted in Equation 45 and this procedure will be repeated until one gets a difference smaller than 0.009 between the d_b calculated with Equation 56 and the d_b from the previous run. The longshore sediment transport was calculated only for the sectors B (with an average coastal orientation of 40º) and H (with an average coastal orientation of 165º), since these have nearshore sediments able to suffer transport in the surf zone. They also have bathymetric contours relatively parallel to the shore, which would not introduce significant errors in the calculation of the refraction coefficient (K_r), the angle (α_b) between wave crests and shoreline at breaker line, the wave breaker height (H_{sb}) and the breaker depth (d_b). The complex bathymetry of the channel Faial-Pico and the sheltering effect of Pico Island would introduce significant errors in the calculation of the longshore drift in sector E and for that reason it was not estimated.

Table 21 shows the calculation of the wave breaker height (H_{sb}) and the breaker depth (d_b) for sector B and Table 23 the same calculation for sector H. Table 22 shows the calculation of the longshore sediment transport for sector B

where it was used the waves from W, N and NW and Table 24 shows the same calculation for sector H where it was used the waves from W, S and SW. The longshore sediment transport (Q_{LS}) that appears in Tables 22 and 24 was calculated assuming that all wave directions have the same frequency, which is not the case. Therefore the real longshore sediment transport (Q_{LSt}) was calculated considering the annual wave frequency of each wave direction (f_{ws} in Tables 22 and 24).

The net longshore drift for sector B is 1.478 km^3 per year in the NE direction. Although the NE waves apparently do not contribute to the longshore transport in the sector B (due to its costal orientation) if they suffer refraction, they could eventually invert the transport to the SW direction. The net longshore drift for sector H is 0.363 km^3 per year in the NW direction. The direction of the longshore transport in sector B and H should be taken into account when decisions regarding the dredging licensing will be decided. For instance, the SE part of sector H does not have beaches, but dredging too near the shore may put in risk the beach of Varadouro (in the NW part of this sector) since the net transport in this sector is in the NW direction.

Although in the other shelf sectors there could not be longshore transport due to lack of sand and gravels nearshore, during extreme storm events wave-induced currents might affect the sea-floor at depths where the bottom is covered by sand and gravels. In the Figure 185 the annual average wave regime and the respective affected coastal sectors are drawn. A brief analysis of the data permits to infer which would be the net transport directions based on the annual frequency and annual average heights of the set of waves that affect each costal sector. Figure 186 represents the longshore transport of sediment that occurs mostly during extreme storm events. The few exceptions are the shelf sectors B, E and H which transport can occur all over the year, because they have sand and gravels nearshore. The bold black lines represent the barriers to sediment transport across different shelf sectors. Therefore, for shelf sectors A1, A2, C+D, E, F+G the net longshore transport would be respectively, SE, E, SSE, S and E, because the higher and more frequent waves would probably transport sediments in these directions (Figures 185 and 186). During these extreme storm events there is also

Table 21 - Calculation of the wave breaker height (H_{sb}) and the breaker depth (d_b) for sector B

	L_0 (m)	d/L_0	d/L	$tan\beta$	T (s)	L (m)	C_{g0} (m/s)	C_g (m/s)	K_s	C_0 (m/s)	C (m/s)	$sin\ \alpha_0$	K_r	H_{sb} (m)	α_b (°)	a	b	yb	d_b (m)
W																			
	165.500	0.012	0.044	0.037	10.3	45.066	8.034	4.262	1.373	16.068	4.375	0.175	0.870	3.585	10.080	22.173	1.051	0.974	3.679
	165.500	0.022	0.061	0.037	10.3	60.459	8.034	5.598	1.198	16.068	5.870	0.235	0.866	3.113	13.581	22.173	1.051	0.984	3.162
	165.500	0.019	0.056	0.037	10.3	56.239	8.034	5.242	1.238	16.068	5.460	0.218	0.867	3.222	12.617	22.173	1.051	0.982	3.280
	165.500	0.020	0.057	0.037	10.3	57.240	8.034	5.327	1.228	16.068	5.557	0.222	0.867	3.195	12.845	22.173	1.051	0.983	3.251
	165.500	0.020	0.057	0.037	10.3	56.992	8.034	5.306	1.231	16.068	5.533	0.221	0.867	3.201	12.788	22.173	1.051	0.983	3.258
N																			
	129.184	0.015	0.050	0.037	9.1	39.672	7.098	4.217	1.297	14.196	4.360	0.235	0.785	2.036	13.606	22.173	1.051	0.995	2.046
	129.184	0.016	0.051	0.037	9.1	40.105	7.098	4.260	1.291	14.196	4.407	0.238	0.784	2.024	13.758	22.173	1.051	0.995	2.033
	129.184	0.016	0.051	0.037	9.1	39.988	7.098	4.249	1.293	14.196	4.394	0.237	0.784	2.027	13.717	22.173	1.051	0.995	2.037
	129.184	0.016	0.051	0.037	9.1	40.017	7.098	4.252	1.292	14.196	4.397	0.237	0.784	2.026	13.727	22.173	1.051	0.995	2.036
	129.184	0.016	0.051	0.037	9.1	40.010	7.098	4.251	1.292	14.196	4.397	0.237	0.784	2.027	13.724	22.173	1.051	0.995	2.036
NW																			
	159.136	0.013	0.045	0.037	10.1	44.165	7.878	4.256	1.361	15.756	4.373	0.024	0.998	3.395	1.386	22.173	1.051	0.976	3.480
	159.136	0.022	0.060	0.037	10.1	57.682	7.878	5.451	1.202	15.756	5.711	0.032	0.998	3.000	1.810	22.173	1.051	0.984	3.048
	159.136	0.019	0.056	0.037	10.1	54.138	7.878	5.145	1.237	15.756	5.360	0.030	0.998	3.088	1.699	22.173	1.051	0.982	3.143
	159.136	0.020	0.057	0.037	10.1	54.942	7.878	5.215	1.229	15.756	5.440	0.030	0.998	3.067	1.724	22.173	1.051	0.983	3.120
	159.136	0.020	0.057	0.037	10.1	54.756	7.878	5.199	1.231	15.756	5.421	0.030	0.998	3.072	1.719	22.173	1.051	0.983	3.126

Table 22 - Calculation of the longshore sediment transport for sector B

	d_{50} (mm)	D_d	s	θ_{cr}	H_b (m)	θ_m	θ_{wsf}	θ_{wr}	$\hat{\theta}_{cr}$	θ_{max}	$f(\alpha_b)$	Q_{LS1} (m^3/s)	Q_{LS2a} (m^3/s)	Q_{LS} (km^3/year)	f_{ws} (%)	Q_{LSt} (km^3/year)
W	0.500	12174.269	3.116	0.055	2.263	0.004	0.002	0.033	26.764	0.032	0.337	0.010	0.330	10.394	23.779	3.581
N	0.500	12174.269	3.116	0.055	1.433	0.002	0.001	0.023	39.618	0.022	0.360	0.003	0.122	3.855	16.101	0.899
NW	0.500	12174.269	3.116	0.055	2.172	0.000	0.002	0.032	200.984	0.032	0.046	0.000	0.041	1.281	29.139	0.541

Table 23 - Calculation of the wave breaker height (H_{sb}) and the breaker depth (d_b) for sector H

	L_0 (m)	d/L_0	d/L	$tan\beta$	T (s)	L (m)	C_{g0} (m/s)	C_g (m/s)	K_s	C_0 (m/s)	C (m/s)	$sin\ \alpha_0$	K_r	H_{sb} (m)	α_b (º)	a	b	yb	d_b (m)
W																			
	165.500	0.012	0.044	0.057	10.300	45.066	8.034	4.262	1.373	16.068	4.375	0.070	0.874	3.602	4.041	29.010	1.175	1.074	3.353
	165.500	0.020	0.058	0.057	10.300	57.844	8.034	5.378	1.222	16.068	5.616	0.090	0.874	3.205	5.190	29.010	1.175	1.085	2.953
	165.500	0.018	0.054	0.057	10.300	54.426	8.034	5.085	1.257	16.068	5.284	0.085	0.874	3.296	4.883	29.010	1.175	1.083	3.044
	165.500	0.018	0.055	0.057	10.300	55.223	8.034	5.155	1.248	16.068	5.361	0.086	0.874	3.274	4.954	29.010	1.175	1.083	3.022
	165.500	0.018	0.055	0.057	10.300	55.029	8.034	5.138	1.250	16.068	5.343	0.086	0.874	3.279	4.937	29.010	1.175	1.083	3.027
SW																			
	134.924	0.015	0.049	0.057	9.300	40.572	7.254	4.225	1.310	14.508	4.363	0.260	0.864	3.395	15.095	29.010	1.175	1.058	3.208
	134.924	0.024	0.063	0.057	9.300	50.892	7.254	5.201	1.181	14.508	5.472	0.327	0.856	3.033	19.066	29.010	1.175	1.071	2.833
	134.924	0.021	0.059	0.057	9.300	47.967	7.254	4.931	1.213	14.508	5.158	0.308	0.859	3.124	17.932	29.010	1.175	1.068	2.926
	134.924	0.022	0.060	0.057	9.300	48.715	7.254	5.001	1.204	14.508	5.238	0.313	0.858	3.100	18.221	29.010	1.175	1.069	2.901
	134.924	0.022	0.060	0.057	9.300	48.515	7.254	4.983	1.207	14.508	5.217	0.311	0.858	3.106	18.144	29.010	1.175	1.068	2.908
S																			
	110.074	0.018	0.055	0.057	8.400	36.513	6.552	4.181	1.252	13.104	4.347	0.320	0.857	2.682	18.688	29.010	1.175	1.062	2.525
	110.074	0.023	0.062	0.057	8.400	40.821	6.552	4.627	1.190	13.104	4.860	0.358	0.852	2.533	20.991	29.010	1.175	1.068	2.371
	110.074	0.022	0.060	0.057	8.400	39.616	6.552	4.504	1.206	13.104	4.716	0.348	0.853	2.573	20.343	29.010	1.175	1.067	2.412
	110.074	0.022	0.060	0.057	8.400	39.935	6.552	4.537	1.202	13.104	4.754	0.350	0.853	2.562	20.514	29.010	1.175	1.067	2.401
	110.074	0.022	0.060	0.057	8.400	39.850	6.552	4.528	1.203	13.104	4.744	0.350	0.853	2.565	20.469	29.010	1.175	1.067	2.404

Table 24 - Calculation of the longshore sediment transport for sector H

	d_{50} (mm)	D_d	s	θ_{cr}	H_b (m)	θ_m	θ_{wsf}	θ_{wr}	$\hat{\theta}_{cr}$	θ_{max}	$f(\alpha_b)$	Q_{LS1} (m^3/s)	Q_{LS2a} (m^3/s)	Q_{LS} (km^3/year)	f_{ws} (%)	Q_{LSt} (km^3/year)
W	0.403	9820.274	3.116	0.055	2.319	0.003	0.002	0.037	34.516	0.037	0.131	0.003	0.129	4.058	23.779	2.772
SW	0.403	9820.274	3.116	0.055	2.197	0.009	0.002	0.037	10.556	0.036	0.472	0.018	0.416	13.132	7.687	2.900
S	0.403	9820.274	3.116	0.055	1.814	0.009	0.002	0.034	11.547	0.032	0.528	0.013	0.302	9.529	3.344	0.915

the possibility of sediments crossing more than one shelf sector. The less likely passages would be (Figure 186):

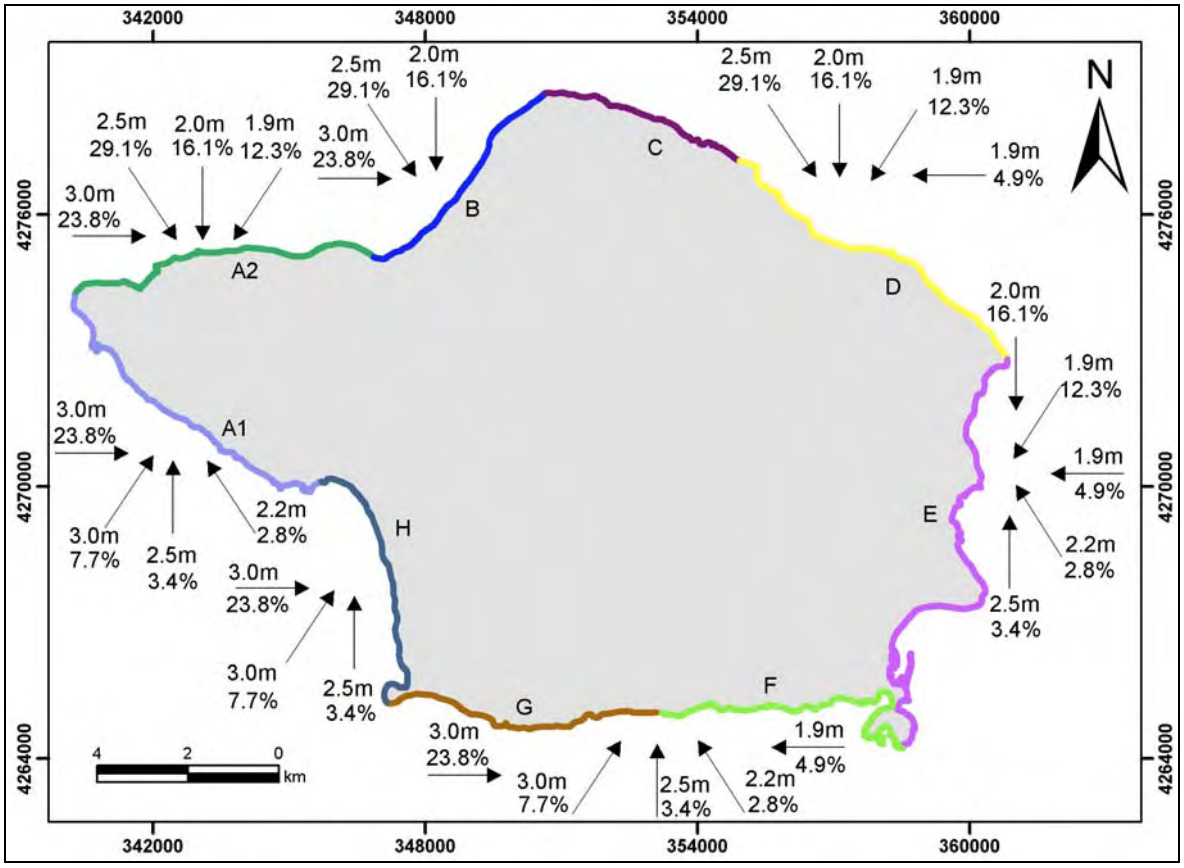

Figure 185 – Annual average wave regime showing wave frequency and wave height affecting the respective shelf sectors. The arrows represent the wave directions that affect each shelf sector.The bold colored lines around the coast of Faial and the black capital letters represent the different shelf sectors.

1. From H to G, because net transport of sediments is on opposite directions for each sector. In addition there are coarse clastic deposits in the intersection of these two sectors that represent bathymetric highs that would stop the sediment passage.
2. From B to C, because there are coarse clastic deposits at the intersection of these two sectors that represent bathymetric highs that would stop the sediment passage.
3. From F to E, because there is a bathymetric embayment in front of Monte da Guia that would act as a sink for sediments trying to cross (see Figure 56 in Chapter 3).

The likely passages (Figure 186) would be from A2 to B, from A1 to H, from C to D, From G to F and eventually from D to E, because there are no evident obstacles impeding the passage. The only one more dubious is the passage from D to E, because there are coarse clastic deposits nearshore up to 50 meters water depth that would prevent sediments crossing above this depth.

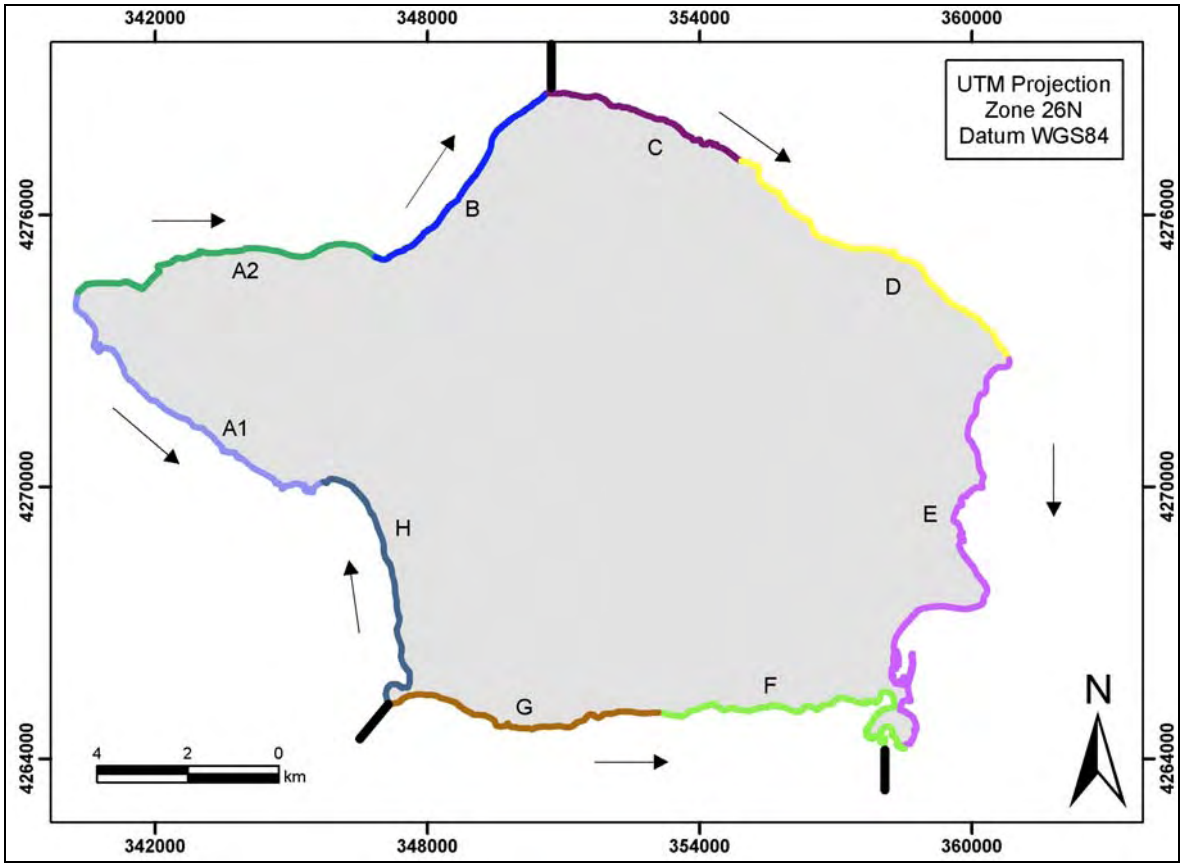

Figure 186 – Net longshore drift on the shelf sectors represented by the arrows. The bold black lines represent shelf features that are barriers to sediment transport. The bold colored lines around the coast of Faial and the black capital letters represent the different shelf sectors.

Chapter 7. Aggregates evaluation

7.1. Introduction

As already discussed in the previous chapters, the offshore deposits of sand and gravel in the Faial shelf appear to result essentially from marine erosion of the coastal cliffs and subaerial erosion of the hydrographic basins. These sediments are then transported from the nearshore areas by downwelling currents directed offshore, that are formed during storms. It is also possible that volcanism, in particular the explosive type, may have contributed in a considerable degree for the resulting deposits, either by syn-eruptive submarine volcaniclastic sedimentation or even by non-eruptive submarine remobilization of the volcaniclastic material. In this chapter, the spatial occurrence of the sand and gravel deposits is described and their quality is assessed for the use as aggregates. Finally, the volume of aggregates is estimated based on the technological and environmental limitations.

7.2. Sand and gravel deposits

The spatial distribution of the sand and gravel deposits of the Faial shelf was characterized in Chapter 3 (Figures 76 and 77) based on the interpretation of the Chirp and Boomer seismic profiles. Although the outer shelf of the Faial Island was not entirely mapped in some sectors, the seismic data often reached 80 meters water depth, which is adequate enough for the assessment of the potential of these sediments as aggregates (see section 7.4.3).

The nearshore areas are often covered with coarse clastic deposits (boulder size) and/or rocky outcrops of lava flows (respectively red and brown colors in Figure 77) to depths of 30 to 50 meters (e.g. shelf sectors C, D, F, G and

H). Further offshore, these shelf sectors are covered with sand and gravel deposits (yellow color in Figure 77). Sector A is almost free of sand and gravel deposits, being constituted mainly by coarse clastic deposits (boulder size) and/or rocky outcrops of lava flows. On the other hand, the sectors B and E have almost their entire area covered by sand and gravel deposits.

The interpretation of the Boomer seismic profiles permitted to map the thickness of the sand and gravel deposits (Figure 187). However, in some areas, due to the poor quality of the Boomer seismic profiles, it was not possible to determine their thickness, although the interpretation of the chirp seismic profiles revealed them to be sand and gravel deposits (light green color in Figure 187). The shelf sectors can be ranked into four decreasing groups in terms of their potential as aggregates. This division is based on the superficial area of the sand and gravel deposits, their thickness and the degree of certainty of the interpretation of the Boomer seismic profiles:

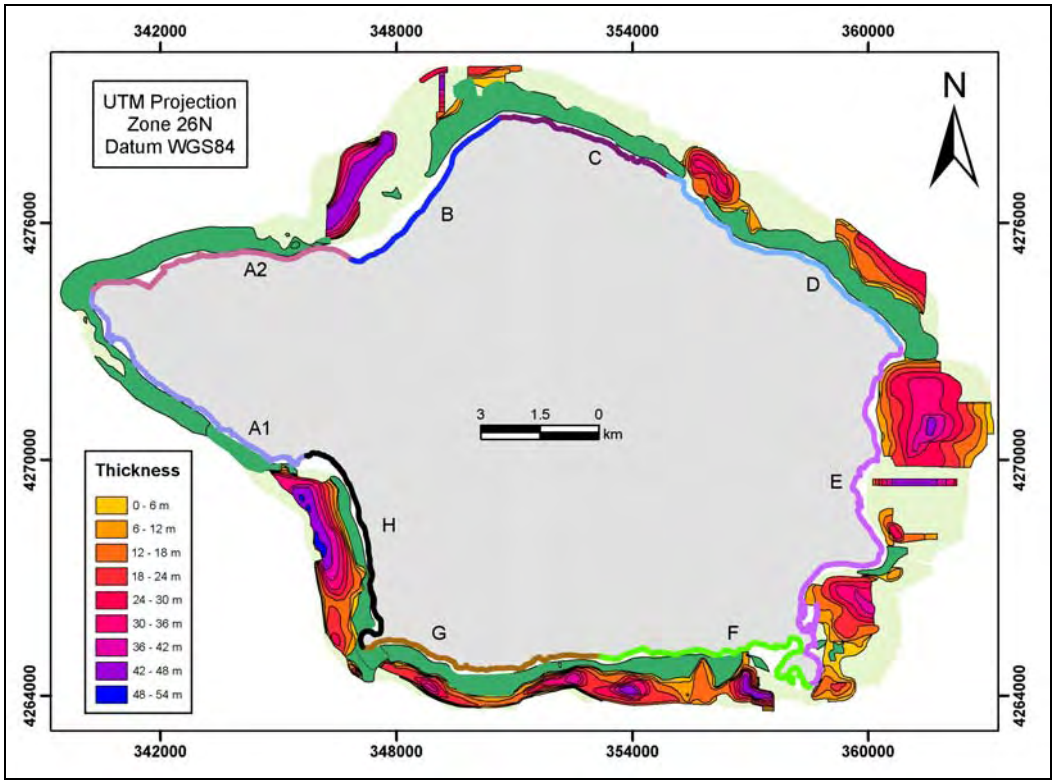

Figure 187 - Sedimentary thickness map produced in ArcGis based on the interpretation of the Boomer seismic profiles (see Chapter 3). Green areas correspond to rocky outcrops/coarse clastic deposits interpreted with the chirp and Boomer seismic profiles. Light green areas correspond to sedimentary areas interpreted with the chirp and Boomer seismic profiles where no information exists about thickness of the deposits due to the poor quality of Boomer seismic profiles.

1. The shelf sectors that have the highest thicknesses and the widest areas of these deposits are sectors B, E and H. From these three sectors, sector H is the most promising because its level of geological assurance is the highest, although it presents the smaller area of sand and gravel deposits. Its shelf area is almost completely characterized in terms of sedimentary thickness. The nearshore areas are formed by coarse clastic deposits (boulder size) and/or rocky outcrops of lava flows up to 20-30 meters water depth on average. Further offshore the sedimentary bodies dominate and can reach a total thickness up to 50 meters. Sector E looks very promising because it has a large area covered by these deposits and they are considerably thick (up to 45 meters). The drawback is that it has a great area of the shelf with uncharacterized deposits in terms of thickness. Less promising than sector E in terms of area, but also with a high thickness of sediments (deposits up to 45 meters thick), is the sector B. However, it is the worst characterized sector of the three, with unknown thickness of the deposits in most of its area.
2. Sector F and G have very small areas of sand and gravel deposits when compared against the sectors B and E. Despite that fact, they show a rather high level of geological assurance because the thickness of their deposits is almost completely mapped. The nearshore areas are formed by coarse clastic deposits (boulder size) and/or rocky outcrops of lava flows up to 30-40 meters water depth on average. Further offshore the sedimentary bodies dominate and can reach up to 40 and 35 meters respectively on sectors F and G.
3. Sectors C and D show less promising results in terms of the sedimentary thickness of their deposits (deposits only up to 30 meters thick). The same happens with their geological assurance, because these sectors have the highest areas of undetermined deposits thickness. They also show a wider belt of coarse clastic deposits (boulder size) and/or rocky outcrops of lava flows that extend up to 40 to 60 meters water depth.
4. Sector A is not promising at all, with only small patches of sand and gravel deposits, in the southwest part of sector A1 and the northeast part of sector A2. Furthermore, these areas are not characterized in terms of sedimentary

thickness which assigns them the lowest degree of geological assurance. To this contributes also the youth of these shelf sectors (less than 10 Ka) which makes very unlikely the existence of thick deposits.

7.3. Aggregates quality and potential applications

The large literature on the classification of mineral resources is a testimony of the complexity of the subject. Nevertheless, the establishment of limiting physical criteria, which are themselves largely conditioned by economic constraints, is necessary before estimation and comparison of the quality and amount of potentially useful prospects can proceed (Geological Society, 2001).

There are however, certain fundamental physical characteristics of aggregates which are relevant to all uses and which are an important part of any aggregate description. These are nominal particle size, particle shape, particle surface texture, color, cleanliness (presence of dust, silt or clay) and presence of surface coatings, encrustations or obviously extraneous material (Geological Society, 2001). In this work, particle size was determined using a laser diffractometer for sands and series of sieves for material coarser than 2 mm. In addition, the samples were submitted to a brief qualitative characterization using macroscopic analysis that looked into color, cleanliness, and the presence of surface coatings and encrustations.

Aggregates can be used for several purposes, to make concrete and mortar, to use in unbound pavement construction, in bituminous bound construction materials and for railway tracks. Concrete may be defined as a mixture of water, cement or binder, and aggregate (a higher percentage of cobbles and pebbles than sand), where the water and cement or binder form the paste and the aggregate forms the inert filler. The term 'mortar' is used in the building industry to denote a mixture of natural sand or other fine aggregate and some binding agent, used as a jointing or a surface plastering and rendering material. Mortars are commonly used for the bedding and jointing of building units such as bricks and blocks (masonry) and also for surface finishes (rendering, plastering

and screeding). In highway and airfield pavements, aggregates (normally pebble to boulder size) are used in various types of unbound or bound materials. Unbound layers are used in the UK mainly for sub-bases or capping, but elsewhere may be used for bases or, in the case of low volume roads, the whole structure. Bituminous mixtures that use both natural and artificial aggregates of coarse and fine sizes are also employed in pavement construction. Railway track formations generally consist essentially of a layer of coarse aggregate, or ballast, in which the sleepers are embedded. The ballast may rest directly on the subgrade or, depending on the bearing capacity, on a layer of blanketing sand (Geological Society, 2001).

From all the applications of aggregates reviewed, only the grading of aggregates required for mortar production fall exactly in the grain-size distribution of the analyzed samples from the Faial shelf. In mortars, sand is the major constituent whilst for the other purposes, pebble to boulders predominate. According to the British Standard 1200 (Geological Society, 2001) the possible occurrence of 'harmful materials such as iron pyrites, salts, coal or other organic impurities, mica, shale and similar laminated materials, and flaky or elongated particles' should be taken into account when produzing mortar. Although cohesiveness is improved by the presence of increased fine material including cement, lime and air-entraining additives, the presence of some silt and clay has the effect of making the mix more workable and also provides the 'fattiness' so typically required by the artisan. However, too much silt and clay can reduce the consistency and thus the workability.

Sediments sampled in the shelf of Faial are normally clean, medium to coarse sands with little percentage or free from silt and clayey material. They are normally constituted by minerals that result from the disintegration of volcanic rocks. According to Cruz (2006) the minerals more common in the volcanic rocks of the Grupo inferior do Complexo Vulcânico dos Cedros, Grupo superior do Complexo Vulcânico dos Cedros and Capelo Volcanic Complex are pyroxene, olivine, amphiboles, plagioclase and alkaline feldspar. These volcanic complexes constitute the majority of the island rocks (in Figure 43 of Chapter 2 the first two correspond respectively to Cedros Volcanic Complex and Caldeira Formation) and

a brief macroscopic analysis of the shelf samples showed a high percentage of dark minerals, without pitting, surface coatings and encrustations. These minerals were not identified in this work, but based on the work of Cruz (2006), they are most likely pyroxene, amphibole and olivine. The samples also showed a variable percentage of carbonate skeletal particles that varied from 0 to 22%. Therefore, it looks like that the shelf deposits of sand and gravels are adequate for mortar use. They can also be used in the production of concrete, unbound and bound pavement construction, because these products require a small amount of sand and gravels in their constitution.

7.4. Assessment of sand and gravel resources

A mineral resource is a concentration of naturally occurring ores and other mineral deposits in such form that economic extraction is currently or potentially feasible. The definition includes those which are potentially economically and technically feasible, and those which are not. This classification was first presented in a diagrammatic way by McKelvey (1972) on what it is colloquially known as 'the McKelvey diagram' (Figure 188). It shows how total resources can be categorized in terms of economic feasibility of extraction (economic constraints) and the degree of geological assurance (the level of available knowledge of the physical characteristics). Therefore, material classified as a *reserve* must be economically and technically feasible to extract. Subsequently, the definition of reserve is unboundedly linked to the extraction techniques available at the present time. Although the definition of reserve is not linked to environmental concerns, today, at least in the develop countries, licenses to exploit mineral resources require an Environmental Impact Statement. The purpose of the assessment is to ensure that decision-makers consider environmental impacts before deciding whether to proceed with the exploitation or not.

In conclusion, one must consider not only the definition of reserve when it comes to assess the volume of aggregates available in the Faial shelf but also the environmental restrictions in the delimiting of the exploitation areas:

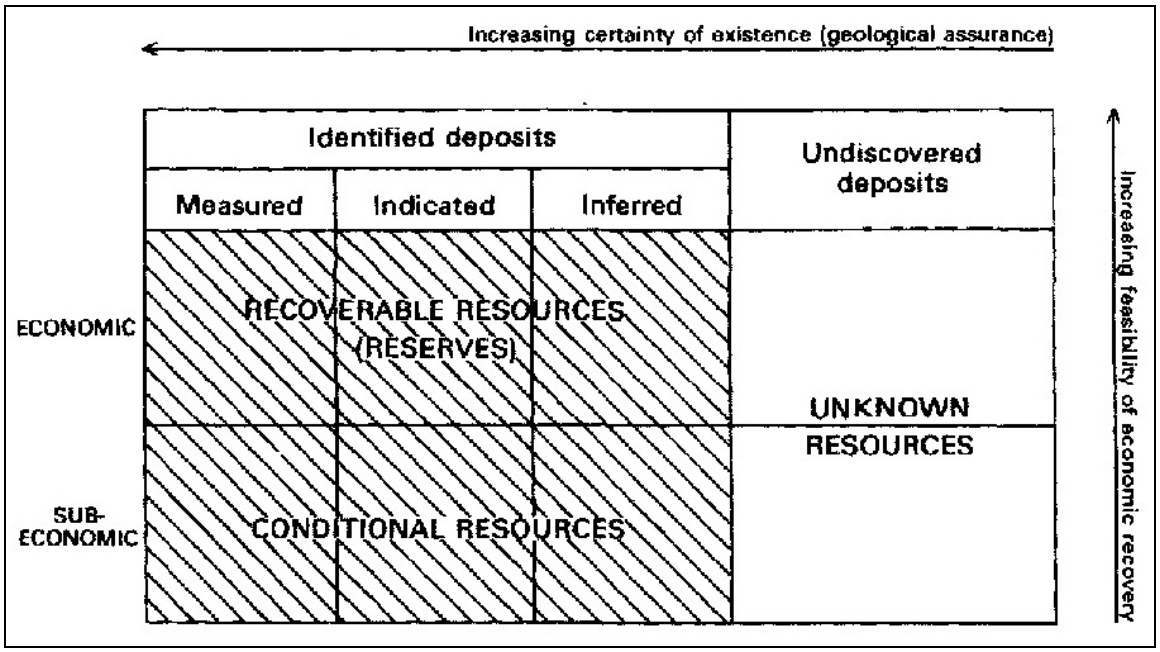

Figure 188 – Classification of mineral resources after Mckelvey (1972).

7.4.1. Technological dredging limitations

Although in Europe there are a variety of marine aggregate extraction dredgers in use, on the continental shelf two kinds of dredgers are the most used for the sand and gravel extraction: anchor dredging and trail dredging (Bellec, 2004; Geological Society, 2001). Anchor dredging, as the name implies, requires the dredging vessel to remain stationary whilst operating. A hole or pit is created in the seabed deposit and production continues while unconsolidated materials fall into the excavation towards the suction head. The main advantage of the method is its suitability to working in the deeper deposits. Its principal disadvantage is the poor accuracy of location, the low efficiency of recovery and the pits that the method tends to leave in the seabed deposit. Trail dredging, is performed while the vessel is underway and excavates the deposit by dragging the dredge head across the surface of the seabed. Unlike anchor dredging the method cuts smooth trenches in the seabed deposit and can be more easily controlled to recover only the payable deposit without penetrating the sub-strata. The more recent technologies permit dredging in much deeper waters with the latest vessels extracting up to 50 m water depth (Bellec, 2004; Geological Society, 2001).

7.4.2. Environmental dredging limitations

The pits and trenches left after dredging are not immutable in time. They tend to infill at a rate that is dictated by the dredged volume, the depth at which the extraction was made (distance to shore) and by the hydrodynamic conditions (mean and wave induced currents) prevailing at those sites. Under certain conditions, the infill process and modifications of the nearshore wave conditions around the dredging sites might have a negative impact in the coastal sediment budget, promoting erosion at the shore. The appropriate sites of extraction should be a compromise between fast regenerating times (which are achieved in shoreface extractions) and minimized impacts on the coastal sediment budget (Kelley et al., 2004). However, other issues should be contemplated in a detailed environmental study of offshore deposits dredging impacts, such as the fauna, flora and water quality; disturbance of cultural heritage sites (e.g., shipwrecks of archaeological interest), etc.

To assess the physical impacts of sand mining on the shoreface and shoreline a detailed knowledge of the hydrodynamic (tide -, wind- and wave-driven flows and wave propagation) and sediment transport processes is required. Mathematical models constitute nowadays a powerful tool to describe the evolution of the seabed as a resultant of interactions between water motion, sediment transport and bed levels changes. An overview of morphodynamic models, namely, coastline models, coastal profile models, coastal area models and local models can be found in de Vriend et al. (1993). Morphodynamic coastal area models (two -dimensional horizontal and three-dimensional) have received in the last two decades an increasing interest. However, major problems are still open: relatively simple equilibrium sand transport formulas are used and the uncertainties associated with the evaluation of sediment fluxes are large; simplifications are required to address the large computational costs required to perform long-term simulations and the choice of representative wave conditions.

In this study, a very simple method was used (see section 6.3.1 in Chapter 6), for the sake of simplicity, to predict the lower limit of the upper shoreface (Hallermeier, 1981) and therefore establish a buffer zone from which no dredging

should occur without putting at risk the shoreline. The disadvantages of sand mining if the extraction sites are located too close to the shore (e.g., in the upper shoreface) are well established and related to negative impacts on the coastal sediment budget enhancing coastal erosion (Kelley et al., 2004).

The analysis of Table 15 in Chapter 6 showed that the lower limit of the upper shoreface is between 10 and 26 m, depending on the direction of the wave propagation. According to Hallermeier (1981) this method only considers the cross-shore redistribution of sediment, which means that the calculated depths are exclusive of the respective wave direction. However, all the sectors in study are affected at least by three to four different wave directions (Figure 189). For instance, the coastal sectors F and G are directly affected by southern waves and have a closure depth of 11 m. However, they are also affected by south-western waves (that produces a 20 m closure depth for costal sectors perpendicular to them) that would certainly produce a higher closure depth if a more advanced transport model was used in the calculations. The same situation happens for all the sectors, which means that each one probably has a higher closure depth than the calculated only with the waves that are perpendicular to them. Therefore, for safety reasons, it was decided to define the limiting shoreward depth of dredging as the one given by the highest closure depth found for the wave directions that affect the coastal segments (e.g. for sector F is 20 m - Figure 189). Subsequently, the 25 m water depth buffer zone was considered for the sectors A, B, C, D and H and the 20 m water depth for the sectors F and G. Establishing a buffer zone for sector E is more complicated since it lies in the western boundary of the Channel Faial-Pico and therefore exhibits a complex bathymetry and suffers the sheltering effect of the neighboring Pico Island. Nevertheless, using the higher value (closure depth of 14m for the NE waves) as a buffer zone would not probably again be very far from the reality.

Although these buffer zones can be regarded as overprotective, they can be easily understood, since the Faial Island suffers from coastal erosion. A detailed survey around the coasts of Faial in the winter of 2003 (Quartau et al., 2005) and the summer of 2004 revealed very few beaches in Faial Island. Most of them are small pocket gravel beaches in the winter with some turning sandy

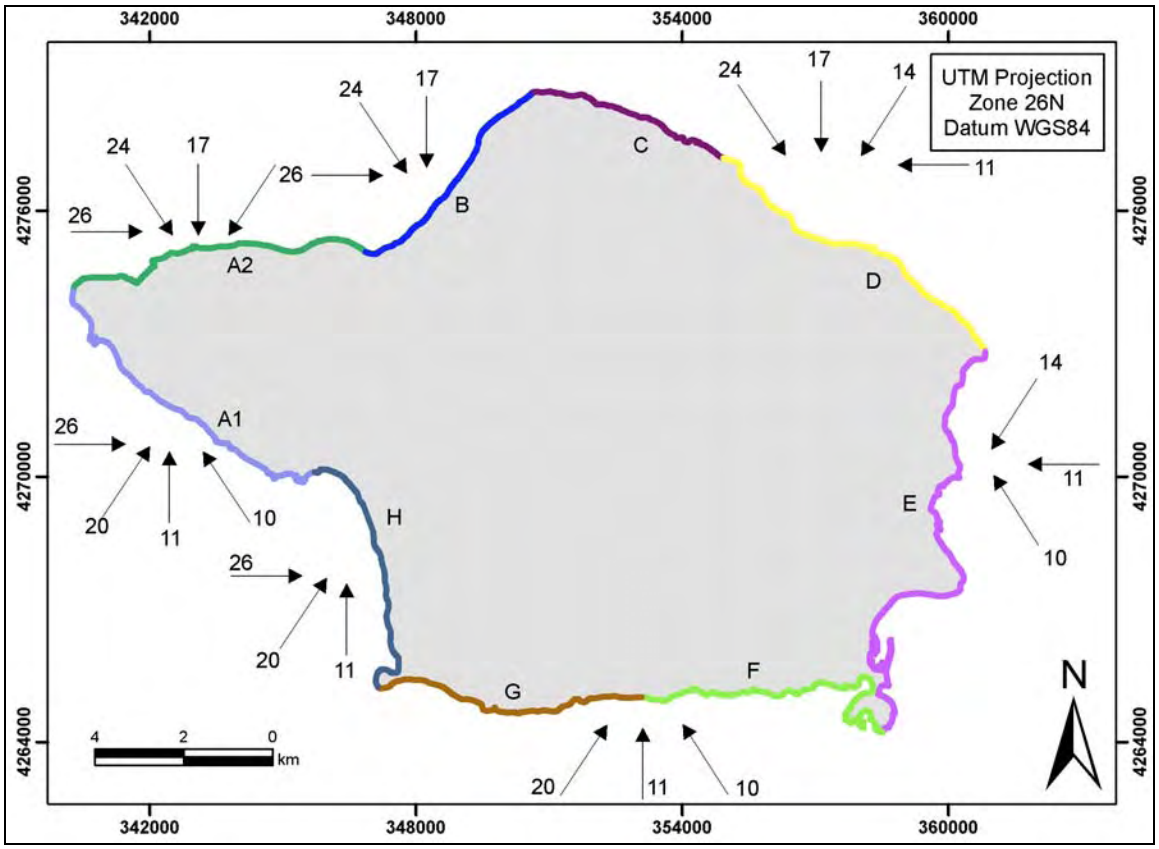

Figure 189 – Wave directions (represented by the arrows) to which each coastal segment is subjected. The bold colored lines and respective letters represent the defined coastal sectors. The numbers next to the arrows represent the closure depth in meters of each coastal segment perpendicular to the respective wave direction.

beaches during the summer. According to local people, sandy beaches are disappearing, turning to permanent gravel beaches even in the summer. Causes for this problem can be attributed to ancient beach backshore extraction of sediments and probably submarine dredging occurring too close to the shore. Extraction pits in Riberinha bay (sector E) have been revealed by a interferometric swath survey that showed scars at 10m depth with 3 meters depression reaching below the surrounding sediment surface (Lafon et al., 2005). These are worrying signs that suggest that the volumes of sand in the upper shoreface required to fill the beaches during summer times are decreasing. The most obvious effect of this will be coastal erosion since beaches act as a protective buffer zone to cliff erosion. Furthermore, the disappearing of these sandy beaches might also have impact on the tourism in the Azores, which has been increasing in the recent years.

7.4.3. Estimation of sand and gravel reserves in the Faial shelf

As already discussed in section 7.2 the more promising shelf sectors in terms of aggregates spatial occurence and geological assurance are in decreasing order, the shelf sectors H, B, E, G, F, C, D and A. Furthermore, the calculation of the sediment volumes was already done for sectors F, G and H in Chapter 6 because the thickness of the sediments in these sectors is almost totally mapped in their extension. It is nevertheless wishful thinking to assume that the total volume of sediments in the Faial shelf would be considered as reserves. A

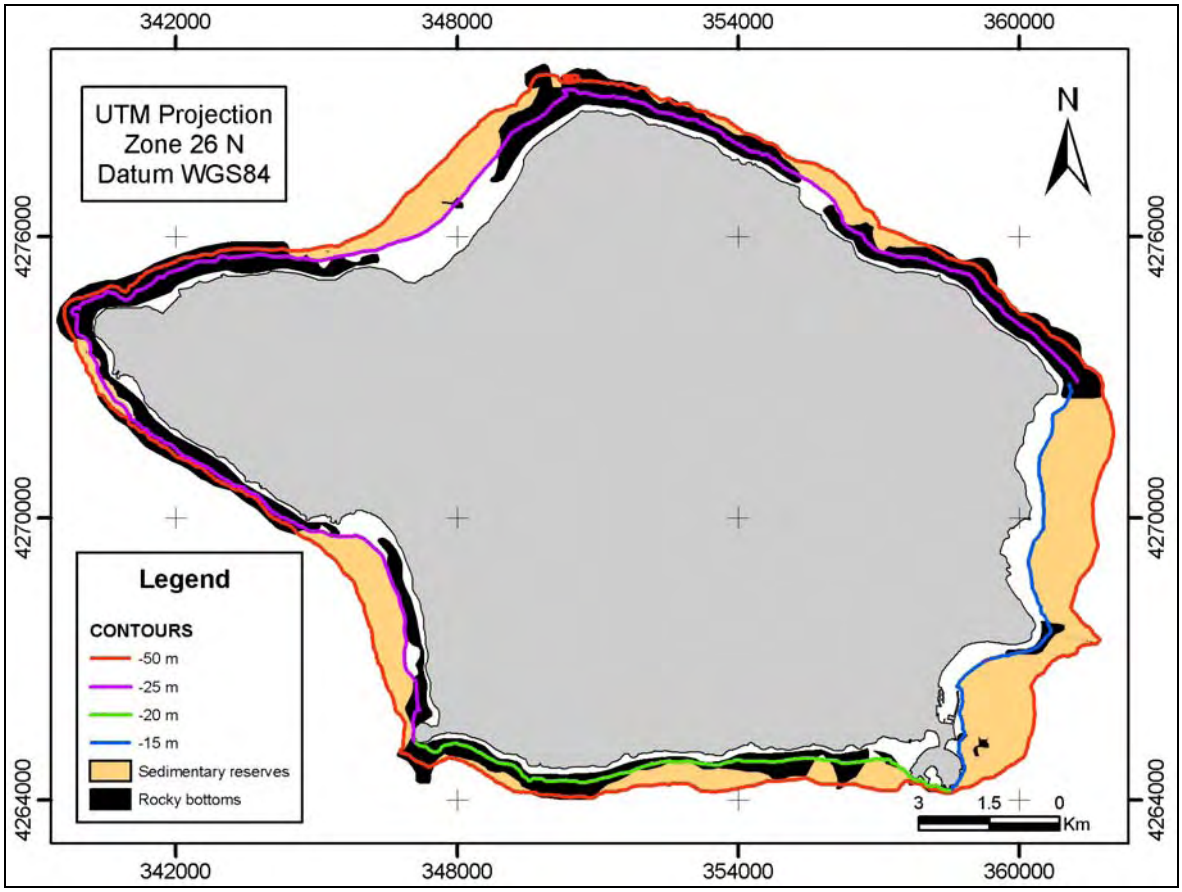

Figure 190 – Buffer zones used in the reserves calculations. Contours show the offshore and shoreward limitations of the areas used for the calculations.

significant part of it may not be dredged because it is either too near the shore (environmental limitations) or too deep in the shelf (technological limitations). In addition, only the superficial part of the deposits would be dredged even if the

anchor dredging method were used which allows deeper penetration into the deposits. Therefore, the sedimentary bottom areas that lie between 25 m and 50 m water depth for sectors A1, A2, B, C, D and H, between 20 m and 50 m water depth for sectors G and H and between 15 m and 50 m water depth for sector E were delimited (Figure 189) to calculate reserve volumes. Although for a significant part of these areas no information exists about the thickness of the deposits, it is very frequent to find at these depths more than 5 meters thickness in the adjacent deposits. The total area of the selected deposits (Figure 190) is 19.2 millions m^2. Assuming that all this area would be dredged at depth of 2 m below the surface a reserve value of 38.4 millions m^3 would be found. Using a dredged depth of 5 m below the surface, a reserve value of 96 millions m^3 could be considered.

Chapter 8. Conclusions and future work

8.1. Main conclusions

8.1.1. Geological characterization of the shelf and its evolution

The geological map of the Faial shelf produced in this work (Figure 77 in Chapter 3) resulted from the interpretation of the available data that included single-beam echo sounder data and high-resolution seismic profiles (Chirp and Boomer). The integrated interpretation of these data showed a shelf normally composed by coarse clastic deposits and lava flows between the shore and 30-50 meters water depth (e.g. shelf sectors C, D, F, G and H). The coarse clastic deposits normally result from the erosion of lava flows. The lava flows in some cases are still well preserved and can be discriminated from the coarse clastic deposits in the chirp records. Nearshore, these coarse clastic deposits may also be the result of the erosion of cliffs mainly composed of non-friable volcanics. Further offshore the sand and gravely deposits dominate and can be mapped till the shelf break. In shelf sectors less volcanically active or with a high degree of subaerial erosion like sectors B, E and western H, these finer deposits are present all over the shelf. Very young shelf sectors (less than 10 Ka), like A1 and A2, show almost no fine sediments and are mainly composed of lava flows and the coarse clastic deposits that result from their erosion.

There were also found evidences of submarine emplacement of lava domes (offshore Morro do Castelo – Figures 65 and 72) and surtseyan cones (offshore Monte da Guia - Figures 64 and 72 and offshore Ponta da Espalamaca – Figures 77 and 100).

The sedimentary bodies composed of sand and gravel deposits have a sigmoidal shape perpendicular to the shore and trend parallel to it (see Figures 73

and 76 in Chapter 3). The highest thicknesses are found at intermediate depths (-40 to -60 m – see Figure 76 in Chapter 3), decreasing towards nearshore and offshore.

8.1.1.1. Shelf width

The trend proposed by Menard (1983) that the shelf width increases with the age of the adjacent coastal sectors was generally confirmed. Therefore, the assumption behind this trend, i.e. that the main mechanism responsible for the origin and development of volcanic islands is abrasional was also validated for the Faial Island. The average rate of widening (0.6 - 1.7 mm/year) for several oceanic volcanic islands compiled by Menard (1983) is smaller than the one measured in the older shelf sectors of the Faial Island (1.9 - 5.3 mm/year). Reasons for this small difference may be accounted for by the time span of the analysis. Faial is a relatively young island (started forming 800 Ka) when compared with the islands that Menard used in his study (most had more than 1 Ma, up to 16 Ma). The shelves in older islands tend to increase slower because as the shelf widens, wave attenuation over it is bigger and that results in less energy reaching the coastline. The differences between short and long term rates also suggested that the age of the shelf sectors has in fact a great influence. Shelf sectors of the young emerged terrain (Capelo Peninsula – 10 Ka) showed higher erosion rates, between 15 and 80 mm/year, probably associated to highstand conditions.

The hypothesis that a major part of the shelf widening occurs during highstand conditions was tested and showed erosion rates between 20 and 52 mm/year. These erosion rates are compatible with the work of Borges (2003) in S. Miguel Island and with the rates found for the sectors A1 and A2 (10 -100 mm/year). Furthermore, if these higher rates (for instance 52 mm/year) were eroding the shelf during the entire cycle of sea-level oscillation, the Faial Island (14 to 21 km wide) would have been completely wiped out within 200 to 300 Ka. Only a very high effusion rate could explain the permanence of the Faial Island above sea-level.

The shelf width has also shown a fairly linear relationship with wave effectiveness (frequency and height) for coastal sectors of the same age (e.g.

between sectors B, C, F and H and between A1 and A2). The absence of a perfect relationship is probably caused by distinct original slopes, volcanic compositions and effusion rates.

8.1.1.2. Shelf break depth and subsidence rates

The depositional shelf break has been found at depths between -65 and -80 m for the shelf sectors adjacent to the Cedros Volcanic Complex. Although the erosional shelf break has only been mapped in the sectors G and H, it showed depths between -90 and -96 m which are compatible with the analysis of the 470 Ka record of sea-level variation (compilation of the curves of Thompson and Goldstein (2006) and Bitanja et al., (2005)). The analysis of that record showed that the sea-level has been a considerable amount of time (16%) at -80 to -90 meters water depth, contributing to the development of a wave-cut surface at these depths. Further east (in the transition for sector F) the erosional shelf break is found at higher depths (between -100 to -115 m). However, the shelf in sector F was most likely formed at the same time as sector D and the subsidence in sector D might explain the higher shelf break depth in the transition from sectors F to G. Therefore, the transition zone between one shelf sector that has suffered subsidence (G) and other that has not (F) is probably smoothed by erosion and for that reason it shows a slow deepening towards the east.

The shelf break at sector D is found at 200 m and a subsidence rate of 0.3 mm/year was calculated based on the age of this sector. Probable causes for this high subsidence rate may be accounted for by tectonic movements related to the transtensional regime of the Faial Fracture Zone, recorded in the graben structures of Pedro Miguel Region. Subsidence might also result from crustal loading of more recent volcanic material erupted from the Caldeira volcano(Cedros Volcanic Complex and Caldeira Formation).

The average shelf break in sectors A1 and A2 is found respectively at 20 and 25 meters water depth. However, the analysis of the sea level record from Thompson and Goldstein (2006) showed that the sea-level was at -38 m around 10 Ka. This means that probably the volcanism in the offshore areas did not occur in a single event. Both shelves might have had lavas prograding offshore until the

sea-level was at the respective present-day shelf break depths which made the start of the abrasion platform later.

An evolutionary model of the Faial shelf is proposed in this work based on the abrasional hypothesis for the origin of the shelf and also in the relations between the shelf width and age of the respective shelf sectors.

8.1.2. Present-day processes occurring in the coast and shelf of Faial Island

8.1.2.1. Coastal erosional processes

The coastline of the Faial Island is mainly composed of rocky cliffs with a sharp angle in the lower parts and accumulation of rock debris at their base. The few existent beaches are small pocket beaches and are mostly pebble and cobble beaches, especially during winter. The cliffs show signs of being retreating mostly by mass-wasting processes related essentially to marine erosion. Earthquakes seem to play also a role in coastal retreating.

8.1.2.2. Shelf sedimentary model

The geometry of the sand and gravel deposits suggests (Figure 130B in Chapter 4) that these were formed during the present highstand condition and therefore they can be classified as a Highstand System Tract according to sequence stratigraphy models. The formation of these bodies was associated to the existence of storm-generated currents that transported sediments seaward. The lack of preservation of the previous system tracts in the shelf of Faial has also been discussed and several factors have been used to justify the failed preservation: narrow and high slope shelf that provides little space for accommodation of sediments, wave- to storm-dominated shelf that easily transports sediments offshore during sea level fall and rise, low subaerial erosion and sea-level fall below the shelf break during Lowstands.

Bedforms with mound-like morphology (see Figures 59 and 77) were found in the sectors C, D and H. These are normally parallel to the coastline and are

found at intermediate water depths between the coarse clastic deposits and the sandy and gravely sediments. The interpretation of the chirp echo characters, suggests that they are composed of finer sediments than those from the surrounding sea floor, probably fine sands. Possible causes for the generation of this bedforms may be related to seaward bottom currents that transport finer sediments at the base of the coarse clastic deposits.

A large sand-wave field was found in sector E (Figures 70, 71 and 99 in Chapter 3). The sand-wave crests have the same direction as the graben structures of Pedro Miguel Region, trending WNW-ESE. It is possible that the graben faults extended offshore and their movements originated a stepping se-floor favoring the emplacement of the sand waves. Offshore Ponta da Espalamaca the chirp echo interpretation revealed submarine cones that confirm the WNW-ESE lineament seen on the hydrographic map (see section 2.4 and Figure 41 in Chapter 2) that extends to the Madalena village, which according to Nunes (1999) is formed by cones of the surtseyan type.

8.1.2.3. Competition between erosive and constructional processes in the shelf of Faial

Shelf sector F shows a good example of the competition between opposing infilling processes (mainly volcanic progradation) and widening processes (cliff retreat) during the shelf growth. Onshore volcanism in this sector is very recent (less than 30 Ka) which should result in a more immature shelf since erosion did not have enough time to modeled it more. However, it is as mature as some much older shelf sectors (e.g. shelf sectors C and G – 470 Ka), showing few lava flows, a large area with coarse clastic deposits and high thickness of sediments. The explanation for the high maturity of the shelf sector F is related to its older initiation, which probably began 800 ka ago.

The time and emplacement of lava flows in the shelf will generate different types of shelf geology:

1. Nearshore predominance of coarse clastic deposits up to 30-50 meters water depth and below these depths predominance of sand and gravel deposits (Figure

135 in Chapter 4). The lava flows have emplaced before the present sea-level and were eroded during the sea-level oscillations. The sand and gravel deposits were formed during the present highstand.

2. Nearshore predominance of lava flows up to 30-50 meters water depth and below these depths predominance of sand and gravel deposits (Figure 136 in Chapter 4). First, the sand and gravel deposits form during the present highstand. Then, over the sedimentary deposits there is volcanic progradation from subaerial source that penetrates the sea and reduces the shelf.

3. The shelf is dominated by lavas intercalated with coarse clastic deposits (e.g. shelf sectors A1 and A2). Very recent shelf formed during the last sea-level rise with volcanism occurring at the same time.

8.1.2.4. Sources of sediments

The presence or absence of the coarse clastic deposits on the shelf appears to be mainly related to the erosion of prograded volcanics. The nearshore clastic deposits may also be related to the erosion of less friable cliffs. The origin of the sand and gravel deposits finer deposits was widely discussed in Chapters 4 and 5. It seems that marine erosion of friable cliffs and erosion of the hydrographic basins are the major responsibles for the input of sediments into the shelf. Other mechanisms were also discussed as possible sources of fine sediments on the shelf, although the lack of detailed knowledge of the subaerial geological evolution of the island makes this hypothesis difficult to test. These mechanisms may be related to syn-eruptive sedimentation or non-eruptive remobilization of volcaniclastic fine material from subaerial origin.

8.1.2.5. Shelf break retreat

In high slope areas, evidences of mass-wasting processes near the shelf break were found. These were revealed by embayments in the bathymetric map produced in this work and by the analysis of the high-resolution chirp seismic profiles (Figures 83, 84 and 89 in Chapter 3 and Figure 136 in Chapter4). These can be related to seismicity and high sedimentation rates with both processes

acting together on the failure of the shelf break.

8.1.3. Shelf sedimentary dynamics

The sediment sampling acquired on the scope of this thesis permitted the mapping of the variability of the sediment texture and composition of the finer sediments of the Faial shelf (sand and gravel).

The data shows that the sediments are in general relatively coarse, ranging from medium sands to granules and that there is an offshore coarsening trend of the sediments. The transition from medium sands to coarse sands and granules is made between 40 and 60 meters water depth. Offshore of these depths there is an increase of the mean size and standard deviation. The skewness is fairly constant around zero and the kurtosis is less constant with values between 1 and 1.5. Several mechanisms have been discussed to explain the odd offshore coarsening trend, but the conjugation of two of them seems to be most likely. A very energetic event or group of events with a very long returning period (more than one year) transport coarse sediments across the entire shelf of Faial through downwelling currents. Winnowing of fine sediments at the shelf break zone provokes the coarsening trend below 50 meters water depth.

Simple mathematical formulations were used to derive the offshore limits of the upper and lower shoreface. The seaward limits of the upper shoreface were between 10 and 26 meters water depth, depending on the shelf sectors orientation. The offshore limits of the lower shoreface showed depths between -29 and -49 m. The higher depth value limits of the lower shoreface, near the 50 meters water depth, apparently correspond to the transition depth of the sediment grain-size (to sediment coarser than 1 Φ offshore) which gives a broader support for the calculation.

The grain settling velocity approach was used to predict the entrainment threshold of sediments in the shelf of Faial and showed that during low recurrence storms sediments can be entrained even at very high depths, between 84 to 164 meters water depth depending on the grain size. During yearly storms, a significant part of the sediments are not entrained below 50 meters water depth

which suggests that only during extreme and low occurrence storm events (in this case that occur only 12 hours each 14 years) all the sediments of the Faial shelf are entrained and transported all over the shelf.

The net longshore drift was calculated for sectors B and H which are the ones that showed nearshore fine sediments and bathymetric contours relatively parallel to the shore. The net longshore drift is 1.478 km^3 per year in the NE direction for sector B and 0.363 km^3 per year in the NW direction for sector H. During storms it is possible that the sand and gravely deposits on the other sectors at depths below 30 to 50 meters also suffered transport. Therefore, for each sector it was analyzed which were the waves that affect them (higher and more frequent) to try to infer the longshore transport of sediments at these higher depths. The results show that the shelf sectors A1, A2, C+D, E, F+G would have net longshore transport respectively directed to SE, E, SSE, S and E (Figures 185 and 186).

8.1.4. Aggregates evaluation

The offshore limit of the upper shoreface (15 to 25 meters water depth) and the dredging technological limitations (50 m water depth) were used to define the areas of possible aggregate exploitation. The -50 m was used because it is the depth that the more recent technologies permit dredging. The offshore limit of the upper shoreface was used as the depth where no significant cross-shore sediment transport occurs during a normal year. Therefore, these two boundaries were used to calculate the amount of aggregate reserves assuming that the dredging would occur a few meters below the sedimentary sea-bottom. If the area in consideration would be dredged at a depth of 2 m below the surface a reserve value of 38.4 millions m^3 would be found. Using a dredged depth of 5 m below the surface, a reserve value of 96 millions m^3 would be considered.

The sediment proprieties were also discussed for their use as aggregates. Their grain-size distribution shows that they are most suitable for the use in the production of mortar. They can also be used in the production of concrete, unbound and bound pavement construction, because these products require a small amount of sand and granules in their constitution. The sediments have a

very insignificant percentage of finer material (normally less than 1% of silt and clay).

8.2. Future work

The interpretation of the data acquired during this PhD work permitted the construction of the first geological map of the Faial shelf, to better understand which are the processes responsible for the present-day shelf, and to infer the influence of these processes in the origin and evolution of the shelf. Nevertheless, the data did not always completely cover the shelf area and even when it did some unresolved issues remained, because of the poor quality or inadequacy of the data. Therefore, new field-work is required to fill in the data gaps and promote a better understanding of the various processes involved.

The depositional shelf break was not entirely mapped and only an insignificant part of the slope was covered. A multibeam survey in the outer shelf and upper slope would allow mapping the depositional shelf break, to check the existence of other mass-wasting processes responsible for the shelf break retreat and to better understand the shelf to slope sedimentation.

The sedimentary deposits of sand and gravel were not mapped in its full extension and the shape and depth of the erosional shelf break remained unknown almost everywhere. The depth at which the erosional shelf break is would show if the island has subsided and, if true, whether some shelf sectors of the island have suffered subsidence in detriment of others.

A side-scan sonar (SSS) survey would map the remaining gaps between the seismic track-lines and at the same time would serve to calibrate the bottom-echoes derived from the interpretation of the chirp seismic profiles. The SSS is also a good method to discriminate between the coarse clastic deposits and the lava flows. Furthermore, it would facilitate the distinction between the different sand and gravely bottoms, providing a more suitable mapping of the shelf grain-size distribution.

A more detailed sediment sampling of the shelf would also be useful, not only to fill the gaps (especially between the shore and the -20 m), but also to infer

sediment transport pathways using the grain-size trends methods such as the popular Gao and Collins (1992) method.

The analysis of consecutive aerial photo surveys covering different time periods would permit to estimate net cliff erosion rates and to compare these values with the cliff retreat estimation made during this work.

Finally, a core campaign would be most useful in selected places of the shelf. It would be important to support two of the main assumptions of this work. These cores might reveal tempestite bed deposits which would give a broader support to the suggestion made in this work that the Faial shelf is a wave to storm dominated type. It might also check if the sand and gravel deposits are in fact highstand deposits as their geometry suggests. The fossil assemblage would also allow the definition of their age.

References

Abdel-Monem, A., Fernandez, L.A. and Boone, G.M. 1968. Pliocene-Pleistocene minimum K-Ar ages of the older eruptive centres, Eastern Azores. *Trans. Am. Geophys. Union*, **49**.

Abdel-Monem, A., Fernandez, L.A. and Boone, G.M. 1975. K-Ar ages from the eastern Azores group (Santa Maria, S. Miguel and the Formigas islands). *Lithos*, **8**: 247-254.

Alves, M. 1992. Condições oceanográficas na região dos Açores. Sua influência nas pescas demersais e pelágicas, Dept. Oceanografia e Pescas, Horta.

Amos, C., Li, M. and Choung, K. 1996. Storm-generated, hummocky stratification on the outer-Scotian Shelf. *Geo-Marine Letters*, **16**: 85-94.

Andrade, C., Borges, P. and Freitas, M.C. 2006. Historical tsunami in the Azores archipelago (Portugal). *Journal of Volcanology and Geothermal Research*, **156**: 172-185.

Andrade, C., Teixeira, S., Reis, R. and Freitas, C. 1996. The record of storminess of the Portuguese NW coast in newspapers sources. In: *Partnership in Coastal Management* (Eds J. Taussik and J. Mitchell), pp. 159-166. Samara Publishing Limited, Cardigan.

Argus, D.F., Gordon, R.G., DeMets, C. and Stein, S. 1989. Closure of the Africa-Eurasia-North America plate motion circuit and the tectonics of the Gloria fault. *Journal of Geophysical Research*, **94**: 5585-5602.

Assistant Secretary of Defense 2001. Global Positioning System. Standard positioning service performance standard, Department of Defense, Washington DC.

Azevedo, J.M.M., Alves, E.I. and Dias, J.F.L. 2003. Contributo para a interpretação vulcanoestrutural da ilha do Corvo, Açores. In: *VI Congresso Nacional de Geologia* (Ed DCT-FCT), *Ciências da Terra*, **Volume Especial V**, pp. A5-A8, Monte da Caparica.

Azevedo, J.M.M., Portugal Ferreira, M.R. and Martins, J.A. 1991. The emergent volcanism of Flores Island, Azores. *Arquipélago*, **9**: 37-46.

Bascon, W. 1951. The relationship between sand size and beachface slope. *Trans. American Geophysical Union*, **32**: 866-874.

Bassett, S.E., Milne, G.A., Mitrovica, J.X. and Clark, P.U. 2005. Ice Sheet and Solid Earth Influences on Far-Field Sea-Level Histories. *Science*, **309**: 925-928.

Bastos, L., Osorio, J., Barbeito, A. and Hein, G. 1998. Results from geodetic measurements in the western part of the African-Eurasian plate boundary. *Tectonophysics*, **294**: 261-269.

Bellec, V. 2004. Report Task 1.5: Review of extraction techniques. EUMARSAND: Evaluation and environmental impact of extraction, Renard Centre of Marine Geology, Gent.

Bettencourt, M.L. (Ed), 1979. *O clima dos Açores como recurso natural, especialmente em agricultura e indústria de turismo*. (Ed INMG), *O clima de Portugal*, Lisboa, 103 pp.
Bingham, R. and Haines, K. 2006. Mean dynamic topography: intercomparisons and errors. *Philosophical Transactions of the Royal Society A: Mathematical, Physical and Engineering Sciences*, **364**: 903-916.
Bintanja, R., van de Wal, R.S.W. and Oerlemans, J. 2005. Modeled atmospheric temperatures and global sea levels over the past million years. *Nature*, **437**: 125-128.
Borges, J.F., Bezzeghoud, M., Buforn, E., Pro, C. and Fitas, A. 2007. The 1980, 1997 and 1998 Azores earthquakes and some seismo-tectonic implications. *Tectonophysics*, **435**: 37-54.
Borges, P. 2003. *Ambientes litorais nos Grupos Central e Oriental do arquipélago dos Açores*. Tese de Doutoramento, Universidade dos Açores, Ponta Delgada, 413 pp.
Bouriak, S. 2003. Processing of seismic data and development of geophysical software. INGMARDEP 19/FCT/2003, Dept. Geologia Marinha, IGM, Alfragide.
Bray, M.J. and Hooke, J.M. 1997. Prediction of soft-cliff retreat with accelerating sea-level rise. *Journal of Coastal Research*, **13**: 453-467.
Bryant, E. 2001. *Tsunami - the Underrated Hazard*. Cambridge University Press, Cambridge, 320 pp.
Buforn, E., Udías, A. and Colombás, M.A. 1988. Seismicity source mechanisms and tectonics of the Azores-Gibraltar plate boundary. *Tectonophysics*, **152**: 89-118.
Calvert, A.T., Moore, R.B., McGeehin, J.P. and Rodrigues da Silva, A.M. 2006. Volcanic history and 40Ar/39Ar and 14C geochronology of Terceira Island, Azores, Portugal. *Journal of Volcanology and Geothermal Research*, **156**: 103-115.
Campan, A., Royer, J.-Y., Gente, P., Olivet, J.-L. and Muller, R.D. 1993. Evolution of the Azores-Gibraltar plate boundary for the last 36 Ma. *Eos*, **74**.
Cannat, M., Briais, A., Deplus, C., Escartin, J., Georgen, J., Lin, J., Mercouriev, S., Meyzen, C., Muller, M. and Pouliquen, G. 1999. Mid-Atlantic Ridge-Azores hotspot interactions: along-axis migration of a hotspot-derived event of enhanced magmatism 10 to 4 Ma ago. *Earth and Planetary Science Letters*, **173**: 257-269.
Capobianco, M., Hanson, H., Larson, M., Steetzel, H., Stive, M.J.F., Chatelus, Y., Aarninkhof, S. and Karambas, T. 2002. Nourishment design and evaluation: applicability of model concepts. *Coastal Engineering*, **47**: 113-135.
Carey, J.S., Swift, D.J.P., Steckler, M.S., Reed, C.W. and Niedoroda, A. 1999. High-resolution sequence stratigraphic modeling 2: effects of sedimentation processes. In: *Numerical experiments in stratigraphy: recent advances in stratigraphic and sedimentologic computer simulations*, *SEPM Spec. Publ.* , **62**, pp. 151-164.
Carter, D.J.T. 1982. Prediction of wave height and period for a constant wind velocity using the JONSWAP results. *Ocean Engineering*, **9**: 17-33.
Carvalho, F. 2002. Apuramentos climatológicos mensais em Açores central no período 1989-2002, Instituto de Meteorologia, Lisboa.
Carvalho, F. 2003. Elementos do clima de agitação marítima no grupo central dos Açores, Instituto de Meteorologia, Lisboa.

Cattaneo, A. and Steel, R.J. 2003. Transgressive deposits: a review of their variability. *Earth-Science Reviews*, **62**: 187-228.
Catuneanu, O. 2002. Sequence stratigraphy of clastic systems: concepts, merits, and pitfalls. *Journal of African Earth Sciences*, **35**: 1-43.
Chappell, J. 1983. Evidence for smoothly falling sea level relative to north Queensland, Australia, during the past 6,000 yr. *Nature*, **302**: 406-408.
Chappell, J. and Shackleton, N.J. 1986. Oxygen isotopes and sea level. *Nature*, **324**: 137-140.
Chough, S.K., Lee, S.H., Kim, J.W., Park, S.C., Yoo, D.G., Han, H.S., Yoon, S.H., Oh, S.B., Kim, Y.B. and Back, G.G. 1997. Chirp (2-7-kHz) echo characters in the Ulleung Basin. *Geoscience Journal*, **1**: 143-153.
Chovelon, P. 1982. *Évolution volcanotectonique des iles de Faial et de Pico, Archipel des Açores - Atlantique Nord*. Thèse de Docteur 3ème Cycle, Université de Paris-Sud, Paris, 193 pp.
Coastal Engineering Research Centre 1984. *Shore protection manual*. U.S. Army Corp of Engineers, Washington DC.
Cole, P.D., Guest, J.E. and Duncan, A.M. 1996. Capelinhos: the disappearing volcano. *Geology Today*, **12**: 68-72.
Cole, P.D., Guest, J.E., Duncan, A.M. and Pacheco, J.-M. 2001. Capelinhos 1957-1958, Faial, Azores: deposits formed by an emergent surtseyan eruption. *Bulletin of Volcanology*, **63**: 204-220.
Cookman, J.L. and Flemings, P.B. 2001. STORMSED1.0: hydrodynamics and sediment transport in a 2-D, steady-state, wind- and wave-driven coastal circulation model. *Computers & Geosciences*, **27**: 647-674.
Coutagne, A. 1954. Quelques considérations sur le pouvoir évaporant de l'atmosphére, l'déficit d'écoulement effectif et le deficit d'écoulement maximum. *Houille Blanche*, **7**: 360–369.
Coutinho, R. 2000. *Elementos para a monitorização sismovulcâncica da ilha do Faial (Açores). Caracterização hidrogeológica e avaliação de anomalias de Rn associadas a fenómenos de desgaseificação*. Tese de Doutoramento, Universidade dos Açores, Ponta Delgada, 343 pp.
Cowell, P.J., Hanslow, D.J. and Meleo, J.F. 1999. The shoreface. In: *Handbook of beach and shoreface morphodynamics* (Ed A.D. Short), pp. 39-71. Wiley and Sons, Chichester.
Crowley, T.J. 1981. Temperature and circulation changes in the eastern North Atlantic during the last 150,000 years: Evidence from the planktonic foraminiferal record. *Marine Micropaleontology*, **6**: 97-129.
Cruz, M.I.F.S.d. 2006. Contribuição para o estudo geoquímico do Complexo vulcânico dos cedros, Ilha do Faial. Master thesis, Universidade dos Açores, Ponta Delgada, 105 pp.
Cullen, R.A. and Moore, P. 2001. A spectral optimally interpolated mean sea surface from satellite radar altimetry. *Journal of Geodesy*, **V75**: 188-198.
Damgaard, J.S. and Soulsby, R.L. 1997. Longshore bed-load transport. In: *25th International Conference of Coastal Engineering*, **3**, pp. 3614-2627. ASCE, Orlando.
Damuth, J.E. 1975. Echo character of the Western Equatorial Atlantic floor and its relationship to the dispersal distribution of terrigenous sediments. *Marine Geology*, **18**: 17-45.

Damuth, J.E. 1980. Use of high-frequency (3.5-12kHz) echograms in the study of near-bottom sedimentation processes in the deep-sea: a review. *Marine Geology*, **38**: 51-75.
Damuth, J.E. and Embley, R.W. 1981. Mass-transport processes on Amazon Cone: Western equatorial Atlantic. *Am. Assoc. Petrol. Geol. Bull.*, **65**: 629-643.
Damuth, J.E. and Hayes, D.E. 1977. Echo character of the east Brazilian continental margin and its relationship to sedimentary processes. *Marine Geology*, **24**: 73-95.
Davis, J.R.A. and Hayes, M.O. 1984. What is a wave-dominated coast? *Marine Geology*, **60**: 313.
De Lange, W.P., Prasetya, G.S. and Healy, T.R. 2001. Modelling of Tsunamis Generated by Pyroclastic Flows (Ignimbrites). *Natural Hazards*, **24**: 251-266.
Dean, R.G. and Dalrymple, R.A. 1991. *Water wave mechanics for Engineers and Scientists*. Advanced series on Ocean Engineering, **2**. World Scientific Publishing, Singapore, 353 pp.
DeMets, C., Gordon, R., Argus, D. and Stein, S. 1990. Current plate motions. *Geophys. J. R. Astron. Soc.*, **101**: 425-478.
Dennielou, B., Auffret, G.A., Boelaert, A., Richter, T., Garlan, T. and Kerbrat, R. 1999. Control of the Mid-Atlantic ridge and the Gulf Stream on the Quaternary sedimentation on the Azores Plateau. *Comptes Rendus de l'Academie des Sciences - Series IIA - Earth and Planetary Science*, **328**: 831-837.
Dessert, C., Dupre, B., Gaillardet, J., Francois, L.M. and Allegre, C.J. 2003. Basalt weathering laws and the impact of basalt weathering on the global carbon cycle. *Chemical Geology*, **202**: 257-273.
de Vriend, H.J., Zyserman, J., Nicholson, J., Roelvink, J.A., Pechon, P. and Southgate, H.N. 1993. Medium-term 2DH coastal area modelling. Coastal Engineering, 21: 193-224.
Dickson, M.E. 2004. The development of talus slopes around Lord Howe island and implications for the history of island planation. *Australian Geographer*, **V35**: 223-238.
Dietz, R.B. and Menard, H.W. 1951. Origin of abrupt change in slope at continental shelf margin *AAPG Bulletin*, **35**: 1994-2016.
Douglas, G.R., Whalley, W.B. and McGreevy, J.P. 1991. Rock properties as controls on free-face debris fall activity. *Permafrost and Periglacial Processes*, **2**: 311-329.
Dunbar, G.B. and Barrett, P.J. 2005. Estimating palaeobathymetry of wave-graded continental shelves from sediment texture. *Sedimentology*, **52**: 253-269.
Einsele, G. 1990. Deep-reaching liquefaction potential of marine slope sediments as a prerequisite for gravity mass flows? (Results from the DSDP). *Marine Geology*, **91**: 267-279.
Eisma, D. 1988. An introduction to the geology of continental shelves. In: *Continental shelves* (Eds H. Postma and J.J. Zijlstra), *Ecosystems of the world 27*, pp. 39-91. Elsevier Science Publishers B. V., Amsterdam.
Embry, A.F. 1995. Sequence boundaries and sequence hierarchies: problems and proposals. In: *Sequence Stratigraphy on the Northwest European Margin* (Eds R.J. Steel, V.L. Felt, E.P. Johannessen and C. Mathieu), **Special Publication 5**, pp. 1-11. Norwegian Petroleum Society.

Emery, K.O. 1968. Relict sediments on continental shelves of the world. *AAPG Bulletin*, **52**: 445-464.
Emery, K.O. 1980. Continental margins - classification and petroleum prospects. *Am. Assoc. Petrol. Geol. Bull.*, **64**: 297-315.
Emery, K.O. and Kuhn, G.G. 1982. Sea cliffs: Their processes, profiles, and classification. *Geological Society of America Bulletin*, **93**: 644-654.
Farrell, W.E. and Clark, J.A. 1976. On postglacial sea level. *Geophysical Journal of the Royal Astronomical Society*, **46**: 647–667.
Feraud, G., Kaneoka, I. and Allègre, C.J. 1980. K-Ar ages and stress pattern in the Azores: geodynamic implications. *Earth and Planetary Science Letters*, **46**: 275-286.
Feraud, G., Schmincke, H.-U., Lietz, J., Gostaud, J., Pritchard, G. and Bleil, U. 1984. New K-Ar ages, chemical analyses and magnetic data of rocks from the islands of Santa Maria (Azores), Porto Santo (Madeira archipelago) and Gran Canaria (Canary islands). *Arquipélago*, **5**: 213-240.
Fernandes, M.J., Bastos, L. and Catalão, J. 2000. The Role of Multi-Mission ERS Altimetry in the Determination of the Marine Geoid in the Azores. *Marine Geodesy*, **23**: 1-16.
Fernandes, R.M.S., Bastos, L., Ambrosius, B.A.C., Noomen, R., Matheussen, S. and Baptista, P. 2004. Recent Geodetic Results in the Azores Triple Junction Region. *Pure and Applied Geophysics*, **161**: 683-699.
Fernandes, R.M.S., Bastos, L., Miranda, J.M., Lourenco, N., Ambrosius, B.A.C., Noomen, R. and Simons, W. 2006. Defining the plate boundaries in the Azores region. *Journal of Volcanology and Geothermal Research*, **156**: 1-9.
Ferreira, D.B. 1981. Les méchanismes des pluies et les types de temps de saisons fraiches aux Açores. *Finisterra*, **16**: 15-61.
Ferreira, M.P. and Martins, J.A. 1983. Estudos de inversão paleo-magnéticas na ilha Terceira, Açores. In: *I Congresso Nacional de Geologia*, pp. 4, Aveiro.
Fleming, A., Summerfield, M.A., Stone, J.O., Fifield, L.K. and Cresswell, R.G. 1999. Denudation rates for the southern Drakensberg escarpment, SE Africa, derived from in-situ-produced cosmogenic ^{36}Cl: initial results. *Journal of the Geological Society*, **156**: 209-212.
Folk, R.L. 1954. The distinction between grain size and mineral composition in sedimentary rock nomenclature. *Journal of Geology*, **62**: 344-359.
Folk, R.L. 1974. *Petrology of Sedimentary Rocks*. Hemphill Publishing Co., Austin, Texas, 184 pp.
Folk, R.L. and Ward, W.C. 1957. Brazos River bar - a study in the significance of grain size parameters. *Journal of Sedimentary Petrology*, **27**: 3-26.
Fontes, J.C., Pereira, L.S. and Smith, R.E. 2004. Runoff and erosion in volcanic soils of Azores: simulation with OPUS. *Catena*, **56**: 199-212.
Forjaz, V.H. 1988. *Azores study tour*, 26 pp.
Gagan, M.K., Chivas, A.R. and Herczeg, A.L. 1990. Shelf-wide erosion, deposition, and suspended sediment transport during Cyclone Winifred, central Great Barrier Reef, Australia. *Journal of Sedimentary Petrology*, **60**: 456-470.
Gagan, M.K., Johnson, D.P. and Carter, R.M. 1988. The Cyclone Winifred storm bed, central Great Barrier Reef shelf, Australia. *Journal of Sedimentary Petrology*, **58**: 845-856.

Galloway, W.E. and Hodbay, D.K. 1996. Terrigenous shelf systems. In: *Terrigenous clastic depositional systems. Applications to fossil fuel and groundwater resources* (Eds W.E. Galloway and D.K. Hodbay) 2nd edn, pp. 159-185. Springer-Verlag, Berlin.

Gao, S. and Collins, M. 1992. Net sediment transport patterns inferred from grain-size trends, based upon definition of "transport vectors". *Sedimentary Geology*, **81**: 47-60.

Gao, S. and Collins, M.B. 1994. Analysis of grain size trends, for defining sediment transport pathways in marine environments. *Journal of Coastal Research*, **10**: 70-78.

Geological Society. 2001. Aggregates. Sand, gravel and crushed rock aggregates for construction purposes. Geological Society Engineering Geology Special Publications, **17**. Geological Society, London, 330 pp.

Gould, W.J. 1985. Physical oceanography of the Azores front. *Progress In Oceanography*, **14**: 167.

Haggar, J.P. 1988. The structure, composition and status of the cloud forests of Pico Island in the Azores. *Biological Conservation*, **46**: 7-22.

Hallermeier, R.J. 1981. A profile zonation for seasonal sand beaches from wave climate. *Coastal Engineering*, **4**: 253-277.

Hamilton, E.L. and Bachman, R.T. 1982. Sound velocity and related properties in marine sediments. *The Journal of the Acoustical Society of America*, **72**: 1891-1904.

Hayes, M.O. 1967. Relationship between coastal climate and bottom sediment type on the inner continental shelf. *Marine Geology*, **5**: 111-132.

Hayes, M.O. 1979. Barrier island morphology as a function of tidal and wave regimes In: *Barrier islands from the Gulf of St. Lawrence to the Gulf of Mexico* (Ed S.P. Leatherman), pp. 1-29. Academic Press, New York.

Hedberg, H.D. 1970. Continental margins from viewpoint of the petroleum geologist. *Am. Assoc. Petrol. Geol. Bull.*, **54**: 3-43.

Hernández-Molina, F.J., Fernández-Salas, L.M., Lobo, F., Somoza, L., Díaz-del-Río, V. and Alveirinho Dias, J.M. 2000. The infralittoral prograding wedge: a new large-scale progradational sedimentary body in shallow marine environments. *Geo-Marine Letters*, **20**: 109-117.

Inman, D.L. and Brush, B.M. 1973. The coastal challenge. *Science*, **181**: 20-32.

Instituto Geográfico do Exército 2001a. Feteira (Faial-Açores) - Folha 6. In: *Carta Militar de Portugal - Série M889* 2nd edn. Instituto Geográfico do Exército, Lisboa.

Instituto Geográfico do Exército 2001b. Horta (Faial-Açores) - Folha 7. In: *Carta Militar de Portugal - Série M889* 2nd edn. Instituto Geográfico do Exército, Lisboa.

Instituto Geográfico do Exército 2001c. Pedro Miguel (Faial-Açores) - Folha 5. In: *Carta Militar de Portugal - Série M889* 2nd edn. Instituto Geográfico do Exército, Lisboa.

Instituto Geográfico do Exército 2001d. Praia do Norte (Faial-Açores) - Folha 4. In: *Carta Militar de Portugal - Série M889* 2nd edn. Instituto Geográfico do Exército, Lisboa.

Instituto Hidrográfico 1999. Ilha do Faial e Canal do Faial. In: *Carta da Série Internacional - Oceânico Atlântico Norte. Arquipélago dos Açores* (Ed Instituto Hidrográfico) 1st edn, Lisboa.

Instituto Hidrográfico (Ed), 2000. *Arquipélago dos Açores*, 2nd edn, *Roteiro da Costa de Portugal* Instituto Hidrográfico, Lisboa.
Instituto Hidrográfico 2005. Tratamentos de dados de agitação marítima. Açores/Terceira - Fevereiro 2005, Instituto Hidrográfico, Lisboa.
International Council for the Exploration of the Sea 2000. Report of the working group on the effects of extraction of marine sediments on the marine ecosystem. Ref. CM 2000/E:07, Gdansk.
IOC IHO and BODC 2003. Centenary Edition of the GEBCO Digital Atlas, published on CD-ROM on behalf of the Intergovernmental Oceanographic Commission and the International Hydrographic Organization as part of the General Bathymetric Chart of the Oceans. British Oceanographic Data Centre, Liverpool, U.K.
Jacobsen, E.E. and Schwartz, M.L. 1981. The use of geomorphic indicators to determine the direction of net shore-drift. *Shore and Beach*, **49**: 38-43.
Johnson, C.L., Wijbrans, J.R., Constable, C.G., Gee, J., Staudigel, H., Tauxe, L., Forjaz, V.-H. and Salgueiro, M. 1998. 40Ar/39Ar ages and paleomagnetism of Sao Miguel lavas, Azores. *Earth and Planetary Science Letters*, **160**: 637-649.
Johnson, H.D. and Baldwin, C.T. 1986. Shallow siliclastic seas. In: *Sedimentary environments and facies* (Ed H.G. Reading) 2nd edn, pp. 229-282. Blackwell Scientific Publications, Oxford.
Keating, B.H. and McGuire, W.J. 2000. Island Edifice Failures and Associated Tsunami Hazards. *Pure and Applied Geophysics*, **157**: 899-955.
Kelley, S.W., Ramsey, J.S. and Byrnes, M.R. 2004. Evaluating shoreline response to offshore sand mining for beach nourishment. Journal of Coastal Research, **20**: 89-100.
Klein, B. and Siedler, G. 1989. On the origin of the Azores Current. *Journal of Geophysical Research*, **94**: 6159-6168.
Krause, D.C. and Watkins, N.D. 1970. North Atlantic crustal genesis in the vicinity of the Azores. *Geophys. J. R. Astron. Soc.*, **19**: 261-283.
Krumbein, W.C. 1938. Size frequency distribution of sediments and the normal phi curve. *Journal of Sedimentary Petrology*, **7**: 3-17.
Laberg, J.S. and Vorren, T.O. 1993. A Late Pleistocene submarine slide on the Bear Island Trough Mouth Fan. *Geo-Marine Letters*, **13**: 227-234.
Lafon, V., José, F., Tempera, F., Macedo, L. and Martins, A. 2005. Summertime morphodynamics of two beaches presenting different wave exposure - Faial island, Azores, Portugal. In: 5th International Conference on Coastal Dynamics, Barcelone.
Lambeck, K. and Chappell, J. 2001. Sea level change through the last glacial cycle. *Science*, **292**: 679-686.
Laughton, A.S. and Whitmarsh, R.B. 1974. The Azores-Gibraltar plate boundary. In: *Geodynamics of Iceland and the North Atlantic area* (Ed L. Kristjansson), pp. 63-81. Reidel, Dordretch.
Le Friant, A., Harford, C.L., Deplus, C., Boudon, G., Sparks, R.J.S., Herd, R.A. and Komorowski, J.-C. 2004. Geomorphological evolution of Monserrat (West Indies): importance of flank collapse and erosional processes. *Journal of the Geological Society*, **161**: 147-160.
Le Roux, J.P. 1994a. An alternative approach to the identification of net sediment transport paths based on grain-size trends. *Sedimentary Geology*, **94**: 97-107.

Le Roux, J.P. 1994b. Net sediment transport patterns inferred from grain-size trends, based upon definition of "transport vectors"--comment. *Sedimentary Geology*, **90**: 153-156.
Le Roux, J.P. 2001. A simple method to predict the threshold of particle transport under oscillatory waves. *Sedimentary Geology*, **143**: 59-70.
Le Roux, J.P. 2005. Grains in motion: A review. *Sedimentary Geology*, **178**: 285-313.
Lee, G.-h., Nicholls, R.J. and Birkemeier, W.A. 1998. Storm-driven variability of the beach-nearshore profile at Duck, North Carolina, USA, 1981-1991. *Marine Geology*, **148**: 163-177.
Lee, S.H., Chough, S.K., Back, G.G. and Kim, Y.B. 2002. Chirp (2-7-kHz) echo characters of the South Korea Plateau, East Sea: styles of mass movement and sedimentary gravity flow. *Marine Geology*, **184**: 227-247.
Leeder, M. 1999. *Sedimentology and sedimentary basins: from turbulence to tectonics*, Oxford, 592 pp.
Léon, S.P. and Soares, C.G. 2005 On the sheltering effect of islands in ocean wave models *JOURNAL OF GEOPHYSICAL RESEARCH-OCEANS*, **110 (C9): Art. No. C09020 SEP 28**
Lighty, R.G., Macintyre, I.G. and Stuckenrath, R. 1982. Acropora palmata reef framework: A reliable indicator of sea level in the western atlantic for the past 10,000 years. *Coral Reefs*, **V1**: 125-130.
Lisiecki, L.E. and Raymo, M.E. 2005. A Pliocene-Pleistocene stack of 57 globally distributed benthic $\delta^{18}O$ records. *Paleoceanography*, **20**: 1-17.
Lourenço, N., Miranda, J.M., Luís, J.F., Ribeiro, A., Mendes Victor, L.A., Madeira, J. and Needham, H.D. 1998. Morpho-tectonic analysis of the Azores Volcanic Plateau from a new bathymetric compilation of the area. *Marine Geophysical Researches*, **20**: 141-156.
Louvat, P. and Allègre, C.J. 1998. Riverine erosion rates on São Miguel volcanic island, Azores archipelago. *Chemical Geology*, **148**: 177-200.
Luis, J.F., Miranda, J.M., Galdeano, A. and Patriat, P. 1998. Constraints on the structure of the Azores spreading center from gravity data. *Marine Geophysical Researches*, **20**: 157-170.
Luis, J.F., Miranda, J.M., Galdeano, A., Patriat, P., Rossignol, J.C. and Mendes Victor, L.A. 1994. The Azores triple junction evolution since 10 Ma from an aeromagnetic survey of the Mid-Atlantic Ridge. *Earth and Planetary Science Letters*, **125**: 439-459.
Machado, F. and Freire, T. 1985. Cone dos Capelinhos em 1981. *Açoreana*, **6**: 261-266.
Madeira, J. 1998. *Estudos de neotectónica nas ilhas do Faial, Pico e S. Jorge: uma contribuição para o conhecimento geodinâmico da junção tripla dos Açores*. Tese de Doutoramento, Universidade de Lisboa, Lisboa, 428 pp.
Madeira, J. and Brum da Silveira, A. 2003. Active tectonics and first paleosismological results in Faial, Pico e S. Jorge islands (Azores, Portugal). *Annals of Geophysics*, **46**: 733-761.
Madeira, J. and Ribeiro, A. 1990. Geodynamic models for the Azores triple junction: a contribution from tectonics. *Tectonophysics*, **184**: 405-415.

Madeira, J., Soares, A.M.M., Silveira, A.B.d. and Serralheiro, A. 1995. Radiocarbon dating recent volcanic activity on Faial Island (Azores). *Radiocarbon*, **37**: 139-147.

Madruga, J., Pinheiro, J. and Madeira, M. 2001. Pedologia. In: *Plano Regional da Água* (Ed Direcção Regional do Ordenamento do Território e Recursos Hídricos/Secretaria Regional do Ambiente), pp. 1-75. Departamento de Ciências Agrárias/Universidade dos Açores.

Malamud, B.D., Turcotte, D.L., Guzzeti, F. and Reichenbach, P. 2004. Landslides, earthquakes and erosion. *Earth and Planetary Science Letters*, **229**: 45-59.

Malheiro, A. 2006. Geological hazards in the Azores archipelago: Volcanic terrain instability and human vulnerability. *Journal of Volcanology and Geothermal Research*, **156**: 158-171.

Masselink, G. and Hughes, M.G. 2003. *Introduction to coastal processes and geomorphology*. Arnold, London, 354 pp.

Mckelvey, V.E. 1972. Mineral resource estimates and public policy. American Scientist, 30: 32-40.

McKenzie, D. 1972. Active tectonics of the Mediterranean region. *Geophys. J. R. Astron. Soc.*, **30**: 109-185.

McLaren, P. 1981. An interpretation of trends in grain size measures. *Journal of Sedimentary Petrology*, **51**: 611-624.

McLaren, P. and Bowles, D. 1985. The effects of sediment transport on grain-size distributions. *Journal of Sedimentary Petrology*, **55**: 457-470.

Menard, H.W. 1983. Insular erosion, isostasy, and subsidence. *Science*, **220**: 913-918.

Menard, H.W. 1986. *Islands*. Scientific American Books, New York, 230 pp.

Milne, G.A. and Mitrovica, J.X. 1998a. The influence of time-dependent ocean-continent geometry on predictions of post-glacial sea level change in Australia and New Zealand. *Geophysical research letters*, **25**: 793-796.

Milne, G.A. and Mitrovica, J.X. 1998b. Postglacial sea-level change on a rotating Earth. *Geophysical Journal International*, **133**: 1-19.

Milne, G.A., Mitrovica, J.X. and Davis, J.L. 1999. Near-field hydro-isostasy: the implementation of a revised sea-level equation. *Geophysical Journal International*, **139**: 464-482.

Milne, G.A., Mitrovica, J.X. and Schrag, D.P. 2002. Estimating past continental ice volume from sea-level data. *Quaternary Science Reviews*, **21**: 361-376.

Miranda, J.M., Victor, L.A.M., Simões, J.Z., Luis, J.F., Matias, L., Shimamura, H., Shiobara, H., Nemoto, H., Mochizuki, H., Hirn, A. and Lépine, J.C. 1998. Tectonic setting of the Azores Plateau deduced from a OBS survey. *Marine Geophysical Researches*, **20**: 171-182.

Mitchell, N.C., Beier, C., Rosin, P., Quartau, R. and Tempera, F. 2007. Submarine lava flows around the coasts of Pico Island, Azores. In: *EGU 2007*, **Geophysical Research Abstracts, Vol. 9**, pp. 02351, Viena.

Mitchell, N.C., Beier, C., Rosin, P., Quartau, R. and Tempera, F. in press. Lava penetrating water: submarine lava flows around the coasts of Pico Island, Azores. *Geochemistry, Geophysics, Geosystems*.

Mitchell, N.C., Dade, W.B. and Masson, D.G. 2003a. Erosion of the submarine flanks of the Canary Islands. *Journal of Geophysical Research*, **108**: 3-1 - 3-11.

Mitchell, N.C., Schmidt, T., Isidro, E., Tempera, F., Cardigos, F., Nunes, J.C. and Figueiredo, J. 2003b. Multibeam sonar survey of the central Azores volcanic islands. *InterRidge News*, **12**: 30-32.
Mitchum Jr., R.M., Vail, P.R. and Sangree, J.B. 1977a. Seismic stratigraphy and global changes in sea level, Part 6: Stratigraphic interpretation of seismic reflection patterns in depositional sequences. In: *Seismic stratigraphy - applications to hydrocarbon exploration* (Ed C.E. Payton), **AAPG Mem. 26**, pp. 117-133. AAPG, Tulsa.
Mitchum Jr., R.M., Vail, P.R. and Thompson III, S. 1977b. Seismic stratigraphy and global changes of sea level, Part 2: The depositional sequence as a basic unit for stratigraphic analysis. In: *Seismic stratigraphy - applications to hydrocarbon exploration* (Ed C.E. Payton), **AAPG Mem. 26**, pp. 53-62. AAPG, Tulsa.
Montaggioni, L.F., Cabioch, G., Camoin, G.F., Bard, E., Laurenti, A.R., Faure, G., Déjardin, P. and Récy, J. 1997. Continuous record of reef growth over the past 14 k.y. on the mid-Pacific island of Tahiti. *Geology*, **25**: 555–558.
Moore, J.G. and Fornari, D.J. 1984. Drowned reefs as indicators of the rate of subsidence of the island of Hawaii. *Journal of Geology*, **92**: 752-759.
Moore, J.G., Philips, R.L., Grigg, R.W., Peterson, D.W. and Swanson, D.A. 1973. Flow of lava into the sea, 1969-1971, Kilauea volcano, Hawaii. *Geological Society of America Bulletin*, **84**: 537-546.
Muecke, G.K., Ade-Hall, J.M., Aumento, F., MacDonald, A., Opdyke, N. and Lowrie, W. 1974. Deep drilling in active geothermal area in the Azores. *Nature*, **252**: 281-285.
Mulder, T. and Cochonat, P. 1996. Classification of offshore mass movements. *Journal of Sedimentary Research*, **66**: 43-57.
Müller, G. and Heidelberg, M.G. 1971. A bomba de carbonatos, um sistema simples para determinação do teor em carbonatos contidos em sedimentos, solos e outros materiais. *Neues Jahrbuch der Mineralogie*, **10**: 466-469.
Nicholls, R.J., Birkemeier, W.A. and Lee, G.-h. 1998. Evaluation of depth of closure using data from Duck, NC, USA. *Marine Geology*, **148**: 179.
Niedoroda, A.W., Swift, D.J.P. and Hopkins, T.S. 1985. The Shoreface. In: *Coastal sedimentary environments* (Ed R.A. Davis) 2nd edn, pp. 533-624. Springer-Verlag, New York.
Nittrouer, C.A. and Wright, L.D. 1994. Transport of particles across continental shelves. *Reviews of Geophysics*, **32**: 85-113.
Nott, J., Young, R. and McDougall, I. 1996. Wearing down, wearing back, and gorge extension in the long-term denudation of a highland mass: Quantitative evidence from the Shoalhaven catchment, Southeast Australia. *Journal of Geology*, **104**: 224.
Nunes, J.C. 1999. *A actividade vulcânica na ilha do Pico do Plistocénico Superior ao Holocénico: mecanismo eruptivo e hazard vulcânico*. Tese de Doutoramento, Universidade dos Açores, Ponta Delgada, 357 pp.
Nunes, J.C., Forjaz, V.H. and Oliveira, C.S. 2004. Catálogo sísmico da região dos Açores (1850-1998) (Eds P. Lourenço and J.O. Barros), *Livro de Actas do 6º Encontro nacional de sismologia e engenharia sísmica*, pp. 349-357. Universidade do Minho, Braga.

O'Grady, D.B., Syvitski, J.P.M., Pratson, L.F. and Sarg, J.F. 2000. Categorizing the morphologic variability of siliciclastic passive continental margins. *Geology*, **28**: 201-210.

Ollitrault, M. 1995. La circulation génerale de L'Atlantique Nord subtropical vers 700m de profondeur, révélée par des flotteurs dérivants de subsurface. *C. R. Academie des Sciences Paris*, **321**: 153-160.

Pacheco, J.M. 2001. *Processos associados ao desenvolvimento de erupções vulcânicas hidromagmáticas explosivas na ilha do Faial e sua interpretação numa perspectiva de avaliação do Hazard e minimização de risco*. PhD thesis, Universidade dos Açores, Ponta Delgada, 330 pp.

Pagarete, J., Teixeira, J.T., B., M.V., Antunes, C. and Ribeiro, H. 1998. The importance of classical geodetic observations for analyzing the geodynamic behaviour of the Azores archipelago. *Tectonophysics*, **294**: 281-290.

Papadopoulos, G.A. and Imamura, F. 2001. A proposal for a new tsunami intensity scale. In: *Proceedings of the International Tsunami Symposium*, pp. 569–577, Washington.

Paulay, G. and McEdward, L.R. 1990. A simulation model of island reef morphology: the effects of sea level fluctuations, growth, subsidence and erosion. *Coral reefs*, **9**: 51-62.

Pflaumann, U., Sarnthein, M., Chapman, M., d'Abreu, L., Funnell, B., Huels, M., Kiefer, T., Maslin, M., Schulz, H., Swallow, J., Kreveld, S.v., Vautravers, M., Vogelsang, E. and Weinelt, M. 2003. Glacial North Atlantic: Sea-surface conditions reconstructed by GLAMAP 2000. *Paleoceanography*, **18**: 10.1-10.21.

Pickrill, R.A. 1983. Wave-built shelves on some low-energy coasts. *Marine Geology*, **51**: 193-216.

Plint, A.G. and Nummedal, D. 2000. The falling stage systems tract: recognition and importance in sequence stratigraphic analysis. In: *Sedimentary Response to Forced Regression* (Eds D. Hunt and R.L. Gawthorpe), **172**, pp. 1-17. Geol. Soc. London Speci. Publ.

Poizot, E., Mear, Y., Thomas, M. and Garnaud, S. 2006. The application of geostatistics in defining the characteristic distance for grain size trend analysis. *Computers & Geosciences*, **32**: 360-370.

Poppe, L.J., Eliason, A.H. and Hastings, M.E. 2003. A Visual Basic program to classify sediments based on gravel-sand-silt-clays ratios. *Computers & Geosciences*, **29**.

Poppe, L.J., Eliason, A.H. and Hastings, M.E. 2004. A Visual Basic Program to Generate Sediment Grain-Size Statistics and to Extrapolate Particle Distributions. *Computers & Geosciences*, **30**: 791-795.

Posamentier, H.W. and Vail, P.R. 1988. Eustatic controls on clastic deposition. II. Sequence and systems tract models. In: *Sea Level Changes: An Integrated Approach* (Eds C.K. Wilgus et al.), *SEPM Special Publication*, **42**, pp. 125-154.

Pratson, L.F. and Coakley, B.J. 1996. A model for the headward erosion of submarine canyons induced by downslope-eroding sediment flows. *Geological Society of America Bulletin*, **108**: 225-234.

Pratson, L.F. and Laine, E.P. 1989. The relative importance of gravity induced versus current-controled sedimentation during the Quaternary along the mideast US outer continental margin revealed by 3.5 kHz echo character. *Marine Geology*, **89**: 87-126.

Pratson, L.F., Ryan, W.B.F., Mountain, G.S. and Twichell, D.C. 1994. Submarine canyon initiation by downslope-eroding sediment flows: Evidence in late Cenozoic strata on the New Jersey continental slope. *Geol. Soc. Am. Bull.*, **106**: 395-412.

Quartau, R. and Curado, F. 2002. Projecto Gemas – Relatório da campanha FAPI2 realizada ao largo do Pico. Relatório Técnico INGMARDEP 15/2002, Dept. Geologia Marinha - IGM, Lisboa.

Quartau, R., Curado, F., Bouriak, S., Monteiro, J.H. and Pinheiro, L. 2003. Projecto Gemas – Localização e distribuição de areias em redor da ilha do Pico. Relatório Técnico INGMARDEP 16/2003, Dept. Geologia Marinha - IGM, Lisboa.

Quartau, R., Curado, F., Cunha, T., Pinheiro, L. and Monteiro, J.H. 2002. Projecto Gemas – Localização e distribuição de areias em redor da ilha do Faial. Relatório Técnico INGMARDEP 5/2002, Dept. Geologia Marinha - IGM, Lisboa.

Quartau, R., Curado, F., Duarte, H., Muiños, S. and Pinto, C. 2005a. Projecto Gemas – Relatório da campanha de sísmica de reflexão (SAMI-1) realizada ao largo da ilha de S. Miguel. Relatório Técnico INGMARDEP 3/2005, Dept. Geologia Marinha - INETI, I.P., Lisboa.

Quartau, R., Curado, F., Duarte, H. and Pinto, C. 2006. Projecto Gemas – Localização e distribuição de areias em redor da ilha de S. Miguel. Relatório Técnico INGMARDEP 1/2006, Dept. Geologia Marinha - INETI, I.P., Lisboa.

Quartau, R., Duarte, H. and Brito, P. 2005b. Projecto Gemas – Relatório da campanha de amostragem de sedimentos (FAPI-3) realizada na plataforma e na orla costeira das ilhas do Faial e do Pico. Relatório Técnico INGMARDEP 2/2005, Dept. Geologia Marinha - INETI, I.P., Lisboa.

Quiquerez, A., Allemand, P., Dromart, G. and J.-P.Garcia 2004. Impact of storms on mixed carbonate and siliciclastic shelves: insights from combined diffusive and fluid flow transport stratigraphic forward model. *Basin Research*, **16**: 431-449.

Reineck, H.-E. and Singh, I.B. 1975. *Depositional Sedimentary Environments*. Springer-Verlag, Berlin, 439 pp.

Ribeiro, A. 2002. *Soft plate and impact tectonics*. Springer-Verlag, Berlin, 324 pp.

Richards, K.S. and Lorriman, N.R. 1987. Basal erosion and mass movement. In: *Slope Stability* (Eds M.G. Anderson and K.S. Richards), pp. 331–357. Wiley, New York.

Rine, J.M., Tillman, R.W., Culver, S.J. and Swift, D.J.P. 1991. Generation of late Holocene sand ridges on the middle continental shelf of New Jersey, USA - evidence for formation in mid-shelf setting based on comparisons with a nearshore ridge. In: *Shelf sand and sandstone bodies: geometry, facies and sequence stratigraphy* (Eds D.J.P. Swift, G.F. Oertel, R.W. Tillman and J.A. Thorne), *Special publication of the International Association of Sedimentologists*, **14**, pp. 395-423. Blackell Scientific Publications, Oxford.

Santos, F.D., Valente, M.A., Miranda, P.M.A., Aguiar, A., Azevedo, E.B., Tomé, A.R. and Coelho, F. 2004. Climate change scenarios in the Azores and Madeira Islands. *World Resource Review*, **16**: 473-491.

Santos, R.S., Hawkins, S., Monteiro, L.R., Alves, M. and Isidro, E.J. 1995. Case studies and reviews. Marine research, resources and conservation in the Azores. *Aquatic conservation: Marine and Freshwater ecosystems*, **5**: 311-354.

Schiebel, R., Schmucker, B., Alves, M. and Hemleben, C. 2002. Tracking the recent and late Pleistocene Azores front by the distribution of plantick foraminifers. *Journal of Marine Systems*, **37**: 213-227.
Schneider, J.-L. 2000. Volcaniclastic sedimentation in submarine settings: products and processes. In: *Volcaniclastic Rocks, from Magma to Sediments* (Eds H. Leyrit and C. Montenat), pp. 175-192. Gordon and Breach Science Publishers, Amsterdam.
Searle, R. 1980. Tectonic pattern of the Azores spreading centre and triple junction. *Earth and Planetary Science Letters*, **51**: 415-434.
Shepard, F.P. 1973. *Submarine Geology*. Harper & Row, New York, 517 pp.
Siddall, M. 2005. Palaeoclimate: The riddle of the sediments. *Nature*, **437**: 39-41.
Siddall, M., Rohling, E.J., Almogi-Labin, A., Hemleben, C., Meishner, D., Schmeizer, I. and Smeed, D.A. 2003. Sea-level fluctuactions during the last glacial cycle. *Nature*, **423**: 853-857.
Soulsby, R.L. 1997. *Dynamics of marine sands, a manual for practical applications*. Thomas Telford Ltd, London, 249 pp.
Southard, J.B. and Stanley, D.J. 1976. Shelf-break processes and sedimentation. In: *Marine sediment transport and environmental management* (Eds D.J. Stanley and D.J.P. Swift), pp. 351-377. John Wiley & Sons, New York.
Stanley, D.J., Addy, S.K. and Behrens, E.W. 1983. The mudline: Variability of its position relative to shelfbreak. In: *The shelfbreak: Critical interface on continental margins* (Eds D.J. Stanley and G.T. Moore), **Spec. Publ. 33**, pp. 279-298. Society of Economic Paleontologists and Mineralogists, Tulsa, Oklahoma.
Steckler, M.S. 1999. High-resolution sequence stratigraphic modeling 1: the interplay of sedimentation, erosion and subsidence. In: *Numerical experiments in stratigraphy: recent advances in stratigraphic and sedimentologic computer simulations*, *SEPM Spec. Publ.* , **62**, pp. 139-149.
Steckler, M.S., Reynolds, D.J., Coakley, B.J., Swift, B.A. and Jarrard, R.D. 1993. Modeling passive margin sequence stratigraphy. In: *Sequence stratigraphy and facies associations* (Eds H.W. Posamentier, C.P. Summerhayes, B.U. Haq and G.P. Allen), *Special publication of the International Association of Sedimentologists*, **18**, pp. 19-41.
Stive, M.J.F., DeVriend, H.J., Nicholls, R.J. and Capobianco, M. 1992. Shore nourishment and the active zone; a time scale dependent view. In: *23rd Coastal Engineering Conference*, pp. 2464-2473. ASCE, New York.
Storms, J.E.A., Weltje, G.J., van Dijke, J.J., Geel, C.R. and Kroonenberg, S.B. 2002. Process-Response Modeling of Wave-Dominated Coastal Systems: Simulating Evolution and Stratigraphy on Geological Timescales. *Journal of Sedimentary Research*, **72**: 226-239.
Stretch, R.C., Mitchell, N.C. and Portaro, R.A. 2006. A morphometric analysis of the submarine volcanic ridge south-east of Pico Island, Azores. *Journal of Volcanology and Geothermal Research*, **156**: 35-54.
Sunamura, T. 1976. Feedback relationship in wave erosion of laboratory rocky coast. *Journal of Geology*, **84**: 427-437.
Sunamura, T. 1977. A relationship between wave-induced cliff erosion and erosive rate of waves. *Journal of Geology*, **85**: 613-618.
Sunamura, T. 1978. A model of the development of continental shelves having erosional origin. *Geological Society of America Bulletin*, **89**: 504-510.

Sunamura, T. 1992. *Geomorphology of rocky coasts*. Coastal Morphology and Research. John Wiley & Sons Ltd., Chichester, 302 pp.
Swift, D.J.P., Stanley, D.J. and Curray, J.R. 1971. Relict sediments on continental shelves: a reconsideration. *Journal of Geology*, **79**: 322-346.
Swift, D.J.P. and Thorne, J.A. 1991. Sedimentation on continental margins, I: a general model for shelf sedimentation. In: *Shelf sand and sandstone bodies: geometry, facies and sequence stratigraphy* (Eds D.J.P. Swift, G.F. Oertel, R.W. Tillman and J.A. Thorne), *Special publication of the International Association of Sedimentologists*, **14**, pp. 3-31. Blackell Scientific Publications, Oxford.
Taggart, B.E. and Schwartz, M.L. 1988. Net-shore drift direction determination: A systematic approach. *Journal of Shoreline Management*, **3**: 285-309.
Teixeira, F.C. 2001. Projecto Gemas – Relatório da campanha FAPI1-2001 realizada ao largo do Faial. Relatório Técnico INGMARDEP 13/2001, Dept. Geologia Marinha - IGM, Lisboa.
Thompson, W.G. and Goldstein, S.L. 2006. A radiometric calibration of the SPECMAP timescale. *Quaternary Science Reviews*, **25**: 3207-3215.
Thorne, J.A. and Swift, D.J.P. 1991. Sedimentation on continental margins, II: application of the regime concept. In: *Shelf sand and sandstone bodies: geometry, facies and sequence stratigraphy* (Eds D.J.P. Swift, G.F. Oertel, R.W. Tillman and J.A. Thorne), *Special publication of International Association of Sedimentologists*, **14**, pp. 33-58. Blackell Scientific Publications, Oxford.
Thornthwaite, C.W. 1948. An approach toward a national classification of climate. *Geographical Review*, **38**: 55-94.
Tilling, R.I. 1985. Volcanoes. In: *http://pubs.usgs.gov/gip/volc/*. United States Geological Survey.
Trenhaile, A.S. 1987. *The geomorphology of rocky coasts*. Oxford University Press, Oxford, 393 pp.
Trenhaile, A.S. 2001. Modeling the Quaternary evolution of shore platforms and erosional continental shelves. *Earth Surface Processes and Landforms*, **26**: 1103-1128.
Tucker, M.J. 1991. *Waves in Ocean Engineering: Measurement, analysis, interpretation*. Ellis Horwood Series in Marine Science. Ellis Horwood Limited, Chichester, 431 pp.
Turc, L. 1955. Le bilan d'eau des sols: relations entre les precipitations, l'evaporation et l'écoulement. *Annals of Agronomy*, **5**: 491-596.
U.S. Army Corp of Engineers 2003a. Estimation of nearshore waves. Part II - Chapter 3. In: *Coastal Engineering manual*, Washington DC.
U.S. Army Corp of Engineers 2003b. Water wave mechanics. Part II - Chapter 1. In: *Coastal Engineering manual*, Washington DC.
Udías, A. 1980. Seismic stresses in the region Azores-Spain-Western Mediterranean. *Rock Mechanics*, **9**: 75-84.
Udías, A., Espinoza, A.F., Mezcua, J., Buforn, E., Vegas, R., Nishenko, S.P., Martinez-Solares, J.M. and Lopez-Arroyo, A. 1986. Seismicity and tectonics of the North African-Eurasian plate boundary (Azores-Iberia-Tunisia). 86-626, U. S. Geol. Surv.

Vail, P.R., Audemard, F., Bowman, S.A., Einsele, G. and Perez-Cruz, G. 1991. The stratigraphic signatures of tectonics, eustasy and sedimentation. In: *Cycles and events in stratigraphy* (Eds G. Einsele, W. Ricken and A. Seilacher), pp. 617-659. Springer-Verlag, Berlin.

Vail, P.R., Mitchum Jr., R.M. and Thompson III, S. 1977. Seismic stratigraphy and global changes of sea level, Part 3: Relative changes of sea level from coastal onlap. In: *Seismic stratigraphy - applications to hydrocarbon exploration* (Ed C.E. Payton), **AAPG Mem. 26**, pp. 63-81. AAPG, Tulsa.

Valadão, P., Gaspar, J.L., Queiroz, G. and Ferreira, T. 2002. Landslides density map of S. Miguel Island, Azores archipelago. *Natural Hazards and Earth System Sciences*, **2**: 51-56.

Van Wagoner, J.C., Posamentier, H.W., Mitchum Jr., R.M., Vail, P.R., Sarg, J.F., Loutit, T.S. and Handenbol, J. 1988. An overview of the fundamentals of sequence stratigraphy and key definitions. In: *Sea level changes: An integrated approach* (Eds C.K. Wilgus et al.), *SEPM Special Publication*, **42**, pp. 39-45.

Vanney, J.-R. and Stanley, D.J. 1983. Shelfbreak physiography: an overview. In: *The shelfbreak: Critical interface on Continental Margins* (Eds D.J. Stanley and G.T. Moore), **Spec. Publ. 33**, pp. 1-24. Society of Economic Paleontologists and Mineralogists, Tulsa, Oklahoma.

Vogt, P.R. and Jung, W.Y. 2004. The Terceira Rift as hyper-slow, hotspot-dominated oblique spreading axis: A comparison with other slow-spreading plate boundaries. *Earth and Planetary Science Letters*, **218**: 77-90.

Wear, C.M., Stanley, D.J. and Boula, J.E. 1974. Shelfbreak physiography between Wilmington and Norfolk canyons. *Marine Technology Society Journal*, **8(4)**: 37-48.

Weggel, J.R. 1972. Maximum breaker height. *Journal of Waterways, Harbours and Coastal Engineering*, **98**.

Wentworth, C.K. 1922. A scale of grade and class terms for clastic systems. *Journal of Geology*, **30**: 377-392.

White, W.M., Schilling, J.-G. and Hart, S.R. 1976. Evidence for the Azores mantle plume from strontium isotope geochemistry of the Central North Atlantic. *Nature*, **263**: 659-663.

Woodroffe, C. and McLean, R. 1990. Microatolls and recent sea level change on coral atolls. *Nature*, **344**: 531.

Young, R.W. 1983. The tempo of geomorphological change: evidence from southeastern Australia. *Journal of Geology*, **91**: 221-230.

Young, R.W. and McDougall, I. 1985. The age, extent, and geomorphological significance of the Sassafras basalt, southeastern New South Wales. *Australian Journal of Earth Sciences*, **32**: 323-331.

Young, R.W. and Wray, R.A.L. 2000. Contribution to the theory of scarpland development from observations in central Queensland, Australia. *Journal of Geology*, **108**: 705-719.

Youssef, W.B.H. 2005. *Caractérisation in situ de l'environnement physique des habitats benthiques occupés par Codium elisabethae au sein de sites d'études particuliers (Faial, Açores)*, Université de Liège, Liège, 94 pp.

Zecchin, M. 2007. The architectural variability of small-scale cycles in shelf and ramp clastic systems: The controlling factors. *Earth-Science Reviews*, **84**: 21-55.